DEPARTAMENT OF PHYSICS
SCHOOL OF SCIENCE AND TECNOLOGY

DIRECT DETECTION OF ORGANIC AND BIOLOGICAL CONTAMINANTS IN INTERNATIONAL SPACE STATIONS

JORGE MANUEL DIAS FERNANDES

Master in Medicinal Chemistry

DOCTORATE IN BIOMEDICAL ENGINEERING

NOVA University Lisbon

april, 2022

DEPARTAMENT OF PHYSICS
SCHOOL OF SCIENCE AND TECNOLOGY

Direct Detection of Organic and Biological Contaminants in International Space Stations

JORGE MANUEL DIAS FERNANDES

Master in Medicinal Chemistry & BSc in Biochemistry

Adviser: Valentina Borissovna Vassilenko
Assistant Professor, NOVA University of Lisbon

Co-adviser: Viktor Fetter
Systems Engineer, AIRBUS Defense and Space

Examination Committee:

Chair: José Paulo Moreira dos Santos,
Full Professor, NOVA University Lisbon

Rapporteurs: Ana Luísa Marques Paixão de Carvalho Maulvault,
Auxiliary Researcher, Instituto Português do Mar e da Atmosfera

Nuno Miguel Ratola Neto,
Principal Researcher, Faculdade de Engenharia da Universidade do Porto

Adviser: Valentina Borissovna Vassilenko,
Assistant Professor, NOVA University of Lisbon

Members: Regina Maria Brandão de Oliveira Duarte,
Principal Researcher, Centro de Estudos do Ambiente e do Mar, Universidade de Aveiro

José Paulo Moreira dos Santos,
Full Professor, NOVA University Lisbon

DOCTORATE IN BIOMEDICAL ENGENEERING

NOVA University Lisbon
april, 2022

Direct Detection of Organic and Biological Contaminants in International Space Stations

ACKNOWLEDGMENTS

I express my gratitude to Professor Valentina Vassilenko, my academic supervisor for supporting me and my work throughout four years of scientific challenges with her insight, feedback, and aid in academic and scientific aspects. Also, for giving me this opportunity to work in a scientific project related to space, in an international setting and, the opportunity to work in the SIRIUS-17 mission. Her support, aid and knowledge provided strength and precision to this dissertation and work, as well as her patience and effort to overcome academic barriers and problems. An appreciation and thanks also to Viktor Fetter, from Airbus, for receiving me with an open mind and making complicated processes and tasks work with simplicity and objectivity, for allowing me to explore this dissertation subject with him, and for valuing my work enough, to allow me to contribute to the dissertation of two Master students, Peter Roth, and Marcel Wolf.

A special acknowledgement and gratitude are also due to all my research colleagues, Paulo Bonifacio, Hojat Lofti, Andreia, Serrano, Anna Poplavska, Pedro Moura, and Paulo Santos for sharing several hours, days, months and years for challenges, successes, cooperation, support, and assistance, and for creating a hard-working group which faced several challenges and hurdles with compassion and empathy. To Paulo Santos especially, for providing a relaxed environment where amusement and laughter were constant and appreciated, as well as for his friendship and understanding. I would like to also thank a great friend, João Rodrigues, which supported me in my scientific efforts as well has my other goals and objectives in life and helped me improve as a person and scientist with a creative and constant desire to discuss any subject with me. To Cátia Cepeda for her encouraging words and advice.

To Marlene Leite, I am grateful for her companionship and love which provided me with immense support during several challenges and frustration while making achievements and celebrations much more enriching and fulfilling.

A big thanks to every staff member I worked with from the Laboratory for Instrumentation, Biomedical Engineering and Radiation Physics (LIBPhys) and the Department of Physics from NOVA School of Science and Technology of NOVA University of Lisbon, which supported through paperwork, materials requisite, and several other minor but important tasks. I also give my gratitude for everyone at G.A.S. Gesellschaft für analytische Sensorsysteme for receiving me warmth and compassion during my early lessons about Ion Mobility spectrometry.

The staff of the Institute for Biomedical Problems of the Russian Academy of Science which helped me during my stay in Moscow with translations, support, and companionship which lasted a full month for the SIRIUS-17 mission. Special to Dimitri Ozerov for helping me everything involving customs and transporting of a scientific instrument and allowing me to share his time with me during working hours and outside working hours.

A special thanks to every single member of the Laboratório de Análises, REQUIMTE – LAQV, from NOVA School of Science and Technology, NOVA University of Lisbon for all the help provided and willingness to aid my scientific research, especially Carla Rodrigues and Nuno Costa. An acknowledgment must also be given for the availability and help provided by Prof. Ana Luisa Fernando, in gathering and obtaining several samples of pure substances for measurements.

Also, to Prof. Mário Diniz for his enormous drive to work, which motivated me to work harder, his desire to discuss and support every single project, task and assignment related to my dissertation and his humble and caring support as a human being and a scientist.

"Persistence is very important. You should not give up unless you are forced to give up."

- Elon Musk.

"It's not worth doing something unless someone, somewhere, would much rather you weren't doing it."

"So much universe, and so little time."

- Terry Pratchett.

ABSTRACT

Detailed, sensitive, and selective monitoring of potentially toxic substances is currently essential to establish suitable health conditions for long-term occupation of spacecrafts, especially since space agencies have plans for habitable stations on the Lunar surface and the human exploration of Mars. Furthermore, as occupation periods increase in spacecrafts, classified as small closed-habitats, novel risks and hazards to health can originate from toxic compounds released by materials, surfaces and microorganisms and contaminate and degrade air, water, life supports and electronic systems. Under microgravity, high radiation and limited resources and rescue options during spaceflight it is critical it constantly monitor environmental conditions to quickly detect toxic compounds and identify bacterial or fungal contamination with high sensitivity and selectivity.

The current monitorization aboard the International Space Station (ISS) is mainly performed off-fline on ground facilities, which delays or offers insufficient time to implement counter measurements. Thus, a demand for novel technologies for in-situ, online detection, and monitorization of a large spectrum of compounds in trace concentrations with minimal resources became vital for mission success. A potential analytical technology capable of filling all necessary requirements is, Ion Mobility Spectroscopy (IMS), which after recent improvements and widespread applications, became a valuable tool for direct detection, quantification, and analysis of Volatile Organic Compounds (VOCs) in ppb_v or ppt_v from several biological matrices without sample preparation and chemical reagents.

Hence, this dissertation aims to examine and evaluate Gas Chromatography coupled with IMS (GC-IMS) as a possible tool to monitor spacecraft environmental conditions in several stages, incorporating air monitoring in ISS analogous conditions, food control and identification of microbial contaminations. Likewise, GC-IMS sensitivity and selectively for VOC detection is investigated, through the development of adequate sampling methodologies, a quantification protocol, establishment, and development of a VOC library for compound identification and a preliminary tool for automatic data processing.

Keywords: International Space Station, Ion mobility spectrometry, biological contamination, space toxicology, volatile organic compounds, space exploration.

RESUMO

Atualmente, a monitoração detalhada, sensível e seletiva de substâncias potencialmente tóxicas é essencial para criar condições de saúde adequadas durante a ocupação prolongada de naves e estações espaciais, especialmente considerando os planos de criar estações habitáveis na Lua e a exploração de Marte. Além disso, o aumento da duração da ocupação de naves espaciais, classificados como espaços confinados, acarretam novos riscos para a saúde humana, devido à libertação de compostos tóxicos de materiais, superfícies e microrganismos, contaminando ar, água e sistemas eletrónicos e de suporte de vida. Aliás, durante voo espacial, microgravidade, elevados níveis de radiação e recursos e opções de resgate limitadas atribuem uma enorme importância à monitorização constante das condições ambientais, à deteção rápida e precisa de compostos tóxicos e, à identificação de contaminações bacterianas ou fúngicas.

A monitoração abordo da Estação Espacial Internacional (ISS) é realizada principalmente *off-line*, em instalações terrestres, atrasando ou impossibilitando a implementação de medidas de mitigação. Assim, novas tecnologias para monitorizarem e detetarem *in-situ*, um grande espectro de compostos em concentrações residuais com o mínimo de recursos, tornaram-se críticas para o sucesso das missões. A Espectroscopia de Mobilidade Iônica (IMS) é uma tecnologia analítica, potencialmente capaz responder a tais exigências, e avanços recentes e utilização generalizada, tornaram-na uma ferramenta relevante na deteção direta, quantificação e análise de Compostos Orgânicos Voláteis (VOCs), em ppb_v ou ppt_v, de várias origens biológicas sem preparação de amostra e reagentes químicos.

Assim, pretende-se examinar e avaliar a Cromatografia Gasosa acoplada com IMS (GC-IMS) para monitorizar condições ambientais em naves espaciais através da monitorização de ar em condições idênticas à ISS, controlo de alimentos e identificação de contaminações microbianas. Também, a sensibilidade e seletividade da GC-IMS na deteção de VOCs é investigada, pelo desenvolvimento de metodologias de amostragem, métodos de quantificação, conceição e desenvolvimento de uma biblioteca de VOCs para identificação e uma ferramenta preliminar para processamento automático de dados.

Palavras chave: Estação espacial internacional, espectrometria mobilidade iónica, contaminações biológicas, toxicologia espacial, compostos orgânicos voláteis, exploração espacial.

CONTENTS

ACKNOWLEDGMENTS V

ABSTRACT IX

RESUMO XI

CONTENTS XIII

LIST OF FIGURES XVII

LIST OF TABLES XXVII

ACRONYMS XXIX

CHAPTER 1. GLOBAL PREFACE: SUBJECT, SCOPE, AIM AND STRUCTURE 1

1.1 Subject 3

1.2 Scope & Focus 3

1.3 Motivation & Aim 4

1.4 Structure Outline 5

1.5 Scientific Outputs 6

CHAPTER 2. INTERNATIONAL SPACE STATION: ENVIRONMENT & MONITORIZATION 9

2.1 Structure and Assembly 11

2.2 Operation and Life Support Systems 14

2.3 State-of-the-art: Monitorization of Contaminants 24

2.3.1 Contaminants in the International Space Station 24

2.3.2 Microbial surveys and Microbial Ecology of the ISS 28

2.3.3 Strategies for Monitoring Contaminants Aboard the ISS 37

2.3.4 Mass and Ion Mobility Spectrometry in Space Exploration 45

2.4 Research in Space and its Future 50

CHAPTER 3. ION MOBILITY SPECTROMETRY: HISTORY, PRINCIPLES, & APPLICATIONS 53

3.1 Ion Mobility Spectrometry: History & Principle 55

3.2 Ion Mobility Spectrometry: Current instrumentation 64

3.2.1 Drift time ion mobility spectrometry (DTIMS) 65

3.2.2 Travelling wave Ion Mobility Spectrometry (TWIMS) 66

3.2.3 High field asymmetric waveform ion mobility spectrometry (FAIMS) 67

3.2.4 Trapped Ion Mobility Spectrometry (TIMS) 69

3.2.5 Aspiration Ion Mobility Spectrometry (AIMS) 69

3.2.6 Differential mobility Analysers (DMA) 70

3.3 Ion Mobility Spectrometry: Hyphenated Methods 72

3.3.1 Coupled Ion Mobility Spectrometry with Mass Spectrometry (IMS-MS) 72

3.3.2 Pre-separation Methods Coupled with Ion Mobility Spectrometry (GC-IMS) 74

3.4 Ion Mobility Spectrometry: Versatility and Applications 74

3.4.1 Military and Security: explosives, warfare agents and drugs 75

3.4.2 Industrial and Environmental: air quality monitorization 77

3.4.3 Medicine: breath, skin, urine, faeces and COVID 79

3.4.4 Microbiology: bacteria and fungi identification 82

3.4.5 Foodomics: food quality and adulteration 84
CHAPTER 4. GAS ANALYSIS, CALIBRATION & APPARATUS: METHODS & MATERIALS 87
4.1 Gas Analysis with Ion Mobility Spectrometry 89
4.2 Headspace Analysis of Volatile Organic Compounds 93
4.2.1 Static Headspace Methods 94
4.2.2 Dynamic and Purge Headspace Methods 95
4.3 Generation of Calibration Gas Standards 97
4.3.1 Understanding the Units of Measurement Employed 98
4.3.2 Static Systems to Generate Standard Gas Mixtures 100
4.3.3 Dynamic Systems to Generate Standard Gas Mixtures 104
4.3.4 The suitability of permeation tubes for IMS calibration 109
4.3.5 Calculation of Detection and Quantification Capabilities 113
4.4 Ion Mobility Spectrometry: Experimental Parameters & Data 117
4.4.1 Effects of Experimental parameters 118
4.4.2 Generalized Aspects of IMS Data Analysis 122
4.4.3 Chemometric & IMS Data Analysis Methods 125
4.5 Selected Ion Mobility Spectrometer 134
4.5.1 Ion Mobility Spectrometer: Technical data & housing structure 135
4.5.2 Operation and Graphical User Interface 140
4.5.3 Associated Software for data analysis 143
CHAPTER 5. DETECTION AND IDENTIFICATION OF CONTAMINANTS: RESULTS 147
5.1 Preliminary Tests and Analytical Assessment/Evaluation 149
5.1.1 Distinction between different volatile organic compounds emission 149
5.1.2 Carrier Flow Influence on Separation of Volatile Organic Compounds 151
5.1.3 Analysing Indoor Air Variations in Ventilated and Unventilated Conditions 155
5.1.4 Examination of emission due to microbial contamination 157
5.2 The SIRIUS-17 Experiment 160
5.2.1 Structure of the Ground-based Experimental Complex 160
5.2.2 Overall Goals and Experimental Schedule 163
5.2.3 Analysis of the Volatile Organic Compound Emission 164
5.2.4 Identification of detected volatile organic compounds 168
5.2.5 General analytical performance and conclusions 170
5.3 The Breath Stress Experiment 172
5.3.1 Exhaled breath analysis and mental stress 172
5.3.2 Goals, experimental design, methodology and stimulus 174
5.3.3 Breath sampling, breath analysis and stress monitoring 176
5.4 Microbial Detection and Identification 179
5.4.1 Initial Detection and Characterization of Bacterial Metabolites 179
5.4.2 On-line Monitoring of Microbial Growth in Liquid Media 184
5.5 Food Quality Control and Seaweeds 191
5.5.1 Microbial Degradation of Fish and GC-IMS as a Tool for Quality Control 191
5.5.2 Seaweeds: A Promising Superfood for Space Exploration and GC-IMS 195
5.6 Construction of a VOC database: VOC Library 203
5.6.1 Important Compounds to be Detected in the International Space Station 204
5.6.2 Compounds and Methodology Used to Gather Data 206
5.6.3 VOC Database: Creation and Development 206
5.6.4 Drift Time Data from Different VOC Functional Groups 210
5.7 Gas Calibration procedure and estimation curves 213
5.7.1 Development of a Method for Gas Calibration 213
5.7.2 Description of the Gas Calibration Protocol 214

5.7.3 Application of the developed protocol for VOC calibration 215
5.8 Development of a software for data processing 223
5.8.1 IMS Data formats, importance, and value 223
5.8.2 Early algorithm for peak detection and quantification 225
5.8.3 Current algorithm and future development 229
CHAPTER 6. OUTLOOK ON THE COMPETENCES OF IMS: DISCUSSION & CONCLUSIONS 231
6.1 Overall Assessment 233
6.2 Evaluation of GC-IMS capabilities 233
6.2.1 Continuous Environmental Air Monitoring in Spacecrafts 233
6.2.2 Microbial identification and monitorization of microbial growth 234
6.2.3 Food spoilage by microorganisms and food production in space 234
6.2.4 Development of a VOC database for compound identification 235
6.2.5 VOC Calibration in low concentrations for monitorization 236
6.2.6 Data processing tools for complex samples and results 236
6.2.7 The potential of IMS in Health Monitoring 237
6.3 Future work and perspective 237
REFERENCES 239
A. APPENDIXES 249
APPENDIX I. Supplementary data: Figures 251
APPENDIX II. Statistical data: SIRIUS-17 & Seaweeds 261

LIST OF FIGURES

Figure 2.1 — International Space Station structure depicting modules and configuration as of Nov 2021. Modules are identified with corresponding structural name or abbreviation. Blue and black rectangles indicate solar panels, dashed lines refer to the established connection between modules and text colour identifies elements created by each space agency [8]. 13

Figure 2.2 — On-Orbit ISS ECLS Hardware distribution as of February 2010. Differences and module distribution of life support systems between the Russian (left of PMA-1) and US orbital segments (right of PMA-1) [11]. 16

Figure 2.3 — The Simplified Life Support Systems Schematic. Shows all life support system elements [21]. 20

Figure 2.4 — Illustration of the ISS showing its mass, habitable volume, speed, wingspan (equal to an American football filed), and the structures responsible for power generations and their respective output. [23] 21

Figure 2.5 — ISS bacterial isolation frequency in pre- and in-flight surface and air samples since 1998 to 2011. Inset illustrates the top 3 most frequently isolated genera of bacteria [50]. 29

Figure 2.6 — ISS fungal isolation frequency in pre- and in-flight surface and air samples since 1998 to 2011. Inset illustrates the top 3 most frequently isolated genera of fungi [50] 30

Figure 2.7 — Most abundant organisms in the international space station and their human association [52]. ... 31

Figure 2.8 — Relative abundances of the most common bacterial families found on surfaces of the ISS. Pie chart containing information from the most abundant microbes' families in 15 ISS surfaces [52]. 32

Figure 2.9 — ISS schematic displaying all eight locations sampled over three flights. Location #1, port panel next to cupola (Node 3); location #2, waste and hygiene compartment (node 3); location #3, advanced resistive exercise device (ARED) foot platform (node 3); location #4, dining table (node 1); location #5, zero G stowage rack (node 1); location #6, permanent multipurpose module (PMM) port 1 (PMM); location #7, panel near portable water dispenser (LAB); and location #8, port crew quarters, bump out exterior aft wall (node 2) [52]. 33

Figure 2.10 — Cultivable bacterial and fungal burden from eight locations on the ISS over a 14-month period. Bar graph representing the CFU/m^2 based on location showing the number of bacteria isolated on Reasoner's 2A agar and Blood Agar Plates were averaged to obtain a number for "Bacteria." Bars represent the average CFU/m^2 at each location with the capped lines showing the lowest and highest value in that group (N = 3). The differences in averages observed in (a, b) were not statistically significantly [52]. 34

Figure 2.11 — Diagram summarizing different strategies for monitoing contaminants in spacecrafts, including the ISS, in terms of mission duration; Short, days or few weeks or Long, six months or more. 38

Figure 2.12 —. Adhesive sheet for microbial monitoring in the space habitat. 1. Photograph of the adhesive sheet; 2. Attach the adhesive area to the sampling site and press; 3. peel the adhesive sheet off the sampling site [72]..... 43
Figure 2.13 —. Microbial monitoring strategy summary for spacecrafts and payloads [79]..... 44
Figure 2.14 — A simplified scheme of the operation systems and principle of mass spectrometry [78]. 47
Figure 2.15 — A block diagram for the VOA based on GC-IMS for both nonpolar and polar detection of VOCs [103]. 49
Figure 3.1 — Important historical development of the field Ion Mobility [94]. A distinction is made in the publication frequency for both time and space-dispersive IM-MS publications. (Left) Histogram showing the number of publications per year in ion mobility and ion mobility-mass spectrometry with focus on IM-MS (scale is truncated at 300). (Right) Historical milestones for the development of ion mobility and IM-MS technologies and instrumentation..... 56
Figure 3.2 — Summarized events within a traditional ion mobility spectrometer equipped with a membrane inlet and a bidirectional flow system (top) and (a) Bidirectional gas flow ion mobility spectrometer and (b) unidirectional gas flow ion mobility spectrometer schematic (bottom) [96]..... 58
Figure 3.3 — Three examples of the possible representation of IMS spectra including their respective axis. (a) Single IMS spectrum or 2D Graph, [103] (b) Heatmap representation, [104] (c) 3D representation (Height denotes intensity) [105]..... 63
Figure 3.4 — A summary of IMS's working principle, showing a GC-IMS drift tube scheme on top and below the ionization reactions taking place in a drift tube without, analyte, with analyte and high analyte load [97, 106]. 64
Figure 3.5 — Schematic diagram of an ion mobility spectrometer (IMS) with a corona discharge source [109]. 66
Figure 3.6 — Ion mobility spectrometry layouts of mobility tubes and operational principles of several instrumentation types. **(A)** Schematic of an Ion mobility–mass spectrometer device; **(Ba)** A simplified schematic for a Drift time ion mobility spectrometer (DTIMS); **(Bb)** Drift tube diagram for a Travelling wave IMS (TWIMS) instrument; **(Bc)** A representation of a Trapped IMS (TIMS) drift tube and operational steps [107]; **(b)** Schematic of an Aspiration IMS (AIMS) and its spectrum; **(c)** Operation, spectra, and drift tube structure of a Differential mobility Spectrometry (DMS) [111]. High field asymmetric waveform ion mobility spectrometer (FAIMS) drift tube is comparable in to DMS(Table 3.1). DMS referes to a planar (p-FAIMS) electrode configuration and FAIMS to a cylindrical (c-FAIMS electrode configuration [108]..... 68
Figure 3.7 — IMS technology variations with applied electronic field and gas dynamics. Relative parameters of each IMS platform and key attributes are represented in bullet points, including their ability to measure CCS information, types of electronic field, type of gas flow, ion packet distribution, instrument footprint, and modularity (Adapted). [110]..... 71

Figure 3.8 — Relative numbers of compounds in each class detected in faeces, urine, breath, skin secretions, milk, blood and saliva. (Based on the number of different compounds identified, not upon their relative concentrations.) [121]. 80
Figure 4.1 — The scheme of the entire procedure of GC-IMS analysis including sampling and optional steps [113]. 90
Figure 4.2 — Chemical structure of several types of volatile organic compounds in gas analysis [142]. 93
Figure 4.3 — Diagrams showing the experimental setup for static headspace, dynamic and pudge sampling [146]. 94
Figure 4.4 — A generalized schematic of processes and factors involved in static and dynamic headspace sampling [147]. 96
Figure 4.5 — The different types of methodologies used to produce standard gas mixtures for calibration [157]. 101
Figure 4.6 — A schematic showing a type of permeation device, the permeation process, and its elements [162]. 110
Figure 4.7 — Definitions and guidelines to estimate the limit of detection in analytical method validation [166]. 115
Figure 4.8 — Definitions and guidelines to calculate limit of quantification in analytical method validation [166]. 116
Figure 4.9 — Signal-to-noise examples of an analyte peak of 10:1 ratio (left) and 3:1 ratio (right)..... 117
Figure 4.10 — Humidity effects studied from a single compound, TMA, in a UV-IMS instrument. (a) TMA Spectra at a constant concentration (220 ppb) for measures with varying humidity percentage and (b) the humidity and drift time relationship for reactive ion peaks (RIP) and the TMA monomer in an UV-IMS device [112]. 120
Figure 4.11 — The effect of humidity on the peak intensity of several compounds (left) and the formation of production ion by chemical ionization with ^{3}H in a stand-alone IMS (right). IMS signal intensities of toluenes and chlorobenzenes over the carrier gas moisture level (left). The relationship between reactant ions composition and carrier gas moisture at a constant temperature of 80◦C (right) [169]. 121
Figure 4.12 — General scheme of IMS data analysis workflow, IMS peak response as a normal Gaussian curve and signal-to-noise examples of 10:1 for estimating LOQ and 3:1 for estimating LOD [172]..... 124
Figure 4.13 — A schematic of the operational system of the GC-IMS instrumentation selected for gas analysis [173]. 136
Figure 4.14 — The front view of the GC-IMS device labelling its specific components by number [173]. 137
Figure 4.15 — The back view of the GC-IMS device labelling its specific components by number [173]. 137
Figure 4.16 — Front (top) and rear (bottom) views of the Circular Gas Flow Unit (CGFU) and their component [174]. 139
Figure 4.17 — Windows selection bar showing the five available windows and the selection marked in blue [173]. 140

Figure 4.18 — Default window highlighting seven components: (1) Pressure display, (2) Pump, (3) Averaging; (4), Drift-Voltage (positive/negative), (5) RIP Window, (6) Flow and (7) Temperatures [173].....141
Figure 4.19 — A view of the System Windows containing (1) Measurement Settings Buttons, (2) Device Settings, (3) System Settings, (4) System Information Panel, (5) Sample Loop setting, (6) Cleaning Mode and (7) Standby Mode options [173].....143
Figure 4.20 — The main window and elements of the Laboratory Analytical Viewer (LAV) version 2.2.1. (1) Browser Window, (2) Project Window, (3) Attribute Lists and (4) Spectra region.....144
Figure 5.1 — Headspace spectra of Pepsi Cola (Left), Coca-Cola (Middle) and a room air sample (Right). The signals detected in the sample air, were removed from other spectra. Red squares mark signals unique to Coca-Cola, green squares mark signals with higher intensities in Coca-Cola compared to Pepsi and yellow squares mark signals with higher intensities in Coca-Cola compared to Pepsi. A label is also present for all important signals with retention time in seconds (top) and drift times relatively to RIP position (bottom)).....150
Figure 5.2 — Separation of room air VOCS with a constant EPC2 flow (left) and an EPC2 flow ramp (right). 152
Figure 5.3 — Comparison of the separation effect of four different programs, Test Flow A through D, highlighting the major differences with an orange circle. White squares mark several signals showing flow A and B degree of separation while orange and green squares mark flow C and D degree of separation respectively of the same signals.....153
Figure 5.4 — Headspace measurements of four different toothpaste brands. Headspace samples were measured with Flow D.....154
Figure 5.5 — Total volatile organic compound intensity from indoor air measurements in a total of 48 hours with a period of 24 hours ventilated interval and another 24 hours in an unventilated state.....156
Figure 5.6 — Volatile organic compound emission from freshly squished orange juice over 5 days and an highlight of the characteristic pattern of microbial decomposition from day 2 to day 3.....158
Figure 5.7 — General structures of the Ground-based Experimental Complex (NEK) and layout with all modules labeled by name with a summary of their uses and equipment. The location of the GC-IMS device during the SIRUS-17 experiment is also marked in the image [183].....161
Figure 5.8 — NEK bluepring showing its five modules: habitat, utility, medical composing the main spacecraft, a Martian-lander ship and a simulator of the Martian surface, for a combined volume of 550 m^3 [184]. 162
Figure 5.9 — A picture showing location of the CGFU and GC-IMS apparatus is shown (below left) its respective location in the NEK complex blueprint (right) [183].....165
Figure 5.10 — Signal intensity (volume) of Sir-1, 2, 3, 4, 5, 6 and 8 for all measurements collected during SIRIUS-17.....166
Figure 5.11 — Signal intensity of Sir-7, 9, 10, 11, 12, 14, 20, 21 and 28 for all measurements collected during SIRIUS-17.....167

Figure 5.12 — Signal intensity (volume) in volts for Sir-13, 15, 16, 19, 24, 25, 29, 32 and 33 for all SIRIUS-17 measurements. 167
Figure 5.13 — Signal intensity (volume) in volts for Sir-17, 18, 22, 23, 26, 27, 30, and 31 for all measurements. 168
Figure 5.14 — A 2D plot representing retention, drift times for all signals and the CAS number for the respective identified signals (left) and RIP exemplified by a vertical red line. Spectrum collected during SIRIUS day 2 with detected signals labelled, y axis corresponding to retention time in seconds and x axis the drift time relative to RIP which is seen as continuous red signal at 1.0 (right) 171
Figure 5.15 — Diagrams of neutral and stress session showing each procedure stage, time frames, breath samples (BS) collected and continuous monitorization of Galvanic skin response and central blood pressure. 175
Figure 5.16 — GC-IMS spectra demonstrating signals present in exhaled breath after a neutral stimulus (left) and a stress stimulus (right). Signals labelled with whit rectangles represented the main differences between the two conditions detected through breath analysis. 177
Figure 5.17 — Unsupervised Analysis with Principal Component Analysis (PCA) for all six stress sensitive breath compounds identified through PLS-DA. (A) PCA for the first stimulus (BS02): stress session (black dots) and neutral sessions (white dots). (B) PCA for the second stimulus (BS03): stress session (black dots) and neutral sessions (white dots). Two dimensional PCA is presented in the left and three dimensional PCA is shown in the right side. 178
Figure 5.18 — Diagram for the experimental procedure used to measure bacterial emission of volatile compounds. 180
Figure 5.19 — A schematic summarizing all bacteria, growth media, experimental conditions and total number of swabs collected and measured during this study. 180
Figure 5.20 — Emission spectra from LB medium, cultures of *P. aeruginosa* at 23°C and at 40°C after 24 hours. 181
Figure 5.21 — Emission spectra from LB medium, cultures of *P. aeruginosa* at 23°C and at 40°C after 48 hours. 182
Figure 5.22 — Emission spectra from LB medium, cultures of *E. coli* at 23°C and at 40°C after 24 hours. 183
Figure 5.23 — Emission spectra from LB medium, cultures of *E. coli* at 23°C and at 40°C after 48 hours. 183
Figure 5.24 — Emission patterns for LB medium, *P. aeruginosa*, *E. coli* and a mixture of both bacteria. 184
Figure 5.25 — Steps for cultivation of *E. coli* and *S. aureus* in liquid media, FTM and TSB for on-line analysis. 185
Figure 5.26 — Sterile FTM media emission over 120 hours at 33°C after 2 hours (left), 58 hours (middle) and 100 h (right). Yellow rectangles represent shallow increasing signals, white rectangles represent fast increasing signals and green rectangles represent signals with decreased intensity from the previous measurement. Retention times in seconds and drift time relative to RIP, are shown for each labelled peak. 186
Figure 5.27 — Sterile TSB media emission over 120 hours at 23°C after 2 hours (left), 58 hours (middle) and 100 h (right). Yellow rectangles represent shallow increasing signals, white rectangles represent

fast increasing signals and green rectangles represent signals with decreased intensity from the previous measurement. Retention times in seconds and drift time relative to RIP, are shown for each labelled peak. 187
Figure 5.28 — Emission detected from *Staphylococcus aureus* inoculated in FTM media emission over 120 hours. Red, green, and yellow squares represent signals increasing, decreasing and new from the previous spectrum, respectively. 188
Figure 5.29 — Emission detected from *Staphylococcus aureus* inoculated in TSB media emission over 120 hours. Yellow, red, and green squares mark new signals, increases, and decreases and from the previous spectrum. 189
Figure 5.30 — Emission detected from *Escherichia Coli* inoculated in FTM media emission over 120 hours. Yellow, red, and green squares mark new signals, increases, and decreases and from the previous spectrum. 190
Figure 5.31 — Emission detected from *Escherichia Coli* inoculated in TSB media emission over 120 hours. Yellow, red, and green squares mark new signals, increases, and decreases and from the previous spectrum. 190
Figure 5.32 — Volatile organic emission from Sarda sarda at ambient temperature (23°C) for 3 days. Signals corresponding to ammonia, CAD, PEA, SPD/SPM and TRP/TYR were labelled with green, yellow, pink, red and white, respectively. 193
Figure 5.33 — Volatile organic emissions of *Trachurus trachurus* at ambient temperature (23°C) during 3 days. Marcked signals correspond to ammonia, CAD, PEA, SPD/SPM were labelled with green, yellow, pink, and red, respectively. 194
Figure 5.34 — Volatile organic emissions of *Sardina pilchardus* at ambient temperature (23°C) for 3 days. Signals corresponding to ammonia and CAD were labelled with green and yellow, respectively. 194
Figure 5.35 — Measurements for day 2 of all three species of fish at ambient temperature (23°C). Signals from blank measurements of air are identified with orange squares and fish characteristic signals by green squares. 195
Figure 5.36 — Phycoprints of three seaweeds from each category (red, brown, and green): *Osmundea pinnatifida* (Red seaweed) right, *Ulva rigida* (Green seaweed) centre, *Undaria pinnatifida* (Brown seaweed) left. Red, green, and yellow squares represent unique pattern signals for the red, green, and brown seaweeds respectably. 199
Figure 5.37 — Principal Component Analysis Biplot of Three Seaweeds. PCA biplot of five replicates of the headspace emission of three seaweeds *Osmundea pinnatifida* (Red), *Ulva rigida* (Green) and *Undaria pinnatifida* (Brown) for 10 peak intensities, red specific peaks: r1, r2, r3, green specific: g1, g2, g3, brown specific: b1, b2, b3 and seaweed common peak: sc. Each peak (characteristic) influence on the principal component is represented in the plot with dashed lines and labelled in their corresponding seaweed colour (red, green, and brown). 201
Figure 5.38 — Headspace emission spectra changes over time of *Undaria pinnatifida*. Measurements over time after 1 hour, 2 hours, 3 hours, 24 hours, and 36 hours. Peaks increasing due to acclimatization are

represented with green squares and two predominant new signals appearing at 24 hours re marked in red squares. 202
Figure 5.39 — Volatile organic compound contained in the VOC database between 0 and 500 second of retention time. Each circle represents one signal, which are coloured by compound class and labelled with CAS number and common name. The GC-IMS flow parameters are displayed at the bottom right. 208
Figure 5.40 — Archetypical signal shapes for 3 chemical groups, aldehydes, alchools and ketones (exemplefied by monomer and dimers signals from hexanal (left), hexanol (mid) and hexanone (right)). 209
Figure 5.41 — Drift time distribution of monomer (DTm) and dimer (DTd) signals from several alcohols, aldehydes, and ketones with increasing number of carbon atoms in their chemical structure. Alcohols are represented by the colour red, aldehydes by blue, and ketones by purple, while monomer are marked by a lighter tone and dimer signals have a darker tone from their respective functional group colour. 211
Figure 5.42 — Drift time distribution of monomer (DTm) and dimer (DTd) signals from several saturated aldehydes (Aldehydes) and unsaturated aldehydes (EnAldehydes) with increasing number of carbon atoms. Saturated aldehydes are represented by the colour blue and unsaturated aldehydes by green whereas monomers have a lighter tone and dimers darker tone of their respective aldehyde type. 212
Figure 5.43 — Thermogravimetric analysis for a 2-butanone permeation tube at 40 °C for 65 hours. 216
Figure 5.44 — Logarithmic curves adjusted to signal intensity vs concentration of measurements conducted for 4 permeation tubes containing 2-hexanone. Circles correspond to total signal intensity (volume) of both 2-hexanone monomer and dimer (2-hexanone [T]) and triangles to signal intensity (volume) of 2-hexanone dimer. Logarithmic equations are shown in bold for the total signal intensity and in normal text for the dimer while standard deviations are present for each point in red. 218
Figure 5.45 — Logarithmic curves adjusted to signal intensity vs concentration of measurements conducted for 4 permeation tubes containing 2-butanone. Circles correspond to total signal intensity (volume) of both 2-hexanone monomer and dimer (2-butanone [T]), triangles to signal intensity (volume) of 2-butanone dimer and diamonds to signal intensity of 2-butatnone monomer. Logarithmic equations are shown in bold for the total signal intensity and in normal text for the dimer while standard deviations are present for each point in red. 220
Figure 5.46 — Logarithmic curves adjusted to signal intensity vs concentration of measurements conducted for 4 permeation tubes containing 1-butanol. Circles correspond to total signal intensity (volume) of both butanol monomer and dimer (Butanol [T]) and triangles to signal intensity (volume) of butanol dimer. Logarithmic equations are shown in bold for the total signal intensity and in normal text for the dimer while standard deviations are present for each point in red. 222
Figure 5.47 — Single IMS or 2D spectrum (right) and 3D spectrum or heatmap examples (left) (spectra processed and obtained from LAV of BreathSpec (GC-IMS) measurements). 224

Figure 5.48 — Detected peaks before (left) and after (right) the application of a developed filtering method with the developed algorithm for automatic peak detection and quantification. *Y*-axis represents the retention time in seconds, *x*-axis the drift time in milliseconds with RIP position defined as 0, and detected peak labelled as dashed lines and numbers inside a grey square.....227
Figure 5.49 — Automatically detected IMS peaks and respective intensity (volts) above a threshold of 0.15 volts without noise filtering (left) and after applying a noise filter (right).....228
Figure 5.50 — Schematic actions and methodologies used in the algorithm for automatic peak detection and quantification of GC-IMS spectra.....229

APPENDIX I

Figure A.1 — Culture- and qPCR-based analyses of microbial burden (bacteria). A total of 133 bacterial isolates (A) and 81 fungal isolates (B) that were cultured from eight locations during three flights, were picked for identification. The bar length (middle panel) represents the number of isolates that were identified as a particular species or genus (left panel) and the bar colour indicates the same genus. The colour filled checkerboard (right panel) indicates from which samples the bacteria were cultured in which black represents flight 1, red, flight 2 and black, flight 3 [52].....253
Figure A.2 — Culture- and qPCR-based analyses of microbial burden (fungi). A total of 133 bacterial isolates (A) and 81 fungal isolates (B) that were cultured from eight locations during three flights, were picked for identification. The bar length (middle panel) represents the number of isolates that were identified as a particular species or genus (left panel) and the bar colour indicates the same genus. The colour filled checkerboard (right panel) indicates from which samples the bacteria were cultured in which black represents flight 1, red, flight 2 and black, flight 3 [52].....254
Figure A.3 — Depiction of GSC and SSAS devices used for sampling cabin atmospheres [75]. Right side pictures: Top right, GSC (https://lsda.jsc.nasa.gov/Hardware/hardw/636) and bottom right, SSAS (https://lsda.jsc.nasa.gov/Hardware/hardw/637).....255
Figure A.4 — Calibration Certificate Permeation Tubes showing the permeation rate, substance characteristics, calibration temperature, tube mass and calibration graph from Owlstone Inc. [163].....255
Figure A.5 — Views of the Spectra window highlighting vertical (1), horizontal (3) and view control bars (2) (top) and menus available for program (1), sample (2) and recording options (3) (bottom) [173].....256
Figure A.6 — The five sections of the Substances window from the Breathspec® instrument: (1) Substances List, (2) Substances List Control Panel, (3) Enable Button, (4) Substance Calibration Information Area, (5) Current Loop Settings [173].....257
Figure A.7 — The five sections contained in the Programs window (1) Measurement program List window, (2) Selected Program Window, (3) Selected Program Window Control Panel, (4) Measurement Program Control Panel, (5) Program Repetition and Average Settings [173].....257
Figure A.8 — Heart Rate (top) and Galvanic Skin Response GSR (bottom) mean responses obtained during the Breath Stress expeiment for both stress (red) and relax (blue) sessions.....258
Figure A.9 — Bacterial growth curve showing phases: (i) lag, (ii) exponential, (iii) stationary and (iv) death phases [211].....259

Figure A.10 — Changes over time of characteritic microbial growth signal, (ES 53) for *S. aureus* and *E. coli* inoculated in FTM.....259
Figure A.11 — A fragment of the VOC database developed for volatile organic compound identification of GC-IMS signals showing a colour scheme the alcohol functional group. VP corresponds to vapor pressure, Vm to molar volume, K_0 is the reduced ion mobility constant, Aff. $_{Proton}$ is the proton affinity and OBS are observation.....260

LIST OF TABLES

Table 2.1 — Contaminants found in the ISS atmosphere and their average concentration in mg/m^3 and ppm [43]. 26
Table 3.1 — Summarized characteristics of IMS types highlighting their similarities and differences [108]. 71
Table 4.1 — Summarized steps and methods used in pre-processing 1D, 2D and 3D ion mobility spectrometry datasets [172]. 128
Table 4.2 — Software and toolbox packages used and employed in IMS data analysis including gold and availability [134] 129
Table 4.3 — Summary of pattern recognition methods used in IMS data analysis [172]. 132
Table 4.4 — A summary of GC-IMS and CGFU dimensions, power supply and characteristics [108]. 139
Table 5.1 — GC Column Flow variation for each of the four programs used to test mixture separation. 153
Table 5.2 — Developed and optimized sampling program after several preliminary test in indoor and VOC analysis. 159
Table 5.3 — Time intervals of measurement sets collected during SIRIUS-17 displaying data, experiment days, number of samples (#S), hours and minutes (T) for measurement. 165
Table 5.4 — Retention and drift time of detected signal during SIRIUS-17 and respective identification with CAS number, molecular weight, proton affinity (Aff.$_{proton}$) and Hazard class. 169
Table 5.5 — Biogenic amines drift times, ion mobility constant (K) and reduced ion mobility constant (K_0). 192
Table 5.6 — Compounds identified from the VOC emission of 10 seaweeds. Compound name, CAS number, Drift time (Dt) and retention time (Rt) means, total number of seaweeds in which the compound was identified and the specific species are show by code: *Osmundea pinnatifida* (OP), *Gracilaria gracilis* (GG), *Grateloupia turuturu* (GT) and *Porphyra spp.* (PS), *Ulva rigida* (UR) and *Codium tomentosum* (CT), *Undaria pinnatifida* (UP), *Fucus vesiculosus* (FV), *Bifurcaria bifurcata* (BB) and *Saccorhiza polyschides* (SP) (coloured text corresponds to seaweed colour group). 200
Table 5.7 — Top priority compounds VOCs to be controlled on the RS-ISS defined at the IBMP. Compounds identified and added to the VOC Library are marked by an "x" and compounds measured that provided unidentifiable data are marked by "---". PDK represents maximum allowed concentration from the Russian ("*Predelno dopustimaya koncentraciya'*). 205
Table 5.8 — Summary of the results obtained for four permeation tubes of 2-hexanone to establish a calibration curve. Concentration is represented in parts-per-billion and the respective mean intensity (monomer and dimer signals) for 5 replicates, the standard deviation, hoven temperatures and respective gas flows and emission rate in ng/min for each tube. 217

APPENDIX II

Table A.1 — Data from 33 detectated peaks of all measurements collected during SIRUS-17 with collection times, mean intensity (int.), and standard deviation (SD).....263

Table A.2 — Seaweeds' unique peaks (UnP) on their respective colour group and species specific (x). Each seaweed is represented by a two-letter code and corresponding scientific name, drift (milliseconds) and retention (seconds) time, mean and standard deviation, peak presence in other species (2 letter code), species-specific peaks (x-marked), identified compounds (#CAS), total peaks, and species-specific peak percentages (UnP) relative to the total detected peaks. ∀\ {} represents "all except" the seaweed species inside the braces 267

Table A.3 — Data obtained for three permeation tubes of 2-butanone for the establishment of a calibration curve with concentration represented in parts-per-billion, respective mean intensity (monomer and dimer signals) for 5 replicates, standard deviation, hoven temperatures and respective gas flows and emission rate in ng/min for each tube.....274

Table A.4 — Data obtained for two permeation tubes of 1-butnanol for the establishment of a calibration curve with concentration represented in parts-per-billion, respective mean intensity (monomer and dimer signals) for 5 replicates, standard deviation, hoven temperatures and respective gas flows and emission rate in ng/min for each tube.....274

ACRONYMS

ACC	Air Contamination Control
ACLS	Advanced Closed-Loop System
ACS	Atmosphere Control and Supply
ALS	Alternating Least Squares
ANITA	Analyzing Interferometer for Ambient Air
ANOVA	Analysis of variance
AOAC	Association of Analytical Communities
API-MS	Atmospheric Pressure Ionization - Mass Spectrometry
AQM	Air Quality Monitor
AR	Atmosphere Revitalization
ASI	Italian abbreviation for Italian Space Agency, "Agenzia Spaziale Italiana"
BEAM	Bigelow Expandable Activity Module
BIOSMHARS	Biocontamination Specific Modelling in Habitats Related to Space
BLSS	Bioregenerative Life Support System
BMI	Body-mass Index
BMP	Russian abbreviation for Micro Purification Unit
CAD	Cadaverine
CBA	Charcoal bed assembly
CBEF	Cell Biology Experiment Facility
CBM	Common Berthing Mechanisms
CCAA	Common Cabin Air Assembly
CCS	Collision cross-section
CDRA	Carbon Dioxide Removal Assembly
CGFU	Circular Gas Flow Unit
CNES	"Centre National d'Études Spatiales" also known as the French Space Agency
COPD	Chronic Obstructive Pulmonary Disease
CPA	Combustion products analyser
CSA-CP	Compound specific analyser-combustion products
CSA-H	Compound Specific Analyzer - Hydrazines
CT	Crew Transfer Vehicles
CWQMK	Colorimetric Water Quality Monitoring Kit
DART	Direct analysis in real time
Desert RATS	Parabolic Flight, Desert Research and Technology Studies
DESI	Desorption Electrospray Ionization
DL	Detection limit
DLR	"Deutsches Zentrum für Luft und Raumfahrt", German Aerospace Center

DMA	Differential Mobility Analysers
DMS	Differential Mobility Spectrometer
DSITMS	Direct Sampling Ion Trap Mass Spectrometry
DTIMS	Drift time Ion Mobility Spectrometry
ECLSS	Environmental Control and Life Support System
ELDO	European Launcher Development Organisation
EPA	Environmental Protection Agency
EPC	Electronic Pressure Control Unit
ESA	European Space Agency
ESI	Electrospray Ionization
ESRO	European Space Research Organisation
EURATOM	European Atomic Energy Community
EVA	Extravehicular activity
FAIMS	High-Field Asymmetric Waveform Ion Mobility Spectrometry
FDA	Foods and Drugs Administration
FDS	Fire Detection and Suppression
FEP	Fluorinated ethylene propylene
FGB	Russian abbreviation for Functional Cargo Block, "Funktsionalno-gruzovoy blok"
FMK	Formaldehyde Monitoring Kits
FTIR	Fourier Transform Infrared Spectroscopy
FTM	Fluid Thioglycollate Media
GALCIT	Guggenheim Aeronautical Laboratory California Institute of Technology
GC	Gas Chromatography
GC-M	Gas Chromatography–Mass Spectrometry
GDL	Gas Dynamics Laboratory
GIRD	Russian abbreviation for “Group for the Study of Reactive Motion”
GPU	Graphics Processing Unit
GSC	Grab sample collectors
GSR	Galvanic skin response
HA	Hydrogen atom transfer
HCA	Hierarchical Cluster Analysis
HEPA	High-efficiency particulate air
HERA	Human Exploration Research Analog
HESTIA	Human Exploration Spacecraft Testbed for Integration and Advancement
HIS	Histamine
HMP	Human Microbiome Project
HR	Heart rate
HRP	Human Research Program
IAEA	International Atomic Energy Agency
IBD	Inflammatory Bowel Disease
IBMP	Institute of Biomedical Problems

ICBM	Intercontinental ballistic missile
ICH	International Conference of Harmonisation
IGY	French abbreviation for Geophysical Year, "Année géophysique international"
ILMAH	Inflated lunar Mars analogue habitat
ISAS	Institute of Space and Astronautical Science
ISRU	In-Situ Resource Utilization
ISS	International Space Station
ITS	Integrated Truss Segment
IUPAC	International Union of Pure and Applied Chemistry
JAXA	Japan Aerospace Exploration Agency
JEM	Japanese Experiment Module
JPL	Jet Propulsion Laboratory
k-NN	k-Nearest Neighbour
LAV	Laboratory Analytical Viewer
LB	Luria Broth
LC	Liquid Chromatography
LCV	Leuco crystal violet
LDA	Linear Discriminant Analysis
LOD	Limit of detection
LOQ	Limit of quantification
LOWESS	Locally weighted scatterplot smoothing
LPC	Limiting Permissible Concentration
LV	Latent variables
m/z	Mass-to-charge ratio
MALDI	Matrix-Assisted Laser Desorption/Ionization
MBS	Mobile Remote Servicer Base System
MCA	Major Constituent Analyzer
MCC	Multi-capillary columns
MCR	Multivariate curve resolution
MDS	Multidimensional Scaling
MELFI	Minus Eighty Degree Laboratory Freezer for ISS
MERCCURI	Microbial Ecology Research Combining Citizen and University Researchers
MLM	Multipurpose Laboratory Module
MMH	Monomethyl hydrazine
MORD	Medical Operations Requirements Document
MPCL	Merged peak cluster localization
MRM	Mini-Research Module
MS	Mass Spectrometry
MSS	Mobile Servicing System
MTBE	Methyl-tert butyl ether
MVA	Multi-variate Analysis

MVOC	Microbial Volatile Organic Compound
NASA	National Aeronautics and Space Administration
NBS	National Bureau of Standards
NEEMO-ACC	Aquarius/NEEMO, Human-Rated Altitude Chamber Complex
NEK	"Nezemnyy Eksperimental'nyy Kompleks" (Ground-based Experimental Complex)
NG	Nitroglycerin
NII-3	Scientific-Research Institute 3
NMDS	Non-metric multidimensional scaling
NN	Neural Networks
n-PLSR	n-way Partial Least Squares Regression
NSRL	NASA Space Radiation Lab
OGS	Oxygen generation system
OLIMS	Open Loop Ion Mobility Spectrometry
OMS	Overtone Mobility Spectrometry
OVG-4	Owlstone Calibration Gas Generator 4
PAB	Pseudomonas Agar Base
PASAT	Paced Auditory Serial Addition Test
PC	Principal component
PCA	Principal Component Analysis
PCR	Polymerase Chain Reaction
PCRg	Principal Component Regression
PEA	Phenethylamine
PFA	Perfluoroalkoxy alkane
PFE	Portable fire extinguishers
PIDS	Laboratory Prime-Item Development Specification
PLRP	Pavilion Lake Research Project
PLS	Partial Least Squares
PLS-DA	Partial Least Squares-discriminant Analysis
PLSR	Partial Least Squares Regression
PMA	Pressurised Mating Adapters
PMAZ	Propidium monoazide
PME	Peak model estimation
PMM	Permanent Multipurpose Module
ppb	Parts-per-billion
ppt	Parts-per-trillion
PTFE	Polytetrafluoroethylene
PTR	Proton transfer reaction
PUT	Putrescine
QL	Quantitation limit
RDX	Cyclotrimethylenenitramine ("Royal Demolition eXplosive")
RF	Random Forests

RIP	Reactive Ion Peak
RNII	Rocket Propulsion Research Institute (Russia)
ROS	Russian Orbital Segment
Roskosmos	State Corporation for Space Activities (Russian: "Роскосмос")
r-SVM	recursive Support Vector Machine
S/N	Signal-to-noise ratio
SBA	Sorbet bed assembly
SFOG	Solid-Fuel Oxygen Generator, a system of oxygen generation candles
SIMPLISMA	Simple to use interactive self-modelling mixture analysis
SIRIUS	Scientific International Research In a Unique terrestrial Station
SM	Service Module
SMAC	Spacecraft Maximum Allowable Concentration
SMS	Simulator of the Martian surface
SOM	Self-organizing map
SPD	Spermidine
SPDM	Special Purpose Dexterous Manipulator
s-PLS-DA	sparse-Partial Least Squares-discriminant Analysis
SPM	Spermine
SPME	Solid Phase Microextraction
SRIG	Stacked-ring ion guide
SSAS	Solid sorbent air sampler
SSRMS	Space Station Remote Manipulator System
SVM	Support Vector Machine
TCCA	Trace Contaminants Control Assembly
TCCS	Trace Contaminant Control System
THC	Temperature and Humidity Control
TIC	Total inorganic carbon
TIMS	Ion Mobility Spectrometry
TMIMS	Transversal modulation Ion Mobility Spectrometry
TNT	Trinitrotoluene
TOC	Total organic carbon
TOCA	Total organic carbon Analyser
TOF	Time-of-Flight
TRP	Tryptamine
TSA	Tryptic Soy Agar
TSB	Tryptic Soy Broth
TWIMS	Travelling Wave IMS Ion Mobility Spectrometry
TYR	Tyramine
U.S.S.R.	Union of Soviet Socialist Republics, often referred to as Soviet Union
UDM	Universal Docking Module
UDMH	Unsymmetrical dimethyl hydrazine

UPA	Urine processing Assembly
US	United States (of America)
USOS	United States Orbital Segment
USP	United States Pharmacopoeia
UV	Ultraviolet light
VfR	Verein für Raumschiffahrt (german) - “Society for Spaceship Travel”
VOA	Volatile Organic Compound Analyzer
VOC	Volatile organic compounds
WHO	World Health Organization
WM	Waste Management
WRM	Water Recovery and Management
WST	Watershed transformation

CHAPTER 1.
GLOBAL PREFACE:
Subject, Scope, Aim and Structure

1.1 Subject

Space exploration has seen a renewed interest and investment from space agencies and governments in the last decade. Novel projects and plans have been defined and developed and many others are still in early proposed stages. The motivation behind this the new era of space exploration is guided by the protection of human life and Earth, while taking advantage of the resources available in space.

Hence human health and environmental conditions are critical for the current stage of space exploration, especially considering the current plans for several moon landings, a new space station Russian Orbital Service Station), a small space station in lunar orbit (Lunar Orbital Platform-Gateway) and a habitable station in the Lunar surface (Lunar Surface Innovation Initiative) to ultimately lead to humans landing on Mars.

Recently scientific focus has been given to the assessment of potential hazardous exposures during spaceflight and setting safe limits, which will considerably protect astronaut's health against chemical exposures and microbial contaminants in this high-pressure and unique environment. Moreover, to sustain the human presence in space through the occupation of the International Space Station (ISS) or any other stations and spacecraft, toxicological risks must be measured and managed within the context of isolation, continuous exposures, reuse of air and water, limited resources, and rescue options in the harsh environment of microgravity.

Thus, the subject of this dissertation is to explore a direct method to detect and monitor organic and biological contaminants aboard spacecrafts, which is currently essential for space exploration.

1.2 Scope & Focus

Knowledge and technologies investigated and developed for use and assistance in space exploration have seen enormous discoveries and inventions. Early steps in space exploration were focused in verifying if the human body was able to adapt and survive in space conditions. Once the first humans were sent to space and returned to earth it became obvious the human body could adapt to space conditions, however the development of several system, technologies, control and monitorization of environmental conditions was essential.

The state-of-the-art in space exploration has seen massive changes and discoveries over almost 70 years, which provided several crucial lessons until reaching the current state. The Mir station provided several early lessons in understanding how a spacecraft environment is changed and influenced by the continuous presence of humans. Among those lessons is the risk microorganisms represent for both human health and spacecraft safety. At Mir, *Penicillium chrysogenum* was identified as the source of a fungal infection in a porthole, and closer inspections revealed further contamination behind control panels, inside air ducts, and in other nooks and crannies [1, 2]. *Penicillium chrysogenum* released corrosive acids, such as acetic acid which pitted Mir's titanium, plastic, and glass, and could eventually become a treat to spacecraft's structural integrity. The malfunctioning of a communication device was

even attributed to the fungus and although this contamination was kept under control, its eradication was never achieved and afterwards, Mir visitors, would often make comments about a mildew odour in the spacecraft [3].

Henceforth, strategies and methodologies used currently aboard the ISS were deeply and exhaustively developed from what was learned and observed in the Mir space station and Skylab. Yet, as the ISS gets older, the methods, technologies and approaches used to monitor its environment have changed and evolved into specifically adapted or re-designed systems or technologies.

The scope and focus of this thesis are on the detection of volatile organic compound (VOCs) originating from inherent sources (e.g., off-gassing, thermal degradation, containment leaks, waste products, extravehicular activities, fire extinguishant use, utility chemicals, crew metabolites and from the various systems that provide a habitable environment) and microorganisms.

More precisely, it focuses on the use of Ion Mobility Spectrometry (IMS) to monitor organic and biological contaminants, through the direct detection and quantification of several volatile organic compounds in very low concentrations ranges (ppb_v and/or ppt_v range) without chemicals or reagents.

1.3 Motivation & Aim

The habitation of spacecrafts and stations by humans has its own risks and hazards to health and the success of any mission or scientific effort. A detailed and high level of monitorization is essential to provide good and healthy conditions for long-term occupations of spacecraft and stations. Air, water, and life support systems are the most critical aspects to generate, maintain and monitor in a closed space environment. The presence of toxic compounds both harmful for human health, structures or systems in a spacecraft is a primary feature to monitor aboard spacecrafts and space stations.

Furthermore, access to medication and treatments aboard a spacecraft or station is very scarce and must be sent during scheduled supply launches, if those are regular enough, available, or even possible. Although every structure designed and constructed for low-orbit or outer space goes through a rigorous process to guarantee a sterile environment, the presence of microorganisms is ubiquitous in spacecrafts and stations. Microorganisms are a source of infections, allergies or respiratory problems which hugely increased in an environment where humans are exposed to a high stress environment, high radiation levels, constrained access resources, including food, medication, disinfection products, water, and air.

Several concerning and dangerous incidents were identified during the lifetime of the Russian station Mir, which was decommissioned due to the presence of fungus species corroding and degrading metallic and electric structures. Thereafter, the monitorization of atmospheric compounds and microorganisms became essential and critical future of space exploration, especially for aboard the International Space Station (ISS) continuously occupied for roughly 20 years starting in 2000.

The presence of microorganisms and hazards compounds in the ISS surfaces, water and air is regularly controlled and monitored by collecting samples which are later analysed on Earth laboratories with various techniques. Although this approach has proved sufficient for most of the 20 years of the

ISS several organizations are concerned with the risks this approach still has. Since monitorization is mainly made offline and relies on Earth laboratories, which delays or might not allow sufficient time for astronauts to implement adequate counter measurements.

Thus, a need for online and real-time monitoring approaches and techniques became essential and hugely sought out by the National Aeronautics and Space Administration (NASA), the European Space agency (ESA), and even the Japan Aerospace Exploration Agency (JAXA). Those agencies are looking for an accurate analytical technology which can detect a large spectrum of compounds in low concentration, between ppb and ppt levels, while providing fast and uncomplicated results, in an easy to read and understandable data format without any additional resources.

Hence this dissertation aims to analyse and evaluate IMS capabilities for the detection of volatile organic compounds (VOCs) in ppb and ppt concentrations in consideration with its own limits and the restrictions and requirements for space habitation of the International Space Station and for future spacecrafts in outer space or other celestial bodies. Concretely, the main objectives of this work translate into the development of sampling methods, experimental protocols, and library tools for online analysis of VOCs, in the detection, identification, and quantification of possible biological contaminations in the ISS or similar closed environments.

1.4 Structure Outline

- Chapter 1: Identification of the subject, scope, aims and structure of the thesis.
- Chapter 2: A brief history of space exploration centred on spacecrafts and stations. Design, development, operation, research, and life support systems aboard the International Space Station (ISS), addressing organic and biological contaminants and the current strategies and technologies used to monitor VOCs from inherent sources and microorganisms.
- Chapter 3: The fundamentals of Ion Mobility Spectrometry including principles, instrumentation, coupling with other analytical methods, and applications.
- Chapter 4: A background on gas analysis and calibration methods, experimental aspects data and information on the selected ion mobility spectrometer used.
- Chapter 5: Evaluation of Ion Mobility Spectrometry coupled with gas chromatography to monitor air quality in several sections: (i) a description of the selected instrumentation, (ii) preliminary tests and analytical assessment, (iii) preparation and results obtained during the SIRIUS-17 experiment, (iv) analysing IMS as possible diagnosis tool via exhaled breath analysis, (vi) application of IMS for microbial detection and identification via their VOC emission, (vii) use of IMS for food quality monitorization applied to new food sources for space, specifically seaweeds, (viii) formulation and development of a VOC database for identification of critical VOCs in spacecrafts/stations, (ix) calibration of IMS for a specific set of VOCs via permeation tubes and (x) a preliminary tactic for automatic peak detection and quantification in GC-IMS data.
- Chapter 6: Main conclusions and evaluation of the capabilities and constraints of IMS for VOCs monitorization in space stations and similar closed environments during long periods of time.

1.5 Scientific Outputs

Several SCOPUS referenced[1], and relevant publication originated from this dissertation to bring attention and importance of the scientific community to IMS as monitoring tool.

SCIENTIFIC PAPERS

2022 (Submitted):

Jorge M. Fernandes, Bruno S. Moreira-Leite, Pedro C. Moura, João P. Noronha, Paulina Mata, Mario Dinis and Valentina Vassilenko. Volatile organic compounds "fingerprint" characterization of ten seaweeds by Gas Chromatography-Ion Mobility Spectrometry. "Applied Phycology (Taylor & Francis).

2021:

J. M. Fernandes, Valentina Vassilenko, Pedro C. Moura, and Viktor Fetter, "Gas Chromatography-Ion Mobility Spectrometry Instrument for Medical Applications: A Calibration Protocol for ppb and ppt Concentration Range" {Book Chapter} in 12th Advanced Doctoral Conference on Computing, Electrical and Industrial Systems, Caparica, Portugal, 2021.

P. H. Santos, Valentina Vassilenko, Pedro C. Moura, Carolina Conduto, J. M. Fernandes and Paulo Bonifácio, "Pilot Study for Validation and Differentiation of Alveolar and Esophageal Air" {Book Chapter} in 12th Advanced Doctoral Conference On Computing, Electrical and Industrial Systems, Caparica, Portugal, 2021.

P. H. Santos, V. Vassilenko, P.C. Moura, C. Conduto, J. M. Fernandes, P. Bonifácio "Instrumentation for Differentiation of Exhaled Air" SPIE 12126, Fifteenth International Conference on Correlation Optics, 121262L 2021.

2020:

J. M. Fernandes, P. H. Santos, and V. Vassilenko, "Algorithm for Automatic Peak Detection and Quantification for GC-IMS Spectra" {Book Chapter} in 11th Advanced Doctoral Conference on Computing, Electrical and Industrial Systems, Caparica, Portugal, 2020.

P. H. Santos, Peter Roth, J. M. Fernandes, Viktor Fetter, and V. Vassilenko, "Real-Time Mental Stress Detection through Breath Analysis" {Book Chapter} in 11th Advanced Doctoral Conference on Computing, Electrical and Industrial Systems, Caparica, Portugal, 2020.

P. C. Moura, J. M. Fernandes, P. H. Santos, and V. Vassilenko, "Indoor & Outdoor Air Profiling with GC-IMS" {Book Chapter} in 11th Advanced Doctoral Conference On Computing, Electrical and Industrial Systems, Caparica, Portugal, 2020.

C. Espalha, J. Fernandes, C. Madeira, J.P. Noronha, V. Vassilenko, M.S. Diniz "Comparing the Detection of Histamine by Using GC-MS and ELISA Methods: Clues fora Faster and Direct Detection of

[1] https://www.scopus.com/authid/detail.uri?authorId=57208625493

Biogenic Amines in Seafood Products" in XVI International Symposium on Marine Natural Products | XI European Conference on Marine Natural Products. Marine Drugs 2020, 18, 40. {XVI MaNaPro & XI ECMNP, Peniche, Portugal, September 1 – 5, 2019}

2018:

M. Gonçalves, J. Fernandes, V. Fetter, M. Diniz, and V. Vassilenko, "Novel methodology for quick detection of bacterial metabolites" in 2019 IEEE 6th Portuguese Meeting on Bioengineering (ENBENG), Lisbon, 2019.

C. Espalha, J. Fernandes, M. Diniz, and V. Vassilenko, "Fast and Direct Detection of Biogenic Amines in Fish by GC-IMS Technology" in 2019 IEEE 6th Portuguese Meeting on Bioengineering (ENBENG), Lisbon, 2019.

V. Fetter, V. Vassilenko, J. Fernandes, T. Hummel, D. Tsarkov, A. Pakhomova, L. Moukhamedieva, O. Orlov "Validation of analytical instrumentation for continuous online monitoring of large spectra of VOCs in closed habitat during simulation of space flight" International Astronautical Congress (Proceedings), IAC Volume 2018-October 2018, 69th International Astronautical Congress.

POSTER COMMUNICATIONS

2017 May: 2nd NOVA Biomedical Engineering Workshop

POSTER: Direct detection of biological contaminations in International Space Stations. Valentina Vassilenko, Jorge Fernandes, Victor Fetter, Thomas Hummel, Dmitry Tsarkov, Anna Pakhomova, and Lana Moukhamedieva.

2018 May: 3rd NOVA Biomedical Engineering Workshop

POSTER: Toxicology in closed habitat during Space Flight. Valentina Vassilenko, Jorge Fernandes, Victor Fetter, Thomas Hummel, Dmitry Tsarkov4, Anna Pakhomova, and Lana Moukhamedieva.

CHAPTER 2.
INTERNATIONAL SPACE STATION:
Environment & Monitorization

2.1 Structure and Assembly

The International Space Station (ISS) is the largest single structure humans ever put in space and it was assembled in space between 1998 and 2011. The structure known as ISS has changed over more than 20 decades of existence with increasing modules being added and has been occupied by humans since Nov 2000. Assembly and operation of the ISS are complex processes and involve numerous countries and space agencies responsible to creating and maintaining a safe and healthy habitable closed space inside it which use the station to conduct several scientific projects in an unique, and dangerous environment.

A *Memorandum of Understanding* between NASA and Roskosmos established early plans for the International Space Station to function as a laboratory, observatory, and factory whilst providing, transportation, maintenance, and a low-orbit Station or base for potential missions to the Moon, Mars, asteroids, comets, and over celestial bodies [4]. Even so, not all the planned uses became a reality, and in 2010, a new policy, attributed re-edit the roles of the ISS to serve, scientific research, commercial, diplomatic, and educational functions [5].

The ISS is a joint project of five space agencies NASA (United States), Roskosmos (Russia), JAXA (Japan), ESA (Europe), and CSA (Canada) with, the station uses, and ownership determined by intergovernmental treaties and agreements [4, 6, 7]. At an average altitude of 400 kilometres the station orbits Earth's low orbit, taking nearly 92 minutes to circle around the Earth completing 15.5 orbits per day [5, 8]. Accounting the previous human occupied space station, including several Salyut stations, Mir, and Skylab stations, the ISS is counted as the ninth crewed station [5].

Design, engineering and manufacturing of ISS modules and structures was a world-wide and challenging endeavour, initiated by the first module, Zarya, launched in 1998 by a self-directed rocket. Zarya, (Russian: Заря́, lit. 'Dawn') was developed and launched with the intent of providing electrical power, storage, communications, propulsion, guidance, and altitude control to the ISS during the initial stage of assembly [5, 6, 7]. Although Zarya lacked lifelong term life support functions it was crucial in the early assembly of other modules and once more specialized modules were attached, its function and purpose became primarily a storage module [9].

Unity, a NASA passive module was launched two weeks following Zarya, aboard the Space Shuttle flight STS-88 and was attached to Zarya by astronauts during and extra-vehicular activities (EVAs), contrary to all Russian modules, except Rassvet, which was launched and docked robotically [9, 7]. Unity module possessed two Pressurised Mating Adapters (PMAs), one connecting permanently to Zarya, and another serving has a docking port for the Space Shuttle [9]. Although the first ISS component was launched in 1998, the first long term occupants only arrived in 2000 hence the station remaining uninhabited for two years due to the still operating and inhabited Mir Station [5, 6]. Zvezda launch into orbit in July 2000, enabled permanent habitation of the station, since this module added sleeping quarters, a toilet, kitchen, CO_2 scrubbers, dehumidifier, oxygen generators and exercise equipment, plus data, voice, and television communications with mission control. Zvezda was

preprogramed with commands on board to deploy solar arrays and communication antennas, becoming a passive target for a rendezvous with the existent Zarya-Unity vehicle which was docked via ground control and an automated rendezvous and docking system [9]. Once Zarya-Unity vehicle and Zvezda modules were connected, Zarya's computer transferred control to Zvezda's operating systems [5, 9].

In November 2000 on a Soyuz TM-31, the first residents of the Station arrived, as part of Expedition 1 and established its definite name as the International Space Station after several debates and other terms had already been used to refer to the station [5, 7]. Segments continued to be added to the station and while Expedition 1 was still on going, the station had seen the addition of an Integrated Truss Structure providing Ku-band communication for US television and substantial solar arrays [5, 9, 7]. Expansion continued in the following two years with Soyuz-U rocket delivering the Pirs docking compartment, the Space Shuttles delivered Destiny laboratory, Quest airlock, Canadarm2, its main robot arm, and additional segments of the Integrated Truss Structure (Figure 2.1) [5, 9].

The Space Shuttle Columbia disaster brought the station expansion to a hiatus in 2003, only to be resumed in 2006 with STS-115 flight bringing a second set of solar arrays [5, 7]. Following flights continued to add segments to the Truss Structure and a third set of solar arrays. Now, with a third set of solar arrays, the station's power-generation capabilities allowed accommodation of more pressurized modules. So, two more modules, Harmony node and Columbus laboratory from the European Space Agency were docked and added to the existing ISS structure (Figure 3.1) [9, 7]. Components for Kibō, a composite module from JAXA, came afterwards, and in March 2009, the Integrated Truss Structure was completed with a fourth set of solar arrays followed in July by the last Kibō structure [9]. A third node arrived in Earth's orbit in February 2010 via the Space Shuttle, called Tranquillity, and together with the Cupola, an ESA-built observatory module with seven windows, were docked and assimilated into the Space Station. Rassvet, a Russian module was delivered in 2010 and an extra pressurised module was made part of the station in 2011, named Leonardo, serving has as Multipurpose Logistic Module [9, 7]. Bigelow Expandable Activity Module was the last module to be made part of the ISS through new external contracts made by NASA [10].

So, the ISS is currently made up by the Integrated Truss Structure and 16 pressurised modules: 4 Russian modules (Pirs, Zvezda, Poisk and Rassvet), 9 US modules (Zarya, BEAM (not shown), Leonardo, Harmony, Quest, Tranquillity, Unity, Cupola, and Destiny), 2 Japanese modules (the JEM-ELM-PS and JEM-PM) and 1 European module (Columbus) (Figure 2.1). [9, 8] At the ISS extra-vehicular activities are regularly performed by two or more astronauts in several maintenance activities, equipment changes and replacement among several other scientific endeavours to keep the station operational and in good condition [8].

ISS development has been continuous over the years and assembly of several new Russian modules and elements were planned for 2020 [5, 9]. The station is serviced by several spacecrafts, such as the Russian Soyuz and Progress, the US Dragon and Cygnus and Japanese H-II Transfer Vehicle delivering, astronauts and cosmonauts, provisions, such as cloths, food, scientific equipment and several important payloads for maintenance and repairs [5].

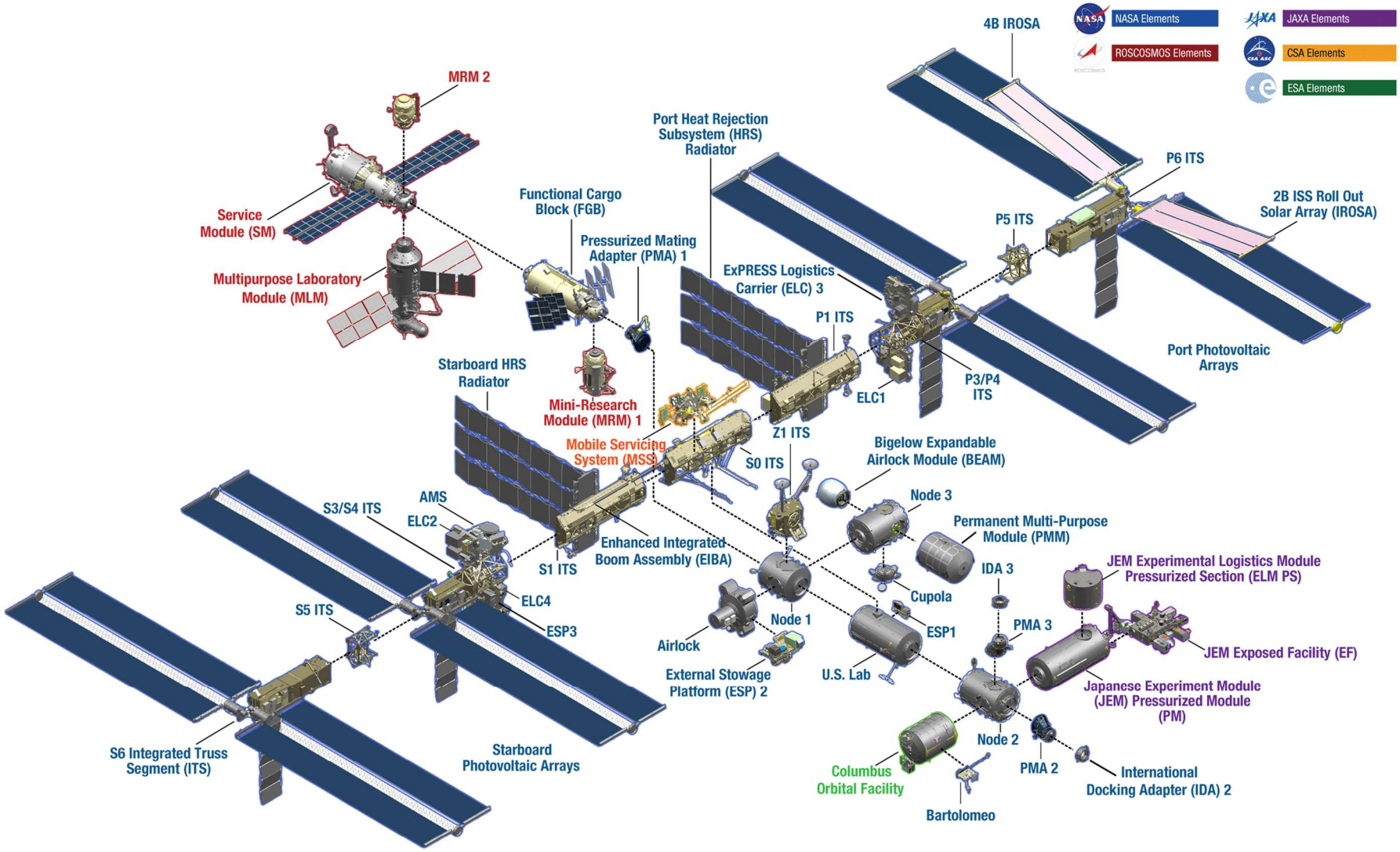

Figure 2.1 — International Space Station structure depicting modules and configuration as of Nov 2021. Modules are identified with corresponding structural name or abbreviation. Blue and black rectangles indicate solar panels, dashed lines refer to the established connection between modules and text colour identifies elements created by each space agency [8].

Moreover, such vehicles also allow pressurised cargo to be returned to Earth for analysis and research in ground facilities with more advanced methods unavailable or impossibly to house in the ISS. Furthermore, the station structure is managed in two sections, one operated by Russia classified as the Russian Orbital Segment (ROS) and a second segment shared by several nations named, United States Orbital Segment (USOS) after the initial US contribute to the station modules [9]. Occupation of the station has surpassed 20 years, making it the longest continuous human presence in low Earth orbit in contrast with Mir's previous record of 9 years and 357 days [9, 8].

NASA has launched two websites to track ISS stats, one allows to track the time the station is in orbit and the cumulative crew time in orbit, { https://spaceflight.nasa.gov/realdata/tracking/index.html }, while the other website allows to track the current position of the station above Earth's surface { https://spotthestation.nasa.gov/tracking_map.cfm }. Every 90 minutes the Station perform one orbit around the Earth traveling at 27,580 km/h leading to a total of 16 sunsets and sunrises experienced abord every 24 hours [8]. Besides being occupied for 20 years, the ISS is also the largest artificial object in space and the largest satellite in low Earth orbit whilst being visible from Earth with the naked eye, and its operation is expected to last until 2030 [7, 8].

The ISS consists of modules and components being developed by a consortium of space agencies, including, Russia, USA, Canada Japan, and a group of European countries, with specific modules built by specific countries however, managed and organized in cooperation (Figure 2.1) [5]. Nonetheless, the ISS is generally separated into two major sections which are connected, but in some ways independent: US/international segments (includes Canadian, Japanese, and European modules) and Russian Segment (Figure 2.1) [9].

2.2 Operation and Life Support Systems

Habitation and operation of the ISS relies on a group of systems called Environmental Control and Life Support System (ECLSS) functioning as life support systems by creating and maintaining a liveable environment in the station [11]. The ECLSS are responsible for controlling atmospheric pressure, fire detection and suppression, oxygen levels, waste management and water supply [9, 11]. Both US and Russian segments hold their own life support systems, which work independently and are organized in slightly different manners.

However, four characteristics are generalized and common across both life support systems: (i) No automatic hatch open/close mechanisms on any hatches; (ii) Fire suppression systems are decentralized and consists of portable fire extinguishers (PFE); (iii) Single equipment failure is not to propagate across RS/USOS interfaces; and (iv) Materials are selected so as to not contaminate the air; i.e., materials have minimal off-gassing [9, 12].

US ECLSS is typically considered as Atmosphere Revitalization (AR), Water Recovery and Management (WRM), metabolic Waste Management (WM), Atmosphere Control and Supply (ACS), Temperature and Humidity Control (THC), and Fire Detection and Suppression (FDS). At the ISS, vacuum resources and exhaust for experiments are also considered part of the ECLSS [9, 13]. Whilst the

Russian ECLSS include food storage and preparation, refrigerators/freezers, extravehicular activity (EVA) support, whole body cleaning, and housekeeping. Moreover, Russians consider thermal control to be a separate system and categorize the ECLS capabilities somewhat differently than US ECLSS. i.e., Russian category translated as "sanitary and hygienic equipment" includes the commode, urinal, hand washers, vacuum cleaner [9, 13].

ISS operation and ECLSS management is coordinated across two segments: the *Russian Orbital Segment (ROS)* and the *US Orbital Segment (USOS)* [12, 9, 7, 8, 13, 14]. The ROS provides the ISS with guidance, navigation, and control; propulsion services; electrical power generation, storage, distribution, and control; communications and data links to ground support facilities and living quarters. ECLS functions include thermal control and heat rejection; data processing, storage, and transportation; housekeeping; personal hygiene; food preparation and storage; EVA; support payload utilities; robotic systems; crew and cargo resupply services; delivery and return of crew, including unplanned crew return capability; and research facilities [9, 11]. A detailed constitution of the ROS includes the following pressurized modules: (Figure 2.1)

- *Zarya:* also known as Functional Cargo Module (FGB, from the Russian name) is a module connecting the ROS and the USOS and initial essentially served several life-support functions. Currently it is owned by the US.
- *Zvezda:* a habitation module for three people, nominally the Service Module (SM).
- *Pirs*: also called Stykovochny Otsek 1 (SO-1) and DC-1 (docking compartment) is a docking module for Soyuz and Progress spacecraft and allows egress and ingress for spacewalks by cosmonauts.
- *Poisk:* also known as the Mini-Research Module 2 (MRM 2) is a docking module of the International Space Station. Its original name was Docking Module 2 (Stykovochniy Otsek 2 (SO-2)), as it is almost identical to Pirs module.
- *Rassvet* or Mini-Research Module 1 (MRM-1) and formerly known as the Docking Cargo Module (DCM) function as a docking port for visiting spacecrafts and stowage module and was only added to the segment in May 2010.

Several other modules were initially designed as part of the ISS but were later cancelled due to engineering problems and budgetary constraints, including, an Universal Docking Module (UDM), laboratory modules – research Modules RM1, RM2, and RM3 planned but never assembled, and modules to connect solar arrays and thermal radiators to the SM: Scientific-Power Platforms (SPP–1 (pressurized) and SPP–2 (unpressurized)) [9, 12]. Likewise, modules such as Nauka, also known as the Multipurpose Laboratory Module (MLM) are planned to be added to the International Space Station and into the ROS, however, have not been launched yet. Hence the current configuration of the ROS may not coincide with this description, but ECLS equipment is expected to be kept as described [9].

ECLSS equipment in the Russian Segment are concentrated in the Service Module, or Zvezda, except for a cabin air analyser (in the FGB), Temperature and Humidity Control (THC) and Fire Detection and Suppression (FDS) are distributed amongst the various modules of the Russian Segment. FDS systems inside the Functional Cargo Block used ionization-type smoke sensors while the

remainder systems use infrared-type detectors. Fire extinguishers are located around the ROS and rely on a foam mixture, and re-breathing masks are provided to the crew to support firefighting cases [11].

The remainder of systems present in the ROS include: a *Micro Purification Unit* (BMP), using a mixture of charcoal and catalytic beds to remove trace contaminants in the cabin air; *Elektron*: an electrolyzer for oxygen production from water creating hydrogen as a by-product, later vented overboard, and a backup system of oxygen generation candles (SFOG); *Vozduk*: a carbon dioxide removal system using regenerable adsorbers with a system of lithium-hydroxide cartridges as a backup; *Waste and Hygiene Compartment* (toilet), which stores in disposable containers, all pre-treated waste (liquid/solid); *cabin air condensate regeneration* system, is used for condensate purification which is later dispensed to the crew as cold and/or warm water; *Pressure control* for cabin air pressure which acts by introducing nitrogen (and oxygen when required); and a *gas analyser* of the cabin air that continuously monitors partial pressures of oxygen, CO_2, water vapor, and hydrogen (Figure 2.2) [11].

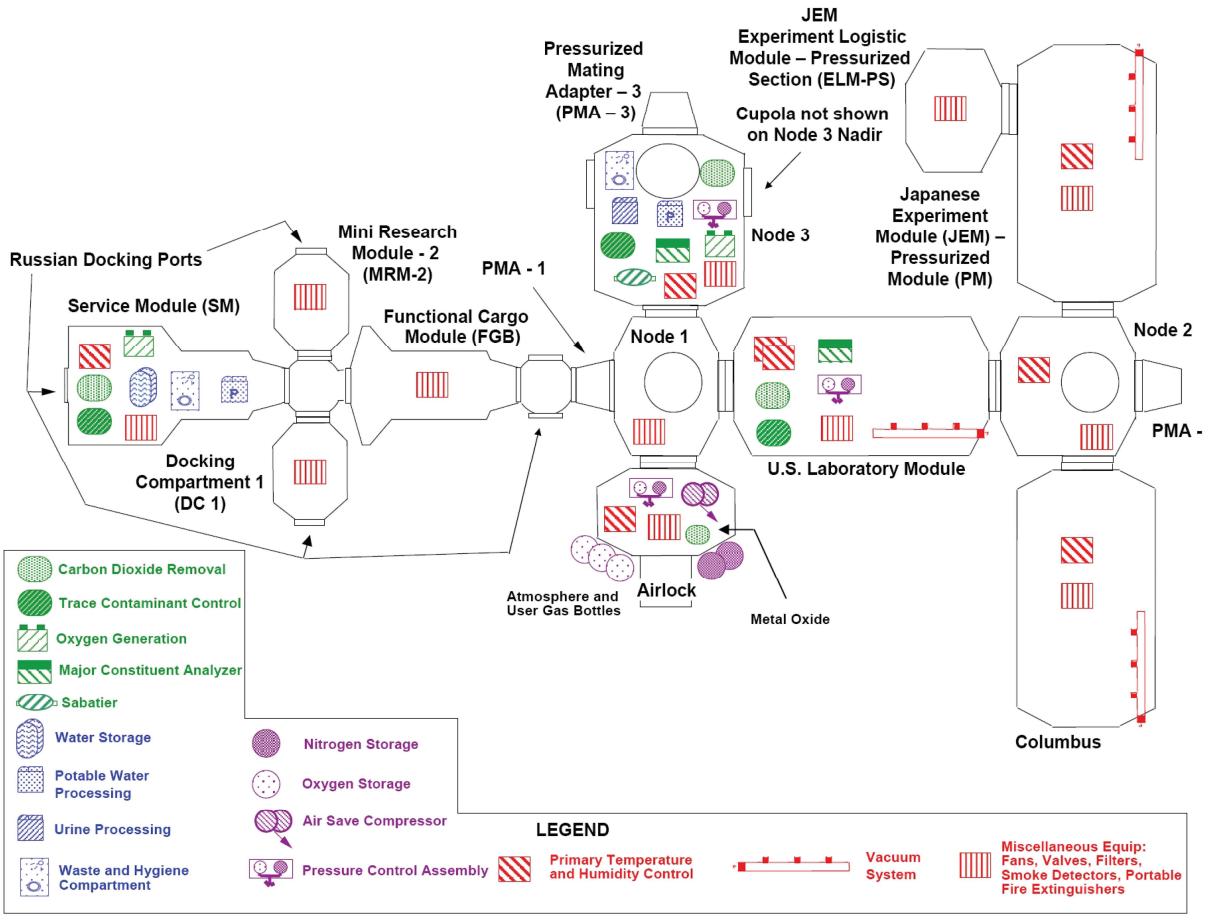

Figure 2.2 — On-Orbit ISS ECLS Hardware distribution as of February 2010. Differences and module distribution of life support systems between the Russian (left of PMA-1) and US orbital segments (right of PMA-1) [11].

All docking compartments share the same ECLS functions: atmospheric pressure measurement, contaminant removal, temperature measurement and control, atmospheric circulation, and intermodule ventilation while also serving as docking ports for Crew Transfer Vehicles (CTV) and airlocks for

Extravehicular Activities (EVA) as well as storage of space suit and equipment. Soyuz and Progress constitute two Crew Transfer Vehicles regularly used and docked to the ISS which have slightly different ECLS equipment [12]. The Soyuz is equipped with basic life support sufficient for short duration transfers between Earth and low-Earth orbit; propulsion; guidance, navigation, and control; and communications capability while also capable of atmospheric pressure measurements and intermodule ventilation. The Progress vehicles are also capable of intermodule ventilation and monitor atmospheric temperature, but able to perform atmospheric supply through storage tanks of resupplied atmosphere gases, control the release of those same gases, control total pressure through sensors able to monitor atmospheric pressure and water supply. The water supply is managed using tanks for storage and delivery of potable water and disposal of wastewater [9, 12, 14].

Additionally, ROS also uses some US-provided equipment for environmental monitoring, including tissue equivalent proportional counter, radiation area monitors, surface sampler kit, microbial air sampler, fungal spore sampler, water microbiology kit, water sampler and archiver and crew contamination protection kit [9, 12].

Similarly, the USOS provides living quarters for three people; electrical power generation, storage, distribution, and control; communications and data links to ground support facilities; environmental control and life support; thermal control and heat rejection; data processing, storage, and transfer; housekeeping; personal hygiene; food preparation and storage; EVA capability; payload utilities; robotic systems; crew and cargo resupply services; and research facilities [9, 11, 12]. The US segment is built around the existence of nodes and additional pressurized modules. Nodes are cylindrical shape modules with 4 ports around their exterior and 1 at each end (total of 6 ports), also called Common Berthing Mechanisms (CBM) [9]. Presently 3 nodes are part of the ISS configuration (Node 1, Node 2, and Node 3) which integrate the USOS composed of the following modules [15]:

USOS Nodes present in the ISS and overall links and functions:

- *Unity (Node 1):* connects the ROS and USOS and serves has the dining room for crewmembers. It is connected to Zarya, the US Destiny Laboratory Module and the Z1 truss and serves. Several systems rely structurally on the Unity module, since more than 50,000 mechanical elements, 216 lines to carry fluids and gases, and 121 internal and external electrical cables were installed in the module [9].
- *Harmony (Node 2):* the central connecting module of the USOS, establishing links with Destiny lab, Kibō, lab and Columbus lab and receiving service vehicles on its nadir and zenith ports, generally, referred to as "utility hub". It holds four sleeping cabins and provides electrical power and data to the segment including power to the station's robotic arm, Canadarm2.
- *Tranquillity (Node 3):* houses the USOS life support systems, a toilet, exercise equipment and two other modules: cupola and Leonardo whilst being connected to Node 1. Tranquillity was initially owned by The European Space Agency and the Italian Space Agency, but ownership was transferred to NASA in 2010. Currently 3 other modules are connected Node

1, the Cupola, the Bigelow Expandable Activity Module (BEAM) and the Leonardo Permanent Multipurpose Module (PMM) [16, 17].

USOS modules function as laboratories for scientific research:

- *Destiny (US Lab):* one of the laboratory modules of the USOS, where experiments related to medical, engineering, biotechnological, physics, materials science and Earth science research are conducted, i.e., Veg-3 experiment: growing edible romaine lettuce and cabbage. It is connected to Unity and Harmony and contains some important research structure, like Minus Eighty Degree Laboratory Freezer for ISS (MELFI) storing samples and reagents on the station under controlled temperature and the Veggie experiment complex [18, 19].
- *Columbus (ESA Lab):* European Space Agency laboratory for research in weightless for fluids, biology, medicine, materials, and Earth sciences. Columbus is berthed to Node 1 and the module is designed for experiments to be conducted outside the module within the vacuum of space by four exterior mounting platforms.
- Kibō, *(JAXA Lab):* officially named Japanese Experiment Module (JEM) was developed by the Japanese Space program and constitutes the largest module currently in the ISS and is berthed to Harmony. It is composed by four parts, the Kibō, main lab, an exposure science platform and two robotic arms. Uniquely it is the only module that allows payloads to be passed to a robotic arm or astronauts at the outside of the station by an airlock. Research at Kibō, include medicine, engineering, biotechnology, physics, materials science, and Earth science.

USOS modules with miscellaneous function and purposes:

- *Quest* Joint Airlock: a module dedicated to operations related to spacewalks, with two parts, an equipment lock, and a crew lock. Necessity of this module arose from the fact that US spacesuits did not fit the previous dedicated space for EVA in the Zvezda module. The Airlock is only accessible from Node 1 "Unity" to which it is berthed.
- *Leonardo* Permanent Multipurpose Module (PMM): attached to Tranquillity's forward-facing side serving as storage of spares, supplies and waste. It was initially berthed to Node 1.
- *Cupola*: a seven windowed cupola attached to Node 3 with six side windows and a direct nadir viewing window equipped with shutters to protect from contamination and collisions with orbital debris or micrometeorites. Accommodates two crewmembers simultaneously and is attached to Node 3's Earth side. Serves also to monitor operations outside the ISS (robotic activities, approach of vehicles, and extravehicular activity (EVA)).
- *Bigelow Expandable Activity Module* (BEAM): an experimental expandable space station module developed by Bigelow Aerospace for NASA. BEAM was berthed to Node 3 on April 2016 and expanded (by inflation) and pressurized in May 2016. BEAM and, its experimental program was developed to test and validate expandable habitat technology in space [10].

Multicomponent structures, adapters, and robotic systems:

- *Integrated Truss Structure Complex* (ITS): constitutes 11 trusses or segments linked together and a separate component, Z1. Z1 is berthed to Unity while the remaining structure

is connected to Destiny. Several unpressurised components are mounted on ITS, including radiators solar arrays, batteries, antennas, electronic and communication equipment, and,

- *Mobile Servicing System (MSS),* a robotic system composed of a Special Purpose Dexterous Manipulator (SPDM, also known as "Dextre" or "Canada hand", a Mobile Remote Servicer Base System (MBS) and a Remote Manipulator System (SSRMS), known as Canadarm2.
- *Pressurized Mating Adapters (PMAs):* space craft adapters for converting CBM to Russian APAS-95 docking ports.

ECLSS equipment in the US orbital Segment is essentially located in Node 3, or Harmony and similarity to the ROS, each USOS modules is equipped with primary Temperature and Humidity Control (THC) and Fire Detection and Suppression (FDS). THC is composed of fans and heat exchanger which transfer water condensate a Water Processing Assembly (WPA) system in Node 3. Equipment for fire detection and suppression include smoke detectors (laser type), portable fire extinguisher (carbon dioxide) and two portable breathing apparatuses that dispense oxygen are available in each module. Additionally, vacuum systems are installed in Destiny, Columbus and Kibō [9, 11, 12].

Node 3 contains hardware responsible for *water reclamation*, a system composed of an Urine processing Assembly (UPA) and Water Processing Assembly (WPA) which re-cycles water from both US and Russian waster and hygiene compartment, Common Cabin Air Assembly (CCAA) and the Air contamination control (ACC), an *Oxygen generation system* (OGS) based on an electrolyser producing oxygen and hydrogen from water originating from the WPA or stored containers, a *Carbon Dioxide Removal Assembly* (CDRA), using lithium-hydroxide canisters, a *Water and Hygiene compartment* (WHC), a close copy of the analogous unit available in the Russian service module, and an *Air contamination control* (ACC) composed of two type of equipment, a Trace Contaminants Control Assembly (TCCA) and a Major Constituent Analyzer (MCA) (Figure 2.2) [9, 11, 12].

The TCA controls trace contaminants in cabin air using charcoal beds, a catalytic oxidizer, and a lithium-hydroxide sorbing bed, while the MCA, continuously monitors oxygen partial pressures, carbon dioxide, hydrogen, methane, nitrogen, and water vapour employing a mass spectrometer. Another MCA responsibility is pressure control, which is achieved by inserting oxygen and nitrogen into the cabin air when needed [9, 11, 12]. Additionally, several types of hand-held equipment are available for the monitorization of specific compounds [11].

Node 3 has also been equipped recently with a system called *Sabatier*, which uses the hydrogen by-product of the OGS and CDRA to produce water and methane, whilst the water is directed to the WPA, methane is vented over-board [11]. Destiny laboratory and Quest airlock are equipped with extra hardware, involved in carbon dioxide removal (CDRA), trace contaminant control, major constituent analyser and pressure control for the Destiny module, while nitrogen and oxygen storage tanks, pressure control, an air save compressor and carbon dioxide removal system are available in the Quest airlock [9, 11, 12]. A simplified life support systems schematic is shown in Figure 2.3.

An additional life support system, the Advanced Closed-Loop System (ACLS) was installed in the Destiny module in 2018. ACLS uses regenerative process for three life support functions: Carbon dioxide removal, Breathable oxygen supply via electrolysis of water and Catalytic conversion of carbon

dioxide with hydrogen to water and methane. Such technology was developed to improve upon the already existing life support systems and create closed loop life support system necessary for human spaceflight beyond low Earth orbit [11, 20]

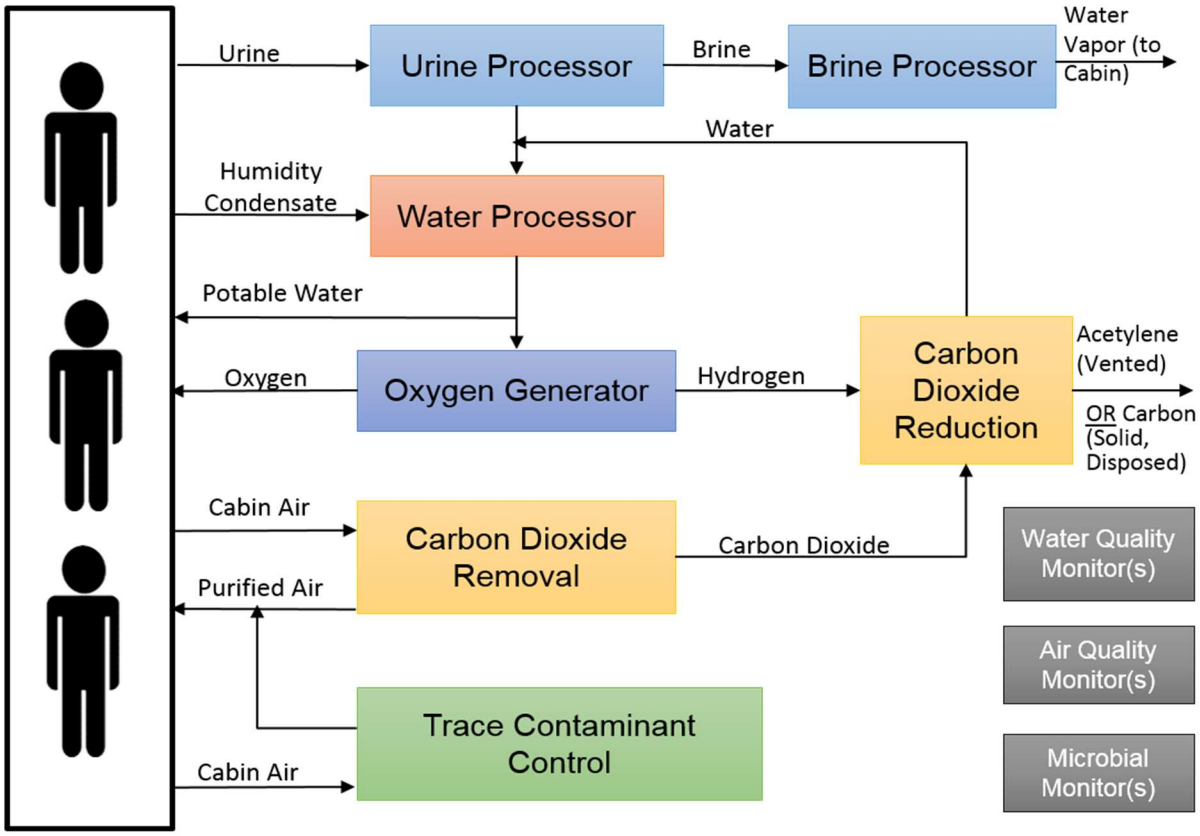

Figure 2.3 — The Simplified Life Support Systems Schematic. Shows all life support system elements [21].

Below the environmental control and life support system main data, in Node 3, is presented [11]:

- Cabin pressure nominal range: T = 14.2 to 14.9 psi.
- Oxygen & nitrogen distribution: P = 93-120 psia, T = 60-113°F (15.5 to 45°C) from Node 1.
- Oxygen Recharge: P = < 1050 psia (max 16 lb/h), T = 25-113 °F (- 4 to 45 °C) from PMA3.
- Nitrogen recharge: P = < 3400 psia (max 3 lb/h), T = 25-113 °F (- 4 to 45 °C) from PMA3.
- Cabin Temperature nominal range: T = 18 to 27 °F (- 8 to -3).
- Cabin air velocity: 3 to 13 meters per minute.
- Heat and humidity control: Common Cabin Air Assembly and Condensing Heat Exchanger.
- Airborne particulate and microbes' removal and disposal: Common Cabin Air Assembly Filters.
- Waste water collection and distribution.
- Fuel cell water and potable water distribution.
- Pre-treated urine: 1 line from W&HC to WRS2, P < 5 psig, T = 65-105 °F (18 to 41 °C).
- Process Water: 4 lines from WRS1 to WRS2.
- Cabin smoke detection: 2 Area smoke detectors.
- External venting lines: CO_2/CH_4, H_2, Major Constituent Analyzer (MCA) and Cabin air.

- Air sampling: from Zen, Port, Stbd, Fwd ports to ARS rack (flow rate 100-400 scc/min).

Life support systems are responsible for sustaining a permanent environment in space which make ISS habitation possible. Systems responsibilities include fresh air, water, food, a habitable climate, waste removal and fire protection [11, 15]. Without oxygen living in the station would not be possible, and although oxygen can be delivered from Earth via spacecrafts, the station systems create breathable oxygen from recycled water. By an electrolysis processes water is split into hydrogen and oxygen, which is mixed with carbon dioxide to create a similar earth atmosphere. Resulting hydrogen reacts with the accumulation CO_2 producing methane has a by-product which is controlled and vented into space [9, 11, 22]. Below, the ISS general data and information is shown [8] (Figure 2.4):

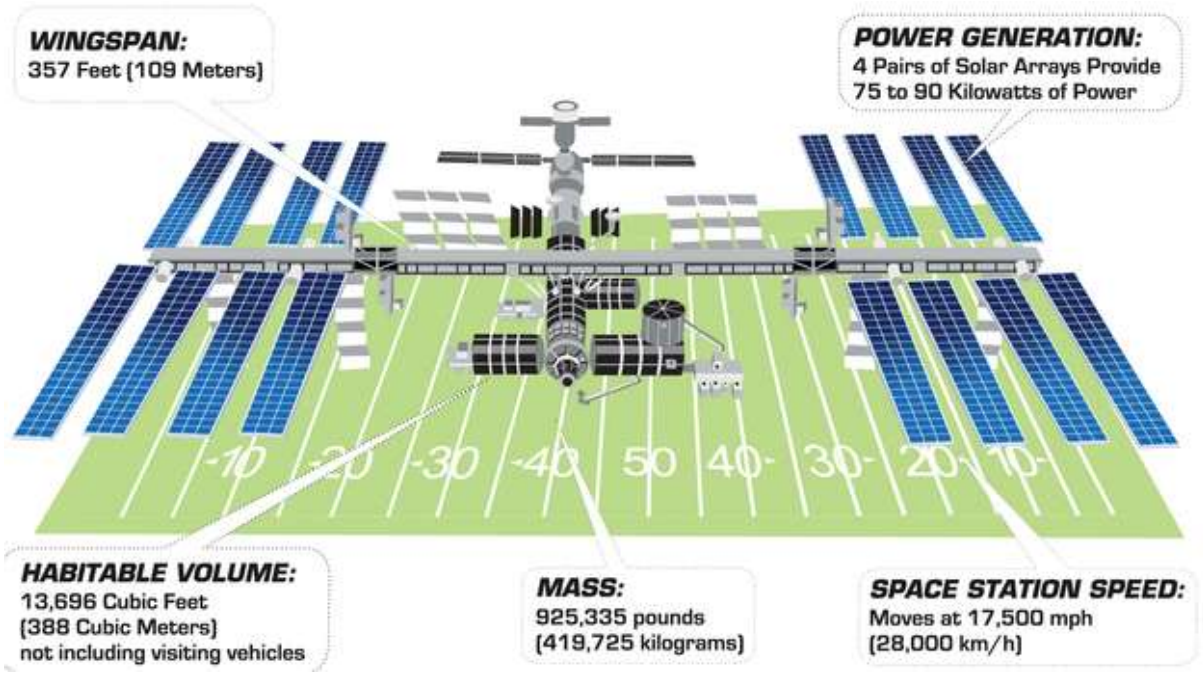

Figure 2.4 — Illustration of the ISS showing its mass, habitable volume, speed, wingspan (equal to an American football field), and the structures responsible for power generations and their respective output. [23]

- Pressurized Module Length: 167.3 feet (73 meters).
- Truss Length: 357.5 feet (109 meters).
- Solar Array Length: 239.4 feet (73 meters).
- Mass: 925 335 pounds (419 725 kilograms).
- Habitable Volume: 13 696 cubic feet (388 cubic meters) not including visiting vehicles.
- Pressurized Volume: 32 333 cubic feet (916 cubic meters).
- With BEAM expanded: 32 898 cubic feet (932 cubic meters).
- Power Generation: 8 solar arrays provide 75 to 90 kilowatts of power.
- More than 50 computers control the systems on the space station.
- Lines of Computer Code: approximately 2.3 million.

- Eight miles (~13 Km) of wire connects electrical power systems aboard the space station.
- On-orbit software monitors (350 000 sensors), ensuring station and crew health and safety.
- The space station has been continuously occupied since November 2000.
- 240 individuals from 19 countries have visited the International Space Station.
- More than 221 spacewalks for construction, maintenance and upgrades conducted since 1998.
- A crew of six live and work, traveling at a speed of 7.66 km/s, orbiting Earth every 90 minutes.
- In 24 hours, the station makes 16 orbits of Earth, traveling through 16 sunrises and sunsets.
- P. Whitson set the record for most total time living and working in space (665 days) on 2017.
- Six spaceships can be connected to the space station at once.

A breathable atmosphere can be created and managed with the life support systems; however, Earth's permanent and stable effects of gravity are not present in the ISS. Since the station travels around Earth at a speed of 27 580 km/h it is in a constant free fall around the planet creating a weightlessness environment in which gravity is reduced often referred to, as microgravity [24]. However, gravity is still present and exerted by earth on the ISS, while in the station, gravity is approximately 90% of the gravity felt on the planet surface [25].

Weightlessness is evident when astronauts are seen float around in the ISS modules and in EVA's, however, this condition can cause some problems, beginning with objects, which can escape inside the modules and float away and hit equipment causing malfunctions. Moreover, weightlessness has an enormous effect on the human body that is accustomed and highly adapted to gravity, therefore once gravity is reduced, a huge effect and toll is exerted on the body including several bodily functions like circulation and digestion [26]. Our bodies are largely composed of fluids that accumulate in its lower part under the influence of gravity. Those fluids are kept in balance by several biological systems, which still function in microgravity and lead to the accumulation of fluids in the top of the body [26, 27]. Therefore, astronauts generally experience headaches, swollen faces, blurry vision, and loss of appetite when they arrive at the station due weightlessness effects [26]. After a few days the human body accommodates and redistributes fluids accordingly to the new conditions, however in the long terms, more severe problems impact the human body including loss of bone and muscle mass [24, 26].

On the station, the human body is also exposed to higher levels of radiation from the sun and other electromagnetic waves moving thought space [26]. Generally, on earth, atmosphere and Earth's magnetic field protect life from such high types of radiation however, aboard the ISS protection had to be implemented in the walls and structure of each module. Nonetheless the structure is not impervious to radiation and astronauts often see flares when their eyes are closed. Radiation can be very harmful and might affect several parts of the body, including eyes, several organs, and even DNA increasing the risk of cancer [26].

Earth's atmosphere not only protects us from radiation but also provides us with a controlled temperature and climate, although temperatures on Earth show changes from season to season and from day to night, in space the temperatures became extremely hot when expose to solar radiation, 120 °C or higher, while in shade it gets as low as -150 °C [28, 29]. The ISS withstands such temperature

on the dark and sunlit sides of our planet while, it maintains a habitable temperature on its interior (~22 °C). This temperature is regulated with heaters, insulation, and liquid ammonia-circulating loops whilst radiators help release excess heat generated by machinery aboard the station [30].

The ISS is surrounded by vacuum which means going outside is enormously different than on Earth, astronauts, regularly must go outside for maintenance and reparations, which requires them to wear spacesuits that protect them from radiation, the enormous temperature changes outside and pressure difference [15]. Moreover, vacuum also means resources must be managed in a much more mindful manner than on earth, water is essential and crucial for continuous habitation and as much as 80 percent of the water aboard is recycled from reclaimed sweat, condensation, and urine [31].

Floating dirt and debris in the ISS could present a hazard since it can damage systems and equipment putting at risk the life support systems or other crucial functions. Moreover, the accumulation of debris, human sweat, and fluids can lead to microbial contamination, with moulds growing in surfaces or even contaminate the water supplies [15]. Therefore, cleaning is much more critical on the ISS and astronauts use various wipes, detergents, and vacuums for, surfaces, filters and even themselves, while trash is collected in bags and stowed in a supply ship that is sent to earth or incinerated [32, 33].

Life in space includes living in a space station of approximately 100m during from six months to almost a year and the ISS is filled with equipment and supplies for 3 to 6 astronauts [15]. Constant monitorization of astronaut's tasks, health and nutrition including an exercise session of 30 minutes on the treadmill and 70 minutes of resistance exercise once a week. Sleeping schedules are also monitored to control mental acuity and general cognitive functions [24, 34]. Beside exercise and sleep, nutrition plays an important role for astronaut's health in the ISS and for future mission to the moon and Mars.

Food is specially prepared for weightlessness which requires changes to prevent it from floating and several types of food are required in the astronauts' diet to counter the effects of microgravity, lack of natural sunlight and effects of cosmic radiation [15]. Moreover, food must be specially treated to last a long time and keep it low in mass, therefore, most food currently sent to the ISS are dehydrated foods. Astronauts do, occasionally get fresh food, such as fruit and vegetables and were even able to eat ice cream for the first time in space during the Skylab program which continues to be eaten in the ISS [35, 36]. Food storage and food production are essential for the ISS and future mission, and must be addressed under the limitation of resources, nutrition requirements. Recent projects are underway in the station to grow vegetables on board and address food and food requirements for Mars and the Moon. [34, 37] As more food is grown in the station food waste and dirt must be managed and controlled, since microorganism like yeast and bacteria grow very easily among wires and commonly used surfaces [38].

Life in space is influenced hugely by microgravity and NASA has provided to the public several videos created in collaboration with the many station residents to educate and demonstrate how the day-to-day life is in microgravity [34, 39]. Moreover, Japan Aerospace Exploration Agency provides us additional details and information on how live is in microgravity in a simplified platform both shedding light on the scientific advances needed to live in space [40].

2.3 State-of-the-art: Monitorization of Contaminants

Air quality is an essential subject in spacecrafts which are partially or fully closed environments that demand a detailed and intensive monitorization to protect both crew and vehicle. In spaceflight it is a breathable atmosphere is imperative and several systems operate to detect, control, and manage pollutants, moreover, since water aboard the ISS is obtained from air condensate, air contaminants can also dramatically affect water quality due to failures or malfunctions of the purification and reclamation processes [41].

Existing works with humans in closed environments have shown that engineering control and current instrumentation are insufficient for a complete crew protection from hazards. Instrumentation to monitor air quality requires further advances, initially to reducing power consumption and size and afterwards in terms of selectivity and sensitivity for contaminants.

Furthermore, the instrumentation characteristics are dependent on the mission with duration being an influent factor, as well as evacuation procedures and available counter measurements after a spacecraft contamination [41, 42]. Air quality and environmental monitoring are complex subjects however, its importance is simply a consequence of the contaminants rate of removal seldom being equal or superior to their generation rate.

2.3.1 Contaminants in the International Space Station

A spacecraft planned for human habitation requires a habitable atmosphere as its fundamental characteristic, providing oxygen and constantly scrubbing CO_2 and other gases to maintain life sustainable and crew member healthy. Atmosphere scrubbing in the US orbital segment is primarily, conducted by a system termed Trace Contaminant Control System (TCCS) on the USOS laboratory and by a micro impurity adsorption device on board the Zvezda module in the ROS, known as BMP from its acronym in the original Russian name.

Those two systems continuously scrub trace contaminants present in the ISS atmosphere, which can be generated by two primary sources, metabolic off-gassing (crew members) and equipment off-gassing. TCCS is part of the Environmental Control and Life Support Systems (ECLSS), and is able to remove trace contaminants from the ISS air and water originating from various sources: e.g. humans, material off-gas products, several systems, chemicals, experiments, leaks, spills, fires, equipment malfunctioning and microorganisms including bacteria and fungi [41, 43, 44].

TCCS and BMP systems were designed and developed with specific air quality standards, the Spacecraft Maximum Allowable Concentration (SMAC) [45], defined by NASA Toxicology in conjunction with the National Research Council of the National Academy of Sciences for each concerning contaminant in any spacecraft [41]. Moreover, cabin material selection, hardware design, manufacturing processes, mission characteristics, crew size and planned activities must conform as well with SMAC constraints for air quality standards. An example is the use of any chemicals aboard the ISS which is subject to an evaluation by ECLS engineers to assure negative impacts to the life support systems and

cabin environment are negligible [41]. Specific ISS design requirements concerning trace contaminant control design and performance are listed and described in the ISS System Specification (SSP-41000Y), the USOS Specification (SSP-41162AN), and the US Laboratory Prime-Item Development Specification or PIDS (S683-29523P).

Trace contaminants must be controlled to less than their respective SMAC for normal equipment off-gassing and metabolic processes from the crew as stated in the ISS System Specification and USOS specifications, while PIDS requires the TCCS specifically to maintain trace atmospheric contaminants concentration from both equipment and crew to less than 90% of individual contaminant SMACs [43]. The TCCS was installed in 2001 and is comprised by a 3-bed system responsible for controlling trace contaminants in the ISS atmosphere which contains approximately 75 000 Kg of equipment and can be occupied by 6 crew members. To maintain the ISS atmosphere, the TCCS uses a three-pronged approach of physical adsorption, thermal catalytic oxidation, and chemical adsorption [43, 46].

Physical adsorption in charcoal bed assembly (CBA) is responsible for the removal of most atmospheric contaminants and are composed of granular activated charcoal treated with approximately 10% phosphoric acid for ammonia removal [43]. Low molecular weight and highly volatile contaminants will sooner or later pass through the charcoal beds, and which are not efficiently removed by physical adsorption and therefore undergo thermal catalytic oxidation in the catalytic oxidizer assembly (COA), composed of palladium-supported catalyst pellets operating at 400°C which are able to oxidize contaminants to carbon dioxide and water by products.

Lastly, halogenated compounds, which can form acid gases (e.g., hydrochloric acid, hydrofluoric acid, and hydrobromic acid), during the catalytic oxidation process and after leaving the COA, are chemically adsorbed, with water and carbon dioxide, in a granular anhydrous lithium hydroxide bed at the sorbet bed assembly (SBA) releasing the purified flow back into the ISS atmosphere [43]. Estimated lifetime expectancy for all the material and operation of the TCCS was deeply studied including charcoal, catalytical beds and atmospheric sample analysis which guarantied TCCS operation for 6 years [43]. Average concentration and respective SMACS and Russian Limiting Permissible Concentration (LPCs) for typical ISS atmosphere contaminants are presented in Table 2.1, concentration averages were obtained by analysis of grab sample containers collected from December 1998 to June 2008 [43, 46]. Although trace contaminants are monitored and controlled to establish a safe and harmless atmosphere in spacecrafts and were highly important in early space exploration mission, generally with short durations, days or weeks, the occupation of space station such as Mir and the ISS have presented environmental control with a novel challenge, biocontamination for microorganism [47].

Spacecraft are designed to provide an internal environment in which physical (gas composition, pressure, temperature, and humidity), chemical (off-gassing), and biological environments are maintained at safe levels, however microorganisms are ubiquitous to human habitation and will occupy spacecrafts, nonetheless. Health and disease prevention have historically been a high priority for space exploration, but the experiences gained from Mir, revealed that microbial contamination of life support system, water and food are as important [47, 48].

Table 2.1 — Contaminants found in the ISS atmosphere and their average concentration in mg/m³ and ppm [43].

Compound	CAS Number	mg/m³ (ppm)	US 180-day SMAC (mg/m³) *	Russian 360-day LPC (mg/m³) **
Aldehydes				
Acetaldehyde	75-07-0	0.342 (0.190)	4	1.0
Propanal	123-38-6	0.047 (0.020)	4 - 8	1.0
Propenal (Acrolein)	107-02-8	0.018 (0.008)	0.03	0.02
Butanal	123-72-8	0.042 (0.014)	4 - 8	1.0
Pentanal	110-62-3	0.031 (0.009)	4 - 8	1.0
Alcohols				
Methanol	67-56-1	0.809 (0.617)	9	0.2
Ethanol	64-17-5	4.25 (2.26)	2000	10.0
Isopropanol	67-63-0	0.271 (0.110)	150	1.5
n-Butanol	71-36-3	0.173 (0.057)	40	0.8
Ketones				
2-Propanone (acetone)	67-64-1	0.324 (0.136)	50	2.0
2-Butanone	78-93-3	0.065 (0.022)	30	0.25
Cyclohexanone	108-94-1	0.047 (0.012)		1.3
Esters				
Ethyl acetate	141-78-6	0.051 (0.014)	-	4.0
Butyl acetate	123-86-4	0.034 (0.007)	-	0.2
Aromatic				
Benzene	71-43-2	0.027 (0.009)	0.2	0.2 (180-d)
Toluene	108-88-3	0.070 (0.018)	60	0.8
m,p-xylenes	179601-23-1	0.040 (0.009)	220	5.0
o-xylene	95-47-6	0.090 (0.021)	220	5.0
Atmospheric gases				
Methane	74-82-8	15.7 (23.9)	3800	3300
Hydrogen	1333-74-0	1.28 (15.5)	340	1600
Carbon monoxide	630-08-0	0.302 (0.264)	10	5.0

*US 180-day Spacecraft Maximum Allowable Concentrations (SMAC) were obtained from JSC 20584.
**Russian 360-day Limiting Permissible Concentrations (LPC) were obtained from Russian State Standard GOST P50804-95.

Total sterilization is simply impossible with human occupancy, however, managing and controlling the presence and spread of microorganism in spacecrafts, is a must for long-term human spaceflight [47, 48, 49, 50]. Moreover, microbial contamination becomes more concerning issue as missions grow in duration or humans develop moon or planet stations. Also, microbial contaminations have different sources, complicating this matter further and further making it a concern and priority. Microbial contaminations can originate from space flight materials during manufacturing and assembly and even with rigorous processes for sterilization microorganisms might survive and will surely grow once human habitation is initiated. Furthermore, external docking vehicles carrying supplies can trigger biological contamination due to the presence of several biological material aboard, e.g., animals, plants and microorganisms for research, and human microbiota as the station or spacecraft is habited [48, 49].

Since the human body contain a large amount of bacteria as commensal microorganisms, this contamination source is perhaps the most important, while several procedures exist to keep the remainder sources in check and controlled, managing the human microbiota spread after several months

or years of human occupation of a spacecraft is more challenging [47, 49]. Surface disinfection using ethanol is impractical and risky for crew and the spacecraft, mainly because ethanol is a huge risk for the breathable atmosphere and a fire hazard therefore, keeping the spread microorganism after habitation is complicated and requires specific methodologies and resources [47, 50].

Human microbiota can spread in the environment through two major channels, (i) air followed by surface sedimentation and (ii) direct transfer to surfaces because most of the microorganism are found in the human skin, mucous membranes, the upper respiratory tract, mouth, nasal cavities and passage and the gastrointestinal tract [48, 49]. Even though most microorganisms are not a serious threat to human health in spacecrafts since they are commensal and part of the human microbiota. However, their presence in a confined and closed space, under high levels of radiations, may lead to adverse effects on the performance of the crew and the integrity of spacecraft instruments, structure and habitat which include infection, allergies, toxicities and degradation of air and water supplies and the corrosion of electrical cables or instrumentation [47, 48, 49]. As results from Mir surveys showed, mutation and proliferation of destructive bacteria and fungi in equipment and structural material can lead to biodegradation of crucial materials and system and eventually, result in system failure endangering the crew's health and wellbeing and even force early spacecraft decommission [49, 50].

The NASA implemented comprehensive microbial analyses of the major risk factors related to microbial contamination aiming to eliminate or mitigate its negative effects. Acceptability requirements were established for food, water, air, surfaces, and crew members in parallel with a robust and meticulous monitoring program verifying if the risks are in the acceptable limits [47, 49, 51]. Nonetheless, prevention is always favoured over mitigation during flight, therefore preventive measures are taken in the early design stages. Water is a huge concern, and when developing a spacecraft, it is required that a system is present to control free water from humidity, condensate, and hygiene activities, because microbes are more likely to grow in the presence of water as it aid metabolic process and even helps in the potential availability of sufficient nutrients [49, 50].

Material and air ventilation for spacecrafts also comes into scrutiny, each design must have materials that do not promote or support microbial growth and, for air filtration is important, since it can greatly reduce the number of airborne bacteria and fungi [49, 50]. Water contamination is controlled by adding a biocide and thermal inactivation of bacteria during water recycling, which is filtrated afterwards to remove any residual biocide and dead microorganisms [47]. Lastly, robust, and regular housekeeping procedures, with periodic cleaning and disinfection, are implemented within the space station habitat as a preventive measure of elevated microbial surface growth [52]. With lessons learned from Mir and the Space Shuttle program, the ISS was designed, constructed, and is managed in a methodical manner that makes it the safest space habitat to this day [47].

Habitation systems and elements aboard the ISS must consider and account for possible microbial contamination, although several different systems are involved in keeping the ISS habitable and its atmosphere breathable keeping those systems cleaned of microbial organisms ensures human can live and work in space. Currently the habitation systems can be divided into seven classes, (i) life support, (ii) environmental monitoring, (iii) crew health, (iv) radiation protection, (v) fire safety, (vi) logistics

and (vii) cross-cutting [51]. Habitation systems are interconnected systems which account for all the needs and requirements for life aboard a spacecraft or station, although some are responsible for providing oxygen, and others preventing fires or managing trash and human waste, their operation must be assured and optimal and, preventing microbial contamination in any systems is a major focus abord the ISS.

Furthermore, as deep space or planetary missions become a possibility in the near future, all the habitation systems will have to be updated and changed for the growing challenges, as well, as monitoring microbial growth and possible mutations [53, 54, 55]. Even if most microorganisms which grow and accumulate in the ISS originated from the human microbiome, exposure to high levels of radiation in Earth's orbit, can alter microorganisms, and possibly result in bacteria and fungi becoming health risks by turning into highly virulent and contagious forms.

Space research on microbial and fungal growth already showed microorganisms adapt to microgravity and alter their growth, how they obtain nutrients, and interact with each other [53, 54, 55, 56]. Several surveys of microorganism communities found in the International Space Station have been performed for the years and aboard several stations, in order to, analyse, control, manage microbial contamination and describe ISS unique environment [47, 49, 52, 57]. Recently an in-depth characterization of the microbial ecology of the ISS environment was conducted and compared with microbial communities' present on Earth's buildings and the human microbiome [52]. Although species-rich, housing at least 12 554 distinct microbial species, the ISS exhibited similar characteristics to surfaces of human homes on earth rather than similarities with the human microbiome. Furthermore, data extracted from this survey concluded the abundance of human pathogens abord the ISS is also analogous with similar environments built on Earth (e.g., analogue environment, NEK, Antarctic Station).

2.3.2 Microbial surveys and Microbial Ecology of the ISS

ISS Microbial characterization was conducted with several experiments; however, two surveys are worth mentioning due to their prolonged sampling and detailed characterization at two different time intervals, firstly from 1998 to 2011 [49, 50] and secondly from 2012 to 2020, a nationwide citizen science project called MERCCURI, Microbial Ecology Research Combining Citizen and University Researchers on ISS [52]. Samples collected from 1998 to 2011 included prefight samples and flight samples from surfaces, air, and water. Surface samples were collected by swabbing a 25 cm^2 area with swab impregnated in phosphate buffer containing Vaseline, air samples were collected with a SAS Super 180 Air Sampler (1 min. at 180 L/min flow rate) and for water a 100 mL water sample was analysed [49, 50]. Microbial growth was conducted in Trypticase Soy Agar (TSA) for bacteria, and Sabouraud dextrose agar for fungi, and total number of microorganisms was counted using the Heterotrophic Plate count (CFU/100 cm^2). Microbial identification included Gram staining, morphologically by microscopy (fungi), 16s rDNA sequencing and Vitek analysis. The Vitek system uses tests cards with 30 or 45 microwells containing either identification substrates or antibiotics [49, 50, 52]. DNA extraction,

duplication, and replication by Polymerase Chain Reaction (PCR), electrophoresis and comparison by BLAST analysis to all GenBank database sequences was done to allow microbial identification [49].

Air and surface samples were essentially dominated by four bacterial genus (Figure 2.5), *Staphylococcus*, *Bacillus*, *Micrococcus* and *Corynebacterium*, and three fungi genus (Figure 2.6), *Penicillium*, *Aspergillus*, and *Hyphomycetes* [49, 50]. A few species of concern, *B. cereus*, *Eikenella corrodens*, and *S. aureus* showing opportunistic pathogenic behaviour, fungi, *A. versicolor* and *Cladosporium* sp. and bacteria, *Flavobacterium indologenes*, *Pseudomonas putida*, and *Xanthomonas malthophila* involved in material biodeterioration were also isolated [49].

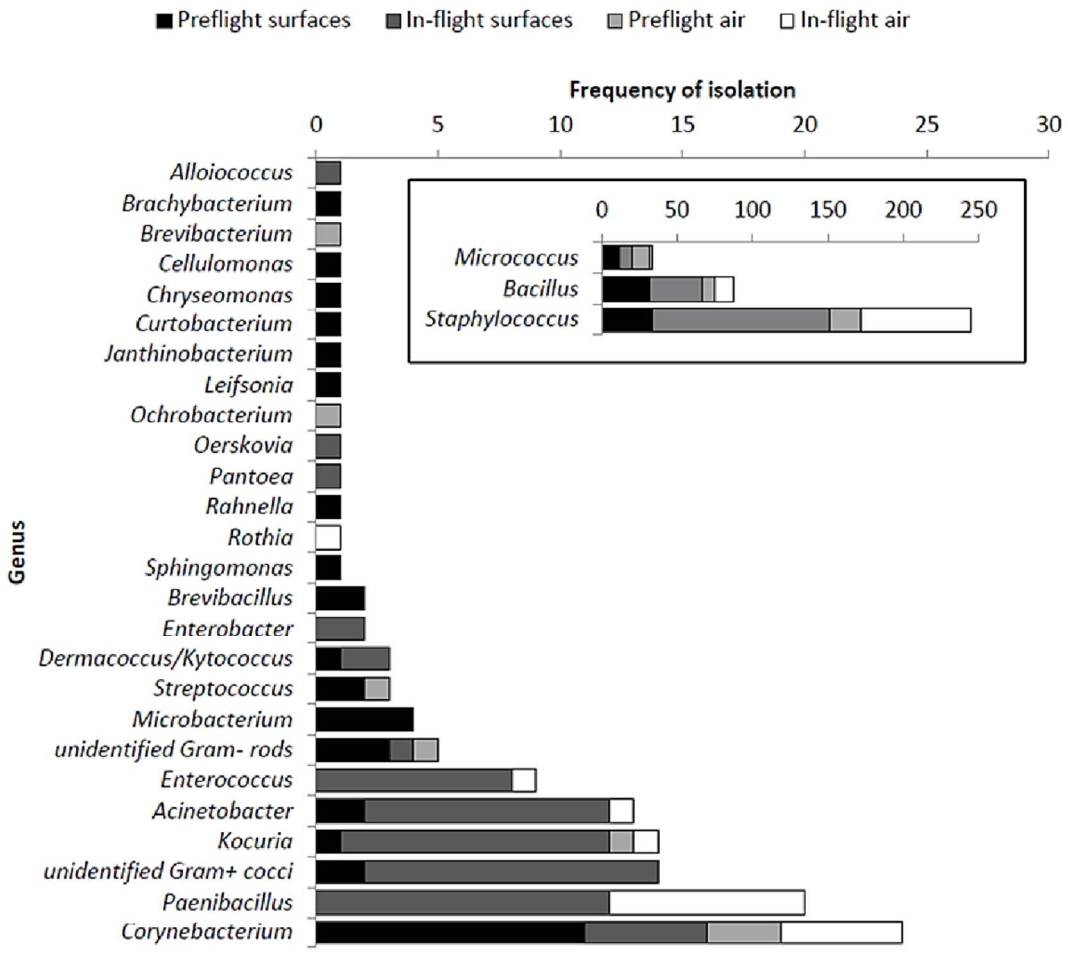

Figure 2.5 — ISS bacterial isolation frequency in pre- and in-flight surface and air samples since 1998 to 2011. Inset illustrates the top 3 most frequently isolated genera of bacteria [50].

Nonetheless, microbial, and fungal concentrations were in most cases below acceptability limits established in the ISS Medical Operations Requirements Document (MORD SSP 50260) whereas main species are typical human microbiota representatives from mucus membranes and skin (*Staphylococcus* sp. and *Corynebacterium* sp.) [49, 50]. Potable water analysis of viable counts in did not exceed 1.0×10^2 CFU/ml and *Sphingomonas* sp. and *Methylobacterium* sp. were the dominant genera, while a molecular analysis was able to recover nucleic acids of non-viable pathogens [49].

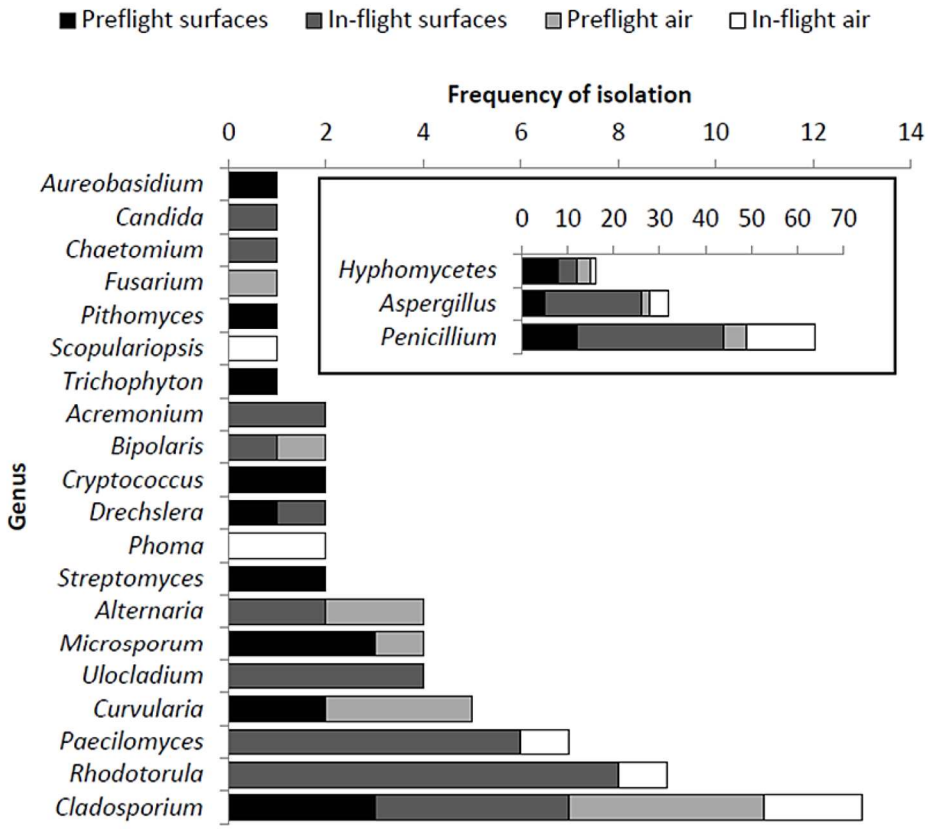

Figure 2.6 — ISS fungal isolation frequency in pre- and in-flight surface and air samples since 1998 to 2011. Inset illustrates the top 3 most frequently isolated genera of fungi [50].

Novikova et al. (2006) collected more than 500 samples from the air, potable water, and surfaces of the ISS during its first six years and created the earliest microbial survey and characterization of the ISS microbial communities. However, such an early survey was unavoidably limited by a reliance on microbial identification by growing microbial species in culture media. Recent culture-independent approaches were implemented abord the ISS, including small-scale 16S rDNA PCR surveys which lead to following survey and microbial characterization in a project called Microbial Ecology Research Combining Citizen and University Researchers on the ISS or MERCCURI for short.

During the MERCCURI project information of the microbial communities living in the ISS during 2011 was gathered and compared to data of homes and the human microbiome [52]. MERCCURI sampling encompassed collection and microbial analysis via 16S rDNA PCR for 15 surfaces on the USOS Harmony and Destiny module (including keyboards, vents, door handles, cell phones, pillows and footholds or equivalents) by swabs. Sequencing and amplification of the 16S rDNA genes from DNA extracted of each swab was used to produce a microbial census of the microbial genus present on each surface sampled. This census provided valuable information although it is important to understand this test does not provide information about the viability of detected bacteria since much of the bacterial DNA on surfaces is typically from dead or non-viable microorganisms [52].

Similarly to the previous survey, human associated microorganisms were the most abundant genus of bacteria located in 15 surfaces (Figure 2.7) in which 93.8% of microbial identified data corresponding

to 19 bacterial orders (Figure 2.8) [52]. Further data analysis also concluded there is no significant differences between samples from the Harmony and Destiny module and the different surface types, hence if a biogeographical pattern exists it is not apparent in those results [52].

Order	% abundance	Dominant Genus	Common habitat	Reference
Actinomycetales	18.3	*Corynebacterium*	Human skin, oral cavity	*Grice et al. (2009)*, *Zaura et al. (2009)*
Bacillales	14	*Staphylococcus*	Human skin, oral cavity	*Grice et al. (2009)*, *Zaura et al. (2009)*
Bacteroidales	12.8	Unclassified Rikenellaceae/S24-7	Animal gut	*Langille et al. (2014)*, *Krych et al. (2015)*
Lactobacillales	11.1	*Streptococcus*	Human oral cavity	*Aas et al. (2005)*
Clostridiales	11	*Finegoldia*	Human skin	*Higaki & Morohashi (2003)*
Pseudomonadales	6.1	*Pseudomonas*	Human skin	*Cogen, Nizet & Gallo (2008)*
Burkholderiales	5.6	Unclassified Comamonadaceae	Environmental	*Willems (2014)*
Neisseriales	2.3	*Neisseria*	Human mucous membranes	*Liu, Tang & Exley (2015)*
Fusobacteriales	2.2	*Fusobacterium*	Human oral cavity	*Schwarzberg et al. (2014)*
Pasteurellales	1.7	*Haemophilus*	Human respiratory tract	*Murphy et al. (2007)*
Verrucomicrobiales	1.6	*Akkermansia*	Human gut	*Belzer & De Vos (2012)*
Flavobacteriales	1.1	*Capnocytophaga*	Human oral cavity	*Zaura et al. (2009)*
Selenomonadales	1	*Selenomonas*	Human oral cavity	*Ribeiro et al. (2011)*
Sphingomonadales	0.9	*Sphingomonas*	Environmental	*Seifried, Wichels & Gerdts (2015)*
Sphingobacteriales	0.8	Unclassified Sphingobacteriales	Environmental	*Steyn et al. (1998)*
Enterobacteriales	0.8	Unclassified Enterobacteraceae	Animal gut	*Linton & Hinton (1988)*
Rhizobiales	0.6	*Methylobacterium*	Environmental	*Knief et al. (2010)*
Campylobacterales	0.6	*Campylobacter*	Animal gut	*Young, Davis & DiRita (2007)*

Figure 2.7 — Most abundant organisms in the international space station and their human association [52].

Although most spacecrafts and cargo undergo rigorous decontamination procedures before launch and rendezvous with the station, it is presumed the dominant source of microbes aboard the ISS originates from human microbiome. Survey authors hypothesized, ISS surface microbial communities were expected to be very similar to human-associated microbes and the Human Microbiome Project (HMP) than Earth home surfaces. However, statistical analysis conducted in this scientific survey, revealed ISS communities were significantly more analogous to Earth home samples than the HMP samples (Student's t -test, p<0:00001) [52].

All 15 collected samples were compared using tight clusters on non-metric multidimensional scaling (NMDS) graphs, a method generally used to visualize the level of similarity between individual cases of a dataset. All samples showed a high degree of similarity, except for one sample, from the starboard crew vent. A combined analysis of the most abundant bacterial families revealed this unique starboard crew vent sample has a higher similarity in microbial composition to human gastrointestinal from the HMP samples when compared with Earth homes. Most abundant families in the starboard crew vent sample included Bacteroidaceae, Ruminococcaceae, and Verrumicrobiaceae which comprised 60.1% of all DNA sequences [52].

This survey concludes the ISS microbial population, although significantly different from Earth homes and the Microbiome Project samples, has a higher similarity with human home surfaces on Earth. ISS surfaces are species-rich with 1 036-4 294 operational taxonomic units (OTUs per sample), an operational definition used to classify groups of closely related individuals without discernible

microbial biogeography, with no observable microbial biogeography. Nonetheless it is suggested the small sample size might be an influencing factor on the lack of any observable microbial biogeography [52].

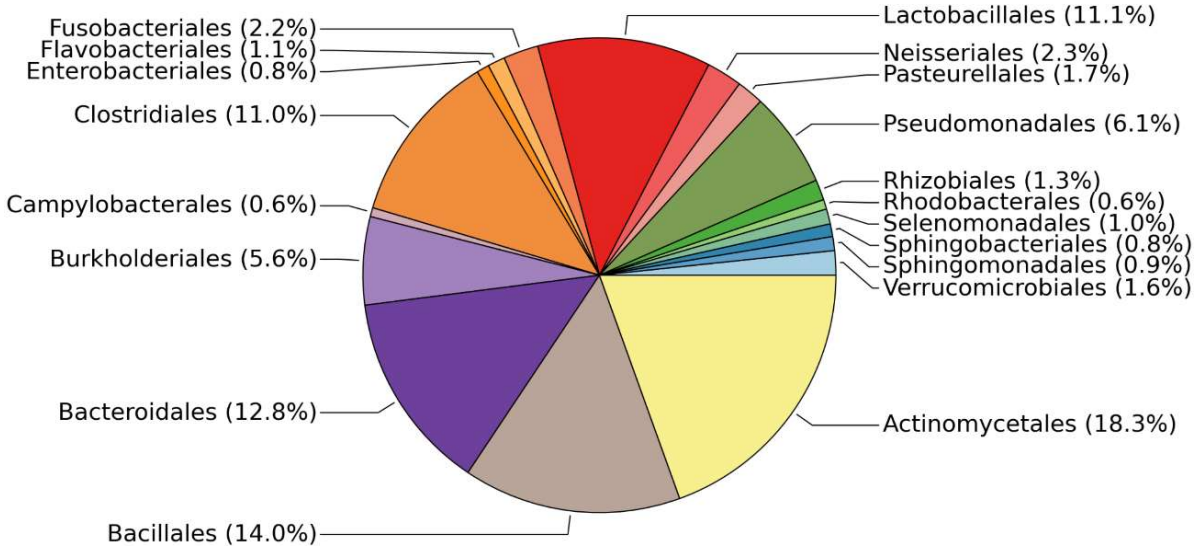

Figure 2.8 — Relative abundances of the most common bacterial families found on surfaces of the ISS. Pie chart containing information from the most abundant microbes' families in 15 ISS surfaces [52].

Aforementioned microbial surveys from the international space station do not account for viable bacterial and fungal organisms providing useful information without distinguishing between viable and non-viable organisms, however, a recent publication presented results from the characterization of the total and viable bacterial and fungal communities associated with the International Space Station surfaces [52].

Presently mandatory microbial monitoring and observational studies of the space station have been performed with traditional methods although many microbes cannot be culture with standard techniques. Therefore, this study applied molecular (polymerase chain reaction (qPCR), targeted amplicon of the 16S rRNA gene and internal transcribed spacer (ITS) region) and culture-based methods to assess microbial communities on various ISS surfaces to attempt to fully characterize the true number and diversity of microorganisms. Distinction between viable and dead cells was also performed by treating half of the samples with propidium monoazide (PMAZ) before DNA extraction. PMAZ higher molecular weight and/or charge, blocks its penetration into cells with intact cell membrane (i.e., viable) but in contrast binds to free floating DNA or DNA inside cells with a compromised cell membrane (i.e., dead cells) and thus distinguishes between intact/viable cells and compromised/dead cells [52].

Eight pre-defined locations (Figure 2.9) were sampled with twenty-four surface wipes during three flight missions in a total of 14 months and returned to Earth for analysis. This comprehensive analysis was used to assess how microbial communities changed over time (temporal distribution) and throughout the SS (spatial distribution) whilst comparing the ISS microbial data with Earth built environmental

microbiome data as the Earth Microbiome Project [96], the Hospital Microbiome Project (Qiita study 10 172) [58], and the Office Succession Study (Qiita study 10 423) [52].

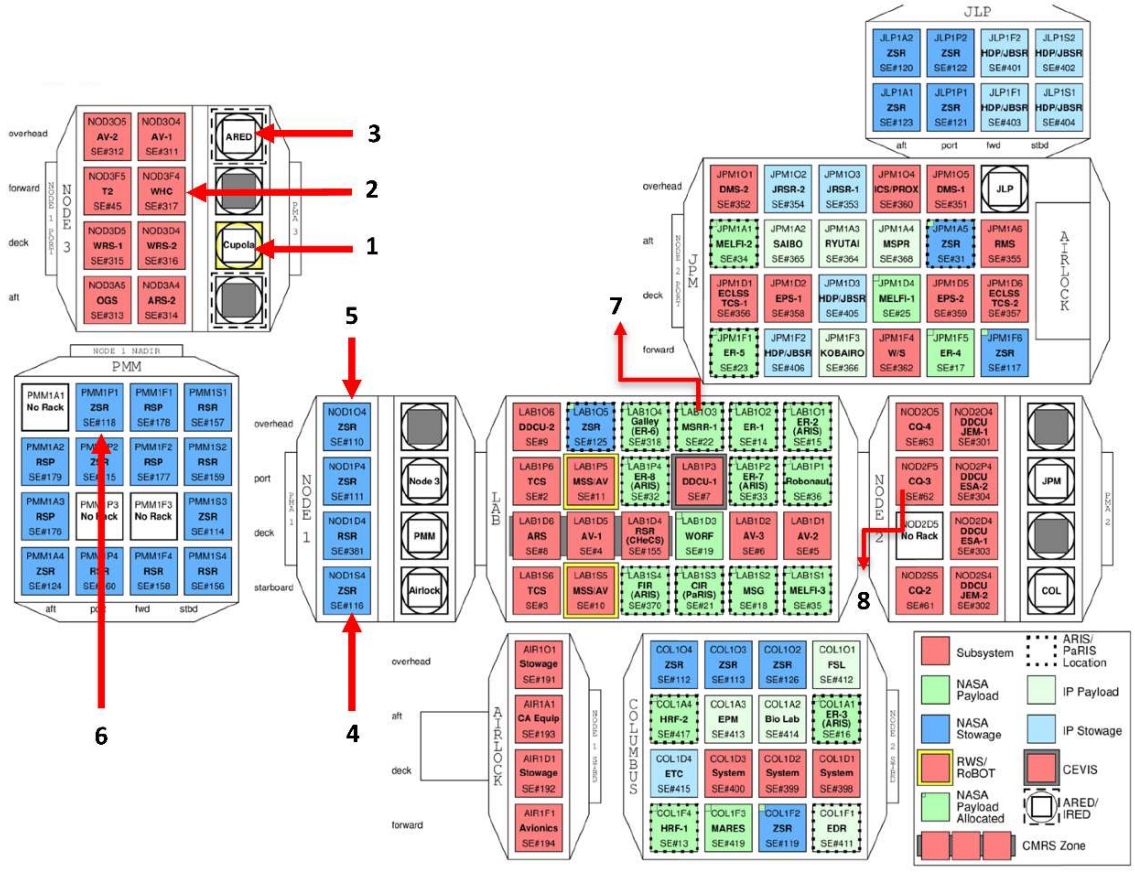

Figure 2.9 — ISS schematic displaying all eight locations sampled over three flights. Location #1, port panel next to cupola (Node 3); location #2, waste and hygiene compartment (node 3); location #3, advanced resistive exercise device (ARED) foot platform (node 3); location #4, dining table (node 1); location #5, zero G stowage rack (node 1); location #6, permanent multipurpose module (PMM) port 1 (PMM); location #7, panel near portable water dispenser (LAB); and location #8, port crew quarters, bump out exterior aft wall (node 2) [52].

The cultivable bacterial and fungal population from ISS samples ranged from 104 to 109 CFU/m^2 which depends on location. Bacterial constitution included *Actinobacteria*, *Firmicutes*, and *Proteobacteria* and fungal constitution was *Ascomycota* and *Basidiomycota* phyla. Moreover, amplicon and cultured-based analysis showed relative differences, with more detected bacteria phyla by the amplicon method but the similar amounts for fungal phyla [52].

Furthermore, temporal changes in bacterial and fungal loads (culture and qPCR) were observed but geographical (locations) differences were absent. Similar results were observed in community composition, reflecting once more changes over time but not locations for bacterial communities while fungal communities remained equal throughout sampling time and locations [52]. However, when bacterial and fungal population were compared, lower values for the fungal community were observed (2 to 3 logs) in all locations expect L6 in which fungal content was 100-fold higher than bacterial load (Figure 2.10). Nonetheless, statistically significant differences were not identified in the overall averages of cultivable counts of bacteria and fungi [52].

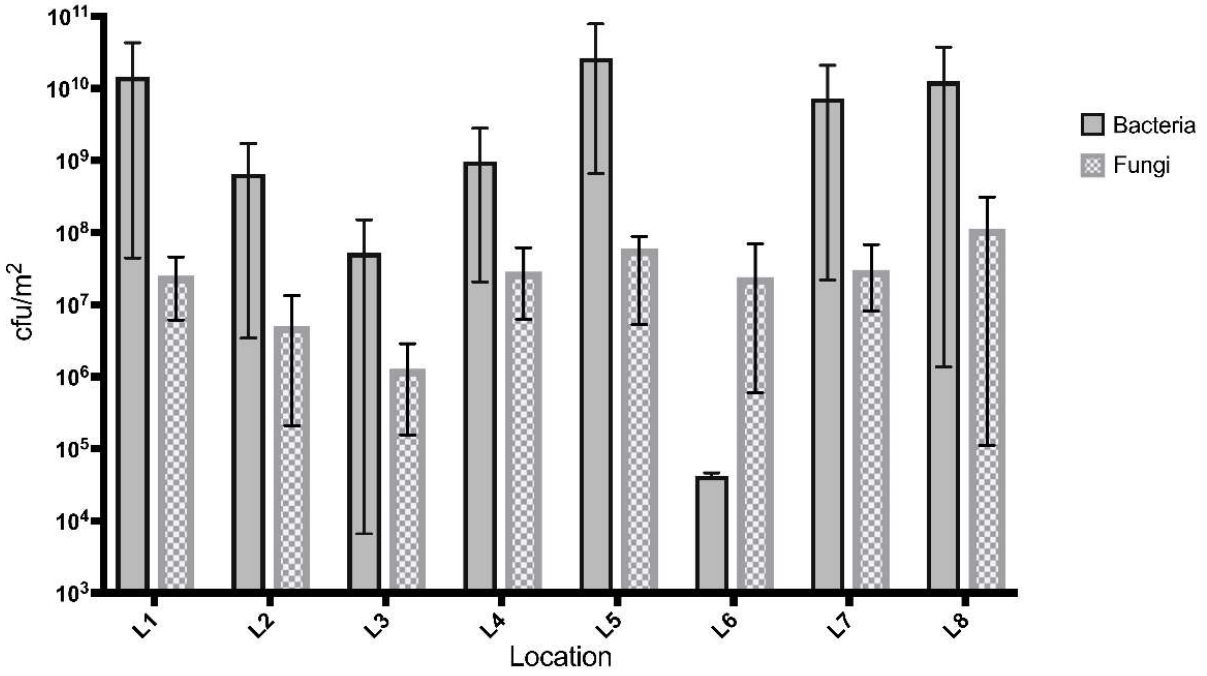

Figure 2.10 — Cultivable bacterial and fungal burden from eight locations on the ISS over a 14-month period. Bar graph representing the CFU/m^2 based on location showing the number of bacteria isolated on Reasoner's 2A agar and Blood Agar Plates were averaged to obtain a number for "Bacteria." Bars represent the average CFU/m^2 at each location with the capped lines showing the lowest and highest value in that group (N = 3). The differences in averages observed in (a, b) were not statistically significantly [52].

The number of bacteria isolated from cultures from 24 surface samples of the ISS was between 6.7×10^3 to 7.8×10^{10} CFU/m^2 while fungi culture ranged from 1.1×10^5 to 3.1×10^8 CFU/m^2, plus roughly 46% intact or viable bacteria and 40% intact or viable fungi could be culture [52].

The growing total bacterial and fungal isolates encompassed 133 bacterial isolates and 81 fungal isolates identified by Sanger sequencing (16S rRNA gene for bacteria; and ITS region for fungi). Bacterial isolates included species from the *Actinobacteria*, *Firmicutes*, and *Proteobacteria* phyla with predominant genius from *Staphylococcus* (26%), *Pantoea* (23%), and *Bacillus* (11%) genius dominated by *Staphylococcus aureus* (10%) and both *Pantoea conspicua* (9%) and *Pantoea gaviniae* (9%). Identified fungal isolates belonged to one phylum, with species from two classes, four families and five genera (*Rhodotorula*, *Penicillium*, *Aspergillus*, *Ulocladium* and *Cryptococcus*) from which two species dominated the total isolates *Rhodotorula mucilaginosa* (41% of total isolates) and *Penicillium chrysogenum* (15% of total isolates) (Appendix I, Figure A.1 and Figure A.2) [52].

Furthermore surface PMAZ-treated samples collected in this survey were compared with two Jet Propulsion Laboratory (JPL) rooms [59], ISS dust [57], ISS High-efficiency particulate air (HEPA) filter and surface samples from an inflated lunar Mars analogue habitat (ILMAH) [52]. Authors concluded the ISS surface microbiome is unique, showing significant differences when compared with all the other human occupied habitats. Afterwards PMAZ-untreated surface samples from the ISS were compared to data from Earth Microbiome Project, hospital environment, and office spaces, revealing them to harbour microbes similar to the human skin but not environmental soil.

Therefore, results of this survey prove ISS surfaces are analogous to Earth built environments while also revealing flight differences among bacterial and fungal communities with relatively small when comparing different environmental sample type. A complete microbial genus summary from the ISS 24 sampled surfaces revealed 121 taxa from which 77 could be assigned to known genera resulting in 68% out of the 77 genera being identified as constituents of the human microbiome while the remaining 32% are found in several soils and water. Furthermore, four unique taxonomic units were present in ISS surfaces, although their total count amounted to only a small percentage of approximately 0.0005 and were identified as *Bacteroides* sp., *Gottschalkia acidurici*, *Paenibacillus thailandensis*, and *Thermus thermophilus*.

This detailed survey strengthens previous studies conducted abord the ISS in the last 20 years and reveal a population of fungi and bacteria living in surfaces that is diverse, changing over time but not between locations. Furthermore, and much like previous microbial surveys mentioned, it was observed microbial organisms growing in the ISS surfaces are dominated by species and genera associated with the human microbiome and earth build environments, once more showing, the ISS is a unique environment which shares a high degree of similarity with our households. Nonetheless, such microorganisms have a potential to become opportunistic pathogens and reenforce the importance of detecting, identifying, and managing viable bacteria and fungi.

This survey led to the first comprehensive catalogue of both total and intact/viable bacteria and fungi found on ISS surfaces, reviewed, and presented herein to elucidate and call attention to the importance of developing technologies, methods, and safety measurements to keep space habitation under safety requirements for longer space exploration mission and future space station, lunar station, and the human exploration of Mars.

Risks associated with microbial contamination of ISS air or surfaces can further be emphasized by various publications about genetic, morphological, and biochemical changes in microbial metabolism. *Escherichia coli* metabolism in space was studied as early as 1991, in a publication of the Journal of General Microbiology, where *E. coli* growth inside the orbiting Biocosmos 2044 satellite was analysed. Microgravity and heavy particle radiation effects on growth parameter, energy metabolism, induction of SOS response, global response to DNA damage, characterized by the arrest of the cell cycle, DNA repair and induced mutagenesis were evaluated [60]. No significant differences were found between *E. coli flight* samples and ground control cultures in terms of growth yield or SOS response, indicating bacterial cells do not require extra energy fighting gravity and cosmic radiation and, therefore show no significant increase in DNA damage [60].

Henceforth it became apparent microbial organisms would have reduced obstacles and enough tools to manage most of the inherent associated changes of a microgravity environment, alerting, in turn to possible risks presented by microorganisms in habitable space station and/or spacecrafts. Subsequently space microbiology grew in importance and more research was conducted to comprehend and characterize microbial biochemistry and genetics.

Several crucial lessons were learned from Mir's microbial communities and their effect in structures and electrical components. Through Mir it became evident both bacterial and fungal species are

potential biodegradors of polymers and might produce biointerference, cause structural damage and eventually the malfunctioning or failure of space systems including life support systems [48, 61]. When Mir was decommissioned some damage to electrical systems and cables was already known to be caused by fungi which metabolically evolved to survive in the nutrient-poor station environment [48].

Ultimately the international space station became a crucial place to test new and growing theories about space microbiology. In the ISS environment microbes experience selective pressures due to microgravity, dehydration, lack or reduced nutrient an increased radiation level which lead to the hypothesis, ISS microbial communities were and had adapted to such and extreme environment. Mora et al. (2016) analysed 8-12 years old dust samples from the ROS focusing on long-term surviving microbes and their extremotolerant potential against dehydration, heat-shock, and clinically relevant antibiotics [62]. In total, 85 bacterial non-pathogenic isolates and 1 fungal isolate were identified and most exhibit robust resistance against heat-shock and clinically relevant antibiotics [62]. Moreover, several studies have demonstrated an increase in growth, virulence and antibiotic resistance showing the danger of uncontrolled microbial communities and a need for more scientific work into the understanding of how microbes grow and change in space [63, 64, 65].

A challenging and abundant problem during Mir's lifetime which is still alarming abord the ISS, are biofilms, surface-associated bacterial communities which form extracellular membranes or environments by secreting small molecules. Effects of spaceflight in biofilm formation and physiology from *Pseudomonas aeruginosa* were studied during two Space Shuttle Atlantis missions, which concluded spaceflight is responsible for an increase of viable cells, biofilm biomass and thickness [53]. Biofilms in microgravity, also showed a characteristic and unique morphology described as column-and-canopy not observed on Earth biofilms. Such changes were observed to be independent from carbon source and phosphate concentration in growth media with flagella-driven mobility being essential for the formation of this new biofilm architecture, representing the first evidence microgravity affects community behaviours of bacteria [53].

Furthermore, a recent study has focused on the interactions between microbial community of the ISS and its crew [66]. A detailed characterization of one crewmember's microbial profile collecting swabs from several body locations (month, nose, ear, skin, and saliva) at eight different time points including pre-, during and post flight and eight different habitable location in the ISS during two missions were collected during flight and after its departure were collected and compared. Results showed skin, nostrils and ear samples had a higher degree of similarity with ISS surfaces when compared with mouth and saliva samples. Also, skin samples showed higher similarity with ISS surfaces during its stay in the station but slight changes after his departure [66].

Microbes can survive and thrive in several types of extreme environments on Earth and as is currently understood also aboard the ISS, a hermetically sealed closed system, under special and unique conditions including microgravity, high levels of radiation, elevated carbon dioxide and air recirculation thought HEPA filters. While microbes present aboard the ISS are likely to have existed since its foundation or have been introduced by new astronauts or payloads, its risks for crew's health are as dangerous and alarming as most cabin air gases or water contaminants.

Control and management of all types of biological contaminants are intrinsic to several habitation systems necessary to maintain both the crew and station health. NASA and Roskosmos have employed complex strategies to monitor biological contaminants over decades of space exploration and habitation, however with the upcoming new era of human exploration, current monitoring needs have shift to specific characteristics directly connected to longer missions where resources are scarce and highly important.

2.3.3 Strategies for Monitoring Contaminants Aboard the ISS

Although strategies for monitoring contaminants change upon mission length its requirements depend on the toxicology of potential contaminants present in air, surfaces, and water. Essentially in short missions (days or few weeks) a strict control of vehicle material selection and a low number of archival samples of air and water collected and later analysed on earth are required, while real-time monitoring in short mission would only be required for a reduced number of important compounds (e.g., oxygen and carbon dioxide) involved in a breathable atmosphere.

Longer missions (6 month or more) much like space stations or planetary landings required different strategies, changing focus into real-time control, whereas reduced archival samples are collected and returned for analysis [41, 42]. Longer missions will also have a substantial increase of distances from Earth, therefore making archival sampling impractical, due to, at best delayed information and surveillance, whilst transforming real-time monitoring into an obligation. Therefore, for insights into cabin air and potable water composition a necessity for autonomous onboard monitoring systems, with artificial intelligence, is essential and will be the initial milestone to make planetary exploration a possibility [41] (Figure 2.11).

Earliest monitoring strategies were simpler and conditional to short duration missions of early humans in spacecrafts, however since the Gemini program, archival air samples have been performed to forensically verify air quality and the performance of the ECLSS, systems designed to maintain a safe balance between generation and removal of air contaminants. Air contaminants can originate aboard a spacecraft from several sources: off gassing, term degradation, containment leaks, waste products, extravehicular activities, fire extinguishant use, utility chemicals, crew metabolites and from the various systems of the life support systems (ECLSS) [41, 67].

Most commonly, air samples are collected with grab sample collectors (GSCs), an electropolished stainless steel container of 300 mL; sorbent tubes in a device named the solid sorbent air sampler (SSAS) (Appendix I, Figure A.3) composed of 8 silica-lined stainless steel tubes containing ¾Tenax and ¼Carboxen; and a Formaldehyde Monitoring Kits (FMK) [41, 67]. The GSC relies on vacuum to draw an air sample into its interior while the SSAS require a small pump to draw air into them over a period of 24 hours. Archival air samples are sent to Earth and analysed on the Toxicology and Environmental Chemistry Laboratory at NASA Johnson Space Center for analyses employing two different protocols for sample analysis of GSC and SSAS. A modified Environmental Protection Agency (EPA) protocol (TO-01) is used for the SSAS sample which only contains volatile organic compounds (VOC), while

the GSCs samples are analysed using the EPA's TO-15 protocol for VOC analysis via gas chromatography–mass spectrometry (GC-MS) and gas chromatography-helium ionization for other gases (i.e. dioxide, carbon monoxide, methane, and hydrogen) using in-house generated protocols [41]. Concentration results are later compared between GSC and SSAS sample and SMACs assessing air quality during each mission. Formaldehyde Monitoring Kits (FMK) contain 12 formaldehyde monitors (10 test units and 2 control units) in a large Ziploc bag and are used to monitor formaldehyde levels, which analysis conducted at the JSC Toxicology Laboratory [67].

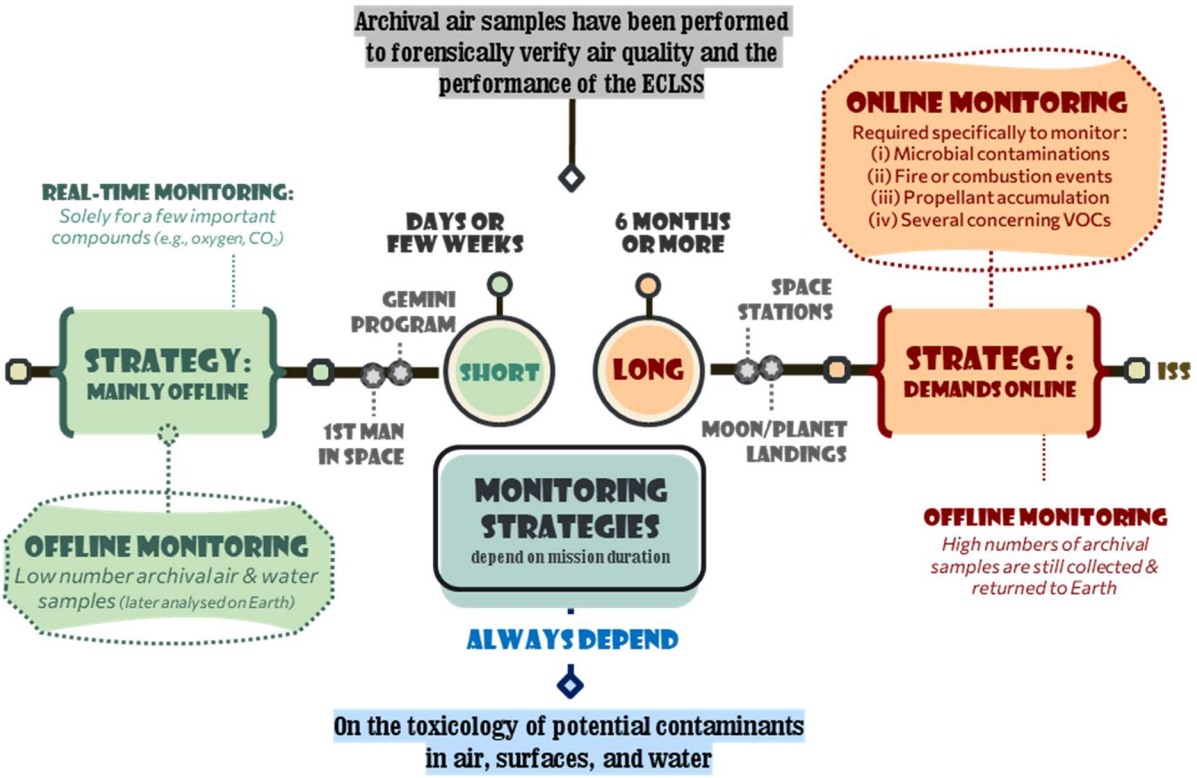

Figure 2.11 — Diagram summarizing different strategies for monitoing contaminants in spacecrafts, including the ISS, in terms of mission duration; Short, days or few weeks or Long, six months or more.

Quickly it became evident archival samples results could be slow, taking 10-14 days at best, while sometimes months could pass between air sampling and analysis, promptly leading to sampling and air quality monitorization to be desired in near real time as a strategy [41]. Real-time air monitoring before 1990 was only conducted for a limited number of compounds, oxygen, carbon dioxide and water condensation measured as a dew point, however, due to a series of incidents, involving space shuttles, NASA was forced to develop the combustion products analyser (CPA) [41, 67].

CPA was the first portable real time monitor device to routinely be used in Shuttle spacecrafts, and only slightly modified from a commercial-off-the-shelf hardware [41]. Structurally it was composed of four electrochemical sensors for monoxide, hydrogen chloride, hydrogen cyanide, and hydrogen fluoride detection and control. CPA was a used as a tool to investigate odours and aid crewmembers deciding on atmosphere safety status after a fire or combustion event and not an alert device.

An upgrade hardware was later developed to replace the CPA and provide tailored fashioned monitorization for combustion released compounds, named therefore as compound specific analyser-combustion products (CSA-CP) [41, 67]. Both systems rely on electrochemical sensors although the CSA-CP had been improved to be more reliable by means of tweaking sensors' cross-sensitivity. Currently CSA-CP is present in the ISS and provides real-time monitoring, nevertheless its electrochemical sensors have a relatively short calibration lifetime of approximately 6 months. Although 6 months is sufficient for the ISS, such time frame is not appropriate for missions further away from Earth with limited access to maintenance materials [41].

Additionally, due to an incident where carbon dioxide accumulated in a module, a portable carbon monoxide detector became a vital necessity aboard the ISS. A commercial unit from Industrial Scientific (which also produces the CSA-CP) based non-dispersive infrared technology was selected as viable instrumentation [41]. Such device expanded from the CSA-CP and became a monitoring tool for real-time control and management of carbon monoxide which is still used aboard the ISS [41, 67]. Specialized instrumentation for two types of propellant related compounds, monomethyl hydrazine (MMH) and unsymmetrical dimethyl hydrazine (UDMH) have also been implemented in the ISS [67]. MMH and UDMH can be introduced into the station after an EVA, and a portable device, named Compound Specific Analyzer - Hydrazines (CSA-H) was developed and currently operates as a battery-powered ion mobility spectrometer in airlocks to detect and quantify (between 80 and 500 parts per billion (ppb)) extravehicular mobile units for possible contaminations by MMH and UDMH [67].

Strategically, archival samples have limited frequency and availability, and aboard the ISS it has been demonstrated and well-understood how important real-time monitorization is for management of volatile organic compounds (VOCs). Hence, at least a reduced number of compounds would have to be monitored in real time when considering the more than 100 compounds detected from archival samples. Therefore, selected compounds would have a defined set of characteristics [41, 67]:

1. VOCs frequently detected at measurable concentrations in spacecraft (e.g., ethanol, acetone, and 2-propanol).
2. VOCs with significant toxicity at low concentrations, even though infrequently detected in spacecraft (e.g., benzene and acrolein).
3. compounds that could affect the ECLS systems (e.g., siloxanes and 2-propanol).

Afterwards a list with approximately 30 priority VOCs was established from aforesaid characteristics and is continuously updated to meet current and changing spacecraft conditions, ECLSS modification and for new material and designs of modules and instrumentation. Limited options existed to monitor such a diverse VOC list, containing alcohols, ketones, aldehydes, C3-C8 alkanes, specific aromatics, chlorofluorocarbons, and siloxanes (section 5.6.1, Table 5.7) [41]. A separation prior to any type of detector would be vital to deal the complexity of the ISS air, and gas chromatography was a preferred candidate for a such a separation technique. Mass spectrometry was a likely candidate as a detector although its, maintenance, calibration, reliability characteristics, need for vacuum and size hindered its optimal operation and usefulness as an ISS volatile organic analyser. In the end, a modified CSA-H using ion mobility spectrometry was developed as an instrument called, Volatile Organic

Compound Analyzer (VOA), a VOC detector coupled with a small low power gas chromatography column [41, 67, 68].

A VOA unit is composed of a pre-concentrator (for improved sensitivity), a gas chromatography (GC) column using nitrogen (available in the ISS) as the carrier gas, and an ion mobility spectrometer as the detector operating at atmospheric pressure. Moreover, an important aspect of the VOA instrument was its VOC calibration remained steady for years while aboard the ISS [41]. This device operated abord the ISS as a VOC detector from 2001 through 2009, later being upgraded, with a commercially available a chip-sized version of the VOA, called a differential mobility spectrometer (DMS) [41]. The final instrument, called the Air Quality Monitor (AQM), was extremely similar to the VOA, containing also a pre-concentrator and a GC column for separation; differing however, in its detector based on DMS [41].

AQM and other types of technology, such as GC/mass spectrometry (GC/MS) and Fourier transform infrared spectroscopy (FTIR) have undergone several research steps in Earth laboratory and have in recent years been flown to the ISS for some experiment in monitoring air contaminants [41, 67]. The GC/MS system showed several problems involving its components, due to instrument complexity, however, a spectroscopy system, Analysing Interferometer for Ambient Air (ANITA) performed well on orbit. Although ANITA operates without a GC separation its size was still relatively large, plus ANITA showed weak sensitivity for most trace VOCs in the air [41]. Still, if ANITA could be reduced in size, a possible combination with a more sensitive VOC detector could be achieved and result in a powerful instrumentation. In contrasts AQM uses air as GC carrier and detector gases and allows a reduction in size and system simplification, however it required maintenance, including replacement every 6 months of 3 sieve cartridges responsible for cleaning its recirculated air [41, 69, 70]. Technological and scientific advancements are currently being made abord the ISS and on Earth to evolve several already existent real-time monitoring devices, including AQM and ANITA as part of a second-generation monitoring systems for use in longer missions, stations, and planetary exploration [41].

Instrumentation selection is based on a few aspects, low power, weight, volume, and reduced reliance on ISS recourses, which are all aspects interconnect with environmental and specific parameters of the demanding task of air quality in space [41, 67]. Furthermore, proper air quality monitorization in spacecrafts and stations requires measurements of several trace gases present with other background gases at higher concentration, while any combination more than the 30 priority trace gases can be present in a wide range of concentration, low ppm (parts per million) or ppb (parts per billion) [41, 67]. Thus, applied measurement techniques must handle or do not suffer from cross-sensitivity problems, chemical poisoning, changes or destruction of its sensor and present reduced impact from system servicing, refilling of consumables or a high frequency for recalibration [41]. In contrast, autonomous operation, automatic data evaluation, reproducibility, stability, and sufficient short response times to slow developments, like leakages events, are key aspects for any measurement technique that might prove useful for the current air quality monitorization aboard the ISS, future missions, spacecrafts, and stations [41, 67].

Besides air, water is also essential for habitation of spacecraft and stations, with its importance being clear and essential for human survival [41, 50]. Monitoring potable water quality involves, guaranteeing restricted inorganic and organic chemical contaminants amount, as well as microbial growth [48, 41]. Equally, to air, water supplies on the station's US segment are conducted by both archival and real-time methods. Teflon bags are used for collection of water samples, later returned to Earth, and analysed within 2 days in the Toxicology and Environmental Chemistry Laboratory at NASA Johnson Space Center in Houston [41, 50]. Water samples undergo a series of analyses employing published (EPA/standard methods) and custom methods (i.e., pH: potentiometric, Iodine: Leuco crystal violet (LCV) (custom), Volatile organics: Purge-and-trap GC/MS, aldehydes, alcohols, and glycols: GC/MS) [41]. In general, archival analysis does not follow recommended analysis times after sampling or volumes required, mostly due to constrains and logistics in returning samples from spaceflight. Although yearly updates from archival water samples indicate onboard systems have consistently produced acceptable quality of potable water with only occasional instances of contamination levels above the ISS Medical Operations Requirements Document (MORD) [41, 50]. Such instances were few and far between which were a consequence of increased levels of silver added to ground-supplied Russian water to inhibit microbial growth [41].

Since early development of the ISS, it was clearly understood real-time monitoring would be required for water, because portable water originates from humidity condensate and wastewater recycling [11, 41, 50]. Real-time monitoring of water quality parameters includes total organic carbon (TOC), total inorganic carbon (TIC), pH and conductivity [41]. A device capable of monitoring each of the previous parameters was delivered to the ISS on 2001 and named TOC analyser (TOCA). However due to use of phosphoric acid and ammonium persulfate in TOCA it required extra containment and, an inability to refurbish the unit on-orbit create a need for a second-generation unit. In 2008 a second generation TOCA unit operating without any hazardous liquid reagents was delivered to the ISS to monitor water quality US water processor assembly [41]. This upgraded TOCA still monitors TOCs in water and water quality aboard the station, on a weekly basis, by oxidizing organic carbon species present to carbon dioxide gas and by measuring its concentration via nondispersive infrared spectroscopy. However, more information about the US Water Recover System is provided by in line conductivity monitors while, concentrations of biocidal compounds (Iodine from the US segment and ionic silver from the Russian Segment) are monitored by the Colorimetric Water Quality Monitoring Kit (CWQMK) [41].

Both systems, TOCA and CWAMK, provide excellent data regarding total organics and biocidal compounds and overall water quality abord the station, however, an inability in determining which compounds are responsible in TOC increases is still absent and, in some instances, it might be imperative to identify specific water contaminants, since some molecules might prove harmless, however, others might create dangerous health risks [41]. Conductivity sensors provide a simple, reliable, and low-cost method in to determine water purity, because it measures the flow of electrons in solution and therefore quantifies metals and ionic species that can carry a charge. Multiple conductivity sensors

are present aboard the ISS including in US Water Recover System, Urine Processor Assembly, and Water Processor Assembly [11, 14, 41].

Although several types of monitoring systems exist abord the International Space Station for air and water quality such instruments and devices all share common characteristics that dependent on the monitoring strategies applied for long habitation of spacecrafts. All monitors must be compact, low power, radiation hardened, need little maintenance, and remain in calibration for long periods of time at the same time as having minimal or no reliance on crew-time and spacecraft resources excluding power [41, 67]. Commercially available instruments are preferred with leeway for modifications and adaptations for the space environment, nonetheless hardware design and function must be simple. Automation in sampling, analytical runs, data analysis and troubleshooting are ideal since it will reduce ground support and crew intervention, informing on how to proceed if any issue arises [41, 67].

A possibility of data from multiple monitors being combined to determine a "health index" is highly desirable. Such health index can alert crewmembers when problems occur and let them sort out and dig further into the data to pinpoint the specific compounds responsible [41, 67]. Furthermore, as plants and vegetables being to be grown in space for food and the possibility of aquaponics for onboard food production is being researched, systems, and instruments capable of monitoring harmful compounds to plants and their growth are ideal [18, 19, 41, 71].

Microbial monitoring in addition to air and water control is critical for crew safety in extended space habitation and life support system operation of transit vehicles, space station and surface habitats [50, 72]. Such structures and spacecrafts are environmentally controlled closed ecosystems under the influence of microgravity and high levels of radiation and research as revealed changes between the relationships between humans and microbes, particularly with evidence of human and microbial physiology changes due to spaceflight adaptation [72].

NASA (National Aeronautics and Space Administration), ESA (European Space Agency) and JAXA (Japan Aerospace Exploration Agency) have developed together specific measurements to monitor, control and counteract biological contamination in spacecrafts and stations, as well as, implemented specific measures to prevent microbial growth and contamination [50, 72]. Continuous monitorization of life support systems and habitats, deployable microbial control, and disinfection, have been implemented, while pre-flight, 2 months to 10 days prior to launches, and quarterly inflight, surface, air and water samples are monitored to aid in the reduction of microorganisms to a minimum in spacecrafts [72]. Swabs are applied in to collect both pre-flight and inflight random surface samples from which microbial enumeration is possible during flight, whereas identification requires ground facilities [48, 49, 41, 72].

Because the current protocol employs a swab approach, requires multiple steps and water to wet each sampled surfaced for effective collection, a need for new sampling devices and simplified procedures has developed. A new device, using an adhesive sheet, an improvement over swabs, simplifying the sampling procedure, has been used for sample collection abord Kibō (Figure 2.12) [72]. Adhesive's ability to collect microbes from metal plates and laptop palm rests made of plastic or another rough

surface was tested and characterized as equivalent to swabs' capabilities. Plus, this adhesive kit also improved and upgraded transport and storage of collected samples [72].

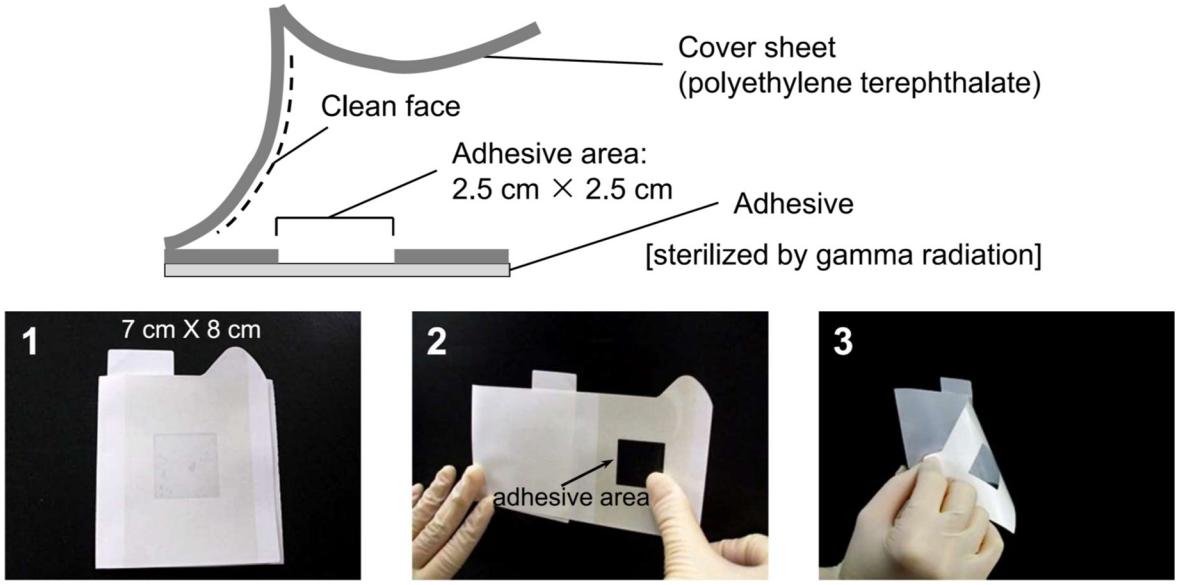

Figure 2.12 —. Adhesive sheet for microbial monitoring in the space habitat. 1. Photograph of the adhesive sheet; 2. Attach the adhesive area to the sampling site and press; 3. peel the adhesive sheet off the sampling site [72].

JAXA has used this new sampling device, the microbe-collecting adhesive sheet in addition to the traditional swabbing method in their continuously bacterial and fungal monitoring of the Kibō module since 2009 (Research title: Microbe). This projected was divided into three phases; (i) September 2009 (Microbe-I), (ii) October 2010 (Microbe-II) and February 2011 (Microbe-II'), and (iii)October 2012 (Microbe-III) from which the Cell Biology Experiment Facility (CBEF; incubator), CBEF door, laptop palm rest, air intake, air diffuser, and handrail were selected as sampled surfaces [72].

Furthermore, NASA employs a strategy of manipulating environmental attributes and parameters to control microbial presence and growth through humidity reduction and free water elimination. This strategy is achieved by maintaining a high-volume exchange, a good air filtration, routinely scheduled housekeeping and by monitoring food products for microorganisms and spoilage [72].

Likewise, rational habitat design can be applied to biocontamination prevention, for instance habitats can be designed to minimize biological aerosol spread under the requirement of reliable models to disperse aerosols from point or diffuse sources in the habitat. An EU-Russia research project, BIOSMHARS, abbreviated from Biocontamination Specific Modelling in Habitats Related to Space aims to develop, calibrate, and validate a mathematical model to predict microbial bio-aerosol dispersion in the BIOS facility, a closed environment used for relevant space research on Earth [72]. In a second phase, the BIOSMHARS intends to develop a versatile and robust modelling tool able to predict airborne microbial contaminant dispersion and deposition in a manned spacecraft in flight. BIOSMHARS can provide a better understanding of microbial dispersal dynamics, survival and proliferation in indoor and confined habitats which will benefit and improve monitoring strategies, management, and control

of microbial flora, and consequently benefiting human health and performance in space conditions and Earth [72].

Currently controlling and monitoring microbial contamination in surfaces, air and water relies on pre-flight and inflight procedures comprised of three phases: (i) sample collection of spacecrafts and payloads, (ii) growth and quantification of colony forming unit (CFU), possible inflight, and (iii) bacterial and fungal identification in ground facilities (Figure 2.13) [50]. This process relies on pre-flight and in flight microbial environmental acceptability limits developed by experts in microbial monitoring and control which were updated and upgraded with data collected from early space exploration and spacecraft habitation [50, 72]. Pre-flight and inflight limits were created to protect astronaut's health and guarantee their safety; however, they are designed to prevent biofouling and keep spacecrafts and station system integrity and operation [50, 72]. Nonetheless, when pre-flight or inflight sample results surpass the limits, remediation or mitigation steps are executed to disinfect and reduce microbial levels to acceptable levels [72].

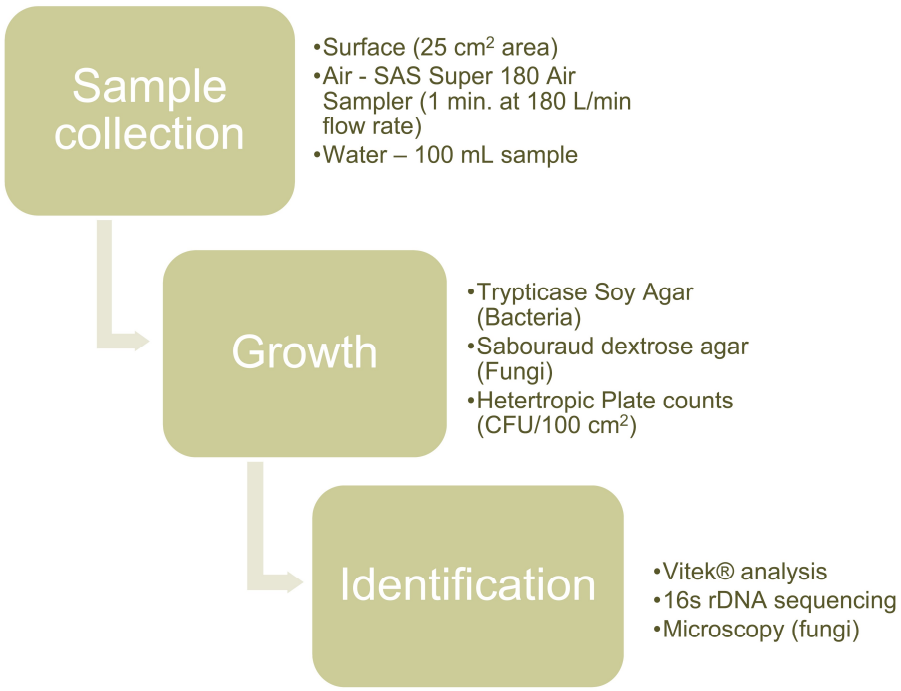

Figure 2.13 —. Microbial monitoring strategy summary for spacecrafts and payloads [79].

Although identification is performed in facilities on Earth, scientific research has been established to create and develop novel molecular techniques to monitor intact microbial population in the microgravity environment that is space [48, 49, 41, 72]. As an example, PCR and amplicon sequencing have recently been proved to be executable in the ISS, however, microbial identification in space conditions required simple, compact, and reliable sample processing instruments, and once such devices are available rapid, real-time microbial detection, functional analysis and species identification are possible for the long duration missions [48, 41, 72]. Even application of electric noses has already been tested in the detection and identification of microorganisms aboard the ISS [73].

Nevertheless, it is evident how important the knowledge collected over decades of the ISS environmental microbiome, has allowed improvements in technology and monitoring strategies [48, 49, 41, 72]. Microbial and trace compound monitoring must be improved if human habitats are to persist in space, and if planetary exploration of Mars and a lunar base are to be established.

As more research into human physiology and microbial presence in spacecrafts is continued several other habitation systems ought to be improved and designed for the new challenges of the current era of space exploration. NASA, ESA and JAXA have presented their roadmaps outlining their plans to improve current systems responsible for (i) Environmental Control & Life Support Systems (ECLSS) and Habitation, (ii) Extravehicular Activity Systems Life Support and Habitation systems, (iii) Human Health and Performance, (iv) Environmental Monitoring, Safety and Emergency Response, (v) Radiation and (vi) Human Systems Integration part of a larger group called Human Health Life Support and Habitation Systems [72]:

The roadmaps for the future of space exploration aim to improved systems for both life support and habitation, as well as more advanced systems for monitoring inorganic and organic volatile organic compounds and microorganisms aboard spacecrafts and stations [74].A need for rapid and robust environmental monitoring tools and systems is evident and management, control and identification of trace compounds and microorganisms is a key subject for all space agencies. Defining correct upper and lower threshold of microbes in air, surface and water is just an example of the status in the strategies for monitoring contaminants in the ISS [74]. However, it is crucial to understand clearer the unique behaviour and changes microgravity causes in microorganisms shedding light on how they persist and survive in such an extreme environment and their impact on human health and spacecraft structures.

2.3.4 Mass and Ion Mobility Spectrometry in Space Exploration

Monitoring air quality on manned space mission has been historically conducted by Mass Spectrometry (MS), which is at present an analytical gold standard for chemical composition analysis and MS has been present in space exploration for decades initially for planetary exploration and to study atmosphere compositions. This analytical technique has supported the US space program from earliest missions into today however, its two main application, monitoring air quality and planetary atmosphere composition, demand special requirements in terms of analytical performance, (sensitivity, selectivity, speed), logistic aspects (space, weight, and power requirements), and operation/deployment in the hardship of a space environment [67, 75].

Mass spectrometry was developed for physical and chemical studies and its use was dominated by physic research from 1890 until 1940 in the fundamental nature of the atom [76]. It was Alfred Nier who tirelessly promoted this technique to people outside the physicist's community. Dennis Schlutter a co-worker of Nier would say "He sort of commercialized the instrument not in the sense that he was trying to sell them, but [he] made them more useful and usable". By 1940 mass spectrometers were commercially available and used by industrial chemists qualitatively to control productions

processes [76]. However, at this time nobody really understood what happened inside the instrument limiting its uses in quantitative analysis which, somewhat made it useless to academic chemists, and its expensiveness led to MS being avoided in chemistry awhile. Only in 1950, due to the work of three scientists Fred McLafferty, Klaus Biemann, and Carl Djerassi did the relationship of mass spectrum to molecular structure became evident, thus expanding MS uses and applications to organic chemistry, biochemistry, and volatile organic compound analysis, among others [76].

MS instrumentation, during the late 1980s and early 1990s, underwent a crucial evolution, changing from complex, room-sized instruments to user-friendly, bench-top equipment [76]. Further research and engineering advances made possible for additional size reductions of mass spectrometers which have been supported by the National Aeronautics and Space Administration. NASA, also, supported miniaturization because it requires analytically powerful instruments for space exploration. GC-MS instruments have been used by NASA to identify and quantify VOC's in ground-based facilities from archival samples in Mercury (1958-63), Apollo (1969-72), Skylab (1972), Space Shuttle (1981-2011), Mir (1995-99) and ISS (2001-current) missions and to study atmospheric constitution of solar system planets in Pioneer Venus (1972-78), Mars Viking Lander (1970-78), Galileo/Jupiter (1989-95), Cassani/Saturn (1997-2004) and Contour/Comets (2002-2008) [75].

Ionization and fragmentation are the basis of mass spectrometry, and thus a mass spectrometer converts individual molecules into ions which are manipulated by external electric and magnetic fields. Because molecules fragment in a unique manner and create an ion fragmentation pattern, structural information for a given molecule can be inferred [77]. Several types of molecules, peptides, proteins, carbohydrates, oligonucleotides, natural products, and drug metabolites can be studied and analysed by MS and recreating their fragment patterns, identifying their respective molecular weights and chemical structures. Molecules are firstly ionized, and their respective ions are sorted and separated according to their mass and charge, traveling in a vacuum tube to be analysed and measured in a detector (Figure 2.14) , creating a chart [78]. Ions are very reactive and short-lived; therefore, their formation and manipulation must be done in vacuum and low pressures of approximately 10-5 to 10-8 torr (less than a billionth of an atmosphere - 760 torr (mm of mercury) [77, 78].

The three main steps occur in any mass spectrometer, establishing its working principle: (i) ionization, accomplished by a high energy beam of electrons, (ii) ion separation, by accelerating and focusing ions on a beam which afterwards is bent by an external magnetic field, and (iii) detected electronically in a Faraday plate type detector, while respective information is stored and analysed by a computer. A mass spectrometer operation is outlined in the diagram of Figure 2.14 [78].

Gases and liquids are generally leaked into the ion source from a reservoir while non-volatiles solids may be introduced directly, however, for complex sample mixtures, a gas chromatography column is regularly used to pre-separate its constituents by molecular weight and relative affinity to a stationary phase [78]. While at a mass spectrometer's tube, a magnetic field, with a specific strength allows ions of different mass to be progressively focused into the detector, while lighter ions deflect more than heavier ions. MS instruments must be specifically developed for space application and several types of mass analyser have been adapted for this uniquely environment, including time-of-flight

(TOF), sector instruments, quadrupole arrays, quadrupole ion traps and cylindrical ion trap mass spectrometers [75].

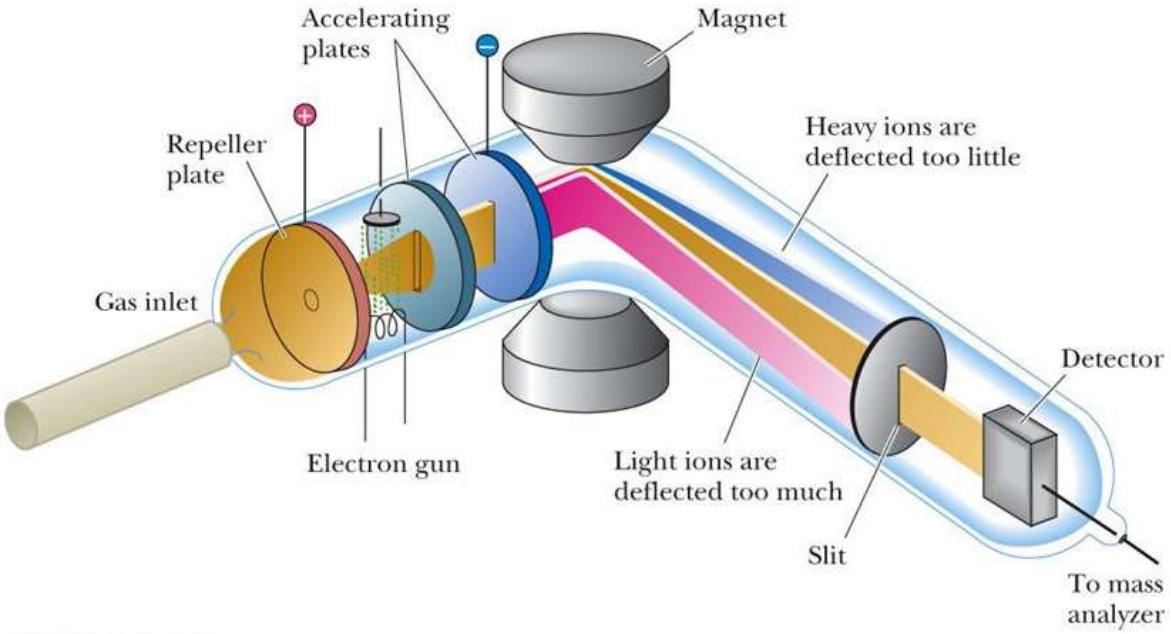

Figure 2.14 — A simplified scheme of the operation systems and principle of mass spectrometry [78].

Besides planetary exploration and air quality monitorization, MS has been used for secondary applications in space, such as analysis of human breath to study microgravity effects on the respiratory system and functions, identify propellant leaks prior to launches of the Space Shuttle and to validate the performance of the trace contaminant removal (Life support system). Moreover, MS has also been proposed to identify and monitor any coolant or fuel leaks external to a spacecraft during extravehicular activity (EVA) [75].

Nevertheless, developing any instrument for space applications is a challenging task because of a mandatory necessity to operate under microgravity, exposure to high G forces, vibrations, and high impact shocks during take-off and landing. Likewise, any analytical instrumentation operational in space conditions requires a highly reliable operation, advanced automation, redundancy, and limited disposables [75]. In the case of instruments for planetary missions, they must account for exposure to radiation, corrosive molecules (molecular oxygen, radicals and, or other reactive species), vacuum, and large variations in temperature and pressure [75].

Although MS instruments have been proven to be a great success in planetary missions, especially since space vacuum can be used to reduce resource demands, several traits and factors that would reduce cost and enhance performance for planetary exploration work against its use in manned mission and spacecrafts. Thus, this led to MS being used sparsely and cautiously in manned missions and several space programs, essentially because of its elevated cost, reliance on large a range of resources and a suspected unreliability in the analysis of complex spacecraft atmospheres [75]. In manned missions and

spacecrafts MS must often operate in a complex atmosphere of trace organic contaminants with high humidity levels, carbon dioxide, hydrogen and methane, all factors limiting MS suitability [75].

Suitability evaluation of MS instruments or other analytical technology for spacecrafts environments and manned missions is dependent on several practical aspects, including size, weight, power requirements, analytical performance including sensitivity, selectivity, precision and accuracy, speed, and cycle times [75, 79]. Moreover, when selecting and developing an instrument for a specific mission, scientist and engineers always consider how each technology supports the mission scientific objectives, costs, readiness to meet often inflexible constrains, and all those factors have progressively reduced MS use in manned missions [75].

Until 1990 GC-MS was used for the analysis of archival air samples, however, during the Shuttle program a series of incidents that degraded cabin air quality steered NASA to develop the first portable real time air monitor device, the Combustion Products Analyzer (CPA) [75]. MS was never a viable analytical candidate for the CPA, which is compose of several electrochemical sensors to detect CO and HCl after a fire [75]. Afterwards, during NASA and Roskosmos cooperated in several Mir missions, Direct Sampling Ion Trap Mass Spectrometry (DSITMS) and GC-MS analysis of archival samples were conducted as part of a technology development study. DSITMS compared to GC-MS offered faster response times and simpler hardware since it required neither an air concentrator nor a gas chromatography however its drawback included a lack of selectivity [75].

Although DSITMS proved capable of detecting most contaminants several levels below their SMAC values, it was unable to identify important compounds such as hydrogen, ethylene, formaldehyde, and the xylene isomers, which fell below its detectable mass range and was particularly prone to interference from nitrogen [75]. Eventually, development of a portable DSITMS was dropped, due to a lack of automation and a need for significant advances in pumping technology and miniaturization, which never allowed for the creation of a viable device for in-situ monitoring of spacecraft's cabin air through this analytical technique [75].

Throughout ISS development and assembly numerous technologies have been considered for monitoring cabin air, including, Fourier Transform Infrared Spectroscopy (FTIR), and mass spectrometry [75]. Initially those instruments were considered and evaluated against a list of more than 200 compounds derived from analysis of contaminants and material off-gassing during previous missions. However, additional information from NASA toxicologists that considered compound frequency in spacecrafts, their potential concentration and toxicity made possible to reduce this list to a manageable 30 VOC's [75]. Hence, target compounds for the ISS were divided into permanent gases (i.e., oxygen, nitrogen, carbon dioxide, etc.), still essentially monitored by MS and, VOC's (i.e., methanol, xylenes, benzene, etc.) which could not all be identified and quantified accurately by GC-MS in-situ [75].

Nevertheless, GC-MS is still recognized as one of the most powerful techniques for monitoring cabin air due to its sensitivity and ability identify a wide assortment of VOCs from retention time and mass spectral data [75, 79]. However, once the ISS grew in volume and frequency of habitation, and future plans for a Martian landing and a moon station, the use of MS became limiting and concerning because it might be able to provide enough information for the next phases of space exploration [75,

79]. Hence. limited resources and longer mission durations aboard the ISS prompted the development of a new instrumentation, the Volatile Organic Analyzer (VOA) for monitoring VOCs in situ [68, 75, 79, 80]. The aim of the VOA was to monitor slow accumulation of contaminants in the atmosphere and effectiveness of decontamination and contingency efforts following a leak or concerning event aboard the spacecraft [75, 80].

Though GC-MS still appeared promising for the VOA due to its analytical capabilities, wide acceptance and use in the detection of trace VOCs, however a rapid progress in the development of IMS instrumentation and technology joined with its growing use in detections of chemical and biological agents by military operation and explosives detection at airports, made it a viable consideration [75, 79]. IMS does not required vacuum, a major advantage in contrast with GC-MS, while also implying size, weight, power, and cost reductions [75]. Furthermore, IMS capabilities met performance requirements and eventually was selected for the basis of a VOA for the ISS. VOA's most important task would be to deliver data to the crew and ground scientists to verify the return of air quality to its nominal state after a contingency event [75, 80].

Even so IMS represented a major side-step from previous practice of monitoring VOCs in spacecrafts and manned missions, while still requiring major efforts to make it suitable for space applications at this unique environment. NASA in collaboration with academia and industry formulated a proposal and strategy for the development of a device which was eventually created for the ISS (Figure 2.15) [75, 80].

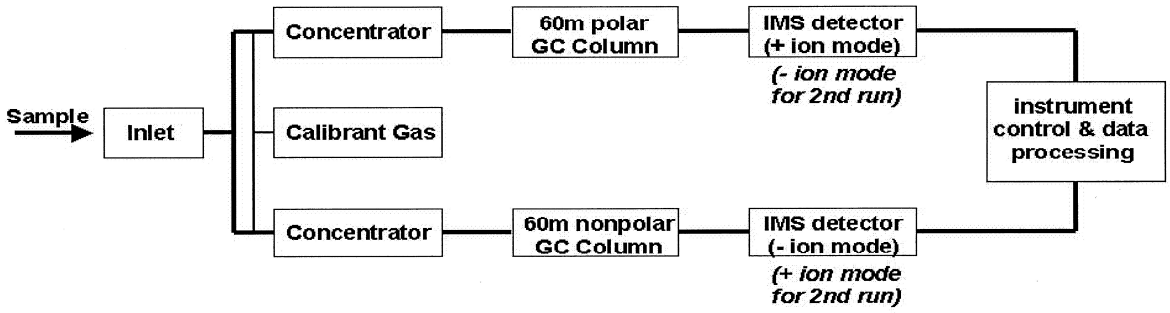

Figure 2.15 — A block diagram for the VOA based on GC-IMS for both nonpolar and polar detection of VOCs [103].

A prototype VOA was first flown during in a Shuttle to evaluate its components, engineering, construction, and competence to operate in microgravity, from which enough results and information for the development a VOA device for the ISS were obtained [75, 80]. An effort to develop and test a smaller, simpler second-generation VOA with improved analytical capabilities has been initiated in 2002 and is still ongoing aboard the ISS [75, 80, 81]. Additionally, ESA is also developing a modified off-the-shelf FTIR device, known as ANITA (Analysing Interferometer for Ambient Air) for early detection and monitoring of toxic, harmful, or unpleasant VOCs [75, 82].

During 2002 a proposal to validate the VOA operation aboard the ISS was executed since it was required that VOA results agreed with other air sample analysis, largely collected by GSCs and analysed by GC-MS [81]. VOA operation was only achieved periodically due to software interface problems

and, several tests were therefore conducted in an attempt of also improving its software. The results allow to conclude the VOA was a stable analytical device that could effectively monitor trace compounds aboard the ISS if kept clean [81].

Further VOA tests were performed in the ISS until 2009, prior to ceasing operations in July 2009, two years after its projected 5-year lifetime, a point in which the development of an operational Air Quality Monitor (AQM) replaced the VOA [80]. AQM and VOA are both based on IMS technologies; however, this new device was developed to test if differential mobility spectrometry (DMS) technologies would allow a more suitable instrumentation for space [69, 80]. However, at this juncture it is evident the necessity of further developments in hardware, software and general scientific research related to IMS to achieve an instrumentation that meets all the required criteria for space operation.

Likewise, the current stage of development of a Fourier transforms infrared (FTIR) spectroscopy device, ANITA, is in equal grounds with VOA/AQM instrumentations. On 2014 it was demonstrated that ANITA could continuously monitor air quality on the International Space Station (ISS), however, this instrumentation showed software and hardware developments were still necessary, and are currently underway, in order to make it a viable long-term option [82].

Hitherto GC-IMS is viewed as a more promising technology for monitoring spacecraft VOC's mainly due to its simplicity (lack of vacuum), flexibility, better reliability, and its ability to operate in degraded environments in comparison with GC-MS, still seen as a potentially powerful tool [75, 79]. Yet GC-IMS still has one important shortcoming, its limited ability to provide enough information for identifying a true unknown compound without a linked databases for VOC identification.

Currently it is also clear that an instrument to be used to monitor life support systems and environmental conditions must have an autonomous operation and a user interface with several levels of control [75, 79]. IMS technologies are still undeveloped in an autonomous operation and requires further developments in software for instrument control, data analysis, self-optimization, and diagnosis.

Confidently, space agencies such as NASA and ESA, are focused in developing and accessing new approaches, such as IMS for future missions, spacecrafts, and stations, because currently there is an enormous demand for in-situ monitoring tools for toxic, harmful, and undesired VOC's aboard spacecrafts in prolonged occupation. Therefore, this will most likely lead to novel or unexplored technologies being researched and studied as a path to revolutionize air quality monitorization in Earth and Space [75, 79].

2.4 Research in Space and its Future

The International Space Station became an enormous research platform in outer space, an orbiting laboratory that provides a unique environment to conduct multidisciplinary research and technological development. Research from several space agency partners is made aboard in this unique structure in several space exploration areas, including basic outer space discoveries and studies, and although each space station partner has their respective goals in scientific research, a unified goal is shared among them, to extend the obtained knowledge for the betterment of humanity [83, 84].

From the evolution of our planet and the life it houses, engineering, environmental and technological advancements, including the study of the physiological effects of spaceflight on the human body and nutrition have been conducted in the ISS. The station contributes annually to scientific developments and research for both space exploration as well as Earth improvements and advancements. Moreover, ISS has been used as an education platform to encourage, inspire, and motivate young students to pursue math, science, and engineering as a career [84, 85]. Space offers unique conditions and possibilities to study human physiology biology, material and physical sciences and the knowledge acquired in the station has been continuously transferred into benefits for society in health, socio-economic and environmental areas [85].

Early spaceflight studies have driven development and advancement in medical instruments and diagnosis for osteoporosis, muscle atrophy and nutrition, while material and radiation studies have already improved our knowledge of combustion, dust particle behaviour and filtering material which are important for high efficient energy production, environmental protection, including air and water purification techniques [84, 86, 87].

Several ISS modules including Columbus, Destiny, Kibō or the Japanese Experiment Module, Poisk or Mini-Research Module 2, Rassvet or Mini-Research Module 1 are devoted to scientific activities and astronauts work daily in several scientific experiments during their habitation of the station [9, 15, 87, 88]. In twenty years of existence and habitation more than 3000 scientific experiments were conducted aboard the ISS by over 4000 researcher from more than 100 different countries, more than 1000 flames have been created during the Advanced Combustion via Microgravity Experiments ACME experiment in order to study and improve combustion on Earth, over 150 billion particle have been measured in aid of dark matter research, 8 different types of leafy greens have been grown in microgravity during the Veggie experiments to understand how to grow food in space for future space exploration [9, 18, 86, 89].

Besides on-board research several experiments about life in space are conducted on ground facilities in what are called Analog Missions, field tests conducted in location that have physical similarities to the extreme space conditions and environment [90]. Analog missions are generally a cooperation of NASA with government agencies, academia, and several industry corporations to test new technologies, robotic equipment, vehicles, habitats and behavioural effects of isolation and confinement, nutrition, communications, power generation, mobility, infrastructure, and storage [90, 91]. Some experiments are unfeasible in space, due to insufficient time, money, equipment, and manpower available aboard the ISS, and analogues offer a quick and less expensive test site to evaluate equipment, materials, and food feasibility for spaceflight among other aspects [90].

Early analogue missions were used to prepare humans for leaving Earth's atmosphere, the moon landing, and the permanent stay at stations orbiting Earth, and have included locations such as the Antarctic, oceans, deserts, arctic and volcanic environments [91]. During those missions, data is collected and analysed about strengths, limitations, and the validity of planned human and, or robotic exploration operations and missions [90]. Therefore, analogue mission aims to prepare for current

and future missions and expeditions, including missions to asteroids, Mars, and the Moon while contributing to problem solving in spaceflight life and research [90].

There major types of analogue facilities exist, isolation and confinement analogues (Human Exploration Research Analog (HERA), Nezemnyy Eksperimental'nyy Kompleks, NEK and several Antarctic Station), a bedrest analogue (envihab) and NASA Space Radiation Lab (NSRL) for radiation analogue missions [88, 91]. Nonetheless, several other analogues have been used and include, Human Exploration Spacecraft Testbed for Integration and Advancement (HESTIA), Aquarius/NEEMO, Human-Rated Altitude Chamber Complex (NEEMO-ACC), Parabolic Flight, Desert Research and Technology Studies (Desert RATS), Pavilion Lake Research Project (PLRP), Haughton Mars Project and In-Situ Resource Utilization (ISRU) [91].

Scientific research on the ISS has been controlled by government agencies, however, even from the start, commercial companies' have played important roles in technological development, from food to building spacecrafts. Those companies have grown in intervention and are becoming more and more relevant in the last years. Building the ISS from 1998 to 2011 was a long and expensive path taking funds from governments that eventually lead to the current ISS structure and *modus operandi*. To reduce governmental expenses and make space research more affordable, private companies are currently allowed to dock their own modules to the ISS from which the Bigelow Expandable Activity Module, or BEAM stands out as a success [10, 86]. However, such shift towards privately funded crews and missions does place the ISS in rather strange and uncertainty state.

ISS decommissioning has been discussed previously and is still a huge possibility, while the station was planned to operate only until 2020, the US and Russia showed interest in extending its lifetime for four more years with Russia even stating 2028 as a future date and recently NASA has announced a preliminary date for the decommissioning process of the ISS for January 2031 [88].

However, NASA recently doubled the rate data is sent from the International Space Station to Earth allowing the station to send faster and larger scientific data, which supports an enormous desire to keep space research active and growing [92]. Nonetheless, improvements in data transfer also open possibilities for missions to other planets or the Moon, and NASA is developing a sister program to the Apollo missions, called Artemis with the aim of putting the first woman on the lunar surface by 2024 [93]. Scientific knowledge gathered in the last 22 years of space research aboard the ISS will be employed in missions to father reaches of the cosmos.

Moon missions have seen a revival with China planning to send people to its surface, NASA has plans to develop an outpost in lunar orbit called Gateway for lunar research and a possible base for the human exploration of Mars which will allow further research for planetary exploration. Although the ISS life might be coming to an end the next decade of space exploration and research is alive and well, and with plans for Lunar bases and the human exploration of Mars a new chapter is being written with its foundations on the ISS. Extended lunar stays will build upon the knowledge from the ISS and provided experience and expertise needed for long term mission to other planets, setting a place for the Moon to also function as a base of operations for replenishing essential supplies created from local materials including rocket fuel and oxygen [88].

CHAPTER 3.
ION MOBILITY SPECTROMETRY:
History, Principles, & Applications

Ion Mobility Spectrometry (IMS) is an analytical technique for the detection of trace amounts of volatile organic compounds in a quick and simple way providing both qualitative and quantitative information withing an analysis. Although this technique has more than 50 years recent requirements for space habitation and monitorization of both organic and microbial contamination has propelled it to focus on both space research and earth application. Due to its ability to detect a large array of VOCs from material and microorganisms with minimal resources, IMS, is currently seen as a promising technique to fulfil the requirements for lost space travel and planetary exploration.

Hence this chapter encompasses a background on the technique, its operation principle, current types of instruments including hyphenated methods, and its application in numerous fields, describing the current state-of-the-art.

3.1 Ion Mobility Spectrometry: History & Principle

Ion mobility and mass spectrometry both have their foundations in Thomson's X-ray experiments conducted in the late 1800s [94, 95]. Although IMS was previously known by other names, such as gaseous electrophoresis due to similarities with liquid-phase electrophoresis and plasma chromatography because of its shared similarities with chromatographic separations, both terms were eventually replaced by ion mobility spectrometry [94, 95]. IMS began in 1896, with Thomson and Ernest Rutherford constructing an apparatus to study ion mobilities in several gases by x-ray ionization, which managed to characterize the behaviour of ions under and their respective ion mobilities and established the technique and its final name [94, 95, 96, 97].

IMS was slowly developed until, in the first three decades of the 20th century an intense interest arose in mobility studies allowing a large body of theory on ion kinetics and experimental data to be collected and produced [94, 95]. Tyndall was a crucial contributor in this era, until 1930, and his work would lead to significant improvements to analytical capabilities of ion mobility. This era saw the exploration of several experimental parameters, differences in pressure, temperature, effects of collisions, electric field, accelerating voltage and ion residence time in the drift region [94, 95, 96, 97].

However, a decline in interest for ion mobility followed in the 30's and 40's with the introduction of mass spectrometry, which did not have complicated reactions at the pressures used for mobility studies [94]. Nevertheless, ion mobility was not forgotten, and hybrid IM-MS instruments were developed by several research groups in 1960 for the study of gas-phase ion chemistry [95] (Figure 3.1). While during this decade, ion mobility measurements were also used by Dole in the earliest development of electrospray ionization (ESI). The epoch, between 1948-1970 has been referred to as ion mobility's foundational studies [97] in which several theoretical studies by Mason and Schamp (1958) and Mc Daniel (1964) [95] established the basis of modern IMS. A renewed interest in ion mobility also seen during this period, with focus on three important uses and developments: (i) primitive ion detectors by military forces during and after World War II, (ii) an ionization anemometer sensitive to organic vapours invented in 1948 by Lovelock and (iii) construction of drift tubes similar to modern drift tubes [95].

Eventually, in 1970, IMS was introduced as an analytical tool by Cohen and Karasek, also known as Plasma chromatography, and the first commercialized instrumentations were made for two main purposes, in structure-based characterization and differentiation of chemical isomer [94]. Karasek work also allowed the crucial deduction that ion formation depends on competitive distribution of available charge among the neutral molecules. Eventually it became evident ion formation is based and influenced by gas phase acidity (or basicity), electron affinities or proton affinities, and concentrations. Those discoveries provided huge improvements in both ion mobility, especially instrumentation [98].

Afterwards the focus became the development of sample ionization, improvements in hyphenated technologies and the use and improvement of pre-existing separation techniques for coupling with IMS. For instance, in 1982 laser ionization was applied to ion mobility as a method of generating simplified mobility spectra based on protonated species, and the introduction of ESI and Matrix-assisted laser desorption/ionization (MALDI) in IMS-MS was developed. Afterwards gas or liquid chromatography was coupled to IMS as a pre-separation tool to simplify analysis of complex samples [94, 95, 96, 97].

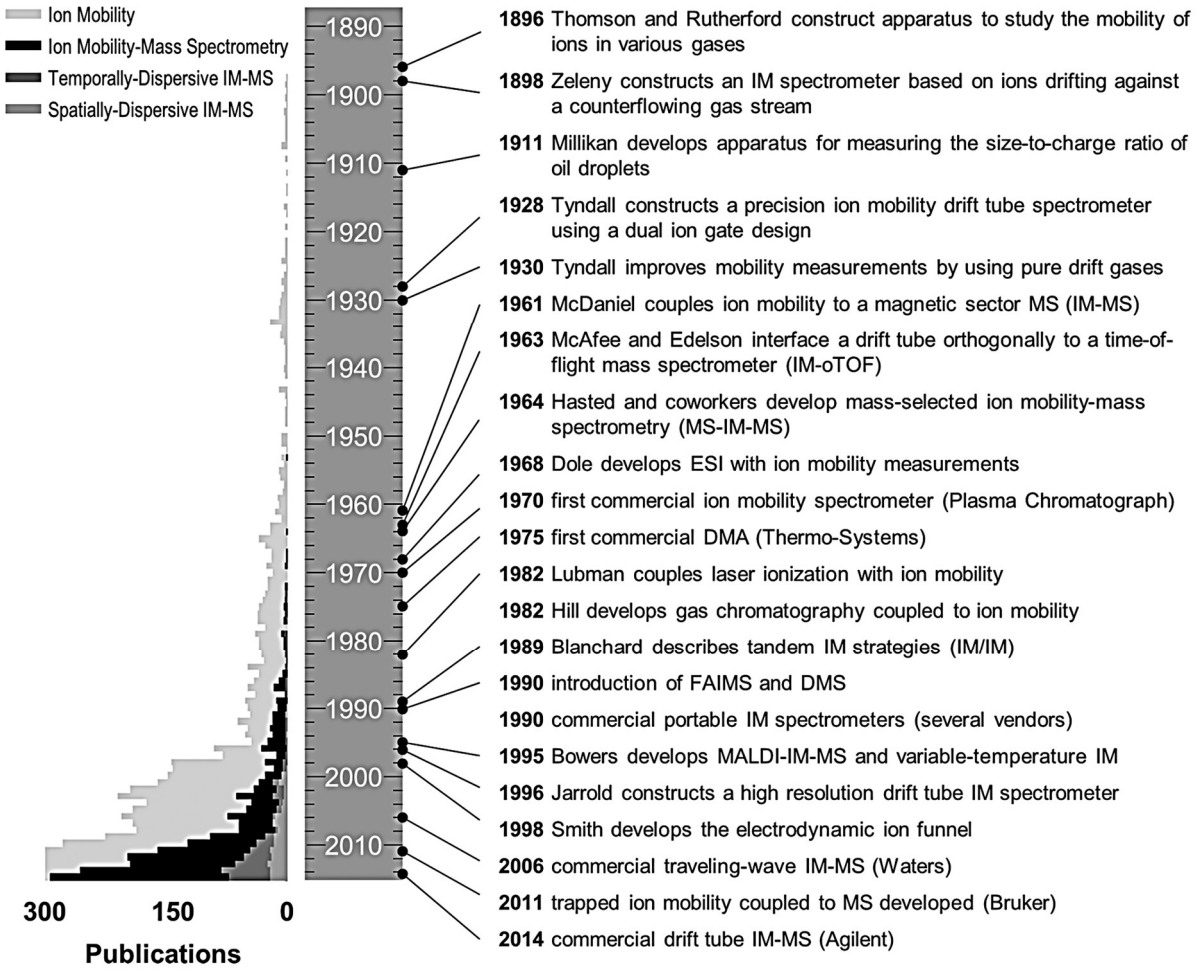

Figure 3.1 — Important historical development of the field Ion Mobility [94]. A distinction is made in the publication frequency for both time and space-dispersive IM-MS publications. (Left) Histogram showing the number of publications per year in ion mobility and ion mobility-mass spectrometry with focus on IM-MS (scale is truncated at 300). (Right) Historical milestones for the development of ion mobility and IM-MS technologies and instrumentation.

In a historical analysis, it is interesting to note the many features associated with modern-day ion mobility technologies were key aspects of early ion mobility instrument design [94]. Although the diversity of ion mobility instrumentations nowadays is enormous, from complex coupled systems, diverse nuances in sampling and sample types, applications to simple ion mobility devices, all instruments share the same basic principle which has existed for approximately 50 years.

In every ion mobility spectrometer, organic molecules are ionized and driven by an electric field against a counterflow of a neutral drift gas until they reach a detector [95]. Since ions travel against a gas flow, their speed in the imposed electrical field is momentarily reduced by collisions between the sample ions and the drift gas. This change between acceleration and deceleration from collisions results in a constant average ion velocity, that depends on the ion's charge, mass, structure, and collision cross sections and, this dependence allows ions to be identified by their arrival time at a detector [95].

Every ion mobility spectrometer consists of simple hardware with three basic units operating at ambient pressure (i) an ionization source, (ii) a drift tube and (iii) a detector (a Faraday plate). A Spectrometer critical component is the drift tube, whereas ions are formed or created and carried to the detector by a constant electric field [94, 95, 96, 97]. The drift tube is maintained at either a positive or negative uniform electric field gradient, leading into the detector [95, 96, 97]. Each drift tube's electric field is created by applying voltage to a set of stacked conducting rings separated with an insulating material and, through its configuration might allow formation of either cations or anions or both simultaneously [94, 95, 96, 97]. The ionization source and the drift tube are separated by a shutter grid which create ion pulses from the two drift tube regions, from the ionization region into the drift region [94, 95, 96, 97].

General IMS operational principles are summarized in Figure 3.2 and include: [96, 99].

i. Transference of sample as vapor into an ion source (radioactive sources: ^{3}H, ^{63}Ni; non-radioactive sources: corona discharges, electrospray, or lasers).
ii. Production of ions from neutral sample molecules at atmospheric pressure.
iii. Injection of an ion swarm into the drift region.
iv. Determination of drift velocities of ions under the influence of an electric field in the drift region and in a supporting atmosphere, the drift gas.
v. Detection of ions and electrical signal storage or display, with or without automated analysis of the result.

IMS working principles results from a simple effect, larger ions, with greater collision cross sections, suffer a higher degree of collisions than smaller ions, therefore take longer to traverse the drift tube. Through this effect, IMS achieves ion separation by shape and size [100]. Hence, this phenomenon seen in all IMS devices is reliant on the crucial parameters from: sample introduction, ion formation and separation at the drift region [96, 100].

In IMS, introduction of a sample can be conducted in several formats, including direct headspace injections, sample vapor adsorption onto a nickel wire, membrane inlet interfaces, permeation tubes, diffusion tubes, gas chromatography for gaseous samples; electrospray ionization, liquid

chromatography for liquid samples; direct analysis in real time (DART), desorption electrospray ionization (DESI), and matrix-assisted laser desorption ionization (MALDI), laser desorption/ablation, for solid samples; direct thermal desorption and solid phase microextraction (SPME), used for both solids or liquid samples [95, 96, 97, 100].

In most IMS instruments two types of gases are defined and inserted, a carrier and a drift gas. The former, also called the source gas is used in the transport of the sample into the ionization region while the latter, generally running counter current to the carrier gas, maintains a clean environment in the drift region, sweeping and purging neutral molecules thus avoiding secondary reactions here [96, 97, 98].

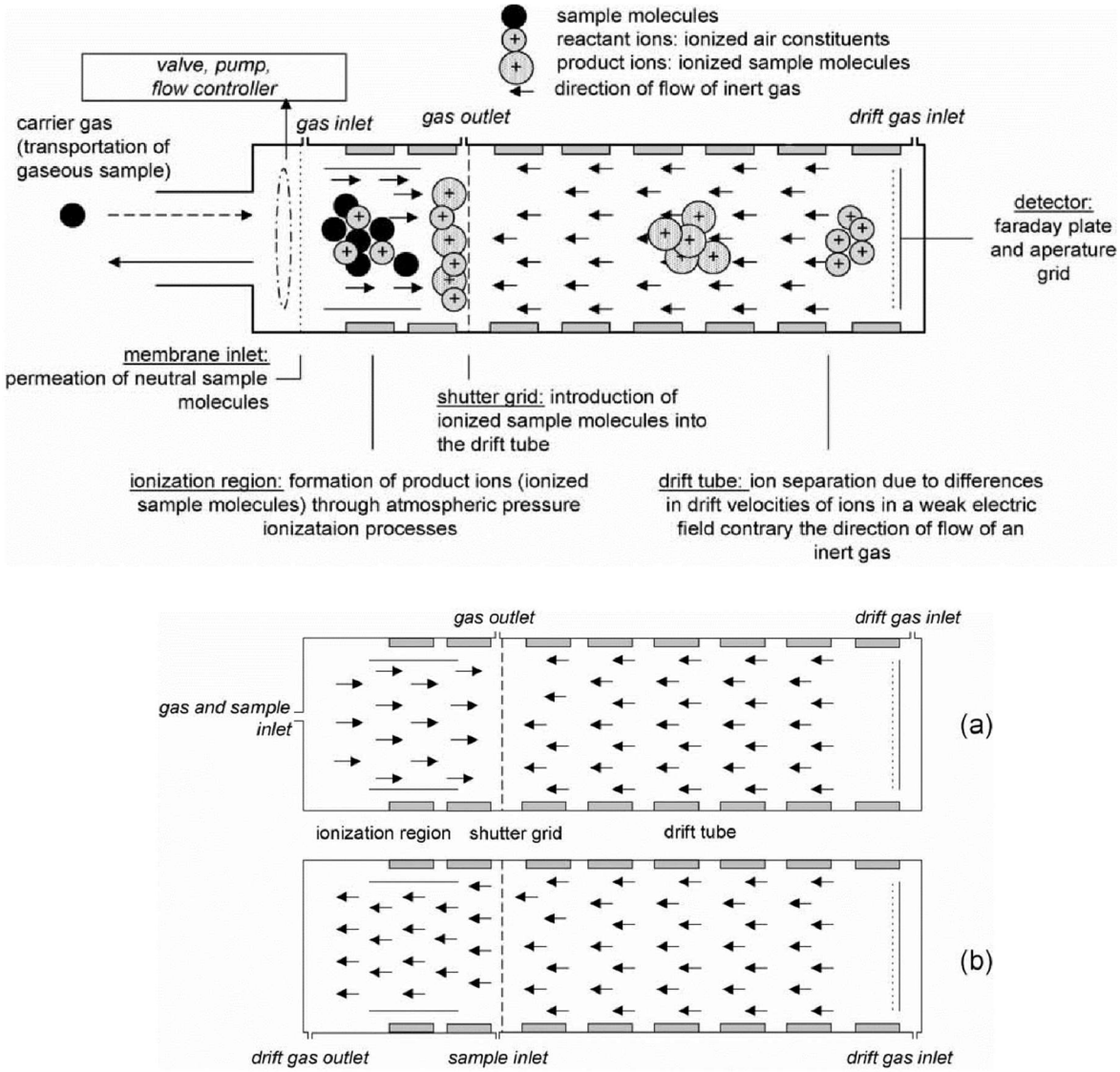

Figure 3.2 — Summarized events within a traditional ion mobility spectrometer equipped with a membrane inlet and a bidirectional flow system (top) and (a) Bidirectional gas flow ion mobility spectrometer and (b) unidirectional gas flow ion mobility spectrometer schematic (bottom) [96].

Moreover, two different gas flows patterns, bidirectional flow, and a unidirectional flow, can be used for sample introductions (Figure 3.2) [95, 96, 97]. A bidirectional flow system operates by

introducing its sample at one end of the drift tube mixed with a carrier gas that travels into the drift region in one direction, while at the detector end, in the opposing direction, a drift gas is inserted, combining with the carrier gas at a shutter grid where a gas outlet is located [95, 96, 97, 100].

A unidirectional flow operates by introducing a sample into the ionization region close to a shutter gird and directly into a drift gas flow coming from the detector side, and exiting at a gas outlet located in the ionization region (Figure 3.2) [96]. Furthermore, in the case of chromatographic methods coupled with ion mobility, selectivity in both the class of compound and amount of sample introduced are attained while also enabling to discriminate between air and water [96, 97].

Ion formation is at IMS's core, and through an ionization source, an initial pool of charge is created which can be dispersed in forming both thermal electrons and, or reactions ions. Ion source commonly used in IMS instrumentation include, thermionic emission, flame ionization, photoionization, surface ionization, laser multiphoton ionization, electrospray, corona-discharge, and β-radiation from radioisotopes (^{63}Ni and ^{3}H) [96, 97, 98]. Sample molecules can be directly ionized (MALDI, UV, and laser ionization) or indirectly by a reaction between the analyte with reactant ions produced by the ionization source through a series of charge transfer reactions (^{63}Ni, ^{3}H, corona discharge, chemical, and electrospray ionization). Nickel 63 radioisotope was the selected ionization source for the first patented IMS instrumentation and is still the most commonly used source in atmospheric pressures [96, 97, 98, 100].

Both ^{63}Ni (a 370 MBq) and ^{3}H (300 MBq) sources emit β-particles from low energy radioactive decay, 17 keV and 5.68 keV respectively, and function as an initiator to the formation of positive and negative reactant ions by atmospheric pressure chemical ionization [100]. This chemical process can be summarized with nitrogen as drift gas by equation (1) in which β-particles ionize drift gas molecules producing thermalized electrons [96, 97, 100].

$$ {}^{3}_{1}\mathrm{H} \rightarrow {}^{3}_{2}\mathrm{He} + \beta^{-} \Longrightarrow \mathrm{N_2} + \beta^{-} \rightarrow \mathrm{N_2}^{+} + \beta' + \mathrm{e}^{-} \qquad (1) $$

This ionized gas reacts with water molecules in trace amounts, in a series of ion-molecule reactions forming reactant ion species $\left[(\mathrm{H_2O})_n\mathrm{H}\right]^{+}$(equation (2)). This step was demonstrated by IMS-mass spectrometric studies which identified the presence of a distribution of water molecules in the reactant ion species [95, 96]. Furthermore, it was also proven this water distribution depends on the temperature and partial pressure of water molecules present in the drift gas. Typically, this distribution ranges from 1 to 6 water molecules, and thus, this phenomenon creates a reaction ions cluster instead of a single discrete ion species [95, 96, 97].

$$ \begin{gathered} \mathrm{N_2}^{+} + 2\mathrm{N_2} \rightarrow \mathrm{N_4}^{+} + \mathrm{N_2} + \mathrm{H_2O} \rightarrow 2\mathrm{N_2} + \mathrm{H_2O}^{+} \\ \mathrm{H_2O}^{+} + \mathrm{H_2O} \rightarrow \mathrm{H_3O}^{+} + \mathrm{OH} \rightarrow \mathrm{H_3O}^{+} + \mathrm{H_2O} + \mathrm{N_2} \\ \mathrm{H_3O}^{+} + \mathrm{H_2O} + \mathrm{N_2} \rightarrow \mathrm{H}^{+}(\mathrm{H_2O})_2 + \mathrm{N_2} + \mathrm{H_2O} \rightarrow \mathrm{H}^{+}(\mathrm{H_2O})_3 + \mathrm{N_2} \end{gathered} \qquad (2) $$

A generalized reactant ion is defined as $[(\mathrm{H_2O})_n\mathrm{H}]^{+}$ which in turn are regularly labelled as a group called the Reactive Ion Peak (RIP) [96, 97]. Furthermore, due to proton transfer two additional positive reaction ions can be formed: $[(\mathrm{H_2O})_n\mathrm{NO}]^{+}$and $[(\mathrm{H_2O})_n\mathrm{NH_4}]^{+}$ resulting from the reaction ion,

between $[(H_2O)_nH]^+$ and ammonia present in the atmosphere [96, 97]. Such ion cluster assemblies should be considered in thermodynamic equilibrium with rapid charge exchange process with clustering and de-clustering rapidly happening.

Once a sample is introduced into the ionization region at atmospheric pressure, product ions are formed, again, via ion-molecules reactions with reactant ions. Proton transfer reactions dominate the process of generation positive product ions which only arise if the sample molecule (M) has a greater proton affinity than the reactant ions (equation (3)).

$$[(H_2O)_xH]^+ + M \rightarrow \left[(H_2O)_yMH\right]^+ + (x-y)H_2O \quad (3)$$

Besides positive reactive ions $[(H_2O)_nH]^+$, negative ions are also being formed in an ionization region, through attachment of a thermalized electron to molecular oxygen, allowing IMS to operate in positive or negative modes. The main reactant ion peak (RIP) produced in the negative mode is $[(H_2O)_nO_2]^-$ however, additional ions can also be produced, for example $[(H_2O)_nO_2O_2]^-$ and $[(H_2O)_n(CO_2)_mO_2]^-$ [95, 96, 97]. Negative product ions are formed from neutral sample molecules (MX) via charge transfer reactions through dissociative and associative electron attachments (equation(4)): [96, 97]

$$\begin{aligned} MX + [(H_2O)_nO_2]^- &\rightarrow M + X^- + nH_2O + O_2 \\ MX + [(H_2O)_nO_2]^- &\rightarrow (MX)O_2^- + nH_2O \end{aligned} \quad (4)$$

In negative mode, electron affinity drives ionization and relative response factors, hence aromatic hydrocarbons, carboxylic acids, nitro-alkanes, or nitro-aromatic compounds and halocarbons exhibit favourable responses while alkanes, alkenes, among others show poor responses [96].

A degree of selectivity in ionization can be imposed in an ionization region by the addition of a doping material to the drift gas. Doping is sparsely used, however in some instances it can improve detectability or remove interferences. For instance, NH_3 can be used as a doping agent/gas, to selectively increasing the formation of the $[(H_2O)_nNH_4]^+$ reactant ion, which is capable of ionizing compounds with higher proton affinity than ammonia [96, 97, 100]. Other examples of dopants used include acetone for chemical warfare agents, chlorinated solvents for explosives detection and nicotinamide for narcotics detection [97, 100]. Product ion formation by chemical ionization might also occur in the ionization region by several mechanisms, electron transfer and charge exchange (proton transfer reaction (PTR)), decomposition (e.g., proton abstraction or hydrogen atom transfer (HAT), nucleophilic displacement, and clustering or adduct formation [96, 97, 100].

An ion mobility spectrum is merely the detected signals, represented as peaks, which correspond to product ions accompanied by the RIP, which are the result of interacting kinetic and thermodynamic processes inside two regions of the drift tube, ionization, and drift region [96, 97, 101]. Concentration, residence times and temperature relationships are key factors controlling cluster ion distribution and ion separation, and directly hinge on the nature of the reaction ion chemistry.

Experimental conditions, substance physicochemical properties and concentration, can form additional product ions in ion mobility spectra [96, 97, 101]. Increasing concentration and residence time

inside the ionization region and drift tube creates a tendency for protonated monomers, $\left[(H_2O)_nMH\right]^+$, to transform into protonated dimers and, even perhaps form trimers or larger cluster ions (equation (5)) [96, 97, 101].

$$[(N_2)_n(H_2O)_mH]^+ + M \rightleftharpoons \left[(N_2)_{(n-i)}(H_2O)_{(m-k)}M_2H\right]^+ + iN_2 + kH_2O \quad (5)$$

Trimer and tetramers product ions are frequently formed but commonly undetected in mobility spectra due to their short lifetimes, generally smaller than drift times in ordinary drift tubes, yet in sub-ambient temperature, below 10°C, proton-bound trimers are frequently stabilized and observed in mobility spectra [96]. This remark allows to define a drift region as, an ion filter based upon ion dissociation under kinetic control and, therefore an ion´s lifetime ought to be long enough for an ion swarm/cluster to transit through the drift region into the detector and be observed in an ion mobility spectrum [96, 97, 100].

Hence, product ions, created in the ionization region are only separated in the drift region of the drift tube by its electric field. A traditional drift tube is made of a series of stainless-stell guard rings connected by 1 MΩ or 0.5 MΩ resistors, while intercalated by insulating quartz, glass, or ceramic rings, in a stack format to create a completely enclosed tube. Voltage gradients in IMS drift tubes are typically between 1–500 V cm^{-1} depending on drift gas pressure values, and the flow of product ions is controlled by a shutter grid [95, 96, 97].

Shutter grids, also called ion gates, are a set of parallel wires that prevent ions from migrating from the ionization source into the drift region. Those gates are electronically open for a few tenths of a millisecond by equalising the shutter grid potential with the electric field and closed when it has a higher potential [96, 97]. Once inside the drift region, ions, in response to the electric field, move faster or slower depending on their individual mobilities and arrive at the detector at different times [96, 97].

Ion mobilities (K, $cm^2\ s^{-1}\ V^{-1}$) are, consequently, determined by their velocity (vd, $cm^2\ s^{-1}$) under an electrical field, (E, V cm^{-1}) in a drift gas. Considering each ion requires a certain time (t_d, s) to travel the tubes' length (d, cm) into the detector, equation (6) is simplified into equation (7) [95, 97, 98].

$$v_d = KE \quad (6)$$

$$K = {}^{d}/_{t_d E} \quad (7)$$

However, ion mobilities are commonly expressed in a reduced mobility (K_0) representing a correction to standard conditions of temperature (T, Kelvin) and pressure (P, Torr) (equation (8)) [95, 97].

$$K_0 = K\frac{273 \times P}{T \times 760} \quad (8)$$

While equation (9) represents ion mobilities in relation to experimental conditions and analyte characteristics, where q is an ion's charge, N is number density of the drift gas, μ reduced mass of the ion, k the Boltzmann constant, T temperature of the drift gas and Ω_D is ions' collision cross section (i.e., size and shape) [95, 97, 98].

$$K_0 = \left(\frac{3q}{16N}\right) \times \left(\frac{2\pi}{\mu kT}\right)^{1/2} \times \frac{1}{\Omega_D} \quad (9)$$

This equation shows, the ion mobility constant is determined by an ion's reduced mass, charge and collisions cross section at a given drift gas pressure and temperature. Large ions show an approximated, Ω, to a simple hard sphere collision cross section, whereas for smaller ions attractive components from ion/neutral molecules interaction must be put into consideration to established collision cross section equations [97, 100]. Furthermore, molecular modelling in conjunction with simulated hard spheres and generalized equations for smaller ion, can be used to create accurate approximations of ion mobilities and permit the prediction structure/mobility correlation [100].

The relationship between K_0 and Ω is only verified at low field limits, in which the electrical field strength (E) to buffer gas density number (N) ratio is small, below 2 Td (1 Td (Townsend) is 10-17 C cm^2), and the mobility measured is independent of drift field [95, 97, 98]. Thus, higher values of E/N signify ion mobility is not constant and becomes field dependent. This phenomenon became the principle of ion separation in differential mobility (DMS) or high-field asymmetric waveform ion mobility spectrometry (FAIMS), which was first recognized by Buryakov in 1993. Therefore, both DMS and FAIMS rely on having sufficient difference between high field and low field mobilities of two ions for separation and are important techniques in trace analysis and structural studies [95, 97, 98].

After traveling through the drift tube, product ion passes a grid located immediately in front of a Faraday plate detector. The grid function is to help reduce the capacitive response of the collector to incoming ions in atmospheric pressure IMS, since ions arrive in a tighter distribution than they would in the absence of the grid [100]. Particularly, product ion misidentification or masking of analyte responses in ion mobility spectrometry analysis, occurs by two basic pathways, firstly by an analyte failing to form a detectable ion in the presence of an interferant which is more easily ionized, and lastly, when detectable ions are both formed by an analyte and an interfering compound with similar collisional and cross-sectional areas and consequential overlapping K_0 values [97, 98].

Once ions arrive at the detector and its corresponding signal is processed, an IMS spectrum can be generated with the aid of automated computer tools. A spectrum is the output data of a single IMS measurement, and is a vector S, (z_0, z_1, …, z_N) of signal intensities, z_i measured in equidistant time point dt_i, where $i \in \{1 \dots N\}$ [97, 99, 102].

Often such data is presented as a 2D graph, or spectrum, of intensity *vs* time, where product ions can be identified as peaks in signals acquired from the IMS detector. However, modern IMS devices commonly use a pre-separation technique, gas chromatography (GC), leading to an additional dimension in the resulting IMS spectrum [99, 102].

A GC-IMS measurement becomes a series of R one dimensional IMS spectra recorded at equidistant retention time point rt_k, $k \in \{1 \dots R\}$, which corresponds to a mathematical matrix containing a series of 2D spectrum every instance a retention time is processed, or every time the IMS shutter grid is opened [99, 102]. GC-IMS spectra can be represented in three common formats, as a matrix (equation (10)), an heatmap, or a 3D graphic.

$$M_{IMS} = \begin{bmatrix} z_{11} & \cdots & z_{21} & \cdots & z_{31} & \cdots & z_{N1} \\ z_{12} & \cdots & z_{22} & \cdots & z_{32} & \cdots & z_{N2} \\ \vdots & \cdots & \vdots & \cdots & \vdots & \cdots & \vdots \\ z_{1R} & \cdots & z_{2R} & \cdots & z_{3R} & \cdots & z_{NR} \end{bmatrix} \quad (10)$$

Within M_{IMS} each data point z_{ij} denotes the signal intensity at a specific drift time d_{ti} and specific retention time r_{tj} [99, 102], whereas in a heatmap retention time is represented in the y-axis, drift time in the x-axis and a colour code scheme is used for signal intensity.

In a 3D graph, the colour code of the heatmap is replaced by a numerical scale on the z-axis, therefore encompassing data from three variables: (a) retention time (t_r) of a gas chromatographic column; (b) drift time (t_d) for the separation of analytes in the drift tube and; (c) intensity (I) detected at a Faraday plate. Retention time is frequently expressed in seconds, drift time in relation to the RIP and intensity in volts. Generally, 2D plots are termed spectrum (singular) and 3D plots or heatmaps, are called spectra (plural) (Figure 3.3).

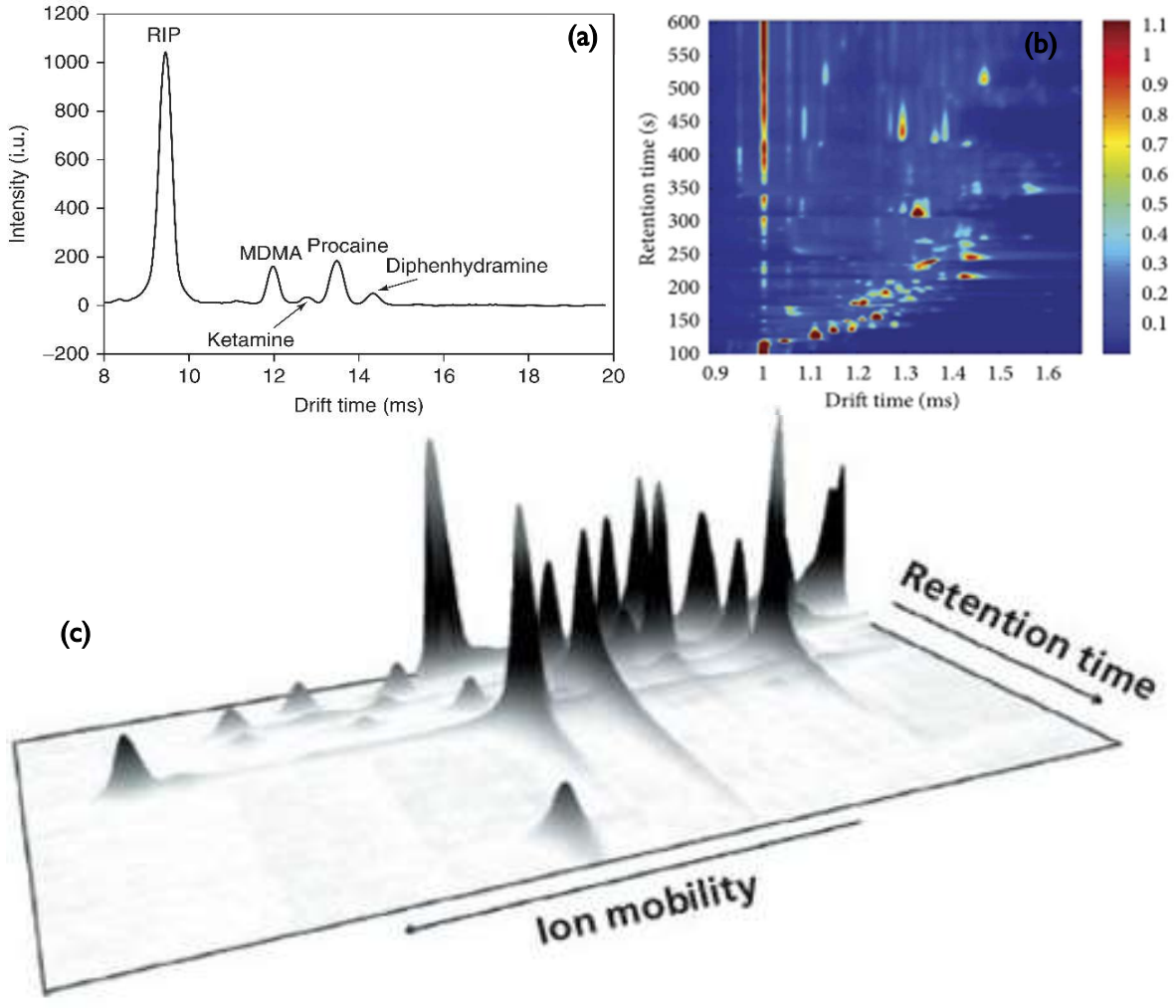

Figure 3.3 — Three examples of the possible representation of IMS spectra including their respective axis. (a) Single IMS spectrum or 2D Graph, [103] (b) Heatmap representation, [104] (c) 3D representation (Height denotes intensity) [105].

A basic summary of the operation principle of an IMS instrumentation is presented in (Figure 3.4), where it is showing a schematic for a drift tube coupled with a gas chromatography, a spectral representation and respective chemical reactions occurring for the formation of reactant ions, the formation of product ions from an analyte and the occurrence of dimer in the presence of high analyte load.

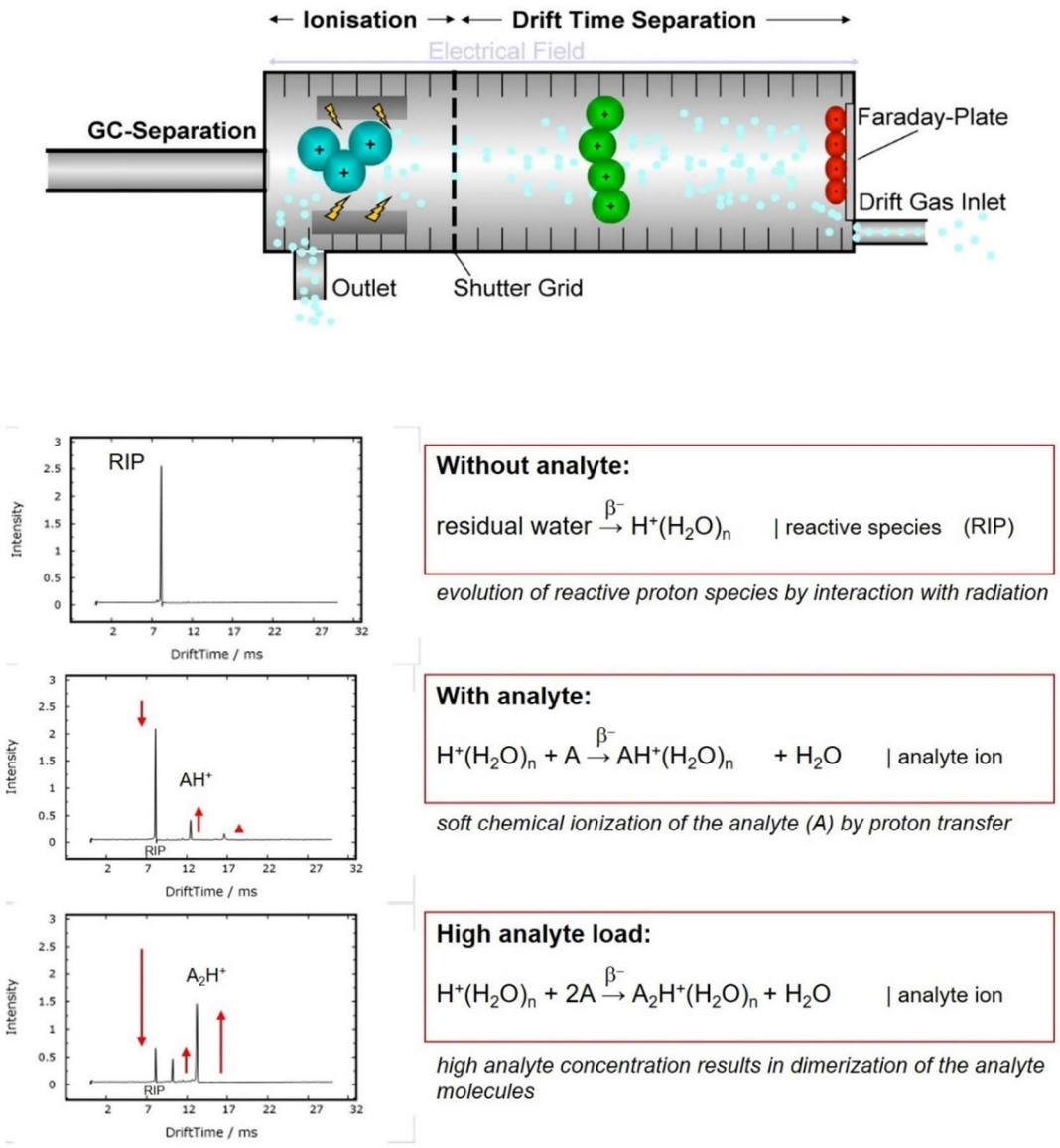

Figure 3.4 — A summary of IMS's working principle, showing a GC-IMS drift tube scheme on top and below the ionization reactions taking place in a drift tube without, analyte, with analyte and high analyte load [97, 106].

3.2 Ion Mobility Spectrometry: Current instrumentation

All existing IMS instrumentation is based on the previously described principle of ion separation by using an electrical field in a specific drift tube. A variety of IMS instruments or types, with different drift tubes and instrumentation formats exist, although, recently emphasis has been given to standalone instruments and specific coupling with other techniques such as GC or mass spectrometry.

A short and generalized description of 8 different IMS instrumentation types (Drift time ion mobility spectrometry (DTIMS), Travelling wave IMS (TWIMS), High field asymmetric waveform ion mobility spectrometry (FAIMS), Trapped IMS (TIMS), Aspiration Ion Mobility Spectrometry (AIMS) or Open loop IMS (OLIMS), Differential mobility analysers (DMA), Transversal modulation IMS (TMIMS), Overtone mobility spectrometry (OMS)) will be given while considering commercial availability [107].

3.2.1 Drift time ion mobility spectrometry (DTIMS)

A drift time ion mobility spectrometer is a traditional IMS instrumentation type, and its operation principle was described in detail in *Ion Mobility Spectrometry: Current instrumentation*. Any DTIMS equipment is configured to move ions through a drift tube under a homogeneous and continuous electric field created by a series of stacked-ring electrodes. Two types of gases are used in any DTIMS drift tube, a carrier gas, which transports any sample into an ionization region (e.g., purified air and nitrogen), and a drift gas (usually nitrogen, helium, or argon) flowing against the carrier from the detector side of a drift tube. This drift gas counter-current removes non-ionized molecules out of the drift region and creates a resistance through collisions to ion injected via an electronic gate [107, 108].

Flexibility in DTIMS instruments is generally seen in drift tube, length, electrical field strength and ionization sources. Two types of ionization sources exist, radioactive or photoionization, and comparatively both exhibit advantages and disadvantages. Radioactive sources, (^{63}Ni or ^{3}H) do not require a power supply and are suitable for portable instruments even though they might come with a few risks, bureaucratic complications due to governmental regulations and require samples in vapor phase [97, 108]. However, ^{3}H, tritium sources, specifically, are devoid of bureaucratic complications for radioactive sources, in Europe, because it produces a radiation energy below the exemption limits of the International Atomic Energy Agency (IAEA) resp. European Atomic Energy Community (EURATOM) [107, 108].

Photoionization, however, is unencumbered by any possible legislative burden and allow detection of compounds with proton affinities below that of water, an impossibility with radioactive sources [97, 108]. Those advantages are only possible due to the process of photoionization, which consists of irradiating a compound with ultraviolet light (UV). UV light ionizes any analyte molecule with ionization potential lower or equal to the photon energy, typically 8–12 eV [108]. Furthermore, UV ionization show a larger linear dynamic range in contrast with ^{63}Ni, implying a reduced influence of noise in the detected signal.

UV photoionization, however, is not as sensitive as atmospheric pressure chemical ionization by radioactive sources, and generally addition of dopants gases for a secondary ionisation process is frequent to enhance sensitivity [107, 108]. Other limitations of any photoionization source are their limited lifetimes and increasing power requirements related to the use of UV lamps [108].

A few other ionization techniques used in IMS instruments include matrix-assisted laser desorption/ionisation (MALDI), electrospray ionization (ESI) and corona discharge (Figure 3.5),

thermal/surface ionisation, whereas MALDI and ESI have allowed the extension of IMS into the analysis of biomolecules and polymers [97, 108].

Commercial devices using DTIMS are abundant and common including the following examples: IONSCAN 400B102 from Smiths Detection, a part of Smiths Group Plc.; RAID M100103 from Bruker Corp.; QS-H150 from Implant Sciences Corp.; IMS-ODOR105, BreathSpec® and FlavourSpec® from G.A.S. *Gesellschaft für analytische Sensorsysteme* mbH; IMS Engine from Photonis;106 HPIMS™ from Excellims Corp.;107 GDA108 series from AIRSENSE Analytics GmbH; EN3300 Illicit Substance Detector and E5000 (GC-IMS) from Scintrex Trace Corp.; Air Sentry® II110 from Particle Measuring Systems Inc.; VG-Test111 from 3QBD Ltd; and BioScout112 from B&S Analytik GmbH [108].

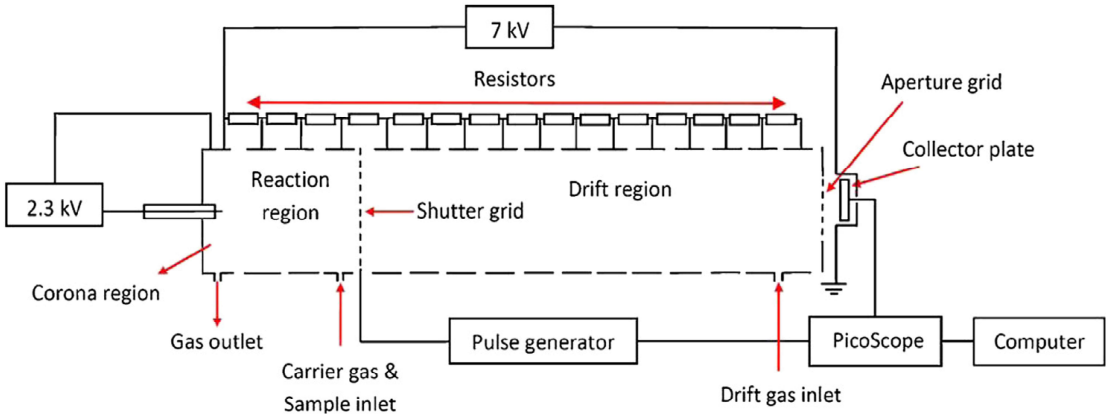

Figure 3.5 — Schematic diagram of an ion mobility spectrometer (IMS) with a corona discharge source [109].

3.2.2 Travelling wave Ion Mobility Spectrometry (TWIMS)

Ordinarily IMS electric fields are uniform, however, traveling wave ion mobility spectrometry (TWIMS) is a type of ion mobility spectrometry where a non-uniform electric field is applied in a drift tube [97, 107, 108]. This IMS drift tube type consists of a stacked-ring ion guide (SRIG) to which a travelling voltage wave is applied, hence ions will travel at a constant speed along the central axis of the stack under the influence of periodic potential oscillations (Figure 3.6). The electric field, generally a radio frequency, is only applied in a small drift tube region, which moves along the extension of the drift tube producing a wave responsible for pushing ions towards a detector [108]. Opposite phases of a radio frequency voltage are applied to adjacent rings to radially confine ions and create high transmission efficiency, which permits this IMS type to operate without the requirement of a high total drift voltage [97, 107, 108].

Since ions are propelled by a repeating pattern of voltage pulses superimposed to each electrode in succession after a fixed pulsed dwell time from one end of the device to the other forming a traveling wave, no counter current gas is used in TWIMS [108]. Ion mobility separation is achieved by altering the speed and magnitude of the traveling wave, because ions experience the field of an approaching wave and begin their drift through the gas in the directions of the wave [97, 108]. Much like DTIMS, ions are separated by their size, because smaller ions have less collision with gas molecules than larger

ions which get slowed and arrive later at the detector [107, 108]. Complex mixtures, for example, are separated by sending several traveling waves through the device in quick successions [108].

However, since TWIMS operation is conducted in the low-field limit, calibration of the ion's drift times is required under defined conditions (gas type/pressure, travelling wave speed or height, etc.) because the relationship between Ω and K_0 in equation(9) is no longer true due to the constantly changing electric field [97, 108]. Therefore, TWIMS optimal calibration require measurements of analytes of similar physical and chemical features with known Ω to guarantee conditions are suitable for both calibration and analysis [108].

Nevertheless, TWIMS ability to function with and without collision cross-sections calibration has found application as both a separation device and a structural tool. TWIMS is always hyphenated with mass spectrometry and an example of a commercially available TWIMS-MS instrumentation is the Synapt G2-S instrument from Waters Corp. which has been used in proteins, protein complexes, microRNA analysis and transition-metal complexes studies [108].

Furthermore, Overtone Mobility Spectrometry (OMS) is a recent IMS type which shows similarities with TWIMS, because both use a pulsed sequence of potentials repeating spatially along the drift tube. However, in OMS some ions are eliminated instead of separated by the wave in elimination regions [108]. OMS will not be described here in further detail due to its recent development and diminished information.

3.2.3 High field asymmetric waveform ion mobility spectrometry (FAIMS)

Rather than a time-based separation, high Field Asymmetric waveform Ion Mobility Spectrometry (FAIMS) is a spatial electrical mobility spectrometer [108]. FAIMAS implements a strong time-dependent electric field as a periodic asymmetric waveform which exploits differences between mobilities at high and low electric fields (>30 Td, >7500 V cm^{-1}) [97, 108]. As such, in FAIMS it is crucial to attain an intense electrical field of reasonable voltages, and therefore, small drift tubes gap sizes are used [108]. FAIMS can, thus be interpreted as a millimetre range miniaturization of the IMS drift tube gap and are frequently seen in miniaturized and portable formats [108]. Miniaturization and portability are active areas of development for all types of IMS instrumentation and several portable instrument types are currently available commercially, including, miniaturized DTIMS, Trapped IMS (TIMS), and FAIMS [97, 108].

FAIMS operate as mobility filters, when a periodic waveform is applied to separate ions under a parallel gas flow [110]. Alternation between high and low electric field strengths creates a process that filters for a particular analyte's change in mobility with field strength as opposed to absolute mobility. So, ions in FAIMS are filtered by a high asymmetric electric field, ideally with a rectangular shape called a dispersion field [97, 108]. Once a specific compensation voltage of intensity, E_C, is superimposed to a dispersion filed, a particular ion with a particular K(E) can be detect. Any other ions, with different K(E) will be lost to the filter electrodes and scanning E_C will produce the spectrum of species present

in a sample [97, 108]. However, FAIMS, due to asymmetric waveforms is unable to provide CCS values and ion structure itself may change during wave oscillations [110].

FAIMS instruments can have two main types of electrode configuration, planar (p-FAIMS) and cylindrical (c-FAIMS) [108]. The planar version is also known as Differential Mobility Spectrometry (DMS) and consists of two flat parallel electrodes (300 µm to 50 mm) gaped by an analytical region (35 µm to 2 mm for DMS and 1.5 to 3 mm for c-FAIMS) where ions are transported by a gas flow perpendicular to the electrical field [97, 108].

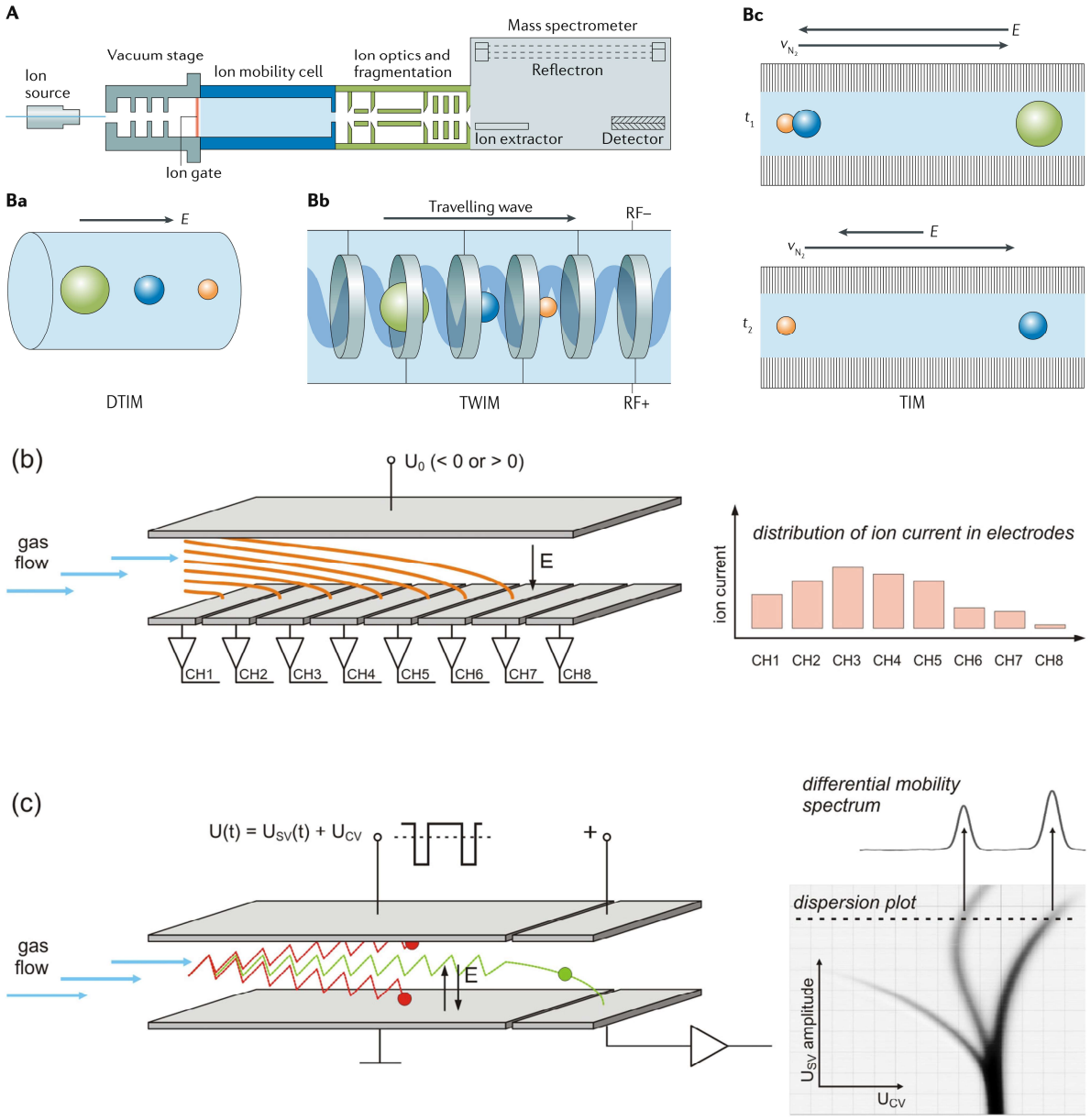

Figure 3.6 — Ion mobility spectrometry layouts of mobility tubes and operational principles of several instrumentation types. **(A)** Schematic of an Ion mobility–mass spectrometer device; **(Ba)** A simplified schematic for a Drift time ion mobility spectrometer (DTIMS); **(Bb)** Drift tube diagram for a Travelling wave IMS (TWIMS) instrument; **(Bc)** A representation of a Trapped IMS (TIMS) drift tube and operational steps [107]; **(b)** Schematic of an Aspiration IMS (AIMS) and its spectrum; **(c)** Operation, spectra, and drift tube structure of a Differential mobility Spectrometry (DMS) [111]. High field asymmetric waveform ion mobility spectrometer (FAIMS) drift tube is comparable in to DMS(Table 3.1). DMS referes to a planar (p-FAIMS) electrode configuration and FAIMS to a cylindrical (c-FAIMS electrode configuration [108].

FAIMS main advantage is, ions can be introduced into the sensor constantly, permitting real-time and continuous monitoring and sample sensing, while both positive and negative ions detection can occur simultaneously. Although simultaneous positive and negative detection is only achieved at the cost of increasing electronic complexity [108]. FAIMS, due to its characteristics and operation mode, is commonly used in tandem formats, including, FAIMS-MS, FAIMS-IMS, IMS-FAIMS and FAIMS-FAIMS [97, 108].

Stand-alone FAIMS device examples commercially available include MO-2M130 from Bahia 21; EGIS™ Defender Explosives Trace™ Detection System from Thermo Fisher Scientific Inc.; Juno® from Chemring Group Plc.; and Lonestar Portable Analyser from Owlstone Nanotech Incfrom. Whereas hyphenated instruments with MS, FAIMS-MS are available in from a few companies, for example the Thermo Scientific™ FAIMS interface from Thermo Fisher Scientific Inc., the SelexION™ Technology from AB Sciex and the UltraFAIMS from Owlstone Inc [97, 108].

3.2.4 Trapped Ion Mobility Spectrometry (TIMS)

A fourth type, called Trapped IMS (TIMS) operates in a different format than previous types, TIMS functions, by using a non-uniform electric field to hold ions stationary against a moving drift gas [97, 108]. TIMS principle relies on drift forces being compensated by an electric field to sperate ions according to their size-to-charge ratio [97, 108]. A TIMS drift tube is composed of three regions, an entrance funnel, a mobility analyser sections and an exit funnel (Figure 3.6) [108].

Different process occurs in each region, the first step (filling), is executed in the entrance funnel, to which ion are injected and focused onto a mobility analyser section. Afterwards, in the analyser sections, an increasing weak electric field along the axial section is created while a radio frequency is applied to the electrodes to confines ions radially (separation) [97, 107, 108]. Separation is performed only in this section since ions are trapped in regions where their drift force is compensated by the electric filed force due to the increase of the electric field along the device axis [107, 108]. Once ions are trapped in different axial positions accordingly to their size-to-charge ratio, the electric field is decreased allowing ions to elude from high to low size-to-charge ratios (elution) into a detector or even into a coupled MS analyser. Ion mobilities are therefore defined by drift gas velocity, ion confinement and the electric field ramp speed [97, 108].

TIMS commercialized devices include several instruments from Morpho Detection Inc. (a subsidiary of SAFRAN Group and the General Electric Company), Itemiser® DX, EntyScan®, MobileTrace® and Hardened MobileTrace® [108].

3.2.5 Aspiration Ion Mobility Spectrometry (AIMS)

Aspiration IMS (AIMS) is also known as open loop IMS (OLIMS) and is akin to FAIMS, since ions are also separated in space instead of drift time [97, 108]. AIMS original designs were composed of three cylindrical electrodes, one central and two external, but modern instruments have been

simplified into a planer form. In AIMS ions are carried in a stream of flowing gas into two parallel plates with several electrodes, normally 8, for ion collections (Figure 3.6) [97, 107, 108].

AIMS electric field is transversal to gas flow and separation is achieved through the influence of ion mobilities into ion trajectories [108]. Low mobility ions are transported further inside the tube, while high mobility ions collide with the first detector plates. Electric field polarity is inverted in short intervals creating a cycle of one second in which polarity is changed from positive and negative polarity once, therefore making possible the detection of both positive and negative ions [97, 108]. The resulting distribution of ion clusters colliding with electrodes is transformed into a pattern of currents, (pA) measured from eight positive and eight negative electrodes [108]. AIMS is, however, limited by space charge effects and diffusion since both factors cause poor spatial separation, which can normally be minimized by increasing flow rates [97, 108].

AIMS is frequently used in military applications, first responders, and industrial users worldwide and not commonly used in scientific research [97, 108]. AIMS instruments are handheld, rapid, sensitive and have low energy requirements, since they are frequently used as field detector and to identify chemical warfare agents, pesticides, organic species released by the human body and toxic industrial chemicals [97, 108]. Two commercialized examples of AIMS/OIMS instruments include the ChemPro100i from Environics Oy and the ChemRAE from RAE Systems [108].

3.2.6 Differential mobility Analysers (DMA)

The last IMS type, referred to as Differential Mobility Analysers (DMA) are similar to DTIMS, because both systems utilize constant electric fields and are able to measure K as a primary method, and similar to OLIMS since ion with different electrical mobilities are separated in space [97, 108, 110]. OLIMS and DMA are also similar in their configurations, however two crucial differences exist between both types [108].

In DMA all ions must travel the same distance to a detector and in OLIMS different ions travel different distances [108]. Secondly, in DMA ions migrate between two electrodes held at different potentials while transported by a stream of gas (initially clean) flowing parallel to the electrodes in contrast with 8 positive and negative electrodes in OLIMS [108]. The classification of ions in DMA is done using high carrier flow rates which leads to the use of space instead of time of drift and might have the advantage of achieving higher resolving powers and sensitivities [108]. Cylindrical and planner DMS instruments exist, while the former is mainly used in the analysis of sub-micrometre aerosols and the latter, is regularly coupled with several atmospheric pressure ionization-mass spectrometry (API-MS) systems [97, 108, 110].

Operation of DMA devices is done in ambient pressure, and have well-characterized unidirectional gas flows, which scanned for the detection of molecules of choice [110]. DMA can perform measurements impossible with DTIMS and is typically applied in the detection of very large analytes, such as aerosol particles, antibodies, viruses, and other macromolecules (ca. tens to hundreds of nm^2). [110] However, DMA is not applied to screen and detected small molecule such as lipids and small

metabolites [110]. Transversal modulation IMS (TMIMS) is often referred as stand-alone IMS type, but since it separates ions according to their mobility using only electrical fields, it is frequently treated as a subtype of DMA and can be understood through DMA [108].

IONER High Resolution IMS152 from Ramem S.A.; DMA153 from SEADM S.L.; and SMPS Model 3938 (ref. 154) from TSI are some examples of commercially available devices of stand-alone DMS, while an instrument, DMA from SEADM S.L. can be hyphenated with several MS types. DMS has also been hyphenated with DTIMS and condensation particle counter (CPC) [97, 108].

A summarized table of IMS types is presented in Table 3.1, showing characteristics for each type clarifying the similarities and differences between each IMS type. Both OMS TMIMS are not shown in this table due to their relative recent existence [108]. While a visual summary of variations between IMS platforms, including drift tube format and electronic field behaviour, is shown in Figure 3.7.

Table 3.1 — Summarized characteristics of IMS types highlighting their similarities and differences [108].

	Drift Time IMS	Traveling-wave IMS	High-field asymmetric waveform ion mobility spectrometers	Trapped IMS	Open loop IMS (IMS)	Differential mobility analysers
Acronym	DTIMS	TWIMS	FAIMS	TIMS	OLIMS	DMA
Drift/transport gas	Yes	Yes	Yes	Yes	No	Yes, high fluid velocity field is required.
Dopants	Common (*e.g.* acetone, ammonia, 2-butanol, dichloromethane)	No	Uncommon (*e.g.* water, dichloromethane)	Common	Uncommon (not in commercial use)	Uncommon
Pressure	Ambient (~1 bar)	0.025–3 mbar	Ambient (~1 bar)	2.6–3.4 mbar	Ambient (~1 bar)	80 mbar–1 bar
Temperature	Ambient (~300 K)	~360 K	Ambient (~300 K)	Ambient (~300 K)	Ambient (~300 K)	Ambient (~300 K)
Electric field *E*	Uniform low *E*	Moving and non-uniform low *E*	Alternating asymmetric high/low *E*	RF low *E*	Uniform low *E*	Uniform high *E*
Humidity affected	Yes	Yes	Yes	Yes	Yes	Yes
Hyphenated techniques	MCC-IMS, IMS-MS, GC-IMS-MS, LC-IMS-MS	TWIMS-MS	GC-FAIMS, FAIMS-MS, ESI-FAIMS, Py-FAIMS	TIMS-MS	OLIMS-MS	DMA-MS
References	168–171	114,117 and 164	43,172 and 173	137 and 138	140 and 142	149,174 and 175

[a] Not shown for Overtone Mobility Spectrometry (OMS) and Transversal Modulation IMS (TMIMS) as they are relatively new techniques.

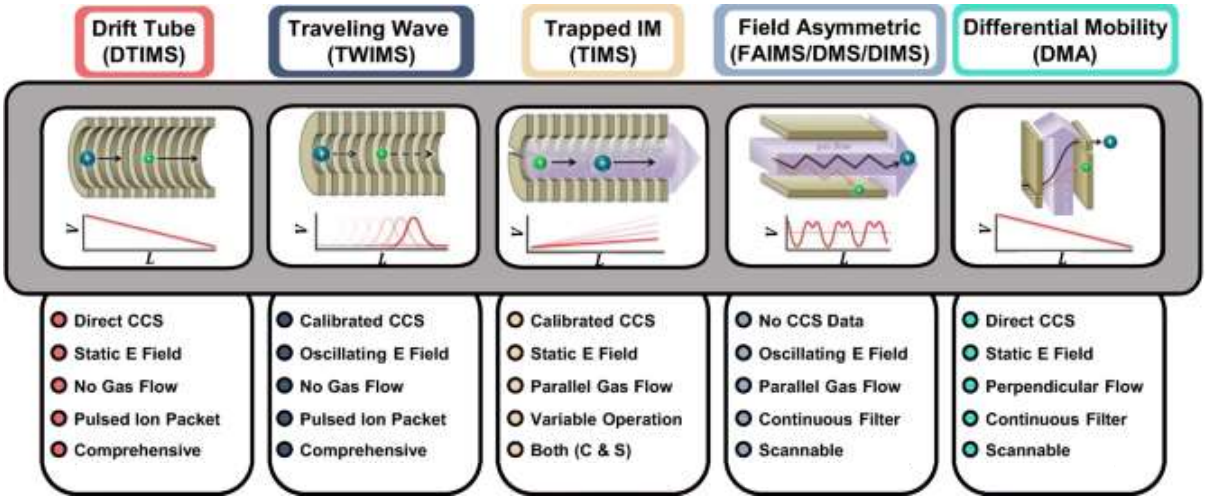

Figure 3.7 — IMS technology variations with applied electronic field and gas dynamics. Relative parameters of each IMS platform and key attributes are represented in bullet points, including their ability to measure CCS information, types of electronic field, type of gas flow, ion packet distribution, instrument footprint, and modularity (Adapted). [110].

3.3 Ion Mobility Spectrometry: Hyphenated Methods

Stand-alone IMS device have become rare, and most recent research and applications relying on IMS combined with other methods with sample components separated in two or more elements of the measurement system. IMS detectors on their own does not have a very high selectivity and when complex samples, e.g., biological samples, are processed, an extra separation is often required. Hence several types of hyphenated instruments and methods are often coupled with IMS to deal with such complexity [97, 112]. Analysis of complex mixtures with ion mobility alone, is frequently not enough for the identification of each analyte present, since analytes often have similar or even equal mobility [97, 112]. Moreover, spectra resulting for solo IMS analysis of complex samples generates complex spectra with several peaks overlapping and hindering compounds identification. This limitation can, however, be bypassed by hyphenating other analytical techniques with IMS [112].

Two hyphenated strategies are frequently used: (i) ion identity confirmation while using IMS as a pre-filter for MS systems and (ii) sample pre-separation prior to IMS analysis, which functions as a detector. In gas-phase, gas chromatography (GC) and multi-capillary columns (MCC) have been commonly used as pre-separation techniques, while in liquid-phase, liquid chromatography (LC) is often used prior to IMS coupled with mass spectrometry [97, 112].

Pre-separation methods linked each analyte into two parameters, a specific drift time or ion mobility and an elution time, or retention time, related to the pre-separation column type and characteristics [97]. Both retention and drift time are characteristic to a particular analyte at specific temperatures, pressures, column length, polarity, and flow rates, thus by using a fixed set of those parameters compound identification is achieved in an unknown sample [97, 112].

Gas chromatography ion mobility (GC-IMS) requires appropriate column selection and detectors for desired samples type analysis. However, GC and IMS are hugely favoured for coupling, since both require similar dynamic characteristics and functions in the same gas flow ranges [97, 112]. Whereas IMS incorporation between LC and MS creates multiple advantages for complex sample analysis. IMS-MS analysis have high-speed measurements across a given LC peak allowing for multiple analysis, highly reproducible drift times and produced an increase in peak capacity because it creates an orthogonality degree to both LC and MS [112].

Hyphenated methods allowed IMS to evolute into an inexpensive and powerful technique with high sensitivity and selectivity for the detection of gas samples at lower ng L^{-1} (ppbv) levels in ambient pressure and temperature [97, 112]. So, IMS matured into a wide range of applications, from chemical warfare agents to biological and clinical analysis, even into applications in medicine, including diagnosis, therapy, and medication control through breath analysis of metabolites [97, 112].

3.3.1 Coupled Ion Mobility Spectrometry with Mass Spectrometry (IMS-MS)

Although IMS-MS hyphenated methods will not be a focus subject herein, a brief description of this coupling approach will be given. Earliest configurations of ion mobility spectrometry were coupled

IMS/MS instruments, combined to provide definitive ion identification in mobility spectra. Recently other aspects combining IMS, and MS have been recognized, especially since the mobility of an ion is complimentary to ion mass which reveals data on the shape and conformation of substances. Such feat was achieved by the implementation of electrospray ionization in ion mobility spectrometers which allows the characterization of biomolecules [97, 100, 112].

Mass spectrometry is highly established in the field of chemical analysis and analytical science, where it measures the mass-to-charge ratio (m/z) of molecular ions, a characteristic defined by the mass number, m, divided by the charge number, z, for a respective ion [112, 100]. A direct correlation can be established between m/z units and the molecular weight of a compound, enabling identification through spectra's de-convolution of peaks and cross-referencing data with databases like NIST or Wiley Mass Spectral Libraries [112]. Thus, an IMS-MS instrument functions by separating ions based on their size-to-charge ratio by IMS while ions are detected according to their mass-to-charge (m/z) ratios through mass spectrometry (MS). During this process a two-dimension separation is created based on size and mass which becomes advantageous due to IMS ability to separate isomers of the same compounds for later MS identification [97, 112].

Most IMS-MS instruments are used for aqueous and solid samples such as proteins, lipids, alcohols and recently even for peptides oligosaccharides and virus [112]. However, those instruments are rarely used in applications related with volatile organic compounds since the connections between IMS drift tubes and a mass spectrometer require careful consideration of vacuum system performance and ion optics for the interface section [97, 112]. Thus, large drift tube operated at low pressures (below 10 Torr) in non-clustering gas atmospheres are usually used in IMS-MS instruments, combined with a variety of mass spectrometers (e.g., quadrupoles, time-of-flight, Fourier transform ion cyclotron resonance and ion traps) for the study of biomolecules [97, 100, 112]. In respect to ion mobility types in IMS-MS system, DTIMS, travelling-wave IMS (TWIMS) and FAIMS remain the main types used [112].

Moreover, low-pressure drift tubes are also less often combined with two mass spectrometers in an MS/IMS/MS configuration, where selected ion, by their mass, from the first mass spectrometer are directed into the drift tube to be separated and transferred into the second mass spectrometer for mass analysis and identification [97, 100, 112].

The frequency of IMS coupling with MS dominates this field, however, tandem IMS system have recently been explored in peptides and proteomic studies. MS tandem combinations include DTIMS, FAIMS and DMS creating systems such as, IMS-IMS, DMS-IMS, IMS-DMS, DMS-DMS and multidimensional IMS (IMS-IMS-MS and 3D IMS-IMS-IMS-MS) [100, 112].

Parallel studies involving GC-IMS, and GC-MS experiments and data have also been conducted for analyte identification. GC-IMS chromatograms accompanied by GC/MS measurements were used to create software approaches for aligning GC/IMS and GC/MS spectra and identify compounds indirectly through GC and MS data [112].

3.3.2 Pre-separation Methods Coupled with Ion Mobility Spectrometry (GC-IMS)

The other hyphenation strategy consists in adding a pre-separation unit, such as liquid or gas chromatography prior to the ion mobility system [112]. Often, a multi-capillary column (MCC), takes the place of regular gas chromatography columns, however, MCCs can still be understood as multiple gas chromatographs set together with short length (~cm) [112, 113]. An example of this type of column includes a weak polar 17 cm long multi-capillary column, MCC-OV5 from Multichrom, former Sibertech. Ltd., Novosibirsk, Russia. This column is composed of 1000 capillary bundles from glass with 40 µm inner diameter each coated with 0.2 µm of stationary phase film [112]. When comparing MCC columns with regular GC columns, the former shows advantages in processing higher sample flows obtaining higher intensities while effectively separating analytes from water vapor however, MCC columns might be limited in availability and higher in cost [112, 113]. In humid samples, MCC pre-separation reduces negative effects of ion clustering during ionization leading to improved detection and sensitivity, which makes MCC suitable for biological and medical samples. MCC columns, due to their small size and speed of separation, are often employed in portable GC-IMS instruments [97, 112, 113, 114].

Anyway, MCC and GC columns when coupled with IMS both improve sensitivity (up to ppt_v levels) and selectivity significantly, ideal for complex mixtures with and without high humidity [97, 112, 113]. The separation and detection process of a GC-IMS instrument is described in five phases, (i) sample introduction, (ii) compound separation, (iii) ion generation, (iv) ion separation and (v) ion detection [97, 112]. This interface creates the benefit of tuning detection to selectively monitor drift times or ion mobilities, much like a mass spectrometer can is used to monitor ion masses, tailoring the instrument to fit the separation demands of a given challenge or problem [112, 113].

Often GC is coupled with conventional drift time IMS or FAIMS where the effect of the columns is to separate different molecules by different times [97, 112]. This separation is a product of different affinities of compounds with the GC stationary phase, leading to shorter or longer times for them to completely pass through the column, often referred as elution [97, 112, 113, 114]. Hence, multidimensional separation is attained relying on both chromatographic retention times and drift times. Since separation by GC occurs in a minutes to seconds time scale and ion mobility spectrometry separation happens in a millisecond time scale, multiple IMS spectra are acquired for each gas chromatographic peak. Once both retention and drift time data are assimilated, 3D chromatograms often coded in a colour scale, are produced with information on the volatile organic compounds present in the analysed sample [112, 113].

3.4 Ion Mobility Spectrometry: Versatility and Applications

Ion mobility spectrometry has been extensively exploited by academic laboratories in the past, which could create and develop their own systems, however, once MS vendors implemented IMS into their instrumentation, new analytical possibilities were seen, especially in the analysis of complex

samples or even high-throughput analysis (automated equipment to rapidly test large numbers of samples for biological activity at the model organism, cellular, pathway, or molecular level).

Several IMS systems have been developed over the decades based on two major approaches: drift time IMS (DTIMS) and differential IMS (DMS), also referred to as "field asymmetric waveform ion mobility spectrometry" (FAIMS). DTIMS and DMS are both based on a unique feature of charged molecules, their specific motion in an electric field while being transported by a neutral gas. Although DMS and FAIMS are generally coupled with low resolution MS, acting as a filter to improve quantification during for the monitorization of selected reactions, DTIMS is coupled with high resolution MS to generate and apply Collision Cross Section libraries in analyte identification [96, 108, 111, 115].

Essentially IMS instruments separate positively and/or negatively charged analytes by size-to-charge ratio, associated with collisional cross section (CCS). Because IMS can operate at atmospheric or reduced pressure, is ideal for small portable and inexpensive devices which opens a wide range of applications [96, 108, 111, 115]. The earliest application of IMS included ambient analysis in airport and transportation security to detect explosives and illicit drugs. Recently, IMS applications have progressed into air quality analysis, food control, medical diagnostics, process control, environmental analysis, and forensic analysis and its importance grew in research and field applications [96, 111, 115].

Even though IMS was established more than 50 years ago, its applications and uses were not fully explored for a long time, because military and government restriction limited commercial availability of instruments and research. Recently those limitations have been partially or totally removed, and scientist initiated an expanding exploration of IMS applications and versatility.

IMS versatility is in essence due to very low detection limits and high sensitivity offered by hyphenation with several other analytical methods, and instrumentation advances allowing miniaturization and portability [96, 108, 111, 115]. In perspective, IMS can be considered a new and emerging technology, especially when its interface with mass spectrometry and/or chromatography are considered, and its innate characteristics and simplicity still assure a strategic and continuous place in analytical fields [96, 115]. The exploration and expansion of IMS applications by the scientific community is re-emerging, reinforced, intensified, and increasing in several scientific areas discussed in the following subcategories [96, 108, 111, 115].

3.4.1 Military and Security: explosives, warfare agents and drugs

The detection of narcotics, warfare agents and explosives, is perhaps the most favoured IMS application overall. Development was initially driven by governments and military agencies and resulted in the deployment and use of IMS devices in large numbers. Several IMS devices are routinely used to screen vehicles, items, or individuals for explosives prior to them boarding a ship, aircraft, or enter a military installation. Those devices are so versatile that vehicles, clothing, briefcases, purses, or any other object that can be driven or carried can be screened and checked with high degrees of confidence. IMS detectors can also be used to screen suspicious letters, packages, parcels and pallets of all

shapes and sizes to detect and identify explosives in seconds, preventing for example mail bombs, a specific method used by terrorists [96, 108, 111, 115].

Generally, most detectors are based on trapped ion mobility spectrometry (TIMS) but also include stand-alone IMS or even GC-IMS devices. Examples of IMS detectors for trace detection of explosives available on the market today include the Vapor Tracer and EntryScan from GE Ion Track, and the GC-IONSCAN and IONSCAN 400B from Smiths Detection [115]. Furthermore, The GE Ion Track Itemiser, a desktop detection system for the detection of trace quantities of narcotics and explosives is regularly used by the United Kingdom's HM Customs and Excise and the Jamaican government in controlling cocaine couriers from smuggling drugs onto flights [115].

Moreover, IMS instrumentation has been refined to produce simple and reliable field analysers for military use, which have been extensively deployed, probably being the most significant case of effectively converting a laboratory instrument into a practical system worthy for the field analysis [96, 115]. The first hand-held chemical agent monitor system developed by Smiths Detection was deployed by the US Army and became the first example of large-scale adoption of IMS in the detection of chemical agents in the field [115]. The choice of this system was driven by the fact that nerve agents (e.g., sarin) are primarily derivatives of organophosphorus compounds with strong proton affinities and can therefore, be detected with excellent sensitivity and specificity in the positive ion mode, greatly diminishing false alarms from other proton accepting compounds present in the atmosphere [115]. Detection limits of nerve agents for those instruments are typically in the low ppb or ppt range [96].

Blister agents (e.g., mustard gas) however, have low proton affinity but contain halogen atoms which can form negative product ions due to their high electron affinity, are detected in the negative ion mode. Thus, an IMS instrumentation can detect both nerve and blister agents by changing ion modes, which has resulted in the use of lightweight chemical agent detectors based on mobility spectrometers by nearly all armed forces in the US, EU, and other nations worldwide [96].

In respect to the detection of explosives, which are mainly nitro organic compounds, such as trinitrotoluene (TNT), nitro-glycerine (NG), or cyclotrimethylenenitramine (RDX), IMS accomplishes their detection because those compounds form, among other ions, [MH]- product ions or negative fragment ions which can be determined in the negative mode [96, 115]. Although the detection limits are low, withing ng or pg range, detection is limited due to low vapor pressures of some compounds and require the use of appropriate sampling strategies [96]. This limitation is commonly overcome by particle collectors combined with thermal desorption (e.g., Solid phase microextraction (SPME)) to allow rapid screening of humans, luggage and/or cargo [96, 111, 115].

Drugs are detected in a similar experimental arrangement as explosive compounds with comparable detection limits [96, 111]. However, illicit drugs are detected with excellent levels of sensitivity in the positive mode, because the presence of nitrogen functional groups produce $[MH]^+$ product ion with high proton affinities [96, 115].

Obviously, information regarding explosives, warfare agents and drug detection is limited and controlled by both military and governmental agencies, however the usefulness and advantages of

employing IMS instruments in this application field are clear and strengthened by its world-wide and frequent use.

3.4.2 Industrial and Environmental: air quality monitorization

On-site determination of a broad range of chemical compounds in environmental and industrial analysis with IMS has been motivated and facilitated by instruments with high density of information, excellent detection limits and portability. In this application, IMS allows on-site monitoring of both industrial and environmental samples while quickly accessing concentrations and spatial distribution of substances without requiring sampling and transportation of samples to a laboratory. Therefore, IMS is especially suited for monitoring air and environment quality in real-time applications because of its millisecond speed response, excellent selectivity, and low cost [115].

Even though other sensors, including photoionization detectors, surface acoustic wave sensors, and electronic noses are less expensive comparatively to IMS analysers, such techniques normally provide sum signals that require data processing to evaluate measurements, while IMS provides a high level of quantitative and qualitative details without further steps. However, for solitary mobility spectrometers, caution with calibration is necessary and essential [96, 111, 115]. Nevertheless, the analytical capability of ion mobility spectrometers, including sensitivity and selectivity for on-site, on-line, or *in situ* measurements are repeatedly preferred when compared with conventional analytical procedures for industrial and environmental monitorization [96, 111, 115, 116].

The detection of aliphatic and aromatic hydrocarbons, halocarbons, and oxygenated hydrocarbons in environmental and industrial is a prime example of IMS analysers utility and application in monitoring health hazards for both industrial hygiene and environmental protections [96, 116]. Specifically, IMS has been used in the determination of methyl-*tert*-butyl ether (MTBE) in water samples. MTBE is a flammable liquid and a widespread additive for unleaded gasoline since the 1980's to improve its octane number, which potentially yields higher engine power [96]. This widespread use has resulted in the contamination of groundwater at industrial sites and neighbouring regions [96, 116].

An on-line procedure was developed to selectively determine MTBE without chromatographic separation by using a membrane inlet capable of extracting MTBE from water samples [96]. Because no sample preparation is required in this procedure, analytical results are available within 5 minutes with detection limits of 100 mg/L. Later this procedure was improved to allow the determination of MTBE between 10 mg/L and 100 mg/L. This second screening procedure was further used in quantitative determination of monoaromatic compounds (benzene, toluene, xylene) with detection limits around 600 mg/L.

Moreover, a GC-IMS method was later developed using a membrane inlet for the analysis and monitorization of complex samples with enhanced concentrations of benzene, toluene, and xylene, and coupling with multi-capillary columns facilitated the successful use of GC-IMS in the quantitative determination of BTEX compounds (benzene, toluene, xylene, and ethylbenzene) in air and water [96, 116]. Fast determination, within 1 minute, of volatile halogenated compounds (e.g., dichloroethylene,

trichloroethylene and tetrachloroethylene) is also possible with a GC-IMS system. Particularly, Solid-phase micro-extraction (SPME) is use instead of a membrane inlet, to determine such VOCs in liquid samples [96]. In the case of halogenate benzenes in environmental samples stand-alone ion mobility spectrometers with corona-discharge ionization have been utilized [96, 116]. Corona discharge ionization and photoionization are frequently used in characterization of petrochemical fuels, polychlorinated biphenyls, phthalates, different pesticides, and the wood preservative pentachlorophenol with detection limits between ng or mg levels [96].

Spectrometers with laser desorption/ionization have been shown to be useful in the rapid determination of polycyclic aromatic hydrocarbons and potentially establish a valuable method for the detection of low volatility substances in industrial processes and for continuously monitoring water, air, and process streams [96]. The determination of acidic and corrosive gases, particular hydrogen fluoride (HF) using negative polarity and methyl salicylate as a reagent gas is an example of the use of IMS in industrial analysis, reaching a detection limit of 0.5 ppm [96]. Methyl salicylate allows distinction of HF product ions from negative reactant ions because the reactant ion peak drift time is displaced by the formation of adduct ions between the methyl salicylate and reactant ions (O_2^-). Hydrogen chloride (HCl), ammonia (NH_3), and bromine are examples of other reactive gases determined and monitored via IMS instruments [96].

Detection and determination of sulphur hexafluoride (SF_6) represents a prime example of IMS potential for monitorization, control, management, and risk assessment in an industrial setting [96, 116]. Sulphur hexafluoride is used in electrical switches at large hydroelectric station, where the performance of the electrical switch is dependent upon the electrical discharge properties of this compound inside insulating gas switches [116]. Decomposition of sulphur hexafluoride due to arcing and discharges changing its properties is unfortunately a huge economic concern, because it causes accumulation of impurities and leads to unpredictable and catastrophic switch failure [96, 116]. Gas quality and decomposition is detected continuously by miniaturized IMS drift tubes placed inside each switch. As decomposition increases the drift time value of the SF_6 product ion peak changes due to increasing concentration of decomposition products and through this change in drift time, switch failure can be anticipated and prevented by scheduling routine maintenance [96, 116].

Additionally, because IMS can identify plasticizers, solvents, and polymers on silicon surfaces it is also, used for air quality control and management of cleanrooms, air control in operating rooms (anaesthetics) and recirculated or controlled atmospheres, monitor remediation processes and to verify cleaning process in the pharmaceutical industry [96]. IMS has even recently been used to determine pesticides in indoor and outdoor air showing its versatility and sizeable application range [117].

Although IMS is utilized in air quality control and monitorisation of specific compounds or processes in both industrial and environmental settings, a generalized approach to air quality has not been fully explored or described in literature. While specifically, in air quality control abord spacecrafts and space exploration IMS is used in an instrument called Compound Specific Analyzer - Hydrazines (CSA-H) responsible to monitor the accumulation of two propellants and the ongoing development and validation an Air Quality Monitor (AQM) based on differential mobility spectrometry [68, 81].

3.4.3 Medicine: breath, skin, urine, faeces and COVID

A recent application of IMS is in medicine, particularly in the quick diagnosis of different diseases. IMS is especially sensitive to heteroatoms and organic compounds ions which makes it useful in the detection of volatile organic compounds from the human metabolome, human microbiota, and, or foreigner microorganisms [96, 116, 118, 119]. The requirements of clinical practice including fast, safe, low cost, real-time, and non-invasive methods to diagnose different diseases are all met by IMS instruments, especially MCC-IMS and GC-IMS detectors which are robust, secure, highly sensitive and compact size instruments. Therefore, an enormous interest has been placed in developing IMS devices to operate as a diagnostic tool of third millennium medicine [116, 118].

Complex mixtures of proteome, metabolome, complete organisms (e.g., bacteria and viruses) have gained a focus in IMS analysis. Plus, monitoring anaesthetic agents, drugs, pharmaceuticals, as well as volatile compounds in human body fluids (e.g., sweat, urine, faeces), skin and exhaled breath have been recently analysed and studied by IMS in order to provide information on human health [116, 118, 119]. Hence, applications of ion mobility spectrometry in medicine include the study of complex mixtures of organic compounds for the reliable non-invasive diagnosis of diseases including asthma, pneumonia, inflammatory lung, bronchial carcinoma, chronic obstructive pulmonary disease (COPD), renal failure, colorectal cancer, non-alcoholic fatty liver disease, or metabolic disorders, COVID-19, as well as medication and therapy control [116, 118, 119, 120]. While pharmaceutical applications of IMS include analysis of over-the-counter-drugs, quality assessment, and cleaning verification [116].

Lung diseases and associated infections can be recognized by exploring exhaled air, as is example a study of COPD with MCC-IMS. Nevertheless, the potential of breath analysis is largely dependent two factors, (i) precise breath sampling with controlled parameters including restrictions to eating, smoking, or drinking beverages prior sample collection and (ii) successful application of computational approaches to find specific disease VOCs, or biomarkers which allow classification of patients into disease-specific profile groups [116, 118]. Therefore, to find specific disease VOCs (also referred to as biomarkers) in breath or other bodily fluids an understanding of all volatile organic compounds emanating from the human body must be explored and understood. In 2014 a review paper was publishing where 1840 VOCs were assigned to breath (872), saliva (359), blood (154), milk (256), skin secretions (532) urine (279), and faeces (381) from apparently healthy individuals (Figure 3.8) [121].

Evidently research of VOCs emanation from the human body and its fluids is essential and important for medicine and for IMS. Although further work is required in this field, IMS is already being explored and developed as a diagnosis tool and to monitor human health through VOCs emanation from the human body. A specific example for COPD diagnosis, evaluating exhaled breath from 84 volunteers, healthy or suffering from COPD or bronchial carcinoma with an MCC-IMS instrument allowed to differentiate COPD patients based on 28-scoring VOCs [118]. While another study using GC-IMS, established a group of three VOCs with significant differences between healthy and control patients with COPD thus, indicating potential for early detection and diagnosis [116].

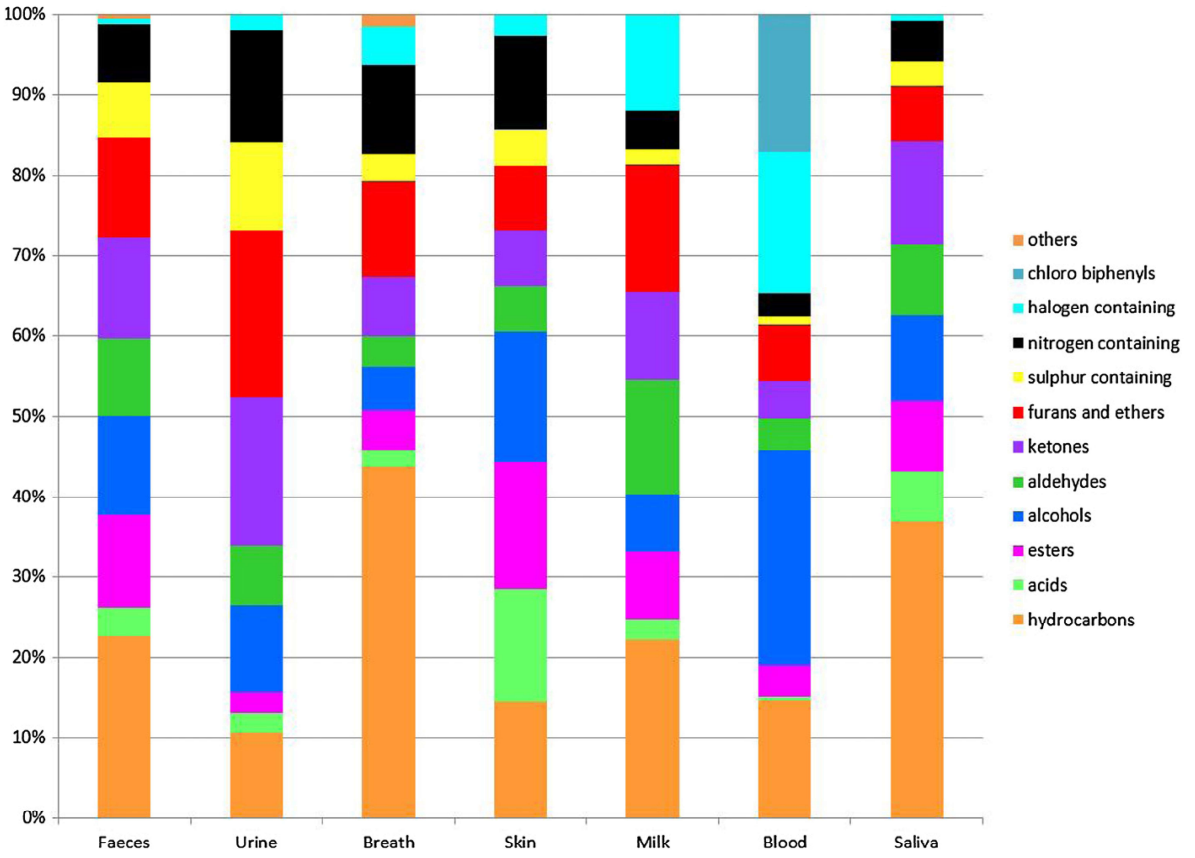

Figure 3.8 — Relative numbers of compounds in each class detected in faeces, urine, breath, skin secretions, milk, blood and saliva. (Based on the number of different compounds identified, not upon their relative concentrations.) [121].

Renal failure might also be detectable using IMS via exhaled breath analysis, since a study, with 28 patients with or without renal failure showed 13 compounds that accumulated with decreasing renal function [116, 118]. Therefore, renal failure induces a characteristic fingerprint in exhaled breath which can probably be used for diagnosis. Lung cancer has also been studied through exhaled breath analysis with IMS, and results have shown a typical spectrum of patients with lung cancer exists and is different from healthy controls [116, 118]. Other diseases such as Sarcoidosis, an inflammatory disease initiated with lung inflammation that further spreads to other organs, have also been studied with MCC-IMS. An example study included samples from 9 patients with sarcoidosis and suspicion of sarcoidosis due to mediastinal lymph node enlargement analysing VOCs in exhaled breath via MCC-IMS [118]. Patients with sarcoidosis showed a highly consistent and different distribution of metabolites in exhaled air when compared with subjects suffering from specific mediastinal lymph node enlargement. Additionally, breath analysis by IMS has also been explored as a real-time monitoring tool for aesthetic gases and depth of anaesthesia during surgeries [116].

Recently a feasibility study for the diagnosis of COVID-19 by the analysis of breath with GC-IMS has been conducted in Edinburgh, UK, and Dortmund, Germany [120]. A single breath sample was collected from 98 adult patients with possible COVID-19 at hospital presentation and corrected for environmental contaminants. Multi-variate analysis and further comparison with GC-IMS databases

identified potential breath-biomarkers of COVID-19 belonging to three classes, aldehydes (ethanal, octanal), ketones (acetone, butanone), and methanol [120]. Those compounds allowed discrimination of COVID-19 infections from other conditions such as asthma, COPD, bacterial pneumonia, and cardiac conditions, with 80% and 81.5% accuracy in Edinburgh and Dortmund, respectively [120]. Since the identity of the group of marker compounds is related to COVID-19 derangement of breath-biochemistry by ketosis, gastrointestinal effects, and inflammatory processes, it is possible this approach can result in rapid diagnosis of COVID-19 once further development and validation can be conducted, creating a much-needed method for a fast diagnosis [120].

Although exhaled breath has been a focus for non-invasive and fast medical diagnosis, urine, skin, and faeces are also being explored as a gateway to understand metabolic process and disease states which can aid in the identification of bacterial infections, gut problems, gut microbiota changes and metabolic disorders like diabetes mellitus, cirrhosis, and liver cancer [116, 118].

Skin and urine volatile organic emissions have even been explored as a tool to detect humans trapped in collapsed buildings for rescue or for the detection of human smuggling associated with cross-border crimes [119, 122, 123]. Two studies serve as examples, the first involving skin and urine emissions evaluating IMS as a suitable tool for the detection of humans during rescue operations after earthquakes or other disasters and, a second involving skin and breath emissions for the detection of smuggling migrants inside shipping containers or trucks [122, 123]. The former study explored an MCC-IMS in the analysis of the headspace of human urine and the permeation of VOCs from urine vapour in mimicked rubble quartz sand [122]. Fourteen compounds were identified in urine headspace although only seven were omnipresent while eleven compounds were detected to permeate through the quartz layer with acetone, 3-methyl-2-butanone, 2-heptanone and octanal showing particular interest because they exhibited the shortest permeation times [122].

For the latter study, an in-house GC-IMS device was investigated as tool for locating hidden migrants through volatiles organic compounds emitted from breath and skin [123]. Volatile emissions were collected under conditions that mimic entrapment and 17 omnipresent volatile compounds were identified and quantified as markers of human presence. The seventeen compounds included 7 aldehydes (acrolein, 2-methylpropanal, 3-methylbutanal, 2-ethacrolein, n-hexanal, n-heptanal, benzaldehyde), 3 ketones (acetone, 2-pentanone, 4-methyl-2-pentanone), 5 esters (ethyl formate, ethyl propionate, vinyl butyrate, butyl acetate, ethyl isovalerate), one alcohol (2-methyl-1-propanol) and one organic acid (acetic acid) showing limits of detections ranging from 0.05 to 7.2 ppb and relative standard deviation from 0.6 to 11%, enough to detect those markers in field conditions [123].

Likewise gut microbiota changes have been studied via IMS analysis of urine and faeces volatile organic compounds for intestinal health research and metabolic profiles related to inflammatory bowel disease (IBD), bile acid diarrhoea, renal, liver, and neurodegenerative diseases [116, 118] Because IBD pathogenesis involves bacterial polysaccharide fermentation IMS, specifically FAIMS, was used in a study to establish a fermentation profile to distinguish between complete and partial bowel cleansing. Distinction between conditions relied on monitoring changes in patients fermentone (β-damascenone) and track bacterial recolonization [118]. FAIMS was also used in the development of a diagnosis for

bile acid diarrhoea and ulcerative colitis by urine analysis, with statistical differences being found between bile acid diarrhoea vs. ulcerative colitis and healthy controls.

Moreover, altered expression of N-linked glycan associated with cancer has been researched by IMS-MS in the human serum of 81 volunteers, 28 with cirrhosis of the liver, 25 with liver cancer, and 28 apparently healthy [118]. Analysis by principal component analysis differentiated liver cancer patients from the other subjects by IMS profiles. Similarly, Parkinson's like disease in rat models was studied by IMS-MS and metabolic differences were found by principal component analysis between samples and healthy controls [118].

The scent of disease is a growing field of research linked to IMS analysis of volatile organic compounds associated with the human body (breath, blood, skin, faeces, and urine) and as disease-specific VOCs are identified and characterized enormous and important possibilities for medical diagnosis of infectious and metabolic diseases, genetic disorders and other kinds of diseases arise [118, 124]. The role of IMS in exploring the scent of disease and medical diagnosis is still largely uncharted but this analytical technique shows promise in both, old and recent health concerns, and even in managing and evaluating therapeutical and treatment practices [116, 118, 124].

3.4.4 Microbiology: bacteria and fungi identification

Bacterial and fungal infections are primarily treated by an initial administration of broad-spectrum antibiotics followed by narrow-spectrum therapy once the microbiological diagnostic results are available [125, 126]. At present two to four days are expected between the sampling of a suspicious infection and the result of microbial diagnostics which can create delays in the identification of pathogens causing, often, a late or unsuitable therapy being initiated for patients [125]. Hence, an optimal therapy by identifying as early as possible the pathogen would lessen bad outcomes and hospitalization costs, inappropriate and over treatment by antibiotics and reduce the risk of pathogen resistance [125, 126].

The current method for microbial identification is the classical use of bacterial and fungal characterization combined with biochemical and susceptibility tests which often are unable to provide results early enough to manage and guide antibiotic administration in early stages of treatment [118, 126]. Ion mobility spectrometry has been explored for a fast and accurate application in bacteria and fungi species identification and resultant infections through the determination of their characteristic volatile metabolomes [125, 126]. Metabolic profiling of bacteria and fungi species is associated with subtract biodegradation to several products, including VOCs which can consequently be detected in the headspace of microbial cultures [125, 126].

The first scientific evidence of microbial VOCs has been presented in 1921 and 1976 but its role and interest as a medical application has only gained importance and focus on recent decades with IMS being continuously explored for microbial identification in medical applications and other areas related to microorganisms [125]. An MCC-IMS, for example, has been tested for rapid discrimination of 15 clinically relevant human pathogens grown for 24 hours in Columbia sheep blood agar by analysing the headspace of those cultures [125]. The results provided by MCC-IMS were cross-validated and

evaluated by gas chromatography–mass spectrometry, GC-MS analysis which also served the purpose of assigning volatile compounds to unknown MCC-IMS signals. All strains investigated showed different VOC patterns via MCC-IMS in positive and negative ion modes with one stain of *Proteus mirabilis* showing 21 specific signals, the highest value observed. This study and several other show the enormous potential for IMS analysis in microbial identification through metabolic profiling in a fast (in hours) and cost-effective method [125, 126, 127, 128]. Although bacterial identification is more prevalent in medical or health related applications, studies of microbial profiling by IMS have transverse into other areas, including agricultural, indoor air toxicity and characterization of metabolites and metabolic process in the identification of fungal and bacterial species in biochemistry [129, 130, 131, 132].

In a more industrial setting, a closed-loop GC-IMS was used to non-invasively monitor bacterial growth in a bioreactor for auto-induced protein production [133]. Bioreactors, uniquely designed for industrial scale, have numerous applications in the productions of biomass or biochemically active substances including pharmaceuticals, flavouring compounds, or bioethanol [133]. The biochemical environment in bioreactors must be continuously controlled within narrow limits to ensure a constant high quality and quantity of products. Sensitive, preferably non-invasively sensors able to continuously monitor important parameters are desired in this field [133].

A study analysed a bioreactor's exhaust gas produced from the bacterial growth and auto-induced protein production of recombinant Escherichia coli BL21 by a compact closed-loop GC-IMS [133]. This apparatus was developed and built-in house allowing exhaust gas to be sampled every 20 min comparing the intensity of different IMS peak with additional online and offline data (e.g., oxygen consumption, optical density or the fluorescence of a GPF-labelled protein produced by the bacteria after auto-induction). The GC-IMS was proven to be suitable to monitor dynamic changes in the exhaust gas composition coming from the bioreactor with reproducible results allowing metabolic states to be identified for the growth and auto-inducing phases based on the emission of microbial VOCs [133].

In agricultural applications the characterization of volatile metabolites formed by moulds on barley was analysed by IMS to monitor and prevent field or storage spoilage of barley seeds, a major cause economic losses in, food processing, malting facilities and breweries [130]. While detecting mould makers in indoor air which can cause health problems such as skin and eye irritations, allergic reactions, headaches, breathing difficulties, and amplification of asthma symptoms are possible applications currently being explored with IMS [128, 131]. Furthermore, another IMS application has been explored in identifying concealed fungal contamination in building material like wood via microbial volatile organic compound profiling [132].

Bacterial and fungi identification via IMS depends on a group of compounds referred to as microbial volatile organic compounds (MVOC), a variety of compounds formed by fungal and bacterial metabolism [134, 125]. Although over 200 compounds have been identified as microbial VOCs, none can be considered exclusive to a specific microorganism or microbial species [134]. However, a total of 15 compounds have been classified as common MVOCs through the analysis of indoor air from highly humid environments with identified microbial damage [134]:

- 2-Methyl-1-propanol
- 3-Methyl-1-butanol
- 3-Methyl-2-butanol
- 2-Pentanol
- 3-Octanol
- 1-Octen-3-ol
- 2-Octen-1-ol
- 3-Methylfuran
- 2-Hexanone
- 2-Heptanone
- 3-Octanone
- 2-Methylisoborneol
- Geosmin
- Dimethyl disulphide
- 2-Isopropyl-3-methoxy-pyrazine

Because MVOCs are produced from both primary (e.g., DNA, amino and fatty acids synthesis) and secondary metabolisms (reactions following the primary metabolism) of fungi and bacteria, their generation is greatly affected by species, growth phase and conditions (e.g., nutrient source, pH, humidity, and temperature) [134, 125]. The generation and release of MVCOs is extremely complex since their origin depend on several metabolic pathways and environmental conditions. However, establishing emission patterns with qualitative and/or quantitative information from several MVOCs is seen as a viable approach for microbial identification in specific and controlled conditions [134, 125].

3.4.5 Foodomics: food quality and adulteration

The last decade has seen numerous developments and innovative uses and application of ion mobility spectrometry in foodomics [135]. Assessment of food freshness has been a focal application of IMS, in which the degree of spoilage from several food products (e.g., fish, beef, chicken and pork) has been investigated [135]. Even determination of odorants responsible for "off-flavour levels in wine", olive oil grade classification, detection of pathogenic microorganisms, pesticides toxins, harmful chemicals, drugs, and adulteration of agricultural products have been studied with IMS [135, 136].

Food freshness and spoilage has been studied with IMS by evaluating levels of volatile nitrogen compounds, focused on biogenic amines formed in amino acid degradation by enzymatic and microbial processes. Trimethylamine, putrescine, cadaverine, spermidine and spermine, are biogenic amines, with high proton affinities and have been used in a qualitative method to evaluate freshness of fish products with a handheld GC-IMS [135]. Hexane measured with an ion mobility spectrometer has also been used to describe a multivariate modelling of fish freshness index, while putrescine and cadaverine levels have been determined in chicken meat by GC-DMS in meat spoilage [135].

The analysis, through IMS, of the earthy odorant 2,4,6-trichloroanisole (2,4,6-TCA) which causes off-flavour in wine has been explored recently in a few publications based on two approaches [135]. The first approach includes the use of ionic liquid based single-drop micro-extraction to selective preconcentrate 2,4,6-TCA and its determination by GC-IMS, while the second approach used a GC/DMS. Both approaches relied on measuring samples in the negative ion mode and were sensitive enough to measure 2,4,6-TCA at below the human olfactory threshold level [137]. However, in some cases the analyte measure was not an ion uniquely attributed to 2,4,6-TCA but a chloride ion [135].

Furthermore, several examples in the determination of toxic and harmful substance in food include the determination of insecticides (malathion, ethion, and dichlorovos), aflatoxins B1 and B2, caffeine, theophylline, ochratoxin A in licorice root, nitrites, and nitrates in potato samples by electro-

spray ionization IMS and malathion and dichlorovos on cherry tomatoes after extraction with acetone by a handheld IMS [135]. Solid phase desorption coupled with a GC-IMS in negative ion mode has been used to determine residues of seven commonly used types of pesticides in fruits and with FAIMS to determine chemical warfare agents in food products. Three veterinary drugs residues in chicken meat have been determined by an IMS device using a corona discharge ionization source after being treated with solid phase extraction and several active ingredients, including acetaminophen, aspartame, thiamin have been determined in counter drugs and beverages [135].

Detection of food adulteration and falsified product classification is another area where the use of IMS has been growing rapidly [135]. Examples include the determination of volatile compounds from Iberian pig meat products to verify their feeding regime, in a pig farm or out in open range [138]. The headspace of fat samples heated for 40 min at 150 °C was examined by IMS and principal component analysis with only 2.3% samples being misclassified [135, 138].

Olive oil classification is another example of IMS applications for food adulteration and falsified classification [135, 139]. Grade classification has been achieved through the analysis of aldehyde content by IMS with UV ionization and MCC-IMS. A successful classification rate of 87% among 98 olive oil samples was achieved with MCC-IMS and chemometric methods could classify olive oil into three groups (extra virgin olive oil, olive, and pomace olive oil) [139].

To summarize, IMS applications are spread through several areas, including industrial and environmental control of toxic substances, non-invasive medical diagnosis, in security and military activities, to characterizing microbial volatile organic compounds and even in food related areas including adulteration and quality control. This diversity makes IMS versatility obvious even showing that several instrumentation types can be applied to different applications and samples.

However, IMS suffers from some setbacks related to its enormous versatility, mainly because transferability between instruments is often problematic and scarcely explored. A generalized database or substance library containing drift times of volatile organic compounds is current non-existent. Plus IMS, generally, still requires a prior qualitative analysis to be performed by either measuring substance standards or through cross validation with other analytical techniques (commonly relying on GC-MS coupled measurements and analysis) to provide accurate quantitative data. Lastly, a lack of well-defined and established methods for quantitative analysis and widespread methods for data is apparent and persistent which is limiting to the processes of identifying and quantifying VOCs and the establishment of biomarkers and, or emission fingerprints.

The conception of suitable and controlled sampling approaches, the implementation of generalized drift time and pattern databases with well described qualitative and quantitative methodologies, and the creation of powerful data evaluation software with sophisticated chemometrics for ion mobility spectrometry are vital steps to establish IMS as a rapid, selective, and sensitive analytical tool in many relevant applications, currently demanding accurate and fast detection of VOCs.

CHAPTER 4.
GAS ANALYSIS, CALIBRATION & APPARATUS:
Methods & Materials

Gas analysis by stand-alone ion mobility spectrometry instruments is unable to provide the best results for complex samples involved in the current range of applications and research, because direct sample introduction will lead to clustering in the ionization and drift regions. Therefore, complex humid samples require the use of pre-separation which has been dominated by gas chromatography including capillary or multi-capillary columns. Hence the current research involved in complex and humid samples from several sources and their gas analysis with coupled gas chromatography and ion mobility spectrometry needs to be described, understood, and optimized for each application.

4.1 Gas Analysis with Ion Mobility Spectrometry

The potential of ion mobility spectrometry as an analytical technique for identification and quantification of gas-phase compounds is augmented by its coupling with gas chromatographic pre-separation. This pre-separation is a must for research and applications involving complex and humid mixtures, since in-line pre-separation greatly improves to ppb_v and ppt_v concentration ranges [96, 97, 108, 112, 113, 114].

A general procedure for gas analysis with IMS as a detector begins with sampling, which must be carried out in a controlled way and adjusted to application as is the case of pre-separation with gas chromatography for complex mixtures [97, 112, 113]. However, using pre-separation by chromatographic methods is not viable with continuous sample introduction and normally a gas-phase sample is introduced via a sample volume of variable size [97, 108, 113]. This variable size volume is achieved in a sample loop system which receives samples through injection or continuous flow into a sample loop with a specific volume size [97, 113, 114]. Commonly a 6-way valve is used to control sample volume introduced into the GC column from the sample loop [113, 114]. This system determines the sample volume introduced into the GC column for analysis by controlling the amount of time the 6-way valve remains in each of its two possible conformations [113]. The default position blocks any flow into the GC column and drift tube while a gas-phase sample is being introduced into the sample loop, once the valve switches to its second configuration the volume inside the sample loop is re-directed into the GC column and consequently into the drift tube [113, 114].

The influence of the sample volume in sensitivity is positive in one aspect, a higher volume means more sample and negative in its impact to GC resolution, because higher volumes will translate into boarder peaks [113, 114]. This results in sample volumes generally used of 1 mL for GC-IMS analysis of complex samples and 5 to 10 mL in samples with extremely low concentration [97, 113]. Therefore, sample value must be adapted to each particular application since a compromise must be met to avoid negative effects on GC resolution whilst maintaining a good enough sensitivity [113].

A generalized perspective of the several modules that are operated and controlled by suitable measurement and data acquisition software can be described in seven steps: (1) Gas-phase sampling, (2) an Optional pre-concentration phase, (3) Sample introduction into the analytical system, (4) Pre-separation by suitable GC columns, (5) Sample ionization, (6) Ion separation by different mobilities and (7) Ion detection (Figure 4.1) [113, 114]. Those steps put together form a procedure for GC-IMS

analysis from sampling to data acquisition. Nevertheless, some specific steps might be only optional when considering specific applications of the IMS analysis and related sampling and sample type [113].

Gas-phase sampling is conducted through a portion of the sample volume since continuous introduction is not possible when coupling with pre-separation techniques is involved (gas chromatography). However, this sample volume must be flushed prior and posterior to any measurement to remove or prevent any memory effects [97, 113, 114]. Flushing is generally achieved by circulating air through the sample inlet and loop, often achieved with a pump or a continuous flow of the selected carrier gas.

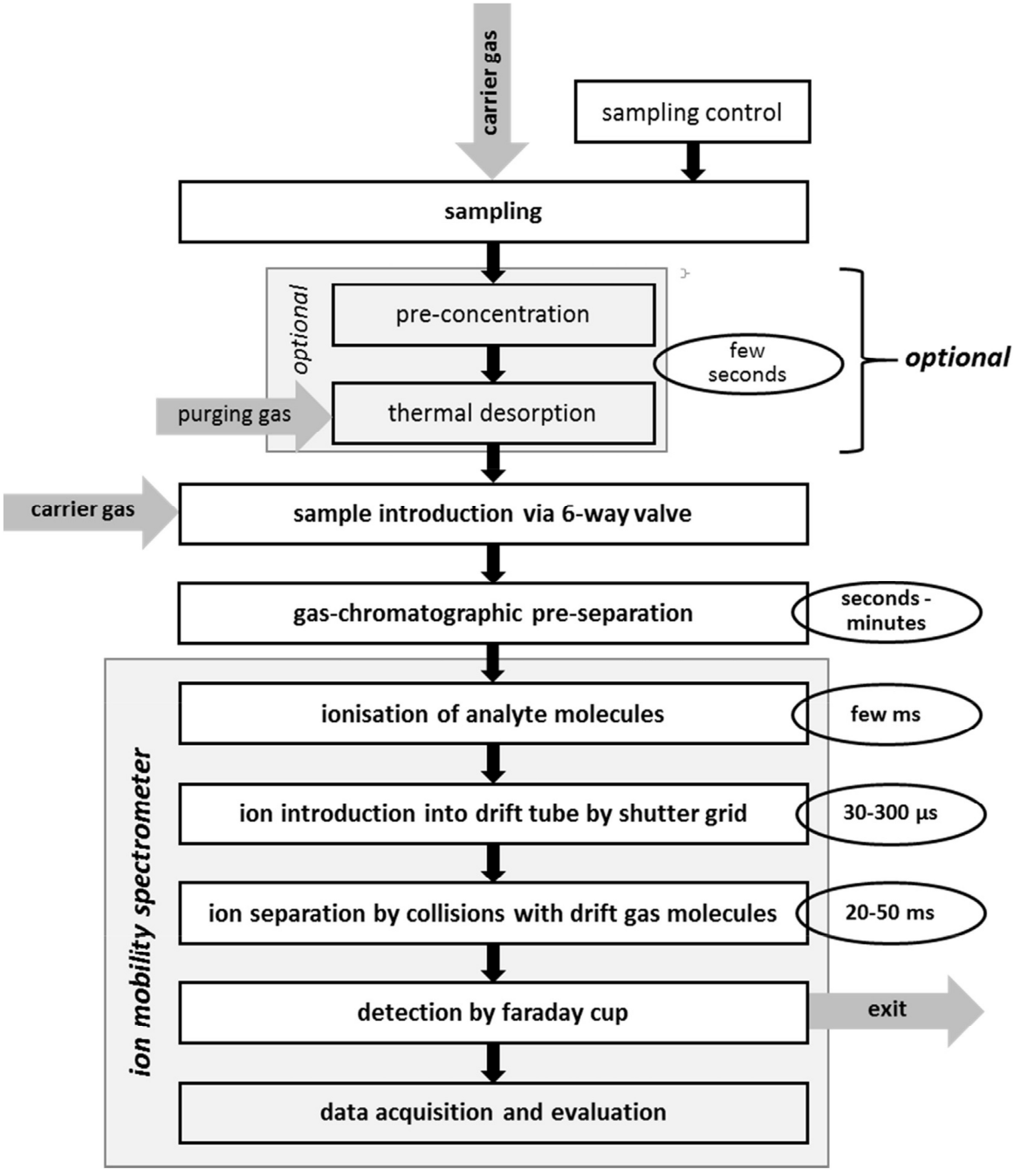

Figure 4.1 — The scheme of the entire procedure of GC-IMS analysis including sampling and optional steps [113].

When analysing solid or liquid samples that can be characterized by their volatile organic compounds, headspace analysis is the most common method, in which a small aliquot of solid or liquid sample is placed inside a chamber or vial at a constant temperature [97, 112, 113, 114]. The headspace inside the vial is injected or flushed into the analytical system using a carrier gas flow. Specific applications might require detailed sampling control by using varying signals from a process or collection instrument. Breath analysis is an obvious example, because if the aim is to analyse exhaled breath, a previous system must guarantee, through appropriate control parameters, that at least an exhalation flow or volume is being sampled an not air from other regions of the respiratory tract [97, 112, 113].

Pre-concentration is used when limits of detection well below ppb_v or ppt_v ranges are intended with GC-IMS in gas analysis of humid and complex samples [112, 113, 114]. Although limits of detection can be improved through changes in ionization due to its reliance on compounds proton/electron affinity and sample volume, the improved sensitivity is often reduced or insufficient. Specific pre-concentration units can be built into an instrument or samples can be processed via adsorption material such as Tenax® and solid-phase micro extraction (SPME) an in the case of HovaCAL, a calibration gas generator, limits of detection were extended to the ppq_v ranges [96, 112, 113].

The use of GC columns for pre-separation is dominant in several application related to air quality, foodomics, breath analysis, medicine, biology, and process control, to mention a few [96, 112, 113]. However, GC columns in commercial IMS are operated isothermally as opposed to the dominant use of GC ovens observed in several mass spectrometry instruments [97, 108, 113]. Size and complexity of a GC oven would hinder and reduce the potential for small and mobile ion mobility spectrometers. Hence, some advantages of a GC oven are replicated by applying a flow program to an isothermally operated column while avoiding its size and complexity limitations [113, 114]. Furthermore, a GC column is always considered and selected in accord with the analysis context, both in terms of application and sample type, whereas capillary and multi-capillary columns are included alongside different lengths and stationary phases [96, 97, 108, 113].

The selection of a column type and length is based on sample complexity, humidity, and analysis time, while column stationary phase considers the specific compound or group of compounds to be detected [96, 113, 114]. Moreover, GC columns contribution is not exclusively for sensitivity by reducing clustering ionization at IMS drift region, but also selectively, since retention time for a determined compound is acquired and permits identification [97, 108, 113, 114].

Ionization of gas-phase samples for ion mobility separation is mostly done by β-radiation sources, although some less used ionization sources might be beneficial in other aspects and instances. The reactant ions formed during ionization are protonated water clusters in the positive mode, which enables ionization of any analyte with higher proton affinity. Whereas in the negative mode, under a drift gas of purified, negatively charged oxygen molecules are produced as reactive ions through electron transfer.

Photoionization by UV light is often used for analysis of specific compound, such as Terpenes, which are ionized directly but it provides lower sensitivity of only positive ions [97, 108, 113]. Corona discharge is also another method of ionization and produces reactant ions from the ionization of drift

gas molecules, often nitrogen, comparable to radioactive ionization sources [96, 97, 108, 112, 113]. Corona discharge shows one particular disadvantage, the degradation of discharge needles which limits its use and applicability causing this ionization method to be less common for IMS instruments [97, 108, 113, 114]. Although legal restriction and irrational concerns might have limited the use of radioactive sources, nowadays sources employed in ion mobility spectrometers have very low activity. The main advantages of radioactive sources compared to other ionization methods are long-term stability while granting an independence from additional power supplies [97, 113, 114].

The succeeding step to ionization is ion separation via different mobilities and, although both phases occur in the IMS drift tube, the aspect influencing ion separation are linked to the drift tube length and the electric field characteristics [97, 108, 113]. Generally, analysis involves a fixed drift tube length, however, in an experiment, a modular drift tube was designed with changeable length from 6 to 24 cm in 3 cm steps in an attempt to optimize resolving power by drift length and electrical field [108, 113]. A longer drift tube might help improve selectivity while simultaneously decreasing sensitivity due to increasing loss of ion to the walls [113]. As a result, any drift tube set-up is adapted to meet the requirement of a certain applications while considering optimal values of selectivity (or resolution) and sensitivity for compounds of interest [113].

Nearly all ion separations and detections are either performed in the positive or negative mode, according to chemical characteristics of the compounds of interest [96, 97, 108, 112, 113]. However, specific applications might require simultaneous detection of both negative and positive ions [108, 112, 113, 114]. Both polarities are normally measured in two subsequent sample introductions after changing polarity or with the use of two drift tubes of different polarity operated in parallel [113, 114]. Remarkably dual IMS instruments have been designed to allow the ionization source and sample introduction to be located at the middle of a drift tube and detect positive and negative ions at opposite ends of the drift tube [108, 112, 113]. This type of system enables detection of positive and negative ion from a single, unique sample, advantageous in certain analysis where sampling is limited, highly valuable or when changes over time can result in sample transformations between positive and negative mode measurements [112, 113].

Another approach used for simultaneous detection of both polarities includes the use of two parallel tubes and splitting the sample or by rapidly switching the electrical field during a measurement [113]. Furthermore, ion separation can also be aided in terms of sensitivity and, or selectivity by using dopant gases in the ionization source. Dopant gases change ionization chemistry and reactions producing reactant ion peaks (RIPs) in terms of proton or electron affinities increasing detectability of compounds. Generally, dopant gases are used to avoid modifying instruments modification and can prove remarkably efficient to detect specific compounds in specialized applications [108, 112, 113].

The potential of ion mobility spectrometry in gas analysis is evident from its capabilities as an analytical technique for identification and quantification of VOCs which, when coupled with other analytical tools, especially chromatographic pre-separation shows significant improvements in selectivity [97, 108, 112, 113]. This combination makes possible the analysis of complex humid mixtures of volatile organic compounds in low concentration ranges (ppb and ppt) and once appropriate substance

databases are implemented and followed by data evaluation with dedicated software the usefulness of GC-IMS for rapid, selective, and sensitive analysis in many applications becomes clearer [96, 97, 108, 112, 113].

4.2 Headspace Analysis of Volatile Organic Compounds

The concept of volatile organic compounds (VOCs) is defined by the World Health Organization (WHO) as compounds with a boiling point below 250 degrees Celsius at standard atmospheric pressure (101.3 kPa) [140, 141]. This classification can be further subdivided into two groups, very volatile organic compounds, mainly gases, with boiling points between 0 and 100°C and volatile compounds with boiling points between 100 and 250°C which can originate from air, water body surfaces or solid surfaces [140]. Physical and chemical properties of volatile organic compounds combined with their mean lifetime in the atmosphere, between a few minutes to several months, allow their dispersion across large distances from their emission source [140, 141]. Aromatic hydrocarbons, aliphatics, aldehydes, ketones, ethers, acids, and alcohols, with diverse functional groups (e.g., halogens, oxygen, sulphur, nitrogen, or phosphorus, excluding carbon oxides and carbonates) are classified as volatile organics (Figure 4.2) [140, 141, 142].

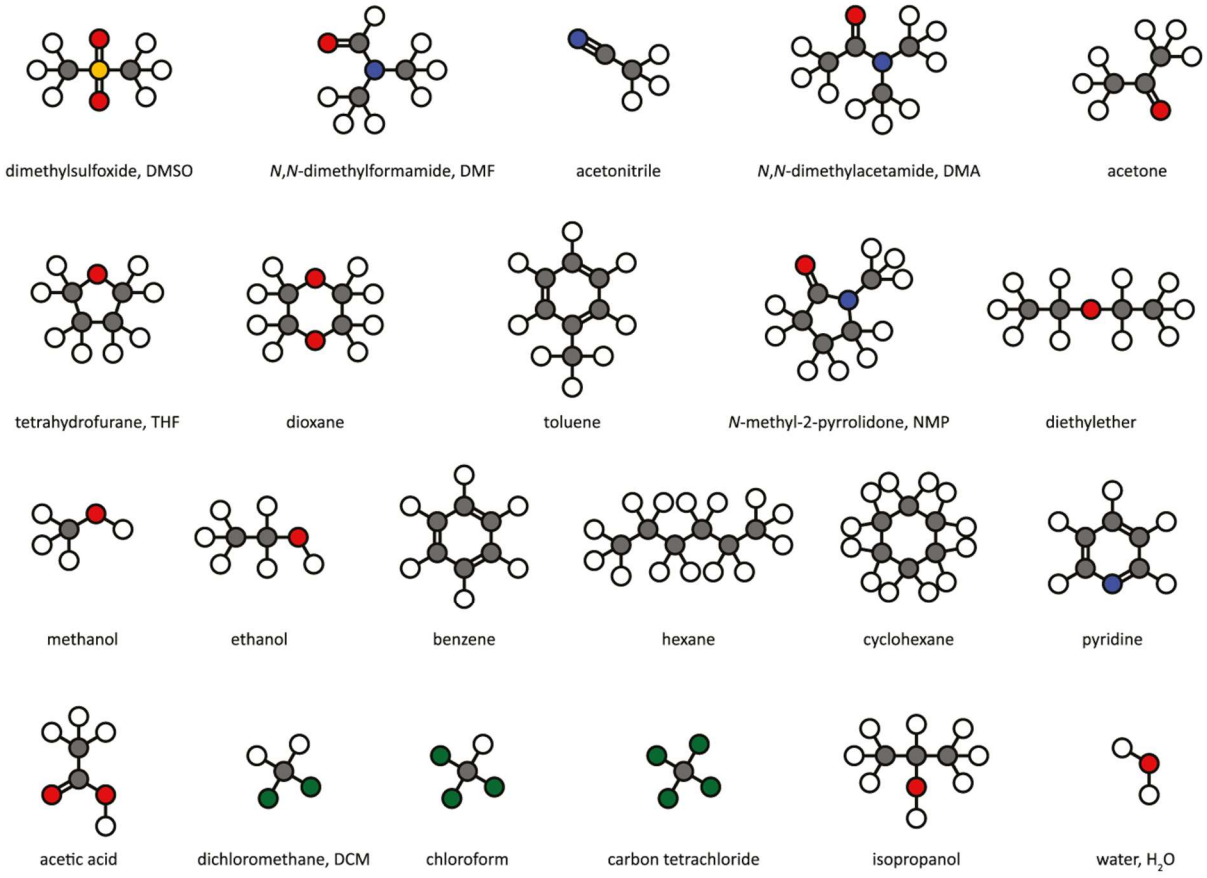

Figure 4.2 — Chemical structure of several types of volatile organic compounds in gas analysis [142].

Volatile organic compounds are plentiful and ubiquitous including natural occurring and human-made chemical compounds with several sources (off-gassing from various types of materials: plywood, particleboard and glues, paint, polish and other wood finishing products solvents and cleaning products, smoke from candles, stoves or cigarettes, vehicle traffic, industrial processes, animal farms, plants, forest fires, human and microbial metabolomes) [140, 141, 142]. Although rather inert lipophilic compounds, VOCs can pass through biological membranes such as skin or through human airways and enter the body showing different levels of toxicity based on their biotransformation [140, 141].

The analysis of volatile organic compounds from complex sample mixtures is normally conducted through a fast and clean method called headspace analysis [140, 143, 144, 145]. This method isolates non-volatile components in a sample from volatile compound by the headspace or vapor portion of a sample inside a vial, container, or chamber. Headspace analysis can be well understood as the analysis of VOCs originating from liquid or solids without a direct sampling of the matrix [143, 144, 145]. The objective of headspace analysis can be to evaluate, identify and quantify individual components in a sample or relate emission profiles to other characteristics like odour or aroma [140, 143, 144, 145].

Liquids or solids for direct gas chromatography impose laborious pre-treatment and clean-up prior to their injection to a GC column [140, 143, 144]. Through headspace analysis, the often-improper state of liquid and solid samples for GC is overcome by sampling headspace components, and directly inject them into a GC column [143, 144, 145]. A calibration calculation can later be applied to convert measured component concentration with values associated with the original sample [140, 143, 145]. Three essential types of sampling procedures exist for headspace analysis, (i) static headspace, (ii) dynamic headspace, and (iii) purge methods, and all methods can be used with GC coupled to IMS and mass spectrometry (Figure 4.3) [140, 143, 146, 147].

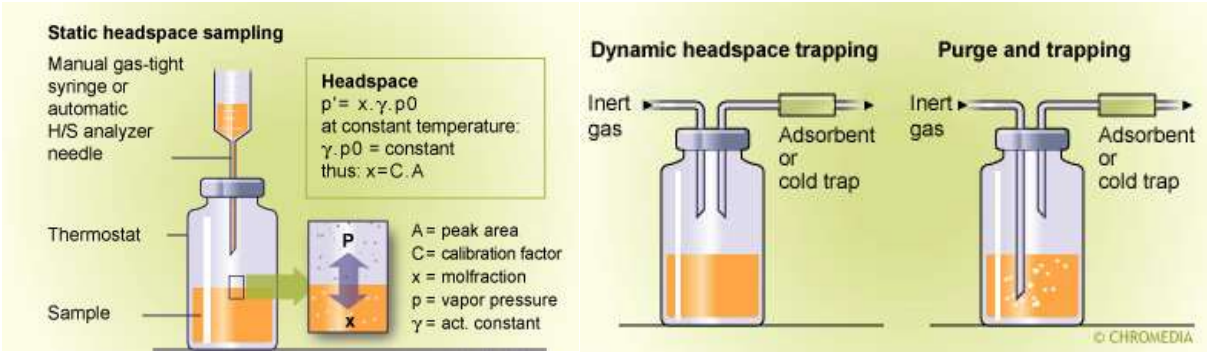

Figure 4.3 — Diagrams showing the experimental setup for static headspace, dynamic and pudge sampling [146].

4.2.1 Static Headspace Methods

Static headspace is a simple method, that can be carried manually with gas-tight syringe or automatically with a 6-port valve system [143, 146, 147]. In this method a sample is left inside a closed container at a controlled temperature until the saturation of the vessel headspace with analyte vapor.

Headspace saturation is a time-dependent process that also depends on analyte vapor pressures, sample concentration and sample temperature [143, 146, 147, 148]. Although while vapor concentration build-up is still increasing, the volume of headspace is important, but once the headspace is saturated, headspace equilibrium is reached, the respective volume concentration will be equal throughout any volume [146, 147, 148, 149].

A compound vapor pressure is the pressure at which the gas phase of an analyte is in equilibrium with its liquid phase and can be used to understand how quickly volatile organic compound evaporate and, in turn their volatility [143, 146, 147]. Higher vapor pressures imply higher volatility and therefore makes such analytes more volatile compounds. The boiling point can also be used to understand compound volatility since it relates to vapor pressure in the fact that a boiling point is the temperature at which the compounds vapor pressure is the same as environmental pressure [143, 146]. Low volatility compounds might be hard to detect, however, increasing sample temperature changes a compound vapor pressure and increases evaporation and consequently their detectability. Changing sample temperature is a direct approach to affect sensitivity in any headspace analysis and the time needed to reach headspace equilibrium, since temperature influences all analyte vapor pressure and evaporation rates (Figure 4.4) [143, 146, 147]. However, for samples containing water or in solution, increases or decreases in sample temperature might affect analyte solubility positively or negatively and increase or decrease humidity levels [146, 147].

The calculation of the saturated headspace concentration for a specific analyte can be done by the following expression $C = V_p/P \times 10^6$, where V_p is the analyte vapor pressure in mmHg at the sample temperature, P is the pressure of the container, (760 mmHg at standard atmospheric pressure) and C is the analyte concentration in the headspace in parts-per-million (ppm) [146, 147]. Furthermore, when the Henry's law is applicable the concentration of each component in the headspace is related to their respective concentration in a liquid or solid sample by the relationship in equation (11) [146].

$$C_{0\,(\text{liquid})} = \frac{C_{i\,(\text{gas})} \times (K \times V_L + V_G)}{V_L} \qquad (11)$$

$C_{0\,(\text{liquid})}$ corresponds to the original concentration of a component in the liquid samples, $C_{i\,(\text{gas})}$ is the concentration in the headspace in the gas-phase, K is the partition coefficient; V_L the liquid sample volume and V_G is the volume of the headspace gas. A careful calibration should, however, be performed over a range of relevant concentration for accuracy in the calculation of the liquid concentration of a compound. Besides temperature and pressure, matrix composition of the sample also has a significant impact in headspace equilibrium and mass transfer of volatile compounds into the headspace, whereas matrix effects like homogeneity, salt concentration, solvent type, solid particles, adsorption effects and pH values are included and should be considered during calibration [143, 146, 147].

4.2.2 Dynamic and Purge Headspace Methods

The dynamic headspace sampling method is similar to static headspace and differs from the previous method because the headspace of a vessel is continuously swept into an analyser via a clear purge

flow (Figure 4.4). [143, 147, 150]. Dynamic headspace involves purging the headspace of a sample with a known inert gas volume to remove volatile compounds from a liquid or solid sample, however, compounds with a strong affinity for the sample matrix might prove to be difficult to extract into its headspace [143, 147, 150]. Evaporation occurs at the surface of the sample which makes surface area a key factor involved in mass transfer into the headspace (Figure 4.4). Although wider containers with lager surface areas can lead to an increase in the amount of analyte moving into the detector, keeping the surface area constant between samples is more imperative to ensure coherent results [143, 150]. Consequently, solid samples are melted or dissolved, when possible, or placed in the vessel in a powder form before sampling in dynamic headspace [147, 150].

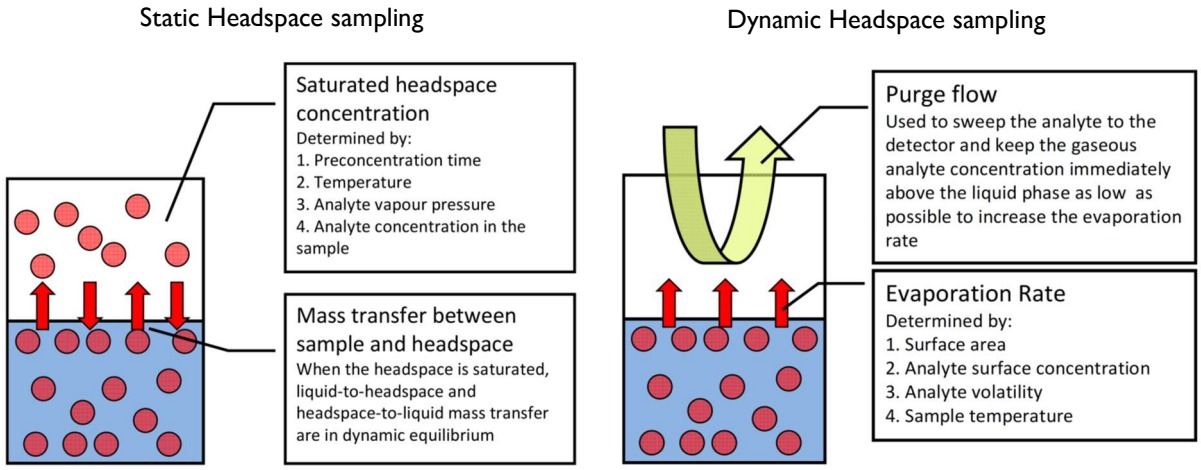

Figure 4.4 — A generalized schematic of processes and factors involved in static and dynamic headspace sampling [147].

Since transport of analyte molecules from the bulk of a liquid to its surface layers is a diffusion-limited process it can be slow with reduce mass transfer speed from the liquid surface to the headspace [143, 147, 150]. The use of magnetic stirrers to homogenize a sample during analysis is a common solution used to overcome this problem while mass transfer rate into the headspace is also increased via a purge flow sweeping the analyte vapor into the analyser [143, 150]. This purge flow can be directly driven into the analyser or prior to entering the analyser pass through a tube packed with a sorbent material (e.g., Tenax TA) scrubbed or cold trap (Figure 4.4) [143, 147, 150].

A boundary layer of high concentration air above the liquid surface might form which can be reduced through a high flow rate or a dip tube. The dip tube approach reduces the distance from the purge flow inlet and the liquid surface, thus creating a flow that travels the entire headspace [143, 147, 150]. Headspace replacement is increased with higher purge flow rates since the penetration into the sample vessel is higher and it can be calculated with equation (12) [143, 150].

$$N = f/b - s \tag{12}$$

Where N is the number of headspace replacement per minute, f is the sample flow rate (ml/min), b is the vessel volume and s the sample volume in ml. To calculate the headspace concentration, C in

ng/ml, in a dynamic sampling method equation (13) is used, dividing mass transfer rate, MT in ng/min by the purge flow rate, F_{purge} in ml/min [143, 147, 150].

$$C = MT/F_{purge} \quad (13)$$

The purge sampling method is analogous to the dynamic headspace sampling, however in this case, the purge gas is passed through the sample and not only the headspace and most system for dynamic headspace sampling can be used for purge sampling after small modifications [143, 150]. Automatic systems for both purge and dynamic headspace methods are available and enable measurements of concentration ranges from ppb to ppt levels.

The use of static dynamic or purge methods for gas analysis in GC-IMS allows VOCS in liquid and solid samples to be identified and quantified in their gas-phase [143, 147, 150]. However, the identification of detected signals in GC-IMS is only achievable by comparing measurement data with suitable databases of ion mobility drift times and retention times, in consideration with the specific GC column, temperature and flows used [113]. Even though a few databases are available or can be estimated from model calculations its use is still hindered by slight deviation in experimental setup which led to significant variations in ion mobility values [113]. Hence databases often need to be developed for each experimental setup through headspace analysis of several VOCs of interests for a particular research or practical application.

In general, the identification of IMS and GC-IMS unknown signals is performed by parallel sampling of adsorption tubes through GC-MS allowing signals from both analyses to be compared to propose possible compounds later validated by measurements of pure reference analytes [113]. This approach can be time-consuming, complex and require multiple instrumentations, expertise, and logistics to obtain results. However, the previously described methods pose a simpler and faster method to identify ion mobility constants and retention times of GC-IMS unknown signals through pure reference analysis. Static and dynamic methods can both be used to identify unknown signals and empirically build VOC databases [113]. Information contained in those databases, such drift times, ion mobility constants and retention times, can further be used for automatic data evaluation and immediate interpretation after, or during a specific GC-IMS analysis.

4.3 Generation of Calibration Gas Standards

Ion mobility spectrometry is also a quantitative analytical technique whereas the intensity of an analyte peak/signal corresponds to a specific concentration value, however creating and delivering concentrations in ppm_v, ppb_v and ppt_v ranges or lower, for the calibration of an ion mobility spectrometer can be challenging. Understanding the meaning of ppb and ppt is crucial to comprehend the degree of sensitivity IMS can provide and to contextualize and evaluate an accurate and precise method for the generation of calibration gas standard.

4.3.1 Understanding the Units of Measurement Employed

The units of measurement ppm, ppb and ppt correspond to the abbreviation of parts-per-million, parts-per-billion, and parts-per-trillion, respectively, which count the number of units of a substance per one million, billion or trillion units of another substance. This notation is used to measure concentrations when a small quantity of a compound can have a big impact and is frequently used to quantify chemical contaminants in soil, water, and air [151, 152].

The use of this notation can be exemplified by a concentration of only 35 ppm of carbon monoxide in the air being poisonous to humans. However, since such type of measurements are involved with very small *vs* very large numbers its conceptualization and meaning might prove complicated to understand immediately [151, 152]. Several analogies can help to visualize and understand better what ppm, ppb and ppt mean:

(i) one part-per-million (ppm) equals: 1 minute in two years, 1 second in 11.5 days, or 1 litre of water in a swimming pool,
(ii) one part-per-billion (ppb) equals: 1 second in 32 years, the first 41 centimetres on a trip to the moon or 1 ml of water in a swimming pool,
(iii) one part-per-trillion (ppt) equals: 1 second in 320 centuries.

Furthermore, part-per-million (ppm), part-per-billion (ppb) and part-per-trillion (ppt) are interchangeable between each other by the following rule: 1 part per million = 1000 parts per billion = 1000 parts per trillion [151, 152, 153, 154]. Another important feature about ppm, ppt or ppt units of measurements is they represent different things for soil, water, and air contaminants [151, 152, 153].

Soil contaminants are regular expressed as the mass of chemical in milligrams, mg, or micrograms, ug, per mass of soil in kilograms, kg, written as mg/kg or ug/kg with respective equivalence of 1 ppm = 1 mg/kg of contaminant in soil, and 1 ppb = 1 ug/kg. (e.g., 6 mg/kg equals 6 ppm or 6000 ppb, which is the same as 6000 ug/kg) [151, 152]. In water analysis, ppm and ppb, correspond to units of the mass of chemical in milligrams, mg, or micrograms, ug, per volume of water in litres, L, represented as mg/L or ug/L which corresponds to 1 ppm = 1 mg/L and 1 ppb = 1 ug/L [151, 152, 153]. An example to demonstrate the interchangeable of units goes as follows, 6 mg/L equals 6 ppm or 6000 ppb, which is equal to 6000 ug/L [151, 152]. Additionally chemicals in water might also be expressed as grams per cubic meter (g/m^3) representing the same as grams per 1000 litres and can be converted to milligrams per litre (mg/L) since 1 g/m^3 = 1 mg/L = 1 ppm, while one milligram per cubic meter (mg/m^3) equals 1 ppb of contaminant in water [151, 152, 153].

Prior to exploring the meaning of ppm, ppb and ppt in air contaminants, it is crucial to understand that such measurement units are defined as a weight (w/w), volume (v/v) basis, or a combination of both (w/v or v/w) [151, 152]. Hence, when dealing with ppm or ppb on a weight (w/w) basis, in a dilute solution of water, a correspondence of a litre of water weighting approximately 1000 g can be established since the solution specific gravity, the density of an object, in this case water, divided by the density of water, equals 1. Through this formula the following equivalences can be established: 1 mg/L

= 1 g/m^3 ≈1 ppm (w/w) 1 µg/L = 1 mg/ m^3 ≈ 1 ppb (w/w), however in concentrated solutions or non-aqueous liquids the specific gravity will not always be a value of one and the previously mentioned relationships do not apply [151, 152].

As a result, to convert µg/L to ppb in a weight (w/w) basis for a solution which specific gravity different than zero a calculation must be performed: dividing the contaminant concentration, µg/L, by the specific gravity of the solution, e.g., 1 µg/L / 1.06 = 0.9 ppb (w/w) where 1.06 is solution specific gravity [151, 152, 153].

Air contaminants are commonly expressed in units of the mass of chemical including milligrams, mg, micrograms, ug, nanograms, ng, or picograms, pg, per volume of air in cubic meter, m^3 which can be converted to part-per-million (ppm) or part-per-billion (ppb) through a conversion factor [151, 152]. Such conversion is based on the molecular weight of each chemical therefore, it will be different between different chemical compounds. The conversion is typically made under the assumption of standard ambient conditions, with a pressure of 1 atm and a temperature of 25 degrees Celsius through the following equations:

$$\begin{aligned}\text{Concentration } (\text{mg/m}^3) &= 0.0409 \text{ x concentration (ppm) x molecular weight} \\ \text{Concentration (ppm)} &= (24.45 \text{ x concentration } (\text{mg/m}^3)) \text{ / molecular weight}\end{aligned} \quad (14)$$

To convert ug/m^3 to part-per-billion (ppb) and vice-versa the same equations can be applied replacing mg/m^3 and ppm for ug/m^3 and ppb, respectively [151, 152, 153]. However, if the concentration is represented in units of volume per volume (v/v) or the relationship between expressing concentration in mixed units of mass per units of volume (e.g., mg/m^3) depends on the compound density another approach is required. Since compound density also depends on its pressure, temperature, and molecular weight a new conversion can be made through the ideal gas law PV = nRT; (P is pressure (atm), V is volume (L), n is the mass of substance (moles), R is the ideal gas constant (0.082 atm L mol^{-1} K^{-1}), T is the absolute temperature (°C + 273) in degrees Kelvin) [151, 152, 153]. Thus, at standard pressure and temperature, 1 atm and 273 K, one ideal gas occupies a volume of 22.4 (equation (15)).

$$\frac{\text{V}}{\text{n}} = \frac{\text{RT}}{\text{P}} = \frac{\left(0.082 \ \frac{\text{atm L}}{\text{mol K}}\right) \times 273 \text{ K}}{1 \text{ atm}} = 22.4 \text{ L/mol} \quad (15)$$

Now, using Boyle's Law which states, P×V = constant or $P_1 \times V_1 = P_2 \times V_2$ for constant temperature conditions and Charles's Law, V/T = constant or $V_1 \times T_1 = V_2 \times T_2$ for constant pressure conditions equation (16) can be established to convert ppm to mg/m^3 and vice-versa [151, 152, 153].

$$\frac{\text{mg}}{\text{m}^3} = \frac{\text{ppm} \times \text{molecular weight}}{22.4 \text{ L/mol}} \times \frac{273}{\text{T(K)}} \times \frac{\text{P(atm)}}{1 \text{ atm}} \quad (16)$$

An important consequence of this equation is that an increase in temperature, which leads to an increase in the volume of the mixture, results in a decrease in concentration, mg/m^3, since the mass of the contaminant is constant [151, 152]. In opposition, an increase in pressure leads to a decrease in

the volume of the mixture which at a constant mass of contaminant creates a concentration increase in mg/m^3.

Although IMS is a quantitative analytical technique its calibration can prove challenging since concentrations as low as ppb and ppt must be generated and feed into an analyser with accuracy and control [113]. Concentration ranges, explained previously, entail a reduced number of molecules from a specific compound in a diluting gas and requires high accuracy in measurements and generation of standard gas mixtures and calibrants [113, 155]. Usually, standard gas mixtures are used as a specific type of reference material in calibration methods through all stages of analytical work in gas analysis, since such mixtures contain a defined and stable amount (or concentration) of analyte and diluting gas, with known sources of errors [113, 155].

Hence, generating standard gas mixtures with known and accurate concentrations is a vital step for the calibration of ion mobility spectrometers. Gas standards, with known concentrations, measured with IMS permit to establish a relationship between IMS signal intensities from a specific compound and an accurate concentration value. Moreover, the behaviour of an IMS signal intensity over a large range of concentration can also be characterized and described through the creations of calibration curves [113, 156]. So, the concept of an IMS calibration method through standard gas mixtures requires, therefore, accuracy, reproducibility, and preferably simplicity in preparation [113, 155, 156].

The current used of methods for generation of gas standard mixtures includes processes classified as static or dynamic (Figure 4.5), and such processes address, deal and account for the complication of weighting gases, volumes changes, temperature, and pressure effects involved with gaseous samples [155, 156, 157, 158]. The main differences between static and dynamic methods for the generation of standard gas mixtures relates to volume size and concentration levels [155, 157, 158]. Static systems are desirable when dealing with comparatively small volumes of a mixture and moderate high concentration levels are intended, while dynamic methods are used to generate a continuous flow of a pure gas or mixture, providing large sample volumes and significantly lower concentration levels [113, 155, 156, 157, 158]. In terms of loss of components to vessel walls, this risk is higher with static system and reduced in dynamic systems because, the latter relies on the equilibrium between the system and a gas stream flow [155, 157, 158].

4.3.2 Static Systems to Generate Standard Gas Mixtures

The use of static or bath system is common for producing standard gas and vapor mixtures and involves introduction of a known weight or volume of a contaminant into a container or vessel of fixed dimensions [157, 158]. Although static system can be used at any desired pressure its laboratory use is frequently limited to systems slightly below or at atmospheric pressure [155, 157, 158]. Through static systems small volumes can be used extensible for calibration and to produce gaseous standards for gas chromatography, mass spectrometry, infrared spectrophotometry, and ion mobility spectrometry [157, 158]. Static systems are divided into two types, pressurized and atmospherics: (a) pressurized static systems include three types, gravimetric, partial pressure, and volumetric methods, whereas

(b) atmospheric pressure methods are classified by their type of chamber or container, establishing single rigid chamber, multiple rigid chambers, and flexible chambers (Figure 4.5) [157, 158].

Gravimetric methods have a long history as standard methods in classical analysis and those used for preparing standard gas mixtures are elementary and have the highest potential to offer the greatest accuracy [157, 158]. Those methods are executed by weighing components into a tared cylinder on a high capacity and sensitivity balance with a high degree of accuracy, however, adsorption and purity variations are not always accountable [158]. Furthermore, weightings are not straightforward and often corrections must be made to account for buoyancy changes due to temperature, pressure, and humidity changes. Gravimetric methods are commonly used in the preparation of commercial primary standard mixtures but are not appropriate for general use in the laboratory [157, 158].

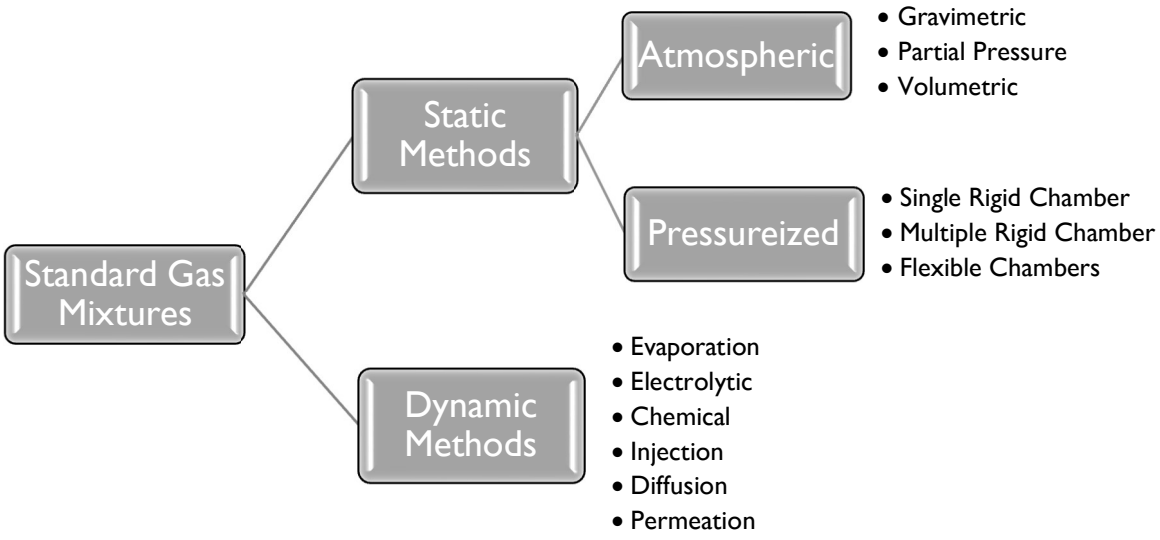

Figure 4.5 — The different types of methodologies used to produce standard gas mixtures for calibration [157].

The preparation of standard mixtures with static systems via partial pressure methods is based on the principle of partial pressures, where a mixture is placed inside a container at atmospheric pressure followed by an increase in pressure [157, 158]. Assuming ideal gas behaviour, the volumetric concentration of a mixture is related to the partial pressure of a component by $p = cP$, where p is the absolute partial pressure, c is the molar fraction and P the absolute total pressure of the mixture [157].However, gases that exhibit ideal behaviour are uncommon at high pressures and the previous formula needs be modified by a compressibility factor (z) resulting in $p = zcP$.

Once the partial pressures of each component and the total pressures are precisely known the concentration in percent by volume of each component can be estimated by $C_{ppm} = 10^6 \times p_n / P$, where C is the concentration and p_n is the partial pressure of a specific component [157]. This method shows some limitations since it is incapable of providing high accuracy and depends on the concentration level, resulting in tolerances usually being listed between 5 and 20%. Other drawbacks of this method include the risks of errors occurring from liquefaction of components and a necessity to dissipate heat generated in the cylinder compression which also requires a complex system [157, 158]. Its

applications have frequently been observed in the preparation of mixtures of nitrogen monoxide, anesthetic agents, carbon dioxide and vinyl chloride [157].

The volumetric method is the third and least used static atmospheric systems to generate standard gas mixtures. This method consists of compressing known flowrates or volumes of gases into a pressure vessel [157, 158]. Concentration of part-per-million range can be achieved via volumetric methods with accuracies of 1 to 10% depending on the chosen technique [157]. Volumetric methods have a few advantages when compared with other static methods, including the ability to easily generate low ppm mixtures of nonreactive, nonadsorbing materials which can also be stored for subsequent use [157, 158].

Pressurized systems for generation of standard gas mixtures include systems with single or multiple rigid chambers and flexible chambers. The single rigid chamber system, the simplest and the most convenient method to produce standard gas mixtures, consists of introducing a specific amount of solvent or gas into a single rigid chamber with a volume known. It allows samples to be vaporized if necessary and adequate mixing. The concentration of a gas contaminant in ppm can be estimated by $C_{ppm} = 10^6 \times v/V$, where v corresponds to the volume of the component and V is the volume of the diluent gas [157]. To maintain an atmospheric pressure as samples are withdrawn, a replacement gas might be introduced to the chamber, therefore, large vessels are used to allow mixture removal without excessive dilution. However, if the concentration changes because of dilution its calculation can be done assuming instantaneous mixing through the following expression: $C = C_o \times \exp(-V_w/V)$, where C is the final concentration, C_o the initial concentration, V_w is the volume of the withdrawn sample and V is the volume of the chamber [157].

A derivation of the single rigid chamber method which has some characteristics of a dynamic system is the exponential dilution flask [157, 158]. Through this method is possible to produce a gas mixture with a component concentration decreasing exponentially over time. The method consists of placing a known amount of a pure compound or standard mixture into a chamber where it is stirred and flushed continuously with a purge gas. The flow of purge gas causes the concentration of the compound to decrease accordingly to this expression: $C = C_o \times \exp(-Qt/V)$, where C_o is the original concentration when t = 0, C is the concentration at time t, Q is the volumetric flowrate at 1 atm, V is the effective volume of the chamber, and t is the time after introducing the sample [157].

This expression is similar to the one previously used in the single rigid chamber method and can be further simplified to $2.303 \times \log(C) = 2.303 \times \log(C_o) - Qt/V$ [157]. However, this method is only considered an excellent method for a limited number of substances, notably permanent gases, like nitrogen, oxygen, or argon [157]. This method assumes no adsorption losses which can be huge a disadvantage at low concentrations, because adsorption losses at low concentration result in a dilution rate that is no longer exponential over time and the method is only applicable to single substances [157, 158]. Furthermore, effective mixing is of high importance for this method, and it can greatly influence the accuracy of results, and even be a significant factor to the method uncertainty, which ranges from 4 to 8% in between 50 to 3 ppm [157]. Lastly uncertainties in the initial concentration

might also pose some challenges for this method, influencing its accuracy in predicting a concentration value [157, 158].

Multiple rigid chambers connected in series can be used in a similar format as the exponential dilution flask to produce higher concentrations of standard gas mixtures [157, 158]. Several identical containers connected in series are filled with a known concentration of a component and when a sample is taken from the last containers, the same amount of a diluent gas is inserted into the first container and mixed. This new mixture formed in the primary container is then directed into the next container where it is mixed and passed to the next container, repeating this until the last container [157, 158]. For example, in a five flasks system, a sample can be extracted from this system and have a concentration 5 times higher compared to an equal volume from a single rigid container [157]. This system is an improvement on the flexibility and usefulness of a single rigid chamber system with, however, a more complex system and a larger space being required.

Non-rigid chambers also called flexible chambers or plastic bags, are an alternative to rigid chamber methods, since they allow the extraction of an entire sample without the need for volume dilution, replacement with air or even pressure changes [157, 158]. Since containers are flexible once a sample is removed from it, its boundaries conform to the final volume inside the container, resulting in negligible internal pressure changes. This type of method is captivating for both field and laboratory use since it allows the calibration of analytical instruments in the field as well as gas samples in remote sites to be sent to the laboratory for analysis [157, 158]. Flexible chambers are less expensive, light, compact, easily portable and require no air dilution during sampling when compared with rigid static systems [157]. However, when using flexible chambers certain considerations, such as sample decomposition, adsorption to and diffusion through the walls must be accounted, especially if samples are stored for long periods of time. Flexible chambers can be described as sealed, flexible-wall container, inflatable to full volume without stretching its boundaries and, generally, possess some type of sample inlet port or septum [157, 158].

Several materials are used to construct flexible chambers including Tedlar®, Kel-F®, Teflon®, and five-layer (polyethylene, polyamid, aluminium foil, polyvinyldechloride, and polyester) polymers and even Mylar®, Saran Wrap®, Scotchpak®, sandwich bags and football bladders have been used, whereas stainless steel, polypropylene valves, or hose clamps are responsible for controlling the entrance and withdrawal of gas from the bags [157]. Flexible chambers materials can also be laminated with other materials, normally aluminium, to seal pores and reduce wall permeability to the sample gases [157, 158]. Generally, materials of flexible chambers show a range of 1 to 20 mm in thickness and its construction should consider an inner layer impermeable to the sample gases and an outer layer impermeable to moisture [157].

Gags constructed for flexible chamber methods must be rolled as tightly as possible to reduce dead volume and should never be filled to completion to reduce wall permeation [157, 158]. Those bags can be filled slowly by adding gas contaminants either into a filling air stream or directly into the bag by a gas-tight syringe through a rubber patch of spectrum. Both gases and liquids can be metered into the bags but when dealing with liquids, its vaporization is required and direct injection into the

container walls must be avoided [157, 158]. A stopcock, pinch clamp or screw-type valve can be used to close the bag and opening, while mixing is normally conducting by kneading the bag for several minutes [157]. Time will slowly lead to the decay of the initial concentration towards zero and this rate of decay can be slower or faster for specific compounds especially during storage times [157, 158]. Sample losses are also influenced by material, nature of the contaminant, relative humidity, and radiation transparency. Sample decay can be reduced by preconditioning the container to the test substances, which requires flushing out the bag several times with the test material with at least six refills being required with at least one remaining inside the bad overnight. Still, in some cases, preconditioning may not show any considerable influence in the rate of decay of a contaminant [157, 158].

4.3.3 Dynamic Systems to Generate Standard Gas Mixtures

Dynamic methods offer a wider variety of methods than static methods for the generation standard gases and vapours, which inevitably translates into dynamic systems have numerous advantages over static methods. The dynamic methods are characterized by their ability to generate a continuous flow of mixture, especially in the case of reactive compounds which show limitation in their storage in static systems [157, 158]. Dynamic methods include evaporation, electrolytic, chemical, injection, diffusion and permeation methods from which permeation and diffusion methods take preference due to their refinement and convenience for both laboratory and field use [155, 157, 158].

Evaporation methods are used in both static and dynamic systems for the generation of standard gas mixtures or vapor atmospheres, however evaporation methods in static systems offer a limited range of volumes when compared with dynamic systems. This method is a prerequisite of injections system adding volatile liquids to gases in both containers and gas streams but is also an important method in dynamics systems [157, 158]. Evaporation methods for dynamic systems involve a diluent gas passing through or over a component that is intended to be vaporized and are frequently used to produce standard atmospheres with known humidity (7 to 98% relative humidity) or in the productions of anaesthetic mixtures in medicine [157, 158].

The important principle of this method is the evaporation rate, which can depend on depth of the column of liquid above the dispersion tube, type of glassware used to inject the gas in a liquid, and the cooling of the liquid happening during the evaporation process [157]. The former can be minimized using a reservoir to replenish the liquid, while the latter requires the system temperature to be controlled and kept constant. For instance, anaesthetic vaporizers used to deliver specific percentage levels of volatile anaesthetics are fabricated with a large copper block surrounding the evaporation chamber, since the high heat capacity and good thermal conductivity of copper ensures the liquid temperature is maintained constant [157]. While another approach used in some vaporizers relies on a bimetallic strip to control the flow of saturated vapor from the evaporation chamber [157].

However, for laboratory applications it is common to immerse the evaporation chamber in a controlled-temperature bath to provide a more precise control of temperature [157, 158]. The earliest example evaporation systems were used to produce moist air by bubbling dry air through a tower

containing distilled water at constant temperature which was later blended with dry air to produce concentrations by volume between 0.0019 and 2.9 % [157]. However, in static systems, constant humidity is achieved by extracting air above certain saturated aqueous solution at specific temperature in an enclosed container [157, 158].

The general *modus operandi* in dynamic systems is defined by allowing all or part of a gas stream to flow through a humidifier with certain saturated aqueous solutions [155, 157, 158]. Different solution can be recombined in a single gas flow is necessary to produce a specific desired humidity level. Mixtures of hydrogen chloride, hydrogen cyanide, benzene, toluene, bromine, hydrogen fluoride, nitric acid and monoethanolamine have been produced through the bubbling method of evaporation while other standard atmospheres of odorous components have been created by allowing a purge gas flow to pass over the component of interest [157, 158]. Errors associated with evaporation methods are minimal when dealing with low vapor pressure compounds since a reduced amount is evaporated thus minimizing dilution and temperature problems and allow accuracies between 5 and 15% [157]. This method of producing standard gas mixtures relies on the assumption that the evaporator flow is always saturated and such fact might not always prove true [157, 158]. However, dynamic evaporation methods can be useful for adding a single volatile compound into a gas stream or flow but should be analysed by an independent analytical method [157, 158].

Certain gases can be synthesized by using electrolytic or coulometric methods in the laboratory [157, 158]. This method is used frequently to generate a gas component of the atmosphere and was adapted from its utilization in analytical chemistry to electrodeposit metal ions from solutions because it can form gases in side-reactions [157]. A solution containing an electrolyte can be electrolyzed when enough potential is applied to two electrodes, arranged in a solution, allowing current to flow. Once the voltage across a solution is increased from zero and reaches a decomposition potential a gas is produced, where its amount from that point on is theoretically a linear function of the applied potential [157]. The selection of electrolytes allows the productions of specific gaseous species when four considerations are addressed: (i) absence of side reactions at the electrode of interest, commonly achieved by providing a pure and plentiful supply of electrolyte (ii) gases produced on the secondary electrode must be inert or diverted from the carrier gas stream to remove any interference, venting the unwanted gases produced in the reaction through one side of a U-shaped container, (ii) minimization of the time needed to reach equilibrium, normally conducted with electrodes in the shape of a thin vertical platinum wire hanging down with a glass bead fused to the tip, and (iv) produced concentration should be as smooth and constant as possible using a small electrode and at least a 45-V source, generating barely visible and continuously gas bubbles [157, 158]. Moreover, current provided into the system should never be lower than 10 μA because it creates irregular gas evolution [157].

Several types of gases can be produced with this method, including nitrogen, oxygen, ozone, nitric oxide, nitric dioxide, arsine, stibine, carbon dioxide and nitrogen in low concentrations with a simple switch [157, 158]. However, electrolytic methods require the construction of systems that might require work of first-rate glass blower and are also limited by the commercial availability of small electrolytic units, which is often scarce [157]. Besides, generation of a component as a function of the

current applied might become non-linear causing difficulties in establishing an accurate concentration estimation. Moreover, the aforementioned factors together a system complexity that can only produce a limited number and type of gases greatly hinder the use of electrolytic methods in standard gas generation particularly for volatile organic compounds and in the calibration of ion mobility spectrometry [156].

A similar method to the electrolytic generation of standard gases is through chemical reactions, where a controlled addition of a contaminant gas into a gas stream is conducted with a chemical reaction [157, 158] . Generally, this chemical method is used to continuously produce gases that are unstable, extremely reactive, commercially unavailable, or highly expensive but can be generated in small mounts in a controlled laboratory environment [157]. The systems and apparatus used for chemical methods are as diverse as possible chemical reactions, however most systems involve gas-liquid or gas-solid reaction systems [157, 158]. Two examples include bubbling nitric oxide (gas) through a solution of permanganate (liquid) to produce nitrogen dioxide and a system of gas-solid that uses dilute chlorine with sodium chlorite to produce chlorine dioxine [157].

Nevertheless, methods using chemical reaction may present several obstacles when compared with other dynamic systems since they require more complex systems due to using at least two reactants, a need have carefully regulated containers for reactions in the case of liquids, and might suffer from issues involved or related to chemical reactions [157, 158]. Hence when using chemical methods to generate standard gases it is crucial the reaction proceeds stoichiometrically to completion, the reactions products are formed in a quick time frame and the presence of additional unwanted products or undesired secondary reactions is inexistent, reduced, or controllable [157]. Again, this method is rarely used to generate standard gases for IMS since it uses complicated systems and requires a large background of chemistry and chemical reactions, which unnecessarily confuses and complicates a calibration method even hindering reproducibility [156].

The most useful and advantageous methods to generate standard gases or mixtures for IMS are among three types: (i) injection, (ii) diffusion, and (iii) permeations methods [155, 156, 157, 158]. Injection methods are a versatile approach to introduce gases and liquids into gas streams by using several injections devices (e.g., pumps, motor-driven syringes, pistons, mechanical dowsers, injectors, and chromatography pumps) [157, 158]. The earliest approach to creating standard gas mixtures with one or more components relied on a motor-driven syringe, and over decades, belt drivers geared mechanisms and syringes have remained a preferred method in many applications [157, 158].

Modern systems have improved in mechanics and automation which can generate gas mixtures with high accuracy and precision during long periods of time. Injection methods allow concentrations to be generated in the part-per-million (ppm) range and have been useful in generating standards for direct-reading instruments, detector tube and dosimeter evaluation, analytical calibration curves for laboratory gas analysers and even in the study of relatively slow chemical reactions, adsorption, and absorption measurements [155, 156, 158]. A general system for injection methods includes a pressure regulated diluent gas supply with a specific flow rate, an injection port where a gas or liquid is introduced through a pump or motor driven syringe or even a gravity feed mechanism, a vaporizer for

liquids, an optional cooling unit to remove or exchange unwanted heat from the vaporization process and a mixing chamber to remove and minimize surges on unevenly flows into the diluent gas [157, 158]. Furthermore, recent systems have an automated control unit present at the injection port to change feeding rates and provide thermostatic control for the vaporizer unit [156, 157, 158].

An early injection system known as Wosthoff gas dosing apparatus, performing sample injection through rotating PTFE valve, cemented the creation and current use of loops systems in both ion mobility spectrometer and mass spectrometers [158]. The Wosthoff gas dosing apparatus consists of feeding a trace component into a valve with a known volume which then rotates 90° to allow a purge gas to sweep it out of the valve and into a diluent flow going driven into a mixing chamber [158]. Through valve volume, rate of rotation and flow of diluent this system can control the dilution level with accuracy showing valuable and usefulness in gas analysers including ion mobility spectrometers [155, 156, 157, 158].

The last two methods, diffusion and permeations methods have some resemblances and are useful and quite simple approaches to produce standard gas mixtures with one or multiple contaminants [157, 158]. Diffusion tubes or cells rely on diffusion of vapour from a tube of accurately known dimensions to generate low concentration of gases. The operation of diffusions tubes or cells functions via evaporation of a liquid and slowly diffusing its vapor through a capillary tube into a gas flow [156, 157, 158]. With knowledge of the rate of diffusion of the vapor and the diluent gas flow rate it is possible to calculate the vapour concentration in the final gas mixture [157, 158]. Diffusion rates can be determined in two approaches, either by weighing the diffusion cell before and after a given time interval to establish the mass of vapor released or by monitoring the liquid meniscus position in the tube over a certain period of time [157, 158].

Equation (17) allows calculation of a diffusion rate through, S the rate of diffusion of vapor out of the capillary tube (g/s), the relative molecular mass of the vapor, M (g/mol), the pressure, P in the diffusion cell at the open end of the tube (atm), A, the cross-sectional area of the diffusion tube (cm^2), the diffusional coefficient D (cm^2/s), the molar gas constant R (ml atm/mol K), the absolute temperature of the diffusion tube T (K), the diffusion path length, L (cm) which corresponds to the distance between the liquid meniscus and the tube end, and p, the partial pressure of diffusion vapor in atm at temperature (T) [157]. Published diffusion coefficients (x) can be found in literature or estimated experimentally through the observation of the change in the liquid level in the capillary over a period of several days via equation (18), where ρ corresponds to the liquid density at a constant temperature T, allowing the diffusion rate to be calculated at a given instance via a simplified formula represented in equation (19) [157].

$$S = \frac{DMPA}{RTL} \times ln\left(\frac{P}{P-p}\right) \tag{17}$$

$$x = \left(\frac{2DMP}{RT\rho}\right) \times ln\left(\frac{P}{P-p}\right) \tag{18}$$

$$S = \frac{x\rho A}{2L} \quad (19)$$

Diffusion tubes are generally laboratory-made equipment with diverse designs, however, diffusion tubes or complete systems with specific, standard dimensions and rates are commercially available as kits or products [156, 157, 158]. However, generation standard gases with diffusion tubes, and permeation tubes both require precise temperature control, normally within ± 0.2 °C to maintain with 1% accuracy for accurate production of standard gas mixture [157, 158].

The use of diffusion tubes allows, in a simple arrangement, for generation of standard gases from almost any liquid, and commercial systems have even been developed with a chamber housing two or more diffusion tubes to create multi-component mixtures [157, 158]. In laboratory use nonetheless, liquids must never be mixed in a single diffusion tube because different evaporation rates can complicate estimations of diffusion rates and final concentrations from the standard gas mixture [157, 158].

Moreover, a diffusion tube system allows productions of standard gas mixtures in a large range of concentration by changing experimental parameters, e.g., diffusion path, diluent gas flowrate and bore of the capillary tube, and although changing tube temperature is an option it must be considered with knowledge that several hours might be required for stable evaporation of the liquid [157, 158]. Thus, changing the diffusion tube temperature should be avoided and normally the simplest parameter that can be adjusted is diffusion path length, which allows concentration equilibrium to be restored after 15- or 20-min [157]. Diffusion tubes have been used to generate gas standard mixtures of hydrocarbons for air pollution studies, trace amounts of water vapor, volatile anaesthetic agents, and a wide range of volatile organic liquids [157, 158].

Even though diffusion methods are simple and precise, their preference above permeations tubes is only observed when permeation tubes are not readily available commercially or when swelling or other adverse effects limit or prevent the use and preparation of permeation tubes. Hence, permeations tubes are regarded as the preferred and desirable method for the generation of standard gas mixtures for several analytical techniques and instruments.

Furthermore, permeation tubes due to their own operation principle allow precision and simplicity when generating extremely low concentrations of standard gas mixtures. Permeation tubes are the most used methods for the calibration of ion mobility spectrometry devices which can, depending on their type of permeation membrane thickness and material, temperature, and flow, provide concentration as low as ppb or ppt ranges, being further diluted if necessary [113].

Several similarities are shared between permeation and diffusion tubes especially the behaviour of tubes in response to temperature changes, which can require quite a long time to reach an equilibrium once the temperature is changed [156, 157, 158]. Like diffusion methods changing the temperature of permeation tubes to produce and generate different concentrations is strongly discouraged because the process of membrane permeation involved in permeation methods is slow and responds at a slow pace to temperature changes [156, 157, 158].

4.3.4 The suitability of permeation tubes for IMS calibration

Permeation methods are founded on the well-known phenomenon of permeation and represent one of the greatest methods to generate standard gas mixtures in ppm and ppb concentrations [155, 156, 157, 158]. This method involves a system centred in a permeation device of cylindrical shape or a tube, made of some type of polymer that contains a compound in liquid phase sealed inside [157, 158]. This chemical contained inside then dissolves in and permeates through the wall of the tube at a constant rate, at a specific temperature, mixes and is carried by a diluent gas flow [157, 158].

Generally, this method and system functions best with gases that can maintain a two-phase equilibrium inside the tube walls. Several compounds, including halocarbons, 2,4-toluenediisocyanate (TDI), benzene and tetrachloroethylene, benzene, and toluene, organo-isocyanates, sulphur dioxide, ethylene, vinyl chloride, hydrogen sulphide and several other volatile organic compounds have been used in permeations methods [156, 157, 158]. Permeation devices can be constructed and assembled in a laboratory environment or are available commercially in several formats, shapes and even as part of larger systems. Those systems can include kits with materials for an individual to build himself permeation tubes and even systems for generating standards gases from permeations devices with structures and systems to control temperature, humidity, and diluent gas flow [156, 157, 158, 159, 160]. Commercially available permeation devices are often accompanied by a certificate showing the permeation rate in pg/min or ng/min and even certify traceability to a standard reference material such as the National Bureau of Standards (NBS) [157, 158].

The use of permeation system is an elegant method for generation of standard gas mixtures and has been used for decades in preparation of primary standards for trace gas analysis since O'Keefe and Ortman first reported it in 1966 [157]. Further alterations and in-depth studies have resulted in its application in instrumental analysis, air pollution and even occupational hygiene work to monitor workers exposure to trace amounts of toxic gases and compounds [157, 158].

The permeation device

A device used for permeation methods is a polymeric tube sealing a liquid or gas compressed to the point of liquefaction, which dissolves into the tube walls and permeates them showing a constant rate at a specific value of temperature [157, 158, 161] . The gas-phase after permeating the tube walls is carried away from by a diluent gas flow into an analytical device. Permeation tubes can be made in the laboratory in a simple process involving sealing a liquid or pressurized gas in a tube through glass beads or stainless steel [157, 158]. However, more modernized approaches include inserting PTFE or other polymer rods into each end of tube and reinforcing them with ferrules to prevent any possible material leakage through the seals (Figure 4.6) [157, 158, 162]. Because leakage can result in a disrupted permeation rate when dealing with lab-made permeation tube is essential to guarantee a strong hold on the PTFE plugs to create quality tubes that show a steady and stable permeation rate [157, 158].

A wide range of commercially available permeation tube can be purchased, and some suppliers even offer the option to manufacture special tubes based on user needs and desires [156, 157, 158, 160]. A certificate always accompanies commercial permeation tubes, containing permeation rates,

substance characteristics, calibration temperature, tube material, dimensions and even the tube mass calibration graph showing details from their tube the construction and certification processes (Appendix I, Figure A.4) [157, 158, 160, 163]. Uncertainties are also presented with commercial permeations tubes which typically are between ±0.5% at 25 °C for NBS standards and never superior to ±1% at 20 or 30 °C [157, 158]. Furthermore, glass vials with permeable tops are also available commercially, offering lower permeation rates when comparing with normal tubes. Those instruments show how the use of different types of Teflon and wall thickness can influence permeation rates and allow different concentrations to be produced through the material aspects of permeations devices [157, 158].

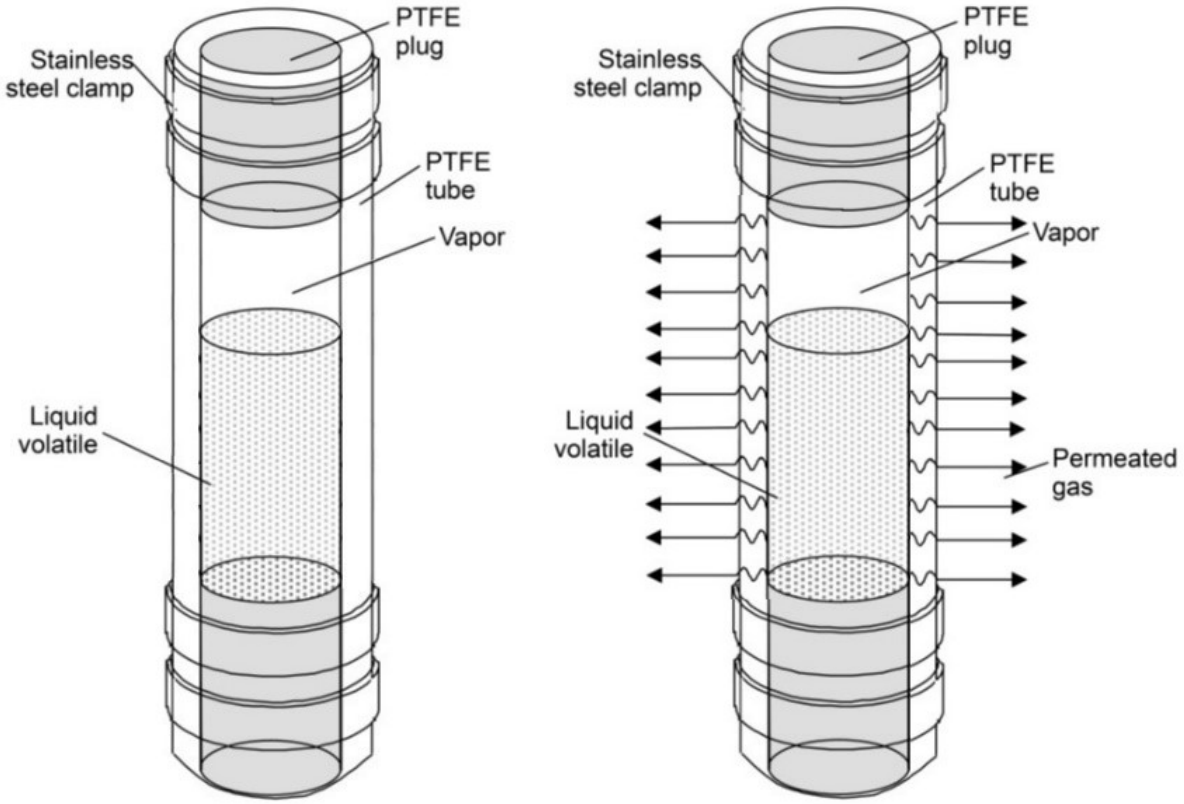

Figure 4.6 — A schematic showing a type of permeation device, the permeation process, and its elements [162].

The robustness and reduce attention needed to guarantee and maintained a precise calibration over their expected lifetimes is an advantage of permeation device, in comparation with other system for generating standard gases [156, 157, 158]. However, during handling any possible contamination of tube surfaces must be avoided using gloves while high humidity during storage is undesired [156, 157, 158]. Humidity can lead to undesired reactions occurring in the inside and walls of the device, whereas certain compounds might be a higher concern due to their reactivity or degradation in the presence of high-water content. Also, certain liquids might show oxygen reactivity and should be stored and used in an oxygen-free atmospheres. Those considerations are of course compound related and when calibrating a permeation device, the diluent gas flow, wall material, temperature and diluent gas must be selected with chemical knowledge of the selected compound properties [156, 157, 158].

A permeation device will always have a finite lifetime because of the continuous permeation process which depends on the volume contained inside the device, the mass of permeant and the permeation rate [156, 157, 158]. In practical terms a device lifetime is an important consideration and can be calculated by Lifetime = 3386 D/R, where R is the permeation rate per centimetre and D is the density of the liquid (g/mL) [157]. This equation assumes the device is kept during its lifetime at the temperature used for calibration, and although low-temperature storage can improve lifetime of permeation devices, extending it until several months, refrigerated storage can lead to invalid calibration and storage at room temperature is favoured [157, 158]. Generally, a permeation device is expected to have a lifetime between weeks or months but once more, it will be related to the material used and the liquid contained inside. Obviously prolonging a permeation tube lifetime also results in reduced permeations rates and can be useful to produce low concentration mixtures without high dilution flows [157, 158].

The permeation rate of any circular permeation tube can be estimated through an equation linked with material properties, dimensions, and temperature, equation (20) where q_s is the emission rate (standard $cm^3\ mm^{-1}$), T is the temperature (K), L is the tube length (cm), P_0 is the reference permeability coefficient of the tube-wall material ($cm^3\ s^{-1}\ cm^{-2}\ torr^{-1}\ cm$), E is the permeation activation energy to sample gas species of the tube-wall material ($cal\ mol^{-1}$), R is the universal gas constant (1.186 $cal\ mol^{-1}\ K^{-1}$), r_i is the internal radius of the tube (cm), r_0 is the outside radius of the tube (cm), $p_0$is the partial pressure of the sample gas inside the tube (torr) and p_i is the partial pressure of the sample gas outside the tube (torr) [157, 158].

$$q_s = 2\pi L P_0 \times \exp(-E/RT) \times \frac{p_i - p_0}{\ln(r_0/r_i)} \quad (20)$$

Permeation is therefore proportional to tube length and shows a logarithmical change with the inverse of the calibration temperature [157, 158]. The only variable that changes in operation is temperature however, it is usually the case with lab-made devices that various constants are not known *a priori*, making it difficult to calculate a desired permeation rate before building and calibrating a tube. To solve this, permeation rates can also be estimated gravimetrically immediately prior to tube calibration and will be addressed in a following section dedicated to the calibration procedure [157, 158].

The permeation system

Systems for preparing standard gas mixtures through permeation devices are often reliant on water-baths to control temperature and glass condensers to hold the permeation tube itself. However, those systems might be recommended and well suited for laboratory work they are somewhat bulky and fragile for field use. Several commercial calibration systems are available and those are more suited for filed but do not forgo its application for laboratory experiments and calibrations [157, 158]. Owlstone Calibration Gas Generator (OVG-4) is a clear example of a modern commercially available permeation system. The OVG-4 was built with two sections, an oven, and a flow control system [160]. Three PTFE permeation tubes with 6cm length and ¼" diameter can be placed inside the oven chamber while the temperature is digitally controlled from 30 to 100°C±0.1 °C in 0.1°C increments [160]. The

sample flow is also digitally controlled between 50 mL/min until 500 mL/min with 1 ml/min increments with an additionally split flow which is manually controlled by a needle value [160].

Any permeation system, be it made or purchased requires a precise temperature control of the tube chamber or container whereas the output concentration can be modified through adjustment in a purge flow gas that carries the emitted compound [157, 158]. A diluent flow after the purge gas flow can be implemented to dilute further the generated concentration. Hence permeation systems can provide a reliable and convenient source to generate standard gas mixtures with special benefits when mixtures are instable in static systems, including cylinders [157, 158].

Since temperature dictates permeation rate, permeation systems must control it with high precision and therefore, permeation systems are developed and constructed to control temperature within ±0.1°C to provide standard gas mixtures with reduced uncertainties during calibration [157]. Temperature control is so critical for permeation systems that holding a constant temperature is a preferable characteristic while mixture concentration is changed by a flowrate of a purge or diluent gas [157, 158]. However, when temperature changes might be necessary, the appropriate course of action is to allow the system a certain time interval for re-equilibrium of the permeation tube to be achieved [157]. Periods of time might include 24 hours for devices used after being stored at low temperatures while for smaller temperature changes 4-6 hours may be sufficient [157]. Of course, said time intervals must be established while accounting for the permeation device material considering its permeation properties and the difference between the boiling point of the compound contained inside the device and the selected temperature for calibration [157, 158]. Tubes produced from fluorinated ethylene propylene (FEP) Teflon, for example, have been described as reaching a plateau of 60-90% of the final equilibrium during the first 4 hours while the final equilibrium was reached only after 10-30h [157].

Moreover, permeation tubes can be used with the other mentioned methods for the generation of standard gas mixtures and have for example been used with chemical reactions systems and with exponential dilutions [157, 158]. The permeation systems offer simplicity, elegance, flexibility, and accuracy to produce standard gas mixtures with single or multiple compounds and have been widely used to calibrate new sampling and analytical devices to monitor personal exposure to toxic substances like sulphur dioxide, chlorine, and vinyl chloride [157]. The wide applications and success of permeations devices and systems can even be seen has a reason for the rapid development of continuous gas phase analysers in the last forty years since their characteristics and capabilities allowed the accurate calibration of low concentrations in a simple format, easily reproduced and even simply made in a laboratory [157, 158]. Permeation systems have even been included in reference methods of analysis for atmospheric emissions from industrial sources in the United States attesting to their usefulness and confidence for calibration purposes [157].

The calibration procedure

The use of permeation methods for generation of standard gas mixtures requires permeations devices and permeation systems, which are either commercially available or can be constructed or assembled in the laboratory [157, 158, 164]. Those are essential for the calibration procedure of any analytical instrumentation through permeation methods and although in commercially available devices

this procedure is simplified and steered with manuals and guides, self-constructed permeation devices require the user to, *a priori*, estimate the permeation rate [157, 158, 160, 164, 165].

The rate of gas permeating a tube can be calculated by equation (23), however when dealing with constructed tubes, it is best to determine the permeation rate gravimetrically [157, 158]. This method monitors over a period of hours or days the amount of mass lost by the tube, which has a direct correspondence with the device permeation rate and considered valid if visible amounts of liquid remain inside the tube [157, 158]. Nevertheless, gravimetric calibration of a permeation device can be a major explanation for errors in dynamic systems and should be conducted with a precision balance and with assurances of constant temperature and pressure of the device being calibrated [157, 158, 164, 165].

Alternatives to a gravimetry calibration, including coulometric methods or, by monitoring absolute pressure above a permeation dive, can be used, although those offer reduced calibration time, in exchange for complex systems with more parts, components and even reagents [157, 158]. Consequently, once a permeation rate for a permeation device is determined the concentration of a standard gas mixture produced can also be determined by equation (21) [157, 158, 164, 165].

$$C = \frac{\mathrm{P}\, M_v}{(R + r)M_r} \tag{21}$$

Where, C (ppm in v/v), is the concentration of the mixture produced, P (pg min^{-1}), the permeation rate at a given temperature, M_v, the molar volume, R (min/L), the flow-rate of the diluent gas, r (min/l), the flow-rate of the purge gas over the device and M_r, the relative molecular mass of the permanent are used [157, 158, 164, 165].

4.3.5 Calculation of Detection and Quantification Capabilities

Detection and quantification capabilities are highly important for the performance and characteristics of any chemical measurement process and essential for applications in research, international commerce, health, and safety. Analytical measurements support several aspects of science and society thus, any possible measurement or analysis needs to be accompanied of respective reliability. Furthermore, any analytical procedures need to address the demands of its intended purpose and provide the user with readily understood results that allow appropriate conclusions to be drawn [166, 167, 168].

The whole lot can be enabled through method validation, where a method can be demonstrated and validated to be fit and suitable for its intended purpose and allow any decision to be taken with confidence. Method validation is described as a process of defining an analytical requirement and confirming that the analytical method under consideration shows performance capabilities consistent with its intended application requirements [166, 167]. Although method validation is crucial for analytical processes knowledge of the exact requirements needed to validate a specific method are somewhat scarce and often confusing, because many of the technical terminology used varies between sectors of analytical measurements, both in their corresponding meaning and determination [166, 167, 168].

Through several more recent protocols and guidelines however, is possible to re-define method validation as a series of tests that prove any possible assumptions from an analytical method leading to establishing and documenting its performance characteristics in order to demonstrate the methods suitability for a specific analytical purpose [166, 167]. A list of performance characteristics of analytical methods includes applicability, selectivity or specificity, calibration, accuracy and recovery, precision, range, limit of quantification, limit of detection, sensitivity and ruggedness or robustness. The definitions of those characteristics can, however, differ between organizations resulting in confusion among analysts [166].

Method validation is furthermore incredibly valuable in allowing methodologies to be transferred between laboratories, which always involves a method being used by many people across the world and on instruments produced by different manufacturers and can cause a decrease in reproducibility and reliability [166]. Those problems can be solved by defining two parameters: limits of detection (LOD) and limits of quantification (LOQ) in which detection and quantification capabilities of any analytical instrument, including ion mobility spectrometers, can be interpreted, understood, and related to applications purposes [166, 168]. Limits of detection and quantification are also required parameters for the calibration of any analytical instrumentation and although the two parameters are related, they have distinct definitions and should not be confused [166, 167, 168].

The intention with both LOD and LOQ is to define the smallest concentration of analyte which can be detected without a guarantee about the bias or imprecision of the result from an analytical method and the concentration value at which quantitation, defined by bias and precision goal is feasible [166, 167]. Although several terms have been used to define limit of detection, typically it represents the lowest concentration of an analyte in a sample that can be detected but may not necessarily be quantifiable under the conditions stated for the analysis [166]. In contrast LOQ is defined as the lowest concentration of an analyte in a sample that can be determined with acceptable precision and accuracy under the conditions stated for the test [166, 167]. Importantly it is crucial to understand that an assay or test is uncapable of accurately measure an analyte concentration down to zero since a sufficient concentration must be present to create an analytical signal which can reliably be distinguished from any signal produced in the analyte absence, also called "noise" [166].

Several methods exist for the estimation of both limits of detection and quantitation limits and several regulatory authorities including the United States Pharmacopoeia (USP), Foods and Drugs Administration (FDA), International Union of Pure and Applied Chemistry (IUPAC), International Conference on Harmonisation (ICH) and Association of Analytical Communities (AOAC) have their own preferred method for both LOD and LOQ [166, 167]. Common methods for LOD and LOQ can be categorized in three groups: (i) Visual definition; (ii) based on signal-to-noise (S/N) ratio and (iii) based on standard deviation of response and slope (Figure 4.7 and Figure 4.8). [166]

The determination of LOD and LOQ based on S/N ratio should only be applied to analysis where a base line noise is present and often classifies the detection limit (DL) and quantitation limit (QL) as 3 and 10 times the noise level, respectively [166, 167]. While methods based on standard deviation of response and slope include a calculation from the standard deviation of the blank, a calculation from

the calibration line at low concentrations from $DL\ or\ QL\ = (F \times SD)/b$, where F is a factor of 3.3 and 10 for DL and QL, respectively, SD is the standard deviation of the blank, standard deviation of the ordinate intercept, or residual standard deviation of the linear regression and b represents the regression line slope [166]. Furthermore, estimated limits should be substantiated by the analysis of an adequate number of samples with the corresponding analyte concentration obtained for the LOD and LOQ [166, 167].

Guidelines	ICH	US FDA	AOAC	USP	IUPAC
Definition	Lowest amount of analyte in the sample, which can be detected but not necessarily quantitated under stated experimental conditions	Explicitly not described	Lowest content that can be measured with reasonable statistical certainty	Lowest amount of analyte in the sample, which can be detected but not necessarily quantitated under stated experimental conditions.	Smallest amount of conc. of analyte in the sample that can be reliably distinguished from zero.
Method	1. By visual evaluation 2. Based on S/N ratio Applicable to procedure, which exhibits base line noise Low conc. of analyte is compared with blank 3. Based on S.D. of response and slope LOQ = $3.3\sigma/s$ s – Slope of calibration curve σ – S.D. of response; can be obtained by Standard deviation of blank response Residual standard deviation of the regression line Standard deviation of the y-intercept of the regression line $S_{y/x}$ i.e. standard error of estimate	Not described	Based on more than 20 blank readings	For non-instrumental: Analysis of sample with known concentration of analyte and by establishing minimum concentration at which analyte can be reliably detected. For instrumental: Process for non-instrumental can be adopted. Detection limit should be sufficiently low for analysis of samples with known concentration of analyte above and below the required detection limit	Not specified
Expression/ calculation	If based on visual examination or S/N ratio - relevant chromatogram is to be presented If by calculation/extrapolation estimate is validated by analysis of suitable no. of samples known to be near or prepared at detection limit	Not specified	The mean value of the matrix blank readings ($n \geq 20$) plus three standard deviations of the mean, expressed in analyte concentration	Not specified	Not specified
Acceptance criteria	S/N ratio > 2–3; not specified in other cases	Not specified	Not specified	Not specified	Not specified

ICH – International Conference on Harmonisation, US FDA – United states food and drug administration; AOAC – Association of Analytical Communities; USP – United States Pharmacopoeia; IUPAC – International Union of Pure and Applied Chemistry

Figure 4.7 — Definitions and guidelines to estimate the limit of detection in analytical method validation [166].

The signal-to-noise approach is generally used to measure noise around an analyte retention time and estimate the concentration of analyte that would yield a signal equal to a specific value of S/N ratio [166, 167]. Noise can be measured both manually, on a chromatogram or by auto integrators, often present in instruments. Accepted signal-to-noise ratios are generally values of 3 for calculating LOD and 10 for LOQ (Figure 4.9) [166]. A test sample with the analyte at the preferred concentration level is required to determine signal-to-noise ratios from S/D = 2H/h, where h corresponds peak-to-peak background noise in a chromatogram over a time equivalent to 20 times the peak width at half-height of the analyte, and H is the height of the analyte peak from the top to the extrapolated baseline [166].

It is important to know this approach requires the system to be free from significant baseline drift or shifts and only works for peak height measurements, which sincerely limits its applicability [166, 167].

Guidelines	ICH	US FDA	AOAC	USP	IUPAC
Definition	Lowest amount of analyte in a sample, which can be quantitatively determined with suitable precision and accuracy.	The lowest amount of analyte that can be quantitatively determined with suitable precision and accuracy also called LLOQ (Lower limit of quantification).	The limit of quantitation is the lowest amount of analyte in a sample, which can be quantitatively determined with precision and accuracy appropriate to analyte and matrix considered	Lowest amount of analyte in a sample, which can be quantitatively determined with suitable precision and accuracy	Not defined
Method	1. By visual evaluation 2. Based on S/N ratio Applicable to procedure, which exhibits base line noise. Low conc. of analyte is compared with blank 3. Based on S.D. of response and slope LOQ = $10\sigma/s$ s – Slope of calibration curve σ – S.D. of response; can be obtained by Standard deviation of blank response Residual standard deviation of the regression line Standard deviation of the y-intercept of the regression line $S_{y/x}$, i.e. standard error of estimate	Preparation of standard curve and lowest conc. on the calibration curve should be accepted as LLOQ if it satisfies following condition. Response at LLOQ = 5 × Response by blank Analyte peak should be identifiable discrete and reproducible with precision of 20% and accuracy of 80%–120%	Not specified	1. By visual evaluation 2. Based on S/N ratio Applicable to procedure, which exhibits base line noise. Low concentration of analyte is compared with blank 3. Based on S.D. of response and slope LOQ = $10\sigma/s$ s – Slope of calibration curve σ – S.D. of response; can be obtained by Standard deviation of blank response Residual standard deviation of the regression line Standard deviation of the y-intercept of the regression line $S_{y/x}$, i.e. standard error of estimate	Not recommended; only recommends expressing uncertainty of measurement as function of concentration
Recommendation	Limit should be validated by analysis of suitable no. of samples known to be near or prepared at quantitation limit.	Not specified	Not specified	Not specified	Not specified
Expression/ calculation	Limits of quantitation and method used for determining should be presented. Expressed as analyte concentration	Not specified	Mean value of the matrix blank reading plus 10 standard deviations of the mean, expressed in analyte concentration.	Expressed as analyte concentration (% or ppb)	Not specified
Acceptance criteria	Not specified	Not specified	Not specified	Not specified	Not specified

ICH – International Conference on Harmonisation, US FDA – United states food and drug administration; AOAC – Association of Analytical Communities; USP – United States Pharmacopoeia; IUPAC – International Union of Pure and Applied Chemistry

Figure 4.8 — Definitions and guidelines to calculate limit of quantification in analytical method validation [166].

The blank determination approach is used when blank analysis gives results with nonzero standard deviation [166, 167]. This approach interprets the consequences of any blank signal being always characterized by a certain signal intensity and therefore, two cases are possible: (i) it is probable an analyte could be detected when in fact its intensity corresponds only to a blank signal (false positive) or background noise, or (ii) an analyte can be assumed as not detected when it is in fact present (false negative) [166].

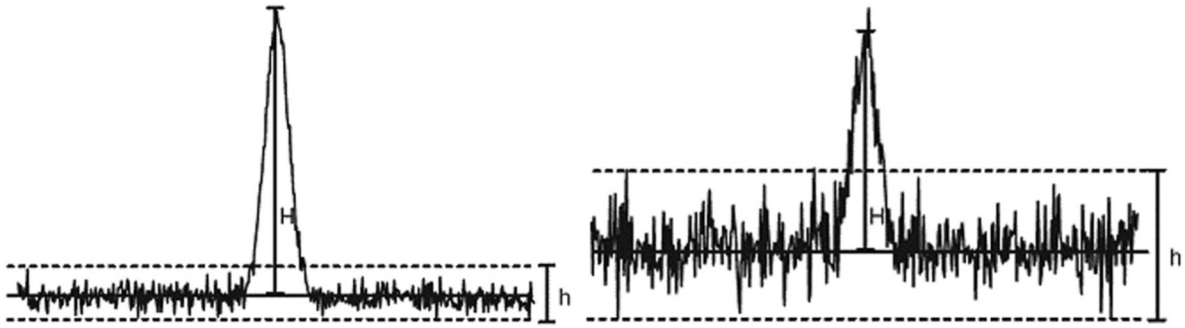

Figure 4.9 — Signal-to-noise examples of an analyte peak of 10:1 ratio (left) and 3:1 ratio (right).

Thus, a limit of detection, LOD with this approach is defined as the analyte concentration with correspondence to a sample blank value plus three standard deviation, $LOD = x_B + 3\sigma_B$ where x_B is the mean concentration of a minimum of 10 blank samples and σ_B is the standard deviation of the blank measurements [166, 167]. While the limit of quantification, LOQ is described as the analyte concentration equal to the sample blank value plus 10 times the standard deviation, $LOD = x_B + 10\sigma_B$ [166]. This approach shows a limitation since there might not be evidence proving low analyte concentration will produce a signal distinguishable from a blank signal (zero concentration) [166, 167].

The Linear regression approach assumes a response of y is linearly related to the standard concentration x, in a limited range of concentrations and therefore can be expressed as $y = a + bx$ [166]. Using this expression and model sensitivity, b and both LOD and LOQ can be obtained whereas LOD is expressed as, $LOD = 3S/b$, and LOQ as, $LOQ = 10S/b$, with S corresponding to the standard deviation of the response and b the slope of the calibration curve [166, 167]. Standard deviation can be calculated by the standard deviation of either y-residuals or y-intercepts of a regression line and a linear regression approach can be applied in any situation, as long has, a linear response is observed, for examples this approach is regularly applied when the analysis method shows an absence of background noise [166, 167].

4.4 Ion Mobility Spectrometry: Experimental Parameters & Data

IMS instrument components, from sample inlet, ion source, ion injector, drift tube type and length, detector characteristics to drift gas flow, play a significant influence in performance and data, and although easily controlled in research instruments, in commercial instruments such components are regularly pre-determined [97, 112]. Besides, instrumentation components, several experimental parameters, including drift gas composition (chemical and humidity), drift gas temperature and pressure, electrical field strength, and changes in the identity of the reactant ions, be it intentionally or unintentionally, significantly affect ion mobility measurements and resulting data [97, 112].

In principle all parameters mentioned are controllable in laboratory or research instruments while temperature and drift gas moisture maybe be controlled in commercial instrument. Perhaps drift gas is the most pertinent experimental parameter since it can dramatically affect separation, where flow

and composition can be optimized for enhanced resolution [112]. Most common drift gases include nitrogen (N_2), purified air (O_2), and combinations of nitrogen and helium (N_2/He) [97, 112].

4.4.1 Effects of Experimental parameters

Drift/Carrier Gas Composition

Drift gas composition leads to variations in ion mobility which can be described by Blanc's law for each ion at a low field in a gas mixture by equation (22), where $K_{máx}$represents the ion mobility in a gas mixture, x_i the abundance of a gas and K_i the mobility in the individual gas [112].

$$\frac{1}{\mathrm{K_{mix}}} = \sum_i \frac{x_i}{K_i} \tag{22}$$

Specific analytical effects produced by changing drift gas composition were first exploited in 1987 by adding trace amounts of ammonia to a carrier gas, nitrogen, in the selective ionization of amines [97, 112]. Afterwards, acetone was used for the selective detection of chemical warfare agents and carbon tetrachloride for the selective detection of explosives [111]. While a combination of acetone and dimethylsulfoxide has been used to selectively detect mixtures of VOCs and organophosphorus compounds. Also, a blend of water, acetone, dimethylsulfoxide was utilized to create specific ionization of indoor ambient atmospheres for the detection of volatile organic compounds [112].

Furthermore, drift gas composition also influences IMS resolution through selective ion–molecule clustering reactions, including the use of hydrogen as a dopant in planar-FAIMS allowing its use in hydrogen-rich planetary atmospheres (e.g., approximately 87 and 96% for Jupiter and Saturn) [112].

In a nutshell, the purpose of using dopant gases, adding trace amounts of a gas to the drift gas, is to reduce ionization interference and selectively ionize specific sample compounds. Dopant gases can be added directly to the ionization region or to the drift region, in the latter case mobilities are modified through dynamic ion–molecule interactions as they drift through the gas [97, 112].

Low-field Strength Effects

The influence of an electrical field, E, of low strength on the movement of ions in a drift region, can be simplified by ions being accelerated via coulombic forces and slowed by collision with neutral gas molecules. However, other factors, such as diffusion loss and space charge effects, might influence the mobility of ions through their transverse of a drift region and lead to ion neutralization hindering detection [97, 112].

Diffusion loss happens through random interactions of ions with neutral gas flow molecules and is a major mechanism responsible for ion neutralization because ions can reach an electrode surface and be neutralized [112]. Both magnitudes of drift times and drift tube effective gap height are important in diffusion loss. As drift time is decreased, sensitivity will be improved, while reduction of the effective gap height will markedly increase diffusion loss [97, 112]. Therefore, selection of the electric field strength, drift tube length, height, and maximum and minimum flow rates are crucial to create optimal conditions to reduce diffusion loss and increase ion detectability. In essence, diffusion loss is

controlled by drift tube length, the filtering region geometry, electric field strength and neutral gas flow rates [112].

Additionally, due to smaller analytical volumes and improvements in ionization efficiencies another phenomenon which might reduce ion detectability is the space charge effect. This effect is marked by ion-ion repulsion that acts to expand the radial dimensions of ion clouds and thus lead to ion clouds interacting with the electrodes. This interaction between ion clouds and electrodes leads to a decrease in ion density over time. In traditional IMS, however, space charge effects are normally reduced and overcome by the effect of thermal diffusion. Space charge effect is also manageable by drift tube dimensions, via both height and length, flow rates and even ionization control with ion shutter opening intervals [97, 112].

High-field strength effects

In ion mobility spectrometry with high-field strengths, interactions between ions and neutral molecules can influence ion velocity, drift time and, thus, ion mobility [97, 112]. High electric fields can potentially have enough energy to change molecular conformation and dipole moments of species, which can both influence ion velocity and create influences in detectability [112]. Moreover, ions moving through a carrier gas can induce a dipole in neutral gas molecules and the resulting ion-dipole interaction can also lead to velocity changes.

Therefore, selecting and defining an electrical field strength should be made with knowledge of those possible electrostatic interactions and their influence in detection and changes to drift times [112]. For FAIMS, a method relying in a high and low asymmetric waveform, both waveform frequency and shape are parameters of great importance for detection. Waveform frequency and shape directly influence ion interactions with the high-field portion of the electric field. Although frequency has been shown to have no effect on ion separation, it directly changes peak intensity, where ion intensity is lower at reduced frequencies and increases as frequencies of higher values are applied [112]. On the other hand, waveform shapes influence ion separation efficiency, with rectangular waveforms showing better results out the two other waveform types: bisinusoidal (referred to as two harmonics) and clipped-sinusoidal (or half sinusoidal) waveforms [112].

Rectangular waveforms have analytically been shown to improve ion separation efficiency, resolution, and/or sensitivity as compared to sinusoidal waveforms, however, electronical devices capable of delivering rectangular pulses for differential ion mobility separations have been scarce due to their necessity of imposing an excessive power load in the system [112].

Humidity, temperature, and pressure effects

Temperature and humidity are the two most valuable parameters in the performance of ion mobility. Although their importance is so big it can hardly be overemphasized, mobility spectrometers remarkably can operate well in a wide range of humidity levels and temperature ranges [112]. However, if both parameters are uncontrolled, responses and reproducibility of results will be difficult to understand and complicate comparisons between laboratories. Such complications arise because the level of confidence for mobility constant values will be hugely affected [112, 169].

Drift time is affected by both temperature and pressure, although pressure creates a linear change in drift times, the same is not observed for temperature causing non-linear change. Both effects of pressure and temperature have an explanation on their influence in clustering reactions, changing collision frequency through their impact in neutral density [112, 169]. The difference between temperature and pressure occurs because temperature can change ion identity by influencing clustering equilibrium and lead to a non-linear behaviour [97, 112].

Humidity levels can have an impact on compound drift time in stand-alone IMS, a study conducted with an UV-IMS revealed drift times increase with increasing water amount in the sample carrier gas. Under those conditions even the formation of dimers is changed, which was only observed in dry conditions (Figure 4.10) [112]. In another study, a stand-alone IMS with a tritium ionization source produced stable drift time values throughout a humidity variation of 0 to 2000 ppm. Drift times remained constant in this range, however, peak intensity was strongly affected by humidity [169].

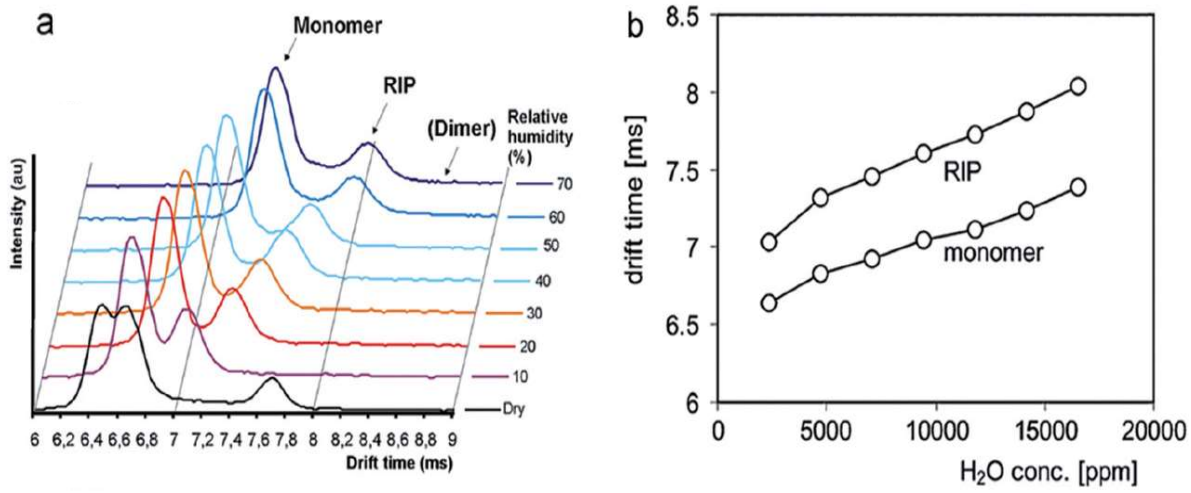

Figure 4.10 — Humidity effects studied from a single compound, TMA, in a UV-IMS instrument. (a) TMA Spectra at a constant concentration (220 ppb) for measures with varying humidity percentage and (b) the humidity and drift time relationship for reactive ion peaks (RIP) and the TMA monomer in an UV-IMS device [112].

Specifically, the nature of ions formed by chemical ionization with ^{3}H in atmospheric conditions was independent of humidity while the relative abundance of product ions is influenced by humidity and depends on the properties of the analysed compounds [112, 169].

Product ions abundance is related to hydration reactions and consequently with ion clusters formations through a dependence on the number of water molecules, n, which change with different carrier gas moisture (Figure 4.11 right) [112, 169]. A study showed amines were comparatively unaffected by humidity whilst chlorinated compounds, toluenes, and ketones exhibited significant decreases in peak intensity with humidity increases (Figure 4.11 left) [169]. Herein, the importance and effectiveness of using gas chromatography becomes evident, since it allows the removal of limitations and setbacks associated with high humidity sample (e.g., exhaled breath or VOCs from food products).

In respect to temperature and pressure effects in ion separation, both are explained and described by the dependence of ion mobility on the gas number density [112]. Gas number density, n/V, is defined

as an intensive quantity used to describe the concentration level of countable objects in physical space with examples including three-dimensional volumetric number density, two-dimensional areal number density, or one-dimensional linear number density.

Pressure and temperature relationships with gas number density involve number density and show an inverse behaviour. Increasing temperature leads to a n/V decrease, consequently increasing the gas number density. While pressure increases create an increase in $_n/V$ that reduces the effective gas number density [112, 169, 170]. Therefore, optimal conditions for ion detections require constant temperature and pressure [112].

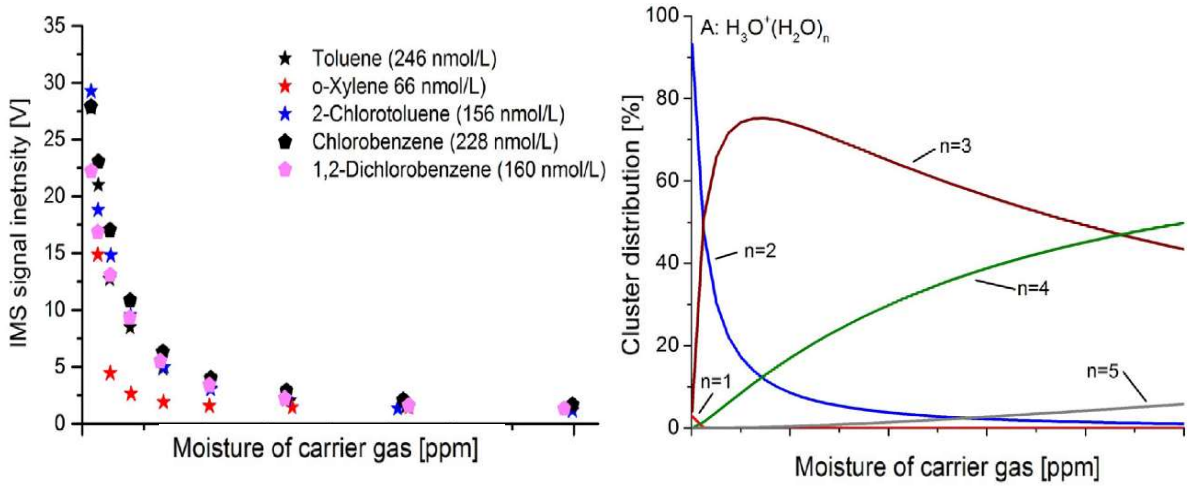

Figure 4.11 — The effect of humidity on the peak intensity of several compounds (left) and the formation of production ion by chemical ionization with ^3H in a stand-alone IMS (right). IMS signal intensities of toluenes and chlorobenzenes over the carrier gas moisture level (left). The relationship between reactant ions composition and carrier gas moisture at a constant temperature of 80◦C (right) [169].

Furthermore, experimental observations have shown drift times are related to temperature in a non-linear behaviour. Much like in humidity effects, this non-linear behaviour is explained due to differences in clustering and hydration, since high temperatures induce a lower degree of clustering by causing neutral gas molecules to detach from ions [112, 169].

Likewise, temperature affects the formation of positive fragment ions which can influence ions stability and impact detection [112, 169, 170]. Temperature effects, due to their relationship with clustering, can vary between functional groups, hence ion mobility measurement at both low and high temperature can improve identification of different compounds from chemical classes [112, 169, 170]. Elevated temperatures, also cause an increase in resolving power which can improve peak separation and compound indentation because of the temperature ability to reduce hydration and clustering effects [112].

In contrast, separation factors are unaffected by pressure since the ion peaks shift is perfect when pressure values are changed but resolving power and resolution are reduced at low pressures (29 Torr to atmospheric pressure) [171]. Low pressures can therefore cause problems when analysing IMS spectra by deforming or overlapping peaks [112, 171].

4.4.2 Generalized Aspects of IMS Data Analysis

Ion mobility measurements produce spectra that include information from the velocity of gaseous ions under the influence of an electrical field and respective signal intensity [97, 112]. Ion velocity is expressed as an arrival time, referred to as drift time (ms) which is regularly normalized to standard temperature and pressure as reduced ion mobility (K_0) or as its inverse reduced ion mobility ($1/K_0$) [97, 112, 172]. All three values are a consequence of ion size, shape, charge, and weight (m/z) [97, 112]. A collision cross-section (CCS) value, a size parameter related to the shape of a molecule can also be expressed, however its frequency is more present in IMS-MS systems and measurements [97, 112, 172]. As ions exist the drift region into a detector, signal peaks are created allowing qualitative information to be created. Drift time, or ions position in spectra, depend on instrumentation types and hardware properties, but ion mobility can always be calculated [97, 112, 172]. However, this relationship between ion mobility and qualitative information is often complex and not well understood yet [172].

A conventional drift time IMS creates data in current versus drift time formant, while GC-IMS data is a function of drift time and retention time intensity often represented in a colour code scheme [112, 172]. A characteristic property of IMS data is the presence of a peak called reactive ion peak (RIP) detected at all retention times when coupled with GC. The RIP is produced by the detection of reactant ions from the ionization of drift gas neutral molecules and is used for analyte ionization in processes of charge transfer [97, 112, 172].

The amount and chemical properties of analytes, such as proton affinity have a direct effect on RIP intensity, which can fluctuate from an intense peak to a signal intensity gap when analytes completely deplete the RIP [172]. Furthermore, analyte concentrations and properties can also create protonated dimers and even trimer ions, however such processes currently lack complete predictability and understanding [97, 112, 172]. So, analyte concentration is expressed as signal intensity from the detector plate in voltage or arbitrary units. This allows quantitative analysis, and thus IMS data provides both the possibility for qualitative (drift time) and quantitative analysis (intensity) [112, 172].

Despite IMS chemical processes lacking a completely understanding, experimental determination of retention times and drift times, or ion mobilities, of VOCs allows databases to be built and used in future analysis of different samples or mixtures [112, 172]. Databases for lipids, peptides and proteins are already publicly available, or available with commercial software, where a collection of chemical compounds and their ion mobilities are included [172].

Thus, peak characteristics are extremely important for both qualitative and quantitative analysis, especially because separation in IMS devices depends on both peak width and position. Peak location is determined by the ions drift time, while peak width is a complex function of the introduction method, diffusion, homogeneity of the electric field, and the engineering of the drift tube [172]. Those factors are vital for peak quality and shape, considered to be a normal Gaussian curve, and influence peak characterization, compound identification and quantification (Figure 4.12) [112, 172].

Peak quality is described better through its aspect ratio, AR, defined as peak height *h* to the width at the base w_b by AR = h/w_d. Hence a peak is easier to distinguish from its neighbouring peak by how tall and narrow it is, but this only allows a comparison if peak appearance is assumed to remaining equal in shape throughout drift times [172]. Resolving power, however, provides more accurate and precise information for comparing peaks because it provides a convenient method to compare the relative ability of an IMS devices to separate closely spaced peaks [172]. Although resolving power is calculated using a single peak, an additional parameter, resolution, R, that uses a direct peak-to-peak separation measurement between two peaks can be utilized. The resolving power allows instrument performance to be compared between laboratories and is defined by equation (23), where t_d is the a peak drift time, and FWHM or $w_{1/2}$ is the Full Width at Half of the Maximum of the peak of interest in the IMS spectrum (Figure 4.12) [172].

$$R_p = \frac{t_d}{FWHM} = \frac{t_d}{w_{1/2}} \tag{23}$$

Peak-to-peak separation, however, is better evaluated through resolution, R, defined by equation (24), in which t_A and t_B are drift times of the ions of interest, and $w_{b,A}$ and $w_{b,B}$ are the peak widths (sec) at the peak base, respectively [172]. Using this equation, the relative ability of an IMS to separate close peaks can be compared. Equation (24) also displays resolution is limited to ion diffusion because peak broadening is a consequence of the diffusion of ions during drift time travel.

$$\mathrm{R} = 2 \times \frac{|t_A - t_B|}{w_{b,A} + w_{b,B}} \tag{24}$$

However, peak broadening can also be a consequence of the initial pulse width and shape; coulomb repulsion; capacitive coupling between approaching ions and the collector plate; field gradient uniformity, temperature gradient; gate depletion/dynamic leakage; pressure fluctuations; and ion–molecule reaction in the drift space [112, 172].

Three other parameters important in IMS spectra and data processing are the limit of detection (LOD), limit of quantification (LOQ) and signal-to-noise ratio (S/N). Although all parameters are related to each other, a clear distinction must be made between LOD and LOQ [172, 166, 167].

The International Conference of Harmonisation (ICH) defines the LOD of an analytical procedure as the lowest amount of analyte in a sample which can be detected but not necessarily quantitated as an exact value, and, LOQ as the lowest amount of analyte in a sample which can be quantitatively determined with suitable precision and accuracy [172, 166, 167]. The determination of LOD and LOQ can be done in three types of approaches: (i) visual evaluation, (ii) based on signal-to-noise and (iii) based on the slope and standard deviation of a response [172]. A visual evaluation can be used for in non-instrumental and instrumental methods by evaluation samples with known concentrations of an analyte and establishing a minimum level that the analyte can reliably be detected [172, 166, 167].

Approaches based on signal-to-noise are only applied to analytical procedures that exhibit baseline noise [172]. Determination of LODs in this approach is done by comparing measured signals from samples with known low concentration of an analyte and blank samples [172, 167]. Through the blank measurements a signal-to-noise ratio is extracted and used to estimate the respective analyte

concentration that values would yield. Generally, a signal-to-noise ratio of three is accepted in the estimation of LODs while a ratio of ten is frequently used for the LOQs. Lastly, signal-to-noise ratio, S/N, is estimated by dividing two times the peak height by the peak-to-peak background noise (2H/h) (Figure 4.12) [172].

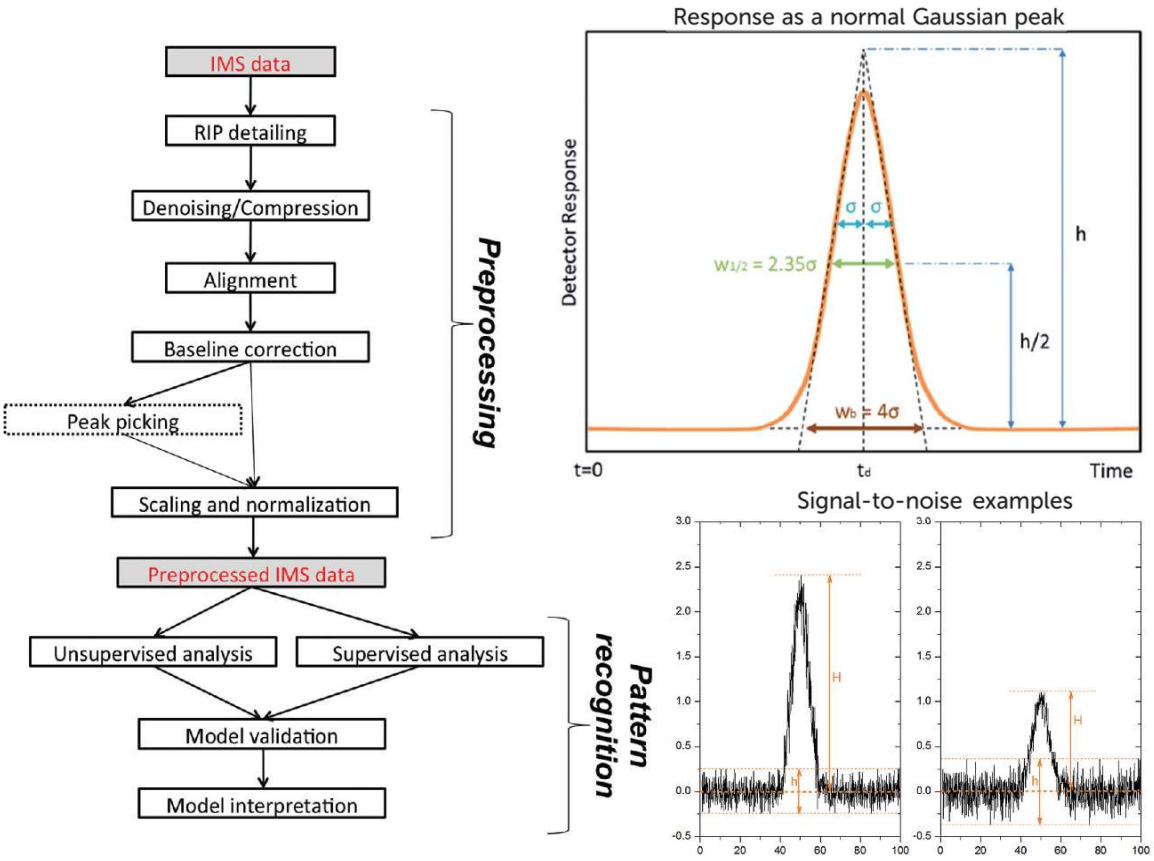

Figure 4.12 — General scheme of IMS data analysis workflow, IMS peak response as a normal Gaussian curve and signal-to-noise examples of 10:1 for estimating LOQ and 3:1 for estimating LOD [172].

The last approach for estimating LOD and LOQ is based on the standard deviation (σ) of the response and slope (S) using the interchangeable relationships in equation (25) [172, 167]. A specific calibration curve using samples of different analyte concentrations must be used for this approach.

$$\mathrm{LOD} = \frac{10\sigma}{3S} \qquad \mathrm{LOQ} = \frac{10\sigma}{S} \qquad \mathrm{LOQ} = 3 \times \mathrm{LOD} \tag{25}$$

Through a regression line of a calibration curve the slope value can be extracted and the calculation of the standard deviation or the y-intercept obtained [172]. Moreover, the standard deviation, σ can be calculated by measuring the magnitude of analytical background response in several blank samples, normally a value of ten samples is considered adequate (equation (25)) [172, 167].

4.4.3 Chemometric & IMS Data Analysis Methods

The evolution of IMS in the last two decades has made it a powerful technique for the detection, at ambient temperatures, of gas samples in lower concentration, ng/L (ppb_v) mainly due to its speed, easy coupling with pre-separation and gas detection method, improved selectivity and potential for miniaturization and portability [97, 112]. However, variation in measured signals between instruments has been a recurrent constraint for IMS developments and research [112].

Extremely low levels of detection can be attained in IMS through comparatively simple and robust instrumentation, without the hurdles of high-vacuum technologies, but IMS data shows challenges from differences in raw signals which eventually require data processing [112, 172]. IMS data is generally high-density and as complex as its system, coupled systems, or its type of sample, and chemometrics, a scientific field for extracting information from chemical system with statistical and other data-driven tool or approaches, is used to process, analyse, and recognize patterns for several applications [112, 172]. Although IMS measurements provide ion drift times, allowing the calculation of ion mobility and collision cross section that led to compound identification and quantification, data analysis is not a simple procedure, since datasets can have different complexities and data analysis can be divided into targeted and non-targeted analysis [172]. Data complexity is a consequence of IMS being coupled with several other techniques, (e.g., gas chromatography and mass spectrometry), sample complexity and signal behaviour [112, 172].

Data from coupling requires the resolution for each separation technique to be retained as analytes pass to subsequent dimensions, which has been solved by increasing sampling frequency as a sample passes from one technique to another. This creates multiple measurements in a subsequent technique within the time frame of a measurement from the previous system. Such strategy is clearly visible in GC-IMS instruments where the analytical timescale of IMS, 10 ms, is much faster than a chromatographic times scale of approximately 1200 seconds [172].

Multidimensional coupling is generally used to increase separation power for complex scientific fields, such as exhaled breath analysis and proteomic, however it also increases the amount of information, retention time and drift time, of analytes per analysis [112, 172]. Data complexity increases with coupling from one dimension (stand-alone IMS) to up to 5 dimensions, with recent systems, which challenges data science and chemometric to infer specific and desired information from system-wide data [172].

A generalized chemometric approach for ion mobility spectral data, applicable for one dimensional or multidimensional IMS can be divided into two stages: (i) pre-processing and (ii) pattern recognition (Figure 4.12) [172]. Pre-processing relates to several approaches to gather, filter, and simplify data, while pattern recognition includes methods to create descriptive models and interpret data. However, it is crucial to understand the selection of appropriate chemometric techniques for IMS pre-processing are dependent on data dimension (1D, 2D, or 3D) while for pattern recognition most methods can be use independently of data dimension [172].

Moreover, the goal and scope of data analysis are also critical in data analysis and influence the selection of chemometric method. Generally, methods can be grouped into targeted analyte analysis and non-targeted analyte analysis, with the former involving analysis for identification or quantification of a selected a target group of analytes, and the latter aims to analyse comprehensively as many sample components as possible without any previous selection [172].

1-Dimension IMS data pre-processing

After any IMS measurements data might be pre-processed to deal with problems such as the presence of interferences or when analytes have a similar ion mobility and environmental changes of peak positions. Both problems can complicate analyte identification and quantification [172]. Usually, data pre-processing is the most time-consuming step of data analysis and can mean the difference between accurate identification/quantification or failure to obtain relevant information from spectra [112, 172]. Target and non-targeted analysis are involved and require different pre-processing methods due to their goals [172].

During targeted analysis one of the first steps includes feature extraction and is commonly used to get important information from more than 1300 data points (1-D). such as isolation of intensity and drift time of select analytes to reduce excess number of data points. Peak deconvolution techniques, mixture analysis and calibration techniques are some of the chemometric techniques used for feature extraction.

Mixture analysis methods can include simple to use interactive self-modelling mixture analysis (SIMPLISMA) or multivariate curve resolution (MCR) with alternating least squares (ALS) for multiple IMS spectra collected over time or different samples [172]. SIMPLISMA functions by locating pure variables, spectra points where a solo analyte peak is present showing a constant level of interference and estimates concentration of the target analytes. Multivariable curve resolution is another method used to deal with interferences and estimate intensities by modulating IMS spectra as a product of concentration profiles of analytes and a matrix of their spectra. For calibration methods implemented in feature extraction, Partial Least Squares (PLS) regression, non-linear PLS neural networks (NN) and Tucker 3 models are commonly used approaches [112, 172].

Data compressing, a feature transformation technique is an alternative to the previous feature extraction approaches. Wavelet transformation is a commonly used method and can be understood as a mathematical transformation for hierarchically decomposing signals [172]. This method is the most common compressing and denoising method applied to IMS since it is extremely suitable for IMS data, because IMS spectral displays uniform gaussian peak shapes easily distinguished from noise [112, 172].

Non-targeted analysis can also be performed in IMS spectra and help directly in the development of unique chemical fingerprints. IMS fingerprints can be created by a single IMS spectrum of a selected sample, averaging IMS data of a single drift time or an interval from a sample collected over time. IMS fingerprint analysis includes both pre-processing and patter recognition [172]. However, non-targeted analysis to pre-process IMS data generally includes five steps: (i) RIP detailing, (ii) Denoising, (iii) Alignment, (iv), Baseline correction and (v) Scaling and normalization [112, 172].

RIP detailing includes processes for removal or minimization of RIP tailing, which in its simplest methods involve cropping IMS spectra region containing tailing [112, 172]. However, such approach leads to loss of information when involving analytes with drift time similar to RIP and alternatives involve fitting a lognormal function to the spectra and subtracting a minimum of 25% quantile intensity, previously determined for each drift time over all spectra [172].

Baseline correction is conducted to allow comparability of spectra, including IMS fingerprints from several samples [172]. This is commonly performed in 1-D IMS by subtracting a "blank" spectrum from sample spectra, but more elaborated methods can be used, such as Asymmetric Least Squares (AsLS), locally weighted scatterplot smoothing (LOWESS), Gaussian smoothing, Savitzky–Golay and wavelets [172]. Such methods do not only remove baseline discrepancies but also improve signal-to-noise ratio. Thus, besides being considered smoothing techniques they also function as denoising methods.

Due to small variations in temperature and pressure, discrepancies can occur in IMS spectra, and can be corrected by alignment methods in the pre-processing phase [112, 172]. Alignment is crucial to create reproducible spectra and results between samples and conditions. Expressing drift times in reduced ion mobility (K_0) or inverse reduced mobility ($1/K_0$) can correct for temperature and pressures variations, however, an internal standard, RIP drift time or mobility constants are also used for spectra alignment. Warping methods such as correlation optimized warping and *icoshift* are other possible methods for spectra alignment [172].

The final step in pre-processing is scaling and normalization and strongly depends on analysis goal and chemometric techniques used afterwards in pattern recognition [112, 172]. Data is often mean-centred but scaling to unit variance, such as min-max scaling, can be used to produced similar contributions from drift times points to IMS fingerprints and pattern recognition models. Logarithmic transformations are also applied to reduce the observed heteroscedasticity of IMS spectra in data scaling [172]. Normalization can be performed by the RIP peak intensity, the maximum intensity, or internal standard peak intensities, but in non-targeted analysis normalization is often averted in proll of using spectra as untreated fingerprints [112, 172].

2D and multi-Dimensional IMS data pre-processing

The combination of IMS with either chromatographic or mass spectrometry techniques produces sample spectra with two-dimensions. As an example, MCC-IMS spectra are data matrixes comprised of more than 200 retention times from MCC and 1000 drift times from IMS filtering, while an IMS-MS matrix is generally comprised of 500 collisions cross sections, from IMS and 2000 mass-to-charge vales from the MS analysis [97, 112, 172]. Therefore, the increase in information is hugely augmented in 2-dimension analysis, and although most 1-Dimensions IMS chemometric approaches are applied to 2D data, some exclusive cases exist due to data complexity and uniqueness. More comprehensive data analysis is often needed when comparing with simple ion mobility spectra with techniques applied to 1D data, being further automated, and redesigned for the increased in data complexity [112, 172].

Essentially in 2-D IMS data analyte peaks are represented in a different format, a peak is composed of several points grouped in a circle or oval shaped regions depending on instrument setup. Wherein

targeted analysis during pre-processing is performed to identify which "spots" belong to the target analytes and afterward quantify its amount. On top of the aforementioned steps, RIP detailing, denoising, baseline correction, alignment, data scaling and normalization, peak picking is an extra and important step applied to 2-D IMS targeted analysis during pre-processing (Table 4.1) [172]. Although most chemometric techniques used for 1-D IMS are applied to 2-D IMS some differences exist for alignment, denoising and baseline corrections in accordance with technique coupled to IMS [172].

Table 4.1 — Summarized steps and methods used in pre-processing 1D, 2D and 3D ion mobility spectrometry datasets [172].

Step	Method	1D	2D	3D
RIP detailing	Data cropping	+	+	+
RIP detailing	Curve fitting	+	+	
RIP detailing	Subtraction of baseline	+	+	
Denoising	Wavelets	+	+	+
Denoising	Savitzky–Golay smoothing	+	+	
Alignment	Correlation optimized warping (COW)	+	+	
Alignment	Correction by mobility of reactant ion peak	+		
Alignment	Correction by temperature and pressure (K_0)	+	+	
Alignment	Linear regression		+	
Baseline correction	Asymmetric least squares (AsLs)	+		
Baseline correction	Subtraction of baseline without peaks	+		
Baseline correction	Locally weighted scatterplot smoothing (LOWESS)	+	+	
Baseline correction	Top-hat filtering		+	
Scaling	log2 transformation and Pareto scaling	+		
Scaling	ln transformation and autoscaling	+		
Scaling	Min–max scaling	+		

A targeted analysis relies heavily on analyte identification and quantification, which makes peak picking, often the last step in pre-processing, and the most important for analytical success. Peak picking is commonly conducted by manual peak annotation but, automated strategies from merged peak cluster localization (MPCL), growing interval merging, wavelet-based multiscale peak detection, watershed transformation (WST) to peak model estimation (PME) have been applied [172].

MPCL procedure relies on IMS chromatogram points being first clustered by *k*-means with Euclidean distance and afterwards merged following a concept for image segmentation. The watershed transformation method has been adapted from the detection of spots in the analysis of electrophoresis images. Herein any IMS spectra is regarded as a landscape with hills and valleys, that is inverted and filled with "water" by an algorithm allowing peak detections as "water-filled" regions [172]. While peak model estimation is described by a model function formed from two shifted inverse Gaussian distributions with an added peak volume parameter [112, 172].

Although a few software examples exist for each strategy type (Visual Now for MPCL, IPHEx software for WST and PEAX for PME) (Table 4.2) currently manual peak annotation by field experts still yields the best results when compared with automated peak picking strategies [172]. However, manual peak picking often takes hours and an optimization in peak picking algorithms would reduce that time to a few seconds. Therefore, further improvement and development in automated tools for peak picking is greatly important to address this limitation in IMS data processing and results.

Table 4.2 — Software and toolbox packages used and employed in IMS data analysis including goal and availability [134]

Name	Goal	Availability
Excellims VisIon	Data visualization, peak finding and referencing of IMS data	Commercial software from Excellims, http://www.excellims.com/products/vision-software/
Visual Now	Data visualization, peak finding and referencing of MCC-IMS data	Commercial software from B&S Analytik, http://www.bs-analytik.de/eprodukte.html
IMMS extension to Drifscope	Preprocessing of IMS spectra onto data formats enabling peptide identification and referencing	Open access, http://code.google.com/p/ion-mobility-ms-tools.html
Amphitrite	Extraction of IMS profiles of single compounds	Open access, http://www.homepages.ucl.ac.uk/~ucbtkth/amphitrite.html
EM-IM	Relating IMS data with electron microscopy data	Open access, http://EMnIM.chem.ox.ac.uk.html
MIMA	Automated identification of MCC-IMS peaks by referencing with GC-MS data	Open access, http://mima.mpi-inf.mpg.de
LC-IMS-MS feature finder	Detection of multidimensional LC-IMS-MS feature	Open access, http://omics.pnl.gov/software/LC-IMS-MS_Feature_Finder.php
Carotta	Unsupervised pattern recognition of MCC-IMS data	Open access, http://carotta.compbio.sdu.dk

In respects to non-targeted analysis of 2-D IMS data its aim is to improve the scope of targeted analysis without the *a priori* set of selected peaks and, or spectral regions. The first non-targeted analysis of IMS data was created for MCC-IMS in 2015 and includes alignment, denoising, compression, baseline correction, region selection and a discriminant analysis as pre-processing chemometric techniques [172]. The main steps of this approach are summarized by seven steps: (1) alignment: correction of drift times to inverse reduced ion mobility values, (2) denoising in RT dimension and 4× compression in IMS dimension with wavelets, (3) baseline correction with top-hat filtering, (4) region selection: RIP region excluded, (5) mask construction: only white and grey regions are included in the further analysis, (6) data unfolding: levels of variables selected during mask construction are reported for all samples (7) pattern recognition with sparse-PLS-DA on the data matrix obtained [172].

An important aspect of this approach is the implementation of data reduction steps, responsible for enabling spectral region selection and an effective classification of different samples by three complementary steps: by compression with wavelet transform (step 2), mask construction (step 5) and variable selection during discriminant analysis with sparse-partial least squares-discriminant analysis (s-PLS-DA) (step 7) [112, 172]. Eventually data size is reduced to 50 relevant variables improving sample classification while also being an option approach to complement targeted approaches.

It is important to understand the development of chemometric techniques for 2-D IMS is being conducted by adapting or modifying other 2-D chromatographic data, GC x GC data, LC x LC data and 2D-electroohoresis to fit 2-D IMS and more complex datasets. Perhaps baseline correction is a good example, since in 2-D IMS baseline drifts can happen in both dimensions, due to RIP properties and peak tailing in both IMS drift time and for example retention time when coupled with GC [112, 172]. Baseline drift is also referred to as background and its corrections is referred to as background elimination. Subtraction methods as asymmetric least squares (AsLS) and wavelets have been extended to 2-D IMS data and applied to baseline correction [172]. Whereas new methods, as the case of top-hat filtering have recently been adapted and implemented for 2-D IMS analysis showing results of outperforming simple subtraction methods because of their ability to remove baseline artifacts in inhomogeneous backgrounds, where MCC-IMS data from breath analysis is included [172].

Data compression is common in 2-D IMS and often produced by wavelets similarly with 1-D IMS pre-processing, however, in two dimensional IMS further options exist [172]. Wavelet transformations can be applied first in one dimension, say IMS and then in the chromatographic dimension or vice-versa and even alternatively apply two-dimensional wavelets in both dimensions simultaneously [112, 172]. The latter case has been shown to be beneficial in pattern recognition.

Equally to baseline drift, distortions may be present in 2-D IMS. For example, in GC-IMS, distortions can occur in both drift and retention time, due to column aging (for retention), temperature and pressure variations (both GC and IMS). In GC variation levels can range from 5 to 25% for retention time and lead to uncertainties or false/incorrect compound identification via retention time and similarly the same can be observed, in a lesser degree of variation for drift time values [134]. The alignment methods normally applied are, correlation optimized warping (retention time), simple linear regressions correcting retention times by flow velocity, monotonic cubit splines base on calibrant samples and multiplicative correction. Nevertheless, currently no simultaneous 2-D alignment methods exist correcting both IMS and retention times variations [172].

Furthermore, scaling and normalization for 2-D IMS and even 3-D IMS are absent, and careful thinking is required to develop fitting guidelines and techniques. This absence is merely a consequence of the relative recent data science analysis of non-targeted analytes in multidimensional IMS [172]. Specifically, for 3-D IMS only recently have multidimensional datasets been produced and analysed in several omics field, such as metabolomics, proteomics, and foodomics. The demands placed onto chemometric techniques for multidimensional datasets analysis and processing are enormous and their current existence is limited [172]. This intricacy complicates the extraction of peak features that can be correlated across multidimensional data, whereas the current software, e.g., for UHPLC-MS and GC-MS, are not equipped for a coupled IMS dimension in multivariate analysis [172].

The current approach applied is to reduce the initial stages of analysis by collapsing the ion mobility dimension, however, a new automated pre-processing strategy including the IMS dimension is being used in LC-IMS-MS. Such strategy has shown promising result in the analysis of saliva and sera where it allowed the extraction of more than 4000 peaks from such dataset types [172].

Pattern recognition techniques

The basis for the selection of patterns recognition techniques in IMS data analysis is decided by the goals and targets of the analysis, the data characteristics (e.g., data dimension or pre-processing), and popularity of chemometric techniques for the specific application [172]. Two types of goals can exist for data analysis, qualitative and quantitative goals. Qualitative goals are associated with data quantitative classification, discrimination, or biomarker detection, whilst quantitative goals essentially are represented by calibration problems.

Pattern recognition is generally initiated with a simple data visualization and exploratory analysis followed by unsupervised chemometrics techniques to provide an unbiased data view, which leads to supervised techniques (that need previous knowledge of analysed data such as sample type or class) [172]. To conclude, pattern recognition results are statistically validated, and interpretation based on

the goals is extrapolated. Both univariate and multivariate statistical techniques of data analysis can be applied in pattern recognition (Table 4.3) [172]. Examples of univariate techniques includes analysis of variance (ANOVA) for one variable at a time (an IMS peak), whereas multivariable involve the analysis of all variables simultaneously. Multivariable techniques are more complex and utilize information proven to be statistically relevant and beneficial to create sensitive and specific statistical models [172].

Herein, several methods used for pattern recognition in IMS data analysis (Table 4.3) will be listed considering the four previously mentioned phases: (i) unsupervised analysis, (ii) supervised analysis, (iii) pattern recognition and (iv) model validation and interpretation [172].

An unsupervised analysis is an exploratory analysis where two types of techniques can be employed, projection and partitional clustering techniques. The most widely utilized projection type explorative analysis is principal component analysis (PCA) [112, 172]. This technique functions by summarizing data into a lesser number of linearly uncorrelated principal components (PCs) that represent samples in a matrix of score and variables by a secondary matrix of PC loadings [172]. Results from PCA are normally represented as a score plot and loading plot where a single point represents a sample and the proximity between points can be interpreted as sample similarity [128, 134]. Therefore, PCA is suited for visualizing high-dimensional datasets due to is ability to reduce data size since it represents data in a limited number of PCs and specifically, is used when a particular source of variation, with interest to the dataset, dominates its content [172].

Another projection technique used is self-organizing maps (SOMs), which construct a non-linear data projection in a low-dimensional display where possible clustering can be observed and identified. SOMs results are normally visually interpretable heatmaps where features are localized according to their profiles and colouring is done by centroid integrated intensity of the features contained [172].

Unsupervised analysis also includes partitional clustering techniques like hierarchical cluster analysis (HCA) and multidimensional scaling (MDS) when the goal is to group samples based on their IMS spectra and peak profile [172]. Clustering techniques can use different similarity measures to partition the dataset into sample clusters, however it always results in using "distances" to access sample similarity and cluster them into ordered groups called hierarchical trees or dendrogram. This method works specifically well when data already has a hierarchical structure such as breath analysis where breath from patients can be clustered and the effect of age and gender can be observed [172]. One alternative to partition datasets is, *k*-means clustering, in which data proximity is also a measuring factor but the user must define the number of clusters before data processing [112, 172]. With a defined number of clusters, *k*-means selects a set of centroids corresponding to where the distances of all samples, to said centroids, is minimized.

In contrast, supervised analysis requires previous knowledge of data. A common example is sample class: including treatment groups or patients, but specific sample properties, such as compound content are also used as previous dataset knowledge [172]. Prior knowledge of data organization is used to evaluate if data contains any related patterns, how strong those patterns are and if they can be used in the predictions of new samples. Fundamentally the goal of supervised techniques is to find a relationship between a matrix of predictors, data matrix X (e.g., IMS peaks in different samples), and

a vector or a matrix of responses, Y vector (e.g., specific compound concentration). Their relationship can be linear or non-linear and determines the type of chemometric methods used in the analysis.

Methods include linear discriminant analysis (LDA), partial-least squares-discriminant analysis (PLS-DA) [112, 172], multivariate linear regression, principal component regression (PCRg), partial least squares regression (PLSR), n-way PLSR (n-PLSR) *k*-nearest neighbour (*k*-NN), neural networks (NN), support vector machine (SVM), random forests (RF), and genetic algorithms [172].

LDA is often used to classify IMS data because it can be performed after PCA analysis, especially on the selected number of principal components (PCA-LDA) [172]. An LDA analysis or other supervised methods can complement, improve, or reveal results otherwise impossible by unsupervised methods, such as the case of olive classification (pomace, virgin, and extra virgin) [136, 172]. In a case study, PCA was unable to provide any obvious separation, but LDA revealed three distinct groups from the analysed samples [136]. The main difference is LDA focuses on finding difference between sample classes while PCA is an exploratory approach where group separation might not result because of the dominant source of variation present [172].

Table 4.3 — Summary of pattern recognition methods used in IMS data analysis [172].

Step	Method
Unsupervised analysis	Principal Component Analysis (PCA)
Unsupervised analysis	Cluster analysis (HCA)
Unsupervised analysis	Multidimensional Scaling (MDS)
Unsupervised analysis	Self-organizing maps (SOM)
Supervised analysis	Partial least squares-discriminant analysis (PLS-DA)
Supervised analysis	Sparse-PLS-DA
Supervised analysis	Linear discriminant analysis (LDA)
Supervised analysis	Recursive support vector machine (r-SVM)
Supervised analysis	Random forests (RF)
Supervised analysis	Genetic algorithms (GA)
Supervised analysis	*k*-Nearest neighbor (*k*-NN)
Supervised analysis	Principal component regression (PCR)
Supervised analysis	Partial least squares regression (PLSR)
Supervised analysis	n-Way partial least squares regression (n-PLSR)

Besides LDA, partial-least squares-discriminant analysis is commonly used for the analysis of IMS data. This method works by dimensionally reduce data to latent variables (LV) in a similar faction to PCs in PCA [172]. Those latent variables are extracted by maximizing covariance between a data matrix X and a model class vector Y which allows PLS-DA to deal with highly collinear data, where IMS data such as "fingerprints" are included [172].

Larger data from some 2-D or multidimensional IMS, however, hamper or complicate pattern recognition techniques, because such datasets are megavariate in nature. This means more than a million variable per sample are present, as well as some redundancy of information caused by several pixels being associated with one compound [172]. Non-targeted analysis is especially victim to mega-variate datasets where computation problems may well arise, due to "out of memory" problems. Pattern recognition in those cases requires long computation times due to the size and complexity associated with datasets and, most chemometric techniques are unsuitable and lead to overfitting and

false positives [172]. Often datasets are reduced in size to deal with this issue and only afterwards, are chemometric techniques applied to data analysis. Therefore, development of novel techniques is desired to address this issue in IMS data analysis and chemometrics of complex datasets.

Data size can be reduced by data compression during both pre-processing and pattern recognition [172]. PCA and PLS are variable reductions approaches that have been somewhat effective however, mask construction, a variable selection approach, is also apply to IMS datasets. Variable reduction is implemented by transforming many redundant variables in latent variables while variable reduction only extracts relevant and important variables. Nevertheless, it is advised to combine different techniques and approaches since it has been proven to increase model performance [172].

In contrast, mask construction selects variables based on predefined criteria that relates to data characteristics and the data analysis goal [172]. Peaks with lower intensities than a set limit of detection (LOD) are an instance where mask construction is used to select only predefined information from IMS datasets. Mask constructions was adapted from image analysis and its results are generally visually expressed with selected variables represented as white spots including information from several peaks of the original data. This allows to visually evaluate common and distinct variables between two sample classes [172]. Techniques for variable selection are very often combined with supervised pattern recognition tools, as is example, sparse-PLS-DA and recursive SVM (r-SVM) [172]. The former joins both variable reduction and variable selection to correlated variables from the same IMS peak for sample classification, while the latter, recursively builds models using different variable subsets and after selects the model with minimum number of variables and minimum cross-validation as a final model [172].

Moreover, pattern recognition is repeatedly combined with validation procedures including both internal and external validation. Internal validation encapsulates the optimization of a technique's parameters, such as the number of latent variables, whereas external validation deals with model generalization and applicability to new samples. Through model validation a specific degree of certainty can be attributed to a model and evaluate/compare different models and chemometric procedures applied onto the same datasets [172].

Validation approaches include resampling methods from which leave-one-out cross-validation, double cross-validation, bootstrapping, and permutation are examples [172]. The choice of resampling methods is made considering the number of available samples in a dataset. Ideally the dataset must be divided into a training set, a validation set and a set of independent tests to evaluate the predictive capabilities of the model [172].

Lastly the relevance of the model findings in the context and application of a specific analysis can be accessed in the final step of IMS data analysis, called model interpretation. Herein, variables selected by a chemometric model can be considered and interpreted as significant for classification or calibration, allowing those variables to be defined as disease biomarkers, bacterial identification compounds, food biomarkers or characteristic VOCs [172].

To conclude, chemometric tools have clear and significant contributions to the expansion and improvement of ion mobility spectrometry and related technologies, in different application and scientific fields. However, a need for a collective effort in developing and creating new well-thought,

comprehensive data analysis strategies is evident [172]. Such novel strategies must consider IMS complex and dimensional data and provide comprehensive and automated compound identification to meet transferability issues between instruments of different manufacturers. Addressing such issues is an essential step to reach a new milestone in the field of ion mobility spectrometry.

4.5 Selected Ion Mobility Spectrometer

The diversity of IMS spectrometer is very vast, and this technique can even be coupled with other analytical tools depending on analytes to be studied and application. For space exploration it is crucial to have a versatile device which has simple instrumentation components and can be adapted easily to a limiting and intense environment. Therefore, an Ion Mobility Spectrometer which operation with simple components and without additional reagents or sampling apparatus is ideal for monitorization of organic and microbial contaminates in spacecrafts. Because Drift Tube Ion Mobility Spectrometers offer control over several experimental aspects, *e.g.,* sample inlet, ion source, ion injector, drift tube type and length, detector characteristics and drift gas flow, reduces unnecessary problems and encumbrances involved with an analytical device. Also, DTIMS can easily be coupled with Gas Chromatography which address the issue of complex samples with trace amounts of numerous VOCs observed in the International Space Station. Lastly DTIMS, due to its particular operation shows an easier approach to address the lack of VOC databases containing ion mobilities and therefore a GC-IMS device ought to be an adequate instrument for the direct detection of organic and biological contaminants aboard space stations.

Hence, an ion mobility spectrometry instrument was chosen and modified from a commercially available instrument with the intention to develop and evaluate its capabilities as a fast, simple, and precise tool to identify, quantify and monitor a large spectrum of toxic, harmful, or vital volatile organic compounds in closed spaces, specifically for the cabin air of spacecrafts. This instrument is based on Gas Chromatography coupled with Ion Mobility Spectrometry since it provides enormous versatility in terms of analysing complex and high humid samples and allows identification and quantification of volatile organic compounds with proton affinity higher than water in ppb and ppt concentration ranges.

The instrumentation selected and used for the development of this thesis was a *BreathSpec*® which represents the synergies of a quick gas chromatography separation and the outstanding sensitivity of an ion mobility spectrometry. The use this IMS instrument enables the detection of volatile organic compounds in highly humid matrices without any special sample preparation with a focus on samples from human exhaled breath. Typically, substances are detectable at ppb_v levels with this instrumentation or even below, at ppt_v, while its results are available within a few minutes. *BreathSpec*® is a product commercially available from G.A.S. (Gesellschaft für analytische Sensorsysteme Dortmund).

Since the purpose of this instrument was for exhaled breath analysis it was installed with a CO_2/O_2 spirometer attached for collecting exhaled breath samples. Hence, an initial modification, was to remove this spirometer, which was easily achieved by simply detaching it from the sample inlet.

Furthermore, software changes were performed to remove the sample operation controlled via the spirometer, because it would no longer operate via the spirometer but via injection or gas flow directed into the sample inlet. Lastly, a specific GC column was installed with the goal of providing a broad-spectrum detection of VOCs, mainly substances commonly found in indoor and outdoor environments, toxic compounds, and microbial volatile organic compounds. The remainder aspects of the *BreathSpec*®, including internal component, software, power requirements and *modus operandi* were kept unchanged and will be described at this juncture.

The *BreathSpec*® is composed of several parametrized components which can be edit or changed to provide an optimization to measurement results in terms of substance separability, detection, quantification, and analyte peak clearness. Furthermore, this instrument can be operated in either negative or positive drift voltage modes. The positive mode will produce a RIP and analyte peaks will be maxima in the respective spectra while in negative mode, an inverted graph will appear, producing minima in spectra for both RIP and analyte peaks. Sample analysis requires a separate analysis for both positive or negative mode, thus two samples are needed for an analysis to include positive and negative modes.

Data acquisition is achieved through user-defined measurement programs that allow several operational parameters of the GC-IMS components to be modified and defined in specific sequences for a measurement run. Measurements can also be acquired in a manual format by a mode designated "Recording" in which all measured data is recorded until the user presses a stop button. The acquired measurements are stored internally in a storage volume inside the *BreathSpec*® or, if activated, in a shared network folder. Additionally, the shared network folder can be integrated into a local area network (LAN) through an Ethernet socket in the back of the device. A USB drive can be plugged into the device allowing the user to copy measurement files from the internal memory of the instrument.

4.5.1 Ion Mobility Spectrometer: Technical data & housing structure

The principal structure of GC-IMS systems inside the *BreathSpec*® consist of a 6-way valve, a loop system that control and directs sample flow into a gas chromatography column coupled with an IMS drift tube (Figure 4.13). The drift gas flowing into the ion mobility tube is supplied by an electronic pressure control unit (EPC1) and a second electronic pressure control unit (EPC2), manages the flow through the 6-way valve supplying carrier gas into the GC column. An exhaust at the end of the IMS drift tube exists for venting both drift and carrier gases while another ventilation outlet, connected to the 6-way valve, controlled with a diaphragm pump is responsible for purging the sample loop between measurements. Furthermore, some components of the system, including both transfer lines (T4 and T5), IMS tube (T1), GC column (T2), 6-way valve and sample loop (T3) are temperature controlled and heated by independent heating systems and can be defined and set by the user at a specific temperature between 30 to 80°C (Figure 4.13) [173].

Sample introduction into the GC IMS system of the *BreathSpec*® is conducted by injection into the sample inlet port at the front of the device housing, it can be drawn into the sample loop by activating a pump or by filling the sample loop through an external gas flow or syringe. Therefore, any

sample, first fills in the sample loop and is afterward carried into the GC column by changing the configuration of the heated 6-port-valve.

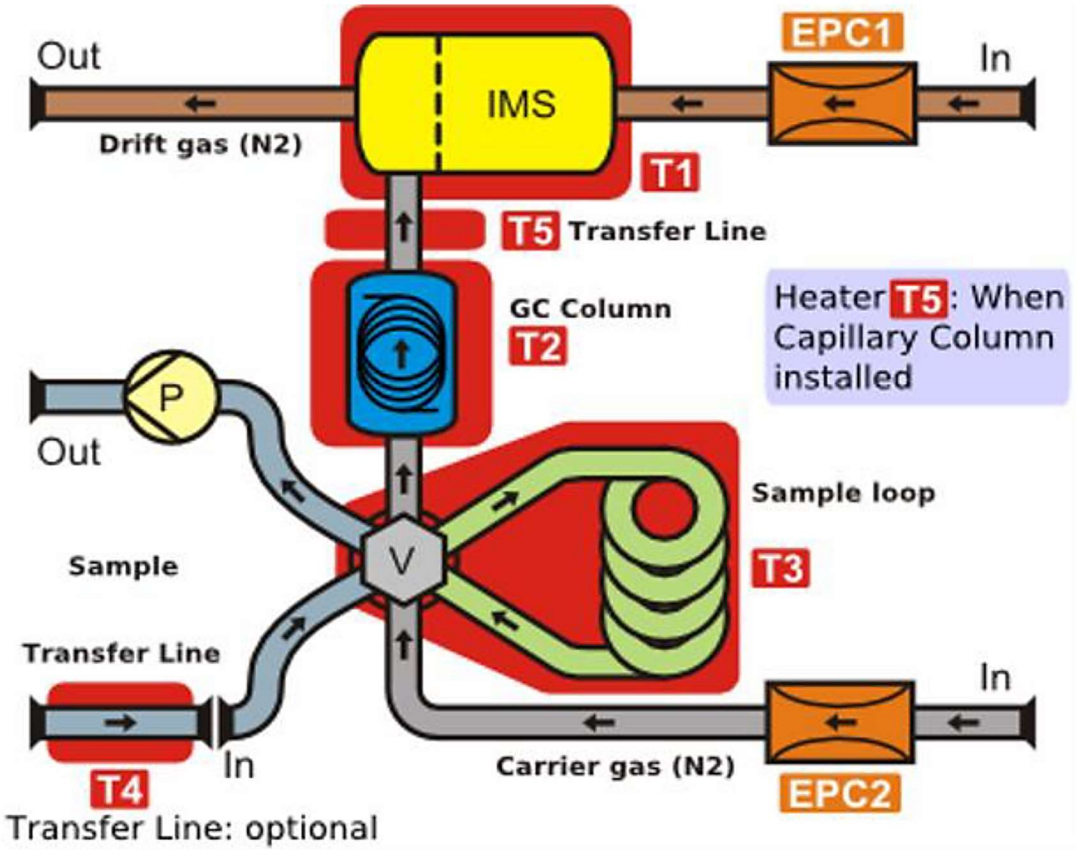

Figure 4.13 — A schematic of the operational system of the GC-IMS instrumentation selected for gas analysis [173].

The valve default position, also called "Fill Loop" has the carrier gas permanently flushing the GC column while the sample gas is passed through the loop by a suction pump resulting in the sample gas being directly routed from the sample inlet to the sample out socket [173]. Afterwards the 6-way valve is switched into its second conformation where the carrier gas, now passing through the sample loop, transports the sample gas from the loop into the GC column (Figure 4.13). Once inside, the GC column substances undergo a preliminary separation by traveling the full column length, eluding subsequently into the ionization region of the IMS drift tube [173]. Here substances are separated under an electrical field by their mass, charge and structure leaving the system via the gas out socket.

A view of the front housing of the GC-IMS can be seen in Figure 4.14, together (1) a Power LED: to indicate whether or not the device is connected to a power supply and is switched on; (2) a USB Socket: USB socket to connect external USB storage volumes (USB drives can be used to export measurement files, import sample name lists, upgrade the device's firmware and to save or load system settings); (3) a Sample in socket: 3 mm Swagelok inlet plug to connect the device to a sample gas source; (4) a 6,4" TFT VGA-Display: to display the graphical user interface; (5) a Push button & rotatory knob: as an input control for actions in the graphical user interface [173].

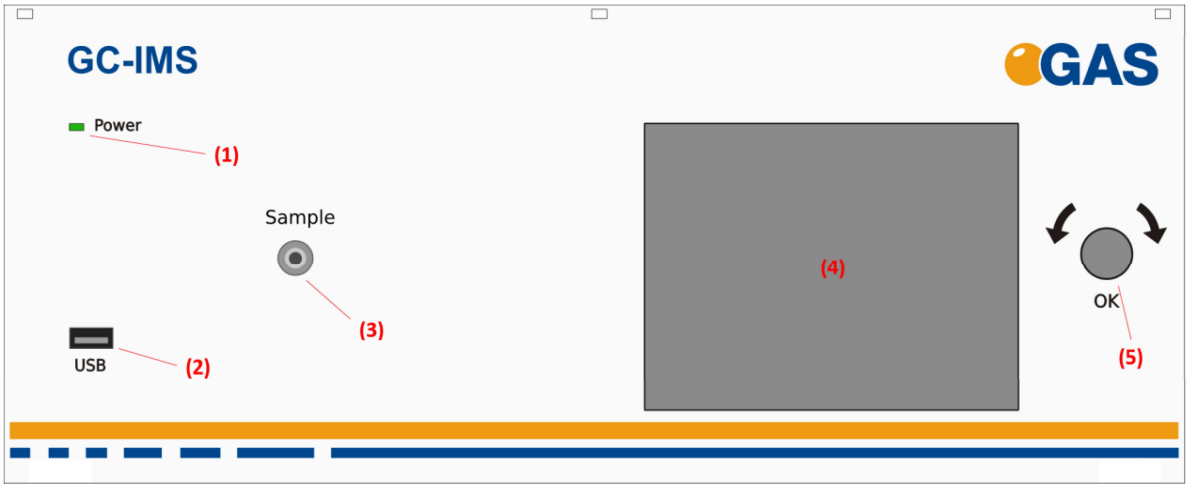

Figure 4.14 — The front view of the GC-IMS device labelling its specific components by number [173].

While Figure 4.15 shows a back view of the device where several components are located: (1) Power Switch: to switch the device on or off; (2) DC-In Socket: a 24V XLR-Connector to link the GC-IMS to a power supply; (3) Signal Converter – I/O Socket: to connect an PLC (Programmable Logic Controller) or other devices (e.g., used to connect an auto-sampler to the GC-IMS or even a Circular Gas Flow Unit (CGFU)); (4) Modem Socket: Socket for connecting an external modem [173].

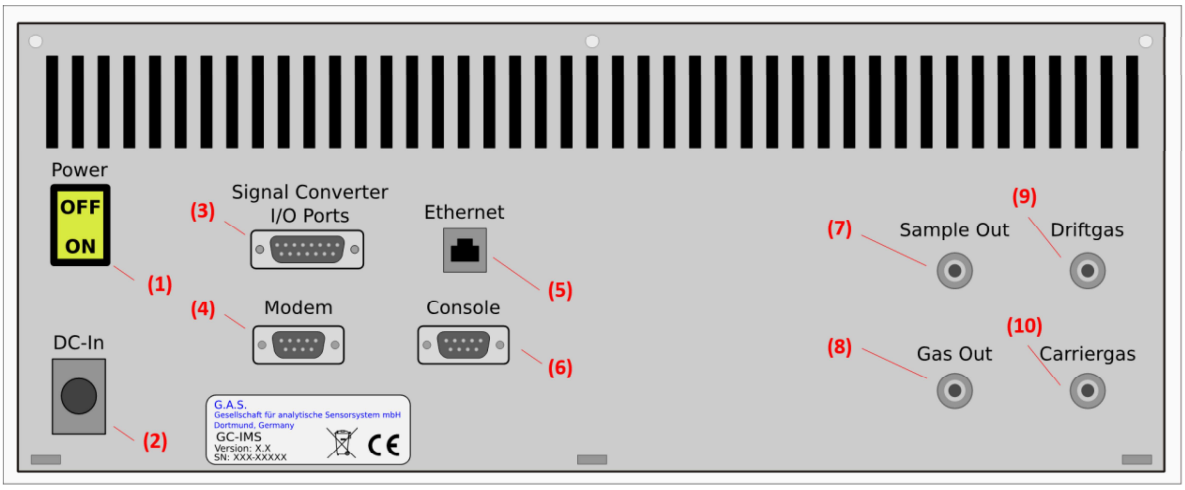

Figure 4.15 — The back view of the GC-IMS device labelling its specific components by number [173].

For service purposes only; a (5) Ethernet Socket: to connect the GC-IMS to a local area network (LAN) to use a shared folder as a storage location for measurement files; (6) a Console Socket: an interface for service purposes only; (7) a Sample Out Socket: 3 mm Swagelok plug to connect the GC-IMS to a laboratory waste gas ventilation system; (8) a Gas Out Socket: 3 mm Swagelok plug to connect the GC-IMS to a laboratory waste gas ventilation system; (9) a Drift gas Socket: 3 mm Swagelok inlet plug used for connecting the GC-IMS to a drift gas source; and (10) a Carrier gas Socket: 3 mm Swagelok inlet plug to connect the GC-IMS to a carrier gas source [173].

Housing dimensions are 184.5 mm height, 449 mm width and 495 mm depth reaching a weight of approximately 15 kg and the GC-IMS power supply requires an input line voltage from 100 to 240 V (AC grounded), resulting in a power consumption of 180 Watts (Table 4.4). Furthermore, it includes an input line frequency between 47-63 Hz, an input current below 2.8 A, an output voltage of 24 VDC, an output current of 9.33 A, [173]. All gas connectors are 3 mm stainless steel Swagelok connectors (drift gas inlet, sample gas in and outlet, carrier gas inlet and IMS gas outlet) while internal hoses are made of Perfluoroalkoxy alkane (PFA) [173]

As previously mentioned, the working principle of the *BreathSpec*® (serial number 3G1-00074) is gas chromatograph coupled with ion mobility Spectrometer (GC-IMS) and uses a β-radiation source (Tritium (^{3}H)) for ionization with an activity energy smaller than 380MBq (below EURATOM exemption limit of 1GBq and therefore requires no license). The drift tube has a length of 9.8 cm with an electric field strength of 500 V/cm and a resolution of approximately 100 and operates at temperatures between 35 and 80°C with its default being 45°C. The drift voltage is switchable between positive and negative modes and has a value of 5kV [173].

The sampling system is a 6-port-valve, containing a sample loop of 1mL which can be operated with temperatures of 35 to 80°C displaying an accuracy of ±1°C and a control accuracy of ±0.1°C. The flow control of the drift gas is done by differential pressure control operating with flow rates between 0 – 500 mL/min (recommended: 150 mL/min) and an input pressure of 3 bar [173]. The carrier gas flow is also controlled by a differential pressure control but only operates with flows between 0 and 150 mL/min (recommended: 50 mL/min) [173].

The GC column present in this device is an MXT-200 column made from stainless steel with a 30 meters length, 0.53 mm of diameter, a particle size of 1µm, a film thickness of 1µm, a temperature range of operation between -20 to 360°C, employing and a mid-polar stationary phase of trifluoropropylmethyl polysiloxane (Table 4.4). However, several GC columns, with different stationary phases and film thickness can be used, including: OV-5 (5% - diphenyl, 95% - dimethylpolysiloxane), non-polar; OV-17 (50% - diphenyl, 50% - dimethylpolysiloxane), weak polar; OV-215 (50% - trifluoropropyl, 50% - dimethylsiloxane), medium polar; OV-225 (50% - cyanopropylmethyl, 50% - phenylmethtylpolysiloxane), polar; or even dedicated column for siloxanes.

Normally both carrier and drift gas of the GC-IMS would be provided with a canister or an in-lab supply of 99% nitrogen or purify oxygen, however, since this instrument is planned for use aboard the ISS or spacecrafts, the traditional method of providing carrier and drift gases must be replaced.

An optional module from G.A.S Dortmund called Circular Gas Flow Unit (CGFU) provides a system for air purification and allows the mobile use of the GC-IMS without the need for any external gas supply. Air purification is achieved through an activated carbon filter, two molecular sieves and a pump.

The CGFU was designed to rest on top of the GC-IMS housing by aid of specific rubber feet and its housing have: 84 mm (Height), 449 mm (Width), 435 mm (Depth) and weighs 6 kg [174]. An input voltage and input current of 24 VDC and 1 A respectively are provided by the GC-IMS (Table 4.4) and its internal hoses are made of Polytetrafluoroethylene (PTFE).

The front panel of this unit contains a power LED (1) which indicates if the device is connected to a power supply and switched on and a fault LED (2) to indicate an internal system error (Figure 4.16) [174]. The rear panel (Figure 4.16) is composed of five connectors: (i) A socket to the IMS: Sub D Socket, to provide power supply and device control via GC-IMS this socket named "To IMS" must be connected to "Signal Converter I/O Port" of the GC-IMS;

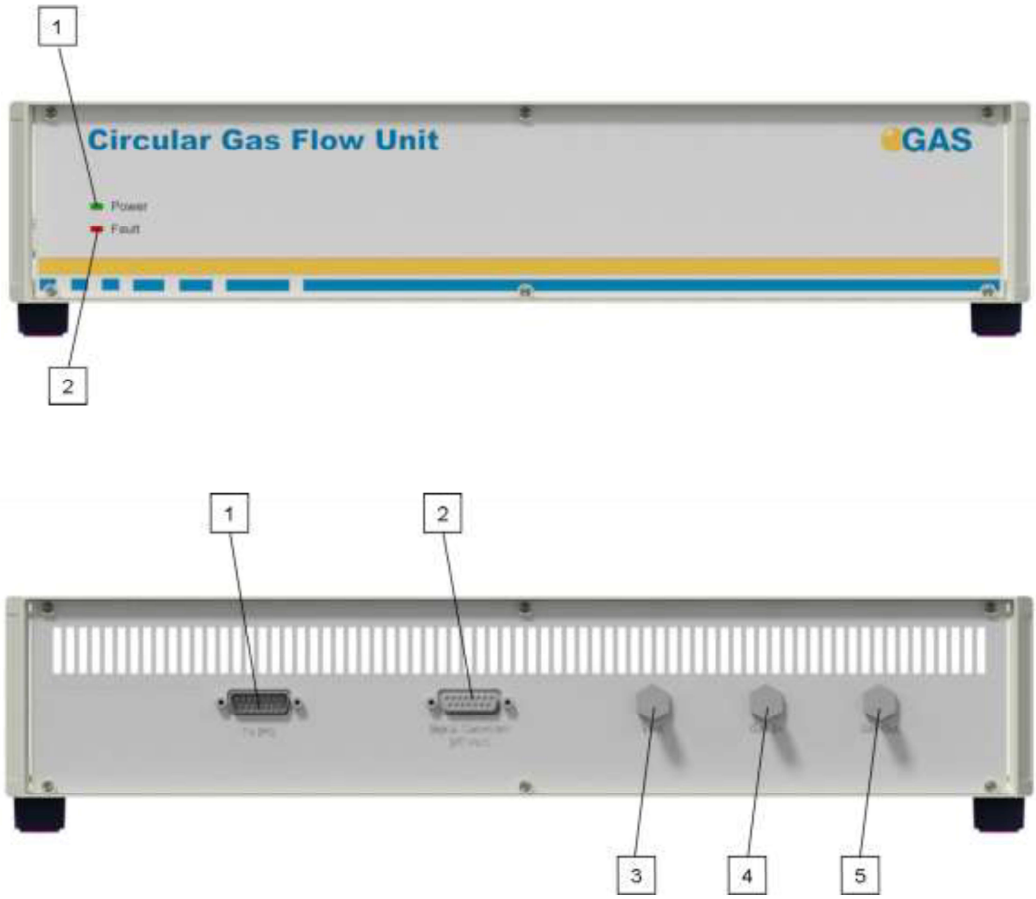

Figure 4.16 — Front (top) and rear (bottom) views of the Circular Gas Flow Unit (CGFU) and their component [174].

Table 4.4 — A summary of GC-IMS and CGFU dimensions, power supply and characteristics [108].

Breathspec®	Gas Chromatography coupled with Ion Mobility spectrometry	
Dimensions	184.5 x 449 x 495 mm (H x W x D)	Weight: 15 kg
Power Supply	Grounded AC, 100 to 240 V	Power consumption: < 180 Watt
GC column	MXT-200, 30 m 0.53 ID mm 1µm DF Polarity: Mid Polar	Stationary Phase: Trifluoropropylme-thyl Polysiloxaner
Ionization Source	Tritium H3 (ß radiation) 300 MBq	Euratom guidelines
Drift voltage	5 kV – polarity switchable	Positive or negative mode
Sampling systems	6-port-valve	Sample loop: 1 mL
IMS parameters	Drift length: 9.8 cm	Electrical field strength: 500 V/cm
Circular Gas Flow Unit	**Purification System to provide carrier and drift gas to the GC-IMS**	
Dimensions	84 x 449 x 495 mm (H x W x D)	Weight: 6 kg
Power Supply	Input voltage & current: 24 VDC, 1 A	Power supplied by the GC-IMS
Filters present	1 carbon activated filter	2 molecular sieves

4.5.2 Operation and Graphical User Interface

The operation of the GC-IMS *BreathSpec*® is conducted through a graphical interface displayed in a TFT screen by a rotatory knob acting also as a push button or simply with the touchscreen. The default screen has three sections, (i) a window selection bar showing the main windows at the top, (ii) a window display area at the center, where content of the selected window is presented and (iii) a status bar at the bottom displaying alerts, messages, and information pop-ups during operation [173]. The window selection bar at the top of the user interface contains five main windows with different functionalities: (1) Spectra window: where data acquisition process is controlled; (2) Defaults window: monitorization and modification of various device parameters and its effects on the current recorded spectra are present; (3) Substances window: parameters for up to 25 substances can be set and managed in this window; (4) Programs window: allows to manage user-defined measurement programs and (5) System window: applications and system specific information are shown (Figure 4.17) [173].

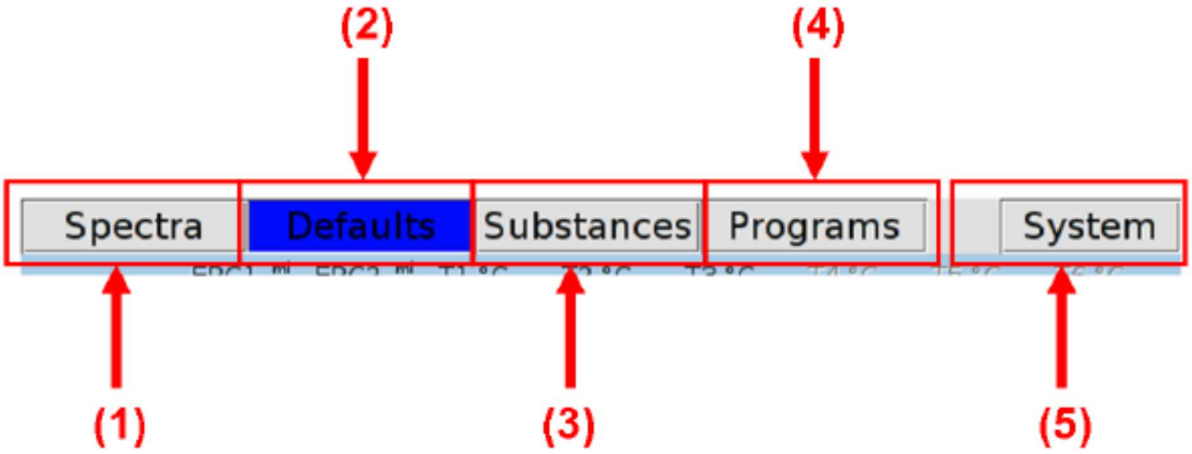

Figure 4.17 — Windows selection bar showing the five available windows and the selection marked in blue [173].

The spectra window is always displayed after the device is initiated and is responsible for controlling and displaying the data acquisition process, hence, the current spectrum is displayed, the recording mode can be activated, and the measurement selected programs can be initiated. In addition, this window contains a vertical and horizontal scrollbar to control the spectrum position in the display region and a view control bar that allows to shift the current view position, up, down, left, right, zoom out and zoom in which can be hidden with a button on the left of this bar (Appendix I, Figure A.5) [173]. While at the left side of this window a program start button showing on top the selected programs is present, a sample option where two options for operating the 6-por-valve can be chosen, either Fill Loop, which operates automatically or toggled manually by the inject option. The last section is a recording check box where live monitoring of measurements can be recorded manually (Appendix I, Figure A.5) [173].

The default window condenses several GC-IMS parameters including electronic pressure controllers (EPC 1 and EPC 2) and heating modules (T1 – T6) of the device displaying current values and allowing control over those parameters (Figure 4.18) [173]. Here is also possible to set the power

percentage of the pump responsible for purging the sample loop. A parameter for the RIP window region for an automatic detection of the RIP is available while the drift voltage can also be changed from positive to negative mode.

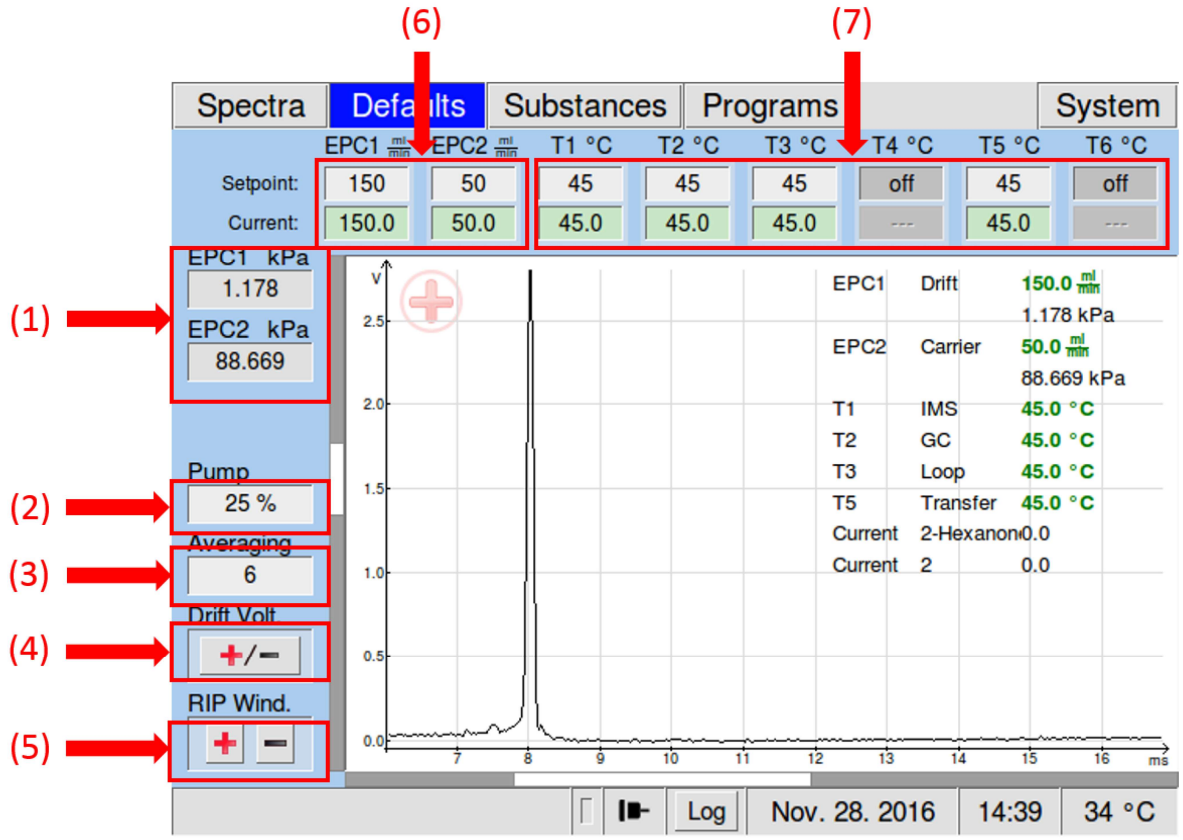

Figure 4.18 — Default window highlighting seven components: (1) Pressure display, (2) Pump, (3) Averaging; (4), Drift-Voltage (positive/negative), (5) RIP Window, (6) Flow and (7) Temperatures [173]

This window can be summarized in seven different regions (Figure 4.18): (1) A pressure display for both EPC1 and EPC2, drift and carrier gas respectively; (2) Pump: setting of the sample-in flow in percent of pump power; (3) an Averaging value, which determines how many raw spectra are averaged to generate one single spectrum in the stored measurement file. This parameter also increases the signal-to-noise ratio where a value of n will result in averaging n+1 spectra; (4) Drift-Voltage: to toggle between positive and negative ionization modes and the current mode is shown in the top left corner of the spectrum view; (5) RIP Window: sets the drift time intervals for RIP detection in both positive and negative modes; (6) Flow: where the input field for Setpoint and current values of EPC1 and EPC2 are and (7) Temperatures: setpoint and current values of the various heating modules in the IMS - (T1), Column (T2), 6-Port valve and loop (T3) and optional transfer line (T5) whereas T4 and T6 modules are not available in this instrument [173].

The third window present in the graphical user display is the Substances window, where a list of detectable substances can be created and edited with a limit of 25 entries. The substances window contains five regions (Appendix I, Figure A.6): (1) Substances List window: where all created substance entries are displayed by name; (2) Substances List Control Panel: containing buttons for creating,

editing and delete substances including changing their order; (3) Enable Button: to enable or disable the detection of the selected substances; (4) Substance Calibration Information Area: displaying the specific substance calibration information including concentration range, average, intensity type, area, search ranges and quantification model; and (5) an optional, Current Loop Settings, where further parameters can be adjusted including error level, and projection area [173].

The following window, named Programs Window is used to create and manage measurement programs by operating five different sections (Appendix I, Figure A.7): (1) Measurement Program List Window displays and lists all created programs by name, while in the (2) Selected Program Window all instructions for a selected programs are displayed in chronological order and includes in its columns all controllable parameters for the device components (V: 6-port-valve, R: recording, E1: drift gas flow, E2, carrier gas flow and P1, pump power percentage) [173]. In the (3) Selected program Window Control Panel, it is possible to create, change or delete actions in a selected program while (4) a Measurement Program Control Panel allows the user to change the programs list order, create, modify, and delete programs [173]. Lastly, at the (5) Program Repetition and Averaging Settings a user can choose its program Averaging value which is appended to the program name in the programs list, and with both entries in "Apply" and "Every", determine how often and in which time-intervals its selected program is executed respectively [173].

The last window is the System Window (Figure 4.19) and contains systems specific information including one section for (1) Measurements containing four buttons: "Copy to USB", to copy all stored measurements to a connected USB volume, a "Delete" button, to delete all internal stored measurements, an "Export" button to activate and set-up a shared folder on a network to store measurements and a "Copy to Remote" button which allows all internal stored measurements to be copied to a connected shared folder [173]. A secondary section, in a Setup action group, is divided into containing (2) Device Settings where a "Device Plan" button containing an overview plan represented in Figure 4.13 is present, Display settings where brightness and screen-saver time-out can be adjusted, Date & Time Set button to edit the date and time of the device clock, Fan regulation Settings where the behaviour of the cooling fan can be controlled, an Overheat Alarm Setting where a threshold temperature can be defined for the overheat alarm and an Inspection button to access inspection and diagnostics functions [173].

The third sections of the System window comprise (3) System Settings, including a Save, Load and Default settings buttons, where the user can save, load, or restore the device system settings to its default conditions, respectively [173]. The last button of this group includes a Firmware Upgrade button to perform a system/firmware upgrade through a connected USB volume. On the right side of the window a (4) System Information Panel is located displaying specific information from the device (e.g., type or device, serial number, date, and IP).

At the bottom on the window three sections each with one button and one editable value allow a user to set a (5) Sample Loop volume in µL, run a (6) Cleaning action with a specific duration in hours, and an option to when should the device enter (7) Standby mode [173].

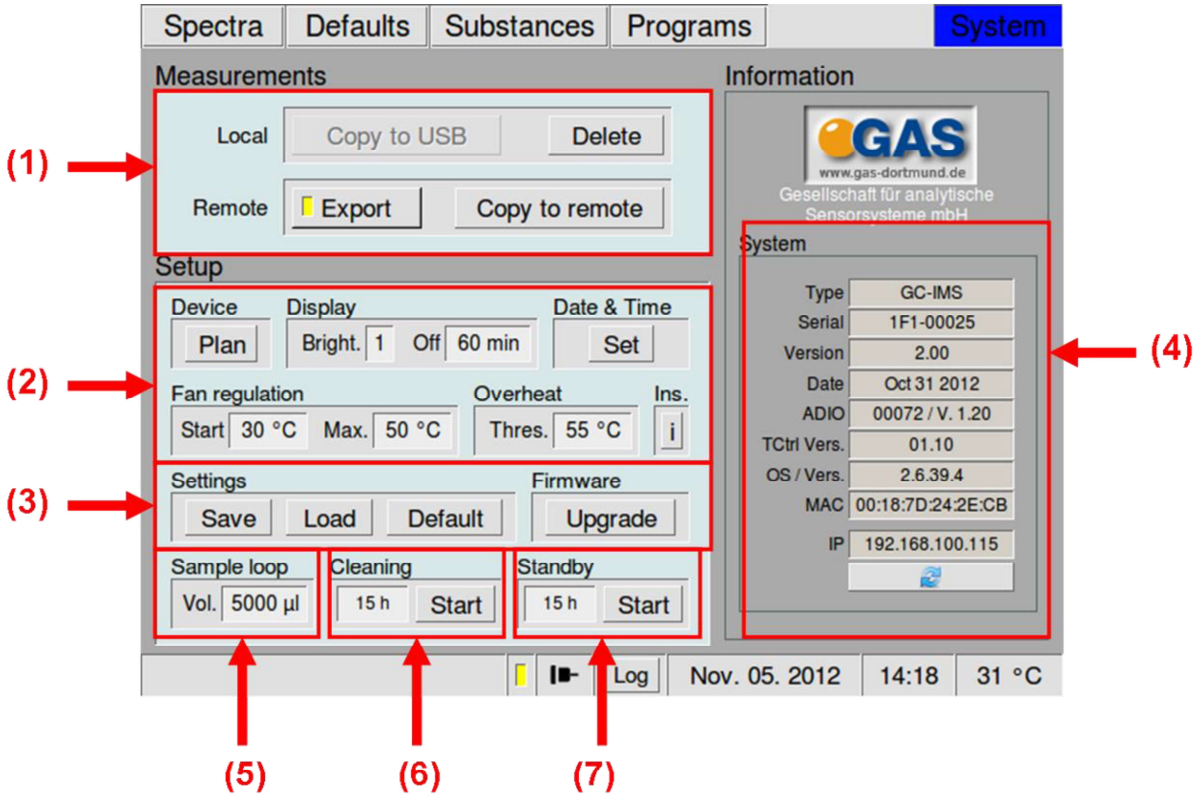

Figure 4.19 — A view of the System Windows containing (1) Measurement Settings Buttons, (2) Device Settings, (3) System Settings, (4) System Information Panel, (5) Sample Loop setting, (6) Cleaning Mode and (7) Standby Mode options [173].

4.5.3 Associated Software for data analysis

A software named Laboratory Analytical Viewer (LAV version 2.2.1) is provided by GAS Dortmund together with the GC-IMS device to allow data visualization and analysis of measurements acquired with any GAS measurement system. Those files are saved in a format with a *".mea"* extension and can be visualized and analysed with several functionalities and options in the LAV software.

The LAV software is composed of 4 main areas (Figure 4.20): (1) a Browser Window to select measurements of interest directly from a computer folder; (2) a Project Window to import measurements from the browser window for an intended analysis; (3) an Attribute list where all relevant information about any selected measurement can be seen, including, name and serial number of the instrument producing the measurement file, flow, temperature, data and even the name and conditions defined in the measurement program; and lastly (4) a Spectra region, where a topographic view together with a single IMS spectrum and ion current view are shown (Figure 4.20).

The topographic view on the software always shows a single measurement, displaying in the *x*-axis the drift time and the retention time in the *y*-axis. Several visualization tools enable to switch on and off the single spectrum view, ion current view, coordinate labelling, crosshair view and tools to zoom in and zoom out the spectra.

Zoom in an out can also be achieved with the shift key and the scroll of the mouse wheel for *x*-axis and with the control key and scroll the mouse wheel for the *y*-axis. On the left side of any spectra,

a colour scaling bar is present, and the visual properties of the colour map can be adjusted to interpret the corresponding intensity of each peak. Apart from the topographic view three other graphical types can be selected, a single IMS spectrum view, an IMS ion current view and a summary view of the measurement with textual information (Figure 4.20).

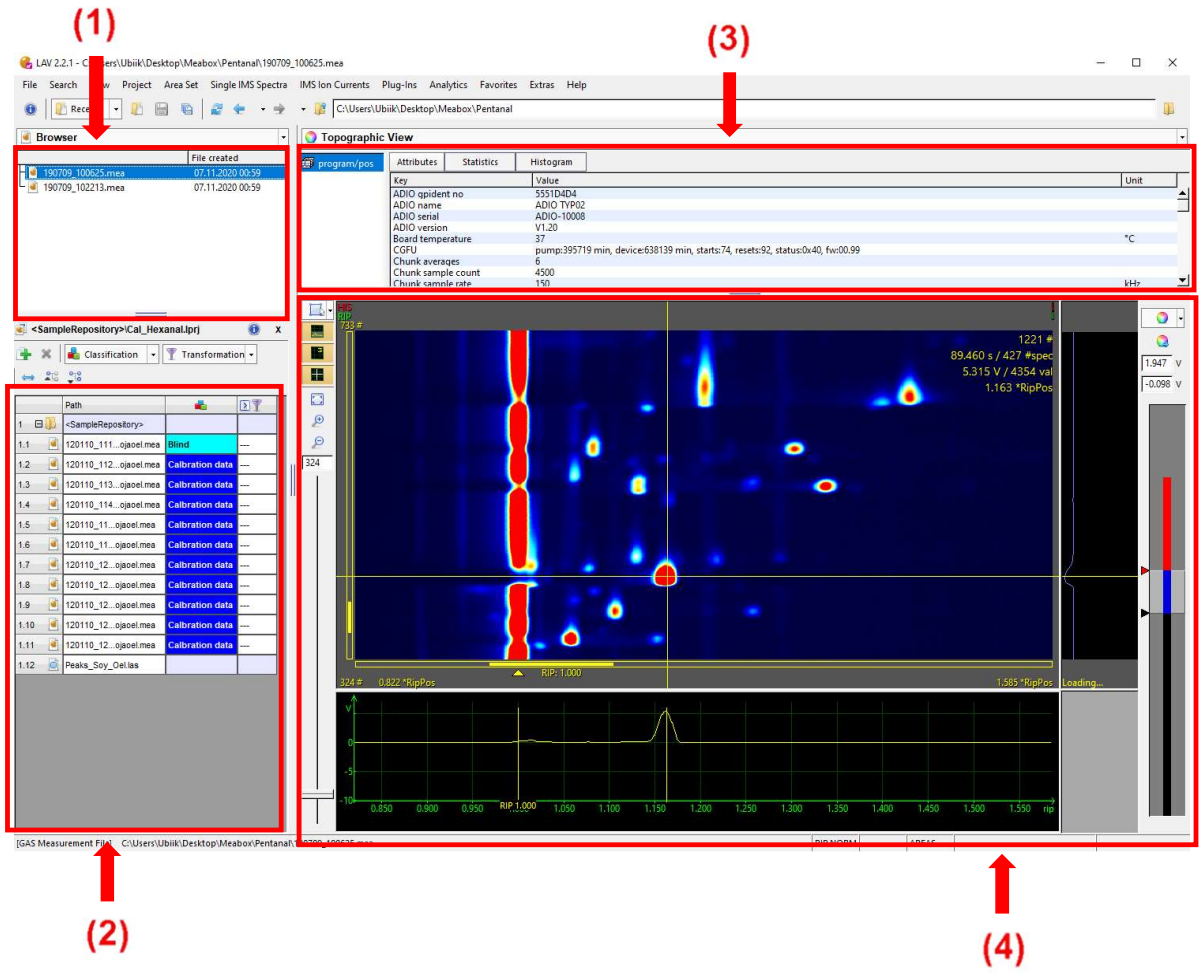

Figure 4.20 — The main window and elements of the Laboratory Analytical Viewer (LAV) version 2.2.1. (1) Browser Window, (2) Project Window, (3) Attribute Lists and (4) Spectra region.

Analysis of measurements always requires files to be added to the project window (Figure 4.20), and it is in this window that all actions performed in the software will take effect. The LAV software allows area sets to be manually added or removed to the measurement files present in the project window. Furthermore, LAV even enables to statistically compare area sets, showing, once an area set is defined by the user, a window with the measurements in the respective project, their intensity and a graph visually representing their intensity. The intensity of each signal in the selected area can be quantified in four formats: volume in area, maximum height range in area, area at maximum height range position in area, and ion current area at maximum height range position in area. Data contained in this stage can also be copied and pasted into an excel file for further analysis and processing.

Any area set created in the software can be saved into a specific file format (*".las"* extension), where the position of each area set are stored and can be used for other analysis. The projects created can also be saved into a specific file but require the selected files to be maintained in the original location when the project file was saved. This type of analysis is done as a preliminary set, and a more useful and detailed analysis can be conducted in the Analysis menu of the software by a quantification module. Likewise, the Analysis menu also allows RIP normalization, meaning all spectra drift times are divided by the drift time of the RIP maxima, resulting in all spectra having their RIP at a value of 1 in the drift time axis.

The quantification module is a dedicated module to create quantification models and perform peak intensity analysis. Once a new model is created, the user can choose a name for the model, an intensity type (i.e., Height above area minimum [V], Height above baseline [V], Volume above area minimum, Volume above baseline, Area at maximum above area minimum, Area at maximum above baseline, Ion current area at maximum above area minimum and Ion current at maximum above baseline), a calibration type (i.e., Exponential, Logarithm or Boltzmann), choose to calculate additional attributes (including RIP drift time and intensity, AIP drift and retention times and RIP drift times and AIP drift and retention times) and load an area set or use the created area set from the current areas marked on the software. Once this step is concluded the user must load the project files and a new window with the desired information will be shown. At this point the user can manually add the concentrations of each measurement and determine a calibration function. A calibration curve will be shown at the bottom and the calibration model can be saved and exported into an excel file. The saved calibration model can later be loaded and is used to calculate concentrations of measurement files.

Several plug-in modules are also available for data visualization and data processing. A plug-in module (CSV Export) exists to convert *mea* files into a CSV file format containing textual information and a mathematical matrix equivalent to the colour map represented in the view area of the LAV software. Another plug-in, named Reporter, allows all measurements in the current project to be plotted and visualized next to each other where further additional visualization options, including a 3D representation can be used. And lastly, a plug-in module, named Gallery, allows visualization of all selected areas from a topographic view side by side which is useful to visualize and analyse characteristic signatures of measurements and LAV software even allows relevant signatures from data and analysis to be saved in a "key" format for later use in classifying measurements.

CHAPTER 5.
DETECTION AND IDENTIFICATION OF CONTAMINANTS:
Results

The detection of contaminants encompassed here, is divided into seven/eight main subjects: (i) evaluation of IMS capabilities under a simulated ISS environment during the SIRIUS-17 experiment (Scientific International Research in a Unique terrestrial Station), (ii) an assessment of IMS analytical capabilities for the detection of VOCs from microorganism; (iii) addressing IMS to monitor food spoilage (iv) exhaled breath analysis with IMS for medical diagnosis (v) development of a database of important VOCs in the context of ISS and space environments; (vi) quantification and calibration of ion mobility spectrometers and (vii) early development of an automatic tool for IMS data processing.

5.1 Preliminary Tests and Analytical Assessment/Evaluation

A series of preliminary tests were firstly conducted to both provide an introduction and initiation for operation and data analysis via an ion mobility spectrometer, more specifically a *Breathspec*® device connected to a Circular Gas Flow Unit (CGFU). Also, the preliminary tests were chosen and designed with the aim of evaluating ion mobility capabilities and analytical characteristics and allow an optimization of sampling programs and approaches.

5.1.1 Distinction between different volatile organic compounds emission

The first preliminary test involved a comparison of two cola-flavoured beverages under the same condition with the selected GC-IMS instrument. Henceforward, the headspace from two cola-flavoured beverages, Pepsi® and Coca-Cola®, was measured under the same flow and temperature with the *Breathspec*® device coupled with the GCFU. Their volatile organic compounds emission was analysed and compared to establish an emission pattern or fingerprint for each beverage and allow their characterization and differentiation. The beverages selected for this test were commercially available cans of regular Coca-Cola® and Pepsi® (33 cL) obtained locally and stored in refrigerated conditions. Each container was removed from refrigeration prior to extraction of a 2 mL volume, place, afterwards into a 20 mL vial. Sample vials were closed and kept away from light and humidity for 24h to achieve headspace equilibrium. The following measurements were performed with a flow program with a total duration of 15 minutes, a constant value of 150 mL for the drift flow and a flow ramp for the carrier flow. The sampling program has a 10 second interval to allow the injection of a 2 mL headspace sample with a syringe into the sample loop of the device. Afterwards the opening of a 6-port valve that leads the sample volume into the GC column and the sample is pre-separated with a flow ramp over 15 min. The starting value for the GC column or carrier flow was set to 10 mL and was increased every two minutes to a maximum of 100 mL as follows: 25:40:50:65:85:100:100 (mL).

Analysis of the headspace spectra from Coca-Cola and Pepsi showed distinct patterns for each beverage. The differences in volatile organic emission between Coca-Cola and Pepsi samples is showing in (Figure 5.1). Twenty-three signals were identified in both beverages indicating a high degree of similarity between the two beverages, however, thirteen of those signals had higher intensity in Coca-Cola and three signals were more intense in Pepsi (Figure 5.1).

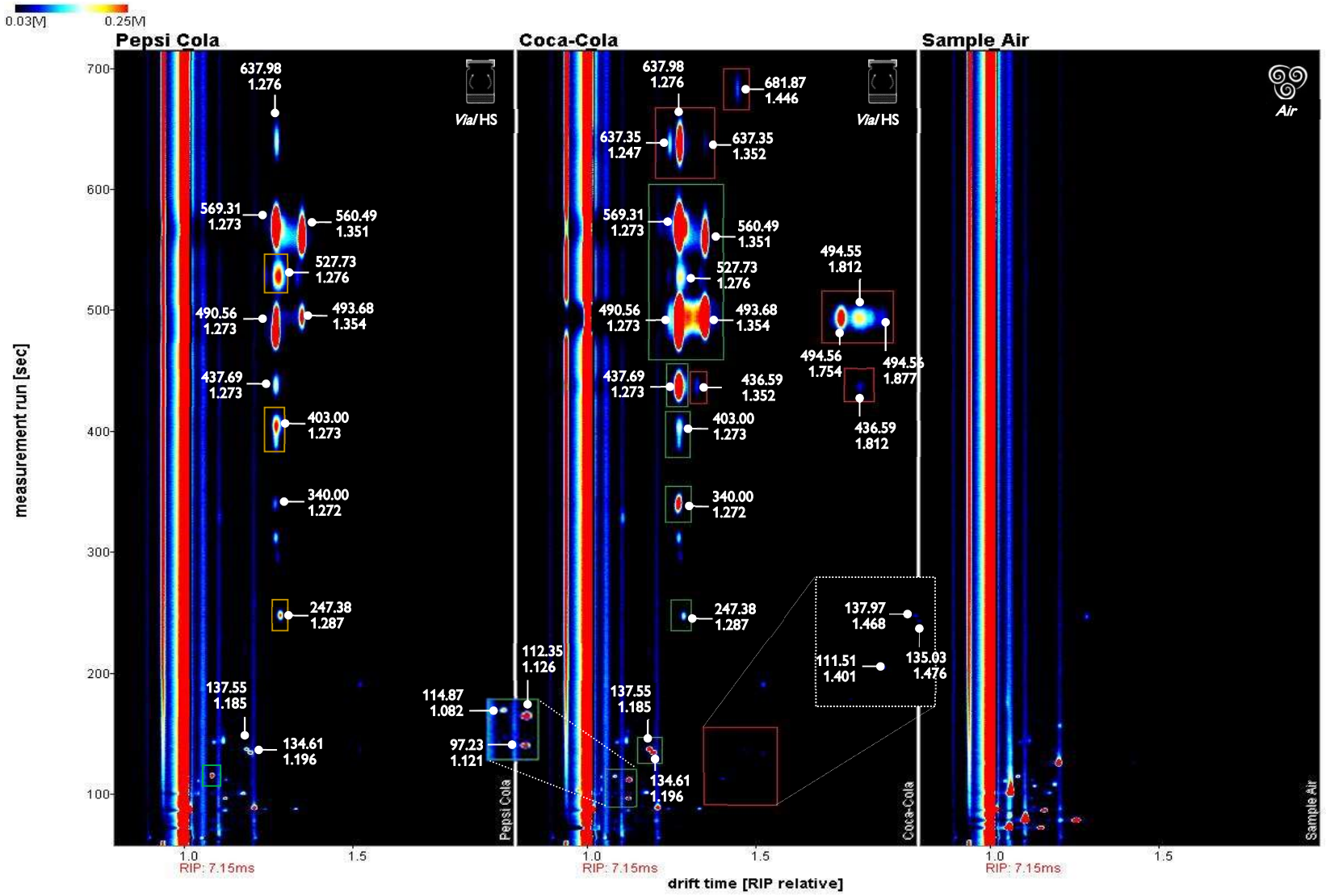

Figure 5.1 — Headspace spectra of Pepsi Cola (Left), Coca-Cola (Middle) and a room air sample (Right). The signals detected in the sample air, were removed from other spectra. Red squares mark signals unique to Coca-Cola, green squares mark signals with higher intensities in Coca-Cola compared to Pepsi and yellow squares mark signals with higher intensities in Coca-Cola compared to Pepsi. A label is also present for all important signals with retention time in seconds (top) and drift times relatively to RIP position (bottom)).

An evident conclusion to be drawn from those preliminary results is the identification of a discernible and characteristic pattern in the headspace of both Coca-Cola and Pepsi. Hence, it is possible to distinguished between beverages by the detection of VOCs present in their headspace with IMS, even implying both beverages have different composition.

Ion mobility spectrometry was therefore able to provide a clear distinction between the two beverages without any prior knowledge of constituents or any complicated steps in sample preparation. Although the identification of signals from both beverages was not yet possible at this early stage, a short literature research, indicated a higher complexity in the volatile emission of Coca-Cola compared with other cola-flavoured beverages, with eugenol and coumarin as predominant odorants in colas followed by moderately emissions of guaiacol, linalool and 1,8-cineole and β-damascenone [175].

Once a preliminary understanding of the detection capabilities and sensitive for volatile organic compound mixtures by the GC-IMS device was obtained further tests followed. The *BreathSpec*® unit was thoroughly tested with a series of mixtures, separation and sampling tests aiming to a develop a procedure with a specific sampling program to be applied in an experiment under simulated conditions of the ISS. This program corresponds to a schedule of actions, automatically performed by the device to control, sample volume, measurement running time, temperature, GC column and drift region flow.

5.1.2 Carrier Flow Influence on Separation of Volatile Organic Compounds

When evaluating the separation capability of the GC column flow an experiment was conducted to establish a carrier gas flow suitable to separate different gas samples in the retention time. The earliest phase of this experiment involved a simple test to assess the differences in separation between two program setups: (i) a constant GC column flow, EPC2, and (ii) an EPC2 flow ramp with increasing value over time (positive slope) (Figure 5.2). The results obtained revealed that using a constant flow for EPC2 would hinder mixture separation, since spectra signals are compressed together making it harder to read and extract precise and accurate data from signals, which indirectly causes further complications in signal identification. Thus, using a flow ramp approach for EPC2 flow will hugely improve separation, however a following test phase was conducted to optimize the flow ramp to better differentiate signals in the retention time dimension.

Four different GC column flow ramps, A, B, C and D were designed, and their separation capabilities were tested with VOCs from a room air sample measured in the Laboratory 106 (Departamento de Física da Faculdade de Ciências e Tecnologia da Universidade Nova de Lisboa) (Table 5.1). This preliminary experiment aimed to clearly separate VOCs in any type of gaseous samples including indoor and outdoor air, headspace sample from liquid and solid samples, such as water, food products and other biological matrixes.

A constant flow value of 150 mL/min for EPC1 was chosen for all flow ramp programs because this flow value is considered standard from the GC-IMS manufacturer and could, probably, facilitate signal identification from other publications and from a commercially available database provided by G.A.S., called GCxIMS Library Tools.

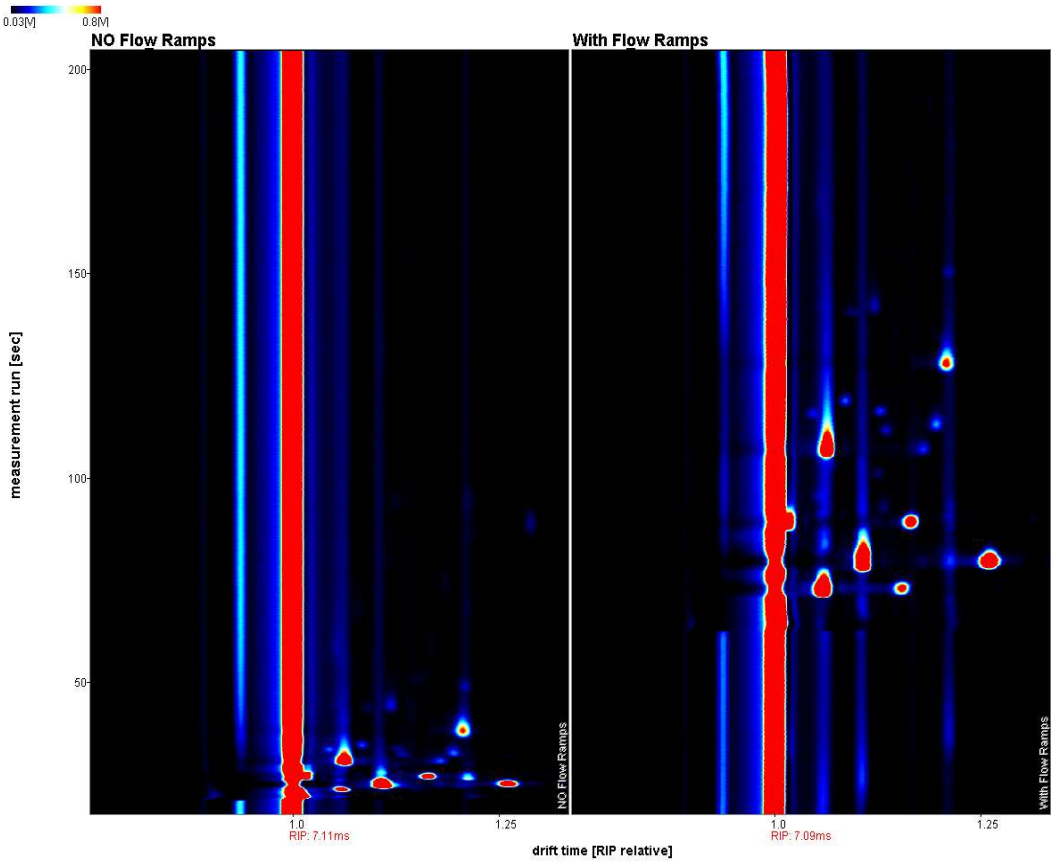

Figure 5.2 — Separation of room air VOCS with a constant EPC2 flow (left) and an EPC2 flow ramp (right).

Air measurements from Laboratory 106 were collected almost consecutively and analysed with each of the four flow ramps in Table 5.1, beginning with flow ramp A and finishing with D. The resulting spectra from this gas analysis were compared in Figure 5.3 and show that flow C and D have the best capabilities for mixture separation.

Nevertheless, in this case a mixture showing a reduced number of peaks at low retention time (low molecular weights) were found, therefore, it only made possible to test this type of separation in a simple air mixture. So, separation capabilities of flow A, B, C and D were tested furtherly by measuring and analysing a different mixture with a higher number of peaks and a larger retention time distribution. Two types of samples were used as examples of complex gas mixtures, (i) the headspace of four brands of toothpastes, individually, and (ii) the previous two cola-flavoured beverages, were tested with all four flow ramps. The selection of toothpastes and cola-flavoured beverages was made because of two main aspects, their diverse composition or signal distribution and easy access.

The four toothpaste brands selected included Colgate®, Aquafresh®, Signal® and Sensodyne® and were measured in triplicate, to ensure repeatability, with flow C and D. Sample preparation was conducted in a similar method as performed for the two cola-flavoured beverages, by placing, inside a 20 mL vial an approximate volume of 2 mL from each toothpaste. Vials were left resting overnight to reach headspace equilibrium, afterwards a volume of 2 mL was extracted with a syringe from each toothpaste sample and injected into the GC-IMS device.

Table 5.1 — GC Column Flow variation for each of the four programs used to test mixture separation.

Time (min)	1	2	3	4	5	6	7	8	9	10	11	12	13	14	15
Flow A (mL/min)	10	25	25	50	50	100	100	100	100	100	100	100	100	100	100
Flow B (mL/min)	10	10	10	50	50	100	100	100	100	100	100	100	100	100	100
Flow C (mL/min)	10	10	10	25	25	25	50	50	50	75	75	75	100	100	100
Flow D (mL/min)	10	10	25	25	35	35	50	50	65	65	85	85	100	100	100

No significant differences were visible between flow C and D in terms of separation in retention time, however, flow D could detect higher molecular weights compounds in the same time frame as flow C. Thus, to complement those results, flow D configuration, was further used to analyse the headspace of two cola-flavoured beverages, previously shown in Figure 5.1. The performance level of this setup was on an equal level to the results obtained for the toothpaste emissions (Figure 5.4) which resulted on the selection of flow D as the best flow setup for simple and complex VOCs in the retention time dimension.

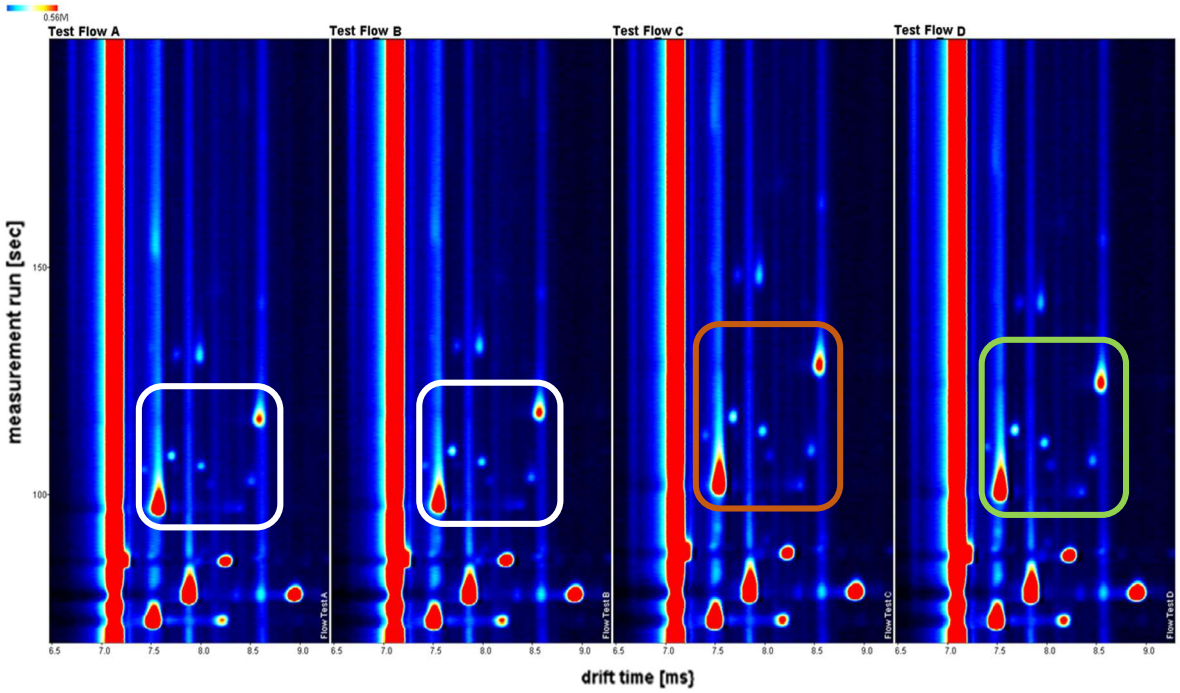

Figure 5.3 — Comparison of the separation effect of four different programs, Test Flow A through D, highlighting the major differences with an orange circle. White squares mark several signals showing flow A and B degree of separation while orange and green squares mark flow C and D degree of separation respectively of the same signals.

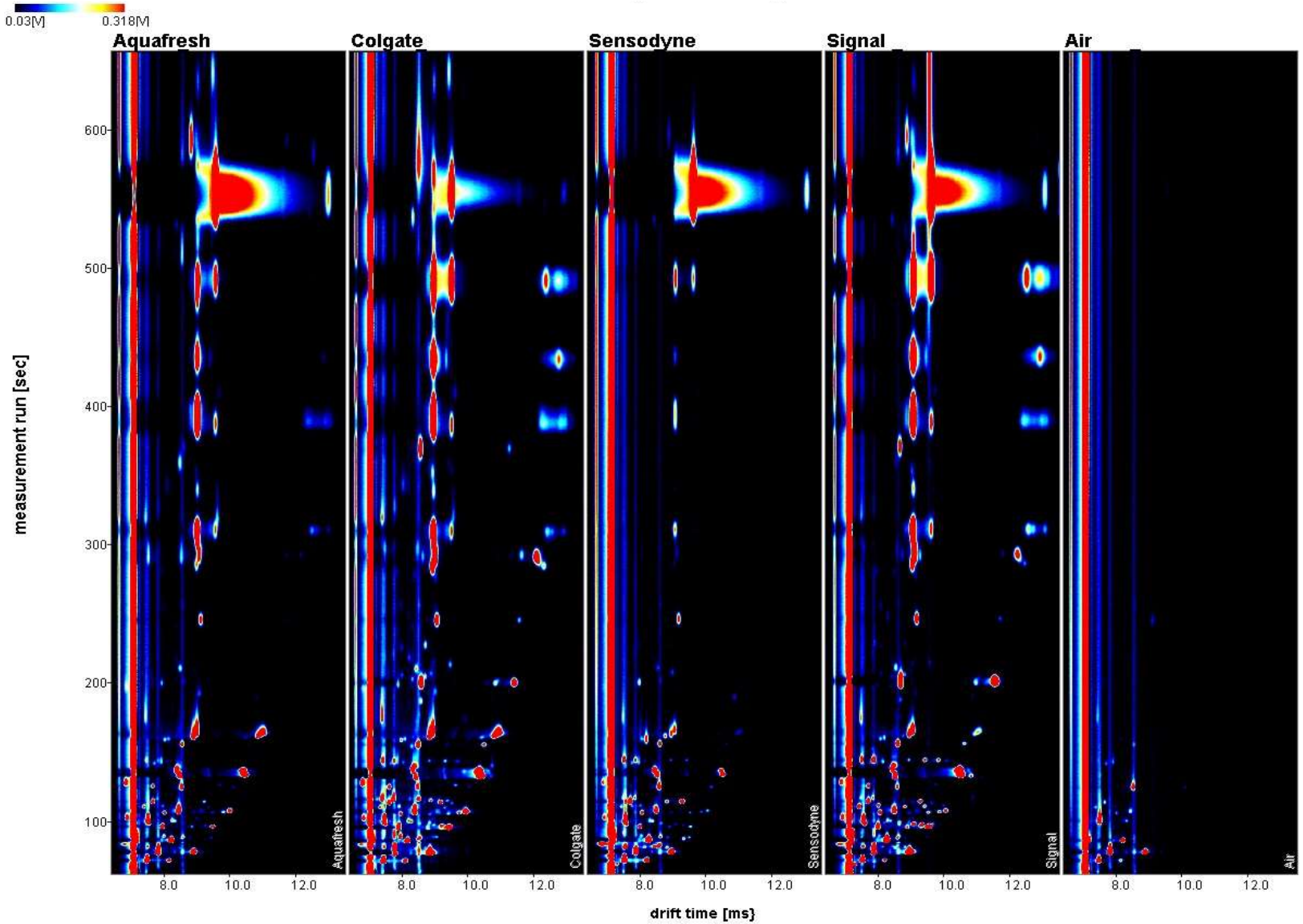

Figure 5.4 — Headspace measurements of four different toothpaste brands. Headspace samples were measured with Flow D.

5.1.3 Analysing Indoor Air Variations in Ventilated and Unventilated Conditions

The previous tests were performed to illustrate IMS abilities to detect and differentiate distinct samples based on their VOC emission and, to establish an effective and useful carrier gas flow setup. Those tests resulted in the selection of flow D setup as the best flow ramp for VOC separation on both simple and complex mixtures. Next, it is crucial to test and analyse how flow D performs when measuring indoor air over a long period of time, hence, flow D was used to measure indoor air inside a room (without any windows) during a period of 48 hours. Sample collection was designed to occur every 2 hours. Moreover, this preliminary test of indoor air, was also developed to analyse how VOCs would behave in the presence and absence of ventilation. Hence, the 48-hour period was divided into two smaller periods of 24 hours. The first 24-hour period had active ventilation inside the room, performed by an air conditioner and the following period of 24 hours the room would remain unventilated.

The room selected for the experiment was, once again the Biomedical Engineering Laboratory 106 at Departamento de Física da Universidade Nova de Lisboa. Laboratory 106 had approximately 75 m^3 (6 m x 3.70 m x 3.40 m) with 2 doors and no windows. Measurements were collected while room ventilation operated via an AC at 27°C and a relative humidity between 50% and 64%. Although the AC temperature was set to 27°C the observed temperature in the Lab varied between 25 to 26°C. The room was kept closed with only three people entering the lab during the full 48 hours, with a maximum time spend inside the laboratory for any occupant not exceeding 5 min. Samples were collected at 16:38h, 18:38h, 20:38h, 22:38h of January 16, 2018, and at 00:38h, 2:38h, 4:38h, 6:38h, 8:38h, 10:38h, 12:38h, 14:38h, 16:38h of January 17, 2018. AC ventilation was turned off after the last measurement was concluded, at 16h55 of January 17. Relative humidity and temperature measured at the end of the last measurement were 50% and 25.3°C respectively.

Room air samples without ventilation began at 17:13 January 17; four measurements were collected on this day, at 17:13h, 19:13h, 21:13h and 23:13h, and remaining measurements were performed on January 18 at 01:13h, 03:13h, 05:13h, 07:13h, 09:13h, 11:13h, 13:13h,15:13h and 17:13h. Relative humidity and temperatures were measured at 17:15h (T: 25.5°C, H: 49%), 9:15h (T: 19.5°C, H: 56.9%), at 12:15h (T: 19.5°C, H: 56.4%), at 15:15h (T: 19.6°C, H: 56.3%) and at 17:32h (T: 19.5°C, H: 56.7%). Air samples were collected without the use of any sampling or injection instrumentation, which means no syringe or tube was used to inject or direct sampled air to the GC-IMS. Hence, sampling was conducted with GC-IMS internal structure, which allows for a direct sampling methodology using a sample loop in combination with a pump and a 6-port-valve. Twenty-eight signals were detected and identified as omnipresent in all air samples (ventilated and unventilated condition).

Relative peak heights, directly correlated to signal intensity, were estimated, and extracted for the 28 signals with LAV software and such data makes it possible to monitor concentration changes of VOCs over time in room air. The total peak intensity was calculated for the 48-hour period and revealed differences between ventilated and unventilated conditions (Figure 5.5).

When ventilated, the total VOC intensity remained stable for the first three measurements (16h38, 18h38 e 20h38), however a decrease was observed afterwards. Hence the total VOC intensity was highest during the first 4 hours of the experiment under ventilated conditions. Later, a relatively small decrease was present during the early hours of the day (from 5h to 7h) and after this period a small increase in the total VOCs is visible until midday (12h38). The total VOC intensity decreases once more after midday until the end of the measurements in ventilated conditions.

A clear difference between ventilated and unventilated conditions can be seen from the results. VOC emission in ventilated and unventilated conditions seems to be affected by time and/or daily variations of temperature, since during the coldest hours, 22h to 7h the total VOC intensity was significantly reduced in comparison with the rest of the day. However, the intensity of all VOCs during unventilated conditions shows more stable values over time marked by a significant increase at the last three measurements collected.

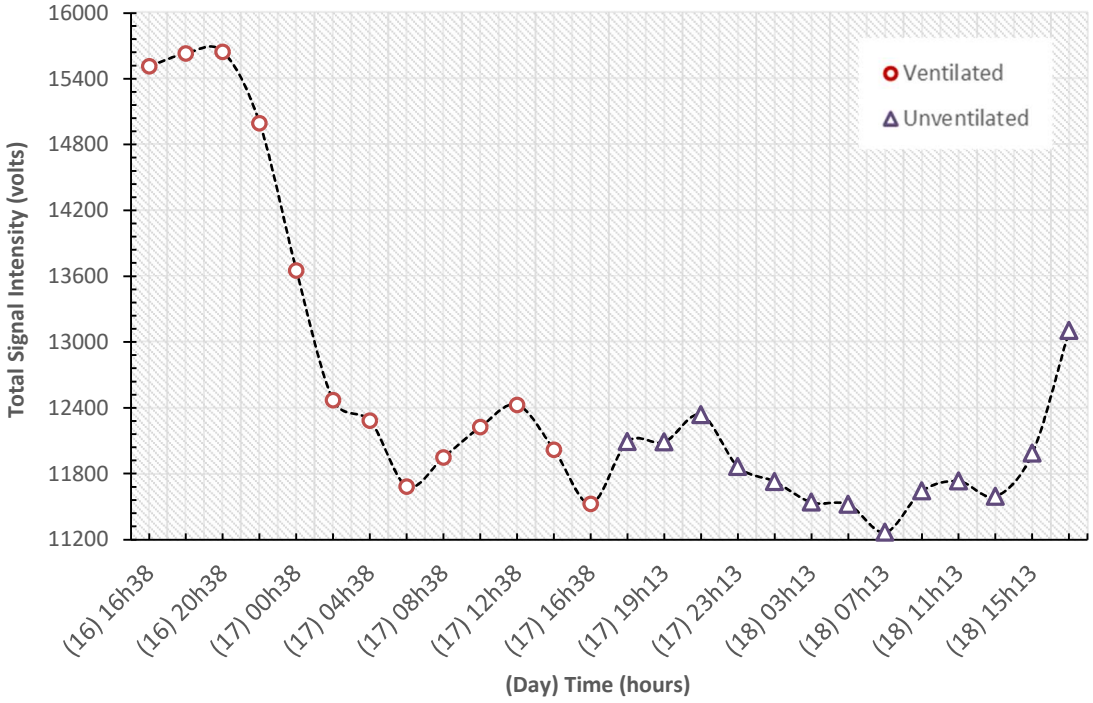

Figure 5.5 — Total volatile organic compound intensity from indoor air measurements in a total of 48 hours with a period of 24 hours ventilated interval and another 24 hours in an unventilated state.

Further analysis of the 28 peaks could provide their possible source and origin within the confines of the laboratory and explain some of the variation observed over the 48-hour period. Therefore, it could be advantageous if further measurements were to be sampled in the absence of any furniture or wallpaper and a comparison between outdoor and indoor air, in order to provide aid in understanding and evaluating how daily environmental changes influence indoor air.

An additional test related to indoor air variation was performed in which air samples were collected without and through a sampling tube, two Teflon tubes with one and two meters in

length were compared and two different locations inside the laboratory were measured. Each sample tube was connected to the sample inlet of the *BreatSpec*® prior collecting a sample.

No major differences were found between measurement localization, tube length and plain sample inlet vs sampling tube. Although measurement location and the presence of a sampling tube showed no significant changes, daily variations of VOC were evident. This fact was also seen during ventilated vs unventilated conditions and indicates a high level of sensibility from the IMS device and a favourable ability to detect and identify VOC changes during long intervals in indoor air.

All data collected and analysed until this stage indicates flow D is a great approach for the separation of VOCs in the retention time dimension, for simple and complex mixtures, as well as, adequate to monitor changes over time. During the preliminary tests described in these sections, flow D was used to monitor air quality and applied in the development of a sampling procedure through the programable option of the GC-IMS. Also, considering this program was designed with the aim of using it in simulated conditions of the ISS a final stage in preliminary testing includes the monitorization of VOC changes due to microbial contamination.

5.1.4 Examination of emission due to microbial contamination

To examine changes in the VOC emission triggered by microbial growth a simple test was designed to monitor the degradation, or spoilage, of freshly squished orange juice. The sampling preparation involved squeezing an orange isolating its juice into a container. From the container 1 mL was collected via pipette and place into a vial (20 mL). Headspace equilibrium was achieved after waiting 3 hours and afterwards a gas volume of 1 mL was collected from the vial using a syringe, and injected into the GC-IMS sample in. Follow-up samples were collected during the subsequent 5 days at approximately the same time as the first measurement. Three replicates were performed for each measurement to ensure repeatability of measurements.

Minimal differences were observed between the VOC emission collected on day 1 and day 2, thus demonstrating an absence of juice degradation during the first 48 hours (Figure 5.6). However, at the third day, a substantial difference was identified, the presence of new and intense signals between retention times of 150 and 180 seconds. On day 4 those newly found signals persisted in the volatile emission of orange juice and only a small intensity decrease was observed on a group of four signals present since day one, marginally above 150 seconds (retention time). The last day measurement was still dominated by the signals found in day 3 which saw an overall intensity increase of most signals with a decrease in signal intensity of signal above 210 seconds.

Those results suggest microbial contamination occurred between day 2 and 3 since at this time frame emission is characterized by the appearance of new signals while accompanied by a visual discoloration of the sample. This visual discoloration evolved into fungal filament during the remainder days of the experiment.

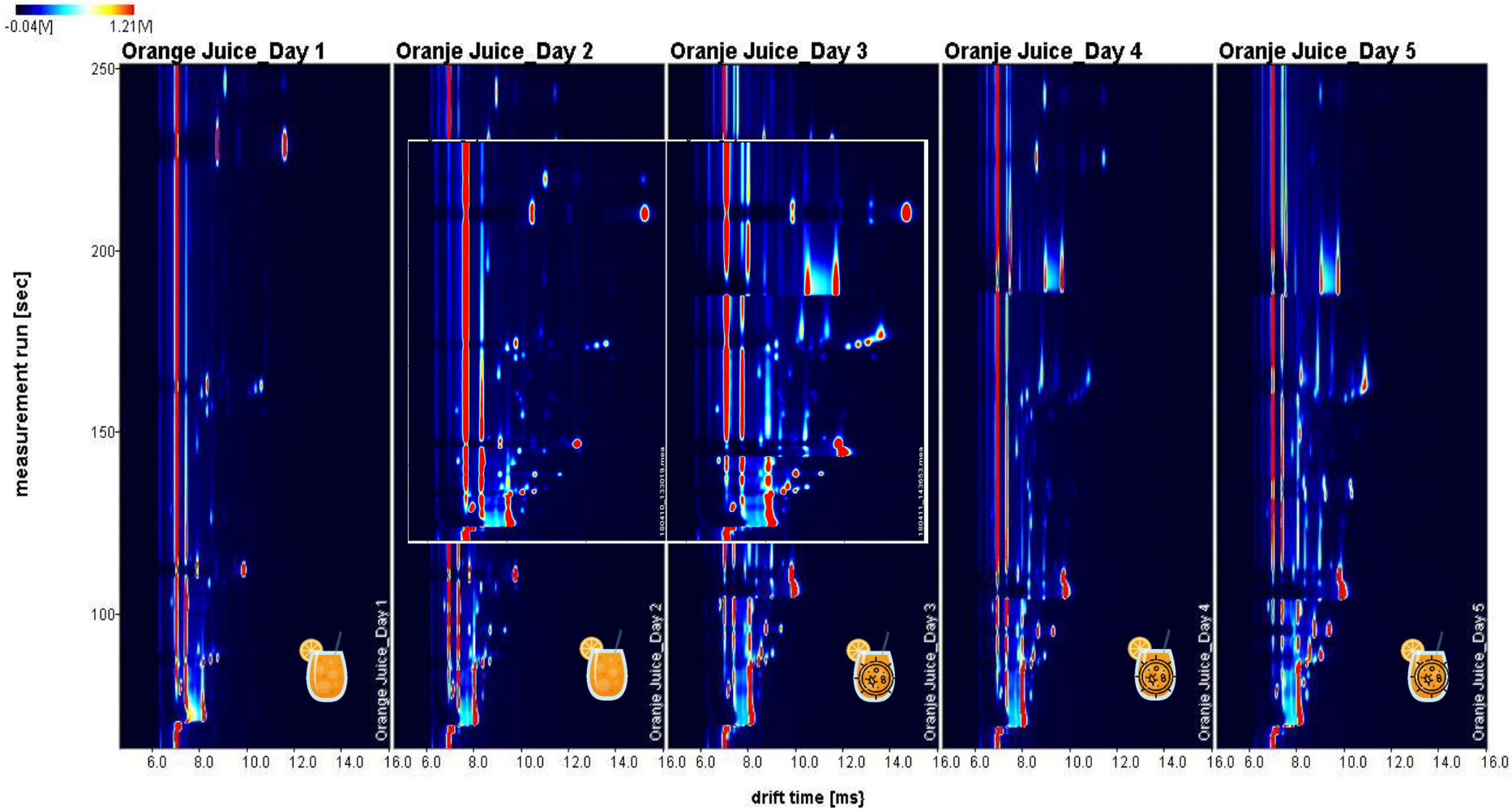

Figure 5.6 — Volatile organic compound emission from freshly squished orange juice over 5 days and an highlight of the characteristic pattern of microbial decomposition from day 2 to day 3.

This last preliminary test showed GC-IMS could also operate as a tool to monitor and characterize changes in VOC emission initiated by microbial degradation and, likewise, validates the selection of flow D as a good separation setup for different types of mixtures under distinct conditions. Consequently, the results of all preliminary tests provide a general perspective on the capabilities and results possible with the analysis of samples with GC-IMS. Those tests also allowed the development and optimization of a sampling program to be used in the monitorization of compounds in simulated conditions of the ISS because it provided a high degree of separation between signals.

Hence an optimized sampling program was developed and added into the GC-IMS programs window with information on several parameterization actions and their schedule over the time frame for sample measurements (15 minutes). The parameters contained in the setup include, program name - TOL-SIRIUS, averaging value, EPC2 flow ramp, corresponding to flow D, EPC1 values, a constant 150 mL/min, starting and stopping times for spectra recording, when to open and close the 6-way valve and when to active the loop purging pump and its corresponding power in percentage (Table 5.2).

Table 5.2 — Developed and optimized sampling program after several preliminary test in indoor and VOC analysis.

NAME	TOL-SIRIUS		**AVERAGES**	6	**Notes:** this program was optimized during a series of preliminary testing phase and is based on flow D setup							
EVERY	--		**Apply**	--								
EPC2 mL/min)	10	10	10	10	25	40	50	65	85	100	100	
EPC1 mL/min)	150	150	150	150	150	150	150	150	150	150	150	
Recording	**REC**										**STOP**	**End**
Valve		**OPEN**	**CLOSE**									
Pump (%)	off		20%								20%	
TIME	**00:00**	**00:10**	**00:14**	**01:00**	**03:00**	**05:00**	**07:00**	**09:00**	**11:00**	**13:00**	**15:00**	**15:00**
	Start Values											

This early phase involves several experiments aiming to comprehensively test ion mobility spectrometry capabilities to detect volatile organic compounds from different sources or origins. Therefore, the primary tests served to quickly access GC-IMS capabilities for: (i) volatile organic compound analysis, including sensitivity and sensibility to minor, and major, differences between diverse sample types and their respective emission patterns, (ii) IMS effectiveness for the separation of simple and complex mixtures and (iii) its usefulness in monitor volatile composition changes over different periods of time in indoor air samples and microbial degradation.

The aim of creating a sampling program, parameterization and approach was primarily to construct a methodology, as adequate as possible, to monitor cabin air change and volatile organic compound emission during an experiment under simulated habitation conditions aboard the ISS. This experiment is named SIRIUS-17 and will now, be discussed in the next segment.

5.2 The SIRIUS-17 Experiment

The SIRIUS-17 experiment is an analog mission from the Scientific International Research In a Unique terrestrial Station (SIRIUS) program, a partnership between NASA's Human Research Program (HRP) and Russia's Institute of Biomedical Problems (IBMP), at Ground-based Experimental Complex (NEK: Nezemnyy Eksperimental'nyy Kompleks). SIRIUS-17 is named due to its duration, a 17-day mission during 2017, beginning on November 7, in which six human participants were isolated and confined in a mock-spacecraft habitat while performing scientific experiments [176, 177, 178].

The SIRIUS missions aim to understand risks of longer and further outwards space travels into our solar system through analog complexes which complement the human research being conducted on the ISS and were created to expand the knowledge of how the human body reacts to, and changes in unique environments [179].

Likewise, NASA's Human Research Program (HRP) is a dedicated program to find and develop the best methods and technologies to support safe and productive human space travel and enable space exploration through the reduction of health and performance risks to astronauts using ground research facilities, the ISS, and analog environments [179, 180]. NASA defines analog missions as field tests in locations with physical similarities to the extreme environment of space. Analog missions have been used in the past to prepare for leaving Earth's atmosphere, the moon landing and permanently orbiting our planet and currently are actively used for deep space destinations including asteroid or Mars [179, 180]. Analog missions are generally performed in cooperation with government agencies, academia, and/or industry to provide NASA with data on strengths and limitations associated with technologies, communications, power generation, infrastructures, behavioural effects due to isolation, confinement, and materials, eventually validating a research design and strategic mission [195, 196].

5.2.1 Structure of the Ground-based Experimental Complex

The NEK complex is a structure of the IBMP from the Russian Academy of Sciences in Moscow, Russia, built in the 1960's and defined as a closed habitat by NASA, where isolation and confinement experiments are conducted. NEK is a unique and multi-compartment facility and offers a pressurized facility which physically isolates crew members from the outside world under limited communication, simulating an actual spaceflight environment, also referred to as an analogue facility. Historically this complex has already housed several isolation studies, including the Mars-500 Project composed of three mission with increasing durations, 14 days, 105-day mission and a final mission which simulated a 520-day human mission to prepare for an unspecified future human spaceflight to Mars [181, 182].

The structure Ground-based Experimental Complex, or NEK, is a medical and technical experimental facility, composed of four modules also known as experimental units, EU, (EU-50, EU-100, EU-150, EU-250) (Figure 5.7) used for different functions, with dedicated structures and equipment and a simulator of the Martian surface (SMS) connected to module EU-50 (Figure 5.8) [183].

Module EU-50 has a total volume of 50 m^3 and is used to simulate a module for landing on the Mars surface with a total occupancy of 3 crew members during 2 to 3 months. EU-50 includes, life support systems, living quarters, a working zone, a kitchen, a bathroom and two transfer tunnels with hatches to access module EU-150 and the SMS.

Module EU-100 has a total volume of 100 m^3 serving as a medical bay and experimental site with several medical equipment installed, life support systems, a working zone, a kitchen, a dining space, a bathroom, a transfer tunnel to the EU-150 module, a hermetical door at the end of the module and an emergency hatch at the opposite end of the module [183].

Module EU-150 has a volume of 150 m^3 and life support systems to accommodate 6 crew members in 6 individual quarters, a living-room for leisure and general gatherings, a kitchen, a bathroom, three transfer tunnels with hatches to access module EU-50, EU-100 and EU-250.

Lastly, module EU-250 has 250 m^3 of volume and life support systems dedicated to storage including tools, dishes, clothes, garbage disposal, food and an experimental greenhouse with a freezer, several shelves for storage, a gym, which is connected to EU-150 and two hermetical sealed doors with metallic stairs at the end of the module for pre-launch loading of food stores [183].

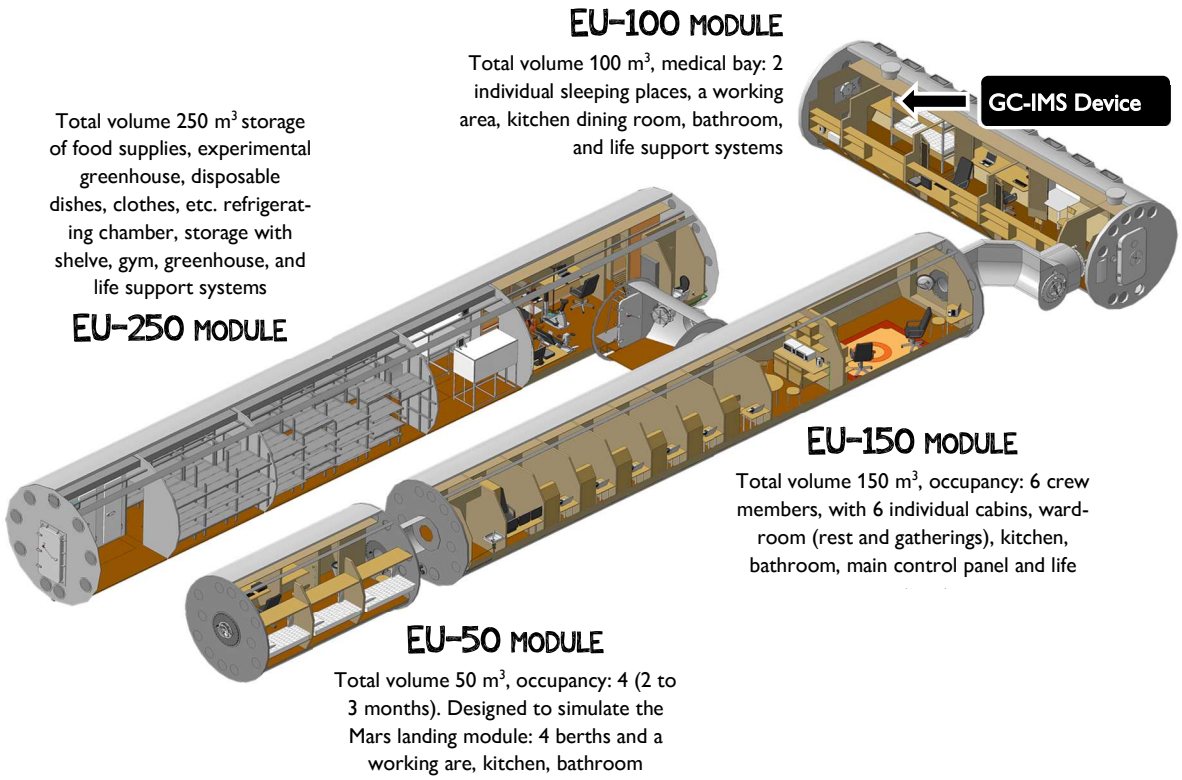

Figure 5.7 — General structures of the Ground-based Experimental Complex (NEK) and layout with all modules labeled by name with a summary of their uses and equipment. The location of the GC-IMS device during the SIRUS-17 experiment is also marked in the image [183].

The SIRUS-17 mission was also designed according to the capabilities of the NEK facility, including planning and integration procedures to identify challenges or issues in a shorter format but avoid such

complications during mission of longer durations. The main objectives for SIRIUS-17 included, identifying types of investigations most suitable for subsequent missions, learn from the integration of international science processes and to elaborate scientific data sharing protocols.

During SIRIUS-17 NASA's Human Research Program, both NASA and IBMP led research to identify preventive measures and technologies to protect astronauts' health during spaceflight. NASA main goal was to determine NEK's suitability as a ground analogue for exploration class spaceflights in future experiments and IBMP goals were to study biomedical and psychological problems in humans associated with isolation and restriction of space.

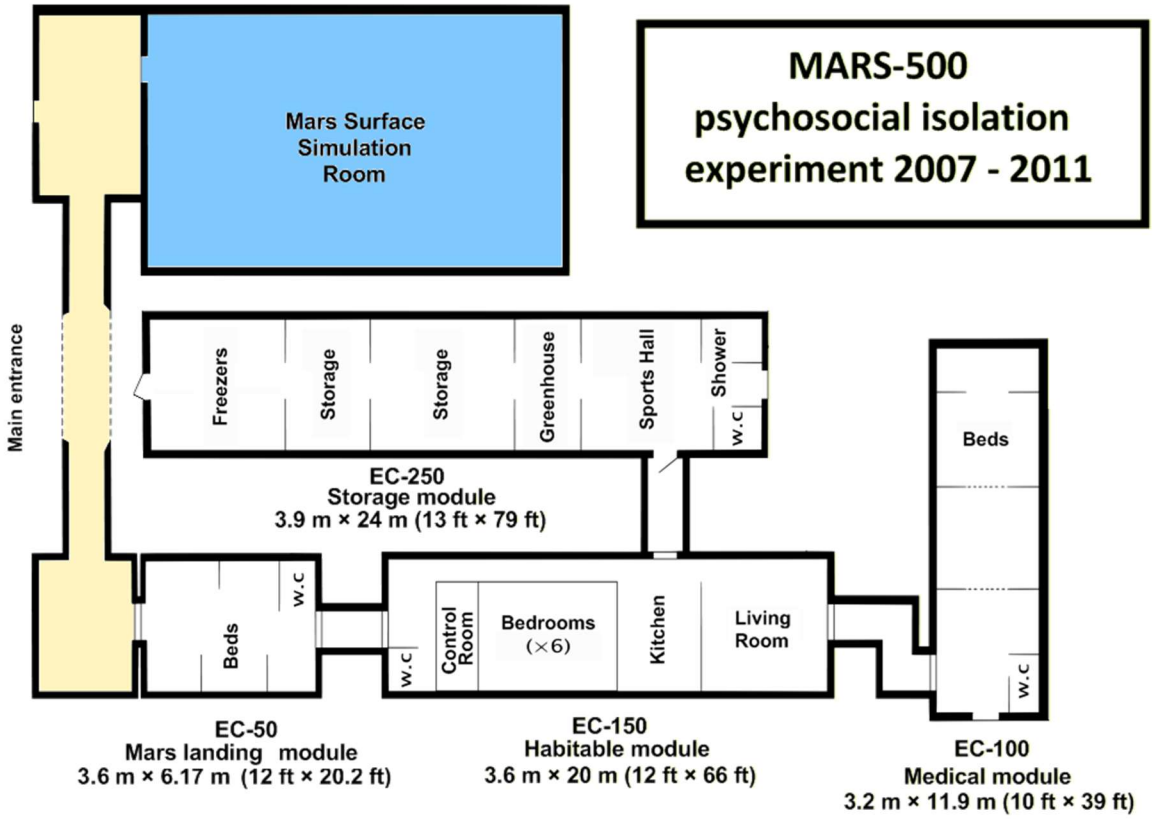

Figure 5.8 — NEK bluepring showing its five modules: habitat, utility, medical composing the main spacecraft, a Martian-lander ship and a simulator of the Martian surface, for a combined volume of 550 m^3 [184].

The SIRIUS-17 experiment included over forty investigations, four by NASA's Human Research Program (HRP) and other from IBMP and the European Space agencies (ESA) hence it offered a great opportunity to access GC-IMS capability for the detection and monitorization of 34 Priority VOCs defined by IBMP's experts to be monitored at the RS-ISS.

The most important line of research conducted during SIRIUS-17 included six types of studies: (i) consolidated studies related to quality of living, health, and psychological condition in isolation, (ii) psychological and psychophysiological studies, (iii) further specific physiological studies, (iv) immunity, metabolic, biochemical, and genetic studies, (v) sanitary/hygienic and microbiological research and (vi) telemedicine [176, 177, 178].

5.2.2 Overall Goals and Experimental Schedule

SIRIUS-17 involved numerous scientific trials including experiments related with sanitary/hygienic and microbiological research which became an incredible opportunity to test GC-IMS as tool to monitor an air quality. The goals in SIRIUS-17 were to sample cabin air several times over the full extent of the 17 days and evaluate GC-IMS sensitivity, sensibility, and analytical performance for the detection of VOCs in an ISS simulated environment [185].

The GC-IMS device together with the CGFU were placed inside the EU-100 module, in dedicated shelf as shown in Figure 5.7. The GC-IMS only required a power outlet for energy supply because the CGFU purifies its carrier and drift gases through a series of filters. Therefore, a constant gas supply of any type was unnecessary. The combination of CGFU and GC-IMS operated continuously with minimal maintenance performed. Initially measurements were planned to be sampled regularly every day at the exact same time, however due conflicts with medical experiments mainly related to earing and noise influence in psychological and psychophysiological status, it was not possible to keep the device continuously operating. Although the noise intensity produced by the GC-IMS was low, it would negatively influence other experiments and an agreement was reached, where the instrumentations would operate outside other experiments timeframes. Hence, before collecting any sample the device would be turned on, and a status verification would be performed by one of the participants, if required a cleaning procedure would be initiated prior to any measurement to unsure accurate results. An uninterruptible power supply was also connected to the GC-IMS and CGFU system in case a power outages or other irregularities could occur guaranteeing measurements would not be lost or interrupted.

Cabin air samples were measured with the previously developed program, TOL-SIRIUS, which controlled sample volume, measurement running time, temperature, GC column and drift region flow. Measurement files generated were stored in the internal memory of the *BreathSpec*® device (GC-IMS) and regularly copied to an USB flash drive as a secondary safety measure. The whole data was examined using the LAV software to provide spectral analysis and visual representation in 2-D or 3-D formats, amongst other functionalities.

The *BreathSpec*® and CGFU were placed inside module 100 of the NEK Habitat and powered on October 31st. An initial system check was preformed and the integrity of all instrument connections, power cables and gas tubes, was carried out. Additionally, instructions were provided to the system operator, Viktor Fetter (flight engineer 2), which remained responsible for operating the GC-IMS during the 17-day isolation. His responsibilities included powering the system, performing a system cleanse and initiate the recording of air samples during the SIRIUS-17. Due to SIRUS-17 aim of simulating isolation conditions aboard the ISS, flight engineer 2, operated the GC-IMS device alone during the 17 days and no additional contact was required, although, a communication line could be established via mission control if unusual issues or problems were identified. To reiterate, air inside EU-100 module was measured with the CGFU/GC-IMS apparatus which worked in an automatic online status under supervision and operations of flight engineer 2, Viktor Fetter.

Each analysis included a measurement set, which corresponds to a group of five measurements made in 80 min with each measurement lasting 15 minutes. Once a measuring program was finished, its data was saved into the BreathSpec®, or GC-IMS, internal memory and copied afterward to a USB flash by the operator. A total of 23 measurement sets were collected throughout several hours on 12 of the 17 days of isolation of SIRIUS-17 (Table 5.3) inside EU-100 module (Figure 5.9).

5.2.3 Analysis of the Volatile Organic Compound Emission

The results reported from the first pilot study on environmental air toxicology monitorization during SIRIUS-17 (Scientific International Research in a Unique Terrestrial Station) at NEK, the Ground-based Experimental Complex of the Institute of Biomedical Problems (IBMP) from 7th to 24th of November 2017 include a total of 23 measurement sets, collected over 12 days from a total of 17 days of isolation. Spectral analysis yield 33 different peaks in total, out of 115 spectra.

Additional data extracted from measurements includes the obtaining relative height and volume (drift time (t_D), retention time (t_R) and intensity (volts)) of each detected peak. Both relative height and volume parameters are quantified in volts and directly correlated with VOC concentration. Also, relative height and volume approaches for signal quantification were compared in all detected peaks. Although general variation and behaviour of signal over all spectra was identical, quantification through relative peak height is limiting in terms of future quantification, because it only considers one dimension of a signal, height. Henceforth, signal volume, which considers signal intensity variation in 3 dimensions, intensity, retention, and drift time was chosen as the most beneficial approach to quantify signals.

Data from each, peak, or signal, was collected and the mean intensity values for each measurement set, with a total of 5 measurements, was estimated with standard deviation. Standard deviations exhibited overall low values with a minimum value of 0.42 and maximum value of 1431.8 in an mean standard deviation of 20.1, for a total of 726 values (Appendix II, Table A.1). The maximum standard deviation was observed for peak Sir-8, which showed a steep increase in intensity between the first and second measurements collected in November 23 at 12 hours.

An odd behaviour was observed during the first measurement set of November 20. A progressive left shift in drift times over retention times was found and, although data could be extracted from spectra, the full measurement set, 5 spectra, were discarded and excluded from the analysis. This shift might be explained by the measurements being initiated before optimal temperatures for analysis were achieved on the GC-IMS.

From November 8 to 14, measurements were recorded on day 1,2,3 and 7, the second week lasted from November 15 to 21 with measurements recorded everyday expect SIRIUS-17 day 12, and the final week consisted of only 2 days of isolation which both had air sample measured. Once all data from week one was analysed and processed a total of three different signal groups could be established based on signal intensities: (i) high intensity signals (Sir-1, 2, 3, 4, 5, 6, 8 and 9), (ii) medium intensity signals (Sir-7, 10, 11, 12, 19, 20, 21, 27, 28 and 33) and (iii) low intensity signals (Sir-13, 14, 15, 16, 17, 18, 22, 23, 24, 25, 26, 29, 30, 31 and 32) (Figure 5.10, Figure 5.11, Figure 5.12 and Figure 5.13).

Table 5.3 — Time intervals of measurement sets collected during SIRIUS-17 displaying data, experiment days, number of samples (#S), hours and minutes (T) for measurement.

Day	NOV 8 SIRIUS D1		NOV 9 SIRIUS D2		NOV 10 SIRIUS D3		NOV 14 SIRIUS D7		NOV 15 SIRIUS D8		NOV 16 SIRIUS D9		NOV 17 SIRIUS D10		NOV 18 SIRIUS D11		NOV 20 SIRIUS D13		NOV 21 SIRIUS D14		NOV 23 SIRIUS D16		NOV 24 SIRIUS D17	
HOURS	#S	T(min)	#S	T(min)	#S	T(min)	#S	T(min)	#S	T(min)	#S	T(min)	#S	T(min)	#S	T(min)	#S	T(min)	#S	T(min)	#S	T(min)	#S	T(min)
07:00	x2	34, 50							x2	38, 54														
08:00	x3	06, 22, 38	x3	21, 37, 53	x3	15, 31, 47	x2	29, 45	x3	10, 26, 42											x1	03	x4	11, 27, 43, 59
09:00			x2	09, 25	x2	03, 19	x3	01, 17, 33			x3	15, 31, 47									x3	19, 35, 51	x2	15 ; 57
10:00							x4	05, 21, 35, 53			x2	03, 16			x1	52					x1	07	x3	13, 29, 45
11:00							x1	09							x4	08, 24, 40, 56							x1	01
12:00																	x1	55			x4	05, 21, 37, 53		
13:00																	x4	11, 27, 43, 59			x1	09		
16:00	x2	36, 52							x1	55														
17:00	x3	08, 24, 40							x3	11, 27, 43							x3	17, 33, 49						
18:00									x1	00			x3	21, 37, 53			x2	05, 21	x1	52				
19:00													x2	09, 25					x4	08, 24, 40, 56				
20:00	x2	31, 47																						
21:00	x3	03, 19, 35																						
22:00													x2	34, 50			x2	41, 57						
23:00									x3	21, 37, 53			x3	06, 22, 38			x3	13, 29, 45			x3	22, 38, 54		
00:00									x2	09, 25											x2	10, 26		

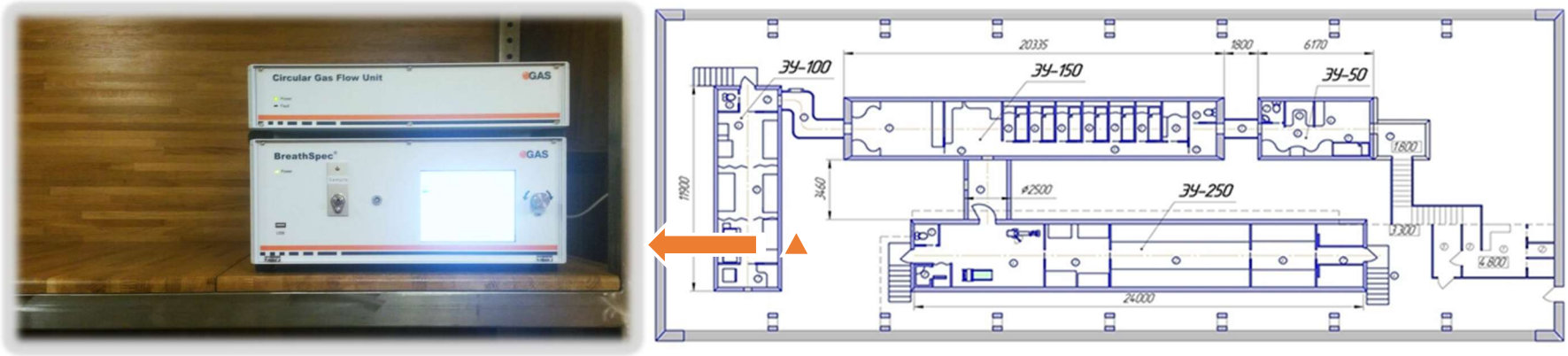

Figure 5.9 — A picture showing location of the CGFU and GC-IMS apparatus is shown (below left) its respective location in the NEK complex blueprint (right) [183]

Overall signal intensities for the second week showed a stabler intensity comparatively with the previous week. The most intense signals during this week were Sir-1, 2, 3, 4, 5, 8, 11, 19 and 27 while the lowest intensity signals were Sir-15, 16, 18, 22, 23, 24, 31 and 32. Medium intensity signals for the second week included Sir-6, 7, 9, 10, 12, 13, 14, 17, 19, 20, 21, 25, 26, 27, 28, 29 and 33. Higher intensities signal however, showed a general behaviour at the end of week 2 characterized by significant increase in intensity during the last two days (day 13 and 14) excluding Sir-8.

During the third and last week of SIRIUS-17 air composition had a similar pattern to the behaviour observed for the last two days of the second week and Sir-1, 2, 3, 4 and 5 were still the strongest signals together with Sir-8, 11 and 27, whereas Sir-14, 15, 16, 17, 18, 22, 23, 24, 25, 30, 31 and 32 showed the lowest intensity in this third week and the remainder of signals, Sir- 6, 7, 9, 10, 12, 13, 19, 20, 21, 26, 28, 29 and 33 can be grouped into a medium intensity set. Sir-8 showed its highest signal during the third week, on day 16 from 12h to 13h followed by a substantial decrease on the later hours of day 16, from 23h22 to 00h26 of day 17. Peculiarly, several signals during this last week show lower intensities than the previous week which might be an indication of removal by ventilation or lower emission rates due to preparations and storage involved with the end of the SIRIUS-17 experiment.

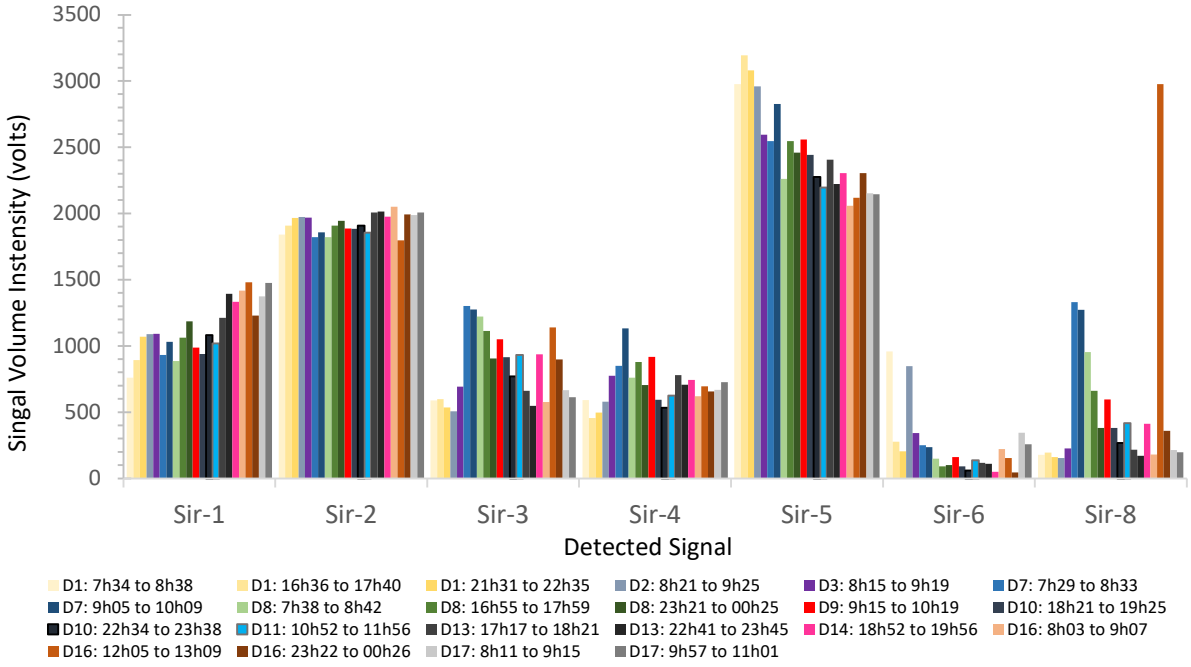

Figure 5.10 — Signal intensity (volume) of Sir-1, 2, 3, 4, 5, 6 and 8 for all measurements collected during SIRIUS-17.

Furthermore, an overall view of all 33 peaks reveals certain peaks have peculiar behaviours over the full extent of SIRIUS-17. Sir-6, for example shows a higher intensity during day 1 and 2 which is followed by a significant decrease afterwards and a reasonably stable stages only changes by a relative increase during the last days of the experiment. However, the most peculiar behaviour occurs for Sir-8, which has a distinctive behaviour, with low intensities during the first week, a moderate increase in intensity during day 7, progressively decreasing during week 2, and in a razor-sharp increase in at midday of day 16.

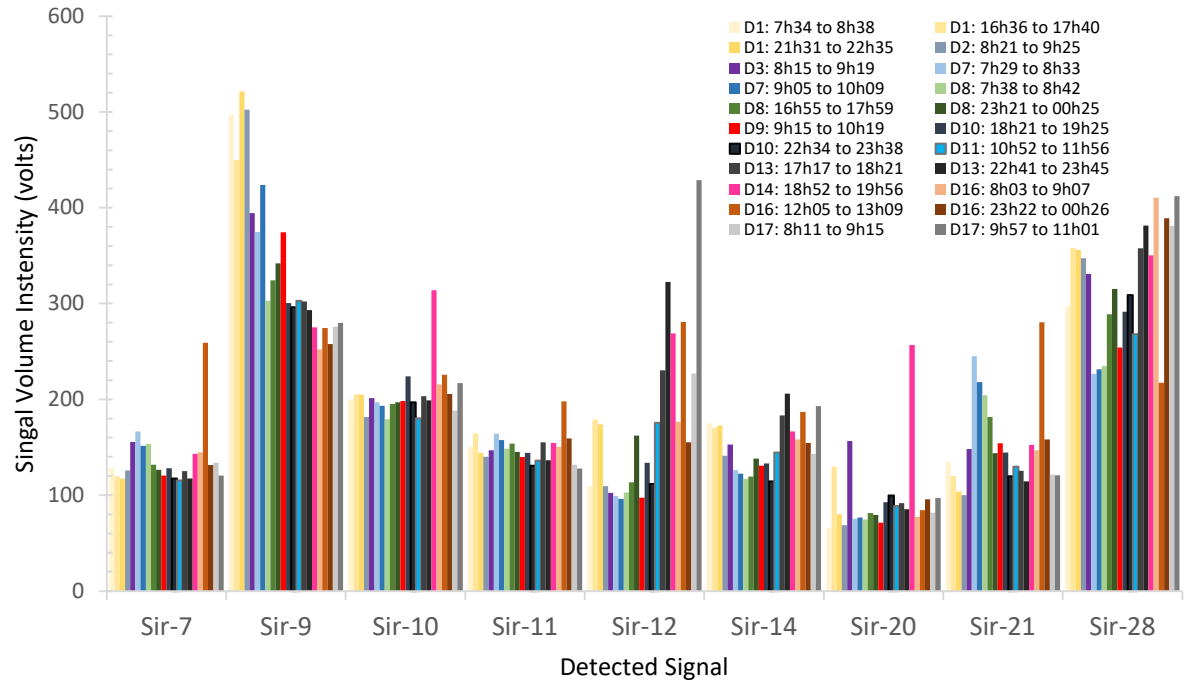

Figure 5.11 — Signal intensity of Sir-7, 9, 10, 11, 12, 14, 20, 21 and 28 for all measurements collected during SIRIUS-17.

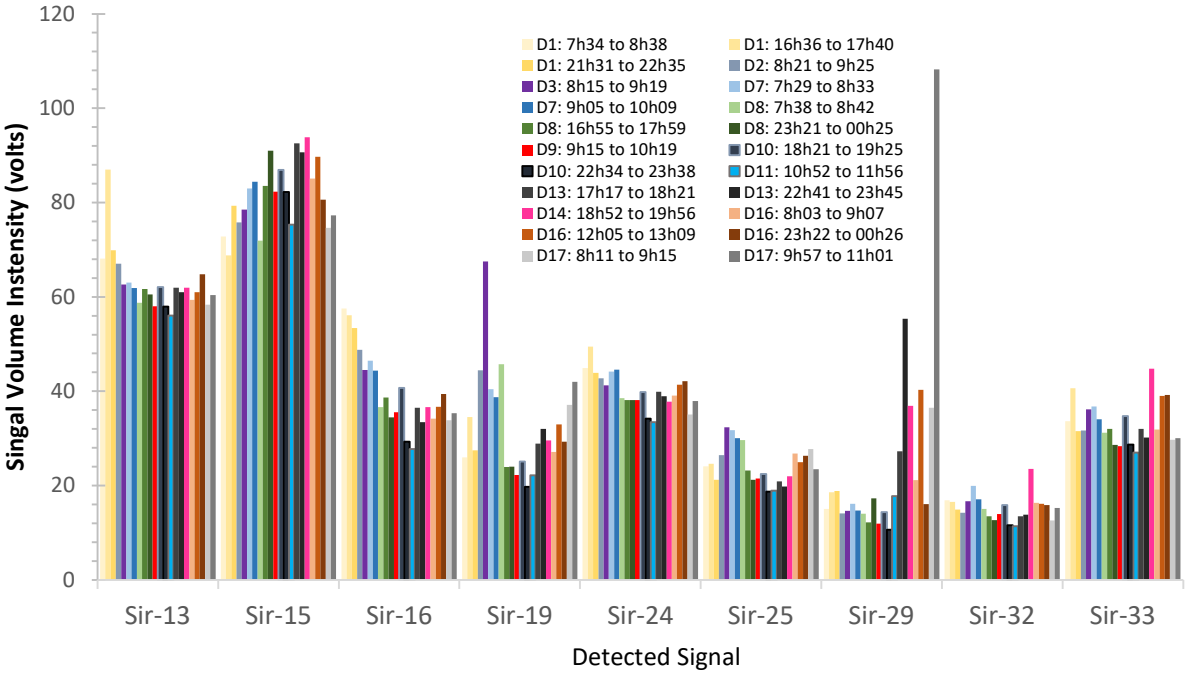

Figure 5.12 — Signal intensity (volume) in volts for Sir-13, 15, 16, 19, 24, 25, 29, 32 and 33 for all SIRIUS-17 measurements.

To summarize a total 33 signals were detected during air monitorization inside EU-100 with three clear groups based on signal intensity; low, medium, and high, and four main behaviours; relatively constant, decreases in intensity, increases in intensity and irregular or abnormal variations. Hence a final, organized based on behaviour and emission intensity can be established for SIRIUS-17 with three levels: (i) unusual signals, Sir-8, Sir-12, Sir-19, Sir-29, remarkable signals, Sir-1, Sir-6, Sir-21, Sir-28 and

unremarkable signals, Sir-4, Sir-5, Sir-9, Sir-11, Sir-13, Sir-15, Sir-20, Sir-18 (Figure 5.10, Figure 5.11, Figure 5.12 and Figure 5.13).

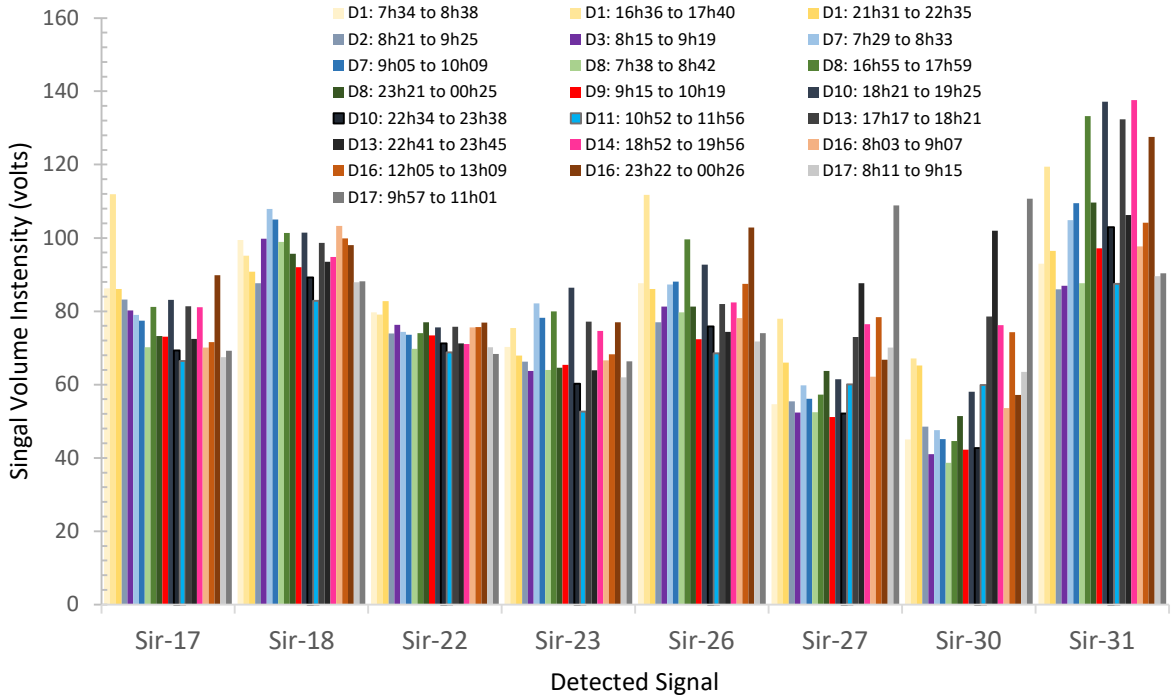

Figure 5.13 — Signal intensity (volume) in volts for Sir-17, 18, 22, 23, 26, 27, 30, and 31 for all measurements.

5.2.4 Identification of detected volatile organic compounds

An early attempt to identify VOCs present in SIRIUS-17 air samples was done with a commercially available tool from G.A.S. named GCxIMS Library tools. Compound identification, in this software, is done by matching both retention times (GC) and drift times (IMS) of a specific signal and cross checking it with retention indexes of a non-restricted version of NIST2014 Retention Index Database with ~400000 annotated Kovats/Lee retention indices for ~83000 compounds. However, current data available at the GCxIMS Library software only allows identification by drift time values because an inability to identifying compounds by retention times arose from the lack of retention times and retention indexes data for GC column use on the *BreathSpec*® (MXT-200).

Retention and drift times extracted from data analysis of all detectable signals from the 115 spectra are presented in Table 5.4 and although a preliminary list of possible compounds could be established from the GCxIMS Library tool, pinpoint a likely candidate was complicated. Therefore, a clear and confident identification of signals was impossible to be achieved through this software.

However, if retention times are further analysed independently, it is possible to affirm that 29 possible substances were detected during SIRIUS-17 with the GC-IMS apparatus, considering signals showing equivalent retention times but different drift times represent dimers or trimers signal from a single volatile organic compound.

Table 5.4 — Retention and drift time of detected signal during SIRIUS-17 and respective identification with CAS number, molecular weight, proton affinity ($Aff._{proton}$) and Hazard class.

Signal	R_t (ms)	D_t (Aust.)	Dt (RIP rel.)	#CAS Number	Name	Mw ($g \cdot mol^{-1}$)	$Aff._{Proton}$	Hazard Class	
Sir-1	73.02	1.1193	1.1530	#64-17-5	Ethanol	46.07 g mol^{-1}	788 kJ mol^{-1}	Health: 2	Flammability: 3
Sir-2	72.3	1.0349	1.0587	#64-17-5	Ethanol	46.07 g mol^{-1}	788 kJ mol^{-1}	Health: 2	Flammability: 3
Sir-3	79.38	1.0763	1.1050	#67-63-0	2-Propanol	60.1 g mol^{-1}		Health: 1	Flammability: 3
Sir-4	89.04	1.1292	1.1641	#67-64-1	Acetone	58.08 g mol^{-1}	823 kJ mol^{-1}	Health: 1	Flammability: 3
Sir-5	103.74	1.0349	1.0587	#64-19-7	Acetic Acid	60.5 g mol^{-1}		Health: 3	Flammability: 2
Sir-6	267.33	1.5480	1.6320						
Sir-7	87.99	1.1686	1.2081						
Sir-8	79.59	1.2144	1.2592	#67-63-0	2-Propanol	60.1 g mol^{-1}		Health: 1	Flammability: 3
Sir-9	103.74	1.1418	1.1781	#64-19-7	Acetic Acid	60.5 g mol^{-1}		Health: 3	Flammability: 2
Sir-10	127.68	1.1686	1.2081	#71-36-3	1-Butanol	74.1 g mol^{-1}		Health: 1	Flammability: 3
Sir-11	116.34	1.0694	1.0972						
Sir-12	112.35	1.0959	1.1268	#141-78-6	Ethyl Acetate	88.1 g mol^{-1}		Health: 1	Flammability: 3
Sir-13	106.89	1.1013	1.1329						
Sir-14	254.52	1.2424	1.2905						
Sir-15	245.7	1.2434	1.2916	#66-25-1	Hexanal	100.16 g mol^{-1}		Health: 2	Flammability: 3
Sir-16	190.89	1.4549	1.5280						
Sir-17	159.6	1.1228	1.1569						
Sir-18	157.08	1.1686	1.2081						
Sir-19	112.98	1.3247	1.3825						
Sir-20	90.3	1.0993	1.1307	#71-23-8	1-Propanol	60.1 g mol^{-1}		Health: 1	Flammability: 3
Sir-21	79.38	1.1686	1.2081	#67-63-0	2-Propanol	60.1 g mol^{-1}		Health: 1	Flammability: 3
Sir-22	109	1.1632	1.2020						
Sir-23	160.89	1.4462	1.5182						
Sir-24	107.5	1.2144	1.2592						
Sir-25	88.62	1.2842	1.3372						
Sir-26	150.57	1.0868	1.1167						
Sir-27	155.82	1.1418	1.1781						
Sir-28	81.69	1.0349	1.0587	#123-38-6	Propanal	58.1 g mol^{-1}		Health: 2	Flammability: 3
Sir-29	112.14	1.3466	1.4070	#141-78-6	Ethyl Acetate	88.1 g mol^{-1}		Health: 1	Flammability: 3
Sir-30	228.27	1.1944	1.2369						
Sir-31	146.58	1.0880	1.1180						
Sir-32	125.37	1.3636	1.4260	#71-36-3	1-Butanol	74.1 g mol^{-1}		Health: 1	Flammability: 3
Sir-33	89.46	1.2383	1.2860	#71-23-8	1-Propanol	60.1 g mol^{-1}		Health: 1	Flammability: 3
TOTAL Signal Identified				**16**	**TOTAL compounds Identified**				**9**
Total Signals Marked				**33**	**% Signals Identified**				**48**

The conclusions of this preliminary identification strengthen the necessity for a VOC database in identification across different IMS instruments and, since the GC-IMS device used herein has been modified, data lacking for the current GC column. Consequently, compound identification was performed via measurements of pure substances which will be described and discussion further along in this dissertation. Compound identification for SIRIUS-17 data resulted in a total of 16 signals recognized as 9 different volatile organic compounds (Table 5.4).

Particularly, Sir-8 was identified as, 2-propanol, a compound commonly used as rubbing alcohol for skin disinfection prior and after blood collection. Flight engineer 2, Viktor Fetter, confirmed several experiments inside module 100 involving blood collection and disinfection had been performed during day 7 and, also confirmed later, an intentional release of rubbing alcohol near the GC-IMS device during day 16 of the SIRIUS mission. The remained of signals were identified as ethyl acetate ethanol, acetone, acetic acid, 1-butanol, 1-propanol, propanal and hexanal and correspond to 48% of the total detected signals in the measured samples from module 100. A dimer and trimer signal were presented for 2-propanol while dimers were found for the remainder compounds except propanal and hexanal.

5.2.5 General analytical performance and conclusions

Results collected during this experiment establish a pilot study for the validation of analytical instrumentation, specifically GC-IMS, for continuous online monitoring of large spectra of VOCs during space flight simulated conditions. Space toxicology in close habitats is a leading subject of research in the current stage of space exploration and aims to protect astronauts' health by measuring possible hazardous during space travel and establish respective safe limits. A crucial aspect in space toxicology is the need for a robust instrumentation and methodology able to monitor and detect known and expected or unexpected volatile organic compounds, in ppb concentration ranges, while providing real-time results.

This pilot study to monitor air quality during SIRIUS-17 showed GC-IMS, as an analytical tool, has a promising value for automatic long-time monitoring of toxicology levels aboard the ISS, spacecrafts, or any other closed spaces. The SIRIUS (Scientific International Research in a Unique Terrestrial Station) experiment, in which SIRIUS-17 is included, consists of a series of analogous missions for space exploration associated with the planned exploration missions to the Moon, Mars and the habitation of the ISS. SIRIUS-17 had six human participants isolated and confined in a mock-spacecraft habitat conducted in Russia's IBMP Ground-based Experimental Complex (NEK) named because of its 17-day duration which started on November 7, 2017, ending on November 24, 2017. Several scientific experiments were conducted during this mission including air quality monitorization inside the NEK habitat, in which cabin air samples and analysis with a GC-IMS instrument, called *Breath-Spec*®.

The developed sampling method and experimental protocol for SIRIUS-17, allowed the detection of 33 different peaks corresponding to 29 VOCs of interest, from analysis of 115 GC-MS spectra, composed of 23 sets with 5 measurements each collected during 12 of the 17-day long experiment (Figure 5.14). A good degree of stability from analytical measurements, 94.78% was obtained since out

of 115 total spectra, only 6 spectra showed irregularities leading to inconsistent and unusable results. Moreover, GC-IMS performance allowed the monitorization of signals over the course of the experiment with overall signals intensity from detected compounds in module100 air increasing mostly with growing days of isolation.

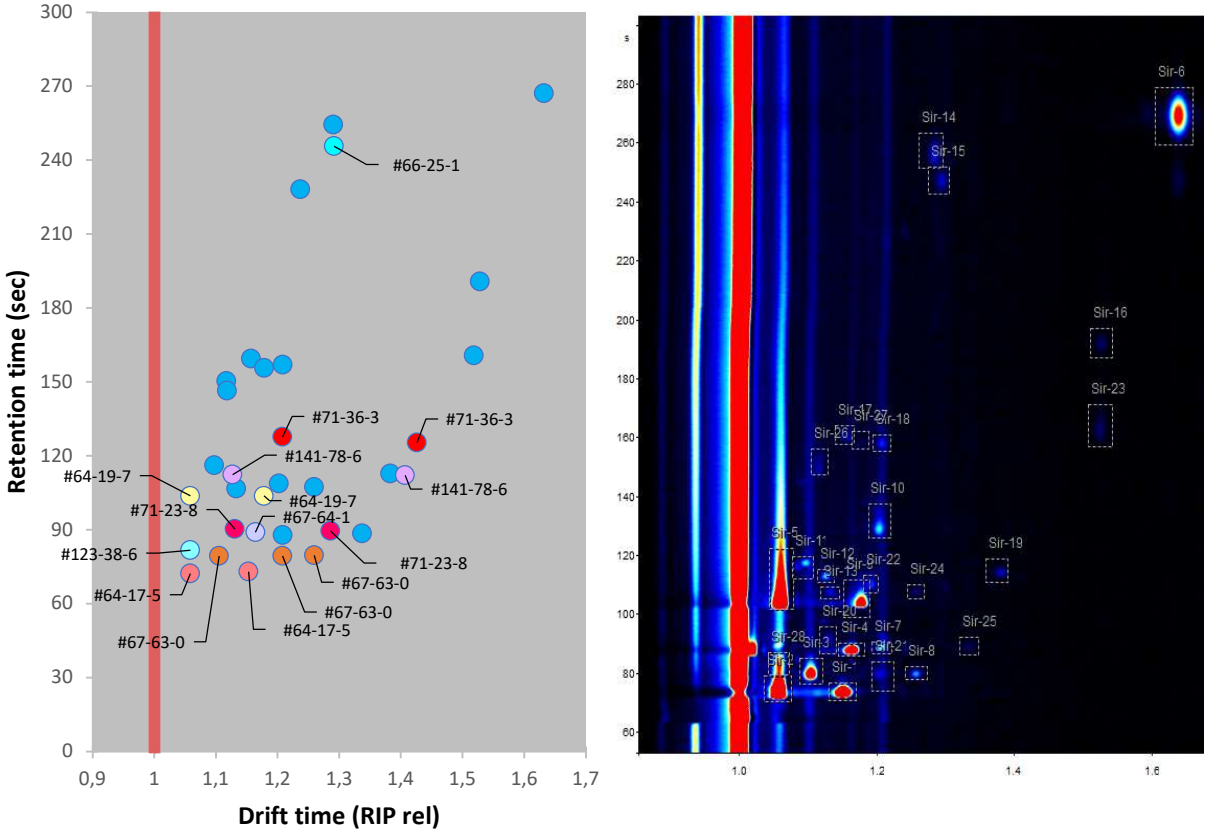

Figure 5.14 — A 2D plot representing retention, drift times for all signals and the CAS number for the respective identified signals (left) and RIP exemplified by a vertical red line. Spectrum collected during SIRIUS day 2 with detected signals labelled, y axis corresponding to retention time in seconds and x axis the drift time relative to RIP which is seen as continuous red signal at 1.0 (right)

Sir-1, 2, 3, 4 and 5 had the highest intensity signal during the full experiment duration and their origin is probably caused by background emissions from structural materials; such has wood or wood agglomerate, plastics from electronic devices or varnishes. Whereas the remainder of the 33 peaks had a more widely distribution in retention times, drift times and intensity variations during the experiment making it hard to speculate their origin.

Sir-8 and Sir-6 for example showed specific behaviours. Sir-8 showed an increase during the last days of the second week and at 16 in the last week, while Sir-6 had a higher intensity during the first recorded measurement decreasing overall afterwards. The source of Sir-8 was attributed to 2-propanol, a compound often used as rubbing alcohol during several medical experiments inside module 100 whereas the intensity variations of other signals could simply be a consequence of continuous human occupation, food products, plants, cleaning processes or even originating from the outgassing of electronic devices and other instruments present in the NEK complex.

The GC-IMS device proved capable of monitoring changes in cabin air constituents and sensing VOC concentration changes over time. While the GCxIMS Library tools could not provide a definite identification for the 33 peaks detected, this challenge was partly resolved afterwards by identifying compounds from pure substance measurements and 48% of the 33 total signals detected were identified as 9 substances. Identification comprised the development of a VOC library containing retention index and drift times for the MXT-200 column and the *BreathSpec*® from compound surveying of pure substances and the construction of a qualitative procedure to establish a relationship between IMS signals and VOC concentration (section 5.6). This last step would allow for acceptable levels of individual chemical contaminants in spacecraft air (SMACs) to be monitored in future and longer missions in spacecrafts and stations (section 5.7). Furthermore, this library was developed considering a list of 32 high priority hazardous VOCs recognized by Airbus as toxic and harmful for human health, performance, and on-board instrumentation.

To conclude SIRIUS-17 results strengthened GC-IMS as a reliable, effective, cheap, fast, and easy-to-use tool to monitor air quality on-line, aboard spacecrafts and closed-spaces and, also for identification and, possibly, quantification of VOCs, which could, in the future help monitor toxicology levels aboard the ISS or other spacecrafts.

5.3 The Breath Stress Experiment

5.3.1 Exhaled breath analysis and mental stress

Breath analysis is a recent research field which has seen a surge in importance and focus due to its tremendous potential as a ground foundation to the establishment of a personalized non-invasive health screening and diagnostics. The creation and development of new sampling instrumentation tools and analytical detection methods has precipitated importance and focus into exhaled breath. Exhaled breath contains a large array of molecules especially with small molecular weight and complex volatile compounds including H_2O, CO_2, NO, NH_3, and VOCs, ketones, aldehydes, alcohols, and hydrocarbons which can be related to regular, irregular, or atypical metabolic processes [186]. This characteristic of breath analysis to monitor biochemical process in the human body in a non-invasive approach has placed it as an emerging and blooming tactic to quickly detect several types of diseases, starting with respiratory infections, and inflammatory conditions such as chronic obstructive pulmonary disease (COPD), and even several types of cancer [186, 187, 188].

Exhaled breath analysis relies on volatile organic compounds generated within the body by metabolic process circulating around the body via blood and cross the alveolar interface to appear in exhaled breath. Measured VOCs are present in trace amounts ranging from parts-per-million by volume (ppm_v) and parts-per-billion by volume (ppb_v) or even lower [188]. However, since exhaled breath analysis is a recent scientific area it shows certain limitations, mainly related to sample collection because, for example, trace compounds produced in the oral cavity, which do not necessarily related to the blood stream can be present in exhaled breath samples [186, 187, 188]. A current need for

standardization of sample collection and analysis is a main issue for the evolution and development of acceptable and accurate monitoring approaches and still hinders the introduction of breath tests in medical diagnosis and monitoring therapeutic stages [186, 188]. Analytical techniques with high levels of sensitivity, accuracy, low analysis times and low detection limits are highly desired and necessary in exhaled breath research and although GC-MS is the gold-standard it has some drawbacks: (i) complex and expensive devices, (ii) requires expert personnel, (iii) longer analysis, (iv) complex sample preparation [186, 187, 188]. However, Ion mobility-based technologies have been explored as a possible and sustainable replacement for mass spectrometry since the innate characteristics and easily understood data originated from IMS prove advantageous in comparison [186, 187, 188].

Identifying disease conditions and states are greatly important for human health on Earth and, even more in spacecrafts and station, however mental stress, high-load and stressful conditions of a spacecraft or station are generally the first concern for astronaut's health and mission success. Monitoring and controlling stressors and stress levels aboard a space station or spacecraft is the frontline to maintain astronauts mental and physical health in check and even mitigate the higher risks to health associated with microgravity and higher radiation levels. Breath analysis has been presented as a non-invasive, real-time approach to monitor and assess stress levels. Although stress has been defined many decades ago by endocrinologist Hans Selye, as an effect of a physiological adaptive response to perceived (psychological) or real (physical) threats or stressors to an organism attempting to return to its own normal homeostatic dynamic equilibrium its boarder concept is more intricate [187].

The overall concept of stress involves several mechanisms activated in response to threats exceeding a given threshold which involves psychological, behavioural, and physiological systems [187]. Two mains stress variants are generally defined, psychological (mental stress) and physical stress with a clear and dominant prevalence for psychological stress in our current society [187]. The brain and peripheral components are both involved in processes occurring in response to stressful condition through the production of several hormones and compounds that elicit the usual stress symptoms: a state of alarm and exhaustion which transforms into muscular tension, irritability, inability to concentrate, headache and an increased heart rate [187]. In case of chronic stress individuals have described an inability to relax, loneliness, isolation, or depression pains, diarrhoea, nausea, dizziness and abuse of alcohol and nicotine [187]. Long term effects of stress have consequences on the human brain and can lead to obesity, metabolic syndrome, type II diabetes mellitus, hypertension, and immunological disruptions [187].

Stressed individuals usually express several compounds, differentially between biological samples, (e.g., blood, saliva, exhaled breath, or breath condensate). Appraisal of specific compounds or their alterations in response to, or associated with stress can be conducted by unobtrusive, real-time methods in humans by exhaled breath metabolomics, also known as "breathomics" [187]. Expensive instrumentation capable of being scalable to a more user-friendly system are usually used in breathomics, including electronic nose-like tools and analytical tools like proton-transfer-reaction MS, selected ion flow tube MS, IMS and laser spectrometry [186, 187, 188]. Additional techniques for accurate sample preparation, sample collection and pre-concentration are often used, although, most are expensive

and unsuited for real-time measurements of exhaled breath. Nevertheless, currently, improvements and developments are in progress to adjust or fit those techniques to real-time measurements [186, 187, 188].

5.3.2 Goals, experimental design, methodology and stimulus

This experiment was conducted as a pilot study to evaluate the performance of a sample collection device, developed in-house to selectively collect samples from the alveolar fraction of the respiratory tree and secondarily to assess IMS capacities to analyse and differentiate breath samples under stress and neutral conditions. The prototype used for sample collection is part of another thesis dissertation between NMT, S.A. and researchers of NOVA School of Science and Technology aiming to develop a device able collect a pre-determined portion of exhaled air through the synchronizing of a previously modelled respiratory cycle and the breathing cycle of the user [189]. The device system is composed of two hardware units, one for hardware communication and an end-user controlled by a specialized and intelligent software built from a machine learning algorithm.

This study was conducted in accordance with the ethical principles of good clinical practice of the Declaration of Helsinki and involved a total of fifteen healthy male non-smokers volunteers (without any occurrences of lung diseases, heart conditions and schizophrenia aged between 20-35 years). Moreover, a series of other conditions were also required for the participation of any volunteers in this study: (a) 2-5 hours of fasting; (b) no prior consumption of any product containing caffeine or taurine; (c) 2-5 hours since the last tooth brushing and mouth wash; (d) minimum of 5 hours of sleep required prior to any test; (e) no hygiene products or perfume used prior to any test and (f) inexistence or only light consumption of alcohol during the 24 hours before sessions.

The study used a randomized cross-over design, which means volunteers were randomly divided in two groups (A and B), attending two experiment sessions (1 and 2). Within each session, participants were exposed to either a stress intervention or a neutral (relax) intervention. The stress intervention was designed to expose subjects to a stressor in the form of a standardized cognitive test, in this case, a Paced Auditory Serial Addition Test (PASAT) which consists of performing a series of mathematical additions from several numbers provided in a paced rhythm by sound. The PASAT is used as the standardized stressor and was initially developed for the evaluation of head injuries consisting of a series of audio files of randomly selected single-digit numbers (between 1 and 9) presented in fixed time intervals [190]. The subject is asked to add the last two mentioned numbers and call out the result. Participation in the PASAT creates anxiety and frustration in subjects however, perceived stress level does not exceed day-to-day stress and is caused simply through high mental workload in an externally controlled pace [191].

During a stress session, the PASAT is performed, firstly with a sound series lasting 2.4 seconds, followed by, a series with a maximum duration of 1.6 seconds. The neutral session consisted of participants watching a video chosen specifically to be actively relaxing and provide a neutral intervention (Figure 5.15).

During session 1, group A was exposed to the stress intervention and group B was exposed to the neutral intervention while in session 2 interventions were reversed and group A was exposed to the neutral intervention and group B was exposed to the stress intervention. Before to any type of measurement each subject was introduced to the experiment and asked to give his written informed consent and volunteers were allowed the possibility to cease the experiment at any time and without any type of justification. Afterwards a questionnaire was conducted to assess each subject personal health background and current health status.

The stress session is first preceded by an explanation of the stressor used and a short training session. Afterwards brachial blood pressure from each subject was measured three times within an interval of 2 minutes to assess their respective baseline blood pressure and is use as reference for the continuous measurements to be performed during stress and neutral interventions. Breath samples, and continuous Galvanic skin response (GSR) and central blood pressure were collected in both stress and neutral session. Before the experiment timer was started, subjects are provided with a few minutes to rest, and establish baselines for GSR and central blood pressure and a breath sample was also collected to serve as exhaled breath baseline (Figure 5.15).

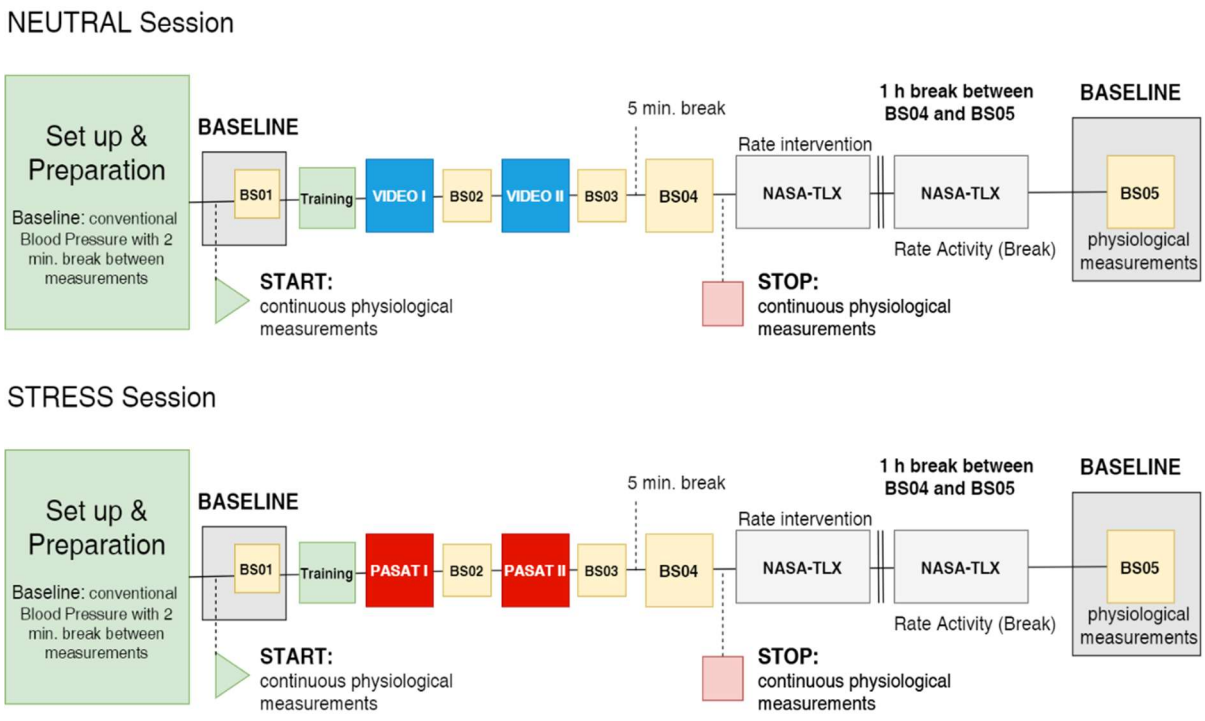

Figure 5.15 — Diagrams of neutral and stress session showing each procedure stage, time frames, breath samples (BS) collected and continuous monitorization of Galvanic skin response and central blood pressure.

Breath samples were measured before any stimulus, directly after the first and second stimulus (stressor/video), 5 minutes after all stimulus and lastly 1 hour after the test has been concluded to monitor long-term effects. Continuous measurements of GSR and central blood pressure are ceased after the fourth breath sample has collected and the timer stopped. The respective equipment is re-moved, and the subject was asked to answer a NASA-TLX questionnaire to rate the intervention

during the fifth breath sample, blood pressure is once more measured to establishing a baseline for each subject after a 1-hour break. The full procedure for both stress and neutral sessions is represented by two diagrams in Figure 5.15 displaying all breath samples collected and when continuous measurements of GSR and central blood pressure are started and stopped.

The devices and technologies used for the measurements involved: (i) a sampler developed by NMT, used for Breath (used previously for clinical studies for breath analysis in nephrology and as part of a PhD project PD/BDE/114550/2016), (ii) GC-IMS, BreathSpec® for gas analysis, (iii) brachial blood pressure was measured with an Omron® blood pressure monitor, (iv) GSR was measured with a Biopac® unit and (v) continuous blood pressure was measured by VasoCheck device (an instrument currently being developed in another doctoral project PD/BDE/114551/2016).

5.3.3 Breath sampling, breath analysis and stress monitoring

Age, body-mass index (BMI), sleep and fasting time were compared between group A and B to assess the homogeneity of the population. Age and BMI both exhibited no significant difference (p-value>0.05) between groups (26.6 ± 5.1 years and 24.4 ± 4.2, respectively). Fasting times were only significantly different (p-value=0.017) between groups within the neutral/relax session with group A showing 3.6 ± 0.8 hours and group B 2.6 ± 0.2 hours and no differences (p-value=0.569) were found between stress sessions. Lastly sleeping times has no significant differences between participants within and between sessions. Hence, study population was considered a single group because no significant or relevant differences were exhibited between participants' cohorts.

Traditional markers for heart rate (HR) and GSR were used to verify stress and relax condition on volunteers during this experimental procedure (Appendix I, Figure A.8). During the relax sessions HR remained constant and stable with no significant changes from the baseline threshold, and both HR and GSR have obvious differences between stress sessions. A higher intensity response is seen in HR and GSR after the first and second stimulus and, average HR showed significant differences between sessions for both stimuli (p-value<0.05) while GSR has no significant differences between sessions. The observation of high variability in HR and GSR after a stressor in comparison with the baseline validates PASAT as a tool to cause phycological stress. Also, NASA-TLX response scores are consistent with HR and GSR results which provides additional confirmation volunteers experienced psychological stress from the PASAT stimulus. NASA-TLX response scores have a range from 0 to 100 and were significantly different between the neutral and stress sessions (13.9 ± 8.5 and 70.4 ± 14.9, respectively) and a higher difference was observed for the stress sessions (42.3 to 94.0) when compared with neutral sessions (5.0 to 28.0).

The sampling program used for breath analysis with GC-IMS was modified from the previous program used in SIRIUS-17. However, due to time constrains and limitations of this experiment a specific program was created to meet all study criteria. Time was hugely important during this experiment, mainly since two stimuli were planned for each session and allowing subjects to wait for prolonged times would have hindered the ability to detect and measure stress indicators in breath. The

breath stress sampling program was created with a total duration of 5 min and constant flows for EPC1 and EPC2, respectively, 150 and 100 mL/min. Data obtained from each breath sample was processed following a specific workflow commonly employed in breath analysis [192]. The first step was to extract numerical values of detected signals from each *mea* file using the LAV software. A group of area sets was therefore obtained manually from all spectra collected and volumes above baseline were estimated for each area yielding a breath matrix with 68 variables representing intensity peaks (or breath VOCs) and was analysed by multi-variate analysis (MVA) considering participants as observations (Figure 5.16).

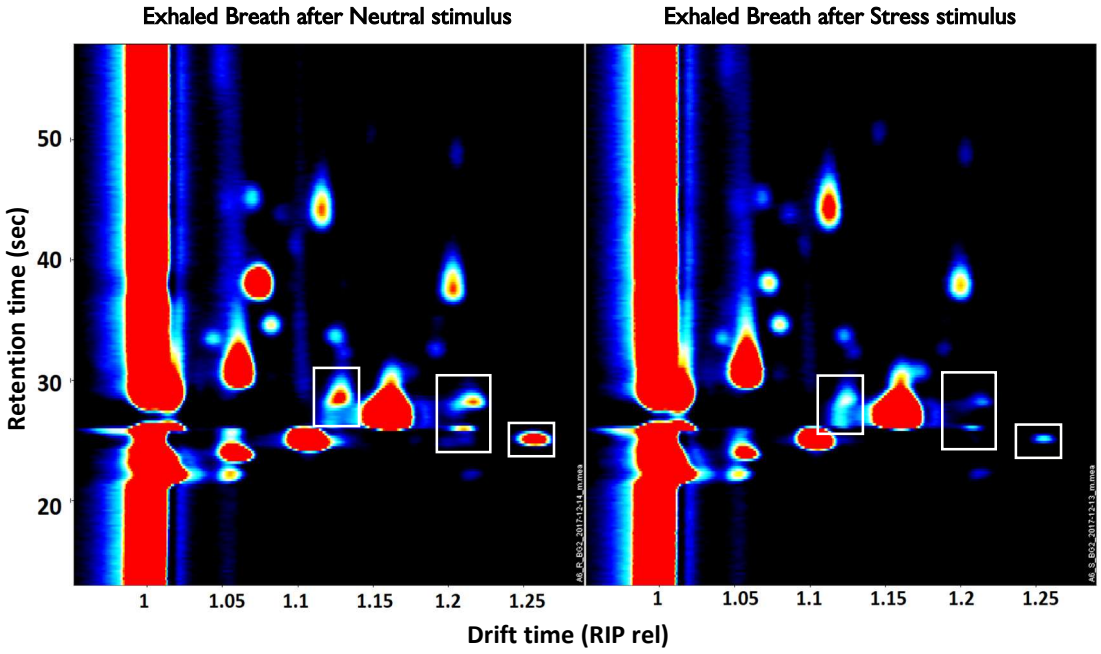

Figure 5.16 — GC-IMS spectra demonstrating signals present in exhaled breath after a neutral stimulus (left) and a stress stimulus (right). Signals labelled with white rectangles represent the main differences between the two conditions detected through breath analysis.

The IBM SPSS Statistics for Windows, version 23 (IBM Corp., Armonk, N.Y., USA) software was used to process all data for the multi-variate analysis. A partial least-square discriminant analysis (PLS-DA) was performed initially for breath samples BS02, BS03, BS04 and BS05 in both stress and neutral sessions. PLS assigned all variables to a solo block with a weighting of 1/√ Block producing a total variance equal to 1 scaled with a pareto variance. The subsequent S-plot of PLS-DA revealed six possible VOC variables changing in response to stimuli interventions which prompted a principal component analysis (PCA) of those six variables (α1 to α6). A comparison through PCA was done for each stimulus between sessions, for example stimulus 1 (neutral) vs stimulus 1 (stress).

Stimulus 1 and 2 corresponding to breath samples BS02 and BS03 produced two score plots where stress and neutral responses cluster together to form individual agglomerates creating a visible separation between breath profiles under stress and neutral conditions (Figure 5.17). The corresponding principal components (PC) for the breath samples collected after the first stimulus were 50.4%

[PC1], 24.9% [PC2] and 16.7% [PC3] of the total explained variance and provided a sensitivity of 61.5% and specificity of 71.4%. In respect to breath samples collected following the second stimulus total variance explained by each PC was 50.6% [PC1], 24.2% [PC2] and 17.5% [PC3] with sensitivity of 78.5% and selectivity of 71.5%. Sample analysis of BS04 and BS05, respectively five and one hour after the second stimulus, exhibited no visible separation between sessions leading to conclude neither mid nor long-term effects caused by stress were identified from breath samples. However, multi-variate analysis indicates a quick response to stress in exhaled breath, consistent with HR and GSR.

From the six signals identified and shown to discriminate the effect of psychological stress by exhaled breath through PLS-DA were linked VOCs via known data cross-referencing. Although retention times for all signals in this experiment cannot be directly correlated with SIRIUS-17 since the EPC2 was a constant value of 100 mL/mn, cross-checking relative positions with other know compounds and their drift time allowed the identification of four compounds.

The signals α2 with drift time (t_D) 1.059 (RIP relative) and retention time (t_R) 24.045 seconds was identified as ethanol (46.07 g/mol), α3 characterized by drift time 1.258 and 25.095 retention time corresponded to 2-propanol (60.10 g/mol). Whereas α4 (t_D: 1.215 and t_R: 28.245) and α6 (t_D: 1.124 and t_R: 29.610) were identified as 1-propanol dimer (60.09 g/mol) and Ethyl acetate monomer (88.11 g/mol) respectively. In respect to α2 and α5 a conclusively identification has not possible, and those signals remain unidentified.

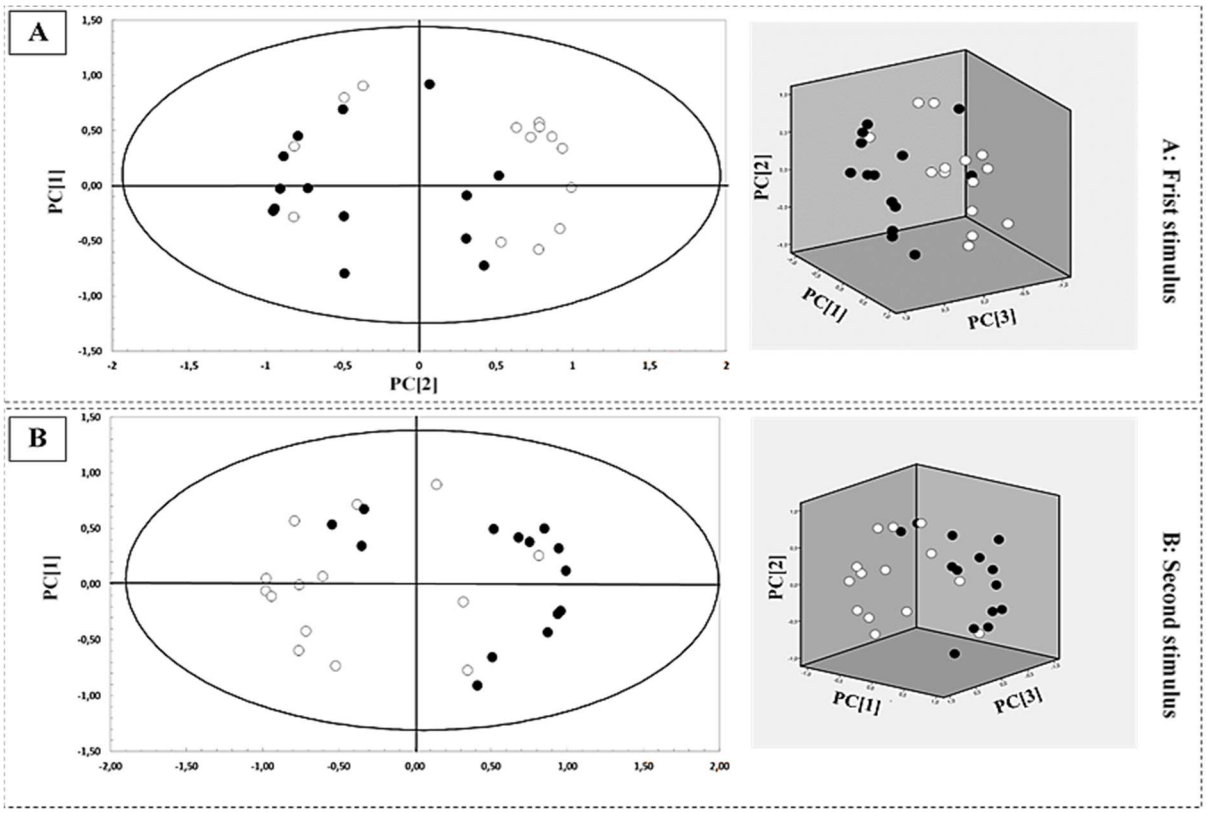

Figure 5.17 — Unsupervised Analysis with Principal Component Analysis (PCA) for all six stress sensitive breath compounds identified through PLS-DA. (A) PCA for the first stimulus (BS02): stress session (black dots) and neutral sessions (white dots). (B) PCA for the second stimulus (BS03): stress session (black dots) and neutral sessions (white dots). Two dimensional PCA is presented in the left and three dimensional PCA is shown in the right side.

Although "Breath Stress" pilot study should be expanded to include a bigger sample size and other age groups, its results demonstrate GC-IMS capabilities for the detection of VOCs in exhaled breath providing high precision and stability. A combination of six signals offered an early classification of stress effect in exhaled breath samples, and although breath analysis has been limited by the lack of accurate and robust instrumentation for sample collection this study shows the potential of IMS has an analytical tool to monitor health in real-time.

Overall, the six-discriminant signals showed a downregulated behaviour after a stress stimulus which might have been caused by increasing heart and respiratory rates during stress. Those are promising results for the use of exhaled breath analysis and VOC profiling as favourable and likely approaches to monitor health aboard spacecrafts and space station as well as on Earth. A deeper and further exploration of exhaled breath and analysis with IMS might augment and strengths, usefulness, and flexibility of this analytical technique for space exploration and planetary occupation by humans.

5.4 Microbial Detection and Identification

5.4.1 Initial Detection and Characterization of Bacterial Metabolites

Initial research was established to evaluate GC-IMS for the detection and characterization of bacterial metabolites by their volatile organic compound emission which involved a collaboration with a master thesis from NOVA University of Lisbon [193]. A direct approach for the detection of microbial organisms would be essential in a tool for air quality control aboard spacecrafts and stations since biological contamination are a high concern and an inevitable problem for space habitation and exploration of other planets.

The aim of this study was to analyse with GC-IMS, the VOC emissions of two common and well characterized microorganisms, *Escherichia coli* and *Pseudomonas aeruginosa* (both Gram-Negative bacteria) grown in solid media. *E. coli* and *P. aeruginosa* are common bacteria which are regularly in contact with humans, *E. coli* is present in human gut and *P. aeruginosa* can sometimes be found in the skin of healthy humans, however, both are opportunistic organisms which can cause serious infections. Also, because both bacteria are Gram-Negative, generally are more resilient to antibodies and antibiotics and, in weak or suppressed immune systems are often responsible for infections.

An experimental procedure was developed to sample, measure and identify specific patterns from both bacteria in different growth media, via a swab sample from grown bacteria in media at room temperature. This swab when placed inside a vial it should contain enough biological material to detect and identify specific patterns of VOCs released by each bacterium grown in solid media.

The procedure is described in five steps (Figure 5.18): (i) a gentle roll back and forth with the head of a cotton swab is done on top of the bacterial culture, (ii) the head of the cotton swab is cut and placed inside a vial with a volume of 20 mL, (iii) the vial is closed and rests at ambient temperature for several minutes to achieve headspace equilibrium, (iv) a 2 mL headspace sample is extracted with a syringe, and (v) the sample inside the syringe is injected into the GC-IMS for analysis.

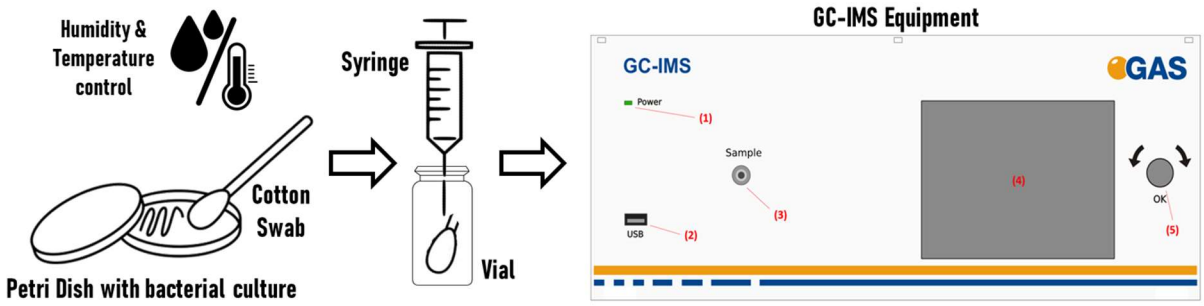

Figure 5.18 — Diagram for the experimental procedure used to measure bacterial emission of volatile compounds.

Additionally, headspace samples for bacterial media were analysed at 40°C and an adjustment was implemented to the previous procedure, replacing step (iii) with a period of heating the vial to 40°C while a direct connection between the vial and the GC-IMS was present through a Teflon tube and, finally, sample analysis was performed by running a sample program in the GC-IMS interface. Three different types of culture media were studied, Tryptic Soy Agar (TSA) and Pseudomonas Agar Base (PAB) media which are specific growth media for *E. coli* and *P. aeruginosa*, respectively, and 'Lisogeny' or Luria Broth (LB) agar was used for the simultaneous growth of both bacteria. A condensed scheme is presented in Figure 5.19 summarizing all bacteria, growth media, experimental conditions and total number of swabs collected and measured during this study is shown.

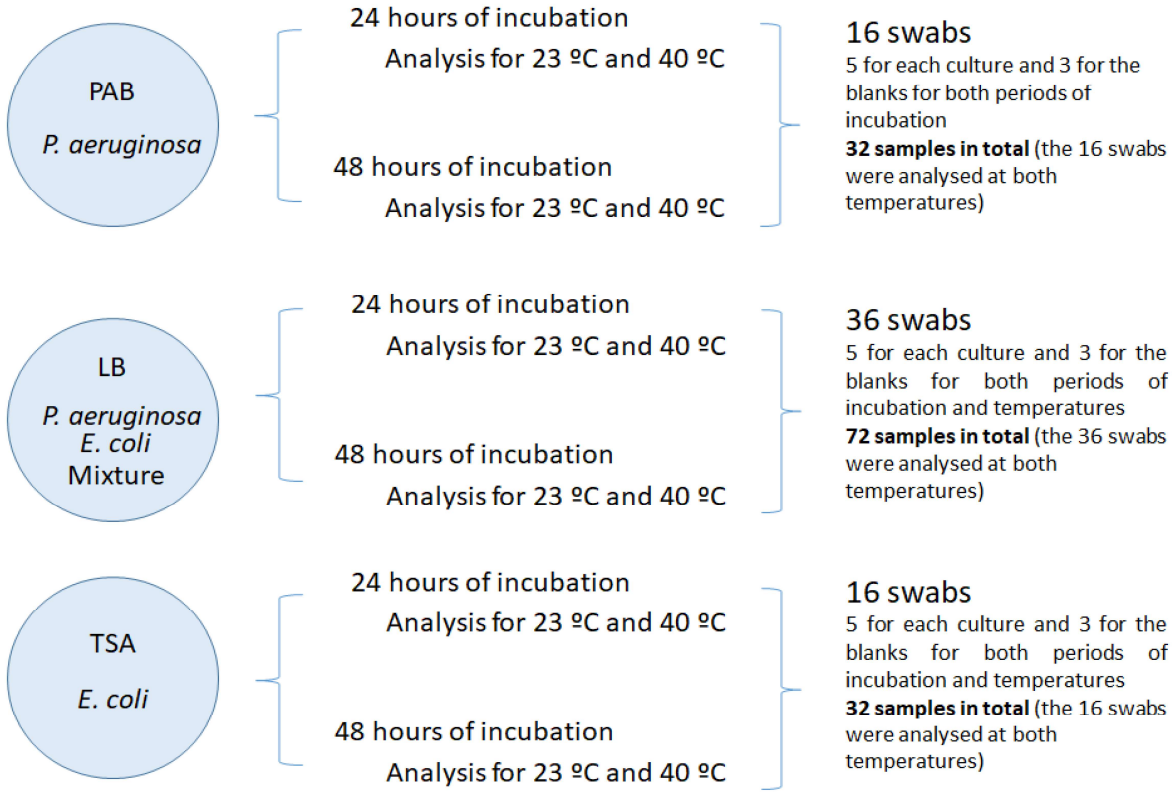

Figure 5.19 — A schematic summarizing all bacteria, growth media, experimental conditions and total number of swabs collected and measured during this study.

The *E. coli* strain used was ATCC 25922 pCU18 while the *P. aeruginosa* strain used was ATCC 27853 and bacteria were incubated at 37°C over a period of 24 hours and 48 hours. Previously to any sample analysis of bacteria growth, culture media were measured to access a background emission and a pattern proving a respective "blank" pattern. The definition of this pattern would allow to identify if VOCs were indeed being produced by bacteria metabolism and if any VOCs from media were changed by microbial growth.

For *P. aeruginosa* grown in LB medium after 24 hours, approximately 30 peaks at room temperature, 23 °C and 33 peaks at 40°C were detected, including new signals and signals with reduction and increases in intensity from blank measurement (medium) (Figure 5.20). A total of 16 signal showed increases and 14 signals decreases at 23°C while 20 and 13 signal increased and decreased respectively, at 40°C. Furthermore, a comparison between 23 and 40°C revealed 11 common signals with reduced intensity and 13 common peaks with increased intensity. The results revealed a common enhancing effect of the temperature which resulted in, signals which decreased from the blank sample to the culture at 23°C, showed a higher decrease at 40°C and, increasing signals from the blank to the culture at 23°C showed higher intensities at the highest temperature (Figure 5.20). A comparison between blank measurements, *P. aeruginosa* grown at 23°C and at 40°C shows similar emission patterns between both temperatures and reveals seven unique signals only present during the bacterial growth.

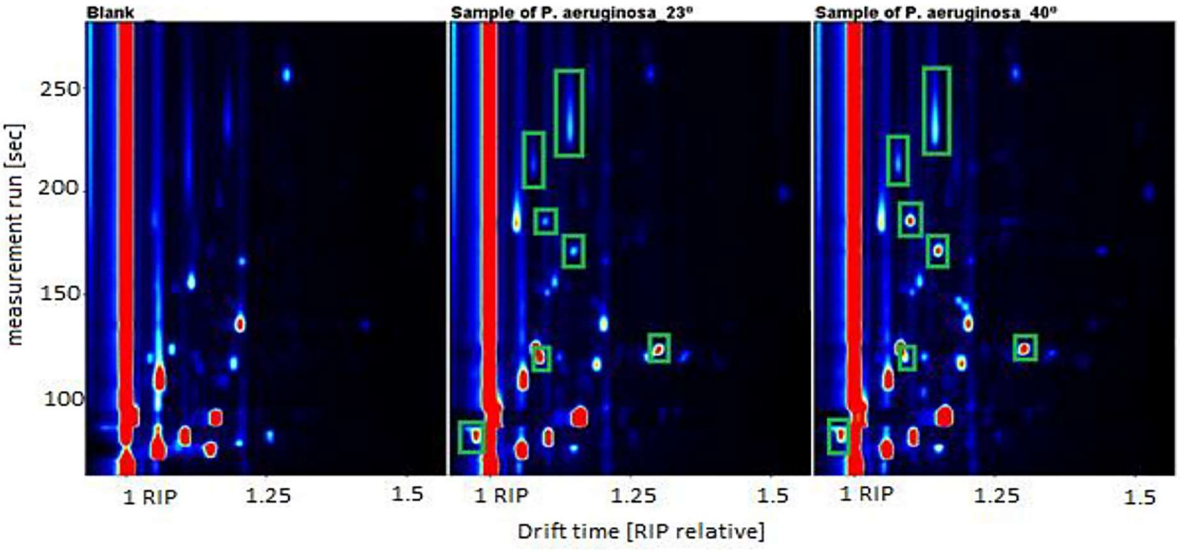

Figure 5.20 — Emission spectra from LB medium, cultures of *P. aeruginosa* at 23°C and at 40°C after 24 hours.

Growth of *P. aeruginosa* in LB medium after 48 hours revealed a VOC emission containing a significantly reduced number of signals, which might have been a consequence of bacteria being less metabolic active, already in a stationary growth phase or microbial senescence (Figure 5.21). A total of 12 signals with significance were detected at 23°C and 15 signals at 40°C. Out of those signals, five showed a decrease in intensity and six an increase in intensity when comparing with media emission. The effect of temperature observed previously, was the same in this situation, with at 40°C having a bigger increase or decrease in intensity compared to the emission at 23°C.

A comparison between emissions from LB medium, culture at 23°C and 40°C, showed only two signals were identified as being uniquely related to the microbial growth of *P. aeruginosa*. The data obtained from *P. aeruginosa* grown at 23°C and 40°C after a 24-hour and 48-hour incubation period show, the emission of this bacterium is incredibly reduced after 48 hours. However, in both periods of time it is still possible to identify signals related to microbial growth showing GC-IMS can identify this microbe via VOC emissions.

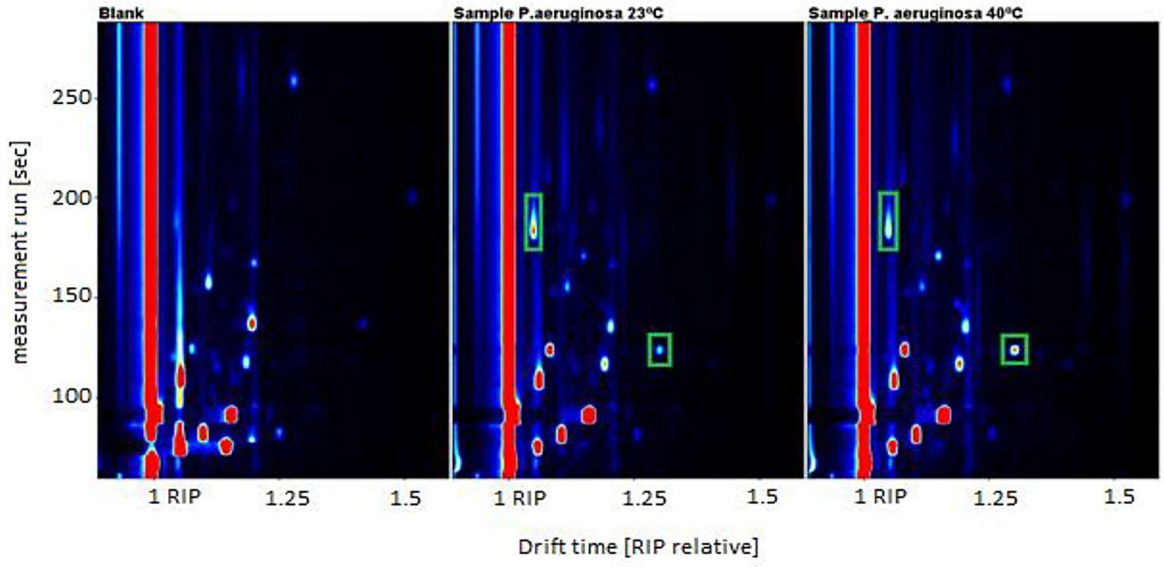

Figure 5.21 — Emission spectra from LB medium, cultures of *P. aeruginosa* at 23°C and at 40°C after 48 hours.

Results from the emissions of *E. coil* grown in LB medium for 24 hours showed a high degree of similarity between the two temperatures, 23 °C and 40 °C. A total of 13 signals showed an intensity decease from the signals present in the blank and 11 signals showing higher intensity from the blank. While at 40°C, 15 signals had a decrease and 15 an increase compared to the medium emission. However, in contrast with *P. aeruginosa* the influence of temperature produced almost no changes in intensity or signal pattern for *E. coli*, possibly because the increase in temperature, of 17°C, might have a smaller influence in *E. coli* metabolism.

The emission pattern for *E. coli* grown over a 24-hour period at 23 °C and 40°C is presented in Figure 5.22. A total of five signals can be identified as uniquely produced due to bacterial growth. Once *E. coli* emission is compared with *P. aeruginosa* emission, significant differences in signal composition are visible without requiring a deep analysis or evaluation.

When *E. coli* was grown for 48 hours at two temperatures (23 °C and 40°C) its emissions show only slight changes. A small reduction in intensity from the unique peaks of *E. coli* detected at 24 hours occurs at 48 hours, and the effect of temperature at 48 hours has little influence in the overall pattern showing only a significant increase of one of the five unique signals (Figure 5.23).

Because signals characteristic of *P. aeruginosa* are reduced after an incubation period of 48h and *E. coli* signals have minimal differences between incubation periods, a mixture of both bacteria was

grown for 24h in LB and at 23°C. This temperature was selected since results for both bacteria are relatively similar between 23 and 40 °C and because 23 °C is similar to all ISS modules temperatures.

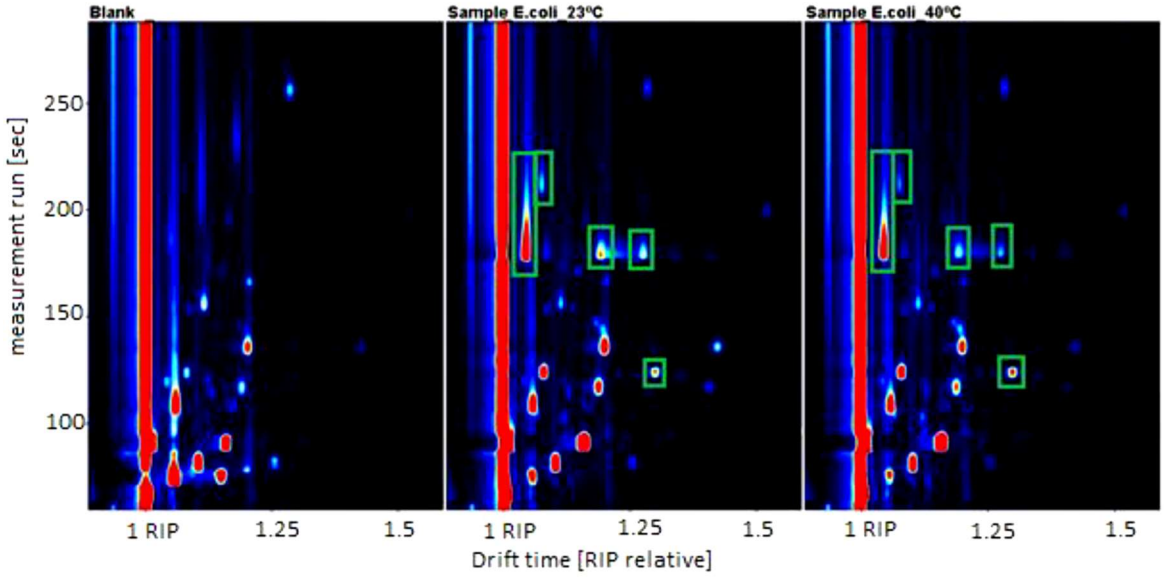

Figure 5.22 — Emission spectra from LB medium, cultures of *E. coli* at 23°C and at 40°C after 24 hours.

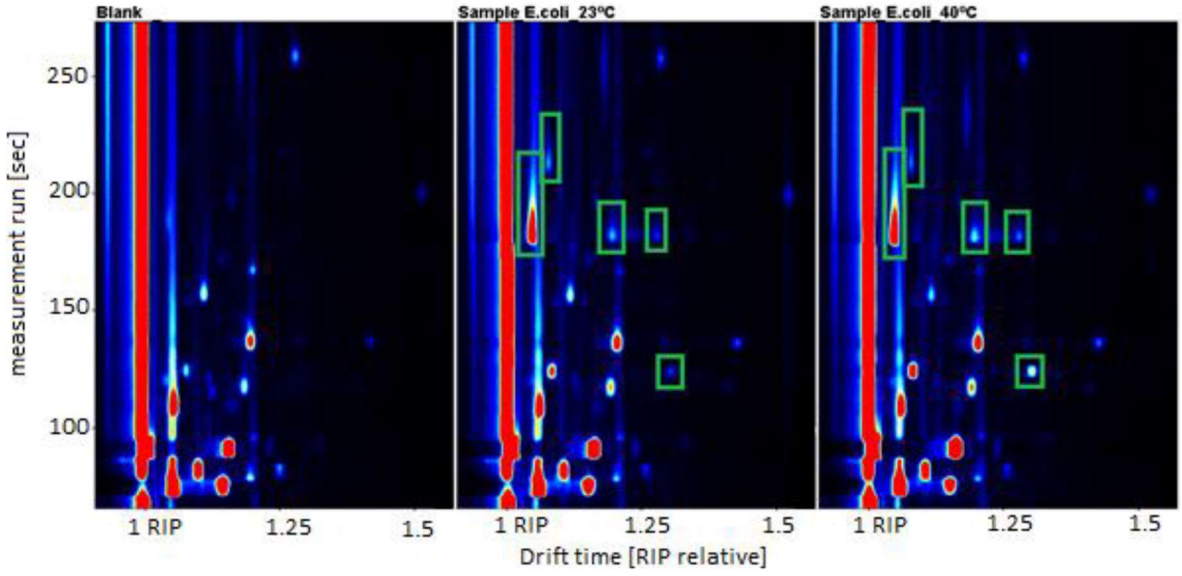

Figure 5.23 — Emission spectra from LB medium, cultures of *E. coli* at 23°C and at 40°C after 48 hours.

A medium of LB was used to simultaneously grow *E. coli* and *P. aeruginosa* for 24 hours at 23°C. In Figure 5.24 several spectra representing VOCs emitted by LB medium, *P. aeruginosa*, *E. coli* and a mixed culture of both bacteria grown for 24 hours are shown. The overall profile of *P. aeruginosa* can be characterized by several signals which either are unique to this bacterium or show intensity changes from the growth medium. Likewise, a group of signals is recognized as the VOC emissions of *E. coli*. Signals marked with green and yellow squares in Figure 5.24 represent bacterial fingerprint constructed from the VOCs emitted during microbial growth at 23°C for 24 hours.

A few signals are shared between individual bacteria emissions which might imply they share similar metabolic pathways producing the same end products. However, a fingerprint established during the microbial growth may perhaps prove different when both bacteria are grown together in the same medium. The emission of VOCs from simultaneous growth of *P. aeruginosa* and *E. coli* does indeed share similar compounds, five signals specifically. Nevertheless, the presence of signals in the mixture is not a complete reflection of each bacterial fingerprint and some signals were absent from the emission of the bacteria mixture.

Moreover, it was interesting to observe some signals had lower intensity in the mixture while a single signal was detected when both bacteria were grown simultaneously. Such observations can be explained by bacteria sharing the same nutrients and resources and perhaps by their interaction leading to a new metabolic pathway that creates a new volatile organic compound.

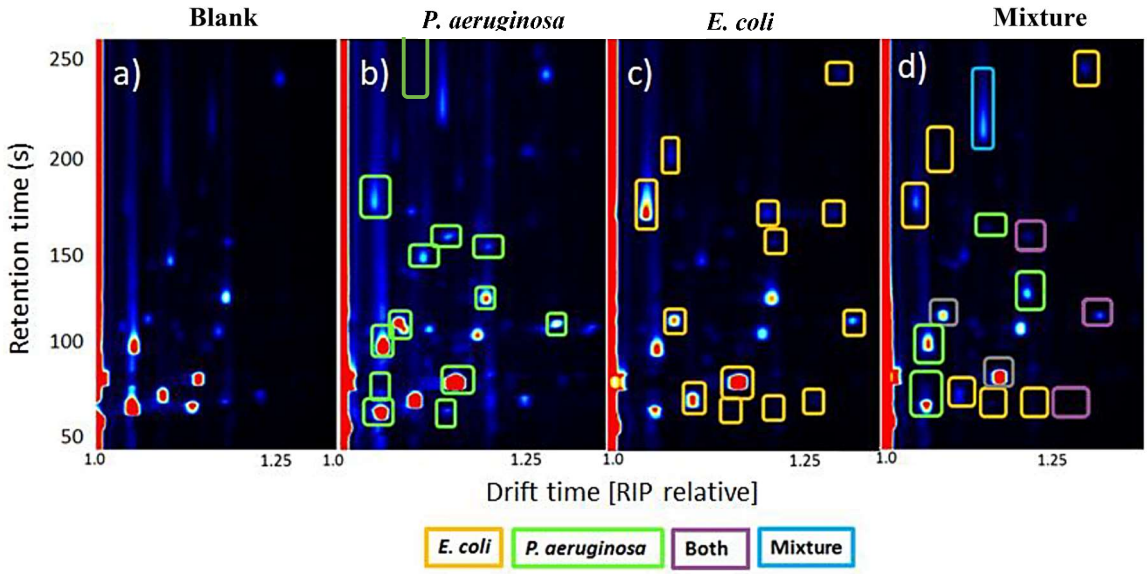

Figure 5.24 — Emission patterns for LB medium, *P. aeruginosa*, *E. coli* and a mixture of both bacteria.

This study was made to evaluate and examine GC-IMS in the detection and identification of bacteria through a qualitative approach from VOC emissions. Because signals emitted from those bacteria were condensed mainly in early retention times, a dedicated sampling program using a constant EPC1 flow (150 mL/min) and a starting EPC2 flow of 10 mL/min, subsequently increased to 25 mL/min until 3 minutes and further increased until a maximum of 40 mL/min and kept constant until 8 minutes. Although changing the flow program might imply compound identification can be hindered the aim herein was merely to qualitatively detect and identify bacterial fingerprints from emissions [193, 194].

5.4.2 On-line Monitoring of Microbial Growth in Liquid Media

A follow up experiment was conducted to monitor microbial growth on-line every hour over a period of 120 hours (or 5 days) (Gram-Negative and Gram-Positive). As opposed to the previous study, microbial growth was achieved in two types of liquid media, Fluid Thioglycollate Media (FTM)

and Tryptic Soy Broth (TSB), with FTM kept between 32 and 35 degrees Celsius and TSB at ambient temperature, 22 to 25°C. Test samples were grouped in pairs of, negative control and a positive sample, where negative controls consisted of sterile media and positive samples corresponded to inoculated media. Each GC-IMS measurement was limited to 6 minutes and 40 seconds to accommodate the total number of samples planned for two types of bacteria grown in two different media.

FTM and TSB media were both inoculated with known and controlled strains of *E. coli* ATCC 10536 (Gram-Negative) and *S. aureus* ATCC 25923 (Gram-Positive). Inoculation of both bacteria was conducted through a method comprised of 8 phases (Figure 5.25): (i) gathering of cryo-cultures from storage, (ii) re-hydration of cryo-culture in nutrition, (iii) cultivation of cryo-culture in brain-heart-bouillon for 24h at 37°C, (iv) 1 µL from the brain-heart suspension is regrown in a Petri dish of Tryptic Soy Agar (TSA) at 32.5°C for 24 hours, establishing a starter culture, (v) a single colony is picked and inoculated in 9ml brain-heart-bouillon for 17h at 32.5°C, (vi) a dilution series is performed to reach a target concentration of 200-600 CFU per ml of NaCl-peptone solvent buffer, a sample is grown in individual TSA Petri dishes and incubated for 24h at 32.5°C and counted, (vii) once the target colony count is at 10 to 30 colonies per 50 µL, inoculation of media is conducted and finally (viii) inoculated liquid media is transferred into dedicated containers into placed their respective conditions for analysis.

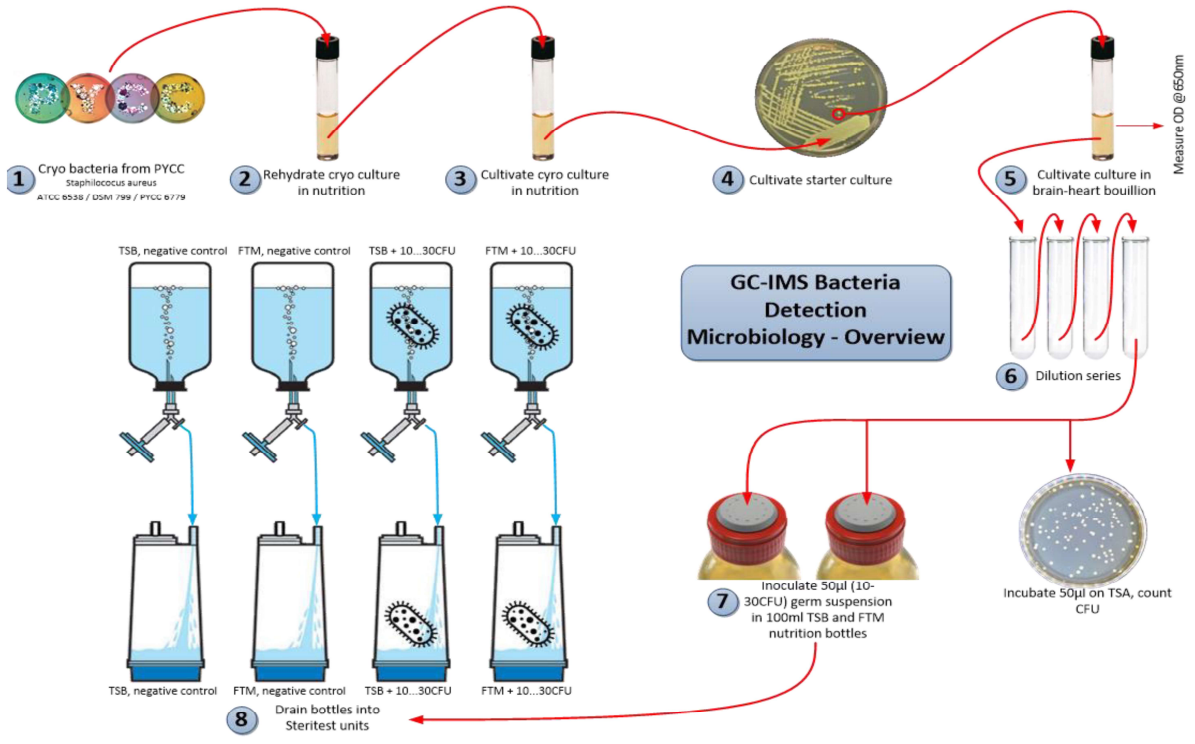

Figure 5.25 — Steps for cultivation of *E. coli* and *S. aureus* in liquid media, FTM and TSB for on-line analysis.

Regarding the GC-IMS sampling program for this experiment it was based on the arrangement used for SIRIUS-17 but was simply cut to approximately 7 minutes to fit time frame constrains, maintaining however respective parameters and values during the first 7 minutes. Sampling took place for both bacteria simultaneously for 5 days and included a total of 9 samples divided into four samples for

FTM at 34°C (#1 FTM [-], #2 FTM [-], #3 FTM *S. aureus* and #4 FTM *E. coli*), four samples for TSB at 22°C (#5 TSB *S. aureus*, #6 TSB *E. coli*. #7 TSB [-] and #8 TSB [-]) and a blank sample.

The emission pattern of FTM and TSB were characterized and revealed a rich pattern with several signals and although some signals are shared a clear difference exist between both media. During the full 120 hours both media emissions showed changes, but FTM showed a higher degree of changes over time (Figure 5.26*).* This was not expected, since both FTM and TSB should show a stable emission, however, after further evaluation, those changes were explained by FTM acclimatizing from ambient temperature to the respective microbial growth temperature of 33°C.

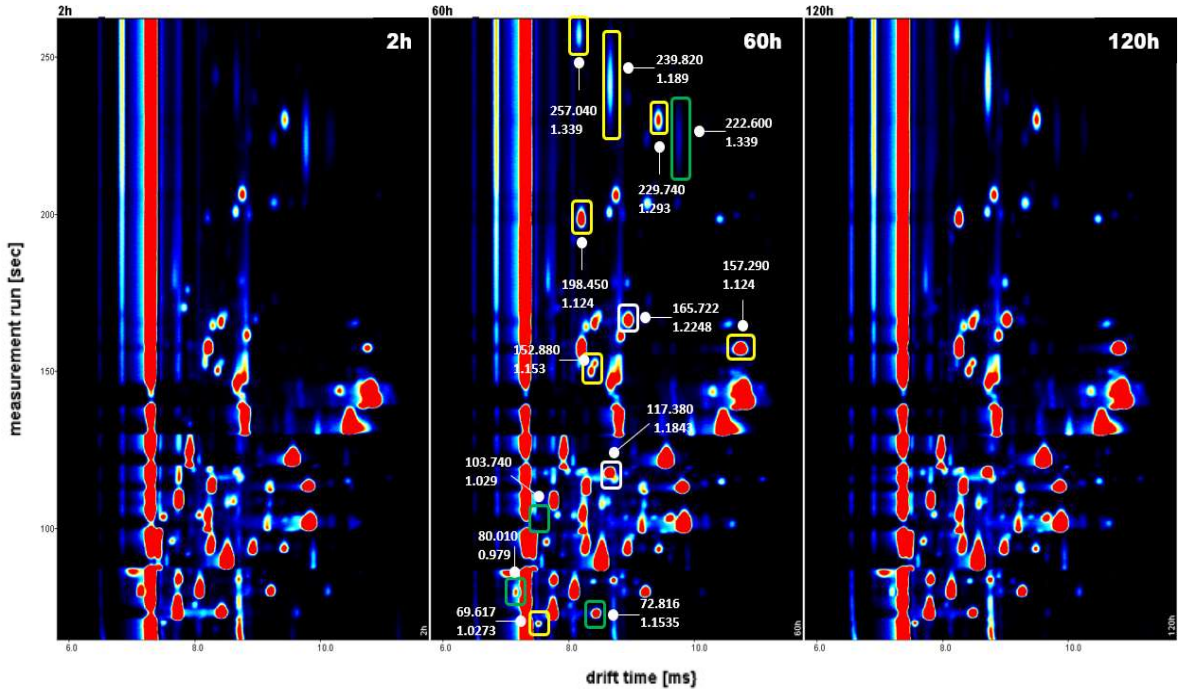

Figure 5.26 — Sterile FTM media emission over 120 hours at 33°C after 2 hours (left), 58 hours (middle) and 100 h (right). Yellow rectangles represent shallow increasing signals, white rectangles represent fast increasing signals and green rectangles represent signals with decreased intensity from the previous measurement. Retention times in seconds and drift time relative to RIP, are shown for each labelled peak.

Although TSB also showed shifts in emission over the 120-hour period, the extent of changes was considerably reduced with only 3 signals showing slight increases and 5 peaks with minor decreases in intensity (Figure 5.27). Since intensity variations, both increases and decreases, are significantly small, it is safe to assume such changes might just be a due to the inability of keeping ambient temperature under control. Nevertheless, TSB and FTM emissions measured produced steady and distinct emission patterns over a 120-hour period and constitutes a good characterization of the blank samples for comparison with inoculated media. Also, it is a good indication for the characterization of microbial growth in liquid media through headspace analysis with GC-IMS in an online approach.

Before analysing measurements of FTM and TSB inoculated with *S. aureus* and *E. coli* it is important to understand the general phases of microbial growth. Bacterial growth is characterized by 4 different phases: (i) lag phase, (ii) exponential phase, (iii) stationary phase and (iv) death phase

(Appendix I, Figure A.9). During the lag phase there is no increase in bacterial count, and no bacterial growth can be identified by optical density measurements, once bacteria reach the exponential phase, the number of bacteria starts growing. Depending on growth conditions and microbial metabolisms, after a certain time, microbial growth reaches a maximum value and bacteria numbers show no increase for hours or days. Eventually bacteria start dying and reach their death phase, in which, viable bacteria numbers decrease leaving behind dead cells, membranes or other cellular components.

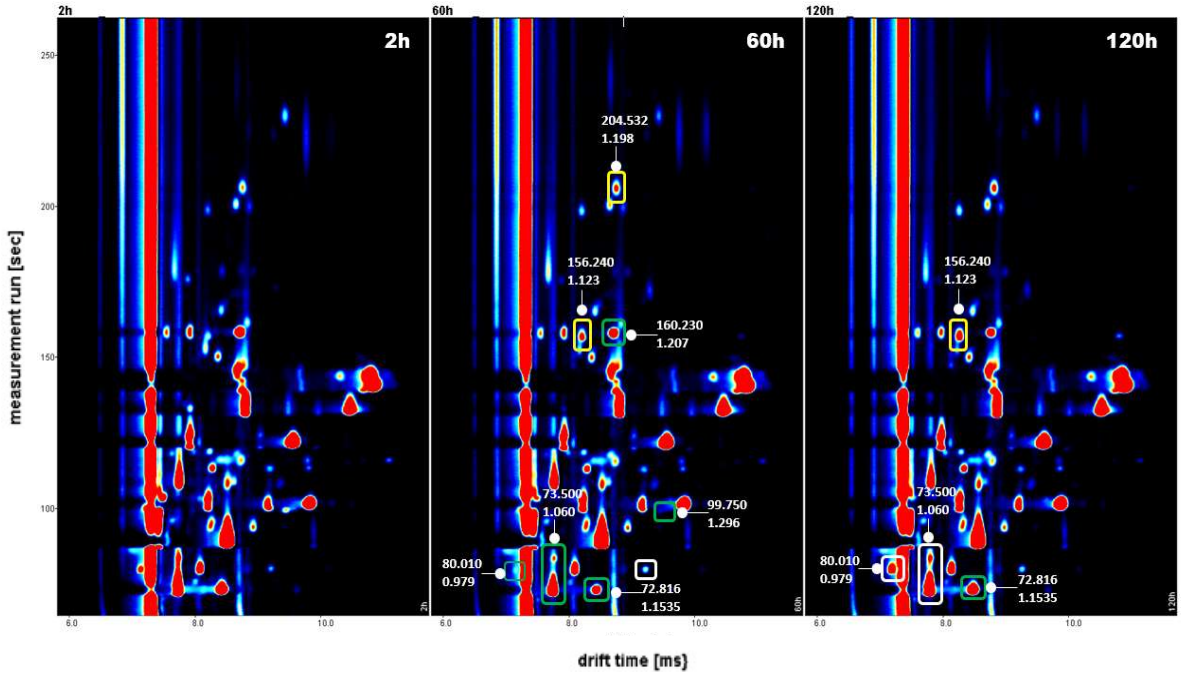

Figure 5.27 — Sterile TSB media emission over 120 hours at 23°C after 2 hours (left), 58 hours (middle) and 100 h (right). Yellow rectangles represent shallow increasing signals, white rectangles represent fast increasing signals and green rectangles represent signals with decreased intensity from the previous measurement. Retention times in seconds and drift time relative to RIP, are shown for each labelled peak.

The growth of *Staphylococcus aureus* (ATCC 25923) in Fluid Thioglycollate Media (FTM) is defined by an emergence of several new signals after 40 hours of growth, and a decrease of several signals from the liquid medium. An overall of 14 news signals appeared after 40 hours of *S. aureus* growth and those signals are characterized by a steep increase in concentration in only 4 hours, followed by a slower and stable increase until 80 hours of growth, remaining somewhat stable afterwards until 120 hours, apart from a small intensity decrease visible (Figure 5.28).

Interestingly the appearance of new signals around 40 hours is also accompanied by a significant decrease of media signals, in which some signals almost disappear completely from the emission spectra. A possible explanation for this could be related to the microbial growth of Staphylococcus aureus reaching its exponential phase. In an exponential phase microorganisms increase fast in microbial numbers, therefore explaining the steep increase in the new signals and consequential a steep decrease in media signals, which at this phase are probably being consumed in high quantities by growing bacteria. Overall, the biggest changes in emission pattern during the growth of *S. aureus* occurs in the first 40 hours most likely caused by intense metabolic rate and processes from microbial growth.

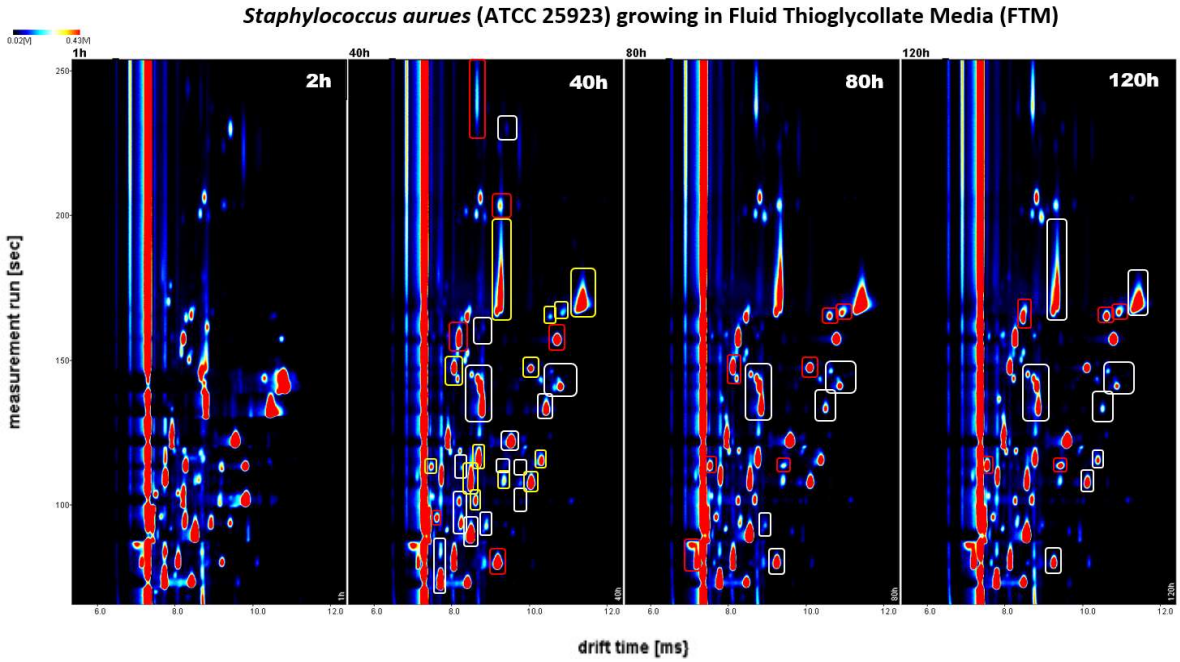

Figure 5.28 — Emission detected from *Staphylococcus aureus* inoculated in FTM media emission over 120 hours. Red, green, and yellow squares represent signals increasing, decreasing and new from the previous spectrum, respectively.

Likewise, the overall reduced activity seen after 40 hours until 120 hours could also signify microbial decline in metabolic rate leading, ultimately, to microbial death. Microbial mortality might have occurred around 110 hours since two signals unique to *S. aureus* growth have a slight decline in intensity until 120 hours. To conclude, *S. aureus* microbial growth changes FTM emission in a clear and discernible way 24 hours after inoculation and almost all alterations are observed in the 40 hours spectra, happen between 24 and 30 hours after incubation, a likely time frame for the exponential growth phase.

Staphylococcus aureus (ATCC 25923) growth in Tryptic Soy Broth (TSB) appears comparatively slower to its growth in Fluid Thioglycollate Media (FTM). Although pattern similarities can be identified from the emission of *S. aureus* in TSB, a clear difference arises from the emission spectra at 2, 40, 80 and 120 hours. Only five unique signals can be identified between 40 and 80 hours of microbial growth, and major differences exists for *Staphylococcus aureus* growing in TSB and FMT after 40 hours (Figure 5.29) TSB growth only produces one unique signal at this time frame and the overall medium emission remains relatively similar to the 2-hour emission. However, in TSB, the most significant growth changes seem to occur only around 80 hours in opposition to the 40-hour time of FTM. Growth in TSB appears to be slower but shows significantly more signals changes in response to microbial growth especially seen by a quick disappearance of signals, an indication media consumption is slower in TSB compared to FTM. Therefore, it could mean, *S. aureus* growth progresses faster into an exponential phase but has a slower stationary phase in FTM when compared with its growth in TSB.

The influence of temperature on *S. aureus* growth could be the principal explanation for difference in growth between TSB and FTM but media composition should not be neglected. The observed growth of *S. aureus* in TSB could simply be a consequence of a substantial lower growth temperature,

23°C in TSB, in contrast with 32°C used in FTM. Moreover, *S. aureus* growth does not appear to produce the exact same compounds in FTM and TSB, which might be explained by different metabolic processes activated by the bacterium between media.

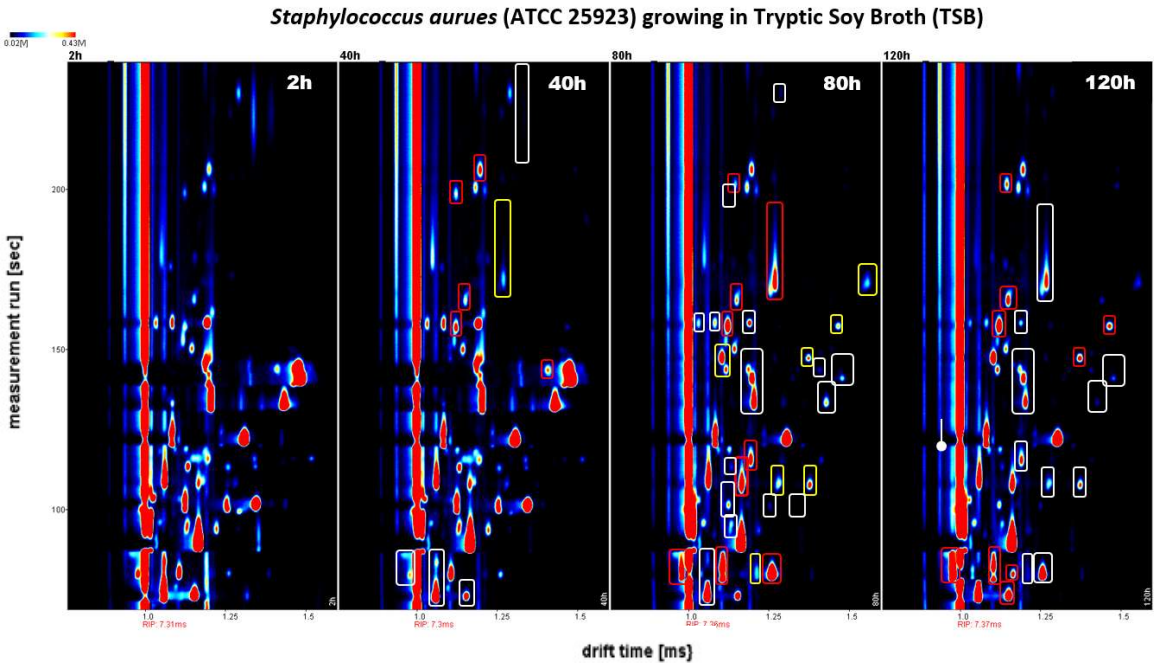

Figure 5.29 — Emission detected from *Staphylococcus aureus* inoculated in TSB media emission over 120 hours. Yellow, red, and green squares mark new signals, increases, and decreases and from the previous spectrum.

The growth of *Escherichia Coli* (ATCC 10536) in Fluid Thioglycollate Media (FTM) was analogous to *S. aureus* growth in FTM and the signals present at 40 hours for *S. aureus* were also visible at the same time in *E. coli* (Figure 5.30). However, emission changes happened at later times for *E. coli*, 30 hours after inoculation in opposition to the 24 hours for *S. aureus*. Comparatively to *S. aureus* growth in FTM several medium signals have steep decreases in intensity during the first 40 hours of *E. coli* microbial growth. However, signals reached a significantly lower intensity than observed in *S. aureus*.

Microbial signals from *E. coli* at 80 and 120 hours show a relative higher intensity comparatively to the same signals at the same times in *S. aureus*. Perhaps *E. coli* growth has a slower exponential phase comparatively to *S. aureus,* but it shows a higher metabolic rate during the stationary phase, explaining the higher degree of media consumption and emission at 80 hours. Finally, the small decline in signal intensities observed at 120 hours could be explained by bacteria entering a senescence or death stage similarly to what occurred in *S. aureus*.

Escherichia coli (ATCC 10536) growth in Tryptic Soy Broth (TSB) is also analogous to *S. aureus* growth in TSB. However, at 40 hours only a small increase in medium signals is visible and one new signal begins to appear on the spectrum. This new signal observed in *E. coli* growth in TSB at 40 hours was also identified in *S. aureus* but showed a significant higher intensity (Figure 5.31). Most emission changes for *E. coli* occur around the 80-hour mark with 8 newfound signals appearing and an overall decrease from several TSB medium signals. A significant decrease in some signals, mainly characteristic

of microbial growth, is visible at the 120-hour mark, once more, pointing out to the possibility of microorganisms dying during the later hours of measurements.

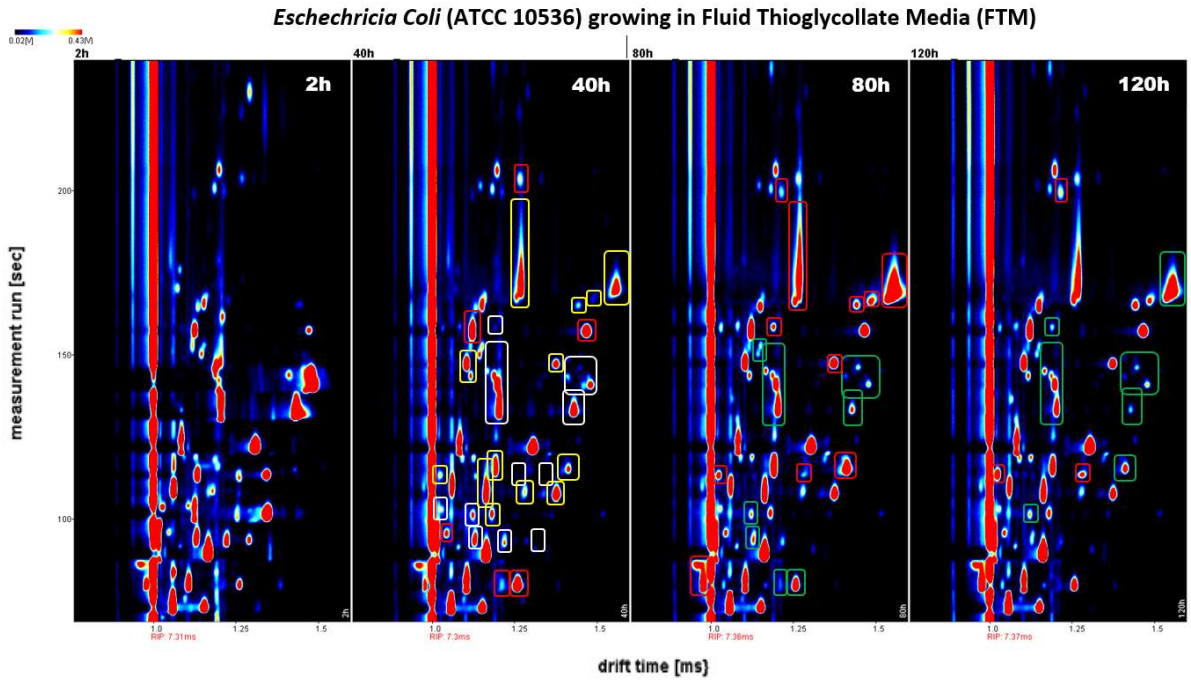

Figure 5.30 — Emission detected from *Escherichia Coli* inoculated in FTM media emission over 120 hours. Yellow, red, and green squares mark new signals, increases, and decreases and from the previous spectrum.

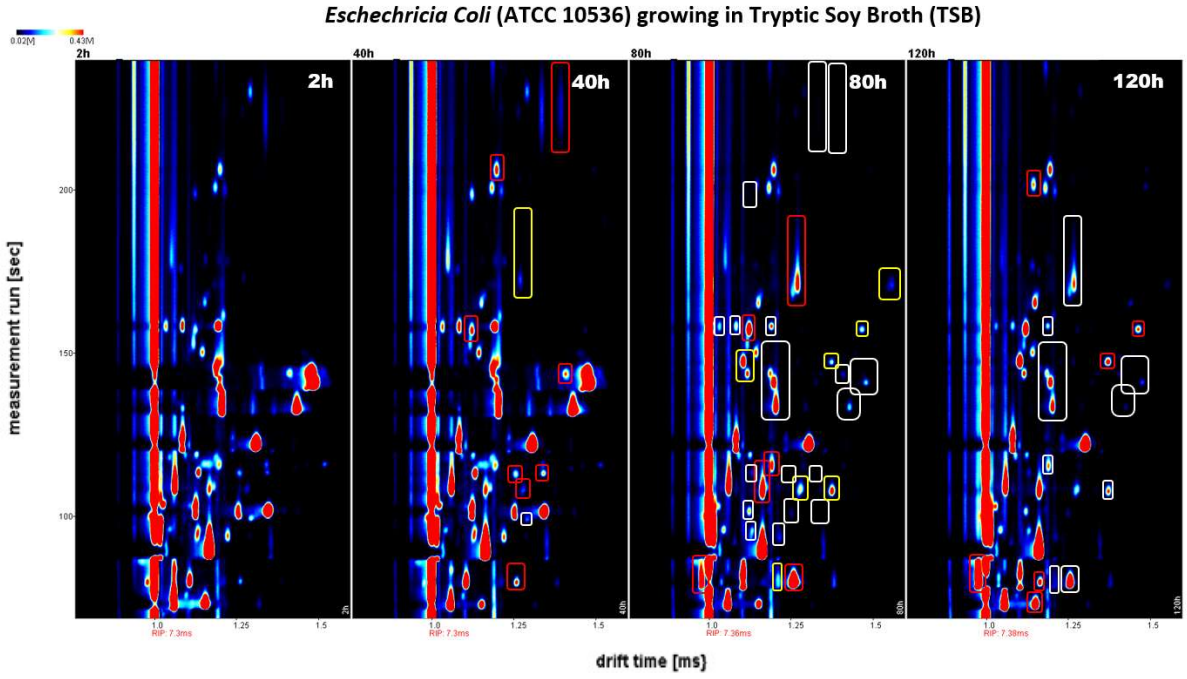

Figure 5.31 — Emission detected from *Escherichia Coli* inoculated in TSB media emission over 120 hours. Yellow, red, and green squares mark new signals, increases, and decreases and from the previous spectrum.

Although *E. coli* growth in TSB is relatively equal to *S. aureus*, *E. coli* growth appears to be slower in TSB because most signals associated with microbial growth show lower intensities values at the

same time, implying *E. coli* metabolism is slower when compared with *S. aureus,* emitting smaller quantities of VOCs at latter times than *S. aureus*. Overall, independently of media, emission changes were similar between bacteria, which might signify a closely comparable metabolism of both bacteria with only minimal differences in emission and intensity rates.

The results of this experiment show GC-IMS can monitor, on-line, the growth of microorganisms in liquid media, encouraging the use of GC-IMS to distinguish overtime emission changes in the head-space of liquids. Furthermore, GC-IMS was highly sensitive to both emission changes from microbes and media, detecting the appearance of both new signals related to microbial growth as well as media emission decreases as bacteria grows and consumes media nutrients.

Lastly, changes detected with GC-IMS analysis agrees almost exactly with microbial phases, since signals uniquely attributed to microbial growth have intensity variations over the 120-hour period matching a microbial growth curve (microbial growth phases: (i) lag phase, (ii) exponential phase, (iii) stationary phase and (iv) death phase) (Appendix I, Figure A.10). This is perceptible from represented timeframes, 2, 40, 80 and 120 hours, in which microbial signals are absent during an early period of time, followed by an almost exponential increase in intensity in a short time interval, reaching after, a stable and almost constant signal intensity until a small decrease in intensity observed at final hours.

5.5 Food Quality Control and Seaweeds

5.5.1 Microbial Degradation of Fish and GC-IMS as a Tool for Quality Control

The possibility of employing GC-IMS as an analytical tool for food quality, especially to monitor microbial growth, spoilage and degradation of plants, fruits, meat, and beverages is a promising for space and planetary exploration. As planetary missions become more important in space exploration so does food, and food production in extreme and challenging environments. The importance of monitoring crops, growth conditions and food quality at end production becomes crucial.

To evaluate GC-IMS for food quality control an early experiment was conducted using fish tissue and emitted VOCs were analysed to detect spoilage through a specific group of compounds, called biogenic amines. Currently biogenic amines are a central concern in the food industry, considering their potential health risk and a growing demand to reduce their permitted limits in food products, including meat and fish and beverages [195]. Biogenic amines include semi and non-volatile amines with the presence of at least one amino group in their molecular structure [195]. Their formation is normally attributed to microbial decarboxylation of the amino acids via enzymatic processes and are naturally present in foods or food products during food processing or storage [195].

The presence of biogenic amines in foods can result in several health problems when high concentrations are produced and present within food products because their toxicity can lead to migraines, headaches, gastric and intestinal problems, and pseudo-allergic responses [195]. Toxicity is mainly caused by the toxicity effects of histamine and tyramine, however, the toxicity of histamine can be enhanced by other amines present in foods, such as cadaverine, putrescine, and tyramine because

those amines are potentiators of histamine's toxicity [195, 196]. Furthermore, most biogenic amines contained in food products remains stable even after cooking, unlike bacteria spoiled food. Amines like spermidine, spermine, tyramine, putrescine, and cadaverine can even give rise to secondary amines after heating, which can, in the presence of nitrites form nitrosamines, chemical products that have high carcinogenic properties [195]. The most important biogenic amines in terms of food toxicity include, histamine (HIS), putrescine (PUT), cadaverine (CAD), tyramine (TYR), tryptamine (TRP), spermine (SPM), spermidine (SPD), and phenethylamine (PEA) where histamine take highest importance [196].

Three difference species of fish, Atlantic bonito, Atlantic horse mackerel and Sardine were purchased from a fish market in Almada, Portugal, already gutted, and transported to the laboratory in a cold box withing 2 hours. Sterile knives were used to prevent any possible contamination during fish tissue preparation which involved cutting a muscle fillet from the three species. A total mass of 0.15 gram of each fish species was weighted and placed into separate vials, sealed afterwards and place at ambient temperature for 4 days. A gas volume of 2 mL was extracted each day, at the same time, from each vial for GC-IMS analysis. This investigation was conducted in collaboration with master thesis from NOVA University of Lisbon [197].

Pure standards of histamine dihydrochloride (CAS No. 56-92-8), putrescine (CAS No. 110-60-1), cadaverine (CAS No. 462-94-2), tyramine (CAS No. 51-67-2), tryptamine (CAS No. 61-54-1), phenethylamine (CAS No. 64-04-0), spermine (CAS No. 71-44-3) and spermidine (CAS No. 124-20-9) from Sigma-Aldrich (Darmstadt, Germany) were measured with a sampling program, also used for fish tissue analysis. The parameters used for the sampling program include a constant carrier gas flow of 50 mL/min and a constant drift gas flow of 150 mL/min for a total of 5 minutes running time.

Pure standards samples were used to identify possible peaks from biogenic amines during the measurements of fish tissue and were measured at room temperature (23°C) and heated to 40°C to test their volatility or volatile sub-products. Data collected from biogenic amines standard measurements contained drift times, ion mobility constants and reduced ion mobility constants and was gathered into a table (Table 5.5) with CAS numbers and abbreviation.

Table 5.5 — Biogenic amines drift times, ion mobility constant (K) and reduced ion mobility constant (K_0).

Biogenic Amine	CAS No.	Drift time (ms)	K ($cm^2V^{-1}s^{-1}$)	K_0 ($cm^2V^{-1}s^{-1}$)
PEA	64-04-0	7.804	2.4613	0.0147
PUT	110-60-1	7.706	2.3037	0.0138
CAD	462-94-2	8.361	2.2971	0.0137
		10.072	1.9071	0.0114
TYR	51-67-2	8.338	2.3037	0.0138
		7.936	2.4204	0.0145
TYR	51-67-2	8.389	2.2900	0.0137
		7.051	2.7241	0.0163
SPM	71-44-3	7.771	2.4718	0.0148
		9.506	2.0206	0.0121
SPD	124-20-9	7.809	2.4597	0.0147
		9.552	2.0109	0.0120

The emission from *Sarda sarda* commonly known as Atlantic bonito is presented in Figure 5.32 showing the first 3 days of food spoilage at ambient temperature. Significant changes are visible between day 1 and day 2 with several intense signals appearing between 24 and 48 hours. Several signals from biogenic amines were identified on the second day, especially, cadaverine, phenethylamine, spermidine, spermine, tryptamine and tyramine (CAD, PEA, SPD SPM, TRP and TYR). Moreover, other signals were significantly increased at the second and on the third day, most amine signals disappeared from the spectra long, resulting in a simpler emission spectrum, but still different from the emission of fresh Atlantic bonito (first day).

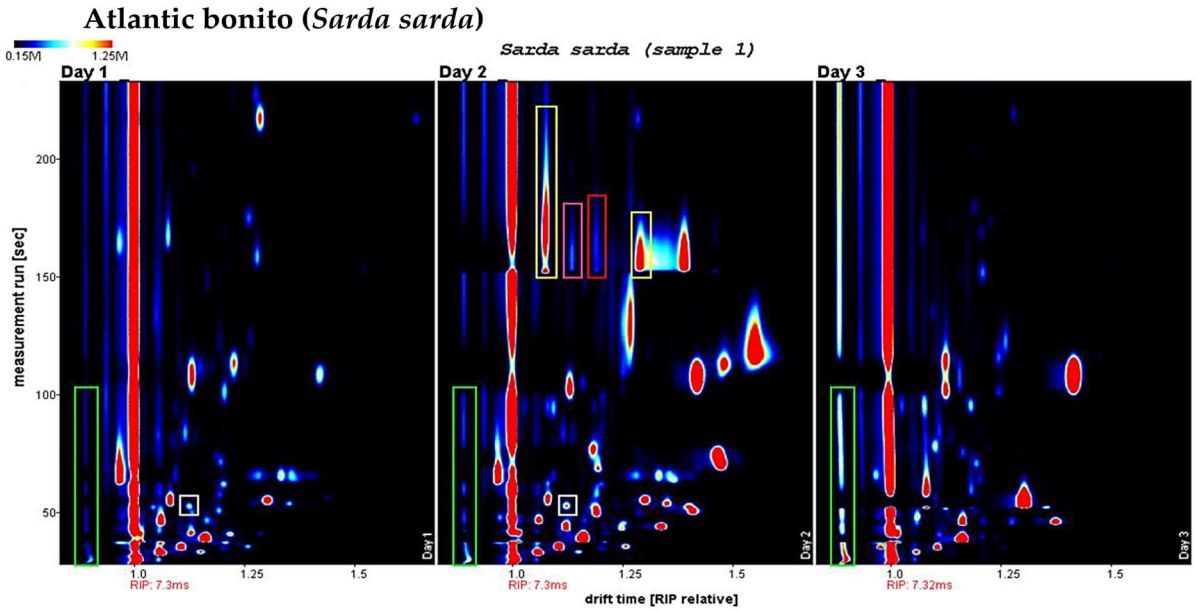

Figure 5.32 — Volatile organic emission from Sarda sarda at ambient temperature (23°C) for 3 days. Signals corresponding to ammonia, CAD, PEA, SPD/SPM and TRP/TYR were labelled with green, yellow, pink, red and white, respectively.

Volatile organic compounds detected from the headspace of fish tissue from Atlantic horse mackerel (*Trachurus trachurus*) are relatively similar to the emission of Atlantic bonito, with the signals from TYR and TRP absent in Atlantic horse mackerel (Figure 5.33). Signal intensity, however, shows generally lower intensities for Atlantic horse mackerel when compared with Atlantic bonito during day 2. Overall, on day 3, more signals were present in horse mackerel than A. bonito and those results might suggest a more complex process of fish degradation for the former fish species.

Finally, the emission of Sardine tissue, presented in Figure 5.34, shows a significantly lower presence of biogenic amines, however, several signals present in both Atlantic bonito and Atlantic horse mackerel are also detected after 2 days of spoilage (including ammonia and CAD). Also, as previously seen for other fish species, day 3 is characterized by a reduction in amine signals and an overall lower count of signals and intensity from the previous day. Generally, Sardine tissue emission during the three days shows lower signals and therefore a lower VOC emission than Atlantic bonito and horse mackerel A general observation for all fish species can be made about the ammonia signals, intensity from this signal was seen to increase over the days, showing a higher intensity after 3 days in all samples.

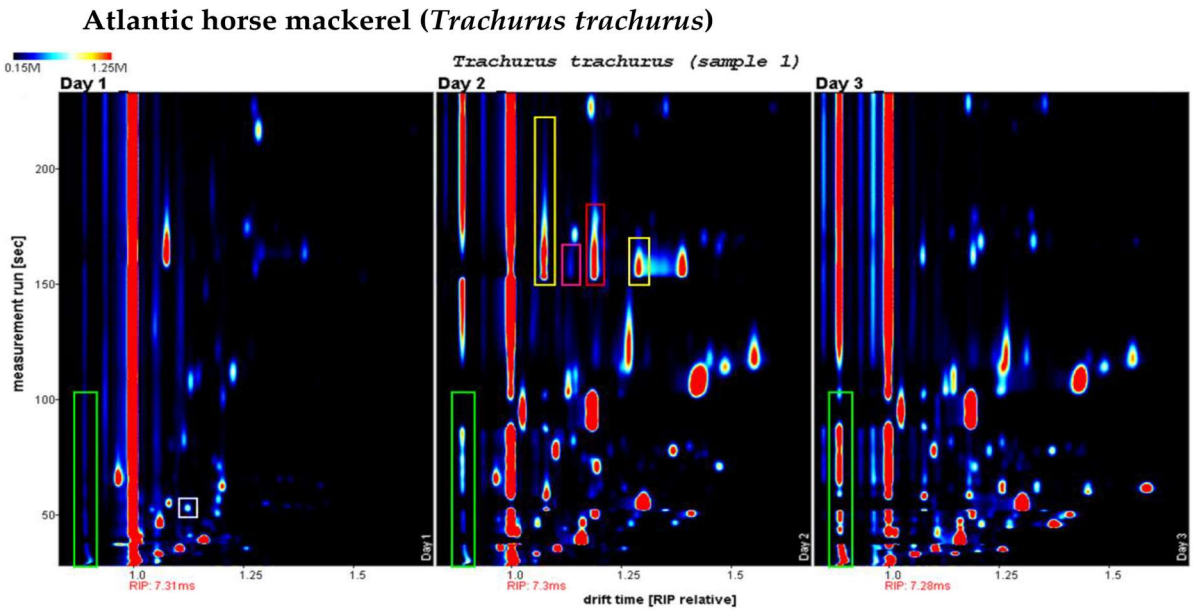

Figure 5.33 — Volatile organic emissions of *Trachurus trachurus* at ambient temperature (23°C) during 3 days. Marcked signals correspond to ammonia, CAD, PEA, SPD/SPM were labelled with green, yellow, pink, and red, respectively.

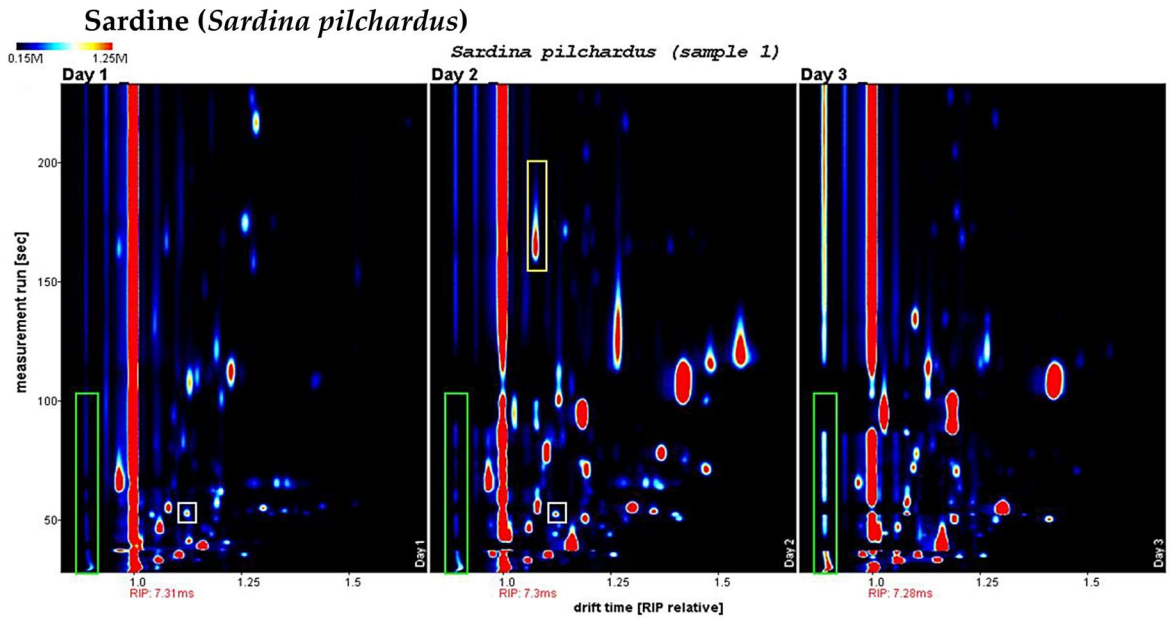

Figure 5.34 — Volatile organic emissions of *Sardina pilchardus* at ambient temperature (23°C) for 3 days. Signals corresponding to ammonia and CAD were labelled with green and yellow, respectively.

Emission for Atlantic bonito, Atlantic horse mackerel and Sardine presented, only show emissions for day 1, 2 and 3 because during day 4 and 5 VOC emission remained significantly stable, and at this point, fish tissue was clearly spoiled and marked by an unpleasant odour characteristic of fish decay.

Fish spoilage seems to occur in all species between 24 and 48 hours with biogenic amines having a relatively lower presence in Sardine and higher incidence in Atlantic bonito. Comparison of VOC emissions during day 2 for all three species shows a higher level of similarity between Atlantic bonito and Atlantic Mackerel, especially above 100 seconds of retention time and a higher similarity between

Sardine and Atlantic bonito below 100 seconds (Figure 5.35). Fish spoilage clearly results in emission changes from fish tissue between day 1 and day 2 and the GC-IMS analysis allows the detection of signals from several biogenic amines which higher intensities during day 2.

The analytical performance of GC-IMS allowed to detected change in the headspace of fish tissue without sample preparation, and the detection of several biogenic amines during the second day of spoilage. Which shows GC-IMS could operate as a tool to control food quality, in a qualitatively approach, by comparing both identified or unidentified signals from VOCs released overtime, or quantitively once a concentration relationship is established between signal intensity and VOC concentration.

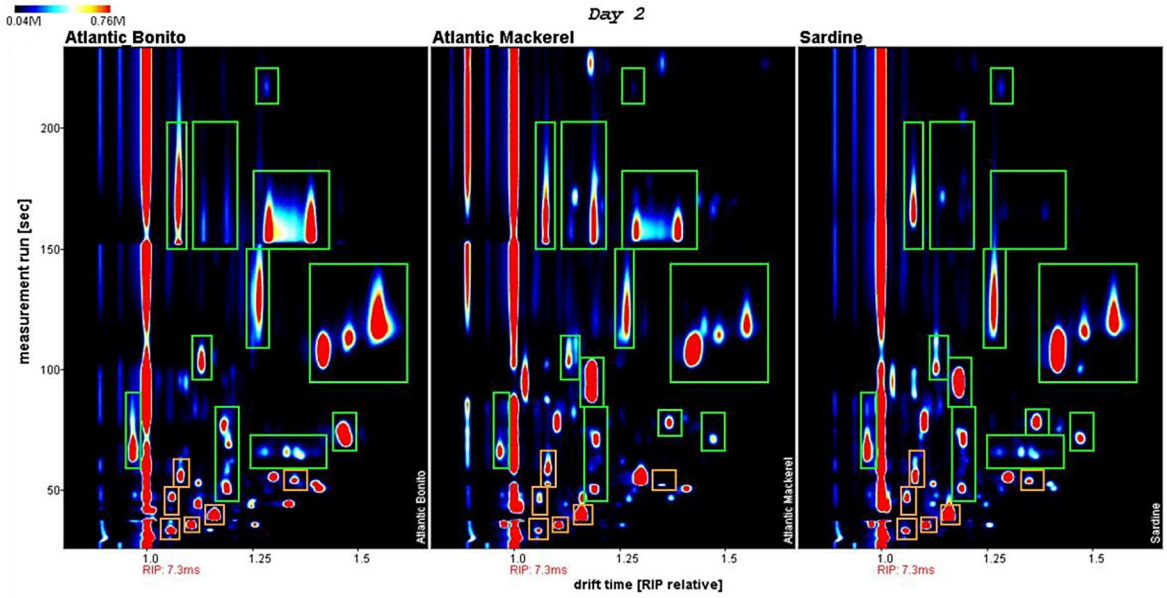

Figure 5.35 — Measurements for day 2 of all three species of fish at ambient temperature (23°C). Signals from blank measurements of air are identified with orange squares and fish characteristic signals by green squares.

5.5.2 Seaweeds: A Promising Superfood for Space Exploration and GC-IMS

The plans of several space agencies for crewed missions to Mars and Moon stations bring new challenges for space exploration and spacecraft or planetary habitation under essential aspects such as life-support systems, food, health, and consumables. Therefore, to sustain Mars exploration and a Moon base, several resources must be generated on site and research into a bioregenerative life support systems (BLSS) is already underway with cyanobacteria feeding on Mars's regolith and its atmosphere [198]. A recent a paper titled "A Low-Pressure, N_2/CO_2 Atmosphere Is Suitable for Cyanobacterium-Based Life-Support Systems on Mars" proposes an approach to grow cyanobacterial biomass under similar condition to Mars surface and cyanobacteria can further be feed to secondary consumers, specifically heterotrophic bacterium *E. coli*. The paper results suggest a mixture of gases extracted from the Martian atmosphere under a tenth of Earth's pressure at sea level is suitable for the development of photobioreactor modules based on cyanobacterium to be used as bioregenerative life-support systems [198, 199, 200, 201] and even as a basis for *on-site* food production.

Moreover, NASA plans to combine aquaculture (rising fish) and hydroponic (growing plants without soil) in an approach termed aquaponics to build a sustainable method of growing fresh plans and a protein source in small fish tanks by a symbiotic relationship between plants, microorganisms, and fishes [199, 201]. Aquaponics conveys importance and focus into aquatic environments for food production in space and planetary surfaces, which can also perform functions as bioregenerative life support systems by relying on cyanobacteria or even algae [199, 201].

Algae are a group of organisms composed mostly of single or multicellular photoautotrophic organisms living in water or humid places, which produce energy by photosynthesis using primarily chlorophyll pigments. Microscopic algae lack true roots, stems, leaves and resemble plant cells whereas, macroscopic algae are comparable to plants in some respects, with similar structures to roots, stems, and leaves but lack flowers and are seedless. Hence macroalgae do not possess embryos or protective structures for their reproductive tissues [202, 203]. Macroalga reproduction is achieved by the production and release of gametes or spores and, in this respect, are more like fungi or bacteria. Simpler macroscopic algae, normally reproduce asexually and some species can have both asexual and sexual reproductions. More complex macroalgae, also called seaweeds, reproduce asexually by producing motile zoospores able to swim off, anchor themselves, and form new individuals. In some instances, a single seaweed section can form a new individual, or reproduce sexually through the formation of sex cells, named gametes, creating a new macroalgae by fusing two gametes [202, 203]. Thus, algae, including microscopic and macroscopic organisms form a diverse group with a large distribution in terms of their size, colour, shape, and reproduction [202].

"Microalgae" is a term cataloguing microscopic organisms which usually are unicellular including cyanobacteria, diatoms, and plankton, while "macroalgae" includes macroscopic organisms that can measure from only a few millimetres to more than 50 meters in length [202, 203]. However, both macroalgae and microalgae are often grouped in accordance with their photosynthetic pigments, establishing green, blue-green, red, and brown algae [204]. Blue green algae are prokaryotic organisms without chloroplasts from the Kingdom Monera and the Cyanobacteria Phylum, while green algae or "chlorophytes" are eukaryotic organisms inserted in the Kingdom Plantae, largely belonging to the Chlorophyta division. Green algae are genetically similar to terrestrial plants and characteristically have chlorophylls a and b, and other accessory pigments, much like plants, as carotenoids. Red or "rhodophyte" algae also belong to the Kingdom Plantae but are, however, part of the Rhodophyta division. Their photosynthetic pigments include chlorophylls a and d, phycobilin, carotenoids and xanthophylls. Brown algae or also called "phaeophyte" algae belong to the Chromist Kingdom, the Ochrophyta division and the Phaeophyceae class with photosynthetic pigments of chlorophyll a and c, and fucoxanthin [204].

Seaweeds are a relevant source of biological resources, exploited in several areas of research and most published research relates to their nutritional or health benefits in food formulations or products. Seaweeds also have a long history in human society as a food resource throughout ancient history in Asia and America and modern uses in sushi, soups sources of food additives and nutrients [202, 203]. An increasing interest in seaweeds as a food ingredient in the Europe and America is relatively recent,

which was driven by a growing awareness of their health benefits and imported foods and culinary dishes from Asia [203, 205].

The organoleptic characteristics of seaweeds derive from a combination of their volatile and non-volatile constituents and as might be expected, not all volatile compounds present in algae are equally important. The degree of contribution of a constituent to flavour depends on the value of their recognition threshold and concentration [206]. For example, most aliphatic hydrocarbons present in seaweeds have no contribution to their aroma profile due to the high odour thresholds, even though those compounds are often the most released VOCs [207].

A study, in cooperation with the Alga4food project of NOVA School of Science and Technology, involved the identification and characterization of VOCs from ten edible seaweeds through the analysis of static headspace with IMS coupled with gas chromatography (GC-IMS). The main aims were to characterize seaweed emissions and to continue exploring GC-IMS in food quality control and analysis of food products related with novel approaches of food production in spacecrafts, stations or plant surfaces and possibly monitor bioregenerative life support system.

The ten seaweeds analysed in this venture included algae from 3 groups: (i) red (Rhodophyta) *Osmundea pinnatifida* (OP; Pepper Dulse), *Gracilaria gracilis* (GG; Slender wart weed), *Grateloupia turuturu* (GT; Devil's tongue weed) and *Porphyra* spp. (PS; Laver); (ii) green (Chlorophyta) *Ulva rigida* (UR; Sea lettuce) and *Codium tomentosum* (CT; Spongeweed); and (iii) brown (Phaeophyceae) *Undaria pinnatifida* (UP; Wakame), *Fucus vesiculosus* (FV; Bladder wrack), *Bifurcaria bifurcata* (BB; Brown forking weed) and *Saccorhiza polyschides* (SP; Furbelows). Seaweed samples were extracted from three different locations in Portugal during the spring of 2019: *Saccorhiza polyschides* was collected from Praia do Norte, Viana do Castelo, *Codium tomentosum*, *Porphyra* spp., *Bifurcaria bifurcata* and *Fucus vesiculosus* were collected from Cabo Mondego, Figueira da Foz and *Gracilaria gracilis*, *Grateloupia turuturu*, *Osmundea pinnatifida*, *Ulva rigida* and *Undaria pinnatifida* were collected from Buarcos, Figueira da Foz.

Once collected, each fresh seaweed sample, was stored at -15 °C and prior to GC-IMS analysis e 0.5 g of each seaweed were cut and placed inside a 20 mL vial. Defrosting was allowed to occur inside the vial during the first hour until ambient temperature (22-25°C) was reached. Injection into the GC-IMS device was conducted afterwards through the collection of a 2 mL volume of the static headspace from each vial using a syringe. Five headspace samples were collected for each seaweed starting one hour after the sample was placed inside a vial and every hour onwards, establishing a total of 5 samples over a 5-hour period for each seaweed species. Each measurement was recorded with the TOL-SIRIUS flow program for 15 min with a constant drift flow of 150 mL/min and a carrier gas flow ramp, with an initial value of 10 mL/min increasing every 2 min in the following sequence, 25, 40, 50, 65, 85, 100 and 100 ml/min. Temperatures were kept at device defaults with the following values: drift tube temperature at 70 °C, GC column at 40 °C and the sample loop at 55 °C.

Moreover, a database of drift and retention times for 41 substances was established and used for peak identification from seaweeds spectra. Analytical grade standards (min. 98% purity) were obtained from Sigma-Aldrich and measured with the previously mentioned program setup used for seaweeds

analysis and SIRIUS-17. Standard measurements for the database were performed by sampling 1 mL of static headspace (in a 20 mL vial) for each pure substance. Due to indigenous characteristics of grade standards (i.e., volatility) the measuring process was optimized, with minor changes, for each compound. Those measurements are part of a VOC database developed over the course of 4 years in this dissertation and will be discussed in detail in the section 5.6 Detected peaks in seaweed samples were identified by cross checking their drift and retention times with data created in the developed database.

The analysis of quintuplet measurements of the VOC emission from the 10 seaweeds showed a clear and unique for each species peak pattern analogous to a fingerprint, that allows individual identification based on a set of points or peaks from the overall pattern. This unique and specific pattern for each seaweed which can be termed "*phycoprint*" (prefix "pycho-", relates to seaweed and "print" refers to any type of pattern marked on a surface or image) and used to distinguish seaweeds. Phycoprints from 3 different seaweeds *Osmundea pinnatifida* (red), *Ulva rigida* (green), and *Undaria pinnatifida* (brown) are showed in Figure 5.36. While a deeper analysis of phycoprints, based on VOC emission pattern, makes it possible to identify a few signals unique to each seaweed species while major intensity difference for several peaks allows a visual discrimination between the three types of seaweeds. Emission patterns from all 10 species showed visible and quantifiable variations between seaweeds, starting with the total number of peaks: *Osmundea pinnatifida* had the highest number of peaks, 105, from all seaweeds, followed by a brown seaweed, *Saccorhiza polyschides*, with 83 total peaks. The lowest number of signals, twenty (20), was observed for a red seaweed, *Porphyra* spp., hence red seaweeds exhibited both the highest and lowest total peaks. The remainder red seaweeds, GT, and GG respectively had 75 and 76 peaks. Whereas green seaweeds, UR, and CT both showed a similar number of peaks, 59 and 50 respectively. Lastly, the in the brown seaweeds group, BB had 77, FV 70 and UP 65 total detected peaks in their emission patterns.

However, phycoptrints are not solely characterized by total number but also by drift and retention times of each peak which create a degree of specificity by a unique pattern of drift and retention time values. Data for drift and retention times from all seaweed signals are shown in Appendix II, Table A.2 and are used to establish a unique pattern of peaks for each seaweed in their group: red, brown, and green. Furthermore, a total of 27 peaks, counting monomers and dimers, were identified as 17 volatile organic compounds (9 VOCs showed dimer) throughout all phycoprints (Table 5.6) by using the aforementioned VOC database. Ethanol, acetone, ethyl acetate, 2-propanol, benzene, and diethyl ether are present in all seaweeds and in indoor air but show significant differences in intensities between air (blank) and samples (seaweed) indicating those VOCs are part of seaweeds emissions.

Hence seaweeds were distinguished by their emission fingerprint in two different levels: inside each group, (i.e., red, green, and brown) and between all species. Distinction was first examined inside each seaweed colour group by comparing phycoprints. This produced a phycoprint portion capable of characterizing and distinguishing each seaweed species inside their respective group (Appendix II, Table A.2). Afterwards, the overall emission of all ten seaweeds was compared between each other to establish unique signals to identify each species among all other seaweeds (Appendix II, Table A.2), therefore establishing a species unique phycoprint with species-specific signals in their VOC emission.

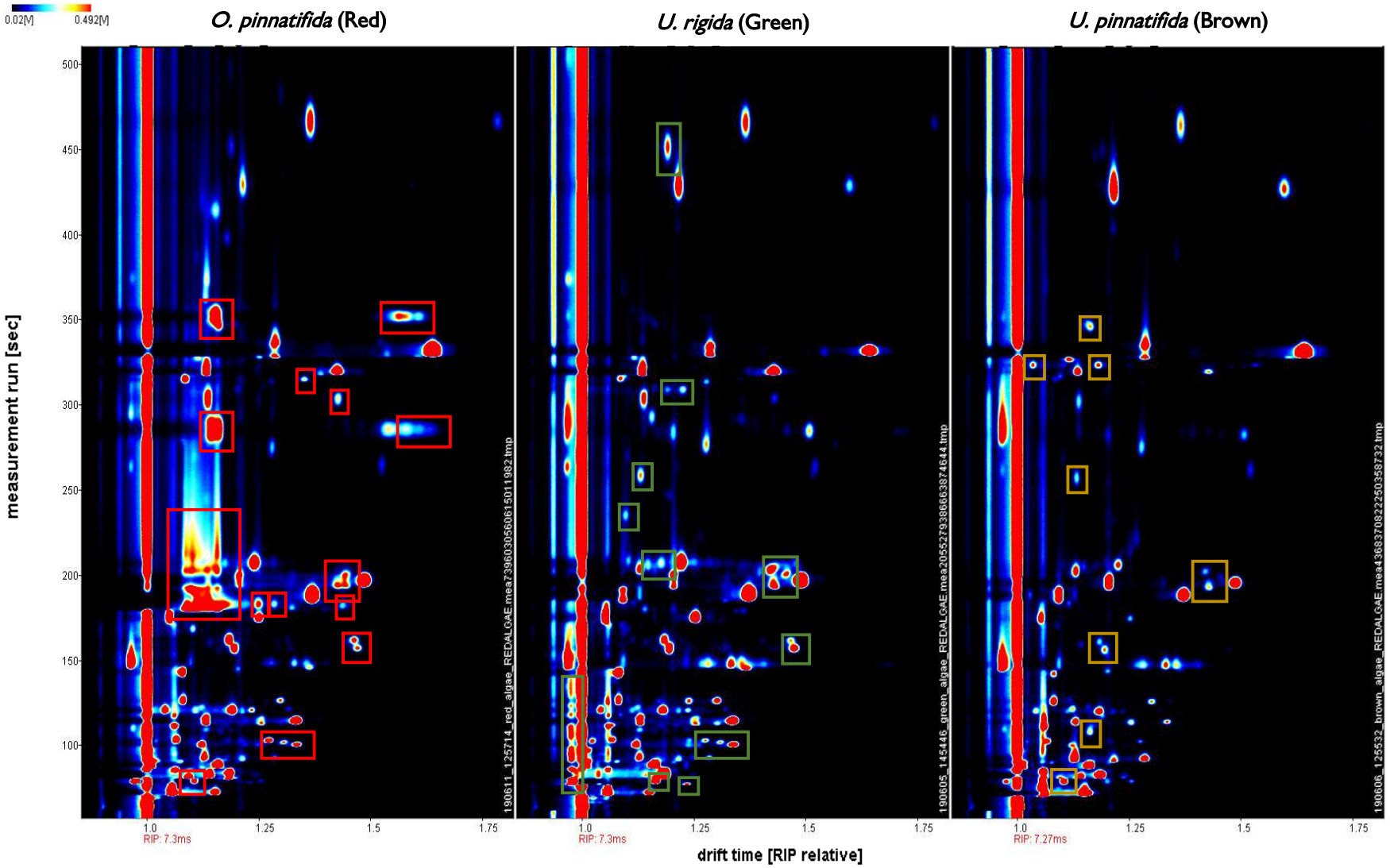

Figure 5.36 — Phycoprints of three seaweeds from each category (red, brown, and green): *Osmundea pinnatifida* (Red seaweed) right, *Ulva rigida* (Green seaweed) centre, *Undaria pinnatifida* (Brown seaweed) left. Red, green, and yellow squares represent unique pattern signals for the red, green, and brown seaweeds respectably.

Table 5.6 — Compounds identified from the VOC emission of 10 seaweeds. Compound name, CAS number, Drift time (Dt) and retention time (Rt) means, total number of seaweeds in which the compound was identified and the specific species are show by code: *Osmundea pinnatifida* (OP), *Gracilaria gracilis* (GG), *Grateloupia turuturu* (GT) and *Porphyra spp.* (PS), *Ulva rigida* (UR) and *Codium tomentosum* (CT), *Undaria pinnatifida* (UP), *Fucus vesiculosus* (FV), *Bifurcaria bifurcata* (BB) and *Saccorhiza polyschides* (SP) (coloured text corresponds to seaweed colour group).

Compound	#CAS N°	Dt mean	Rt mean	Total	Species Presence
Name	#CAS Number	Dt (RIPrel)	Rt (sec)	Seaweeds	Seaweed code
Ethanol	64-17-5	1.057	73.61	10	UP | FV | BB | SP | OP | GG | GT | PS | UR | CT
		1.153	73.15	9	UP | FV | BB | SP | OP | GG | GT | | UR | CT
2-Propanol	67-63-0	1.256	80.29	6	| FV | BB | SP | OP | | GT | PS | |
		1.104	80.54		
Acetone	67-64-1	1.161	89.08	10	UP | FV | BB | SP | OP | GG | GT | PS | UR | CT
Ethyl acetate	141-78-6	1.124	119.39	5	UP | FV | | SP | OP | | | | UR |
		1.402	119.23		
2-Butanone	78-93-3	1.082	122.98	10	UP | FV | BB | SP | OP | GG | GT | PS | UR | CT
		1.302	122.73		
2-Ethylfuran	3208-16-0	1.081	133.52	10	UP | FV | BB | SP | OP | GG | GT | PS | UR | CT
Hexanal	66-25-1	1.286	253.66	10	UP | FV | BB | SP | OP | GG | GT | PS | UR | CT
		1.642	249.88	9	UP | FV | BB | SP | OP | GG | GT | | UR | CT
(2E)-2-Hexenal	6728-26-3	1.216	369.18	9	UP | FV | BB | SP | OP | GG | GT | | UR | CT
		1.598	367.68	7	UP | FV | BB | SP | OP | | GT | | UR |
Heptanal	111-71-7	1.366	405.86	6	UP | | | SP | OP | GG | GT | | UR |
		1.789	405.72	2	| | | | OP | | GT | | |
(2E)-2-Heptenal	18829-55-5	1.300	619.63	5	UP | | | SP | OP | GG | GT | | |
		1.783	613.62	1	| | | | OP | | | | |
(4Z)-4-heptenal	6728-31-0	1.191	391.44	4	| | | SP | OP | | GT | | UR |
2-Pentanone	107-87-9	1.146	173.25	4	| | | | OP | GG | GT | PS | |
		1.439	169.68	2	| | | | OP | GG | | | |
Diethyl ether	141-78-6	1.091	75.60	3	| FV | BB | | | | | | | CT
		1.201	74.76	1	| FV | | | | | | | | |
Benzene	71-43-2	1.113	117.60	2	| | | | | GG | GT | | |
Octanal	124-13-0	1.445	677.04	1	| | | | OP | | | | |
1-Octen-3-one	4312-99-6	1.783	609.42	1	| | | | | GG | | | |
1-Octen-3-ol	3391-86-4	1.207	510.51	1	| | | | | GG | | | |

In respect to compound identification, *U. pinnatifida*, *Bifurcaria bifurcata*, *G. turuturu*, *Porphyra* spp. and *C. tomentosum* had no identified compounds attributed to their unique signals, however, in *Saccorhiza polyschides* one compound, (4Z)-4-heptenal, was identified as unique to this seaweed inside its respective brown group. Additionally, (4Z)-4-heptenal was also identified in the emission of one red and one green seaweed (Table 5.6).

Red seaweeds were established as the only group releasing 2-pentanone, benzene, octanal, 1-octen-3-one and 1-octen-3-ol, but diethyl ether was absent from the phycoprint of all red seaweed. Whereas 2-propanol and (2E-)2-heptenal, were absent from any green seaweed (Table 5.6). Peak intensities from heptanal, (2E)-2-heptenal and 2-pentanone had higher intensities in red seaweeds and diethyl ether was more intense in *F. vesiculosus*, a brown seaweed. Finally, octanal was only found in the red seaweed *O. pinnatifida*, and 1-octen-3-one and 1-octen-3-ol were identified as specific compounds of *G. gracilis*.

Additionally, seaweed emission data for three selected seaweeds, *Osmundea pinnatifida* (red*), Ulva rigida* (green), and *Undaria pinnatifida* (brown) was statically processed by Principal Component Analysis (PCA) (Figure 5.37). Ten peaks, absent from indoor air, were discriminately selected for analysis, with 3 peak sets (3x3) characteristic of each seaweed (red, green, and brown) and one peak common to all three seaweeds.

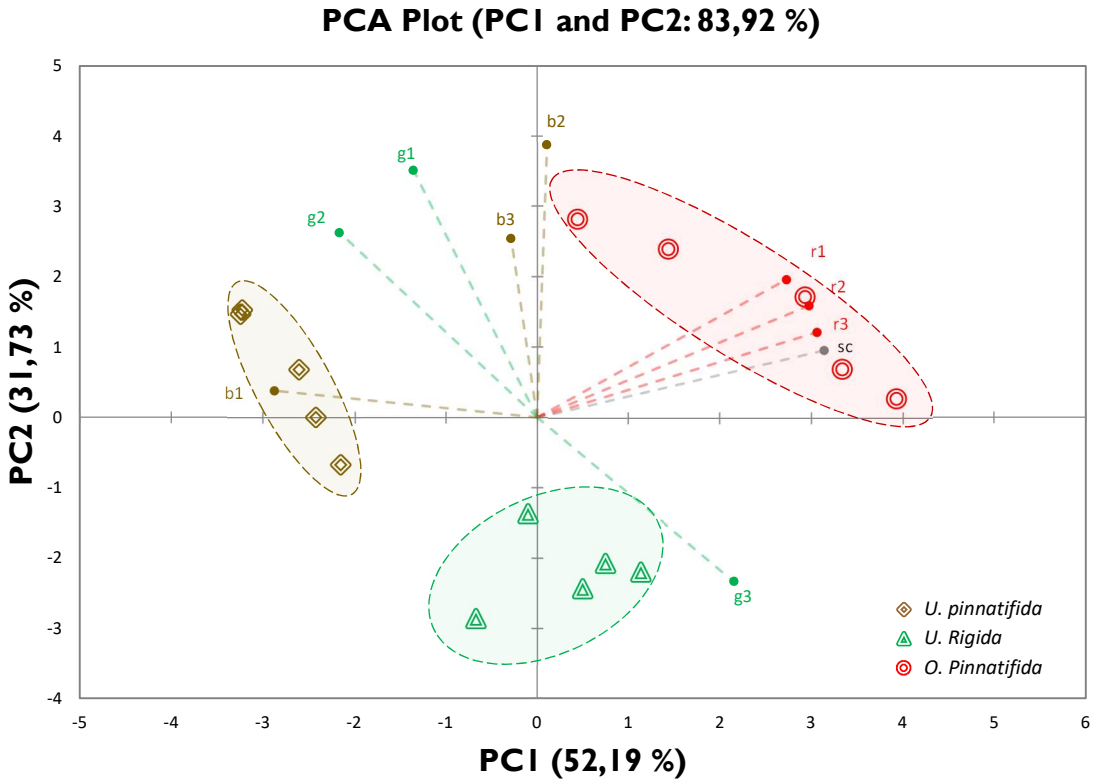

Figure 5.37 — Principal Component Analysis Biplot of Three Seaweeds. PCA biplot of five replicates of the headspace emission of three seaweeds *Osmundea pinnatifida* (Red), *Ulva rigida* (Green) and *Undaria pinnatifida* (Brown) for 10 peak intensities, red specific peaks: r1, r2, r3, green specific: g1, g2, g3, brown specific: b1, b2, b3 and seaweed common peak: sc. Each peak (characteristic) influence on the principal component is represented in the plot with dashed lines and labelled in their corresponding seaweed colour (red, green, and brown).

The peak selection was conducted randomly between each set and PCA was conducted with the Microsoft Excel plug-in XLSTAT with a Pearson Correlation coefficient and a maximum of 9 factors were employed. Red-specific peaks selected were: (r1): Dt 1.785 and Rt 404.96; (r2): Dt 1.43 and Rt 164.21; (r3): Dt 1.472 and Rt 143.84. Brown-specific peaks were (b1): Dt 1.285 and Rt 94.02; (b2): Dt 1.097 and Rt 85.16; (b3): Dt 1.159 and Rt 110.95. Green-specific peaks were (g1): Dt 1.123 and Rt 119.603; (g2): Dt 1.401 and Rt 119.39; (g3): Dt 1.186 and Rt 536.80. While the common peak selected had 1.37 and 161.08 of drift and retention time, respectively. PCA characterized 83% of peak total explained variance with only two principal components, PC1 with 52.19% and PC2 with 31.73%. Red, green, and brown seaweed replicates were visually separated and distributed in the top right, middle-left, and bottom-centre in the PCA plot respectively (Figure 5.37).

Besides characterization of seaweeds VOC emissions, a simultaneous analysis was conducted for a single seaweed species, *Undaria pinnatifida*, to assess emission changes over time (Figure 5.38). Headspace samples were measured at five different times, 1 hour, 2 hours, 3 hours, 24 hours, and 36 hours after a sample was weighted and place in a vial.

Headspace spectra from the first three hours had only minor changes in intensity, which were most likely related to defrosting and acclimatization to ambient temperature (Figure 5.38). However, after 24 hours, two new predominant signals were observed and a significant decrease or even disappearance of some characteristic signals of *Undaria pinnatifida*. Lastly, at 36 hours, seaweed emission is significantly diminished since most seaweed characteristic peaks have disappeared and the overall peak intensity was reduced.

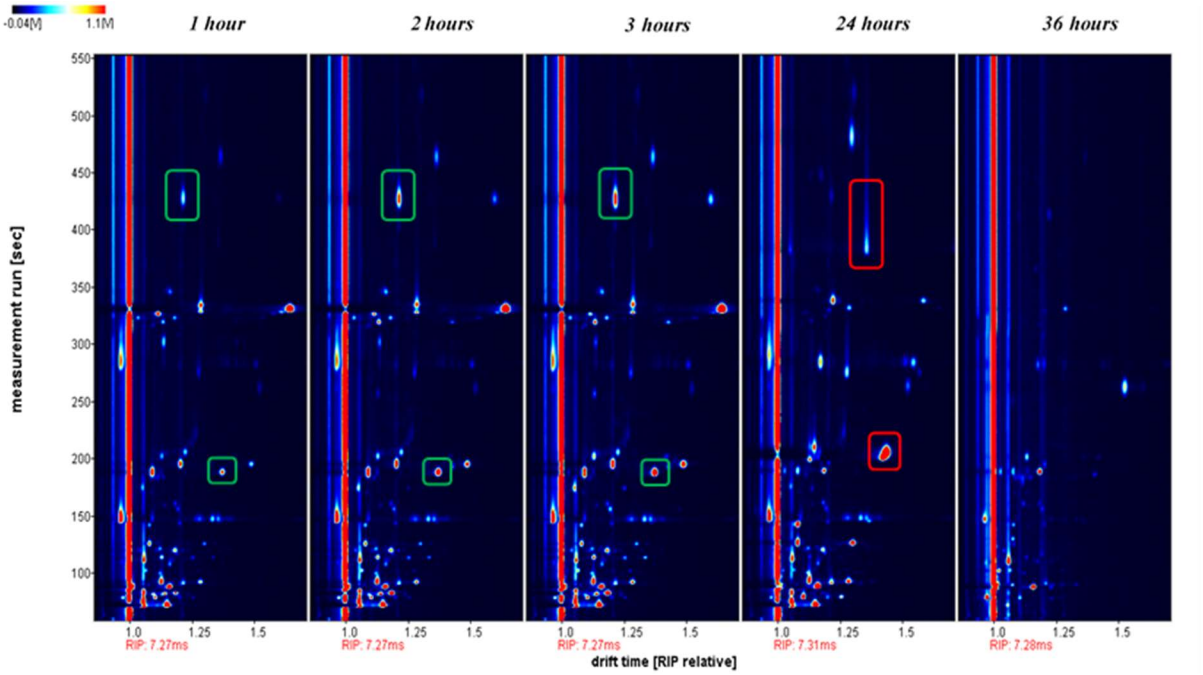

Figure 5.38 — Headspace emission spectra changes over time of *Undaria pinnatifida*. Measurements over time after 1 hour, 2 hours, 3 hours, 24 hours, and 36 hours. Peaks increasing due to acclimatization are represented with green squares and two predominant new signals appearing at 24 hours re marked in red squares.

The results seen in emission for 36 hours indicate seaweed proprieties change greatly between 3 to 24 hours and could be cause by de-hydration, eventually leading to loss of flavour, odour, and texture, events generally involved in spoilage and, or microbial degradation.

GC-IMS analysis of the headspace of ten seaweeds detected distinctive and unique VOC emission for each seaweed, and a topographic map of peaks, termed phycoprint, could even be established for each seaweed measurement. The detected VOC emissions and consequently phycoprint allowed seaweeds species to be identified among their colour group and among all 10 studied species. Each seaweed therefore was characterized by a phycoprint containing common peaks between colour group, but as unique seaweed species as well peaks.

Furthermore, a database of retention and drift times was used to identify phycoprint signals and several signals were attributed to known substances. Sixteen compounds were identified in all seaweed VOC emissions, octanal, 2-pentanone, and (2E)-2-heptanal were unique compounds of *Osmundea pinnatifida*, 1-octen-3-one was unique to *Gracilaria gracilis* and diethyl ether to *Fucus vesiculosus*.

Principal component analysis score plots showed 3 groups, separated visually into the respective red, green, and brown seaweed. PCA explained 83.92% data variance with a set of ten peaks which reinforces the degree of uniqueness and specificity from the characterized phycoprints.

Overall, GC-IMS analysis detected clear and distinctive patterns for all seaweeds and was able to monitor changes during seaweed spoilage over a period of 36 hours. Therefore, due to its high sensitivity and selectivity, low cost, easy operation and portability, GC-IMS can be a suitable tool to characterize, distinguish and assess the food quality of seaweeds and fish tissue. GC-IMS could also be advantageous to monitor seaweeds, plants, or fishes in bioregenerative life support system and food production systems, such as aquaponics in spacecrafts, station.

5.6 Construction of a VOC database: VOC Library

The identity of volatile organic compounds (VOCs) can be secondary or inconsequential in some ion mobility spectrometry (IMS) applications, however for space toxicity knowing the type of compounds present aboard spacecrafts and stations is essential and critical. Space toxicology is a unique discipline with specific attributes for spaceflight, space habitation and missions to, planets, moons, and asteroids [208]. The goal of space toxicology is to protect astronaut's health by assessing potential exposures to chemicals during spaceflight in combination with defined safe limits against chemical exposures. Since spaceflight is unique and unlike any earth environment, astronauts are exposed to distinctive and exclusive health risks due to limited access to resources, rescue, or medical care [208].

Although continuous occupation of the International Space Station (ISS) has been maintained by accessing and managing toxicology risks, continuous exposures, air and water recycling, limited rescue option and the use of highly toxic compounds for propulsion in an isolated environment, it currently requires an online and *in situ* assessment of specific toxic compounds and respective concentrations [208].Therefore, sustaining the human presence in outer space and space exploration of other celestial

bodies lays on the detection and quantification of a large spectra of compounds in low concentrations, ppb and ppt, with versatile, sensitive, and selective analytical tools.

Ion mobility spectrometry has been explored as a possible tool to provide *in situ*, and almost real-time detection and quantification of volatile organic compounds, however, currently a there is lack of a generalized databases of drift times, mobility constants or reduced mobility constants. Making IMS viable for, and useful in space exploration, while providing valuable and beneficial results in space toxicity requires the creation of a database of volatile organic compounds to allow identification of harmful and hazardous compounds in space environments.

5.6.1 Important Compounds to be Detected in the International Space Station

A list of 34 priority volatile organic compounds has been defined to be monitored and managed aboard the Russian segment (RS) of the ISS by IBMP (Institute for Biomedical Problems) experts, where SIRUS-17 was conducted. Several types of compounds are included in this list presented in Table 5.7 expect for siloxanes and heptane. Siloxanes can be detected with ion mobility spectrometry, however, the current GC column used has low affinity for such compounds but G.A.S, which commercializes the *Breathspec*® has dedicated GC-IMS device for siloxanes. Whereas heptane is undetectable with IMS since its proton affinity is lower than water.

Compounds shown in Table 5.7 include the remainder 32 volatile organic compounds from the 34-priority list and 30 have already been detected by IMS, while 2 shown unclear detectability. Additional data (Table 5.7) also includes CAS number, molecular formula, hazard class, molecular weight, detectability by IMS, maximum allowed concentration in spacecrafts ("*Predelno dopustimaya koncentraciya*", PDK), minimum and maximum exposure concentration ranges and if drift and retention times were identified and added to the developed VOC database.

Volatile organic compounds such as ethanol, acetone, 2-butanone, butanol, propanol, ethyl acetate, isobutanol, isopropanol, dichloromethane, benzene, toluene, styrene, ethylbenzene, chlorobenzene, benzonitrile, benzaldehyde, formaldehyde, acetaldehyde, cyclohexanone, are priority compounds to be monitored in the Russian segment of the ISS due to their origin in off-gassing of polymers and electronic materials, leakage from possible instrumentation failure, formed during products of water and air revitalization, reagents or even because they are by-products of scientific experiments conducted aboard the ISS.

A total of 21 compounds were detected with the GC-IMS device and founded the early development and construction of a VOC database named "VOC Library". This database contains drift and retention times for those 21 compounds which allows peak/signal identification from IMS spectra measured with the TOL-SIRUS flow program. Additionally, methanol and formaldehyde were measured to collect their respective drift and retention times, but due to complexities in spectra a clear and efficient signal data could not be established for both VOCs. For methanol, specifically a possible signal appeared to be present but was too close to the RIP to obtain accurate information of drift, retention time and intensity

Table 5.7 — Top priority compounds VOCs to be controlled on the RS-ISS defined at the IBMP. Compounds identified and added to the VOC Library are marked by an "x" and compounds measured that provided unidentifiable data are marked by "---". PDK represents maximum allowed concentration from the Russian ("*Predelno dopustimaya koncentraciya'*").

Identified	CAS number	VOC Name	Molecular Formula	Hazard Class	PKD (mg/m³)	[mg/m³] min	[mg/m³] max	[ppb] min-max	Molecular Weight	Detectable by IMS
x	[64-17-5]	Ethanol	C_2H_6O	4	10 (5,3 ppm)	0.011	35	**5.8-1858**	46.07	**YES**
x	[71-36-3]	1-Butanol	$C_4H_{10}O$	3	0.8 (0.26 ppm)	0.001	7.9	**0.3-2605**	74.123	**YES**
x	[1330-20-7]	*m,o,p* Xylenes	C_8H_{10}	3	5 (1.15 ppm)	0.002	10	**0.5-230**	106.16	**YES**
x	[141-78-6]	Ethyl acetate	$C_4H_8O_2$	4	4 (1.11 ppb)	0.001	15	**0.3-4160**	88.106	**YES**
x	[67-64-1]	Acetone	C_3H_6O	4	1 (0.42 ppm)	0.001	7.2	**0.4-303**	58.08	**YES**
x	[108-88-3]	Toluene	C_7H_8	3	8 (2.12 ppm)	0.003	4.4	**0.8-1343**	92.14	**YES**
x	[78-83-1]	Isobutanol	$C_4H_{10}O$	3	0.1 (0.03 ppm)	0.003	5	**1-165**	74.122	**YES**
x	[67-63-0]	Isopropanol	C_3H_8O	3	1.5 (0.61 ppm)	0.002	3.3	**0.8-1343**	60.1	**YES**
x	[71-43-2]	Benzene	C_6H_6	2	0.2 (0.06 ppm)	0.001	3.221	**0.3-1010**	78.11	**YES**
	[104-76-7]	2-Ethylhexanol	$C_8H_{18}O$	3	0.6 (0.11 ppm)	0.005	10	**0.9-1877**	130.23	**YES**
x	[71-23-8]	1-Propanol	C_3H_8O	3	0.6 (0.24 ppm)	0.002	2.25	**0.8-920**	60.1	**YES**
x	[75-09-2]	Dichloromethane	CH_2Cl	4	6 (1.73 ppm)	0.010	20.2	**2.9-5815**	84.93	**YES**
x	[98-82-8]	Methylethylbenzene	C_9H_{12}	3	0.25 (0.05 ppm)	0.002	0.8	**0.4-163**	120.19	**YES**
	[75-07-0]	Acetaldehyde	C_2H_4O	3	1 (0.56 ppm)	0.001	3.5	**0.6-1943**	44.05	**YES**
x	[124-19-6]	Nonanal	$C_9H_{18}O$	3	0.38 (0.07 ppm)	0.005	0.6	**0.9-103**	142.24	**YES**
x	[108-94-1]	Cyclohexanone	$C_6H_{10}O$	3	1.3 (0.32 ppm)	0.001	2.144	**0.2-534**	98.15	**YES**
x	[100-52-7]	Benzaldehyde	C_7H_6O	3	1 (0.23 ppm)	0.004	1.1	**0.9-253**	106.124	**YES**
	[100-41-4]	Ethylbenzene	C_8H_{10}	4	2 (0.46 ppm)	0.001	5.2	**0.2-1198**	106.17	**YES**
---	[67-56-1]	Methanol	CH_4O	3	0.2 (0.15 ppm)	0.010	0.7	**7.6-534**	32.04	**YES**
x	[124-13-0]	Octanal	$C_8H_{16}O$	2	0.02 (0.004 ppm)	0.004	3.5	**0.8-667**	128.212	**YES**
x	[66-25-1]	Hexanal	$C_6H_{12}O$	3	0,4 (0.10 ppm)	0.001	0.9	**0.2-220**	100.16	**YES**
x	[78-93-3]	2-Butanone	C_4H_8O	4	0.25 (0.08 ppm)	0.005	0.49	**1.7-170**	72.11	**YES**
	[100-42-5]	Styrene	C_8H_8	3	0.25 (0.06 ppm)	0.001	2.662	**0.2-620**	104.15	**YES**
x	[108-90-7]	Chlorobenzene	C_6H_5Cl	3	1.5 (0.33 ppm)	0.001	2.322	**0.2-504**	112.56	**YES**
x	[112-31-2]	Decanal	$C_{10}H_{20}O$	3	0.2 (0.03 ppm)	0.005	0.51	**0.8-80**	156.2	**YES**
	[107-06-2]	1,2 Dichloroethane	$C_2H_4Cl_2$	2	0.05 (0.01 ppm)	0.001	0.241	**0.2-60**	98.96	**YES**
x	[100-47-0]	Benzonitrile	C_6H_5CN	3	0.15 (0.04 ppm)	0.069	0.263	**16-62**	103.04	**YES**
	[84-74-2]	Dibutylphtalate	$C_{16}H_{22}O_4$	2	0.01 (0.001 ppm)	0.002	0.322	**0.2-28**	278.34	**unclear**
	[78-84-2]	Isobutyraldehyde	C_4H_8O	2	0.18 (0.06 ppm)	0.020	0.02	**6.8**	72.11	**YES**
	[107-02-8]	Propenal (acrolein)	C_3H_4O	2	0.1 (0.04 ppm)	0.010	0.5	**4.4-218**	56.06	**YES**
	[2807-30-9]	Propyl Cellosolve	$C_5H_{12}O_2$	3	0.02 (0.005 ppm)	0.001	0.054	**0.2-13**	104.15	**YES**
---	[50-00-0]	Formaldehyde	CH_2O	-	0.05 (0.04 ppm)	-	-		30.031	**unclear**

5.6.2 Compounds and Methodology Used to Gather Data

Every compound measured during the construction and development of the VOC database with drift and retention times, including top priority compounds to be controlled on the RS-ISS, were obtained from several departments at the School of Science and Technology from Nova University of Lisbon. Almost all compounds had been purchased from Sigma-Aldrich or affiliated companies. Hence, compound availably was to a degree limited to compounds present in several laboratories and repositorium's at the physics and chemistry departments of NOVA University of Lisbon. Furthermore, all compounds were obtained had 99% purity and some considerations were implemented during the construction and development of the VOC database in measurements to ensure compound data from each VOCs could be extracted and identified with accuracy and precision.

Identification of drift and retention times from VOCs was performed empirically with measurements from a single sample made for each compound with different volumes, 1 mL, 2mL and 5 mL. This approach was often enough for a fraction of the measured compounds, such as alcohols, which required only 1 mL to be injected and analysed due to their high volatility and detectability by the GC-IMS. Additionally, in some instances, signals could even be identified for compounds by sampling room air after a previous volume had been extracted with a syringe from the sample vial.

Nevertheless, for some compounds, identifying specific signals was not as straightforward, since a few IMS signals would appear in a single measurement from a pure compound. Increasing the injected sample volume would predominantly increase the signal (or signals) from the pure substance and drift and retention times could, empirically, be attributed to the respective VOC. Finally, for some compounds two or even three vials containing liquid samples from different bottles were made and measured to verify any doubts about IMS signal identify and corresponding measured VOC.

Essentially several measurements were conducted for each compound in order to attain sufficient data and permit drift and retention times to be unequivocally extracted and identified. While a few compounds proved more problematic than others, accurate data could be extracted and used added to the construction and development of a VOC database in an empiric method.

VOCs selected for analysis and development of the database was done considering top priority compounds to be controlled in the RS-ISS, VOCs emission from microorganisms (MVOCs) and several common polymers and toxic compounds commonly found in indoor air.

5.6.3 VOC Database: Creation and Development

The construction of the VOC database was done by analysing measurements with LAV software and extracting relevant data for approximately 70 compounds and adding corresponding data (CAS number, compound name, molecular weight, drift time in milliseconds, drift time presented as RIP relative, retention time in seconds, reduced mobility constant, vapour pressure, molecular vapor). Data from VOCs exhibiting mainly monomer and dimer signals however, trimer signals or more were also identified for some substances (e.g., m,o,p-xylenes - trimer signals; limonene and α-pinene 4 signals).

The full list of VOCs already in the current database version include ethanol, 1-propanol, 1-butanol, 1-pentanol, 1-hexanol, 1-heptanol, 1-octanol, 2-propanol (isopropanol), 2-methylpropanol (isobutanol), 3-methyl-butanol, 2-methylbutan-2-ol, 2-aminoethanol (ethanolamine), 1-octen-3-ol, (2E)-2-octen-1-ol, o-xylene, p-xylene, m-xylene, benzene, methylbenzene (toluene), isopropyl-benzene (cumene), nitrobenzene, chlorobenzene, tert-butylbenzene, benzonitrile, diethyl Ether, t-Butyl methyl ether (2-methoxy-2-methylpropane), methyl acrylate (methyl prop-2-enoate), dichloromethane, ethyl Acetate, acetone (2-propanone), 2-butanone, 2-pentanone, 2-hexanone, 2-heptanone, 2-octanone, 1-octen-3-one, cyclohexanone, acetophenone, cistus cyclohexanone, propionaldehyde or propanal, butanal (butyraldehyde), hexanal, heptanal, octanal, nonanal, decanal, (2E)-2-hexenal, (2E)-2-heptenal, (2E)-2-octenal, (2E)-2-nonenal, (4Z)-4-heptenal, pentanedial (glutaraldehyde), 2,4-octadienal, 2,6-nonadienal, β-homocyclocitral, benzaldehyde, phenylacetaldehyde, 2-ethylfuran, 2-pentylfuran, acetic acid (ethanoic acid), propionic acid (propanoic acid), butyric acid (butanoic acid) pentanoic acid (valeric acid), limonene, α-pinene, linalool, α-terpineol and menthol.

The type of compounds included in the VOC database are simple and substituted alcohols, xylenes, benzene derivates, ethers, acrylates, acetates, ketone, cyclic-ketone, aldehydes, unsaturated aldehydes, di-aldehydes (two aldehyde groups), benzaldehydes, furans, acids, and terpenes. The developed VOC database also includes a section to write any possible observation or notes about a specific signal, a tag for each compound class or functional group, and known proton affinities.

VOC database construction and development correspond to the analysis of pure substances involved in space toxicity, plants, food and food spoilage, microorganisms and air contaminant originating from office supplies, furniture, and home materials. Therefore, the results contained here for volatile organic compounds are related to previously described analysis and studies and is an on-going process. Database size is important for space toxicity and other applications of IMS, and further data should be added for more substances or as drift and retention times are uncovered.

In Figure 5.39 compounds detected between 0 and 500 second of retention time are displayed as a visual representation of most volatile organic compound contained in the VOC database. Most of the VOCs included in the database are condensed between this retention time interval and is possible to observe most low molecular weight compounds appear at low retention times with shorter drift times. Another important observation conducted during the analysis of the overall data contained in the VOC Library is a lack of occurring signals between 120 and 180 seconds (retention time). So, it appears compounds eluding at those retention times have escaped detention and remain unidentified in the current database version, which means, a larger spectrum of compounds should be measured to provide knowledge of VOCs contained in interval.

A fragment of the developed VOC database is found in Appendix I Figure A.11, displaying several types of data from each compound and observations for each signal. Moreover, once compounds were grouped by functional chemical group two unusual characteristics became evident. Firstly, visual analysis of all alcohols, ketones and aldehydes signals revealed a characteristic shape for each functional group (Figure 5.40) and secondly data from dimer and monomer signals show a linear distribution, (positive slopes) for drift time values of VOCs belonging to the same chemical family (section 5.6.4).

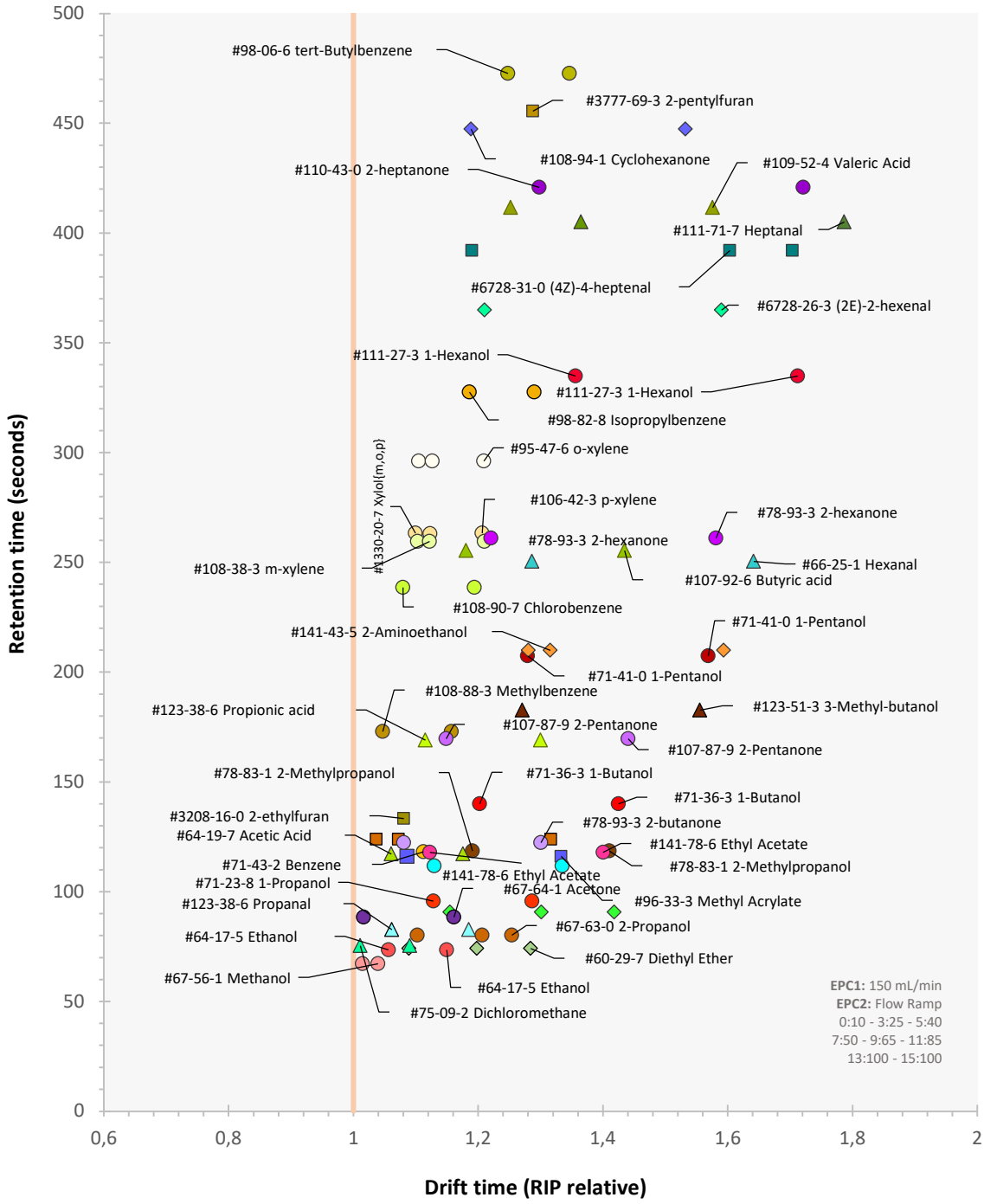

Figure 5.39 — Volatile organic compound contained in the VOC database between 0 and 500 second of retention time. Each circle represents one signal, which are coloured by compound class and labelled with CAS number and common name. The GC-IMS flow parameters are displayed at the bottom right.

The observation unique signal has a particular shape relatable to chemical functional groups could be a consequence of molecular structure, shape, column affinity, electronic distribution, ionization chemistry and collision cross section. A deeper exploration on this subject might provide further information about the processes occurring inside the IMS drift tube and even allow the development of prediction tools for retention and drift times based on the chemical structures of compounds.

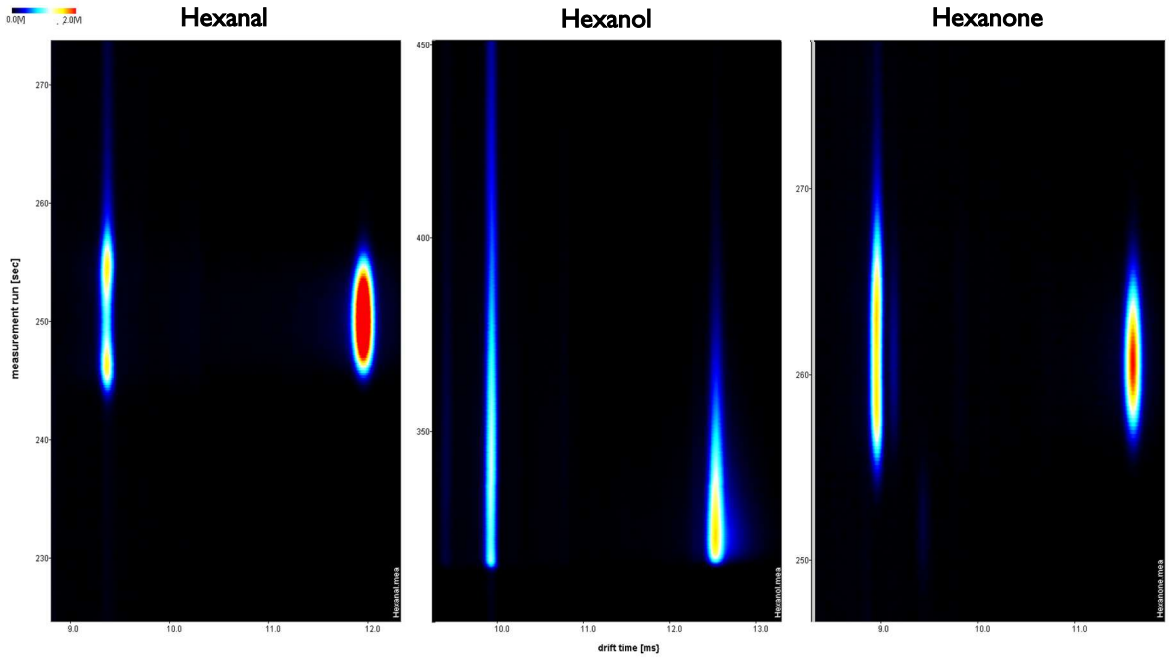

Figure 5.40 — Archetypical signal shapes for 3 chemical groups, aldehydes, alchools and ketones (exemplefied by monomer and dimers signals from hexanal (left), hexanol (mid) and hexanone (right)).

Another observation from data included in the VOC database is pertains to drift and retention time values, which were extracted with LAV software from manually marked spectra areas. Drift and retention time date showed a certain degree of variability with increasing concentration or IMS signal. A higher variability was observed for retention times comparatively with drift times which could be to column properties and compound affinity. Retention time variability increases at higher values compared to smaller times a typical behaviour observed in gas chromatography. Drift times, relative to RIP, showed a maximum inaccuracy of 0.05 which already provides enough accuracy to discern between different compounds. Although further research should be conducted in terms of examining drift and retention time variability as compound concentration increases.

The developed VOC database, called VOC Library has proven incredibly useful in manually identifying signals from samples, however, during its development, became clear that further work is required, be it in growing the database with data from now VOCs, but also, in exploring how IMS signals behave in general and what might problems can arise from variations in retention and drift times.

An automated tool should also be developed for identification of VOCs from GC-IMS spectra since most steps in IMS data processing are still conducted manually and require vast amounts of time. Artificial intelligence and machine learning could be explored for automation and to expand the current knowledge of IMS signals, especially in establishing reduced ion mobility constants as a transferable value between IMS instrumentation, or to create a new constant able to provide accurate identification of VOCs across IMS devices.

The creation and development of this VOC database revealed a necessity to study and compare reduced mobility constants between instrumentation to develop tools or approaches that enable

comparison of data between IMS instruments. Moreover, artificial intelligence and machine learning should also be applied to develop a prediction tool for retention times under different program flows, since currently, this is a considerable hurdle for compound identification in the developed database.

The development of this VOC database provided useful data to identify VOCs for gas samples measured with the previously developed flow program, TOL-SIRIUS. However, during the development of this database it was clear a lot more research and growth is still required and should in fact be given priority and focus as future work.

5.6.4 Drift Time Data from Different VOC Functional Groups

A comprehensive analysis about the variation of drift times over several volatile organic compounds belowing to three functional groups, alcohols, ketones, and aldehyde, uncovered a linear behaviour. The drift time data extracted from both monomer and dimer signals for methanol, ethanol, 1-propanol, 1-butanol, 1-pentanol, 1-hexanol, 1-heptanol and 1-octanol was plotted in Figure 5.41.

The graph also contains the drift times of monomer and dimers signals for several ketones (acetone, 2-butanone, 2-pentanone, 2-hexanone, 2-heptanone and 2-octanone) and aldehydes (propanal, butanal, hexanal, heptanal, octanal, nonanal and decanal). Monomer signals as well as dimer signals for ketones and aldehydes show a linear distribution and therefore, a linear adjustment was fitter to data from each monomer and dimer group of signals for the three functional groups.

An observation can be made from data presented in Figure 5.41, monomer and dimers signals from each functional group show a visual separation. Linear distributions for dimer signals demonstrate a higher slope when compared with monomer, which eventually leads to a separation between dimer and signals as carbon chain number increases. Also, both monomer and dimers of alcohols have a higher drift time value compared with ketones and aldehydes resulting in alcohol data points being above monomer and dimers signals of the other two functional groups signals. In contrast, ketones have the lowest drift time compared with the respective alcohols and aldehydes with the same number of carbons, while aldehydes show intermediate drift times between alcohols and ketones.

Hence results shown in Figure 5.41 for several alcohols, aldehydes and ketones imply their chemical structure and electronic distribution during drift tube separation might have a predictable effect on drift time values. Consequently, the linear behaviour observed by the distribution of drift times from those volatile organic compounds could be used to predict drift time from unknown compounds without requiring measurements of pure substances.

Moreover, difference between drift times from one function group could also prove useful to predict drift times from other functional groups with the same number of carbon atoms in their chemical structure. Further measurements and a deeper data analysis should be conducted to validate this observation. The development of a methodology for predicting RIP relative drift times of volatile organic compounds by their chemical structure might also be possible with further research, eventually establishing a predictive method of drift time values from chemical structures. Predicting drift time values via chemical structure would also improve tools and databases for compound identification.

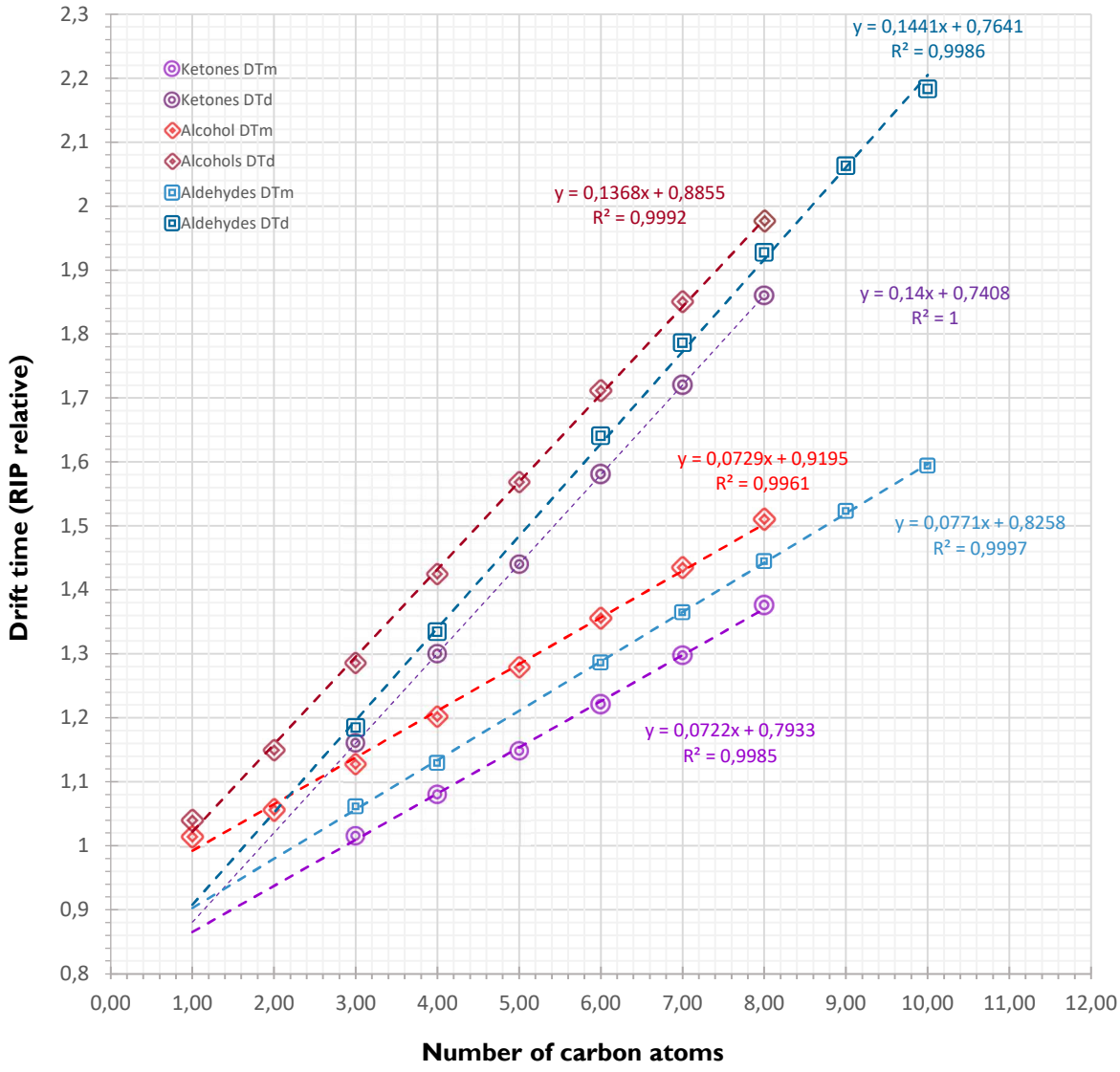

Figure 5.41 — Drift time distribution of monomer (DTm) and dimer (DTd) signals from several alcohols, aldehydes, and ketones with increasing number of carbon atoms in their chemical structure. Alcohols are represented by the colour red, aldehydes by blue, and ketones by purple, while monomer are marked by a lighter tone and dimer signals have a darker tone from their respective functional group colour.

The previous results only included saturated carbon compounds, meaning every compound only had a single bond between all carbon atoms, therefore a comparison between the drift times from saturated aldehydes and unsaturated aldehydes was conducted (Figure 5.42). The saturated aldehydes analysed were propanal, butanal, hexanal, heptanal, octanal, nonanal and decanal while unsaturated aldehydes included 2-hexenal, 2-heptenal, 2-octenal and 2-nonenal.

The drift times of both saturated and unsaturated aldehydes drift times demonstrate, once more, a linear distribution, however unsaturated aldehydes have a higher slope for both monomer and dimer signals when compared with saturated aldehydes. Contrary to what was observed in Figure 5.41, both slopes from the adjusted linear regression of monomer and dimer signals have significant differences, even reaching and interception point for saturated and unsaturated aldehyde dimers.

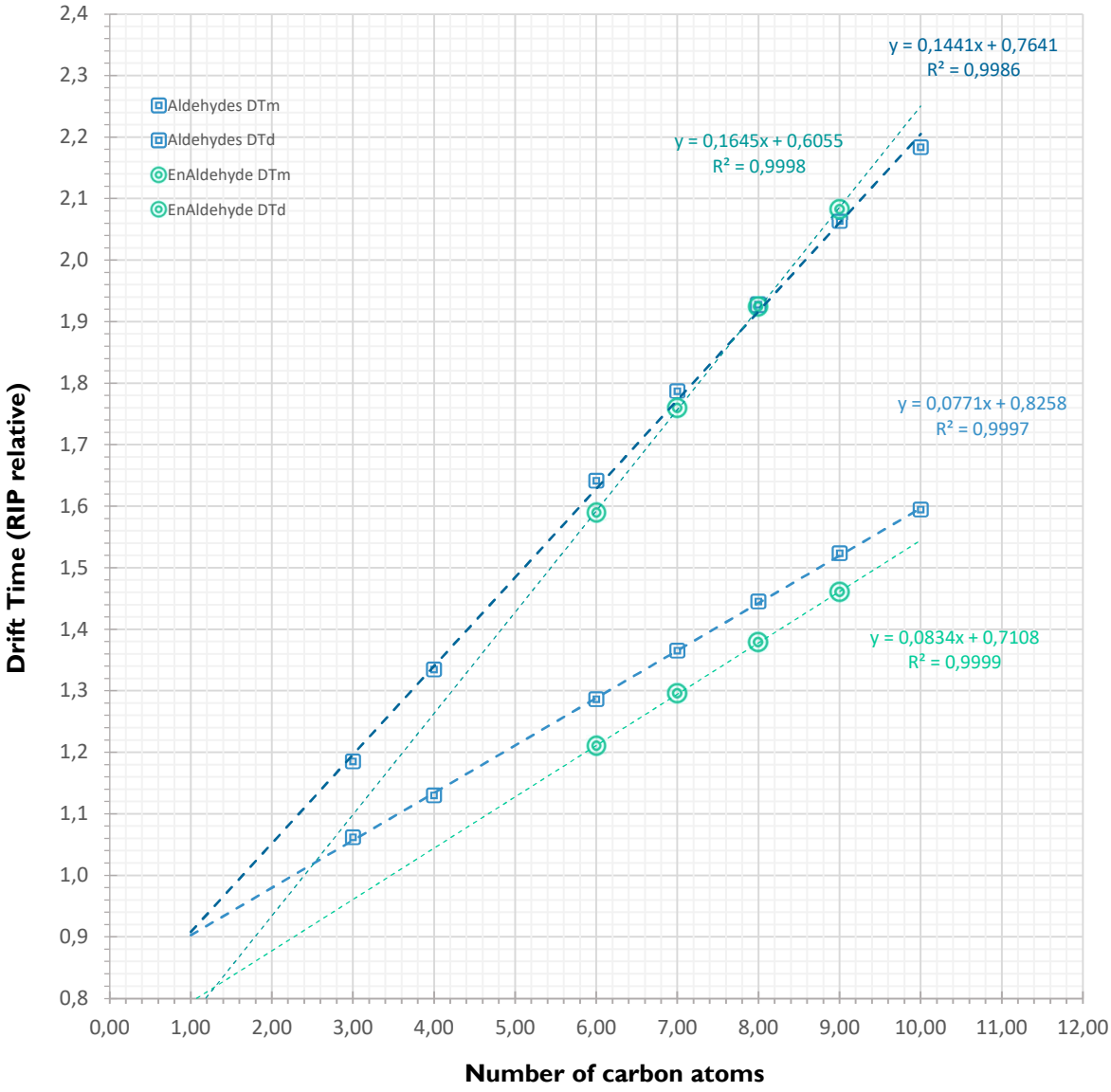

Figure 5.42 — Drift time distribution of monomer (DTm) and dimer (DTd) signals from several saturated aldehydes (Aldehydes) and unsaturated aldehydes (EnAldehydes) with increasing number of carbon atoms. Saturated aldehydes are represented by the colour blue and unsaturated aldehydes by green whereas monomers have a lighter tone and dimers darker tone of their respective aldehyde type.

Overall, the results provide information about the effect of a carbon double bound on the drift time of aldehydes and reveal drift times suffer predictable changes due to differences in chemical structure. All data presented here about drift time values is relatively to RIP and suggest values could be predicted through the chemical structure of VOCs.

Moreover, it is possible, reduced ion mobility constants could be predictable in a similar process which, would help establish a transferable ion mobility constant for compound identification between IMS devices. [209] Since, the relative ion peak, or RIP, can probably be used as a reference for the conditions inside the drift time while variability between instrumentations related to electric field and drift tube length could be adjusted once an in-depth analysis of drift times is conducted between different GC-IMS instruments. [209, 210]

5.7 Gas Calibration procedure and estimation curves

Besides identification of compounds present in cabin air of spacecrafts, quantification of both toxic and non-toxic compounds is also essential to establish and maintain a health and safe environment in spacecrafts and stations. Exposure to toxic substances is highly dependent on exposure levels where concentration is important but also time of exposure plays a crucial factor and through Spacecraft Maximum Allowable Concentrations (SMACs) for selected airborne contaminants environmental conditions and astronauts' health are monitored and controlled. SMACs were developed and established to account for several compounds present in low concentration, although even constant or permanent exposure in low concentrations can lead to short- and long-term health effects and reduce performance hindering health and any mission success. Non-toxic compounds might be important to identify good environmental conditions or changes prior to possible harmful events, including rapid and harmful growth of microbial organisms, degradation of electronic components or other materials present in both life support systems and essential operation systems.

Ion mobility spectrometry has a great analytical flexibility, with low-cost instrumentation compared with other analytical techniques, provides almost real-time monitoring and is high selectivity and sensitivity when coupled with gas chromatography have provided extraordinary detection limit of VOCs, specifically, in low ppb_v and ppt_v concentration. However, without a precise and accurate method for VOC calibration in ppb_v and ppt_v concentrations, IMS utility and suitability for monitoring daily exposure to toxic compounds in Earth and spacecraft environments is constrained. Thus, a calibration protocol was developed to determine a direct relationship between IMS signal intensity and concentration values for three compounds: 2-hexanone, 2-butanone and 1-butanol as example VOCs.

5.7.1 Development of a Method for Gas Calibration

To develop a gas calibration, a simple procedure and suitable method that provides accurate and precise results must be selected from the many methods and approaches from the generation of calibration gases. The available methods to generate standard gases and mixtures include static and dynamic methods, however because static methods are susceptible to gas adsorption from the container surface and concentration ranges for calibration are particularly small including ppb and ppt, static methods are inadequate. Nevertheless, static methods are still used to calibrate instruments at higher ranges of concentration or even for compound identification of retention and drift time.

Hence dynamic methods are the best approach for calibration of standard gases of GC-IMS devices at lost concentration, yet dynamic systems used for calibration are varied, including methods evaporation, electrolytic, chemical, injection, diffusion, and permeation methods. Chemical and electrolytic methods can be influenced by parameters involved in chemical reactions or electrolytic process and require several different materials and complex systems which complicates the calibration procedure. Evaporation, injection, and diffusion methods are based on dedicated and specific containers and although accurate and precise results can be obtained from those methods, their reliance in specific

containers and systems makes them unnecessary complicated for the development of a suitable calibration protocol. Therefore, permeation methods were selected as a viable, simple, accurate and precise method for the calibration of gas standards for a GC-IMS device. The advantages of permeation methods over diffuse and static techniques are linked to the ability of permeation methods to generate low concentrations of volatile gases, liquid or even solids with a stable and constant concentration over a long period of time.

The use of permeation tubes, a dynamic approach included in the permeation methods to generate gas standards, is frequently employed, and involves the construction of permeation tubes, which are monitored by gravimetric methods establishing an emission rate for compounds, at constant temperatures, enclosed inside a polymer tube, generally, PTFE. Inside a PTFE tube, a chemical compound permeates its walls at a constant rate at a specific temperature, afterwards its vapor is mixed and carried by a diluent gas flow and delivered into an analyser. Thus, during the developed protocol it is curtail and essential to have an accurate gravimetric instrument, and a device capable of generating, and maintaining a constant temperature over long periods of time and house a permeation tube with a gas flow. The obvious approach is to take advantage of a thermogravimetric instrument, which can weigh an item with high precision while keeping it at a highly controlled and stable temperature over several days or weeks.

5.7.2 Description of the Gas Calibration Protocol

VOC calibration for the GC-IMS instrument was based on the dynamic method of permeation tubes to produce and generate low concentration ranges between ppb_v and ppt_v by thermogravimetry analysis. The proposed calibration protocol can be explained by creating and filling a permeation tube with a specific pure volatile organic compound which is continuously weighed inside an oven with a constant temperature over several days by a thermogravimetric instrument. When stable mass loss ratio and emission rate from the tube is established different flow values streaming from the thermogravimetric device create different concentrations. Air samples with different concentrations are measured with the GC-IMS and intensity values are extracted and gathered in a plot graph to which a curve is adjusted producing a calibration curve and an expression for the relationship between IMS signal intensity and VOC concentration. A summarized version can be established with five main stages:

1. Cutting materials for permeation tubes,
2. Assembling and filling permeation tubes with the desired compound,
3. Thermogravimetric analysis: establish mass loss ratio and maintain a constant temperature,
4. Flow and temperature variation to generate different concentrations,
5. Creation of a calibration curve and expression to estimate VOC concentration.

Materials used included a Permeation Tube Manufacturing Kit commercially available from Owlstone Inc. composed of 20x mild steel end crimps, 1/4" PTFE tubing, 5mm PTFE end caps, custom crimping tool, crimping vice, spatula for solid sample measurement, 10x pipettes for liquid sample measurement and a tube cutter [159]. The preparations to build permeation tubes involved cutting a

portion of PTFE tubing and end caps and metallic crimps to create a tube of approximately 2 cm of length approximately holding 0.2 mL of a compound. Tube extremities were sealed with 5mm PTFE end caps with 0.5 cm length which were tighten with 0.5 cm length mild steel end crimps by a crimping vise. Therefore, effective length of each tube, which corresponds to the distance between the two interior end plug surfaces was roughly 1 cm. Permeation tubes were constrained to a maximum length of 3 cm indoor to fit into the thermogravimetric instrument since only a maximum height of 3 cm was available inside the device hoven. Consequently, to allow some spacing between the tube and the tube holding space inside thermogravimetric hoven a total length of 2 cm was chosen for permeation tubes. Whereas tube filling was conducted considering liquid quantity inside the tube should be maximum to reduce the formation of any possible air bubbles.

The instrumentation used for thermogravimetric analysis (TGA) was a LABSYS evo TGA 1150® device from Setaram allowing temperature ranges from room temperature to 1150°C with 0.1°C precision, a weighing precision of 0.01 % with 0.02 µg resolution while using purified air as a flow gas. As a result, a calibration system can be defined as comprising the CGFU and GC-IMS coupling, which was connected via its sample inlet to the TGA device via a Teflon tube of 40 centimetres. The thermogravimetric analysis was used to provide an accurate mass loss ratio estimation of permeation tubes, control hoven temperature and flow rate into GC-IMS. Several temperatures were used to create accurate concentration of several VOCs, 40, 60 and 85 °C, while the flow rates used were 25, 50, 100, 150 and 200 mL/min. Since specific temperatures would generate different mass loss ratios, flow rate was only changed once a stable mass loss ratio and emission rate was achieved for each tube, creating different concentration which can be estimated by equation (26) [158, 160].

$$C = \left[{}^{(q_d \times 22.4)}/_{M}\right]/Q \tag{26}$$

Where, C represents concentration in ppm, q_d permeation ratio in ng/min, M molecular weight in g/mol of the volatile organic compound inside the tube, and Q the flow ratio in mL/min, passing through the TGA device into the GC-IMS. Measurements lasted 15 min, using the TOL-SIRIUS program, with 5 replicates being performed for each concentration value, however, depending on the compound, shorter measurement times could be established. Lastly, each gas flow change was interspersed by 15 min before to any measurement to guarantee flow and temperature stability.

5.7.3 Application of the developed protocol for VOC calibration

During the application of the developed protocol several considerations were careful managed controlled. First, construction of each permeation tube was done maintaining, as much as possible, similar dimensions between tubes. Secondly, to avoid leakage crimps were strongly tightened, and the tube laid for 12h at ambient temperature to verify sealing. Once place a tube was inside the TGA hoven, temperature was kept constant over days while the permeation tube would lose mass through it walls by permeation, and a constant flow of 10 mL/min of purified air was circulated inside the TGA device hoven.

A peculiar observation was found during early analysis of mass loss ratio from permeation tubes, when the hoven temperature was set to temperatures close to ambient temperature (25 to 34°C) the permeation tube would never reach a constant and stable loss of mass. An explanation for this might be related to the TGA instrumentation having difficulties keeping a stable temperature in this range because the device operates by detecting the temperature inside the hoven and not the exact temperature of the permeation tube. Thus, only temperatures above 40°C were used during all calibrations of permeation tubes. A constant mass loss ratio due to permeation was achieved for tubes between 4 to 7 days depending on the defined temperatures and the compound inside the tube.

Overall, mass loss ratios were characterized by smaller and more irregular ratio in the early minutes and hours after the permeation tube was placed inside the TGA device. This is a consequence of permeation tubes requiring a certain period to reach equilibrium as acclimatization and permeation occurs. The mass loss through permeation for a tube containing 2-hexanone is show in Figure 5.43. A linear regression was adjusted to the mass variation of the permeation tube over time with a corresponding slope of -0.0047, means, 0.0047 mg were being released from this permeation tube. Hence, emission rates of each permeation tube were estimated through this process for prior to calibration.

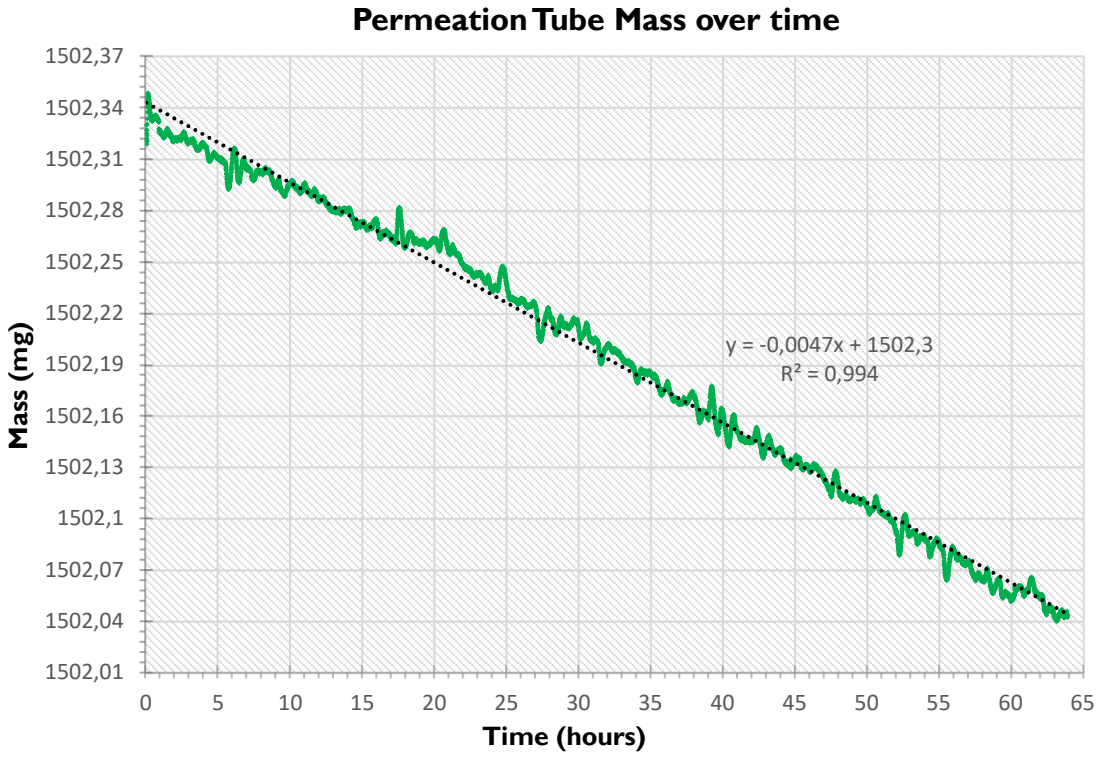

Figure 5.43 — Thermogravimetric analysis for a 2-butanone permeation tube at 40 °C for 65 hours.

Once an emission rate was established for a permeation tube, equation (26) was used to estimate concentrations at a selected flow rate and produce a calibration curve for each volatile organic compound. So, estimation of emission rates via thermogravimetry and the generation of several concentration through flow rate allowed a curve to be created and link to signal intensity from the respective compound concentration generated into the gas flow directed to the GC-IMS.

The first compound selected for calibration was 2-hexanone, with 99% purity, also served as the first application and test of the developed calibration protocol. Temperature values, flow values and tube construction were all tested with 2-hexanone. Eventually four different permeation tubes containing 2-hexanone were constructed and tested with different flows and temperatures.

Permeation tube 1 was place at 85°C achieving an emission rate of approximately 137.6 ng/min which produced four concentration values, 2753, 1376, 918 and 702 ppb by selecting four flow rates, 50, 100, 150 and 200 mL/min, respectively. While permeation tube 2 was place at 60°C reaching an emission rate of approximately 43.2 ng/min resulting in five values of concentration, 1727, 864, 432, 288, 220 ppb by changing flow rates to 25, 50, 100, 150 and 200 mL/min. Tube 3 was analysed at 85°C and reached an emission rate of 126 ng/min and tested for an additional flow rate (25 mL/min) when compared with tube 1. The last tube made for 2-hexanone was thermogravimetrically analysed at 40°C and had an emission rate of 9.1 ng/min reacting concentration of 362, 181, 91, 60 and 46 ppb through the same flow rates previously used. A summarized table containing the results for all created and analysed permeation tube of 2-hexanone is presented in Table 5.8.

Table 5.8 — Summary of the results obtained for four permeation tubes of 2-hexanone to establish a calibration curve. Concentration is represented in parts-per-billion and the respective mean intensity (monomer and dimer signals) for 5 replicates, the standard deviation, hoven temperatures and respective gas flows and emission rate in ng/min for each tube.

Concentration [ppb]	Mean Intensity, 5 replicates) [volts]	Standard deviation	Temperature (°C)	Gas flow (ml/min)
Permeation tube 1	**----**	**Permeation rate**	**(137.6 ng/min)**	**----**
2753	16309.60	47.94	85	50
1376	13840.21	70.28	85	100
918	12403.41	70.42	85	150
702	11394.99	33.99	85	200
Permeation tube 2	**----**	**Permeation rate**	**(43.2 ng/min)**	**----**
1727	13241.45	69.39	60	25
864	10837.40	21.90	60	50
432	8611.60	28.27	60	100
288	7168.54	133.17	60	150
220	6458.79	58.55	60	200
Permeation tube 3	**----**	**Permeation rate**	**(126 ng/min)**	**----**
2521	15247.31	177.88	85	25
2101	14727.63	67.01	85	50
1260	12832.12	250.80	85	100
840	11598.73	18.36	85	150
630	10557.16	107.10	85	200
Permeation tube 4	**----**	**Permeation rate**	**(9.1 ng/min)**	**----**
362	8607.41	46.32	40	25
181	6428.60	48.64	40	50
91	4424.19	45.90	40	100
60	3473.57	47.66	40	150
46	2888.47	49.69	40	200

Analysis with GC-IMS allowed extraction of intensity values 2-hexanone signals, two peaks with the equal retention time but different drift time. Therefore, 2-hexanone showed a monomer and dimer under calibration conditions. Calculation of mean intensities for all concentrations generated with permeation tubes allowed a calibration curve to be adjusted. A plot graph was created with data presented in Table 5.8 for total signal volume of 2-hexanone monomer and dimer (Figure 5.44).

A logarithmic curve was adjusted for both distributions due to the characteristic behaviour of IMS signals therefore establishing a calibration curve for 2-hexanone. The logarithmic curve for 2-hexanone monomer and dimer signal are characterized by the equation, $y = 3261.8 \ln(x) - 10407$ with an R^2 of 0.98 by equation $y = 2594.9 \ln(x) - 9711.1$ with an R^2 of 0.93, respectively.

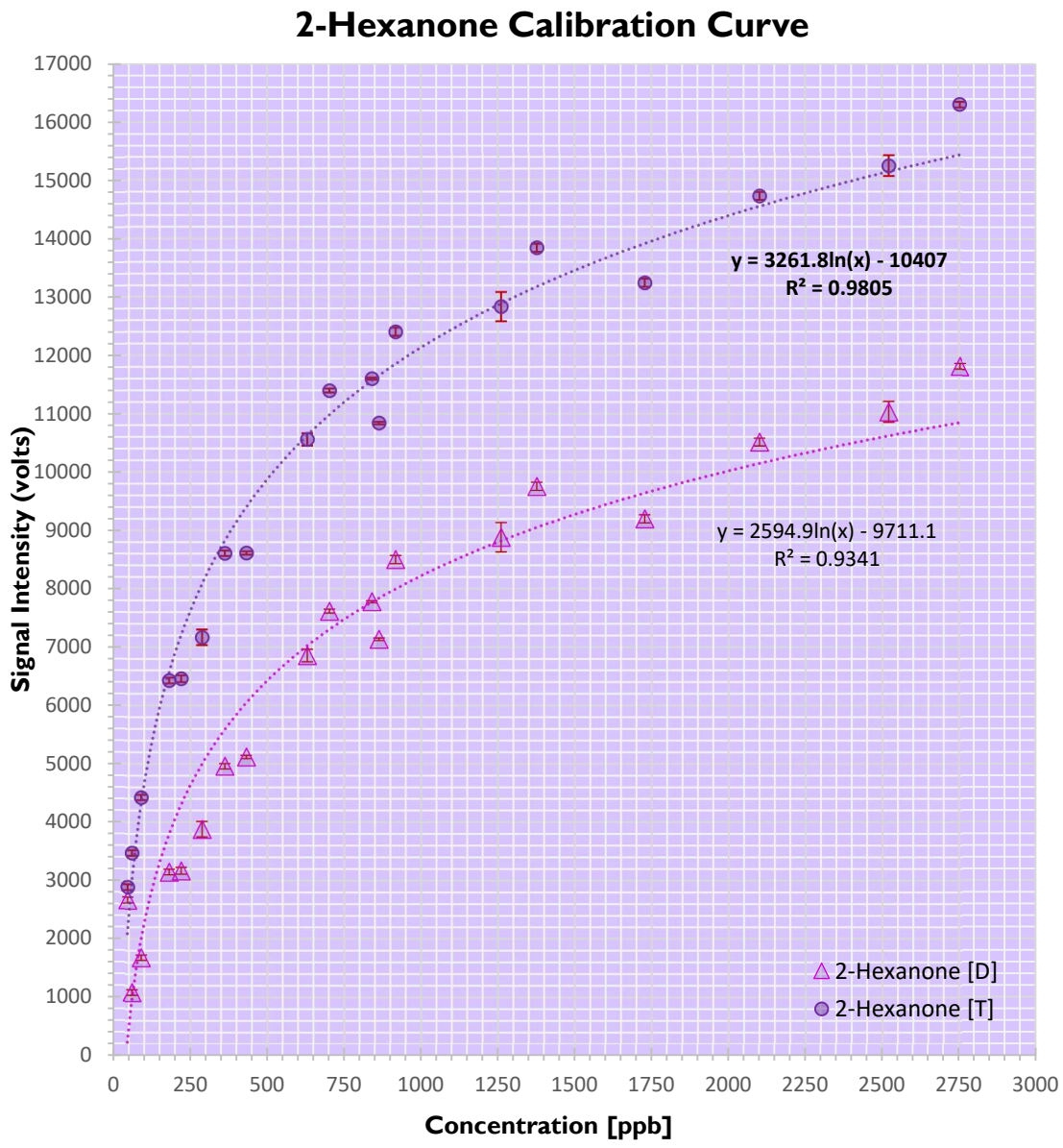

Figure 5.44 — Logarithmic curves adjusted to signal intensity vs concentration of measurements conducted for 4 permeation tubes containing 2-hexanone. Circles correspond to total signal intensity (volume) of both 2-hexanone monomer and dimer (2-hexanone [T]) and triangles to signal intensity (volume) of 2-hexanone dimer. Logarithmic equations are shown in bold for the total signal intensity and in normal text for the dimer while standard deviations are present for each point in red.

In general, low values of standard deviations were observed between measurements which indicates a high degree of stability and repeatability from the GC-IMS device. GC-IMS measurements detected a concentration as low as 46 ppb with a limit of detection (LOD) of 26 ppb estimated by the mean intensity of 10 blank samples. [166, 167]

The detectability of 2-hexanone by GC-IMS may perhaps be much lower than 26 ppb, however the current calibration protocol, due to limitations with the TGA instrumentation, does not allow the generation of concentration lower than 40 ppb. A dilution system must be implemented into the outlet of the TGA flow to allow lower concentrations to be created since, temperatures below 30°C and flow rates below 10 mL/min, are impossible to be established with this TGA instrumentation.

Furthermore, results presented for the 2-hexanone calibration could reach further accuracy, validity, and importance if cross validated with either, samples of known concentrations or through sample analysis by an additional analytical tool, preferably the gold standard, which is mass spectrometry.

The application of this calibration protocol with 2-hexanone also served as an opportunity to evaluate which stages and parameters were crucial for precise and repeatable results. Although permeation tube construction is important, its considerations rely on keeping the permeation tube as tight as possible and with minimum air inside. Tube cutting should be made with the aim of achieving a symmetric permeation tube without any irregularities to avoid an irregular position and pressure on the TGA balance.

Then, for good results it is essential to achieve a stable and constant mass loss ratio from each permeation tube and, even though, the structure of each tube is important, temperature plays a more critical role. Temperature control was performed by the TGA instrument, however, when generating VOC concentrations particular attention should be placed in identifying any oscillation in temperature over time. Emission rates for each tube is also influenced by the compound characteristics and will show slight deviations from tube to tube and the construction of permeation tube still requires some optimization to establish a replicable tube.

Lastly, 2-hexanone measurements verified the requirement of approximately 5 to 10 min, to achieve stability in the IMS detected signal once TGA hoven flow was changed to generate a new concentration. Still, results for 2-hexanone show good stability and consistence, but attention and precautions with all previously mentioned considerations is important. Lessons learned from 2-hexanone calibration, including precautions and consideration were applied for the subsequent calibration of 2-butanone (Figure 5.44) and 1-butanol (Figure 5.46).

The second compound calibrated was 2-butanone, and as with 2-hexanone, two signals are present, a 2-butanone a monomer and a dimer. Although a calibration curve for 2-hexanone and 2-butanone can be established solely on monomer intensity, this method of action is strongly discouraged and can inadequately results. Because both monomer and dimers signals represent the total concentration of compound detected and since dimer-monomer equilibrium is temperature and humidity, dependent among other IMS factors (e.g., carrier gas or ion source), an accurate calibration curve should be established considering both monomer and dimer intensities.

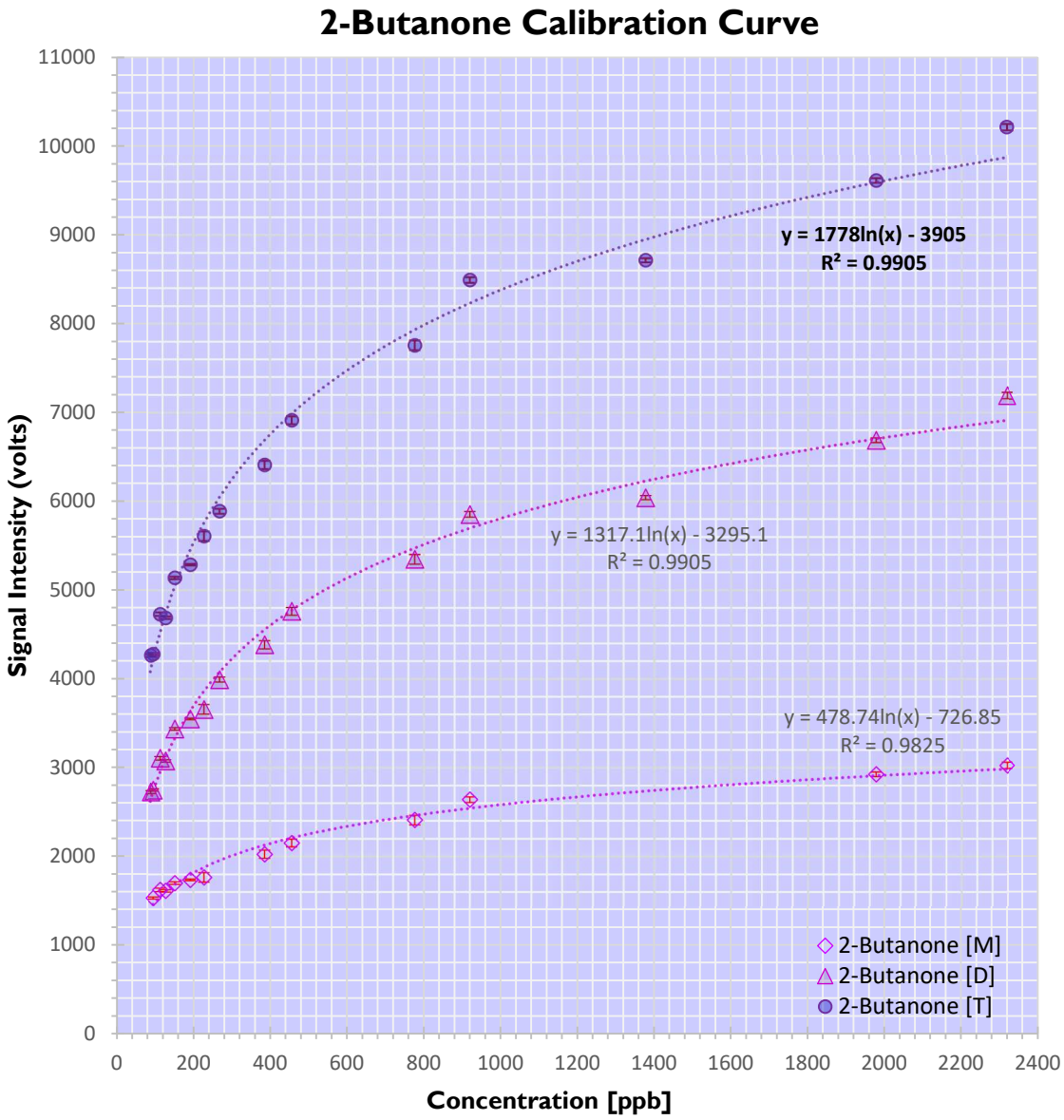

Figure 5.45 — Logarithmic curves adjusted to signal intensity vs concentration of measurements conducted for 4 permeation tubes containing 2-butanone. Circles correspond to total signal intensity (volume) of both 2-hexanone monomer and dimer (2-butanone [T]), triangles to signal intensity (volume) of 2-butanone dimer and diamonds to signal intensity of 2-butatnone monomer. Logarithmic equations are shown in bold for the total signal intensity and in normal text for the dimer while standard deviations are present for each point in red.

The calibration of 2-butanone involved 3 permeation tubes, which produced concentration from 2318 to 89 ppb with low standard deviation values (55 to 9) (Appendix II, Table A.3). The limit of detection for 2-butanone based on signal-to-noise ratio of 10 blank samples resulted in 12 ppb, while a logarithmic expression adjusted to the total signal intensity of monomer and dimer signals yield the expression y = 1778 ln(x) - 3905 with an R^2 of 0.99. This expression allows the determination of 2-butanone concentrations from IMS detected intensities from both dimer and monomer signals and when compared with 2-hexanone expressions, it can be stated, the IMS instrumentation has a higher sensitivity for 2-hexanone but lower limit of detection for 2-butanone.

Signal intensities vs concentration for 2-butanone for monomer, dimer signal and the sum of both signals were plotted in Figure 5.45. The monomer expression adjusted has a lower curvature when compared with the sum and dimer signals expressions. Therefore, sensitivity for 2-butanone concentration through monomer signal can have significantly reduced sensitivity when compared with the signals (dimer, and total intensity). Hence, determining concentration through total signal intensity might prove more sensitive and useful for a greater range of concentrations while, using solely the monomer signal could prove better below 100 ppb.

The last compound, an alcohol, 1-butanol was calibrated the developed protocol and a calibration curve was established. Two permeation tubes were built containing 1-butanol and analysed by thermogravimetry to obtain emission rates and generate several concentrations. Generated concentrates were between 1897 and 14 ppb (Appendix II, Table A.4). The calibration curve for 1-butanol dimer and total signal, sum of dimer and monomer signals, are shown in Figure 5.46. The limit of detection for 1-butanol was estimated as 14 ppb from the standard deviation of 10 blank measurements.

Comparatively, butanol appears to have a scattered distribution of points over the concentration range analysed and the adjusted curves shows an R^2 of 0.8618 and 0.91 for the total intensity and dimer intensity, respectively. An explanation for butanol's lower R^2 of the adjusted curves could easily be a result of analysing a lower range of concentrations and therefore lacking enough points for an accurate adjustment of a logarithmic curve.

Furthermore, it appears IMS signals show a higher variability between 100 and 300 ppb which coincided with the depletion of the monomer signal by its dimer, which is related to monomer-dimer equilibrium. This equilibrium is influenced by temperature and humidity, and the latter parameter could have differed between the two permeation tubes analysed, thus creating signal variations. Anyhow 1-butanol appears to have a significantly higher variability in signals intensity and therefore a reduced accuracy for its present calibration. Hence future calibration needs to be considered with each volatile organic compound properties and behaviours under each the calibration conditions, be it temperature, permeation tube materials, humidity, or concentration ranges.

Furthermore, data collected during the calibration of 2-hexanone, 2-butanone and 1-butanol indicates a need to further study and analyse IMS signal behaviours from both monomers and dimers of different functional groups. Even though the issues observed with butanol, could have been a consequence of small irregularities related with the constructions of permeations tubes or certain peculiarities of 1-butanol, mainly its monomer-dimer behaviour, it is clear VOC calibration might require cross validation through other analytical instruments. Ideally measurements of known concentration from the three tested VOC can be used to help evaluate the accuracy and suitability of the developed protocol and estimation curves. Thus, further research and laboratory analysis needs to be place into the subject of GC-IMS calibration to achieve the required qualities for space exploration and to fully take advantage of IMS quantitative capabilities.

Nevertheless, data produced and analysed here is an early and critical exploration of IMS in terms of quantification and in the development of a simple, accurate and repeatable method in the calibration volatile organic compounds with GC-IMS instruments.

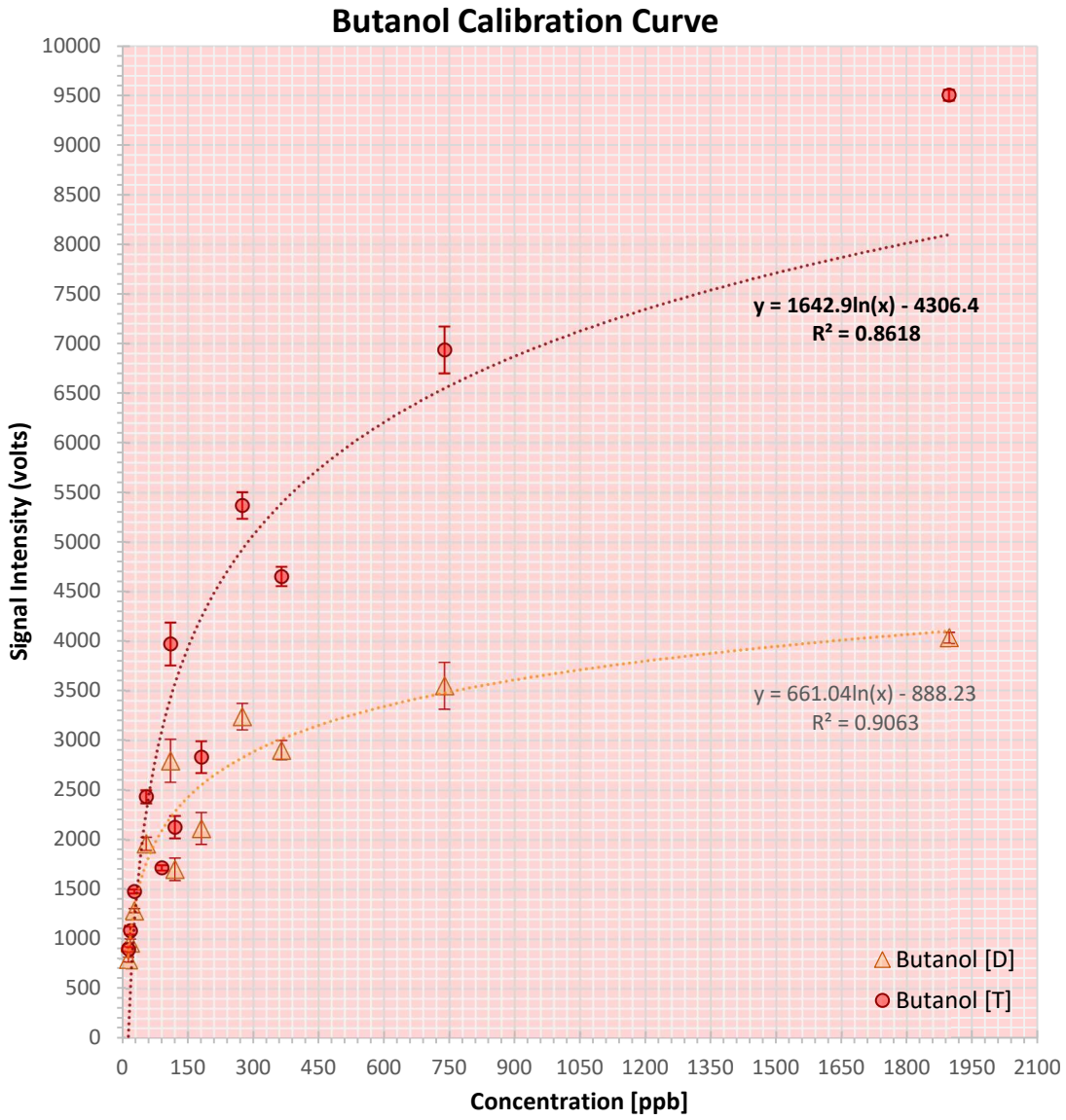

Figure 5.46 — Logarithmic curves adjusted to signal intensity vs concentration of measurements conducted for 4 permeation tubes containing 1-butanol. Circles correspond to total signal intensity (volume) of both butanol monomer and dimer (Butanol [T]) and triangles to signal intensity (volume) of butanol dimer. Logarithmic equations are shown in bold for the total signal intensity and in normal text for the dimer while standard deviations are present for each point in red.

The protocol developed also revealed how important generating low concentration is for IMS calibration and the challenges and limitations of calibration protocols for ppm and ppb ranges. It became evident how important temperature control is during the establishment of emission rates from permeation tubes. Although the tubes used were lab-made the same calibration should be performed with commercially available tubes since inaccuracies or miscalculations on establishing an emission rate can create enormous problems for calibration and further time and efforts need to be expended in future research. A calibration of other types of volatile organic compounds should also be explored.

Even so, when proper conditions are established, calibration is a relatively uncomplicated procedure which can be improved with the use of precise instrumentation and systems therefore allowing GC-IMS to serve as versatile tool for monitoring VOCs in spacecrafts and space environments.

5.8 Development of a software for data processing

Ion mobility spectrometry has been used for almost 50 years with increasing frequency and in a diversity range of applications such as environmental monitorization, medical diagnosis, industrial applications, process control, air quality, food quality and foodomics, detection and classification of microorganisms, to study of chemical structures and characterize biomolecules. Therefore, IMS reached a point where data processing is essential in both research and industry and data processing tools, including, chemometric approaches have increasingly required are slowly becoming a key strategy in research and industrial applications.

Because data processing and chemometric approaches have only been partly explored in IMS and GC-IMS data, an early algorithm for automatic peak detection and quantification for GC-IMS spectra was designed and constructed after all the knowledge gathered during experiments and data generated in this dissertation. The coding language, Python, was used as a foundation for the development of this algorithm which aims to motivate and bring attention to this somewhat unexplored and undeveloped topic from GC-IMS analysis and data processing.

5.8.1 IMS Data formats, importance, and value

Data produced from GC-IMS instruments, especially the *Breathspec*® is frequently represented as a 2D graph or 3D showing drift time (t_D) and retention time (t_R) as *x.* and y-axis, and signal intensity (volts) as a colour map (Figure 5.47). Displayed in the GC-IMS device screen is a spectrum in a 2D format, which represents the *x* and *y*-axis as drift time (ms) and intensity (volts), respectively (Figure 5.47). This representation format is possible also in the LAV software which provides useful information for signal intensity and even signal behaviour between measurements and retention times in instruments coupled with a gas chromatography.

Drift time is sometimes presented in milliseconds (ms) but preferable expressed in relation to the Reactive Ion Peak (RIP) drift time (RIPrel), by dividing a signal drift time by the RIP time (ms). This approach is used because the type of drift gas used, temperatures, humidity, and dopant gases lead to different RIP positions therefore, the employment of drift times relative to RIP position allow a standardized data for drift times which can be used to identify peaks and compounds in measurements from the same instrument. Proprietary software is typically used for signal processing, recording measurements files, visually represent spectra, among several tools to manually analyse spectra, including, data visualization, of single IMS spectra, 2D, 3D spectra or heatmaps, signal quantification, extraction of drift and retention times, manual peak picking tools, compute calibration curves and other general tools and options for data treatment.

The *Breathspec*® specifically stores measurement files in a format denominated a *mea* file which can be seen, analysed and process in the Laboratory Analyser Viewer (LAV) software commercially available from G.A.S. Dortmund (Gesellschaft für analytische Sensorsysteme). This software loads the output files from the GC-IMS device in a *mea* format (extension ".mea") and represents them, in its

default mode, as an heatmap in a window section. In the window peak areas can be marked manually for quantification, extraction of drift and retention times, management of project with several measurements (several *mea* files simultaneously) and option for visual representation of single and multiple files in a project with the help of several plug-ins.

A particular plug-in, "CSV Export", is important for automatic analysis of IMS files and data, because it allows *mea* files to be converted to a CSV file, also called "comma separated values" files. CSV files contain text information from measurements, including flows, temperature, duration, GC column, IMS serial number, among others, and a mathematical matrix with intensity values for a full IMS spectrum. This matrix is represented by the LAV software as an heatmap which displays information as interactive image with a black background and several blue to red dots coded in a colour code from intensity values (Figure 5.47).

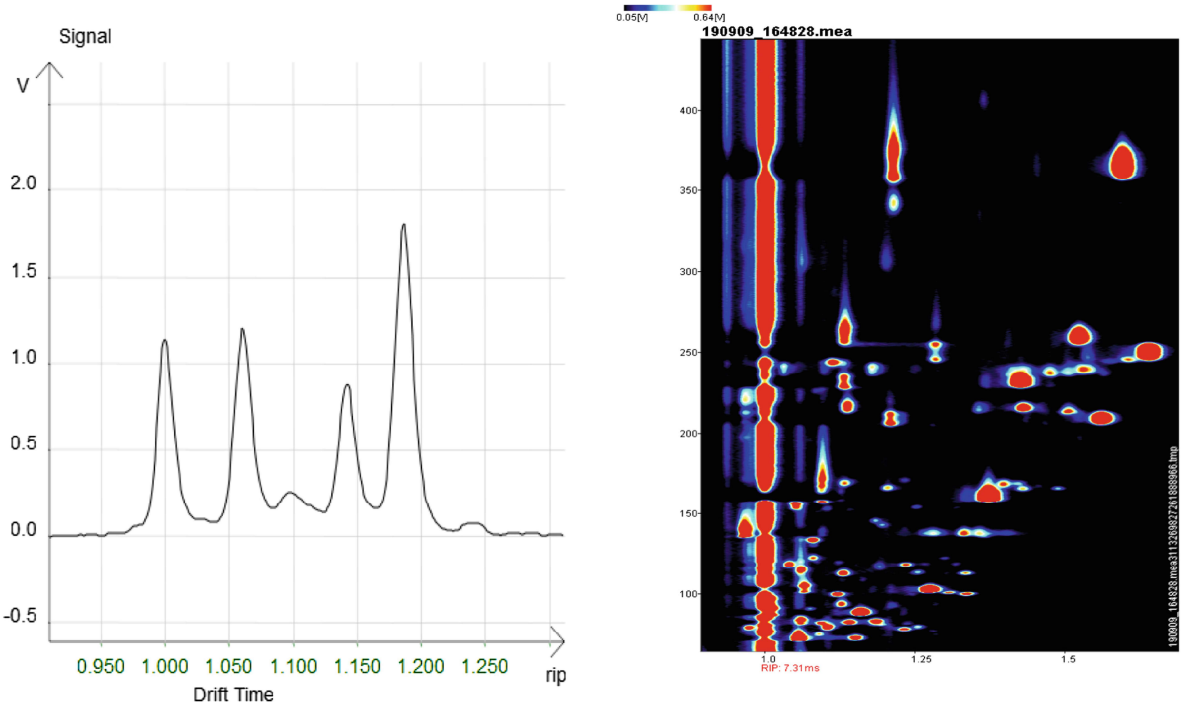

Figure 5.47 — Single IMS or 2D spectrum (right) and 3D spectrum or heatmap examples (left) (spectra processed and obtained from LAV of BreathSpec (GC-IMS) measurements).

Although visual information can be crucial to read and understand IMS data, identify patterns and compounds in measurements, this type of visual representation can complicate and limit automatic data processing and generate undesired results and errors. Hence, an algorithm was developed for automatic peak detection and quantification through the analysis of CSV files converted through the CSV Export plug-in of LAV software. CSV files are highly important since all available information from an IMS measurement is contained in *mea* files and can in a CSV format be read and analysed by several Python libraries. Therefore, using Python tools to process text and numerical data contained in CSV files can prove a simple, easy, and rapid tactic to read GC-IMS files and process its complex information.

The conversion of *mea* files to CSV produces an output file containing 3 lines with 63 columns of textual information separating, by a blank line, a mathematical matrix with 4502 column representing mobility spectra (ms) and several rows corresponding to retention times recorded each 0.21 seconds. The total number of rows will vary according to a measurement run time and the integration of column and rows establishes a GC-IMS spectra because each cell forms has an intensity value. Consequently, the developing of such algorithm relies heavily on the value contained in CSV files and tools to read, extract and process both textual and mathematical information.

Another way of representing and visually understanding what is contained in a CSV file exported from a *mea* file is a vector S = (z_0, z_1, ..., z_n) of signal intensities z_i measured in equidistant time point d_{ti}, i ∈ {1…N} for drift time, combined with a series of R one dimensional IMS spectra recorded at equidistant retention time point, r_{tk}, k ∈ {1…R} for retention time. A representation of this type of data, including the respective textual information contained in each *mea* file is shown below:

$$i_{textual} = \begin{bmatrix} machine & \dots & gas_{drift} & \dots & \dots & Timestamp \\ units & \dots & \dots & kHz & {}^{o}C & \\ data & \dots & Air & \dots & serial & 2019 \dots \\ \dots & & & blank\ line & & \dots \\ \#specnum & RetTime\ [s]\ /\ Drift\ time\ [ms] & & & & \dots \end{bmatrix}$$

$$M_{ims} = \begin{bmatrix} Z_{11} & \cdots & Z_{1n} \\ \vdots & \ddots & \vdots \\ Z_{1R} & \cdots & Z_{nR} \end{bmatrix}$$

5.8.2 Early algorithm for peak detection and quantification

Open-source coding language, Python version 3.7, was used to develop a preliminary algorithm for automatic peak detection and quantification by applying libraries and functions such as: *scikit-image* algorithms collection for image processing; *scipy.ndimage*, multi-dimensional image processing; *pandas* 0.25.3, Python Data Analysis Library; *mathplotlib* 3.1.1, Python 2D plotting library and; *NumPy*, a fundamental package for scientific computing including a standard operator functions. Although some libraries related to imaging processing and analysis, those methods were applied to the spectral mathematical matrix and not to any spectra images from IMS data. This means a theoretical approach of image processing was applied to mathematical data from IMS spectra to detected and quantify peaks automatically.

Four main phases were established in the preliminary algorithm: (i) scanning textual data, (ii) processing the IMS matrix (spectra), (iii) automatic peak detection and (iv) peak filtering and quantification. The algorithm is initiated by using pandas' function to read the CSV file, containing textual and numerical information, and separate both types of information into two different temporary functions. The phase involved in reading text comprehends scanning and selectively printing relevant information contained in a 3-line header. Name and file data, instrument type used, serial number and GC column are all information read and gathered at the end of phase one. However, at this stage no other textual information was presented and considered relevant but the algorithm is easily tailored to include other

information (e.g., carrier gas flow programmed and used in a measurement). An example with two additional lines of text, file origin and format additionally added, can be seen in below:

```
FILE ORIGIN:                    LAV conversion
FILE FORMAT:                    CSV DATA
FILE NAME:                      181114_163532_1.csv
DATE:                           2018 11 14
TIME:                           16 35 32
SAMPLE:
Machine type :                  BreathSpec®
Machine serial :                3G1-00074
GC Column :                     MXT-200. 30m X 0.53mm ID
```

Afterwards, the second phase, involves a few steps for processing the IMS matrix (spectra). RIP position is identified during this phase by locating the highest intensity values in the first retention time column/time. Further processing is performed to extract the drift time column containing the maximum intensity value and is converted after into drift time in milliseconds. The feasibility of this approach relies on recording always starting slightly before any analyte is injected, hence, the information contained inside the first matrix line is solely about intensity of the drift and carrier gas in the absent of any analyte, meaning only the RIP will be present. Furthermore, a secondary step is implemented to establish a RIP window, which involves the identification of column numbers containing an intensity above, 0.280 V and 0.100 V prior (left) and posteriorly (right) from the RIP maximum, respectively. Those values were defined by information gathered from several IMS spectra during this dissertation and provide an accurate method for the identification of a RIP window. Value differences between the left and right side of the RIP are due to the intrinsic RIP characteristics since gas humidity influences intensity values only at the RIP's left side creating a higher limit

To finalize this phase, the full mathematical matrix is reconstructed through the matplotlib functions, achieving a visualization identical to what is seen with the LAV software (Figure 5.48). Similarly, to phase one, additional processing steps can be implemented during this phase to meet user requirements or necessities. Nevertheless, since the algorithm aims to automatically detected and quantify IMS peaks, matrix processing was simplified to provided solely essential conditions for peak detection and quantification.

Automatic peak detection was conducted by a module from a *skimage* library, *skimage.measure.find_contours* (array, level), also referred to as measure. The *skimage* module works by locating iso-valued levels in the IMS matrix from a defined intensities (equal or above a threshold) and obtain clusters of column and row coordinates equal or above the defined value. Clusters can be used afterwards to detect and mark regions on the IMS matrix equal or above the defined threshold, represented with a contour at the threshold value (Figure 5.48).

The threshold value was defined as equal or above 0.150 V and produced a series of contours represented in the left image of Figure 5.48. However, because IMS spectra have some regions with low intensity values, different than zero, but equal intensity values, a number of areas were detected and marked as possible peaks by the algorithm. Those areas are in fact spectra noise which results

from the *skimage* module outputting all region above the defined threshold-value, above 0.150 V, and, to remove spectra noise, an additional step was implemented.

Since all detected and mark regions using the *skimage* module, equal or above 0.150 V, in the IMS matrix do not have a direct equivalence with the effective total number of peaks, a filtering step was needed to removed regions (or contours) corresponding to spectra noise. The tactic employed was to filter noise regions from the total detected peaks with *skimage.measure* through the subtraction of maximum and minimum values contained in each detected region. A threshold of 0.04 volts was defined as an excluding point to be implemented into a filtering tool based on the difference between maximum and minimum values. This threshold value was defined based on noise values and regions observed throughout several IMS spectra, and therefore regions with a max-min difference lower or equal to 0.04 were excluded as effective peaks (Figure 5.48) through a filtering step.

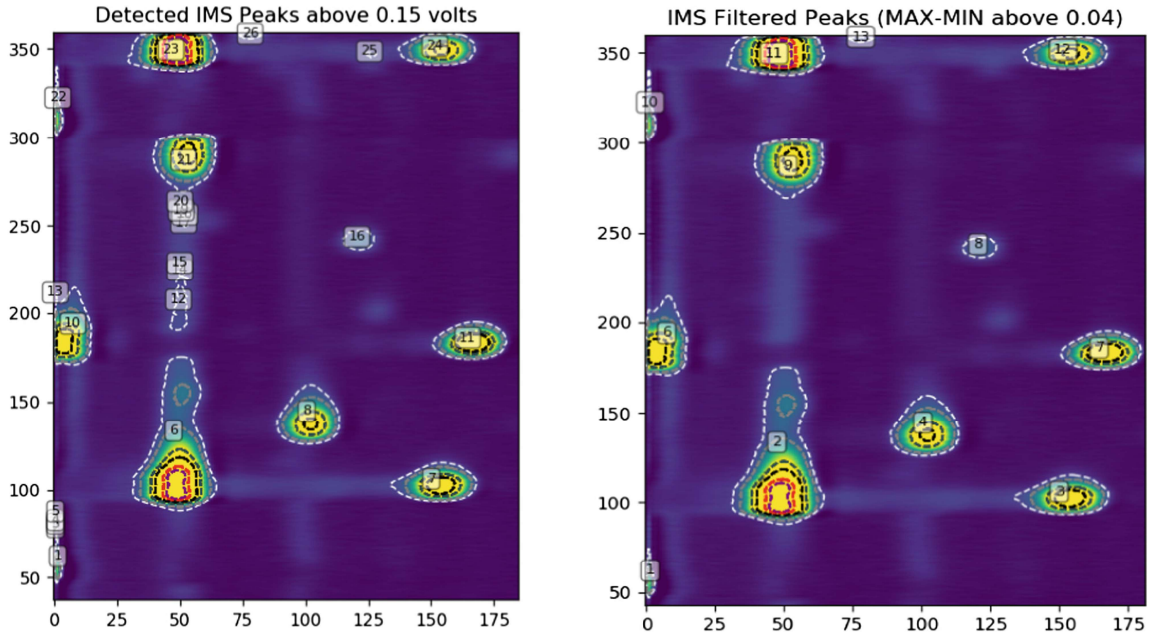

Figure 5.48 — Detected peaks before (left) and after (right) the application of a developed filtering method with the developed algorithm for automatic peak detection and quantification. *Y*-axis represents the retention time in seconds, *x*-axis the drift time in milliseconds with RIP position defined as 0, and detected peak labelled as dashed lines and numbers inside a grey square.

Once the noise filter was implemented into algorithm, the number of detected peaks was reduced, enabling recognition of only effective (real) peaks from the spectra (Figure 5.48). Moreover, users can select and adjust the filtering threshold value to meet their goals and data peculiarities providing an adaptable approach to remove the detection of noise regions as IMS peaks.

At this stage, the algorithm was able to detect peaks and could be expanded to enable automatic quantification of the detected peaks. So, peak intensity was estimated by adding all matrix values within each detected peaks after noise filtering (Figure 5.49). This method of quantification directly corresponds to the option used in LAV software, volume above baseline, during manual data processing and signal quantification.

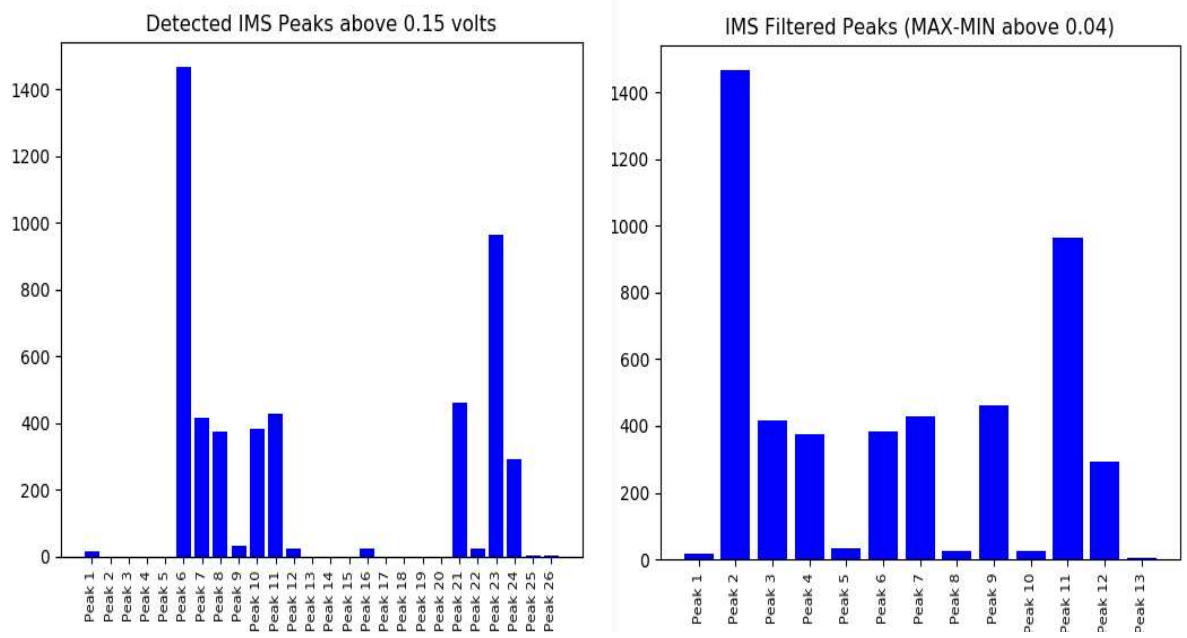

Figure 5.49 — Automatically detected IMS peaks and respective intensity (volts) above a threshold of 0.15 volts without noise filtering (left) and after applying a noise filter (right).

To further improve to improve the automatic peak detection of the develop algorithm, matrix index (column and row) for the maximum value in each effective detected peak was located. This final step of obtaining matrix index values, which can be converted into retention and drift time, is an important step provide to implement peak identification using the developed VOC database in future iteration. Hence, the final output provided by the present algorithm is displayed below, showing filter type, filter threshold, peak numeration before noise filter, maximum intensity value, and column and row index coordinates.

```
FILTER TYPE:                                    MAX-MIN
FILTER APLLIED:                                 0.04 volts
PEAK 1              Max 0.682           COORD (55, 1)
PEAK 6              Max 3.569           COORD (97, 49)
PEAK 7              Max 2.119           COORD (103, 154)
PEAK 8              Max 1.661           COORD (138, 102)
PEAK 9              Max 0.344           COORD (137, 270)
PEAK 10             Max 1.871           COORD (186, 4)
PEAK 11             Max 2.467           COORD (183, 167)
PEAK 16             Max 0.273           COORD (241, 121)
PEAK 21             Max 1.808           COORD (290, 53)
PEAK 22             Max 0.758           COORD (309, 1)
PEAK 23             Max 3.702           COORD (345, 49)
PEAK 24             Max 1.683           COORD (350, 154)
PEAK 26             Max 0.206           COORD (358, 78)
```

5.8.3 Current algorithm and future development

The current state of the developed algorithm includes reading textual and numerical information contained in CSV files converted from *mea* files with LAV plug-in. Through a series of steps illustrated in the diagram of Figure 5.50 the current developed algorithm can automatically detect effective peaks from numerical information and quantify intensity from regions detected as peaks. This algorithm also aims to be an early iteration in the development and designed of software for automatically process data from GC-IMS measurements.

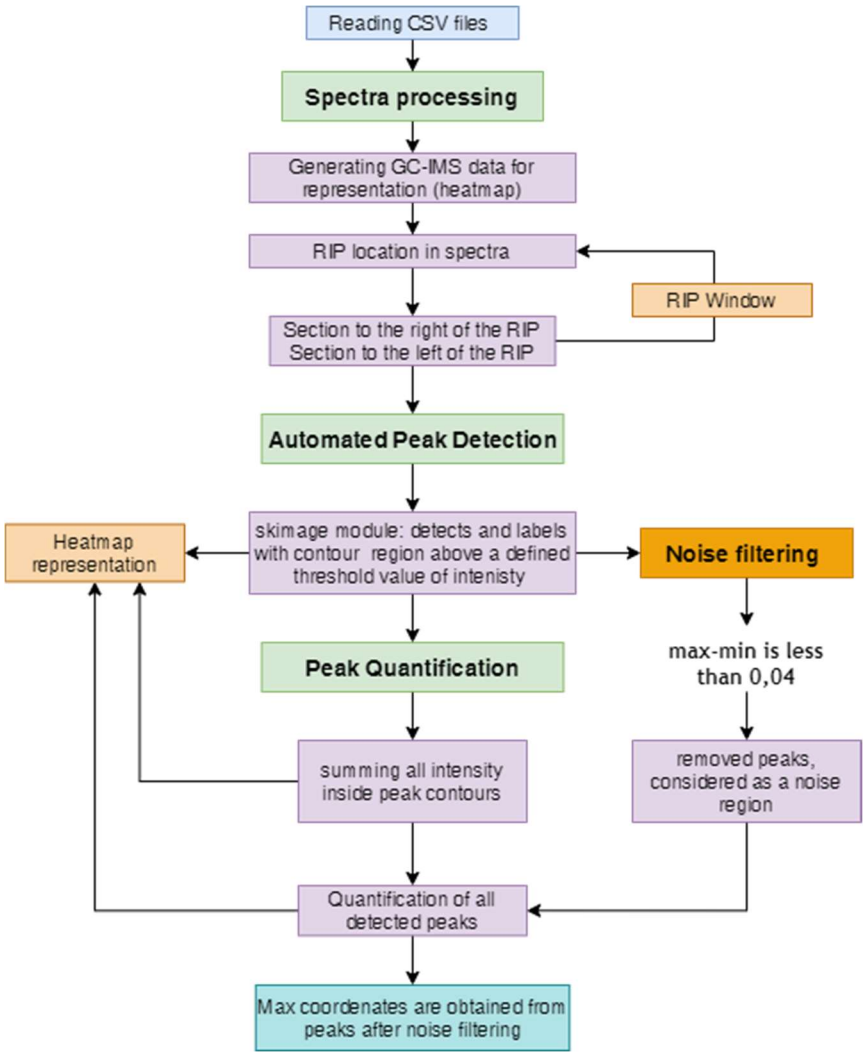

Figure 5.50 — Schematic actions and methodologies used in the algorithm for automatic peak detection and quantification of GC-IMS spectra.

Although still in its early stages the developed, the created algorithm, showed promising results using adaptable approaches to detect, quantify and visually represent results from GC-IMS spectra. However, further coding development is required for this approach to become a useful software in IMS data processing and chemometrics. The automatic detection and quantification of VOCs in GC-IMS spectra has been an area of research ignored or unexplored in the current scientific literature,

which results in computational methodologies to detect, quantify and even deconvolute overlapped peaks being diminished and scarce. Nonetheless, the presented algorithm was developed and designed to account for additional features which should be developed further and, or, implemented in new iterations.

For example, a three-dimensional representation of GC-IMS spectra contained in CSV files was attempted during the development of this algorithm. However, the numerical matrix corresponding to the GC-IMS spectra includes a huge number of intensity values and although normal representation approaches were able to generate a three-dimensional representation, rotation and visual management of this representation was slow and hard to achieve. A possible solution for this would be to either reduce the number of intensity values prior to representation, but information could possibly be lost or altered, or implement secondary tools for data representation and visualization. Two python libraries could prove useful for this task, mainly *VisPy*, a high-performance interactive 2D/3D data visualization library using the computational power of modern Graphics Processing Units (GPUs) to display very large datasets or *MayaVi,* which is a scientific data visualizer associated with Python coding.

Furthermore, deconvolution of potential overlapping peaks needs to be addressed, as this is a major issue in IMS spectra. A solution could be to implement adjusted Gaussian functions for both drift and retention times. However, such step might require further analysis of IMS peak behaviour and establishing common shapes, and overall behaviours for peaks from different functional groups of volatile organic compounds. A crucial step following the deconvolution of peaks would be patter recognition, and statistical analysis via both supervised (e.g., genetic algorithm) and unsupervised analysis, (e.g., Principal component analysis (PCA) or cluster analysis) or even exploring further denoising approaches such as wavelets.

Baseline and spectra subtraction for comparative analysis is also a valuable feature that should be implemented into the current algorithm and even axis scaling is important, including an option to represent spectra in milliseconds, RIP relative, mobility constant and reduced mobility constants.

Moreover, a series of smaller changes can, also be implemented to improve the current state of the algorithm, including estimation of mean and standard deviation of peak maximum coordinates (t_R and t_D), which can enhance peak detectability. Peak maximum coordinate and standard deviation would help establish points, with retention and drift time, specific of VOCs or a region where the respective VOC signals occurs. Henceforth, the algorithm could also be able to automatically detect, quantify, and identify peaks by cross-checked drift and retention times with an GC-IMS libraries (VOC Library) for compound identification and even provide toxicology information from detected VOCs and respective exposure limits or effects on health.

Likewise, an important topic related to retention times generated using different flow programs or GC columns should be tackled by establishing a mechanism to predict retention times from VOCs based on flow programs. Applying machine learning or artificial intelligence may be required to address this topic and from the experience gathered during the development of this preliminary algorithm, both machine learning and artificial intelligence can bring useful solutions and essential improvements in establishing a software for automatic IMS data processing.

CHAPTER 6.
OUTLOOK ON THE COMPETENCES OF IMS:
Discussion & Conclusions

6.1 Overall Assessment

The extensive research conducted in this dissertation explores and evaluates IMS as a feasible, beneficial, and valuable tool for the monitorization of air quality, including biological contaminants aboard spacecrafts and space stations. Hence, IMS versatility was explored in prospectively useful scientific areas, such as exhaled breath for medical diagnosis, quality of food products, particularly seaweeds due to their importance in establishing food production in space, and lastly but not least, identification of microorganisms and consequent characterization of microbial growth.

A clear statement about IMS serving a large array of useful applications and adequate characteristics to work as an on-line analytical technique for spacecrafts can be upheld from the previously presented research. IMS shows desirable aspects, such as low-cost, high sensitivity, hight selectivity, robustness, simplicity and effectiveness for the detection and accurate quantification of VOCs from several matrixes of relevance in the current and future stages of space habitation and exploration.

The GC-IMS technology was evaluated and validated for continuous air monitoring during simulated conditions of spaceflight in SIRIUS-17 showing it is possible to utilize GC-IMS devices as monitoring tool for continuous air in spacecrafts without requiring additional reagents or complex systems [185]. Hence, the main conclusions of this extensive work are presented below for each related subject studied during this dissertation.

6.2 Evaluation of GC-IMS capabilities

Ample scientific research was conducted to evaluate and study ion mobility spectrometry abilities and limitations for serve as a novel analytical technique in monitoring organic and biological contaminants aboard spacecrafts. Preliminary results offered a basic understanding of the selected apparatus and a comprehensive knowledge of its operation and options. Those results served as preparations for a specific experiment involved in a program called SIRIUS, an acronym for "Scientific International Research in Unique Terrestrial Station".

6.2.1 Continuous Environmental Air Monitoring in Spacecrafts

During the first phase of this program an IMS device was used to measure cabin air inside a module from an analogue facility where 6 individuals were isolated in simulated conditions of a spacecraft. This experiment, called SIRIUS-17, lasted 17 days and intended to mimic a trip to the Moon, where several other technologies and studies would be conducted in search of new approaches and methods to be used in space exploration. A high analytical stability was observed from the IMS device during the SIRIUS-17 experiment, detecting a total of 33 different peaks from 115 spectra. While data analysis allowed to detect and affirm 29 substances were detected during measurements, with 16 signals identified as 9 different volatile organic compounds.

During SIRIUS-17 the GC-IMS device proved capable of monitoring cabin air changes over several hours and days while, also detecting variations in VOC concentrations over time. The results collected during SIRIUS-17, reinforced GC-IMS as a reliable, effective, economical, fast, and easy-to-use tool to on-line monitor air quality in spacecrafts and closed-spaces. Nevertheless, the effectiveness of GC-IMS in identifying and quantifying of VOCs in spacecrafts requires additional development, prompting, a devotion of resources and time into developing a VOC database for future compound identification.

Nevertheless, prior to being the development of a VOC database, a greater focus was given to several application of GC-IMS which can prove important or even essential during the next phases of space exploration and habitation. Three dedicated studies were conducted into analysis of three different sample types, (i) microorganisms and (ii) food products including seaweeds. (iii) exhaled breath,

6.2.2 Microbial identification and monitorization of microbial growth

Ensuing subjects and challenges related to spacecrafts and space habitation, GC-IMS was used to analyse emissions from several microorganisms in solid and liquid media. Microbial growth is a concerning issue in long missions in space and a tool to identify and monitor microbial growth is highly desirable and critical for the ISS and future spacecraft and stations. Two phases were included in the analysis of microbial growth with GC-IMS: (i) analysis of the volatile emission of swabs from *E. coli* and *P. aeruginosa* cultures, and continuous analysis of sterile and inoculated liquid media with *E. coli* and *S. aureus*. In both instances the GC-IMS device allowed identification of a clear and distinctive emission pattern, or fingerprint, for each bacteria grown, while continuous analysis of emitted VOCs showed several IMS peaks having intensity changes similar to a microbial growth kinetics or related to growth.

The results observed during microbial studies illustrate an auspicious use of GC-IMS to identify microorganisms, and eventually, microbial monitorization and identification aboard spacecraft, an environment where such contaminations can lead to serious and dangerous outcomes, and require, a simple, clear, and precise method for microbial identification. Notwithstanding, further studies should be conduct with more microorganism species, ideally under analogous ISS conditions to develop and validate GC-IMS has a utensil to monitor biological contaminations in spacecrafts.

6.2.3 Food spoilage by microorganisms and food production in space

Afterwards a study of volatile emissions from food products was conducted with GC-IMS to access its ability to monitor food quality and identify microbial growth and spoilage any food and food products. Three types of fish, Atlantic bonito, Atlantic horse mackerel and Sardine, freshly squished orange juice and ten seaweed species were monitored using a GC-IMS device. Analysis of the orange juice emissions was a preliminary task which yield promising results by showing GC-IMS had adequate capabilities and appropriate methodologies were being applied. A clear change was observed after 2 days in VOC emission for freshly squished orange juice without sample preparation and in minimal analysis time.

Similarity, a distinctive pattern of spoilage for three fish species was detected via GC-IMS, some signals were identified as characteristic of fish spoilage and attributed to several biogenic amines. Lastly, a total of 10 seaweeds species were analysed with GC-IMS to characterize their volatile emission. Seaweed emissions based on characteristic signals defined a *phycoprint*, a pattern unique to every single seaweed species form VOC emission. Several signals were also identified as specific compounds through measurements of pure substances and some identified VOCS were even distinguished as species specific. Subsequently characterization of seaweed spoilage was also achieved by GC-IMS analysis.

Overall, GC-IMS proved excellent in identifying changes in the emission of several food products due to spoilage while providing a fast and simple method to identify different food products, especially seaweeds, based on their emission pattern. The possibility of GC-IMS to monitor food products abord the ISS and on Earth would be another profitable service provided from this technology and provide the first steps to monitor seaweed and plant growth in microgravity.

6.2.4 Development of a VOC database for compound identification

Although analytically, GC-IMS proved fruitful and beneficial in the detection and characterization of VOCs from several origins as previously stated, data processing and databases for compound identification are currently scarce or even absent. Transferability of data between instrumentation has also been a great challenge, so it currently limits GC-IMS used and contributions as an analytical tool in all its applicable areas. Therefore, to combat such limitations and challenges, three major steps were taken during this dissertation to examine and address complications involved with IMS databases and in data analysis. The steps include: (i) development of a VOC database, (ii) establish accurate methods for VOC calibration and (iii) design an algorithm for automatic IMS peak detection and quantification.

The construction of a VOC database was accomplished through empirical measurements of pure substances with the GC-IMS device, including a list of 34 volatile organic compounds established by experts from IBMP (Institute for Biomedical Problems) as priority compounds to be monitored and managed aboard the Russian segment of the ISS. At present, the developed VOC database includes 70 compounds containing data for CAS number, compound name, molecular weight, drift time in milliseconds, drift time presented as RIP relative, retention time in seconds, reduced mobility constant, vapour pressure and molecular vapor. The database incorporates compounds mainly exhibiting monomer and dimer signals but trimer signals and above have also been identified for some substances.

Moreover, a total of 21 compounds, could be included in the VOC database from the priority list of 34 volatile organic compounds established by IBMP experts. Identification of VOCs during this dissertation was attained through the information contained in the VOC database and peculiar behaviour was also observed between drift times of several compound containing the same functional groups. Drift times demonstrated a linear behaviour with carbon chains increments for the same functional group, alluring to a possible predictability of drift times and mobility constant based on chemical structure and collision cross-sections. Moreover, IMS signals appear to have similar shapes between

compounds with the same functional group which should be explored and analysed further as a possibility strategy for automatic peak detection and identification by functional group for unknown compounds.

6.2.5 VOC Calibration in low concentrations for monitorization

Besides unmistakable identification of VOCs, quantification is likewise an essential aspect in maintaining a healthy and stable environment in spacecrafts and to protect materials, systems, and crew. Hence, exact estimation of VOC concentration via IMS signal intensity is required for the ISS and other spacecrafts. An assessment of available methods of calibration for GC-IMS was conducted with the purpose of selecting a simple, accurate and precise procedure to obtain mathematical relations between IMS signals and VOC concentration. The dynamic method of permeation tubes was selected to calibrate the GC-IMS device because it can generate low concentration of gases, liquids, and solids with precision under controlled temperature and gas flows.

Three volatile organic compounds, 2-hexanone, 2-butanone and 1-butanol were used to obtain a calibration curve for the GC-IMS with permeation tubes. The respective limits of detection (LOD), based on signal-to-noise ratio of 10 blank samples, were 26 ppb for 2-hexanone, 12 ppb for 2-butanone and 14 ppb for 1-butanol. All compound showed an exponential behaviour for concentration vs signal intensity, however different equations were obtained entailing different sensitivities of the GC-IMS for the three compounds. This also means, calibration curves must be established for all VOCs to be detected and quantified in spacecrafts, which can be produced in an accurate, fast, and straightforward approach via permeation tubes. Also, this step was an initial stage, and calibration curves should be created for more VOCs, especially, for the list of 34 priority compounds and, further adjustments must be made to evaluate if lower limits of detections can be obtained.

6.2.6 Data processing tools for complex samples and results

The processes of identification and quantification of VOCs generate high amounts of data which often involve professionals and laborious hours, henceforth urging the development of automated tools and software for data processing. Therefore, a methodology for an automated software able to detect and quantify IMS signals was conducted. Using Python coding language, it was possible to develop an algorithm to detect and separate effective signals from spectral noise, while afterwards extracting intensity values from define peak areas and quantifying IMS signals for each peak.

Although, an initial version, the algorithm showed promising results in delivering automated methods to detect and quantify IMS signals and should be further explored to include, deconvolution of potential overlapping peaks, patter recognition, statistical analysis via supervised and unsupervised analysis and the study of signal behaviour and variability (in retention and drift time). A recommendation to implement machine learning and artificial intelligence in the previously developed algorithm is encouraged, since almost every aspect in detecting and quantifying signals can be enhanced and improved from both methods.

6.2.7 The potential of IMS in Health Monitoring

Exhaled breath was analysed with the GC-IMS device after sample collection with a dedicated prototype, created, in another doctorate, to gather breath samples from different regions of the respiratory tract. Two types of stimuli were induced in each subject, a stressor and a relaxer, and breath samples were analysed immediately after a total of 2 stimuli, 5 min and 1 hour after the las stimulus was executed. The results indicated significant statistical differences between exhaled breath after a stressor and relaxer stimuli were induced on a subject. Six-discriminant signals were identified showing a downregulated behaviour after a stressor, likely caused by increased heart and respiratory rate during a stressed condition. Therefore, providing promising results for the use of exhaled breath analysis and VOC profiling with GC-IMS, as a beneficial and prospective approach to monitor health aboard spacecrafts, space stations and, on Earth. Nevertheless, a greater exploration of exhaled breath analysis via IMS should be conducted to improve and strengthen the usefulness and flexibility of this analytical technique in monitoring human health in space, including habitation of planets or moons by humans.

6.3 Future work and perspective

This dissertation also unveils further work is required to transform the use of GC-IMS as a monitoring tool for space stations into a reality. Besides obvious improvements needed in both VOC identification and quantification mainly in sample size, further research into signal behaviour and deeper studies of LODs, GC-IMS will surely require further adjustments, in mechanical characteristics and method validation for applications in spacecrafts. Eventually, it would be beneficial to conduct specialized measurements campaigns with GC-IMS devices, including, (i) continuous monitorization of air after purification directly from revitalization systems at the ISS, (ii) a large analysis and study of VOC detection in IMS negative mode, (iii) a comparatively analysis between cabin air and system air prior and after purification and even, (iv) a comparison between both similar and different IMS instruments in order to evaluate transferability between their detectability, compound identification and quantification processes.

Based on everything learned from this dissertation, I would affirm, IMS possesses potential to server as a new analytical tool needed for space habitation and exploration, and, if enough attention and resources from the scientific community were to be given, GC-IMS could soon be employed in spacecrafts and space station as an on-line monitorization tool for organic and biological contaminants.

REFERENCES

[1] N. Novikova, "Review of the Knowledge of Microbial Contamination of the Russian Manned Spacecraft," *Microbial Ecology,* vol. 47, p. 127–132, 2003.

[2] R. Klintworth, H. Reher, A. Viktorov e D. Bohle, "Biological induced corrosion of materials II: New test methods and experiences from mir station. ,," *Acre Astronautica,* vol. 44, nº 7-12, pp. 569-578, 1999.

[3] C. Adams, "Was the Mir space station being eaten by a mysterious fungus?," The Straight Dope, 13 Jul 2001. [Online]. Available: https://www.straightdope.com/21343445/was-the-em-mir-em-space-station-being-eaten-by-a-mysterious-fungus. [Acedido em 15 Jan 2022].

[4] "Memorandum of Understanding between NASA and the Russian Space Agency Concerning Cooperation on the Civil International Space Station - NASA-RSA Agreement," 29 Jan 1998. [Online]. Available: https://www.nasa.gov/mission_pages/station/structure/elements/nasa_rsa.html. [Acedido em 2020 Jun 28].

[5] J. M. Logsdon, "Space exploration - Encyclopædia Britannica," Encyclopedia Britannica, inc., 1 Jun 2020. [Online]. Available: https://www.britannica.com/science/space-exploration. [Acedido em 2020 Jun 27].

[6] D. M. Harland, J. E. Catchpole e J. Catchpole, Creating the International Space Station, Cornwall: Springer Science & Business Media, 2002.

[7] The Continuing Story of The International Space Station, Cornwall: Springer Science & Business Media, 2002.

[8] M. Garcia, "International Space Station Facts and Figures," 9 April 2020. [Online]. Available: https://www.nasa.gov/feature/facts-and-figures. [Accessed 30 Nov 2021].

[9] National Aeronautics and Space Administration, "Reference guide to the International Space Station – Utlization Edition NP-2015-05-022-JSC," 2015.

[10] National Aeronautics and Space Administration, "Demonstrating Technologies For Deep Space Habitation. Bigelow Expandable Activity Module (BEAM): Facts Sheet NF-2016-03-600-HQ," NASA, 2016.

[11] European Space Agency, "Environment Control and Life Support System (ECLSS): Factsheet ESA-HSO-COU-030," 2010. [Online]. Available: http://wsn.spaceflight.esa.int/docs/Factsheets/30%20ECLSS%20LR.pdf.

[12] P. O. Wieland, Living Together in Space: The Design and Operation of the Life Support Systems on the International Space, vol. 1, Marshall Space Flight Center, Alabama: NASA: National Aeronautics and Space Administration, 1998.

[13] A. Bommenel, Artist, *Diagram of the International Space Station (ISS).* [Art]. AFP, 2019.

[14] R. B. Ernst Messerschmid, Space Stations: Systems and Utilization (ISBN 978-3-642-08479-9), Berlin: Springer, 1999.

[15] Sandra Häuplik-Meusburger, Architecture for Astronauts: An Activity-based Approach, Springer, 2011.

[16] European Space Agency, "Node-3 (Tranquility): Factsheet ESA-HSO-COU-006," [Online]. Available: http://wsn.spaceflight.esa.int/docs/Factsheets/6%20Node%203%20HR%20web.pdf.

[17] C. L. Mansfield, "NASA Receives Tranquility (News)," NASA, [Online]. Available: https://www.nasa.gov/mission_pages/station/behindscenes/tranquility_transfer.html. [Accessed 2020 Jun 26].

[18] National Aeronautics and Space Administration, "Veggie - NASA Factsheet FS-2020-01-007-KSC," [Online]. Available: https://www.nasa.gov/sites/default/files/atoms/files/veggie_fact_sheet_508.pdf.

[19] National Aeronautics and Space Administration, "Veg-03 Project," NASA, [Online]. Available: https://www.nasa.gov/mission_pages/station/research/experiments/explorer/Investigation.html?#id=1159. [Accessed 2020 Jun 26].

[20] "Space flight life support rack," *World Pumps: Applications,* vol. 1, pp. 16-17, 2019.

[21] National Aeronautics and Space Administration, "Life Support Systems," NASA, 4 Aug 2017. [Online]. Available: https://www.nasa.gov/content/life-support-systems. [Acedido em 30 Nov 2021].

[22] M. Starr, "Breathe Deep: How the ISS Keeps Astronauts Alive," CNET, 19 March 2015. [Online]. Available: https://www.cnet.com/news/breathe-deep-how-the-iss-keeps-astronauts-alive/. [Acedido em 3 August 2020].

[23] National Aeronautics and Space Administration (NASA), "Artboard 17 - NASA," 13 Jul 2020. [Online]. Available: https://www.nasa.gov/sites/default/files/atoms/files/iss20_infographic_david_20200713_compressed.pdf. [Acedido em 15 Dec 2021].

[24] European Space Agency, "Life in Space," [Online]. Available: https://www.esa.int/Science_Exploration/Human_and_Robotic_Exploration/Lessons_online/Life_in_Space. [Acedido em 3 Agosto 2020].

[25] Japan Aerospace Exploration Agency - JAXA, "What's Outer Space Like? - Space Station Kids," 2003. [Online]. Available: https://iss.jaxa.jp/kids/en/space/index.html. [Acedido em 3 August 2020].

[26] Arnauld E. Nicogossian, Richard S. Williams, Carolyn L. Huntoon, Charles R. Doarn, James D. Polk, Victor S. Schneider, Space Physiology and Medicine: From Evidence to Practice, New York: Springer, 2016.

[27] A. A. Harrison, Y. A. Clearwater e C. P. (. McKay, From Antarctica to Outer Space: Life in Isolation and Confinement, New York: Springer-Verlag Publishing, 1991.

[28] Japan Aerospace Exploration Agency - JAXA, "Space - Extreme of cold and hot Temperature," 2003. [Online]. Available: https://iss.jaxa.jp/kids/en/space/402.html. [Acedido em 2020 August 3].

[29] F. Craig e M. Mark, "How the International Space Station Works," HowStuffWorks, 2020. [Online]. Available: https://science.howstuffworks.com/international-space-station.htm#pt2. [Acedido em 3 August 2020].

[30] J. Wright, "Cooling System Keeps Space Station Safe, Productive," National Space Agency - NASA, 12 Dec 2013. [Online]. Available: https://www.nasa.gov/content/cooling-system-keeps-space-station-safe-productive. [Acedido em 3 August 2020].

[31] European Space Agency - ESA, "Water in space," 22 March 2019. [Online]. Available: https://www.esa.int/Science_Exploration/Human_and_Robotic_Exploration/International_Space_Station/Water_in_space. [Acedido em 3 August 2020].

[32] A. Clayton C, "The Secret Behind How the ISS Gets Cleaned," Forbes, 2017 March 27. [Online]. Available: https://www.forbes.com/sites/quora/2015/03/27/the-secret-behind-how-the-iss-gets-cleaned/#46128bdb5304. [Acedido em 3 August 2020].

[33] National Aeronautics and Space Administration, "NASA Seeks New Ways to Handle Trash for Deep Space Missions," NASA, 2018 July 9. [Online]. Available: https://www.nasa.gov/feature/nasa-seeks-new-ways-to-handle-trash-for-deep-space-missions. [Acedido em 3 August 2020].

[34] National Aeronautics and Space Administration, "A Day in the Life Aboard the International Space Station," NASA, 13 May 2020. [Online]. Available: https://www.nasa.gov/audience/foreducators/stem-on-station/dayinthelife. [Acedido em 3 August 2020].

[35] D. R. Jenkins, The History of the American Space Shuttle, Pennsylvania: Schiffer Publishing, 2019.

[36] S. M. Smith, J. Davis-Street, L. Neasbitt e S. R. Zwart, Space Nutrition, National Aeronautics and Space Administration, 2012.

[37] A. A. Casaburri, C. A. Gardner e J. A. George, Space Food and Nutrition: An Educator's Guide With Activities in Science and Mathematics, National Aeronautics and Space Administration, 1999.

[38] A. Vaishampayan e E. Grohmann, "Multi-resistant biofilm-forming pathogens on the International Space Station," *Journal of Biosciences ,* vol. 44, nº 5, p. 125, 2019.

[39] Space Station Explores, "Living on the ISS," The Center For The Advancement Of Science In Space, INC., 2011-2020q. [Online]. Available: https://www.spacestationexplorers.org/news-media/videos/. [Acedido em 3 August 2020].

[40] Japan Aerospace Exploration Agency - JAXA, "Life in Space," JAXA, [Online]. Available: https://iss.jaxa.jp/kids/en/life/index.html. [Acedido em 3 August 2020].

[41] T. F. Limero e W. T. Wallace, "What Air and Water Quality Monitoring Is Needed to Protect Crew Health on Spacecraft?," *New Space,* vol. 5, nº 2, pp. 67-78, 2017.

[42] W. T. Wallace, T. Limero, L. J. Loh, P. D. Mudgett e D. B. Gazda, "Monitoring of the Atmosphere on the International Space Station with the Air Quality Monitor," *47th International Conference on Environmental Systems (ICES),* p. 103, 2017.

[43] A. V. Macatangay, J. L. Perry, P. L. Belcher e S. A. Johnson, "Status of the International Space Station (ISS) Trace Contaminant Control System," *SAE Int. J. Aerosp.,* vol. 4, nº 1, pp. 48-54, 2011.

[44] J. Perry, *Trace Contaminant Control During the International Space Station's On-Orbit Assembly and Outfitting,* 2017.

[45] Human Health and Performance Directorate, *Spacecraft Maximum Allowable Concentrations for Airborne Contaminants,* National Aeronautics and Space Administration, 2020.

[46] A. V. Macatangay e J. L. Perry, "Cabin Air Quality On Board Mir and the International Space Station - A Comparison," *37th International Conference on Environmental Systems,* July 2007.

[47] D. Pierson, "Microbial contamination of spacecraft," *Gravitational and Space Biology Bulletin : Publication of the American Society for Gravitational and Space Biology,* vol. 4, nº 2, pp. 1-6, Jun 2001.

[48] N. Novikova, "Review of the Knowledge of Microbial Contamination of the Russian Manned Spacecraft," *Microbial Ecology,* vol. 47, nº 2, pp. 127-132, 2004.

[49] N. Novikova, P. de Boever, S. Poddubko, E. Deshevaya, N. Polikarpov, N. Rakova, I. Coninx e M. Mergeay, "Survey of the environmental biocontamination on board the International Space Station," *Research in Microbiology,* vol. 157, nº 1, pp. 5-12, 2006.

[50] D. Pierson, D. J. Botkin, R. J. Bruce, V. A. Castro, M. J. Smith, C. M. Oubre e C. M. Ott, "Microbial Monitoring of the International Space Station," em *Environmental Monitoring: A Comprehensive Handbook*, River Grove, IL, DHI Publishing, 2012.

[51] R. Gatens e G. A. Ruff, "Environmental Control & Life Support/Fire Safety Systems Maturation Team Status," 2020. [Online]. Available: https://www.nasa.gov/sites/default/files/atoms/files/7-gatens_eclss_firesafety.pdf. [Acedido em 16 Set 2020].

[52] J. Lang, D. Coil, R. Neches, W. Brown, D. Cavalier, M. Severance, J. Hampton-Marcell, J. Gilbert e J. Eisen, "A microbial survey of the International Space Station (ISS)," *PeerJ,* vol. 5, nº e4029, 2017.

[53] W. Kim, F. Tengra, Z. Young, J. Shong, N. Marchand, H. Chan, R. Pangule, M. Parra, J. Dordick, J. Plawsky e C. Collins, "Spaceflight promotes biofilm formation by Pseudomonas aeruginosa.," *PLoS One,* vol. 8, nº 4, p. e62437, 2013.

[54] K. S. Landry, J. M. Morey, B. Bharat, N. M. Haney e S. S. Panesar, "Biofilms—Impacts on Human Health and Its Relevance to Space Travel," *Microorganisms,* vol. 8, nº 7, p. 998, 2020.

[55] R. J. McLean, J. M. Cassanto, M. B. Barnes e J. H. Koo, "Bacterial biofilm formation under microgravity conditions," *FEMS Microbiol Lett,* vol. 195, nº 2, pp. 115-119, 2001.

[56] R. Gilbert, M. Torres, R. Clemens, S. Hateley, R. Hosamani, W. Wade e S. Bhattacharya, "Spaceflight and simulated microgravity conditions increase virulence of Serratia marcescens in the Drosophila melanogaster infection model," *NPJ Microgravity,* vol. 6, nº 4, 2020.

[57] K. Venkateswaran, P. Vaishampayan, J. Cisneros, D. L. Pierson, S. O. Rogers e J. Perry, "International Space Station environmental microbiome — microbial inventories of ISS filter debris," *Appl Microbiol Biotechnol,* vol. 98, pp. 6433-6466, 2014.

[58] S. Lax, N. Sangwan, D. Smith, P. Larsen, K. Handley, M. Richardson e K. Guyton, "Bacterial colonization and succession in a newly opened hospital," *Sci Transl Med,* vol. 9, nº 391, 2017.

[59] A. Checinska, A. J. Probst, P. Vaishampayan, J. R. White, D. Kumar, V. G. Stepanov, G. E. Fox, H. R. Nilsson, D. L. Pierson, J. Perry e K. Venkateswaran, "Microbiomes of the dust particles collected from the International Space Station and Spacecraft Assembly Facilities," *Microbiome,* vol. 3, nº 50, 2015.

[60] P. Bouloc e R. D'Ari, "Escherichia coli metabolism in space," *Journal of General Microbiology,* vol. 137, pp. 2839-2843, 1991.

[61] G. Horneck, D. M. Klaus e R. L. Mancinelli, "Space Microbiology," *Microbiology and Molecular Biology Reviews,* vol. 74, nº 1, p. 121–156, 2010.

[62] M. Mora, A. Perras, T. A. Alekhova, L. Wink, R. Krause, A. Aleksandrova, T. Novozhilova e C. Moissl-Eichinger, "Resilient microorganisms in dust samples of the International Space Station—survival of the adaptation specialists," *Microbiome,* vol. 4, nº 65, 2016.

[63] P. W. Taylor, "Impact of space flight on bacterial virulence and antibiotic susceptibility," *Infection and Drug Resistance ,* vol. 8, nº 8, pp. 249-262, 2015.

[64] J. A. Rosenzweig, O. Abogunde, K. Thomas, A. Lawal, Y.-U. Nguyen, A. Sodipe e O. Jejelowo, "Spaceflight and modeled microgravity effects on microbial growth and virulence," *Appl Microbiol Biotechnol,* vol. 85, nº 4, pp. 885-891, 2010.

[65] B. Huang, D.-G. Li, Y. Huang e C.-T. Liu, "Effects of spaceflight and simulated microgravity on microbial growth and secondary metabolism," *Military Medical Research,* vol. 5, nº 18, 2018.

[66] A. Avila-Herrera, J. Thissen, C. Urbaniak, N. A. Be, D. J. Smith, F. Karouia, S. Mehta, K. Venkateswaran e C. Jaing, "Crewmember microbiome may influence microbial composition of ISS habitable surfaces," *PLOS One,* vol. 15, nº 4, 2020.

[67] J. Trowbridge, L. T. e J. James, "Strategy for Monitoring Trace Contaminants on International Space Station," *SAE Transactions,* vol. 107, nº 1, pp. 866-869, 1998.

[68] T. Limero, E. Reese, P. Cheng e J. Trowbridge, "Preparation of a gas chromatograph-differential mobility spectrometer to measure target volatile organic compounds on the international space station," *International Journal for Ion Mobility Spectrometry ,* vol. 14, nº 81, p. 81–91, 2011.

[69] T. Limero, W. Wallace e J. T. James, "Operational Validation of the Air Quality Monitor on the International Space Station," em *44th International Conference on Environmental Systems*, Tucson, Arizona, USA, 2014.

[70] W. T. Wallace, T. F. Limero e R. L. Gillispie, "Effects of Ambient CO2 on Monitoring of the International Space Station Atmosphere with the Air Quality Monitor," em *48th International Conference on Environmental Systems*, Albuquerque, New Mexico, USA, 2018.

[71] H. R. Smith, "Aquaponics," National Aeronautics and Space Administration (NASA), 20 May 2009. [Online]. Available: https://www.nasa.gov/audience/foreducators/9-12/features/aquaponics.html. [Acedido em 25 Nov 2020].

[72] N. Yamaguchi, M. Roberts, S. Castro, C. Oubre, K. Makimura, N. Leys, E. Grohmann, T. Sugita, T. Ichijo e M. Nasu, "Microbial Monitoring of Crewed Habitats in Space—Current Status and Future Perspectives," *Microbes Environ,* vol. 29, nº 3, pp. 250-260, 2014.

[73] U. Reidt, A. Helwig, G. Müller, L. Plobner, V. Lugmayr, S. Kharin, Y. Smirnov, N. Novikova, J. Lenic, V. Fetter e T. Hummel, "Detection of Microorganisms Onboard the International Space Station Using an Electronic Nose," *Gravitational and Space Research,* vol. 5, nº 2, 2017.

[74] K. Hurlbert, B. Bagdigian, C. Carroll, A. Jeevarajan, M. Kliss e B. Singh, "DRAFT Human Health, Life Support and Habitation Systems," *Technology Area 06, NASA,* 2010.

[75] P. T. Palmer e T. F. Limero, "Mass spectrometry in the U.S. space program: past, present, and future," *J Am Soc Mass Spectrom,* vol. 12, nº 6, pp. 656-675, 2001.

[76] J. Griffiths, "A Brief History of Mass Spectrometry. A few of the great people and major discoveries that have shaped this century-old technique.," *Anal. Chem.,* vol. 80, nº 15, pp. 5678-5683, 2008.

[77] W. Reusch, "Virtual Textbook of Organic Chemistry," 1999. [Online]. Available: https://www2.chemistry.msu.edu/faculty/reusch/VirtTxtJml/intro1.htm. [Acedido em 18 Fev 2021].

[78] D. L. Pavia, G. M. Lampman, G. S. Kriz e J. A. Vyvyan, Introduction to Spectroscopy, Brooks/Cole, Cengage Learning, 2009.

[79] P. V. Johnson, L. W. Beegle, H. I. Kim, G. A. Eiceman e I. Kanik, "Ion mobility spectrometry in space exploration," *International Journal of Mass Spectrometry,* vol. 262, pp. 1-15, 2007.

[80] T. Limero, "Development of the Volatile Organic Analyzer for the International Space Station," em *64th American Chemical Society Southwest Regional Meeting*, Little Rock, Arkansas, 2009.

[81] T. Limero, E. Reese, J. Trowbridge, R. Hohmann e J. T. James, "Validation of the Volatile Organic Analyzer (VOA) Aboard the International Space Station," *SAE Technical Paper,* 2003.

[82] T. Stuffler, H. Mosebach, A. H. D. Kampf, H. Odegard, H. Schumann-Olsen e G. Tan, "The ANITA Air Monitoring Programme and Instrumentation – ISS and other Applications," *SAE Technical Paper ,* 2006.

[83] C. A. Evans, J. A. Robinson, J. Tate-Brown, T. Thumm, J. Crespo-Richey, D. Baumann e J. Rhatigan, "International Space Station Science Research Accomplishments During the Assembly Years: An Analysis of Results from 2000-2008," National Aeronautics and Space Administration, 2009.

[84] International Space Station Program Science Forum, International Space Station Benefits for Humanity 2nd Edition, National Aeronautics and Space Administration, 2017.

[85] J. A. Lewis, "Space Exploration in a Changing International Environment," Center for Strategic and International Studies, Washington, D.C. USA, 2014.

[86] K. Rainey, "Space Station Research & Technology," National Aeronautics and Space Administration, March 2018. [Online]. Available: https://www.nasa.gov/mission_pages/station/research/experiments_category. [Acedido em 31 August 2020].

[87] European Space Agency, "About research in space," European Space Agency, [Online]. Available: https://www.esa.int/Science_Exploration/Human_and_Robotic_Exploration/Research/About_research_in_space. [Acedido em 31 August 2020].

[88] International Space Station Program Science Office, International Space Station Facilities: Research in Space 2017 and Beyond, National Aeronautics and Space Administration, 2019.

[89] National Aeronautics and Space Administration (NASA), *20 Years of Science on the Space Station,* National Aeronautics and Space Administration, 2020.

[90] K. Mars, "Analog Missions," National Aeronautics and Space Administration, May 2019. [Online]. Available: https://www.nasa.gov/analogs/what-are-analog-missions. [Acedido em 31 August 2020].

[91] K. Mars, "Types of Analogs," National Aeronautics and Space Administration, May 2020. [Online]. Available: https://www.nasa.gov/analogs/types-of-analogs. [Acedido em 31 August 2020].

[92] M. D. Peters, "Data Rate Increase on the International Space Station Supports Future Exploration," National Aeronautics and Space Administration, Aug 2019. [Online]. Available: https://www.nasa.gov/feature/goddard/2019/data-rate-increase-on-the-international-space-station-supports-future-exploration. [Acedido em 31 August 2020].

[93] N. Drake, "The future of spaceflight—from orbital vacations to humans on Mars," National Geographic, [Online]. Available: https://www.nationalgeographic.com/science/space/space-exploration/future-spaceflight/. [Acedido em 31 August 2020].

[94] J. C. May e J. A. McLean, "Ion Mobility-Mass Spectrometry: Time-Dispersive Instrumentation," *Anal. Chem.,* vol. 87, nº 3, p. 1422–1436, 2015.

[95] R. Fernandez-maestre, "Ion mobility spectrometry: history, characteristics and applications," *Revista UDCA de Actualidad y Divulgación Cientifica,* vol. 15, nº 2, pp. 467-479, 2012.

[96] H. Borsdorf e G. A. Eiceman, "Ion Mobility Spectrometry: Principles and Applications," *Applied Spectroscopy Reviews,* vol. 41, nº 4, pp. 323-375, 2006.

[97] G. Eiceman, Z. Karpas e H. H. H. Jr., Ion Mobility Spectrometry, Third Edition, Boca Raton, Florida: CRC Press, 2013.

[98] K. A. Daum e S. L. Fox, "Data for Users of Handheld Ion Mobility Spectrometers," (INL/EXT--08-14265), United States America, 2008.

[99] J. M. Fernandes, V. Vassilenko e P. H. Santos, "Algorithm for Automatic Peak Detection and Quantification for GC-IMS Spectra," em *Technological Innovation for Life Improvement. DoCEIS 2020. IFIP Advances in Information and Communication Technology 2020, vol 577, pp.369-377*, Costa da Caparica, Portugal, 2020.

[100] C. S. Creaser, J. R. Griffiths, C. J. Bramwell, S. Noreen, C. A. Hillb e C. L. P. Thomas, "Ion mobility spectrometry: a review. Part 1. Structural analysis by mobility measurement," *Analyst,* vol. 129, nº 11, pp. 984-994, 2004.

[101] G. Kaur-Atwal, G. O'Connor, A. A. Aksenov, V. Bocos-Bintintan, C. L. P. Thomas e C. S. Creaser, "Chemical standards for ion mobility spectrometry: A review," *International Journal for Ion Mobility Spectrometry,* vol. 12, nº 1, pp. 1-14, 2009.

[102] R. Slodzinski, L. Hildebrand e W. Vautz, "Peak Detection Algorithm Based on Second Derivative Properties for Two Dimensional Ion Mobility Spectrometry Signals," em *Fathi M. (eds) Integration of Practice-Oriented Knowledge Technology: Trends and Prospectives. Springer*,, Berlin, Heidelberg, 2013.

[103] K. Z., "Forensic Science Applications of Ion Mobility Spectrometry," *Forensic Sci Rev. ,* vol. 1, nº 2, pp. 103-119, 1989.

[104] "Gas Chromatography-Ion Mobility Spectrometry Detection of Odor Fingerprint as Markers of Rapeseed Oil Refined Grade," *Journal of Analytical Methods in Chemistry,* pp. 1-8, 2019.

[105] U. Perycz, Z. Witkiewicz, M. Maziejuk e J. Puton, "Coupling Gas Chromatography with Ion Mobility Spectrometry," LCGC Europe - MJH Life Sciences™ and Chromatography Online., 2021. [Online]. Available: https://www.chromatographyonline.com/view/coupling-gas-chromatography-ion-mobility-spectrometry. [Acedido em 26 Fev 2021].

[106] GAS Dortmund, "GAS Dortmund - Ion Mobility SpectrometryIMS Working Principle," GAS Dortmund, 2019. [Online]. Available: https://www.gas-dortmund.de/data-live-gas/images/Technology/working_principle.jpg. [Acedido em 26 Fev 2021].

[107] E. Kalenius, M. Groessl e K. Rissanen, "Ion mobility–mass spectrometry of supramolecular complexes and assemblies," *Nature Reviews Chemistry,* vol. 3, nº 1, 2018.

[108] R. Cumeras, E. Figueras, C. E. Davis, J. I. Baumbach e I. Gràcia, "Review on Ion Mobility Spectrometry. Part 1: Current Instrumentation," *Analyst,* vol. 140, n° 5, pp. 1376-1390, 2015.

[109] A. Sheibani e N. Haghpazir, "Application of ion mobility spectrometry for the determination of tramadol in biological samples," *J Food Drug Anal,* vol. 22, n° 4, pp. 500-504, 2014.

[110] J. N. Dodds e E. S. Baker, "Ion Mobility Spectrometry: Fundamental Concepts, Instrumentation, Applications, and the Road Ahead," *Journal of The American Society for Mass Spectrometry,* 2019.

[111] J. Puton e J. Namieśnik, "Ion mobility spectrometry: Current status and application for chemical warfare agents detection," *rends in Analytical Chemistry,* vol. 85, pp. 10-20, 2016.

[112] R. Cumeras, E. Figueras, C. E. Davis, J. I. Baumbach e I. Gràcia, "Review on Ion Mobility Spectrometry. Part 2: Hyphenated Methods and Effects of Experimental Parameters," *The Analyst,* vol. 140, n° 5, pp. 1391-1410, 2015.

[113] W. Vautz, J. Franzke, S. Zampolli, I. Elmi e S. Liedtke, "On the potential of ion mobility spectrometry coupled to GC pre-separation - A tutorial," *Analytica Chimica Acta,* vol. 1024, pp. 52-64, 2018.

[114] A. B. Kanu e H. H. Hill, "Ion Mobility Spectrometry Detection for Gas Chromatography," *Journal of Chromatography A,* vol. 1177, n° 1, pp. 12-27, 2008.

[115] A. B. Kanu e H. H. Hill, "Ion Mobility Spectrometry: Recent Developments and Novel Applications," *LabPlus International,* vol. April/May, pp. 20-26, 2004.

[116] J. I. Baumbach, "Process analysis using ion mobility spectrometry," *Anal Bioanal Chem,* vol. 384, n° 5, pp. 1059-1070, 2006.

[117] D. Gallart-Mateu, S. Armenta e M. d. l. Guardia, "Indoor and outdoor determination of pesticides in air by ion mobility spectrometry," *Talanta,* vol. 161, pp. 632-939, 2016.

[118] K. I. Romero e R. Fernandez-Maestre, "Ion mobility spectrometry: the diagnostic tool of third millennium medicine," *Rev Assoc Med Bras,* vol. 64, n° 9, pp. 861-868, 2018.

[119] V. Ruzsanyi, P. Mochalski, A. Schmid, H. Wiesenhofer, M. Klieber, H. Hinterhuber e A. Amann, "Ion mobility spectrometry for detection of skin volatiles," *J Chromatogr B Analyt Technol Biomed Life Sci.,* vol. 911, n° 1, pp. 84-92, 2012.

[120] D. M. Ruszkiewicz, D. Sanders, R. O'Brien, F. Hempel, M. J. Reed, A. C. Riepe, K. Bailie, E. Brodrick, K. Darnley, R. Ellerkmann, O. Mueller, A. Skarysz, M. Truss, T. Wortelmann, S. Yordanov, C. P. Thomas, B. Schaaf e M. Eddleston, "Diagnosis of COVID-19 by analysis of breath with gas chromatography-ion mobility spectrometry - a feasibility study," *EClinicalMedicine,* vol. 29, p. 100609, 2020.

[121] B. de Lacy Costello, A. Amann, H. Al-Kateb, C. Flynn, W. Filipiak, T. Khalid, D. Osborne e N. M. Ratcliffe, "A review of the volatiles from the healthy human body.," *Journal of Breath Research,* vol. 8, n° 1, p. 014001, 2014.

[122] P. Mochalski, H. Wiesenhofer, M. Allers, S. Zimmermann, A. T. Güntner, N. J. Pineau, W. Lederer, A. Agapiou, C. A. Mayhew e V. Ruzsanyi, "Monitoring of selected skin- and breath-borne volatile organic compounds emitted from the human body using gas chromatography ion mobility spectrometry (GC-IMS)," *J Chromatogr B Analyt Technol Biomed Life Sci.,* vol. 1076, pp. 29-34, 2018.

[123] J. Rudnicka, P. Mochalski, A. Agapiou, M. Statheropoulos, A. Amann e B. Buszewski, "Application of ion mobility spectrometry for the detection of human urine," *Anal Bioanal Chem.,* vol. 398, n° 5, pp. 2031-2038, 2010.

[124] M. Shirasu e K. Touhara, "The scent of disease: volatile organic compounds of the human body related to disease and disorder," *J Biochem.,* vol. 150, n° 3, pp. 257-266, 2011.

[125] M. Jünger, W. Vautz, M. Kuhns, L. Hofmann, S. Ulbricht, J. I. Baumbach, M. Quintel e T. Perl, "Ion mobility spectrometry for microbial volatile organic compounds: a new identification tool for human pathogenic bacteria," *Appl Microbiol Biotechnol.,* vol. 93, n° 6, pp. 2603-2614, 2012.

[126] A. P. Snyder, D. B. Shoff, G. A. Eiceman, D. A. Blyth e J. A. Parsons, "Detection of bacteria by ion mobility spectrometry," *Anal Chem.,* vol. 63, n° 5, pp. 526-529, 1991.

[127] G. B. Smith, G. A. Eiceman, M. K. Walsh, S. A. Critz, E. Andazola, E. Ortega e F. Cadena, "Detection of salmonella typhimurium by hand-held ion mobility spectrometer: A quantitative assessment of response characteristics," *Field Anal Chem Technol,* vol. 1, p. 213–226, 1997.

[128] T. Perl, M. Jünger, W. Vautz, J. Nolte, M. Kuhns, M. B.-v. Zepelin e M. Quintel, "Detection of characteristic metabolites of Aspergillus fumigatus and Candida species using ion mobility spectrometry-metabolic profiling by volatile organic compounds," *Mycoses,* vol. 54, n° 6, pp. 828-837, 2011.

[129] S. Schulz e J. S. Dickschat, "Bacterial volatiles: the smell of small organisms," *Nat Prod Rep.,* vol. 24, nº 4, pp. 814-842, 2007.

[130] A. Erler, D. Riebe, T. Beitz, H.-G. Löhmannsröben, D. Grothusheitkamp, T. Kunz e F.-J. Methner, "Characterization of volatile metabolites formed by molds on barley by mass and ion mobility spectrometry," *J Mass Spectrom,* vol. 55, nº 5, p. e4501, 2020.

[131] V. Ruzsanyi, J. I. Baumbach e G. A.Eiceman, "Detection of the mold markers using ion mobility spectrometry," *Int J Ion Mobil Spectrom,* vol. 6, nº 2, pp. 53-57, 2003.

[132] T. Hübert, C. Tiebe e I. Stephan, "Detection of fungal infestations of wood by ion mobility spectrometry," *nternational Biodeterioration & Biodegradation,* vol. 65, nº 5, pp. 675-681, 2011.

[133] J. Langejuergen, C. Wagner, S. Beutel, T. Hopmeier, T. Scheper e S. Zimmermann, "Non-invasive monitoring of bacterial growth and auto-induced protein production in a bioreactor with a closed-loop GC-IMS," *Int. J. Ion Mobil. Spec.,* vol. 18, pp. 9-15, 2015.

[134] A. Korpi, J. Jarnberg e A.-L. Pasanen, "Microbial Volatile Organic Compounds," *Critical Reviews in Toxicology,* vol. 39, nº 2, p. 139–193, 2009.

[135] Z. Karpas, "Applications of ion mobility spectrometry (IMS) in the field of foodomics," *Food Research International,* vol. 54, nº 1, pp. 1146-1151, 2013.

[136] R. Garrido-Delgado, F. Mercader-Trejo, S. Sielemann, W. D. Bruyn, L. Arce e M. Valcárcel, "Direct classification of olive oils by using two types of ion mobility spectrometers," *Anal. Chim. Acta,* vol. 696, nº 1-2, p. 108–115, 2011.

[137] Z. Karpas, A. V. Guamán, D. Calvo, A. Pardo e S. Marco, "The potential of ion mobility spectrometry (IMS) for detection of 2,4,6-trichloroanisole (2,4,6-TCA) in wine," *Talanta,* vol. 93, pp. 200-205, 2012.

[138] R. Alonso, V. Rodriguez-Estevez, A. Dominguez-Vidal, M. J. Ayora-Canada, L. Arce e M. Valcárcel, "Ion mobility spectrometry of volatile compounds from Iberian pig fat for fast feeding regime authentication," *Talanta,* vol. 76, pp. 591-596, 2008.

[139] R. Garrido-Delgado, F. Mercader-Trejo, S. Sielemann, W. d. Bruyn, L. Arce e M. Valcárcel, "Direct classification of olive oils by using two types of ion mobility spectrometers," *Anal Chim Acta,* vol. 696, nº 1-2, pp. 108-115, 2011.

[140] R. Montero-Montoya, R. López-Vargas e O. Arellano-Aguilar, "Volatile Organic Compounds in Air: Sources, Distribution, Exposure and Associated Illnesses in Children," *Ann Glob Health,* vol. 84, nº 2, pp. 225-238, 2018.

[141] S. S. Anand, B. K. Philip e H. M. Mehendale, "Volatile Organic Compounds," *Encyclopedia of Toxicology,* pp. 967-970, 2014.

[142] S. Papathanasiou, "VOCs inside our homes - See The Air," 8 Set 2015. [Online]. Available: https://seetheair.wordpress.com/2015/09/08/vocs-inside-our-houses/. [Acedido em 27 April 2021].

[143] N. H. Snow e G. C. Slack, "Head-space analysis in modern gas chromatography," *Trends in Analytical Chemistry,* vol. 21, nº 9-10, pp. 608-617, 2002.

[144] B. V. Ioffe, A. G. Vitenberg e I. A. Manatov, Head-Space Analysis and Related Methods in Gas Chromatography, Wiley-Interscience, 1984.

[145] C. J. Denawaka, I. A. Fowlis e J. R. Dean, "Evaluation and application of static headspace-multicapillary column-gas chromatography-ion mobility spectrometry for complex sample analysis," *J Chromatogr A,* vol. 1338, pp. 136-148, 2014.

[146] "Headspace analysis. (2019, June 3). Retrieved April 27, 2021, from," MindTouch, 3 June 2019. [Online]. Available: https://chem.libretexts.org/@go/page/61201. [Acedido em 27 April 2021].

[147] R. Muffett, "Theory of Headspace Sampling," 11 Aug 2011. [Online]. Available: https://support.owlstonenanotech.com/hc/en-us/articles/212366966-Theory-of-Headspace-Sampling. [Acedido em 27 April 2021].

[148] R. Law, "An Introduction to Headspace Sampling in Gas Chromatography," 2014. [Online]. Available: https://www.perkinelmer.com/uk/libraries/GDE_Intro_to_Headspace. [Acedido em 27 April 2021].

[149] Restek, "A Technical Guide for Static Headspace Analysis Using GC," [Online]. Available: https://d1lqgfmy9cwjff.cloudfront.net/csi/pdf/e/rk67.pdf. [Acedido em 27 April 2021].

[150] "Dynamic headspace & purge-and-trap," 3 June 2019. [Online]. Available: https://chem.libretexts.org/@go/page/61203. [Acedido em 27 April 2021].

[151] A. Thompson e B. N. Taylor, "Guide for the Use of the International System of Units (SI)," 2008. [Online]. Available: https://physics.nist.gov/cuu/pdf/sp811.pdf. [Acedido em 10 May 2021].

[152] T. K. Boguski, "Understanding Units of Measurement," 2006. [Online]. Available: https://cfpub.epa.gov/ncer_abstracts/index.cfm/fuseaction/display.files/fileid/14285. [Acedido em 10 May 2021].

[153] "Concentrations of Solutions. (2020, May 29). Retrieved May 9, 2021„" 2 May 2020. [Online]. Available: https://chem.libretexts.org/@go/page/119752. [Acedido em 9 May 2021].

[154] "Measurement Definitions," Providence Water, 2019. [Online]. Available: https://www.provwater.com/water_quality/measurement-definitions. [Acedido em 11 May 2021].

[155] M. Słomińska, P. Konieczka e J. Namieśnik, "New developments in preparation and use of standard gas mixtures," *TrAC Trends in Analytical Chemistry,* vol. 62, p. 135–143, 2014.

[156] B. C. Hauck, C. S. Harden e V. M. McHugh, "Current status and need for standards in ion mobility spectrometry," *International Journal for Ion Mobility Spectrometry,* vol. 21, nº 2, 2018.

[157] R. S. Barratt, "The preparation of standard gas mixtures. A review," *The Analyst,* vol. 106, nº 1265, pp. 817-849, 1981.

[158] G. Nelson, Gas Mixtures: Preparation and Control, CRC Press, 1992.

[159] "How to Build Permeation Tubes," Owlstone Inc, [Online]. Available: https://www.owlstoneinc.com/products/build-your-own-permeation-tubes/. [Acedido em 10 May 21].

[160] B. Boyle, "Generating Calibration Gas Standards with OVG-4 and Permeation Tubes," [Online]. Available: https://www.gasdetection.com/wp-content/uploads/Whitepaper_-_Generating_Calibration_Gas_Standards_with_OVG-4_and_Permeation_Tubes.pdf. [Acedido em 10 May 2021].

[161] Y. Li, T. Täffner, M. Bischoff e B. Niemeyer, "Test Gas Generation from Pure Liquids: An Application-Oriented Overview of Methods in a Nutshell," *International Journal of Chemical Engineering,* pp. 1-6, 2012.

[162] J. Spinhirne e J. A. Koziel, "Generation and calibration of standard gas mixtures for volatile fatty acids using permeation tubes and solid-phase microextraction," *Transactions of the ASAE 46(6):,* vol. 46, nº 6, pp. 1639-1646, 2003.

[163] Owlstone Nanotech Inc, *Generating Explosive Calibration Standards with OVG-4 and Permeation Tubes,* Owlstone Whitepaper.

[164] S. Tumbiolo, L. Vincent, J.-F. Gal e P. Maria, "Thermogravimetric calibration of permeation tubes used for the preparation of gas standards for air pollution analysis," *The Analyst,* vol. 130, nº 10, pp. 1369-1374, 2005.

[165] P. C. Maria, J. F. Gal, M. Balza, E. Peré-Trepat, S. Tumbiolo e J. M. Couret, "Using thermogravimetry for weight loss monitoring of permeation tubes used for generation of trace concentration gas standards," *Anal Chem,* vol. 74, nº 1, pp. 305-307, 2002.

[166] A. Shrivastava, "Methods for the determination of limit of detection and limit of quantitation of the analytical methods," *Chronicles of Young Scientists,* vol. 2, nº 1, pp. 21-25, 2011.

[167] W. Huber, "Basic calculations about the limit of detection and its optimal determination," *Accreditation and Quality Assurance,* vol. 8, nº 5, pp. 213-217, 2003.

[168] D. A. Armbruster e T. Pry, "Limit of blank, limit of detection and limit of quantitation," *Clin Biochem Rev,* vol. Suppl 1, pp. 49-52, 2008.

[169] H. Borsdorf, P. Fiedler e T. Mayer, "The effect of humidity on gas sensing with ion mobility spectrometry," *Sensors and Actuators B: Chemical,* vol. 218, pp. 184-190, 2015.

[170] M. Tabrizchi, "Temperature effects on resolution in ion mobility spectrometry," *Talanta,* vol. 62, nº 1, pp. 65-70, 2004.

[171] M. Tabrizchi e F. Rouholahnejad, "Pressure effects on resolution in ion mobility spectrometry," *Talanta,* vol. 69, nº 1, pp. 87-90, 2006.

[172] E. Szymańska, A. N. Davies e L. M. C. Buydens, "Chemometrics for ion mobility spectrometry data: recent advances and future prospects," *Analyst,* vol. 141, nº 20, pp. 5689-5708, 2016.

[173] G.A.S. - Gesellschaft für analytische Sensorsysteme, User manual GC-IMS, Dortmund, Germany, 2016.

[174] G.A.S. - Gesellschaft für analytische Sensorsysteme, User Manual Circular Gas Flow Unit, Dortmund, Germany, 2015.

[175] C. K. Lorjaroenphon Y, " Characterization of typical potent odorants in cola-flavored carbonated beverages by aroma extract dilution analysis.," Vols. %1 de %228;63(3):769-75., 2015 Jan.

[176] National Aeronautics and Space Administration, "SIRIUS - NASA," 2018. [Online]. Available: https://www.nasa.gov/sites/default/files/atoms/files/sirius-17.pdf. [Acedido em 11 Junho 2021].

[177] Institute for Bio-Medical Problems (IBMP) , "Проект "SIRIUS"," [Online]. Available: http://sirius.imbp.ru/. [Acedido em 11 June 2021].

[178] National Aeronautics and Space Administration, "About NEK & SIRIUS," NASA, 14 Apr 2021. [Online]. Available: https://www.nasa.gov/analogs/nek/about. [Acedido em 11 June 2021].

[179] National Aeronautics and Space Administration, "NASA is "SIRIUS" About Its Analog Missions," NASA, 1 Nov 2017. [Online]. Available: https://www.nasa.gov/feature/nasa-is-sirius-about-its-analog-missions. [Acedido em 11 June 2021].

[180] National Aeronautics and Space Administration, "About Analog Missions," NASA, 16 May 2019. [Online]. Available: https://www.nasa.gov/analogs/what-are-analog-missions. [Acedido em 11 June 2021].

[181] CaroleTafforin, "The Mars-500 crew in daily life activities: An ethological study.," *Acta Astronautica, ,* vol. 91, p. 69–76, 2013.

[182] I. Poláčková Šolcová, I. Šolcová, I. Stuchlíková e Y. Mazehóová, "The story of 520 days on a simulated flight to Mars.," *Acta Astronautica, ,* vol. 126, p. 178–189, 2016.

[183] Institute for Bio-Medical Problems (IBMP), "«Mars-500» project," [Online]. Available: http://mars500.imbp.ru/en/nek.html. [Acedido em 11 June 2021].

[184] "520 Day Mars Mission Simulation by ESA Yields OK," Exo Cruise, 7 10 2015. [Online]. Available: https://dodlithr.blogspot.com/2015/10/mars500-520-day-mars-short-stay-mission.html. [Acedido em 18 Nov 2021].

[185] V. Fetter, V. Vassilenko, J. Fernandes, T. Hummel, D. Tsarkov, O. Orlov, A. Pakhomova e L. Moukhamedieva, "Validation of analytical instrumentation for continuous online monitoring of large spectra of VOCs in closed habitat during simulation of space flight," em *Proceedings of the International Astronautical Congress, IAC*, Bremen, Germany, 2018.

[186] N. V. R., A. K. Mohapatra, U. V. K., R. K. Sinha, R. Nayak, V. B. Kartha e S. Chidangil, "Breath analysis for the screening and diagnosis of diseases," *Applied Spectroscopy Reviews,* 2020.

[187] A. Tonacci, F. Sansone, A. P. Pala e R. Conte, "Ehaled breath analysis in evaluation of psychological stress: A short literature review," *International Journal of Psychology.,* vol. 54, 2018.

[188] C. Lourenço e C. Turner, "Breath Analysis in Disease Diagnosis: Methodological Considerations and Applications," *Metabolites,* vol. 4, nº 2, p. 465–498, 2014.

[189] V. Vassilenko and P. H. C. Santos, "System for controlled and selective sampling of exhaled air and corresponding operating procedure". Portugal Patent WO/2018/047058, 12 09 2016.

[190] D. M. A. Gronwall, "Paced Auditory Serial-Addition Task: A Measure of Recovery from Concussion," *Perceptual and Motor Skills,* vol. 44, nº 2, p. 367–373, 1977 .

[191] T. Tombaugh, "A comprehensive review of the Paced Auditory Serial Addition Test (PASAT)," *Arch. Clin. Neuropsychol.,* vol. 21, nº 1, p. 53–76 , 2006.

[192] D. L. Massart, B. G. M. Vandeginste, S. Deming, Y. Michotte e L. Kaufman, Chemometrics: a Textbook (Data Handling in Science and Technology), vol. 2, Amsterdam: Elsevier, 2003.

[193] M. C. Gonçalves, "Quantitative analysis of contamination of biological origin in direct detection in-situ," *B.S. Thesis, NOVA School of Science and Technology, NOVA University of Lisbon, Caparica, Portugal,* 2018.

[194] M. Goncalves, J. F. V. Fernandes, M. Diniz e V. Vassilenko, " Novel methodology for quick detection of bacterial metabolites," em *IEEE 6th Portuguese Meeting on Bioengineering (ENBENG)*., 2019 .

[195] R. Tofalo, G. Perpetuini, M. Schirone e G. Suzzi, "Biogenic Amines: Toxicology and Health Effect," *Encyclopedia of Food and Health,* pp. 424-429, 2016.

[196] C. Espalha, J. Fernandes, M. Diniz e V. Vassilenko, "Fast and Direct Detection of Biogenic Amines in Fish by GC-IMS Technology," em *IEEE 6th Portuguese Meeting on Bioengineering (ENBENG)*, 2019.

[197] C. Á. Espalha, "Direct Detection of Biogenic Amines from Fish," *B.S. Thesis, NOVA School of Science and Technology, NOVA University of Lisbon, Caparica, Portugal,* 2018.

[198] C. Verseux, C. Heinicke, T. Ramalho, J. Determann, M. Duckhorn, M. Smagin e M. Avila, "A Low-Pressure, N2/CO2 Atmosphere Is Suitable for Cyanobacterium-Based Life-Support Systems on Mars," *Front Microbiol.,* vol. 12, p. 611798, 2021.

[199] National Aeronautics and Space Administration, "Aquaponics," NASA, 19 May 2009. [Online]. Available: https://www.nasa.gov/audience/foreducators/9-12/features/aquaponics.html. [Acedido em 2 Jully 2021].

[200] M. Nelson e C. Shultz, "The potential applications of aquaponics for bioregenerative space life support systems," em *42nd COSPAR Scientific Assembly*, Pasadena, California, USA, 2018.

[201] V. Bluem e F. Paris, "Aquatic food production modules in bioregenerative life support systems based on higher plants," *Advances in Space Research,* vol. 27, nº 9, p. 1513–1522, 2001.

[202] O. G. Mouritsen, Seaweeds: Edible, available & sustainable, 1st ed., vol. 1, Chicago: University of Chicago Press., 2013.

[203] Kaori O'Connor, Seaweed: A Global History (Edible), London, UK: Reaktion Books, 2017.

[204] L. Pereira e F. Correia, Macroalgas Marinhas da Costa Portuguesa: Biodiversidade, ecologia e utilizações, 1st ed., Paris: Nota de Rodapé, 2015.

[205] Mouritsen, O. G., "The emerging science of gastrophysics and its application to the algal cuisine," *Flavour,* vol. 1, n° 1, p. 6, 2012.

[206] E. H. Maarse, Volatile Compounds in Foods and Beverages, 1st ed, New York: Marcel Dekker, Inc., 1991.

[207] M. I. Hosoglu, " Aroma characterization of five microalgae species using solid-phase microextraction and gas chromatography–mass spectrometry/olfactometry," *Food Chem.,* vol. 240, p. 1210–1218, 2017.

[208] N. Khan-Mayberry, J. T. James, R. Tyl e C. Lam, "Space Toxicology," *International Journal of Toxicology,* vol. 30, n° 1, pp. 3-18, 2011.

[209] M. D. Wessel, J. M. Sutter e P. C. Jurs, "Prediction of reduced ion mobility constants of organic compounds from molecular structure," *Anal Chem,* vol. 68, n° 23, pp. 4237-4243, 1996.

[210] R. Fernandez-Maestre, "Accuracy of reduced mobilities and measurement of instrumental parameters in ion mobility spectrometry," *International Journal of Mass Spectrometry,* vol. 421, p. 8–13, 2017.

[211] A. T. Garrison e R. W. Huigens, "Eradicating Bacterial Biofilms with Natural Products and Their Inspired Analogues that Operate Through Unique Mechanisms," *Current Topics in Medicinal Chemistry,* vol. 17, n° 14, pp. 1-8, 2016.

A. APPENDIXES

APPENDIX I.

Supplementary data: Figures

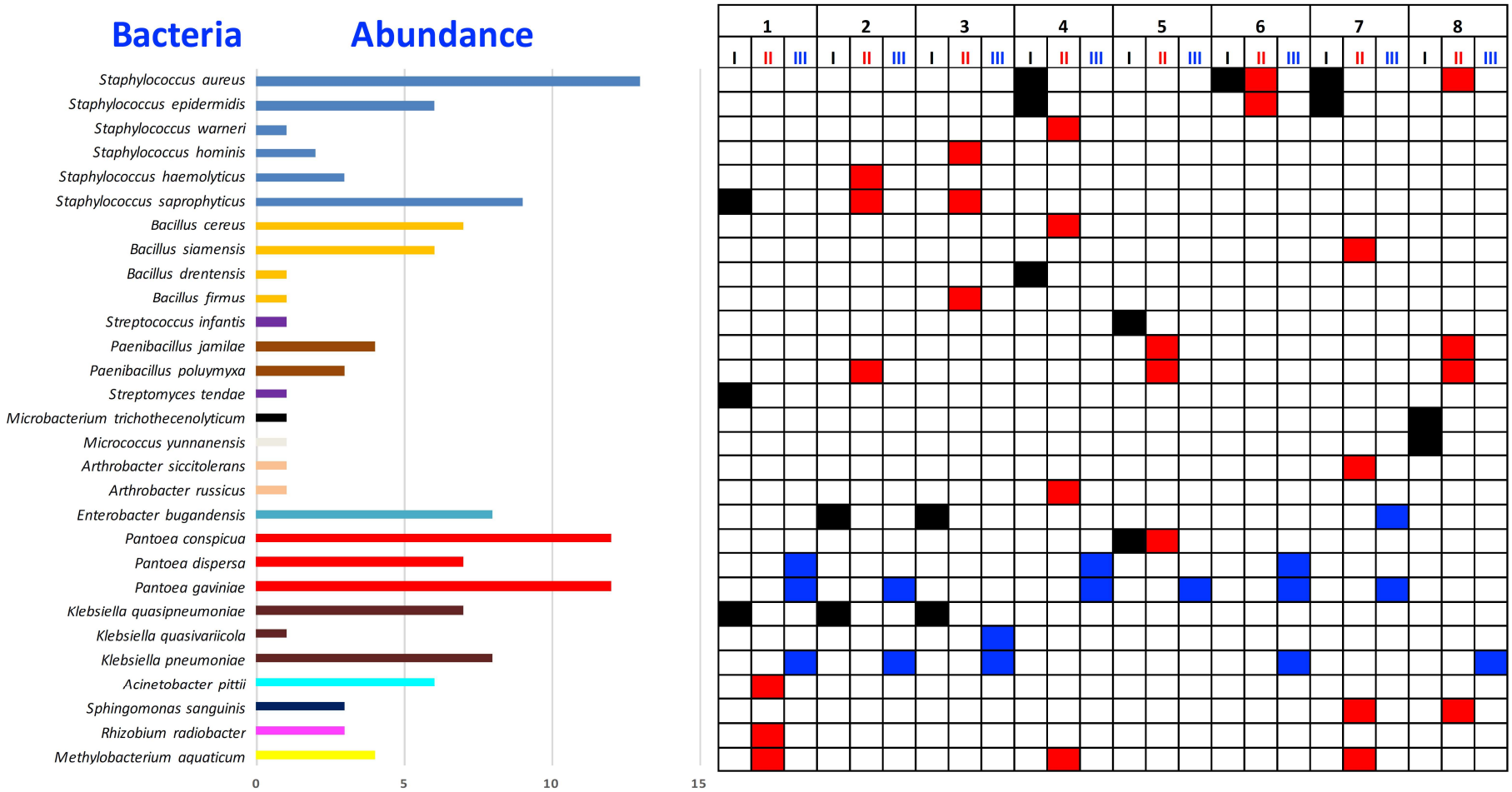

Figure A.1 — Culture- and qPCR-based analyses of microbial burden (bacteria). A total of 133 bacterial isolates (A) and 81 fungal isolates (B) that were cultured from eight locations during three flights, were picked for identification. The bar length (middle panel) represents the number of isolates that were identified as a particular species or genus (left panel) and the bar colour indicates the same genus. The colour filled checkerboard (right panel) indicates from which samples the bacteria were cultured in which black represents flight 1, red, flight 2 and black, flight 3 [52].

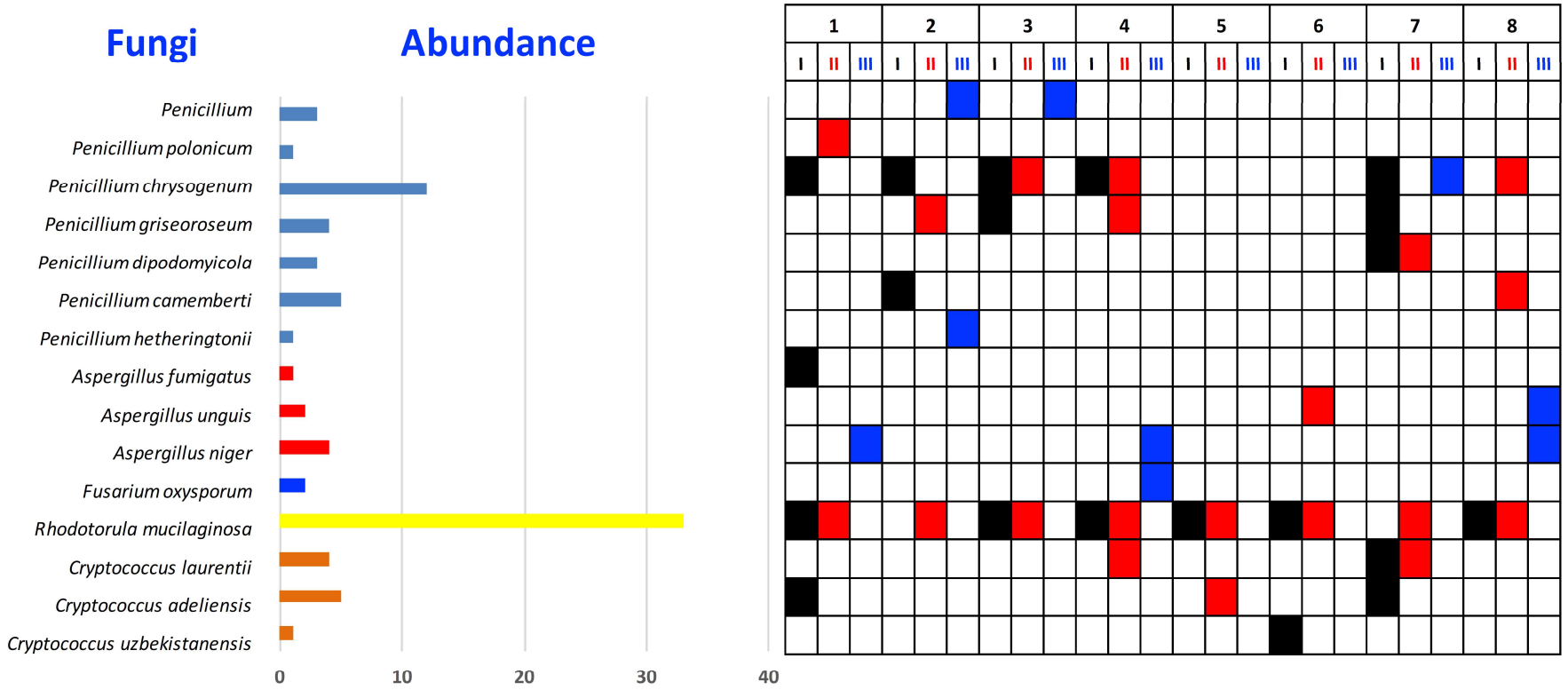

Figure A.2 — Culture- and qPCR-based analyses of microbial burden (fungi). A total of 133 bacterial isolates (A) and 81 fungal isolates (B) that were cultured from eight locations during three flights, were picked for identification. The bar length (middle panel) represents the number of isolates that were identified as a particular species or genus (left panel) and the bar colour indicates the same genus. The colour filled checkerboard (right panel) indicates from which samples the bacteria were cultured in which black represents flight 1, red, flight 2 and black, flight 3 [52]

GRAB SAMPLE CONTAINER (GSC):

0.35 L stainless steel canisters
passivated surfaces
instantaneous "whole air" samples
used for VOC analysis, especially
permanent gases not collected
on sorbent trap

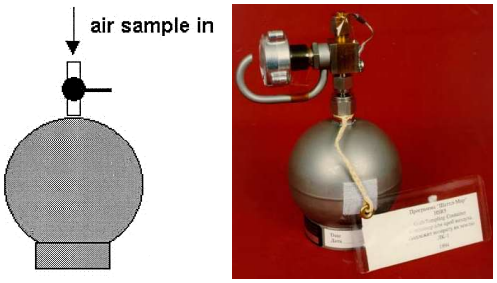

SOLID SORBENT AIR SAMPLER (SSAS):

8 cartridges packed with sorbent agent(s)
battery powered sampling pump
low flow rates (~ 1 mL/min)
24-hour time-averaged samples
used for VOC analysis

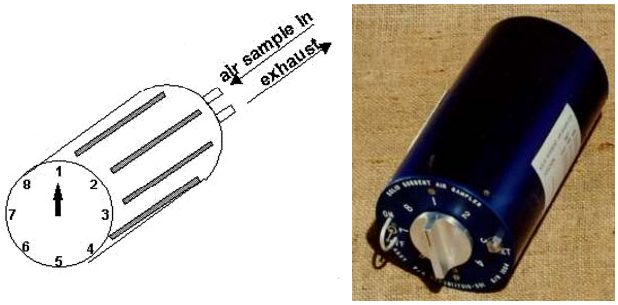

Figure A.3 — Depiction of GSC and SSAS devices used for sampling cabin atmospheres [75]. Right side pictures: Top right, GSC (https://lsda.jsc.nasa.gov/Hardware/hardw/636) and bottom right, SSAS (https://lsda.jsc.nasa.gov/Hardware/hardw/637).

Acetone / Triacetone Triperoxide (TATP) Precursor

Record Tube Mass Measurement

Tube Mass (g)	8.2209

Record Tube Mass

Permeation Tube Calibration Parameters

Analyte	Acetone
Molecular Weight	58.08
Calibration Temperature (°C)	30
Permeation Rate (ng/min)	694
No. DataPoints	6

Manufacturing Information

Operator ID	Rebecca O'Donnell
Tube Serial Number	100-120
Mass Balance ID	E18
OVG-4 ID	OVG1

Tube Mass (g)	Date & Time
8.2311	10/05/2010 12:00
8.2279	12/05/2010 12:00
8.2259	14/05/2010 12:00
8.2230	17/05/2010 12:00
8.2219	18/05/2010 12:00
8.2209	19/05/2010 12:00

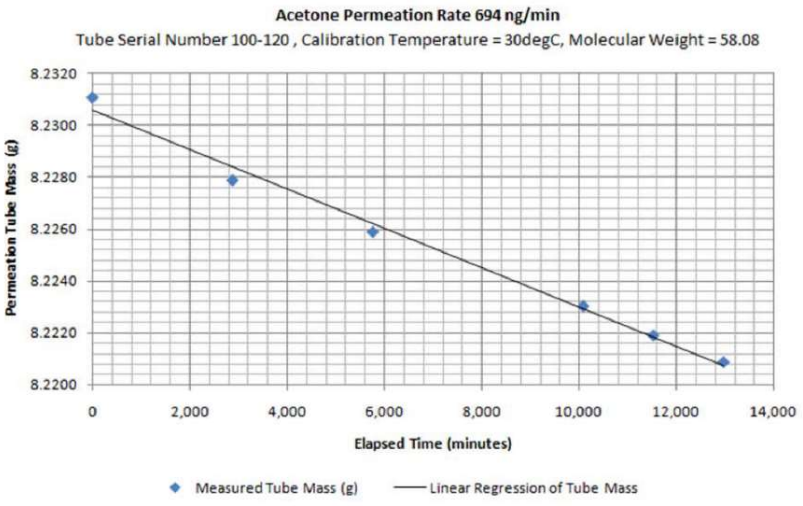

OWLSTONE

Owlstone Nanotech Inc - Permeation Tube Calibration Certificate

C:\Users\Billy.boyle\Desktop\OVG Knowledge Centre\Calibration Certs\[Acetone Permeation Tube Calibration Log.xlsm]Permeation Tube Calibration

Signed: _____ Russell Parris - Chief Application Officer

Date: _____

Figure A.4 — Calibration Certificate Permeation Tubes showing the permeation rate, substance characteristics, calibration temperature, tube mass and calibration graph from Owlstone Inc. [163].

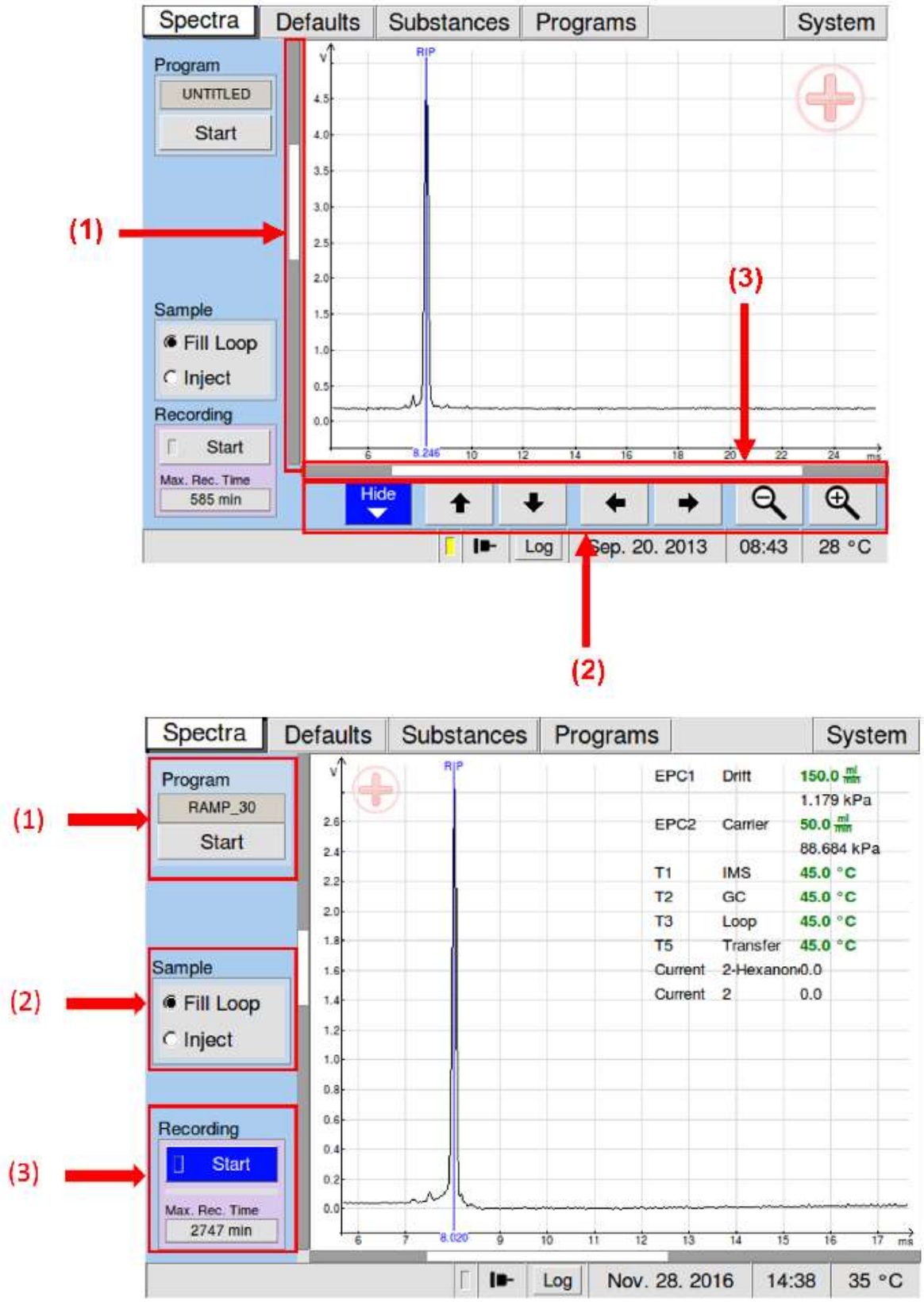

Figure A.5 — Views of the Spectra window highlighting vertical (1), horizontal (3) and view control bars (2) (top) and menus available for program (1), sample (2) and recording options (3) (bottom) [173].

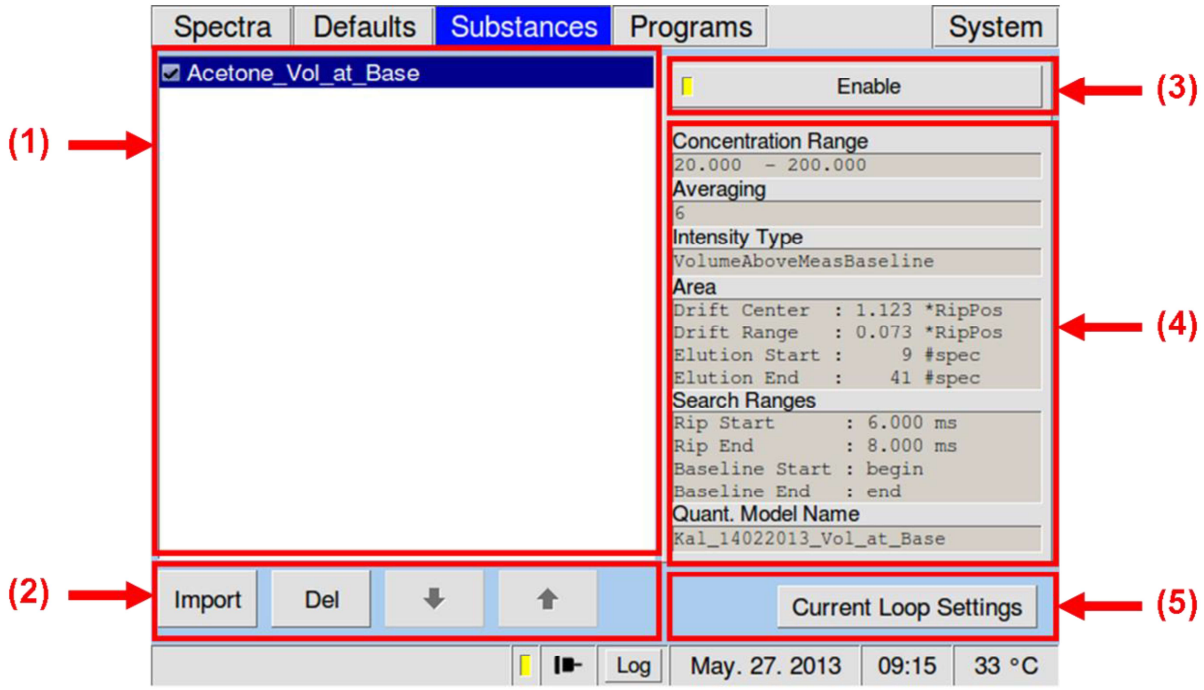

Figure A.6 — The five sections of the Substances window from the Breathspec® instrument: (1) Substances List, (2) Substances List Control Panel, (3) Enable Button, (4) Substance Calibration Information Area, (5) Current Loop Settings [173].

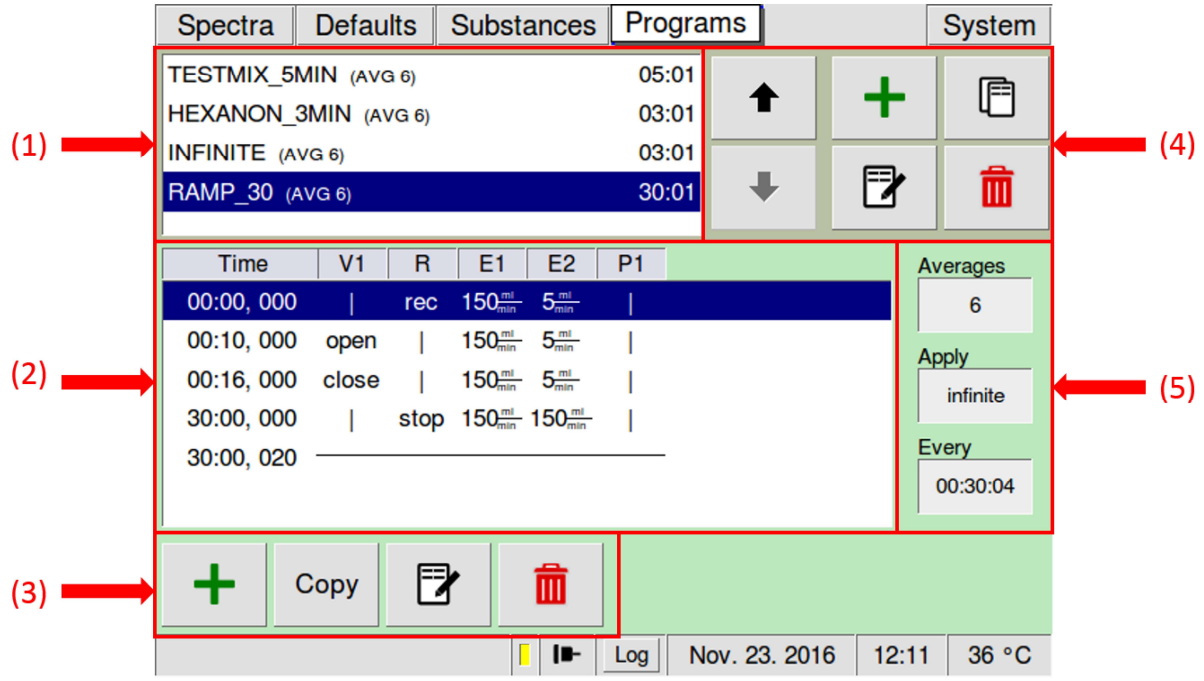

Figure A.7 — The five sections contained in the Programs window (1) Measurement program List window, (2) Selected Program Window, (3) Selected Program Window Control Panel, (4) Measurement Program Control Panel, (5) Program Repetition and Average Settings [173].

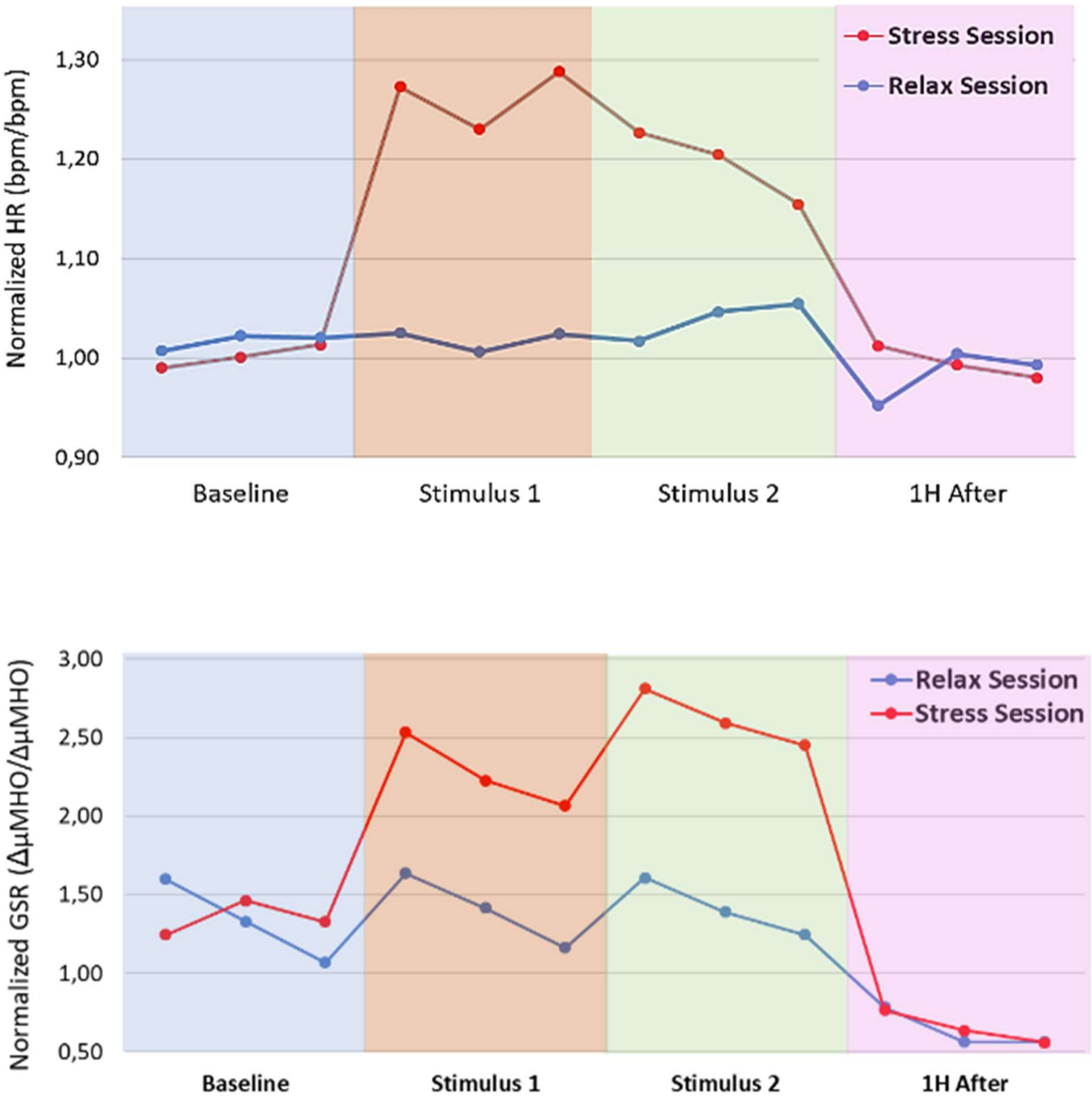

Figure A.8 — Heart Rate (top) and Galvanic Skin Response GSR (bottom) mean responses obtained during the Breath Stress expeiment for both stress (red) and relax (blue) sessions

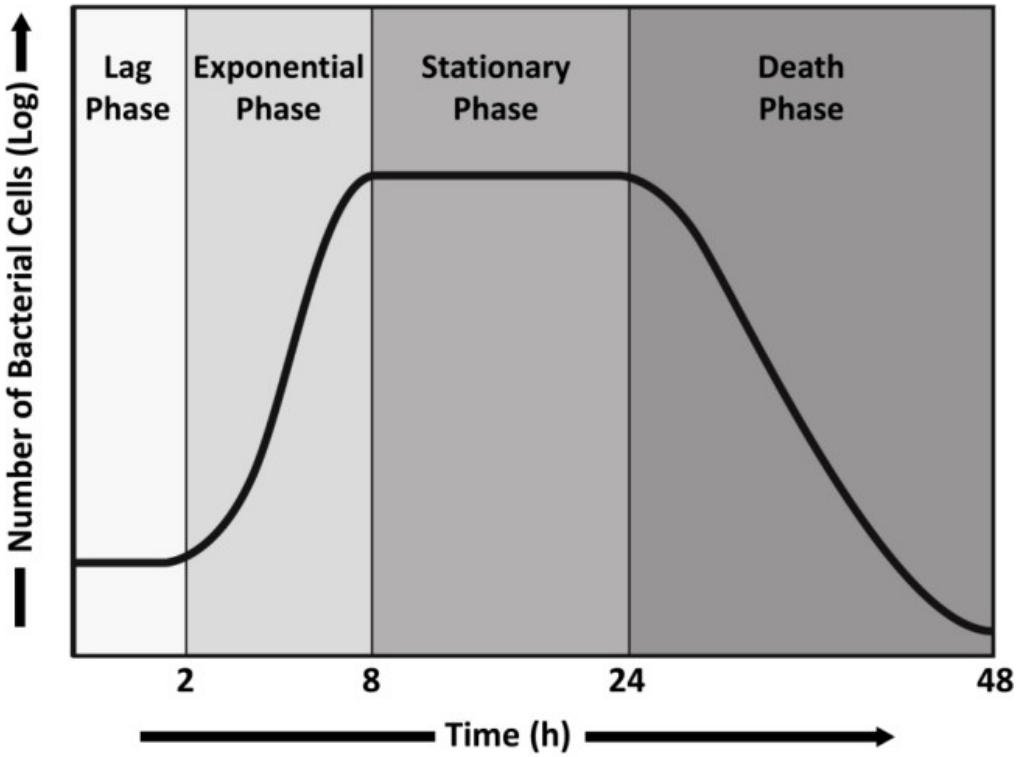

Figure A.9 — Bacterial growth curve showing phases: (i) lag, (ii) exponential, (iii) stationary and (iv) death phases [211].

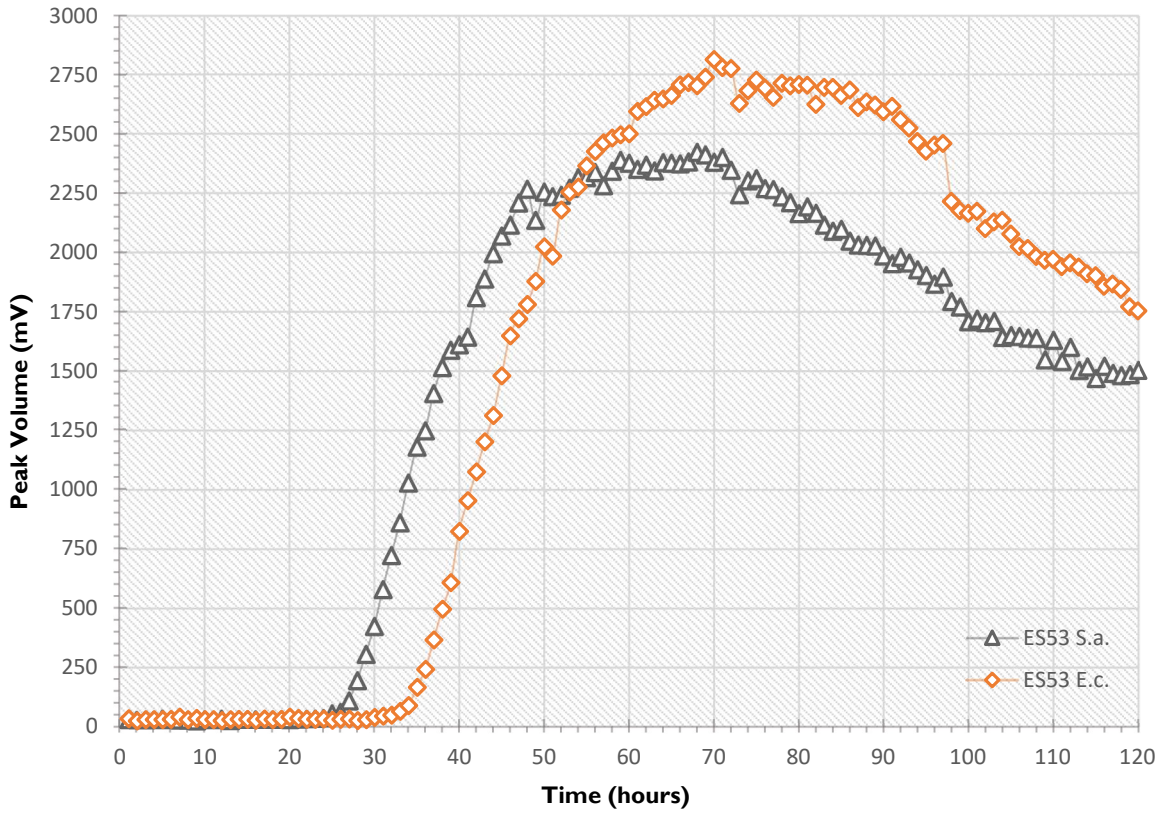

Figure A.10 — Changes over time of characteritic microbial growth signal, (ES 53) for *S. aureus* and *E. coli* inoculated in FTM.

	#CAS	NAME	Mw g·mol⁻	Dt (ms)	RIP Rel	R time	K_0	Vp (mmHg)	T (ºC)	Vm (L/mol)	Aff_{Proton} (NIST WebBook)	OBS.	CLASS	RS-ISS
Simple Alcohols	#67-56-1	*Methanol*	32,04	7,366	1,015	67,2	2,0922	97,65	20	123,2955	754.3 kJ·mol⁻¹	*has a maximum inside the RIP*	*ol*	RS-ISS
				7,546	1,039	67,2	2,0423					*dual signal (has two maxima)*		
	#64-17-5	*Ethanol*	46,07	7,773	1,056	73,50	1,9827	45	20	58,36817	788 kJ·mol⁻¹	*Shows a Dimer and Monomer* 	*ol*	RS-ISS
				8,460	1,149	73,50	1,8217							
	#71-23-8	*1-Propanol*	60,1	8,280	1,128	95,76	1,8613	21	25	74,84433	786,5 kJ·mol⁻¹	*Has a signal in the middle of the two* 	*ol*	RS-ISS
				9,440	1,286	95,76	1,6326					*Coordinates: DT 1,214 and 92,8 RT*		
	#71-36-3	*1-Butanol*	74,12	8,793	1,202	140,07	1,7527	6	20	91,50617	789,2 kJ·mol⁻¹	*dual signal (has two maxima)* 	*ol*	RS-ISS
				10,420	1,425	140,07	1,479					*dual signal (has two maxima)*		
	#71-41-0	*1-Pentanol*	88,15	9,373	1,279	207,48	1,6442	2,2	25	0,27127	795,0 kJ·mol⁻¹	*dual signal (has two maxima)*	*ol*	
				11,493	1,569	207,48	1,3409					*pure substance proved the curve prediction (DT)*		
	#111-27-3	*1-Hexanol*	102,177	9,926	1,356	334,95	1,5526		25	0		*dual signal (has two maxima)*	*ol*	
				12,533	1,712	334,95	1,2297					*dual signal (has two maxima)*		
	#111-70-6	*1-Heptanol*	116,204	10,506	1,435	556,08	1,4669		25	0		*dual signal (has two maxima)*	*ol*	
				13,546	1,851	556,08	1,1377					*dual signal (has two maxima)*		
	#111-87-5	*1-octanol*	130,231	11,046	1,510	937,65	1,3952	0,00794	25	0,00961	799,0 kJ·mol⁻¹	*dual signal (has two maxima)*	*ol*	
				14,456	1,977	937,65	1,0661					*pure substance proved the curve prediction (DT)*		
Substituted Alchool	#67-63-0	*2-Propanol* *Isopropanol*	60,1	8,120	1,103	80,22	1,898	45,4	25	76,4631	796 kJ·mol⁻¹	*Rubbing alchool | Sander ID*	*ol*	RS-ISS
				8,883	1,206	80,22	1,7349					*Isopropanol | isopropyl alcohol*		
				9,236	1,254	80,22	1,6686							
	#78-83-1	*2-Methylpropanol* *Isobutanol*	74,122	8,693	1,191	118,65	1,7729	9,00	20	11,22195	793.7 kJ·mol−1		*ol*	RS-ISS
				10,293	1,410	118,65	1,4973					*Other names used: Isobutyl alcohol or IBA*		
	#123-51-3	*3-Methyl-butanol*	88,148	9,293	1,271	182,7	1,6584		25	0		*dual signal (has two maxima)*	*ol*	
				11,373	1,555	182,7	1,3551					*dual signal (has two maxima)*		
	#75-85-4	*2-Methylbutan-2-ol*	88,15	7,553	1,037	123,9	2,0404		25	0	0.0 kJ·mol−1		*ol*	
				7,813	1,072	123,9	1,9725					*triple signal (has three maxima)*		
				9,593	1,316	123,9	1,6065							
	#141-43-5	*2-Aminoethanol* *Ethanolamine*	61,084	9,340	1,281	210,00	1,65	0,480	20	0,474488		*Amonia signal possible before the RIP*	*ol*	
				9,593	1,315	210,00	1,6065					*Triple signal (three maximum*		
				11,620	1,593	210,00	1,3263					*Cause spetra saturation due to amonina signals*		
	#3391-86-4	*1-octen-3-ol*	128,215	8,8	1,205	504,63	1,7513	0,531	25	0,120682		*dual signal (has two maxima)*	*ol*	
				12,273	1,689	504,63	1,2557					*Dimer has a "fat" signal with a "fog"*		
	#18409-17-1	*(2E)-2-octen-1-ol*	128,21	8,773	1,206	867,93	1,7567	0,107	25			*dual signal (has two maxima)*	*ol*	
				12,3	1,691	867,93	1,253					*Dimer has a "fat" signal with a "fog"*		

Figure A.11 — A fragment of the VOC database developed for volatile organic compound identification of GC-IMS signals showing a colour scheme the alcohol functional group. VP corresponds to vapor pressure, Vm to molar volume, K_0 is the reduced ion mobility constant, Aff. $_{Proton}$ is the proton affinity and OBS are observation.

APPENDIX II.

Statistical data: SIRIUS-17 & Seaweeds

Table A.1 — Data from 33 detectated peaks of all measurements collected during SIRUS-17 with collection times, mean intensity (int.), and standard deviation (SD).

PEAK	DAY ONE						DAY TWO		DAY THREE		DAY SEVEN			
	D1: 7h34-8h38		D1: 16h36-17h40		D1: 21h31-22h35		D2: 8h21-9h25		D3: 8h15-9h19		D7: 7h29-8h33		D7: 9h05-10h09	
	Int. (volt)	SD	Int. (volt)	SD	Int. (volt)	SD	Int. (volt)	SD	Int. (volt)	SD	Int. (volt)	SD	Int. (volt)	SD
Sir-1	760.58	13.66	893.52	66.35	1070.19	23.29	1088.64	13.83	1092.15	102.70	931.83	11.60	1031.32	35.31
Sir-2	1839.18	21.18	1907.31	61.08	1966.18	16.64	1973.76	10.80	1969.13	58.08	1820.71	23.57	1857.43	11.00
Sir-3	588.40	18.96	597.93	17.00	535.19	4.20	506.59	18.08	692.39	71.62	1302.37	10.08	1275.31	12.49
Sir-4	591.53	119.01	455.16	95.28	496.84	10.70	579.75	38.74	775.06	116.80	849.55	322.72	1132.98	91.60
Sir-5	2975.68	464.33	3192.46	214.08	3080.92	188.19	2959.42	176.53	2593.45	469.89	2545.67	466.14	2826.70	40.54
Sir-6	959.03	97.70	276.75	112.25	203.37	11.96	846.95	38.58	341.88	44.74	249.73	22.17	234.59	1.44
Sir-7	128.43	12.66	119.80	12.90	116.95	3.61	125.70	6.55	155.32	5.61	166.62	4.76	151.58	2.06
Sir-8	177.77	26.72	195.89	16.42	160.74	13.71	153.67	18.70	226.72	27.70	1330.95	41.93	1271.91	83.55
Sir-9	497.48	126.38	449.90	64.19	521.44	53.78	502.24	57.46	394.53	102.67	374.55	101.71	423.81	9.90
Sir-10	199.94	10.30	205.17	27.35	205.07	10.32	181.65	10.96	201.34	1.72	196.84	7.05	193.31	3.64
Sir-11	150.32	6.43	164.50	12.72	144.21	5.62	139.99	3.30	146.70	4.17	164.28	2.12	157.55	4.76
Sir-12	109.51	9.30	178.76	9.98	174.00	6.49	109.52	6.27	102.18	1.65	98.91	3.69	96.00	3.23
Sir-13	68.13	1.80	86.96	10.77	69.86	2.02	67.04	2.88	62.59	1.65	63.05	0.63	61.89	0.77
Sir-14	175.02	9.07	170.02	25.14	172.98	8.72	141.20	10.00	152.75	5.17	126.07	2.58	122.29	3.28
Sir-15	72.77	7.40	68.81	13.74	79.32	3.96	75.81	6.13	78.49	2.79	82.98	1.88	84.43	0.76
Sir-16	57.55	14.07	56.11	11.71	53.37	7.26	48.80	8.81	44.53	7.15	46.47	2.52	44.37	1.21
Sir-17	86.29	7.04	111.90	13.26	86.08	8.21	83.24	6.24	80.20	3.42	79.02	1.85	77.44	2.42
Sir-18	99.40	11.38	95.15	6.41	90.78	5.05	87.63	7.94	99.75	5.35	107.92	6.10	105.04	3.43
Sir-19	25.95	7.54	34.54	7.63	27.50	5.79	44.46	12.03	67.51	20.58	40.40	7.02	38.75	2.81
Sir-20	65.93	1.83	129.70	71.37	79.92	2.08	68.63	4.42	156.49	5.37	75.25	3.40	76.74	2.43
Sir-21	134.93	22.42	119.98	10.00	103.61	4.04	100.12	8.72	148.01	8.92	245.12	15.11	218.05	6.16
Sir-22	79.68	1.55	79.11	4.74	82.78	7.90	73.98	4.59	76.33	1.21	74.39	0.60	73.57	1.66
Sir-23	70.28	15.57	75.43	17.30	67.90	13.01	66.24	16.24	63.73	18.04	82.16	14.39	78.22	18.80
Sir-24	44.90	5.39	49.47	5.57	43.93	3.77	42.75	4.35	41.24	2.67	44.19	1.16	44.56	1.15
Sir-25	24.08	5.11	24.61	2.67	21.21	2.57	26.45	2.82	32.36	2.76	31.76	3.31	30.07	1.35
Sir-26	87.64	3.74	111.72	5.93	86.07	8.18	76.98	7.57	81.29	3.81	87.27	6.53	88.05	5.38
Sir-27	54.69	8.16	77.93	8.56	65.98	5.09	55.42	5.63	52.39	3.78	59.82	3.76	56.13	2.34
Sir-28	296.83	2.45	357.84	24.48	355.84	11.71	347.18	7.33	330.88	17.30	226.61	8.13	231.49	10.39
Sir-29	15.03	4.88	18.61	2.24	18.84	2.60	14.11	3.42	14.62	2.34	16.15	1.64	14.72	0.57
Sir-30	45.04	8.52	67.14	4.47	65.23	5.07	48.52	7.14	41.02	4.15	47.60	2.49	45.16	1.19
Sir-31	92.96	5.82	119.42	7.06	96.47	10.05	86.00	9.70	86.98	2.54	104.88	9.22	109.46	7.40
Sir-32	16.90	6.63	16.52	3.51	14.90	3.37	14.24	3.79	16.67	3.64	19.96	2.73	17.08	0.77
Sir-33	33.66	7.63	40.65	5.53	31.54	4.64	31.66	4.84	36.14	2.61	36.80	2.70	34.06	2.02

(continuation) Table A.1 — Data from 33 detectated peaks of all measurements collected during SIRUS-17 with collection times, mean intensity (int.), and standard deviation (SD).

PEAK	DAY EIGHT						DAY NINE		DAY TEN				DAY ELEVEN	
	D8: 7h38-8h42		D8: 16h55-17h59		D8: 23h21-00h25		D9: 9h15-10h19		D9: 9h15-10h19		D10: 22h34-23h38		D11: 10h52-11h56	
	Int. (volt)	SD	Int. (volt)	SD	Int. (volt)	SD	Int. (volt)	SD	Int. (volt)	SD	Int. (volt)	SD	Int. (volt)	SD
Sir-1	885.97	3.62	1061.77	41.02	1185.16	8.05	986.79	15.50	938.53	26.67	1081.79	39.33	1018.04	11.04
Sir-2	1821.51	19.16	1907.42	30.71	1943.71	11.27	1887.19	8.02	1884.77	13.84	1907.72	11.28	1855.70	12.22
Sir-3	1221.30	5.49	1112.24	20.60	904.05	10.28	1049.42	99.80	914.82	15.85	769.39	11.76	931.08	10.07
Sir-4	760.89	157.74	877.33	68.71	704.48	10.34	918.14	37.99	592.70	57.94	533.15	74.33	625.60	56.88
Sir-5	2260.40	390.71	2544.81	132.97	2458.19	146.58	2557.18	155.23	2441.12	74.89	2274.10	59.64	2194.68	153.01
Sir-6	148.01	26.17	89.73	3.37	100.09	43.30	160.58	6.36	91.79	20.84	59.85	15.01	137.35	6.48
Sir-7	153.48	4.03	131.85	4.83	126.27	1.94	120.36	1.33	128.18	7.66	117.24	2.34	115.50	1.80
Sir-8	954.08	8.91	662.00	14.82	381.91	13.23	594.74	132.54	381.50	26.20	267.94	10.93	416.90	13.76
Sir-9	302.89	69.15	324.09	22.11	341.83	29.12	374.30	34.33	300.63	9.11	296.32	7.99	302.84	30.23
Sir-10	179.31	2.28	195.27	9.74	196.96	4.23	198.29	5.87	223.97	14.86	197.01	6.04	180.35	1.59
Sir-11	148.50	2.08	153.72	4.12	145.23	5.11	139.68	1.69	144.03	6.78	130.65	1.73	136.23	10.31
Sir-12	102.68	1.46	113.41	4.26	162.25	3.73	97.27	1.91	133.87	9.90	111.68	2.72	175.37	6.74
Sir-13	58.73	0.89	61.71	1.26	60.53	0.54	58.00	0.54	62.10	3.25	57.96	0.74	56.02	0.72
Sir-14	117.03	1.02	119.35	4.56	138.07	3.01	130.80	2.41	133.13	14.03	114.43	3.04	144.32	4.17
Sir-15	71.89	0.59	83.52	1.88	90.99	0.42	82.33	1.45	86.94	6.83	82.21	1.45	75.34	1.05
Sir-16	36.61	1.25	38.70	3.73	34.44	2.35	35.53	0.71	40.67	10.87	29.30	1.12	27.73	1.25
Sir-17	70.15	1.70	81.16	4.47	73.28	4.12	73.06	1.34	83.09	9.52	69.29	3.14	66.39	1.32
Sir-18	98.89	5.39	101.33	7.64	95.69	3.26	92.03	3.81	101.45	12.08	89.21	5.12	82.86	3.33
Sir-19	45.71	9.31	23.96	3.05	24.05	1.78	22.24	1.16	25.07	7.40	19.71	1.59	22.17	1.99
Sir-20	74.73	2.90	81.44	2.68	79.34	1.43	71.16	1.53	92.59	4.32	99.80	1.09	88.70	0.98
Sir-21	204.12	16.15	181.44	9.66	143.81	5.13	154.02	10.42	144.35	10.88	119.62	5.65	129.76	3.62
Sir-22	69.74	1.37	74.01	0.99	76.97	0.83	73.44	0.66	75.63	3.95	71.26	0.96	68.82	0.54
Sir-23	64.01	12.74	80.00	13.16	64.64	15.24	65.35	15.54	86.41	13.83	60.22	16.46	52.65	13.80
Sir-24	38.51	0.52	38.15	2.04	38.14	0.94	38.10	1.22	39.80	6.58	34.18	1.64	33.43	0.91
Sir-25	29.63	1.74	23.19	2.62	21.23	1.11	21.49	0.67	22.43	4.86	18.75	1.50	18.89	0.66
Sir-26	79.73	2.61	99.63	9.05	81.30	6.93	72.39	2.43	92.70	5.12	75.87	3.02	68.56	0.58
Sir-27	52.46	3.84	57.27	5.85	63.76	2.93	51.17	2.02	61.48	9.66	52.15	3.47	60.02	2.88
Sir-28	234.56	1.69	288.77	5.54	315.14	6.50	254.08	4.88	291.45	5.23	308.84	10.81	268.04	4.37
Sir-29	14.04	2.09	12.22	1.64	17.28	1.24	11.96	0.93	14.34	4.09	10.65	1.32	17.78	1.52
Sir-30	38.63	1.81	44.62	3.73	51.38	2.01	42.23	1.14	58.03	10.57	42.66	2.60	59.89	2.78
Sir-31	87.66	1.20	133.25	11.15	109.63	5.57	97.14	2.83	137.11	13.24	102.89	5.67	87.48	0.87
Sir-32	15.08	2.71	13.47	2.11	12.67	0.86	13.95	1.09	15.85	4.97	11.61	1.39	11.40	0.56
Sir-33	31.18	2.84	32.03	3.74	28.65	1.50	28.34	2.17	34.74	7.50	28.69	2.71	26.99	1.97

(continuation) Table A.1 — Data from 33 detectated peaks of all measurements collected during SIRUS-17 with collection times, mean intensity (int.), and standard deviation (SD).

PEAK	DAY THIRTEEN				DAY FOURTEEN	
	D13: 17h17 to 18h21		D13: 22h41 to 23h45		D14: 18h52 to 19h56	
	Int. (volt)	SD	Int. (volt)	int.	Int. (volt)	SD
Sir-1	1210.90	47.51	1394.23	11.89	1332.86	82.01
Sir-2	2006.80	20.08	2013.03	12.82	1975.11	9.26
Sir-3	660.14	15.35	546.70	5.61	936.96	17.18
Sir-4	778.28	11.10	708.13	11.37	742.95	68.74
Sir-5	2406.21	95.54	2220.76	94.45	2304.64	26.32
Sir-6	118.03	4.43	108.95	44.02	50.79	2.79
Sir-7	125.18	2.48	117.33	2.35	142.98	3.31
Sir-8	215.75	12.87	170.00	5.47	412.96	14.08
Sir-9	302.04	4.59	293.15	13.92	275.12	8.07
Sir-10	203.37	4.95	198.91	6.34	314.01	2.59
Sir-11	155.00	16.43	136.48	4.02	154.55	4.58
Sir-12	230.39	6.25	322.44	13.50	268.83	2.98
Sir-13	61.93	0.92	60.99	0.91	61.96	0.97
Sir-14	183.36	5.89	205.85	8.56	166.66	1.35
Sir-15	92.57	0.88	90.62	1.97	93.86	0.80
Sir-16	36.48	3.56	33.44	2.42	36.66	2.13
Sir-17	81.33	4.28	72.48	3.67	81.08	5.50
Sir-18	98.68	6.27	93.51	5.61	94.77	6.83
Sir-19	28.91	4.93	32.01	3.16	29.56	3.32
Sir-20	91.70	3.22	85.38	1.92	256.59	7.10
Sir-21	125.30	2.79	114.45	5.33	152.44	1.69
Sir-22	75.81	2.95	71.25	1.63	71.07	1.64
Sir-23	77.15	19.27	63.87	15.51	74.61	17.52
Sir-24	39.89	2.52	38.96	1.53	37.80	2.86
Sir-25	20.87	0.87	19.81	0.94	22.01	1.83
Sir-26	81.97	5.54	74.38	7.51	82.44	4.11
Sir-27	73.02	5.64	87.62	6.01	76.47	4.40
Sir-28	357.63	13.89	381.51	3.56	350.26	14.46
Sir-29	27.27	1.45	55.39	5.54	36.90	1.44
Sir-30	78.55	4.14	101.95	6.00	76.19	1.79
Sir-31	132.37	7.61	106.27	7.08	137.60	5.49
Sir-32	13.48	0.97	13.86	0.88	23.54	0.98
Sir-33	31.18	2.84	32.03	28.34	44.78	2.24

(continuation) Table A.1 — Data from 33 detectated peaks of all measurements collected during SIRUS-17 with collection times, mean intensity (int.), and standard deviation (SD).

PEAK	DAY SIXTEEN						DAY SEVENTEEN			
	D16: 8h03 to 9h07		D16: 12h05 to 13h09		D16: 12h05 to 13h09		D17: 8h11 to 9h15		D17: 9h57 to 11h01	
	Int. (volt)	SD	Int. (volt)	SD	Int. (volt)	SD	Int. (volt)	SD	Int. (volt)	SD
Sir-1	1416.59	52.13	1479.89	10.14	1229.06	66.74	1374.08	22.83	1476.36	22.83
Sir-2	2049.74	5.86	1796.52	113.44	1991.64	18.81	1987.98	15.42	2008.05	15.42
Sir-3	575.42	16.26	1139.55	289.54	897.69	23.19	664.83	11.40	611.58	11.40
Sir-4	620.54	26.44	694.47	30.68	656.22	26.19	668.10	121.16	725.98	121.16
Sir-5	2056.89	162.86	2117.61	126.51	2304.14	27.29	2152.79	152.22	2145.47	152.22
Sir-6	222.23	21.64	154.10	11.38	45.42	13.14	343.41	23.48	258.24	23.48
Sir-7	144.75	4.27	258.91	67.24	131.31	3.09	133.59	8.99	120.37	8.99
Sir-8	180.01	12.98	2976.71	1431.79	358.90	20.35	214.19	15.79	196.25	15.79
Sir-9	252.15	20.33	274.51	25.13	257.70	15.55	275.86	28.92	279.80	28.92
Sir-10	215.72	4.92	225.52	4.56	205.46	3.93	188.26	6.90	216.88	6.90
Sir-11	150.36	5.51	197.79	32.46	159.19	5.95	131.80	6.29	127.89	6.29
Sir-12	176.48	40.55	280.67	8.23	155.05	7.10	226.83	100.87	428.86	100.87
Sir-13	59.40	1.37	61.01	2.53	64.81	4.77	58.32	2.94	60.40	2.94
Sir-14	157.99	12.09	186.91	5.63	154.53	8.34	142.98	24.32	192.82	24.32
Sir-15	85.07	0.95	89.67	4.00	80.60	8.97	74.61	4.10	77.25	4.10
Sir-16	34.17	3.00	36.70	7.28	39.39	6.24	33.83	7.33	35.36	7.33
Sir-17	70.14	2.89	71.61	3.20	89.83	11.28	67.44	4.30	69.22	4.30
Sir-18	103.28	7.34	99.84	3.60	98.03	5.70	87.92	5.80	88.22	5.80
Sir-19	27.16	2.19	32.99	3.60	29.28	7.70	37.09	11.91	42.03	11.91
Sir-20	77.37	1.66	84.35	2.26	95.54	10.37	81.60	6.85	96.89	6.85
Sir-21	146.69	19.84	280.43	75.00	158.07	4.96	121.55	6.80	120.88	6.80
Sir-22	75.60	1.48	75.65	1.58	76.87	4.44	70.15	2.74	68.33	2.74
Sir-23	66.60	12.85	68.23	22.32	76.99	15.23	61.98	11.85	66.36	11.85
Sir-24	39.10	2.13	41.38	3.53	42.13	7.05	35.09	3.83	37.89	3.83
Sir-25	26.76	1.58	24.99	2.36	26.33	4.13	27.76	4.78	23.49	4.78
Sir-26	78.11	2.08	87.51	10.53	102.83	10.54	71.76	3.02	74.04	3.02
Sir-27	62.14	6.53	78.37	3.13	66.74	10.66	70.06	15.82	108.86	15.82
Sir-28	410.45	6.32	217.32	97.91	389.19	6.32	380.97	3.22	411.96	3.22
Sir-29	21.14	6.31	40.30	2.52	16.06	2.74	36.48	24.77	108.25	24.77
Sir-30	53.57	7.10	74.29	4.96	57.20	7.19	63.44	19.78	110.68	19.78
Sir-31	97.69	2.87	104.15	12.91	127.52	9.34	89.55	4.11	90.37	4.11
Sir-32	16.34	3.58	16.12	2.55	15.87	4.10	12.63	3.24	15.23	3.24
Sir-33	31.87	3.62	39.04	4.13	39.24	6.20	29.72	4.56	30.03	4.56

Table A.2 — Seaweeds' unique peaks (UnP) on their respective colour group and species specific (x). Each seaweed is represented by a two-letter code and corresponding scientific name, drift (milliseconds) and retention (seconds) time, mean and standard deviation, peak presence in other species (2 letter code), species-specific peaks (x-marked), identified compounds (#CAS), total peaks, and species-specific peak percentages (UnP) relative to the total detected peaks. ∀\ {} represents "all except" the seaweed species inside the braces

ID CODE	Drift time	Retention time	Dt Mean	Dt Mean SD	Rt Mean	Rt Mean SD	Species	Compound	Total Peaks	UnP
	Dt (ms)	Rt (sec)	Dt (RIPrel)	Dt (RIPrel)	Rt (sec)	Rt (sec)	Specifics	#CAS Number	Fingerprint	%
Brown Seaweeds: UP (*Undaria pinnatifida*), **FV** (*Fucus vesiculosus*), **BB** (*Bifurcaria bifurcata*) and **SP** (*Saccorhiza polyschides*)										
UP (*U. pinnatifida*)	1.1042	85.2600	1.1051	0.0004	85.0500	0.5040	OP		**65**	**7.69**
	1.0128	90.9300	1.0091	0.0015	89.1240	2.2848	CT			
	1.0822	85.8900	1.0844	0.0031	85.5960	0.5544	x			
	1.1637	109.6200	1.1638	0.0007	109.8300	0.5880	x			
	1.2030	136.5000	1.2042	0.0006	136.9200	0.5040	x			
FV (F. *vesiculosus*)	1.0577	127.8900	1.0580	0.0005	126.6720	1.6296	x		**70**	**18.57**
	1.1236	85.2600	1.1258	0.0035	84.3360	0.9408	x			
	1.1584	120.1200	1.1593	0.0007	119.9940	0.3696	x			
	1.2014	74.7600	1.2020	0.0013	74.8860	0.1008	x	**#60-29-7**		
	1.2051	90.7200	1.2051	0.0008	90.5520	0.2016	x			
	1.2051	205.3800	1.2053	0.0004	205.6740	0.1848	GT & CT			
	1.3040	491.6100	1.3029	0.0008	490.6440	0.8232	x			
	1.3168	99.9600	1.3159	0.0013	100.1700	0.3360	x			
	1.3442	122.8500	1.3450	0.0006	122.7660	0.2184	OP			
	1.3589	332.6400	1.3578	0.0012	334.9080	4.6368	x			
	1.4826	150.7800	1.4825	0.0013	150.6960	0.4704	x			
	1.4898	164.8500	1.4908	0.0010	164.9760	0.1848	GT			
	1.5760	244.2300	1.5754	0.0013	244.9020	0.3696	x			
BB (*B. bifurcata*)	0.9681	220.0800	0.9709	0.0055	218.4000	1.9950	x		**77**	**19.48**
	1.0957	171.9900	1.0954	0.0014	168.4200	3.5700	OP			
	1.1049	153.3000	1.1036	0.0014	153.3525	0.0788	CT			
	1.1213	99.9600	1.1173	0.0048	99.8025	0.2625	UR			
	1.1331	263.9700	1.1311	0.0024	264.2850	0.7875	x			
	1.2014	307.6500	1.2026	0.0021	306.8100	1.1550	x			
	1.2143	375.4800	1.2120	0.0028	373.5375	2.0475	x			

(continuation) Table A.2 — Seaweeds' unique peaks (UnP) on their respective colour group and species specific (x)

ID CODE	Drift time	Retention time	Dt Mean	Dt Mean SD	Rt Mean	Rt Mean SD	Species	Compound	Total Peaks	UnP
	Dt (ms)	Rt (sec)	Dt (RIPrel)	Dt (RIPrel)	Rt (sec)	Rt (sec)	Specifics	#CAS Number	Fingerprint	%
(continuation) Brown Seaweeds: UP (*Undaria pinnatifida*), **FV** (*Fucus vesiculosus*), **BB** (*Bifurcaria bifurcata*) and **SP** (*Saccorhiza polyschides*)										
BB (*B. bifurcata*) (continuation)	1.2151	342.5100	1.2129	0.0027	341.4075	1.5488	x		**77**	**19.48**
	1.3583	215.8800	1.3589	0.0043	215.1975	0.3675	x			
	1.3983	168.4200	1.3976	0.0022	168.8925	0.9188	x			
	1.4048	137.3400	1.4063	0.0041	137.6025	0.2625	x			
	1.5059	213.5700	1.5088	0.0059	213.9375	0.5513	x			
	1.5241	259.3500	1.5256	0.0047	260.7675	2.3363	x			
	1.5378	246.3300	1.5384	0.0024	247.6950	1.6275	OP			
	1.5616	209.1600	1.5627	0.0044	208.3725	1.0763	x			
SP (*S. polyschides*)	0.9663	197.4000	0.9688	0.0030	197.7024	0.5376	x		**83**	**14.46**
	0.9680	279.0900	0.9699	0.0033	279.3336	0.7056	x			
	1.0082	104.7900	1.0082	0.0000	104.7900	0.0000	x			
	1.0855	226.8000	1.0831	0.0038	226.9848	1.0416	x			
	1.1903	391.6500	1.1898	0.0013	392.0868	0.5208	OP. GT & UR	#6728-31-0		
	1.2049	104.1600	1.2049	0.0013	103.5888	0.5208	x			
	1.2067	522.4800	1.2065	0.0004	521.7492	2.4192	x			
	1.2167	93.4500	1.2165	0.0001	93.4164	0.1512	x			
	1.2768	222.8100	1.2777	0.0011	222.9948	0.2688	OP			
	1.3205	158.9700	1.3219	0.0022	159.2304	0.4032	x			
	1.4581	166.7400	1.4573	0.0015	167.0424	0.3192	OP & CT			
	1.7104	206.2200	1.7150	0.0040	206.2116	0.1344	GT & CT			
Red Seaweeds: OP (*Osmundea pinnatifida*), **GG** *(Gracilaria gracilis)*, **GT** (*Grateloupia turuturu*) and **PS** (*Porphyra* spp.)										
OP (*O. pinnatifida)*	0.9709	110.4600	0.9708	0.0001	110.4600	0.0840	x		**105**	**36.19**
	0.9754	78.1200	0.9783	0.0046	78.0780	0.2352	x			
	1.0684	132.9300	1.0652	0.0037	129.6120	3.9816	x			
	1.0903	156.8700	1.0897	0.0014	156.9960	0.1512	x			
	1.0939	174.7200	1.0950	0.0039	174.5100	1.0080	BB			
	1.0957	81.6900	1.0975	0.0033	81.6060	0.3024	x			

(continuation) Table A.2 — Seaweeds' unique peaks (UnP) on their respective colour group and species specific (x)

ID CODE	Drift time	Retention time	Dt Mean	Dt Mean SD	Rt Mean	Rt Mean SD	Species	Compound	Total Peaks	UnP
	Dt (ms)	Rt (sec)	Dt (RIPrel)	Dt (RIPrel)	Rt (sec)	Rt (sec)	Specifics	#CAS Number	Fingerprint	%
(continuation) Red Seaweeds: OP (*Osmundea pinnatifida*), **GG** *(Gracilaria gracilis)*, **GT** (*Grateloupia turuturu*) and **PS** (*Porphyra* spp.)										
OP (*O. pinnatifida)* (continuation)	1.0985	86.3100	1.0994	0.0026	85.7640	0.3192	UP		**105**	**36.19**
	1.1203	361.6200	1.1234	0.0050	364.6020	9.4584	x			
	1.1231	119.9100	1.1232	0.0003	119.8680	0.2352	SP			
	1.1268	238.1400	1.1218	0.0059	240.4080	2.7216	x			
	1.1295	108.5700	1.1298	0.0004	108.8640	0.1848	x			
	1.1331	318.7800	1.1335	0.0004	318.7380	0.9744	x			
	1.1350	86.1000	1.1307	0.0064	86.1000	0.0000	x			
	1.1385	157.0800	1.1406	0.0025	157.1220	0.3696	x			
	1.1467	206.4300	1.1468	0.0007	206.3880	0.2184	x			
	1.1495	276.5700	1.1492	0.0004	277.2420	0.4536	x			
	1.1568	87.3600	1.1477	0.0073	84.8400	2.0160	x			
	1.1842	147.0000	1.1844	0.0003	146.7480	0.3864	UR			
	1.1887	273.2100	1.1896	0.0011	273.5460	0.2352	x			
	1.1951	143.0100	1.1960	0.0011	143.1360	0.1848	x			
	1.2471	99.9600	1.2473	0.0003	100.0440	0.3528	CT			
	1.2516	243.3900	1.2513	0.0004	243.9360	0.5712	x			
	1.2698	120.9600	1.2715	0.0027	121.0860	0.6048	x			
	1.2772	222.3900	1.2787	0.0017	222.3900	0.7560	SP			
	1.2807	210.0000	1.2808	0.0004	210.5040	0.5208	CT			
	1.2872	157.0800	1.2870	0.0006	157.4160	0.2352	x			
	1.3036	111.3000	1.3055	0.0032	111.8880	0.5376	x			
	1.3382	156.2400	1.3377	0.0003	156.3660	0.1512	x			
	1.3510	121.1700	1.3480	0.0046	121.0020	0.6216	FV			
	1.3901	228.4800	1.3903	0.0007	229.6140	1.1088	x			
	1.4020	119.7000	1.4014	0.0003	119.5320	0.2016	FV&UR			
	1.4321	215.4600	1.4322	0.0004	215.7540	0.2352	x			
	1.4448	677.0400	1.4463	0.0011	679.5600	1.0080	x			
	1.4467	167.5800	1.4448	0.0028	167.4540	0.6552	SP&CT			
	1.5196	367.7100	1.5192	0.0006	370.1880	2.9736	x			

(continuation) Table A.2 — Seaweeds' unique peaks (UnP) on their respective colour group and species specific (x)

ID CODE	Drift time	Retention time	Dt Mean	Dt Mean SD	Rt Mean	Rt Mean SD	Species	Compound	Total Peaks	UnP
	Dt (ms)	Rt (sec)	Dt (RIPrel)	Dt (RIPrel)	Rt (sec)	Rt (sec)	Specifics	#CAS Number	Fingerprint	%
(continuation) Red Seaweeds: OP (*Osmundea pinnatifida*), **GG** *(Gracilaria gracilis)*, **GT** (*Grateloupia turuturu*) and **PS** (*Porphyra* spp.)										
OP (*O. pinnatifida)* (continuation)	1.5378	245.0700	1.5385	0.0006	246.2460	1.1592	BB		**105**	**36.19**
	1.6071	244.2300	1.6095	0.0029	245.4900	0.9240	x	**#124-13-0**		
	1.7831	613.6200	1.7831	0.0013	614.8800	2.0160	x	**#18829-55-5**		
GG *(G. gracilis)*	0.9752	85.6800	0.9774	0.0035	85.4700	0.4200	x		**76**	**32.89**
	1.1261	312.9000	1.1259	0.0005	312.9000	0.8400	x			
	1.1463	233.5200	1.1552	0.0035	231.3780	1.1256	x			
	1.1600	271.3200	1.1588	0.0012	270.9000	0.2520	x			
	1.1645	79.3800	1.1642	0.0005	79.2540	0.1008	x			
	1.2049	199.9200	1.2042	0.0007	199.8360	0.3192	x			
	1.2057	162.7500	1.2054	0.0009	162.8760	0.4536	x			
	1.2067	510.5100	1.2063	0.0009	511.1820	2.0832	x	**#3391-86-4**		
	1.2268	283.2900	1.2268	0.0004	282.7440	0.4032	x			
	1.2351	77.7000	1.2344	0.0007	77.6580	0.0672	UR			
	1.2543	177.6600	1.2544	0.0002	177.2820	0.6384	x			
	1.2570	461.3700	1.2576	0.0006	459.3120	1.6296	x			
	1.2872	318.5700	1.2861	0.0010	318.6960	0.3192	x			
	1.3375	642.1800	1.3381	0.0006	641.3820	1.3776	x			
	1.3649	117.1800	1.3646	0.0005	117.3480	0.2016	x			
	1.4308	141.7500	1.4311	0.0011	141.4560	0.3528	x			
	1.4335	138.3900	1.4329	0.0006	138.5160	0.3696	x			
	1.5672	140.4900	1.5659	0.0012	140.4480	0.0672	x			
	1.7089	200.9700	1.7081	0.0008	200.8020	0.3024	x			
	1.7099	212.5200	1.7083	0.0013	212.1840	0.4032	x			
	1.7693	455.0700	1.7672	0.0018	455.6580	1.3608	x			
	1.7830	609.4200	1.7822	0.0009	609.1260	2.0832	x	**#4312-99-6**		
	1.8801	140.2800	1.8793	0.0009	140.1120	0.0672	x			
	2.0703	202.0200	2.0687	0.0013	202.1460	0.4536	x			
	2.0703	210.2100	2.0688	0.0010	209.8740	0.3696	x			

(continuation) Table A.2 — Seaweeds' unique peaks (UnP) on their respective colour group and species specific (x)

ID CODE	Drift time	Retention time	Dt Mean	Dt Mean SD	Rt Mean	Rt Mean SD	Species	Compound	Total Peaks	UnP
	Dt (ms)	Rt (sec)	Dt (RIPrel)	Dt (RIPrel)	Rt (sec)	Rt (sec)	Specifics	#CAS Number	Fingerprint	%
(continuation) Red Seaweeds: OP (*Osmundea pinnatifida*), **GG** *(Gracilaria gracilis)*, **GT** (*Grateloupia turuturu*) and **PS** (*Porphyra* spp.)										
GT (*G. turuturu*)	1.2051	206.4300	1.2038	0.0005	206.6400	0.2520	FV & CT		**75**	**10.67**
	1.2807	204.5400	1.2798	0.0006	206.3460	1.9152	x			
	1.4057	145.9500	1.4043	0.0007	145.9920	0.0672	x			
	1.4694	145.9500	1.4677	0.0007	145.9500	0.0000	x			
	1.4913	166.3200	1.4897	0.0009	166.0680	0.3024	FV			
	1.5442	537.3900	1.5446	0.0018	538.9440	0.7392	x			
	1.5725	204.7500	1.5718	0.0014	206.6820	1.5624	x			
	1.7120	206.2200	1.7117	0.0042	206.3040	0.1848	SP & CT			
PS (*Porphyra* spp.)	1.1344	262.7100	1.1329	0.0011	262.7520	0.3864	x		**20**	**25.00**
	1.1436	153.3000	1.1423	0.0013	153.0900	0.1680	x			
	1.1600	114.8700	1.1722	0.0146	115.8360	1.4952	x			
	1.2102	209.7900	1.2086	0.0011	209.7060	0.2352	x			
	1.2304	122.8500	1.2287	0.0018	122.5560	0.2688	x			
Green Seaweeds: UR (*Ulva rigida*) and **CT** (*Codium tomentosum*)										
UR (*U. rigida*)	0.9697	139.6500	0.9669	0.0003	139.6920	0.4536	x		**59**	**54.24**
	0.9697	213.3600	0.9678	0.0006	214.4520	0.9912	x			
	0.9761	106.2600	0.9759	0.0027	107.0160	1.5456	x			
	0.9761	127.8900	0.9754	0.0026	128.0160	0.4872	x			
	0.9771	93.6600	0.9772	0.0040	94.8360	1.5456	x			
	0.9771	115.9200	0.9761	0.0026	117.2640	1.7304	x			
	0.9779	86.5200	0.9779	0.0041	86.6460	0.1848	x			
	1.0630	115.5000	1.0604	0.0003	115.8780	0.2184	x			
	1.0887	226.5900	1.0835	0.0032	226.9680	0.3024	SP			
	1.0987	159.3900	1.0954	0.0004	160.1460	0.7392	x			
	1.1243	99.9600	1.1216	0.0004	100.3800	0.4200	BB			
	1.1261	119.4900	1.1235	0.0005	119.5320	0.0672	UP & FV & SP & OP	#141-78-6		
	1.1316	94.5000	1.1286	0.0001	94.6680	0.1344	x			

(continuation) Table A.2 — Seaweeds' unique peaks (UnP) on their respective colour group and species specific (x)

ID CODE	Drift time	Retention time	Dt Mean	Dt Mean SD	Rt Mean	Rt Mean SD	Species	Compound	Total Peaks	UnP
	Dt (ms)	Rt (sec)	Dt (RIPrel)	Dt (RIPrel)	Rt (sec)	Rt (sec)	Specifics	#CAS Number	Fingerprint	%
(continuation) Green Seaweeds: UR (*Ulva rigida*) and **CT** (*Codium tomentosum*)										
UR (*U. rigida*) (continuation)	1.1335	111.9300	1.1306	0.0003	112.3080	0.3696	x		**59**	**54.24**
	1.1408	194.8800	1.1353	0.0034	195.1740	0.3192	x			
	1.1857	82.1100	1.1833	0.0007	82.6140	0.4368	x			
	1.1875	145.9500	1.1917	0.0059	144.8160	0.9072	OP			
	1.1902	117.8100	1.1875	0.0006	117.9360	0.1008	x			
	1.1929	391.4400	1.1924	0.0033	392.7000	0.5880	SP & OP & GT	**#6728-31-0**		
	1.2359	170.7300	1.2318	0.0006	170.7300	0.0000	x			
	1.2369	77.2800	1.2358	0.0037	77.6160	0.2856	GG			
	1.2561	154.1400	1.2533	0.0003	154.3500	0.2520	OP			
	1.2853	138.6000	1.2831	0.0009	138.7260	0.2856	x			
	1.3229	118.6500	1.3196	0.0011	119.1540	0.3192	x			
	1.3394	112.9800	1.3356	0.0008	113.0640	0.1008	x			
	1.3412	100.8000	1.3362	0.0025	100.9260	0.2016	x			
	1.3622	138.3900	1.3583	0.0007	138.8100	0.3360	x			
	1.3696	405.0900	1.3657	0.0005	406.4340	0.6552	∀\ {FV BB PS CT}	**#111-71-7**		
	1.3768	161.2800	1.3741	0.0007	161.5740	0.2688	x			
	1.4043	119.2800	1.4007	0.0003	119.4480	0.0672	FV & OP	**#141-78-6**		
	1.4784	142.8000	1.4724	0.0034	142.9260	0.1848	x			
	1.6019	368.5500	1.5957	0.0020	369.8940	0.7728	∀\ {GG GT CT}	**#6728-26-3**		
∀\ {} represents "all except" the seaweed species inside the braces										
CT (*C. tomentosum*)	1.0109	97.4400	0.9994	0.0004	97.3980	0.1344	x		**50**	**44.00**
	1.0146	90.7200	1.0003	0.0008	92.1900	0.0000	UP			
	1.0912	75.3900	1.0918	0.0005	75.3060	0.1512	FV & BB	**#60-29-7**		
	1.1049	153.3000	1.1008	0.0040	153.0480	0.4872	OP & GT			
	1.1331	169.0500	1.1319	0.0007	169.3440	0.2184	x			
	1.1377	215.8800	1.1381	0.0009	216.2160	0.7728	x			
	1.2024	208.5300	1.2022	0.0012	205.2540	5.1408	FV & GT			
	1.2389	102.9000	1.2471	0.0009	99.8760	0.1512	OP			
	1.2561	138.6000	1.2517	0.0002	141.7500	0.0000	x			
	1.2717	98.9100	1.2706	0.0131	99.7500	0.1680	x			

(continuation) Table A.2 — Seaweeds' unique peaks (UnP) on their respective colour group and species specific (x)

ID CODE	Drift time	Retention time	Dt Mean	Dt Mean SD	Rt Mean	Rt Mean SD	Species	Compound	Total Peaks	UnP
	Dt (ms)	Rt (sec)	Dt (RIPrel)	Dt (RIPrel)	Rt (sec)	Rt (sec)	Specifics	#CAS Number	Fingerprint	%
(continuation) Green Seaweeds: UR (*Ulva rigida*) and **CT** (*Codium tomentosum*)										
CT (*C. tomentosum*) (continuation)	1.2807	210.2100	1.2861	0.0010	218.6520	1.0248	OP		**50**	**44.00**
	1.2826	160.2300	1.2720	0.0110	161.4900	2.4360	x			
	1.3163	142.8000	1.3203	0.0002	143.2200	0.3360	x			
	1.3190	133.5600	1.3121	0.0123	133.6020	0.8736	x			
	1.3245	165.9000	1.3375	0.0023	163.0020	0.7392	x			
	1.3319	163.1700	1.3410	0.0019	161.6160	0.1512	x			
	1.4038	250.5300	1.3965	0.0076	249.4800	0.8400	x			
	1.4212	168.6300	1.4252	0.0028	168.0840	0.7392	FV			
	1.4403	203.2800	1.4379	0.0010	206.6400	1.5960	x			
	1.4567	167.3700	1.4578	0.0051	167.1600	1.0920	SP & OP			
	1.4622	203.4900	1.4767	0.0041	205.7580	3.5784	x			
	1.7074	206.4300	1.7075	0.0006	202.0200	0.0000	SP & GT			

Table A.3 — Data obtained for three permeation tubes of 2-butanone for the establishment of a calibration curve with concentration represented in parts-per-billion, respective mean intensity (monomer and dimer signals) for 5 replicates, standard deviation, hoven temperatures and respective gas flows and emission rate in ng/min for each tube.

Concentration [ppb]	Mean Intensity, 5 replicates) [volts]	Standard deviation	Temperature (°C)	Gas flow (ml/min)
Permeation tube 1	**----**	**Permeation rate**	**(22.7 ng/min)**	**----**
2318	10218.12	35,55	35	10
920	8493.33	31,83	35	25
456	6913.05	43,79	35	50
228	5607.54	53,89	35	100
152	5137.92	14,22	35	150
114	4729.63	19,69	35	200
Permeation tube 2	**----**	**Permeation rate**	**(19.1 ng/min)**	**----**
1977	9613.85	26,07	30	10
776	7757.60	54,10	30	25
386	6410.07	46,54	30	50
192	5286.40	8,99	30	100
128	4688.37	13,71	30	150
96	4280.89	12,43	30	200
Permeation tube 3	**----**	**Permeation rate**	**(13.3 ng/min)**	**----**
1377	8715.31	23,28	25	10
269	5888.26	28,28	25	50
89	4264.08	16,67	25	150

Table A.4 — Data obtained for two permeation tubes of 1-butnanol for the establishment of a calibration curve with concentration represented in parts-per-billion, respective mean intensity (monomer and dimer signals) for 5 replicates, standard deviation, hoven temperatures and respective gas flows and emission rate in ng/min for each tube.

Concentration [ppb]	Mean Intensity, 5 replicates) [volts]	Standard deviation	Temperature (°C)	Gas flow (ml/min)
Permeation tube 1	**----**	**Permeation rate**	**(2.7 ng/min)**	**----**
274.9	5369.20	133.82	40	10
110.0	3973.97	216.32	40	25
54.3	2434.71	66.32	40	50
27.0	1480.55	20.33	40	100
18.0	1086.30	40.31	40	150
13.5	894.77	23.97	40	200
Permeation tube 2	**----**	**Permeation rate**	**(18 ng/min)**	**----**
1896.7	9507.55	53.82	50	10
738.5	6936.07	236.06	50	25
364.8	4654.10	97.42	50	50
180.6	2833.64	160.40	50	100
120.3	2128.33	113.17	50	150
90.1	1717.97	26.23	50	200

2022

JORGE MANUEL DIAS FERNANDES

DIRECT DETECTION OF ORGANIC AND BIOLOGICAL CONTAMINANTS IN INTERNATIONAL SPACE STATIONS